ASPECTS OF THE GEOLOGY AND GEOCHEMISTRY OF THE PROTEROZOIC ROCKS OF THE VALLEY OF A THOUSAND HILLS, KWAZULU NATAL

By

George Charles Milne

Thesis submitted in partial fulfillment of the requirements
for the degree of Doctor of Philosophy

School of Geological and Computer Sciences,
University of Natal, Durban,
South Africa

December 1999

PREFACE

The work described in this thesis was carried out in the School of Geological and Computer Sciences, University of Natal, Durban, from June 1988 to December 1999, under the supervision of Professors A. Kerr and M. Watkeys.

These studies represent original work by the author and have not otherwise been submitted in any form for any degree or diploma to any tertiary institution. Where use has been made of the work of others it has been duly acknowledged in the text.

G.C. Milne

Dedicated to the memory of
Grace Margaret Milne
(1937-1989)

ACKNOWLEDGEMENTS

This project was originally conceived by Alan Kerr, whose enthusiasm provided the initial impetus for the thesis. Following his untimely death this role was taken on by Mike Watkeys. Financial support was provided by the FRD. The completion of this thesis was assisted by numerous individuals and institutions, and in particular I would like to thank Professors E Saggerson, J Krynauw, and F Bell for their advise, the technical staff at the University of Natal for the preparation of thin sections, Rhodes University for the use of their microprobe, the University of Pietermaritzburg for the geochemical analyses, the Geological Survey for the geochemical analyses and the use of their rock drill and Royal Holloway and New Bedford College, London, for REE analyses. A special thanks to Chantelle Goodes, for her assistance with printing several plans. Nothing could have been done, however, without the support of my family who encouraged me through the years.

ABSTRACT

A regional field and geochemical study has allowed the identification of three primary units within the Proterozoic basement of the Valley of a Thousand Hills. The Nagle Dam Formation incorporates several chemically distinct orthogneiss series, characterised by limited intragroup fractionation, and derived from discrete sources. Intrusive into the gneisses are the megacrystic A-type granites of the Mgeni batholith, comprising the biotite granites of the Ximba Suite; the hornblende granites and charnockite of the Mlahlanja Suite; and the medium grained leucogranite of the Nqwadolo Suite. Petrogenetic modelling indicates that these are predominately cumulates. A general model for the A-type granites suggests that they were derived through variable MASH processes on an original within plate type basalt. Enclaves within the Mgeni batholith form a distinct series, the Valley Trust Formation, comprising a nongenetic orthogneiss association of amphibolite and crustal sourced quartzo-feldspathic gneiss and locally derived paragneisses. Interaction between the biotite granite and the pelitic enclaves generated a biotite garnet granite. Geothermobarometry suggests temperatures of metamorphism to a maximum of 770°C for the Nagle Dam Formation and c.850°C at a pressure of 6 kb for the Valley Trust Formation. Potential magmatic temperatures of c.760°C at 5 kb are derived for the Mgeni batholith. High Mn garnets within late veins indicate subsequent intrusion at higher levels.

Derivation of a tectonic model for the Valley of a Thousand Hills is assisted by a revaluation of the chemical tectonic discrimination plots as source or initiator discriminators. These indicate an origin for the Nagle Dam Formation in an arc environment, while the bimodal orthogneiss association of the Valley Trust Formation and the A-type character of the Mgeni batholith suggests their evolution during extensional events. Geothermobarometry defines an isothermal decompression path, possibly generated during a collision event, superimposed on which is a potential midcrustal heating event, resultant on the intrusion of the Mgeni batholith. These data can be integrated with revised lithotectonic data from the southern portion of the Natal Province to derive a regional model. This comprises: the collision of a number of arcs with associated splitting to form backarcs, sedimentation, and failed rift systems; syn-collisional S-type magmatism, contemporaneous with isothermal decompression of the region; and a series of pulses of post-orogenic granites.

TABLE OF CONTENTS

CHAPTER 1

INTRODUCTION

1.1 OBJECTIVES OF THE PRESENT STUDY

The present study was initiated by Prof. A. Kerr as a continuation of the earlier work of Kuyper (1979), Du Toit (1979), Bulley (1981) and Eglington (1987) in the Valley of a Thousand Hills, an area selected as a representative example of the Proterozoic granite-gneiss association of central KwaZulu Natal (Cain 1975). Its aim is to extended the previously limited geochemical data base in the Valley of a Thousand Hills and so allow the more specific geochemical characterisation of the major rock types, distinguish distinct rock groups, identify the nature of the protolith of the metamorphosed lithologies and develop petrogenetic models for selected units. In addition, a geothermobarometric study of the area has been undertaken to produce a quantitative analysis of the conditions of metamorphism of the country rocks and the level of intrusion of the granites.

These data are utilised as the framework for the development of a general model for the geological evolution of the Valley of a Thousand Hills during the Proterozoic, an area largely neglected during recent regional analyses of the Natal Province (for example Thomas 1989a). Ultimately this scheme is extended to provide a comprehensive model for the southern portion of the Natal Province.

1.2 LOCALITY

The present study is centred within the Valley of a Thousand Hills, northwest of Durban, KwaZulu Natal, South Africa (Figure 1.1) and includes the majority of the Proterozoic basement rocks exposed in the 1:50 000 topographical sheets 2930 DA Cato Ridge and 2930 DB Inanda, an area of approximately 600km^2. This area takes the form of a large topographic low, open to the northeast, and surrounded by an escarpment of Phanerozoic sediments, the Natal Group and Karoo Sequence. Its northern and western portions are extremely rugged with prominent granite bornhardts, such as Sithumba and Nqwadolo, and heavily vegetated steep-sided ridges. South of the Nanda plateau the country becomes more subdued, with the Mgeni River developing a marked meander pattern before it exits the Valley of a Thousand Hills through the gorge below Matabetule.

Retreat of the escarpment has left several large outliers of Phanerozoic sediments within the basement exposure. These occur as large, flat topped 'Table Mountains' with distinctive scarp slopes. From Kwa-Matabata to Nanda a series of these combine to form a marked linear feature. This serves to separate the Mgeni River and its tributaries, to the southwest, from the smaller Mdloti River system to the northeast.

1.3 PREVIOUS WORK

The first account of the basement rocks of KwaZulu Natal was in a letter from Sutherland to Sir R.I. Murchison noting the presence of a large northeast - southwest trending '*dyke of granite*' with a '*rough-grained, almost porphyritic*' texture (Sutherland 1855). Subsequently, Griesbach (1871) in his geological map of the Colony of Natal, identified several large occurrences of granite within the major coastal river valleys. The full extent of these rocks in northern KwaZulu Natal was distinguished by Anderson (1902), who believed that the granites and associated metamorphic series formed an integral rock association. Krige (1935), however, in his geology of Durban considered the granites, although gneissose, to be intrusive in nature. On mineralogical grounds he correlated the granites with those of northern KwaZulu Natal and Mpumalanga.

Subsequently, numerous studies were initiated within the Valley of a Thousand Hills and surrounding areas, including Kent (1938), Cherry (1946), Dodson (1950), Matthews (1952), Hargraves (1952), Scheepers (1952), van Straten (1952), Arnett (1953), Lambert (1954), Thompson (1955), Gold (1957) and Davies (1964). These investigations distinguished a series of paragneisses and orthoamphibolites, which were typically correlated with the Tugela Series of northern KwaZulu Natal, and later granites. The granites were initially thought to have formed through metasomatic alteration of the gneisses, but later analysis (Guy 1974; Cain 1975) suggested that they represented a remobilised basement to the associated gneisses.

In 1978 a major mapping programme was initiated in the Valley of a Thousand Hills (Kuyper 1979; Du Toit 1979; Bulley 1981). These authors recognised the fundamental difference between the paragneisses (Nagle Dam Formation) and the granitic rocks, which were viewed as the remobilised basement to the gneisses, portions of which occur as enclaves within the granites.

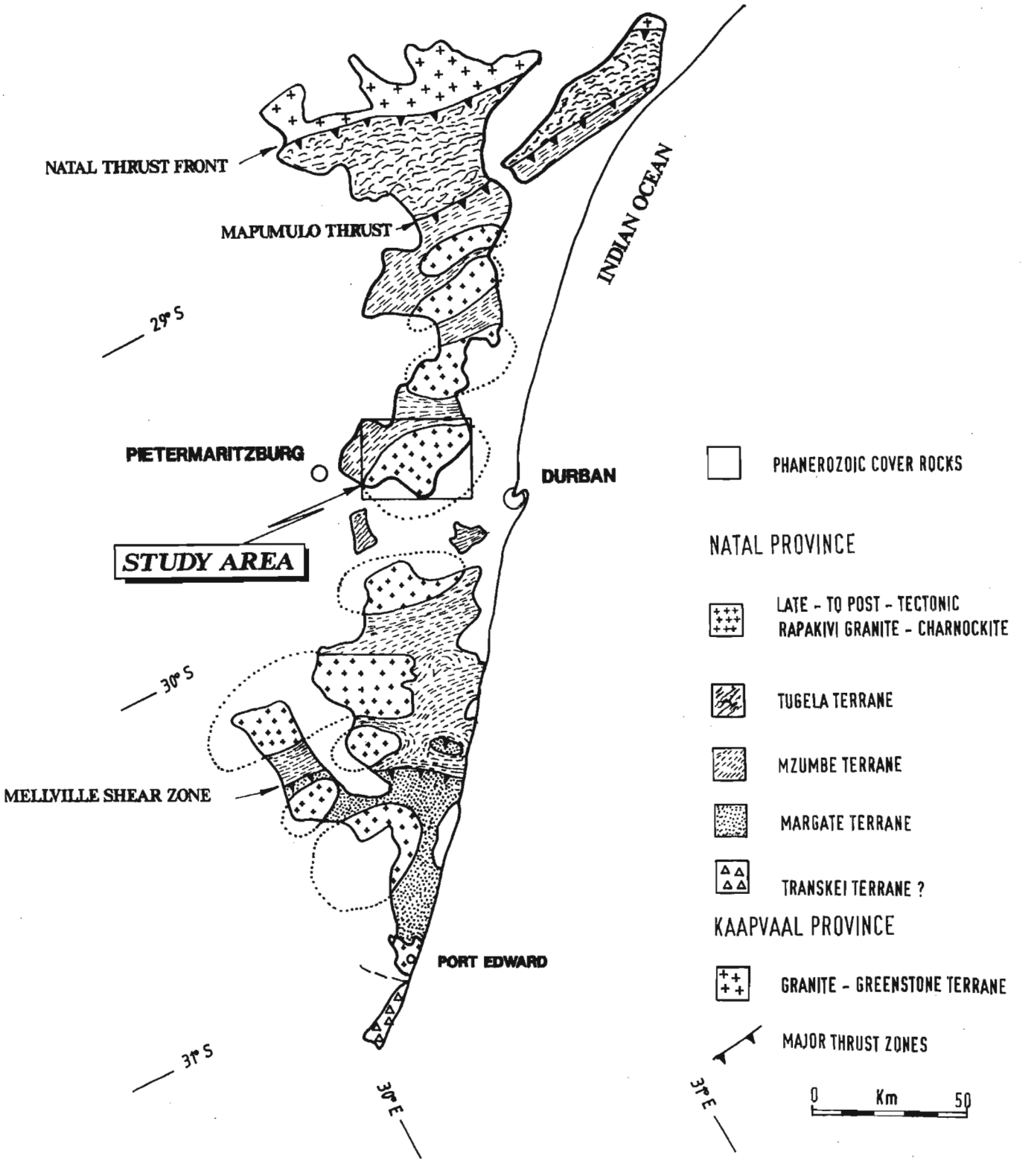

Figure 1.1 Regional geological map of the Natal Province (Thomas 1989a), showing the location of the study area in relation with the principle tectonic subdivisions of the province.

Smaller enclaves were thought to represent restite material. Metamorphism to granulite grade was identified, with the development of charnockites within the granites. Three phases of deformation were distinguished, including the late large scale warping of the granites.

Kuyper (1979) and Du Toit (1979) presented 46 geochemical analyses, predominately from the granites. These defined simple trends on Harker diagrams which were considered to suggest a genetic relationship between the various granites. Kerr (1985), however, proposed that the granites represented three distinct families, comprising:

Suite I - hornblende granite, charnockite, garnet hornblende granite;
Suite II - biotite garnet granite, biotite granite; and
Suite III - late Nqwadolo granite.

This conclusion was supported by the isotopic analyses of Eglington (1987), which showed that each suite possessed distinct initial strontium ratios (Sr_I):

Suite I - Sr_I 0.7042±28;
or 0.7053±8 (Eglington *et al.* 1989a);
Suite II - Sr_I 0.7077±12;
Suite III - Sr_I 0.716±24;

and ages of 1096±180 Ma, or 1029±57 Ma (Eglington *et al.* 1989a), 1001±35 Ma and 1033±18 Ma respectively. Kerr (1985), Milne (1986) and Eglington (1987) noted the distinct chemical characteristics of these granites - high Fe/Mg ratios and enhanced high field strength element (HFSE) concentrations - comparable to those found in the A-type granites of Loiselle and Wones (1979) and Collins *et al.* (1982) which intrude during the end phase of an orogenic event or in an anorogenic setting.

1.4 REGIONAL SETTING

The Proterozoic basement of KwaZulu Natal - the Natal Province (Tankard *et al.* 1982; Thomas 1989a) - is restricted to a narrow, discontinuous inlier trending subparallel to the coast from Port Edward to the Tugela River (Figure 1.1), where Matthews (1972) identified a thrust contact with the Archaean Kaapvaal Craton - the Kaapvaal Province of Thomas (1989a). The lateral extent of the province is concealed by later sedimentary cover but it is typically considered to form an eastern extension of the Proterozoic sequence in Namaqualand (Tankard *et al.* 1982; Goodwin 1991), while the southern margin of the province is thought to be marked by the geophysical Southern Cape conductivity belt and the Beattie magnetic anomaly (De Beer *et al.* 1982; De Beer and Meyer 1983). A possible eastern continuation into Antarctica was proposed by Smith and Hallam (1970), Piper (1974) and Groenewald *et al.* (1991).

Many of the earlier workers, including Du Toit (1954) and Haughton (1969), correlated the basement rocks of KwaZulu Natal with those of Mpumalanga. The regional isotopic study of Nicolaysen and Burger (1965), however, identified a major hiatus between the c.2600 Ma granites in Mpumalanga and the c.1000 Ma granites and metasedimentary rocks of southern KwaZulu Natal. Following the identification of this distinct Proterozoic basement in KwaZulu Natal, a number of authors, including Matthews (1972; 1981a; 1981b), Cain (1975), the South African Committee for Stratigraphy (1980), Milne (1986) and more recently Thomas (1989a), Jacobs *et al.* (1993) and Jacobs and Thomas (1994) have developed and are refining a regional framework for the geological evolution of the Natal Province.

Initially, the Proterozoic basement of KwaZulu Natal was partitioned into a series of zones each characterised by a specific lithological assemblage or grade of metamorphism (Matthews 1981a). Subsequently, Thomas (1989a) proposed that these zones represented four distinct tectonic terranes (Figure 1.1) each separated by a major structural discontinuity, and distinguished by variations in their supercrustal lithologies and early intrusions. This juxtaposition of terranes was considered to represent the cumulation of a series of collision events, involving one or more island arcs, of c.1200 Ma age, and the Kaapvaal Craton (Matthews 1981a; Milne 1986; Jacobs *et al.* 1993; Jacobs and Thomas 1994). Following the fusing of these terranes, c.1100 Ma (Jacobs and Thomas 1994), the province behaved as a single tectonic unit, into which a series of granites intruded, the most prominent of which are the c.1050 Ma (Jacobs and Thomas 1994) rapakivi granite - charnockite batholiths of the Oribi Gorge Suite (Thomas 1988a).

CHAPTER 2

GEOLOGY OF THE VALLEY OF A THOUSAND HILLS

2.1 INTRODUCTION

In this section the field appearance, petrography and mineral chemistry of the principle lithologies present within the Valley of a Thousand Hills will be described.

Kerr (1985) distinguished two major units within the Valley of a Thousand Hills:

1) the Nagle Dam Formation, which occupies the northern portion of the area, and consists predominately of migmatised banded biotite and hornblende-biotite gneisses, with lesser amphibolite, quartzo-feldspathic gneiss and pelitic gneiss. Meta-ultrabasic, quartzite, marble and small manganiferous bodies are of minor significance (described in detail by Kent 1938; Davies 1964). At least three phases of deformation and metamorphism that reached granulite grade have been recognised (Bulley 1981); and
2) the Mgeni megacrystic granite (Mgeni batholith), a series of granites characterised by large feldspar megacrysts - believed to be a member of the Oribi Gorge Suite of post-orogenic granites (Thomas 1989a) - which intrudes the gneisses of the Mapumulo Group.

Within these granites a number of enclaves were identified, predominately an amphibolite - pelitic gneiss association, correlated with the Nagle Dam Formation, and quartzo-feldspathic gneiss, believed to be feeder dykes to the Nqwadolo granite (Kuyper 1979), metamorphosed to granulite grade. Although small enclaves occur in all the granites, large enclaves are restricted to the megacrystic granites, and in the southwest of the batholith form major septa separating individual plutons.

Lithological and chemical differences between the enclaves found within the main body of the Mgeni batholith and the country rock gneisses, however, do not support their correlation (Section 4.3.3). Rather, the enclaves are considered to represent a separate unit - the Valley Trust Formation. The numerous small enclaves present in the contact zone of the Mgeni batholith and the larger enclaves included within the granite veins intruding the Nagle Dam Formation are, however, viewed as a portion of the Nagle Dam Formation.

Three primary units have therefore been recognised during the present study:

1) the gneisses of the Nagle Dam Formation;
2) the enclaves of the Valley Trust Formation; and
3) the granites of the Mgeni batholith.

These are summarised in Table 2.1 and Figure 2.1. To facilitate in the analysis of these units an extensive field sampling programme was initiated, from which specific samples were selected for microprobe analysis of their mineral phases and geochemical analysis. These latter are given the prefix UND or NQ (for a series of samples collected from the Nqwadolo Suite), and the results are given in Appendix 2 (Microprobe Analyses) and Appendix 3 (Geochemical Analyses). The position of these samples are given on the geochemical sample locality plan in Appendix 3. Other samples, which were not selected for geochemical analysis are given the prefix NDF (Nagle Dam and Valley Trust Formations), XS (Ximba Suite) and MS (Mlahlanja Suite). The location of those which are discussed in this section are given on the geochemical sample locality plan in Appendix 3.

2.2 THE MAPUMULO GROUP

2.2.1 NAGLE DAM FORMATION

a) Biotite Hornblende Gneiss

A grey, medium grained, commonly migmatised, biotite hornblende gneiss comprises the majority of the Nagle Dam Formation. It consists predominately of quartz, plagioclase feldspar (An_{25-40}), perthitic K-feldspar, biotite and hornblende (Appendix 1), with accessory opaque ore, apatite, zircon and allanite. Secondary prehnite, chlorite (after biotite), sphene (around ore), muscovite and carbonate may be present. Individual enclaves within the contact zone of the Mgeni batholith may, however, differ conspicuously from this norm, and mafic rich gneiss, orthopyroxene bearing gneiss, chlorite (after biotite) muscovite gneiss and porphyroblastic gneiss have been identified.

Thin sections are usually seriate, with the mafic minerals characteristically smaller than the associated quartzo-feldspathic material, or inequigranular, with the development of quartz and plagioclase megacrysts. Mineral contacts are predominately interlobate. A lepidoblastic or nematoblastic texture is developed, depending on the individual mineralogy of the section. Variations

Table 2.1. Stratigraphic nomenclature of the Proterozoic basement of the Valley of a Thousand Hills.

LITHOSTRATIGRAPHIC UNIT	PRINCIPLE LITHOLOGIES	UNITS
Mgeni batholith		
Nqwadolo Suite	Mafic poor biotite granite	Nqwadolo pluton
Mlahlanja Suite	Garnet hornblende granite Hornblende granite - charnockite Hornblende granite	Spitskop, Matata plutons Sansikane, Egugwini plutons Mlangakhuta, eNyoni plutons
Ximba Suite	Biotite $\pm$ garnet $\pm$ hornblende granite	Ximba pluton
Mapumulo Group		
Valley Trust Formation	Pelitic gneiss Amphibolite Quartzo-feldspathic gneiss	
Nagle Dam Formation	Biotite hornblende gneiss Quartzo-feldspathic gneiss Amphibolite	

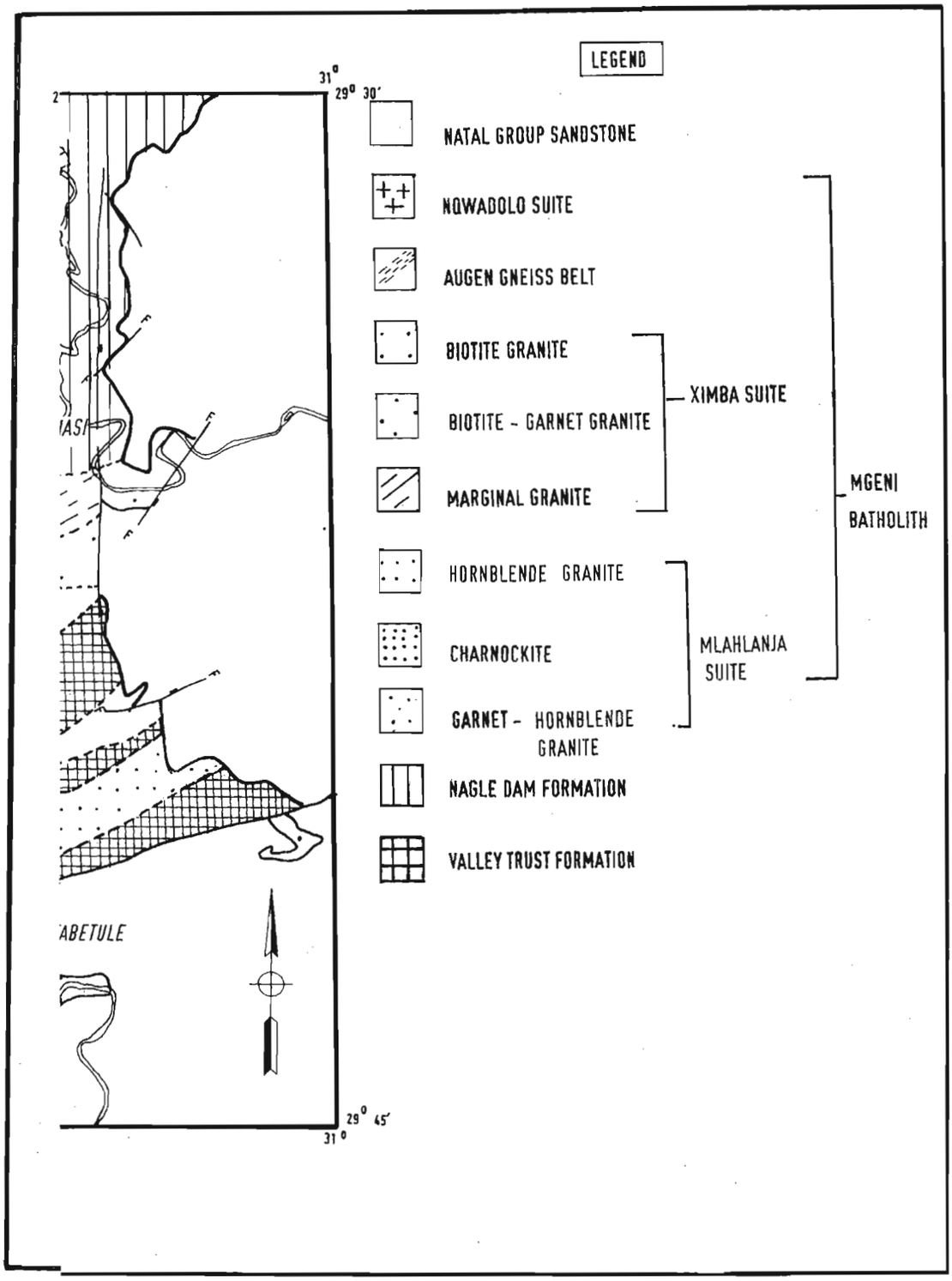
LEGEND
31°
29° 30'
NATAL GROUP SANDSTONE
NQWADOLO SUITE
AUGEN GNEISS BELT
BIOTITE GRANITE
BIOTITE - GARNET GRANITE
MARGINAL GRANITE
XIMBA SUITE
MGENI BATHOLITH
HORNBLENDE GRANITE
CHARNOCKITE
GARNET - HORNBLENDE GRANITE
MLAHLANJA SUITE
NAGLE DAM FORMATION
VALLEY TRUST FORMATION
ABETULE
29° 45'
31°

isand Hills

in mafic mineral orientations suggest the existence of a second fabric.

Microprobe analyses of the plagioclase and biotite are available from a marginal enclave (NDF2) within the Mgeni batholith (Appendix 2). These are an andesine (An_{33-36}) and annite (Figure 2.2) respectively, with the biotite exhibiting a low iron (Fe/Fe+Mg = 0.33-0.42) and total alumina (Al_{TOT} = 2.48-2.58) content.

b) Quartzo-feldspathic Gneiss

In outcrop the quartzo-feldspathic gneiss is typically white or red in colour and consists predominately of medium grained felsic minerals, quartz, perthitic microcline and oligoclase, with minor biotite (Appendix 1). Accessory amounts of opaque ore, zircon, apatite and allanite occur, the latter being particularly abundant in the enclaves within the marginal granite. Elongate felsic minerals and biotite define a crude foliation. Bulley (1981) described two large occurrences adjacent to the Mgeni and Glendale batholiths, but the former has since been reinterpreted as a portion of the Mgeni batholith (A Kerr, 1988, pers. comm.[1]).

It is texturally complex, with individual samples displaying a heterogranular granoblastic texture, or in those thin sections with abundant biotite, a lepidoblastic texture. Elongate quartz may also define a fabric. The localised occurrence of biotite in individual thin sections produces a gneissose texture. Typically the mineral size distribution is seriate, although the actual size of the crystals differ greatly. Mineral contacts are variable with interlobate and amoeboid contacts developed.

Microprobe analyses of the feldspars (Appendix 2) from a sample (UND 309) collected within the main gneiss belt indicate that the plagioclase is an oligoclase (c.An_{24-27}), frequently with an albite margin (c.An_{1-5}), rarely an albite. The K-feldspar is highly potassic, typically with limited solid solution ($Or_{91-100}Ab_{0-9}An_0$), although individual analyses possess a significant sodium content ($Or_{23}Ab_{76}An_1$).

c) Amphibolite

The amphibolite occurs predominately as a component of an association of distinct lithologies, and in particular pelitic gneiss, at Sanvula (Davies 1964) and below Tafamasi (Bulley 1981). Numerous scattered, smaller exposures also occur associated with the biotite hornblende gneiss and within the marginal granite of the Mgeni batholith. It is a medium grained dark rock, comprising plagioclase (c.An_{40}), hornblende and quartz, occasionally with diopside and biotite (Appendix 1). Opaque ore is a common accessory mineral. A crude gneissosity, which may be deformed, is frequently developed. Hornblendite and a medium grained two pyroxene amphibolite are present within the marginal granite of the Mgeni batholith.

The amphibolite typically possesses a foliated equigranular medium-grained nematoblastic polygonal texture although the mafic portions of a thin section and the more mafic samples are coarser grained than the felsic sections. The pyroxene amphibolite is markedly inequigranular. A gneissose texture marked by variations in the hornblende/plagioclase ratio or the presence of mineralogically distinct layers is present in individual thin sections. Particularly well-defined are plagioclase ± diopside or quartz ± diopside zones alternating with hornblende dominant layers. Triple point contacts are found between the plagioclase and hornblende, but rarely with the pyroxene which tends to display rounded contacts, and especially with the plagioclase.

One sample of the amphibolite was selected for microprobe analysis - UND 320 - from below Odlameni (Appendix 2). The plagioclase is an andesine (c.An_{42-48}), with individual analyses displaying considerable solid solution ($An_9Ab_{72}Or_{19}$). The amphibole is magnesium (Fe/Fe+Mg = 0.39-0.41, Fe^{3+} = 0.48-0.71), with a low alkali content. Following the terminology of Leake (1997) it is a calcic amphibole ($(Ca+Na)_B>1$, $Na_B<0.5$ and $(Na+K)_A>0.50$) and on the classification diagram of Leake (1997) plots in the edenite field (Figure 2.3). The clinopyroxene is also magnesium rich (Fe/Fe+Mg = 0.28-0.29), with a high nonquadrilateral component (Al_2O_3 = 1.54-1.63%, Na_2O = 0.39-0.40%) and plots in the diopside field on the pyroxene classification diagram of Morimoto (1988).

d) Pelitic Gneiss

Pelitic gneiss has been reported from several localities within the Nagle Dam Formation and the marginal phase of the Mgeni batholith, and in particular Phangendays (Kuyper 1979) and Tafamasi (Bulley 1981). The present study has found that it is medium grained with a poorly to well defined gneissose texture, consisting essentially of plagioclase (An_{27-35}), quartz, perthitic K-feldspar (microcline and orthoclase), a

[1] Prof A Kerr, University of Natal, deceased

Figure 2.2 Classification of the biotites from the Mapumulo Group and the granites of the Mgeni batholith, after Deer *et al.* (1971).

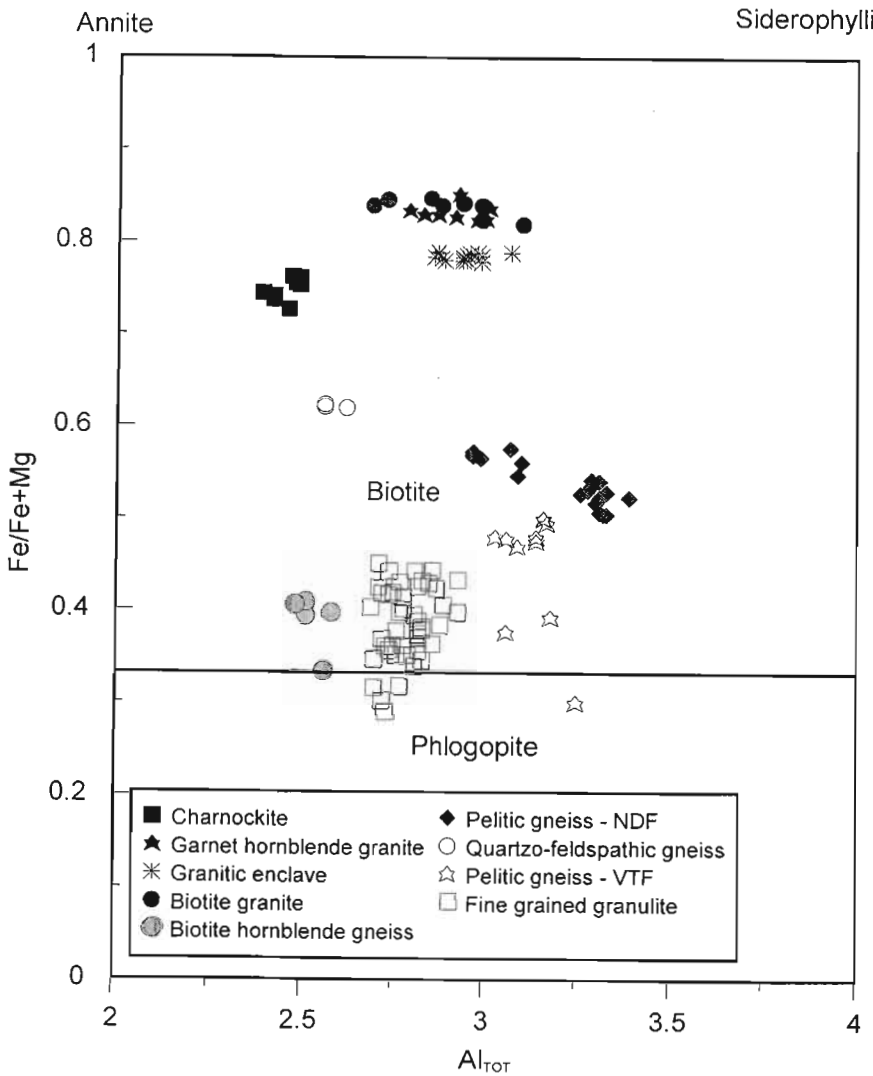

Figure 2.3. Classification of the amphiboles from the Mapumulo Group and the granites of the Mlahlanja Suite, after Leake (1997). Fe^{3+} calculated by the method of Holland and Blundy (1994).

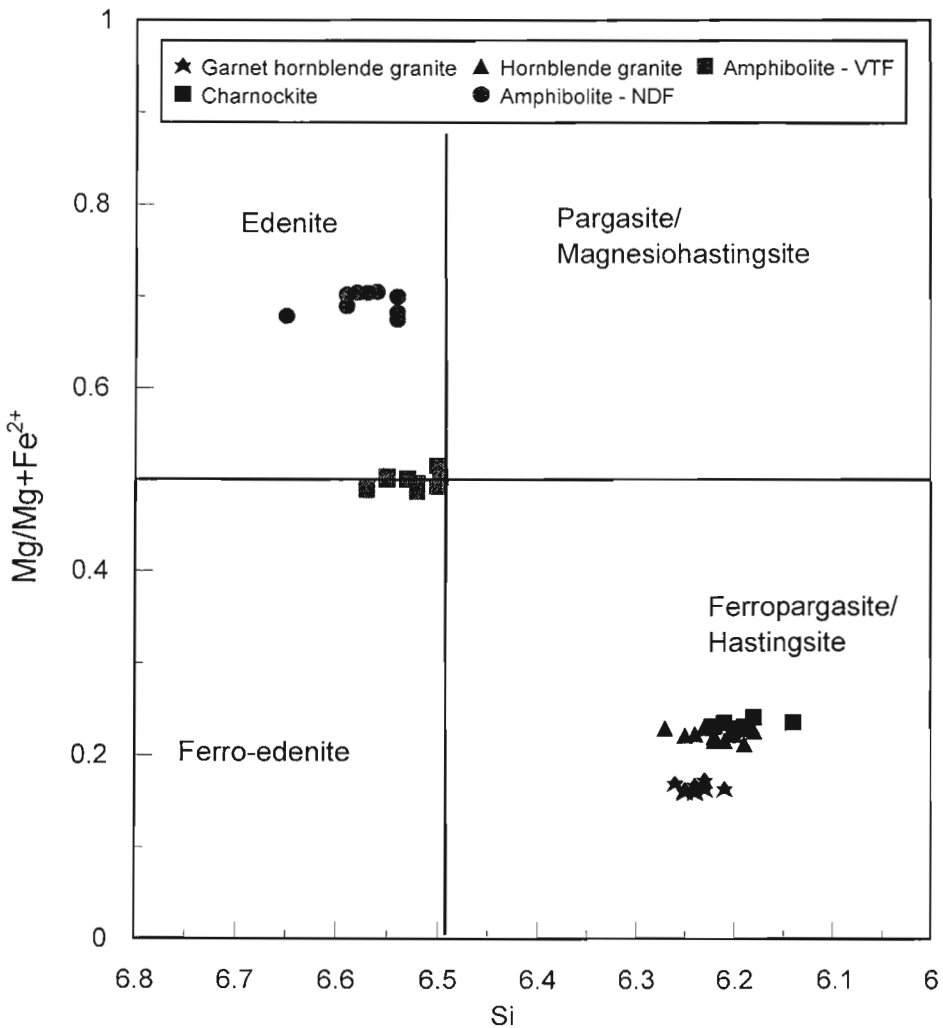

characteristically high biotite content and garnet (Appendix 1), with accessory opaque ore, zircon and apatite.

A gneissose texture is distinguished by major variations in the biotite concentration and the size of the felsic minerals, which are typically larger in the leucosome, although plagioclase megacrysts may occur associated with the melanosome. In addition, plagioclase appears to be more altered and muscovite more abundant in the leucosome. Garnet is ubiquitous.

Within individual layers the pelitic gneiss displays a well developed lepidoblastic texture. The mineral size distribution is variable, with the biotite-rich melanosome being more equigranular than the seriate biotite-poor leucosome. Mineral contacts are typically interlobate, but are amoeboid in quartz-rich zones. Evidence for the development of a second fabric is recorded in the variation of mafic mineral orientations.

Two samples of the pelitic gneiss were selected for microprobe analysis, one a marginal enclave within the granite at Phangendays (NDF 60) and the other from Tafamasi (NDF 8) (Appendix 2). The plagioclase is an andesine (c.An_{32-39}) with no apparent zonation. The high total alumina content (Al_{TOT} = 2.97-3.39) of the biotite places it within the siderophyllite sector of the ideal biotite plane (Figure 2.2), while its high titanium content (Ti = 0.33-0.47) is characteristic of biotite from the granulite grade (Guidotti 1984). Analyses from the different samples are chemically distinct, and in particular the biotite from sample NDF 60 possesses relatively high alumina contents but low iron. Individual analyses may display potassium loss. The garnet is an almandine, with high pyrope and lesser spessartine and grossular components ($Alm_{67-69}Spess_{9-12}Py_{14-18}Gross_{4-5}$), and a marginal sector enriched in alumina, iron and manganese but depleted in silica and magnesium ($Alm_{70.5}Spess_{15.5}Py_9Gross_5$). These features are typical of diffusion zoning in garnet (Tracy 1982) that underwent retrograde breakdown to form biotite at upper amphibolite conditions (Tracy *et al.* 1976; Hollister 1977).

2.2.2 VALLEY TRUST FORMATION

The majority of the Valley Trust Formation occurs as distinct raft swarms at Stanco to the southwest of the Nqwadolo Mountain and at Bethlehem-Merryland in the southern portion of the batholith (Kuyper 1979; Du Toit 1979) extending along strike for several kilometres (Figure 2.1). Ubiquitous occurrences of smaller mafic-rich enclaves have, however, been described beyond the limits of these major raft swarms. All tend to extend parallel to the fabric in the granite.

Following the terminology of Didier and Barbarin (1991), the majority of these enclaves are xenoliths, with highly variable shapes, strongly dependent upon their mineralogy, or schlieren. The smaller biotite-rich enclaves described by Kuyper (1979), Du Toit (1979) and Bulley (1981), however, are surmicaceous enclaves. Rarely, felsic microgranular enclaves are distinguished.

a) Amphibolite

The amphibolite occurs predominantly within the major raft swarms identified by Kuyper (1979) and Du Toit (1979), closely associated with the pelitic gneiss. It is typically medium grained with a marked foliation and a crude gneissosity. Contacts with the pelitic gneiss and the granites are sharp, but on a local scale display the effects of intense deformation. This results in the reduction of the amphibolitic bodies to a series of small (c.1m) boudinaged pods.

Two major mineralogical varieties have been distinguished (Appendix 1):

1) plagioclase hornblende amphibolite; and
2) two pyroxene amphibolite.

The former appears to be relatively rare, with the majority of the amphibolite samples collected being pyroxene bearing with distinct brown hornblende.

The amphibolite displays a grano-nematoblastic texture, slightly inequigranular, with a seriate distribution of crystal sizes. They are broadly homogeneous, but mineralogical layering, and the presence of localised preferential enrichment of specific phases, particularly hornblende, are noted, with the development of a crude gneissosity. A well defined lineation is produced by the elongate nature of the composite minerals. Interlobate crystal contacts are widely developed, but triple point contacts may be present between the major minerals, particularly at analogous junctions.

One sample was selected for microprobe analysis (UND 357), collected adjacent to the large pelitic gneiss enclave in Figure 2.4 (Appendix 2). The plagioclase is a labradorite (An_{60-62}), with more calcic margins (An_{60-66}). The amphibole possesses moderate iron (FeO = 18.59-19.49%, Fe/Fe+Mg =

0.54-0.55, Fe^{3+} = 0.33-0.54) and total alkali concentrations ($(Na+K)_{TOT}$ = 0.54-0.60). Following the terminology of Leake (1997) it is a calcic amphibole ($(Ca+Na)_B>1$, $Na_B<0.5$ and $(Na+K)_A>0.50$) and on the classification diagram of Leake plots across the boundary separating the edenite and ferroedenite fields (Figure 2.3). Slight, but variable, differences exist between the Fe/Mg ratio of the core and margin of individual amphiboles. These analyses are somewhat similar to those obtained by Du Toit (1979), although the latter are typically higher in alumina and iron but lower in magnesium and calcium than the present analyses. The orthopyroxene is iron rich (Fe/Fe+Mg = 0.57-0.58), with a low nonquadrilateral component (TiO_2 = 0.03-0.11%, Al_2O_3 = 0.45-0.64%, Na_2O = 0-0.03%). The clinopyroxene possesses a high nonquadrilateral component (Al_2O_3 = 0.89-1.13%, Na_2O = 0.21-0.25%) and moderate iron levels (FeO = 13-86-14.36%, Fe/Fe+Mg = 0.42-0.43). On the pyroxene classification diagram of Morimoto (1988) these plot in the ferrosilite and diopside fields, respectively.

b) Pelitic Gneiss

The pelitic gneiss is dark grey and medium-grained with a prominent, multiply deformed, gneissic fabric. In most outcrops it forms a negative feature, being eroded preferentially to the surrounding granite. Contacts parallel to the fabric in the granite are sharp but may be undulatory with sporadic marginal inclusions of megacrystic feldspar. The lateral extremities of the enclaves, however, may display partial disassociation and mixing with the granite (Figure 2.4). This process produces a zone of darker than normal granite within which small enclaves of dark biotite gneiss are found.

The typical pelitic gneiss consists predominately of quartz, feldspar, biotite, garnet, sillimanite and cordierite (Appendix 1). It possesses a lepidophyroblastic texture, defined by the marked elongation of the biotite and sillimanite crystals and porphyroblasts of garnet and sillimanite, with individual sillimanite needles reaching 10cm in length. In more quartzo-feldspathic varieties this becomes a grano-(lepido)-porphyroblastic texture. Sulphide mineralisation is locally pronounced.

It is highly heterogeneous, with the development of marked mineralogically and texturally specific domains, and in particular zones characterised by:

1) fine grained homogeneous biotite + sillimanite + cordierite + quartz + feldspar;
2) biotite + sillimanite folia; and
3) coarse quartz+microcline-perthite+plagioclase ($c.An_{31}$)+garnet leucosomes, probably generated through partial melting (Powell and Downes 1990).

The biotite gneiss differs markedly from the typical pelitic gneiss, with a darker colour than the norm, a poorly defined gneissosity, a finer grain size with few garnets, no sillimanite or cordierite and no apparent associated leucosome. In section it displays a granolepidoblastic texture, with the lineation defined by the marked parallelism of the elongate red brown biotite laths. Typically it is equigranular, or slightly seriate, although individual plagioclase crystals may be larger than the average (Appendix 1).

Two sections of the pelitic gneiss were selected for microprobe analysis, samples NDF 56 and UND 374. Both were collected from the large enclave pictured in Figure 2.4, with the latter situated adjacent to a significant concentration of the granitic partial melt (Appendix 2).

The plagioclase is an oligoclase (An_{22-28}), with slightly more sodic margins. The K-feldspar is extremely variable in composition, due to varying degrees of perthite exsolution, typically potassic (K_2O>13%), but with a substantial sodium content (1.1-2.6%). Unexsolved K-feldspar possesses sodium contents to a maximum of 4 percent.

The biotite possesses a high alumina content (Al_{TOT} = 3.03-3.35), but is low in iron (Fe/Fe+Mg = 0.3-0.5). It therefore plots in the biotite field, with extension into the phlogopite field, but towards the siderophyllite portion of the ideal biotite plane (Figure 2.2). The garnet from both sections is an almandine, but that from sample NDF 56 ($Alm_{70-77}Spess_{1-2}Py_{20-25}Gross_{2-3}$) possesses substantially more pyrope than the garnet from sample UND 374 ($Alm_{75-77}Spess_{2-3}Py_{18-19}Gross_{3-4}$). No zonation has been identified within sample NDF 56. Only core analyses are available from sample UND 374.

Two samples of the garnet partial melt, NDF 92A and UND 93, were collected for microprobe analysis of their garnet, the former adjacent to the pelitic gneiss and the latter from a large granitic mass within the core of the enclave (Appendix 2). These are almandine, but with variable solid solution characteristics, NDF 92A possessing less almandine and grossular but more pyrope ($Alm_{75-77}Spess_{2-3}Py_{18-20}Gross_3$) than UND 93 ($Alm_{77-79}Spess_{2-3}Py_{13-14}Gross_{5-7}$,). The garnet from sample NDF 92A is somewhat similar to that from

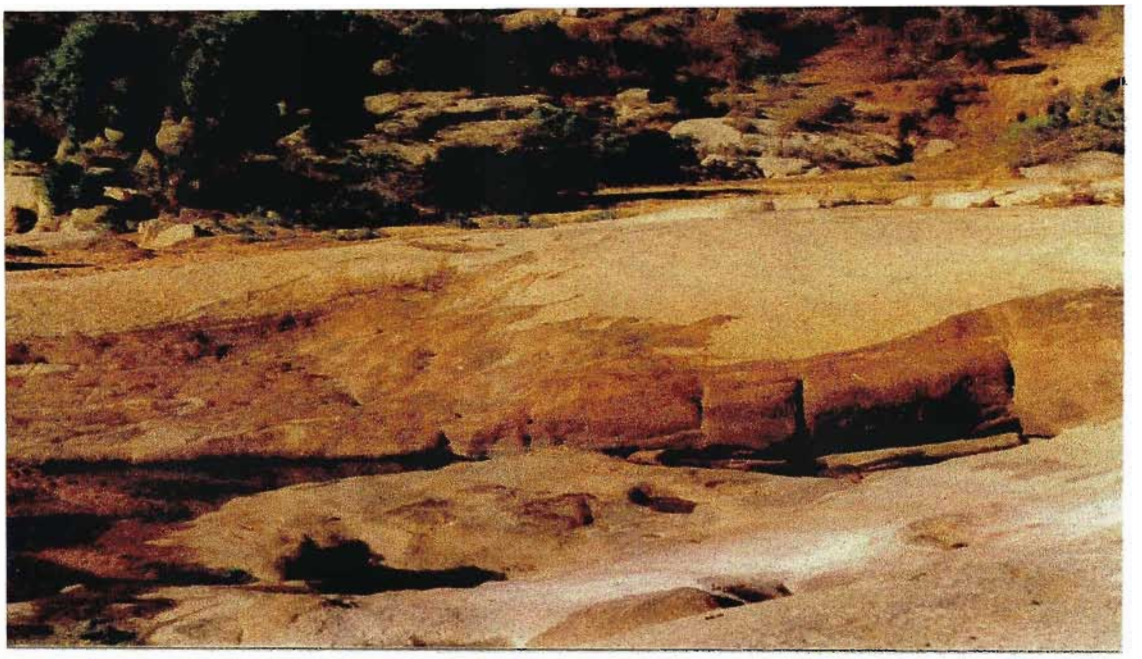

Figure 2.4. Pelitic enclave within the biotite garnet granite of the Ximba Suite, displaying lateral disassociation.

the juxtaposed pelitic gneiss.

c) Quartzo-feldspathic Gneiss

Du Toit (1979) and Kuyper (1979) noted the presence of a series of quartzo-feldspathic granitoid gneisses within the southern portion of the Mgeni batholith. These were considered to represent a phase of the granite, while smaller enclaves were viewed as feeder dykes to the Nqwadolo granite. Bulley (1981), however, suggested that the large quartzo-feldspathic body at Nduzula was an enclave. Subsequent field work has demonstrated the development of granite veining within the quartzo-feldspathic gneiss indicating that it represents an early series of supercrustals. Sharp contacts with the granite are observed, but an example of a discordant contact noted by Kuyper (1979) has been reinterpreted as a fault contact (A Kerr, 1988, pers. comm.[1]).

The white or pink quartzo-feldspathic gneiss consists of medium grained quartz, microcline or microcline microperthite, albite or oligoclase with minor biotite and garnet (Appendix 1), the elongation of which defines a crude fabric. The texture is granoblastic and inequigranular, with feldspar megacrysts. These latter are relatively common in the 'porphyroblastic' quartzo-feldspathic gneiss of Kuyper (1979) and Du Toit (1979), but are less abundant in the smaller bodies found in the northern portion of the Mgeni batholith. Individual thin sections display evidence of shearing, with the development of patches of finer grained quartzo-feldspathic material around remnant larger crystals.

Two samples of the quartzo-feldspathic gneiss were selected for microprobe analysis, UND 302 from a biotite-poor gneiss within the hornblende granite phase of the Sansikane pluton and UND 42 from a biotite-rich megacrystic enclave in the eastern portion of the batholith (Appendix 2).

The K-feldspar is orthoclase rich, with a variable albite content (3-14%). The plagioclase may be an albite (UND 42) or an oligoclase (UND 302), rarely an albite. A marginal zone with a higher albite content is present around the oligioclase.

Analytical totals are low for the majority of the biotite analyses, with declining potassium and silica but increasing iron and magnesium concentrations with progressive alteration. Unaltered biotite plots within the annite sector of the ideal biotite plane (Figure 2.2). It differs from the typical metamorphic biotite analyses of Deer *et al.* (1971), with low alumina (Al_{TOT} = 2.56-2.62) but high iron (Fe/Fe+Mg = 0.62) contents. Similarly, it does not plot with the granulite grade biotites of Giudotti (1984). Rather it is comparable with biotite analyses from granitic rocks.

[1]Prof A Kerr, University of Natal, deceased

d) Fine Grained Granulite

Kuyper (1979) described a fine grained hypersthene quartz gneiss, with prominent mineralogical banding and a plagioclase amphibolite with a well developed palimpsest texture. These, with other identified lithologies, are now considered to form a portion of a fine-grained granulite association.

The fine-grained granulite series is mineralogically complex (Appendix 1). Occasional samples are amphibolitic in composition, but the majority of the samples collected consist of garnet + biotite $\pm$ orthopyroxene $\pm$ sillimanite in a felsic granoblastic groundmass. Variations in the mineral assemblage, and primarily the presence or absence of sillimanite and orthopyroxene, which occur in separate mineralogical domains, allow the division of these latter samples. Three principle mineralogical groups have, therefore, been identified within this series:

1) biotite - garnet - orthopyroxene granulite;
2) biotite - garnet - sillimanite granulite; and
3) amphibolitic granulite.

The former may be further subdivided on the basis of distinct mineralogies and textures. Insufficient data are available from the amphibolitic granulite to allow the determination of a similar scheme, but rather suggest the progressive development of the amphibolitic granulite from the original dolerite.

Biotite - Garnet $\pm$ Orthopyroxene $\pm$ Sillimanite Granulite

These are grey, fine grained rocks, occasionally megascopically banded through the presence or absence of porphyroblastic garnet.

The orthopyroxene bearing granulite is mineralogically and texturally highly variable. Three distinct classes have been identified:

1) strongly banded garnet - bearing;
2) weakly banded garnet - bearing; and
3) nongarnetiferous granulite;

the latter corresponding with the hypersthene quartz gneiss described by Kuyper (1979) (quartz + hypersthene + biotite). The biotite garnet sillimanite granulite (Appendix 1) possesses less marked banding than the orthopyroxene bearing granulite, but is equally mineralogically variable.

Weakly banded samples are relatively homogeneous, with the banding defined by the presence or absence of garnet. Within the strongly banded granulite, however, fine banding is demarcated by major mineralogical variations, in particular of biotite, and sharp contacts, marked by marginal concentrations of mafic minerals. Within these prominent bands, finer banding can be distinguished, by changes in the mafic or felsic mineralogy, or by the presence of monomineralic layers, in particular of biotite or orthopyroxene.

Modal analyses of these rocks and selected individual layers are given in Appendix 1.

These rocks display a well-developed fabric, as defined by the parallelism of the biotite and smaller monomineralic bands, in addition to the prominent gneissosity of the more pronounced mineral bands. Intersecting foliations are possibly related to the development of discrete mineral assemblages. Felsic mineral contacts, however, are typically triple points, as are those between the felsic minerals and the mafic minerals such as orthopyroxene in the felsic-rich layers. Typically a granoblastic-lepidoblastic texture is developed, with equigranular-seriate crystal sizes. Individual crystals display polygonal-interlobate shapes. In garnet-rich layers the texture is grano- (lepido) porphyroblastic, with the garnet and sillimanite occurring as porphyroblasts.

Four samples of the fine grained granulite (NDF67, NDF67a, NDF69 and NDF70), the majority being orthopyroxene bearing, were selected for microprobe analysis (Appendix 2).

The orthopyroxene analytical totals are typically low, but suggest that the pyroxene from each section is distinct, although nonquadrilateral component concentrations are uniformly high. In particular alumina concentrations in excess of 6 percent have been identified. On the classification diagram of Morimoto (1988) they plot in the enstatite field, with iron/magnesium ratios of 0.39-0.47. Within individual sections the orthopyroxene composition is closely related to the adjacent mineralogy. In particular the presence of garnet is marked by a slight increase in the magnesium concentration of the orthopyroxene, but depletion in iron. The presence of biotite does not appear to have a similar effect on orthopyroxene composition.

The biotite composition is highly variable, both between and within sections, but all possess moderate iron (Fe/Fe+Mg = 0.29-0.45) and alumina (Al_{TOT} = 2.69-2.93) concentrations. In the

ideal biotite plane they plot predominately within the biotite field, but with extension into the phlogopite field (Figure 2.2). Their high Ti (Ti= 0.34-0.96) content is characteristic of biotites from granulite grade pelitic schists (Guidotti 1984). The associated mineralogy, and in particular the presence of garnet, exercises a strong control on biotite composition, resulting in lower iron, but higher magnesium concentrations in adjacent biotites, similar in style to that identified by Tracy (1982) for diffusion zoning developed between biotite-garnet pairs within the granulite facies.

The garnet is an almandine (0.57-0.69) with a large pyrope (0.27-0.41) component, although average analyses from each section are distinct and analyses within an individual section are markedly variable. Zonation takes the form of an increase in iron and a decrease in magnesium in a thin marginal rim, as noted by Tracy (1982) from granulite grade garnet. No significant calcium or manganese zonation is apparent.

Amphibolitic Granulite

Kuyper (1979) described a plagioclase amphibolite with palimpsest texture, which he believed represented a lower grade equivalent of the pyroxene amphibolite. During the present study, however, a series of dark fine grained amphibolitic rocks have been identified, which suggest that the plagioclase amphibolite of Kuyper may represent an initial stage of recrystallisation from an original dolerite.

Thin section analysis reveals the presence of two distinct mineral assemblages (Appendix 1):

Assemblage 1 - plagioclase$_1$ (c.An$_{57}$) + clinopyroxene$_1$ + orthopyroxene$_1$ with a palimpsest subophitic texture;
Assemblage 2 - hornblende + orthopyroxene$_2$ + clinopyroxene$_2$ + plagioclase$_2$ (c.An$_{54}$) $\pm$ quartz $\pm$ garnet;

with Assemblage 2 systematically replacing Assemblage 1.

The original subophitic texture is altered with recrystallisation and the increasing size of the new mineral phases to a grano-porphyroblastic texture, the porphyroblastic phase in these latter sections being the augite of Assemblage 1. The completely altered sections are granoblastic to grano-nematoblastic, with a lesser range of mineral sizes. Marked mineral layering occurs, however, defined by the concentration of specific mineral phases.

e) Biotite Hornblende Gneiss

Kuyper (1979), Du Toit (1979) and Bulley (1981) noted the occurrence of small (c.20cm in length), dark enclaves of biotite-hornblende gneiss. These are elongated parallel to the foliation in the surrounding granites, contacts with which are sharp, but irregular, undulating around adjoining megacrysts, which may occur included within the enclave.

They consist of plagioclase (c.An$_{30}$), K-feldspar, quartz, hornblende and biotite (Appendix 1), the quartz and plagioclase occurring as porphyroblasts (possibly inclusions from the granite) and possess a grano-lepidoblastic texture, with a prominent lineation defined by parallel biotite laths and elongate concentrations of biotite. Grain contacts are irregular to interlobate with embayments.

f) Granitic Enclaves

Rare small, c.50 cm long, granitic enclaves have been identified within the granites of the Ximba Suite. These are distinguished in the field from the quartzo-feldspathic gneiss by their well developed gneissosity, much higher mafic content and the presence of abundant garnet. Contacts with the granite are sharp, cutting the fabric of the enclave.

They are coarse grained, and consist essentially of K-feldspar (perthitic microcline), plagioclase (c. An$_{27}$) and quartz, with lesser biotite and garnet (Appendix 1), and accessory allanite, zircon and apatite. Minor amounts of secondary chlorite, prehnite, muscovite and carbonate are also present. Parallelism of the felsic minerals and the small mafic mineral clots impart a well defined fabric. Concentrations of the mafic phases occur adjacent to the contact of the enclave and the enclosing granite.

A large range of crystal sizes are present, with most mineral phases possessing megacrystic tendencies. Individual megacrysts, and in particular the quartz and K-feldspar megacrysts, may consist of groupings of smaller crystals. These megacrysts are, however, smaller than those found in the megacrystic granites. Rapakivi and antirapakivi textures may be present.

One sample (UND 330), was collected for microprobe analysis (Appendix 2). The biotite exhibits extreme iron enrichment (Fe/Fe+Mg=0.78-0.79), at levels comparable with

biotite from rapakivi and A-type granites (Anderson and Bender 1989; Abdel-Rahman 1994) rather than the calc-alkaline granites (Pitcher *et al.* 1985). All analyses plot in the biotite field of the ideal biotite plane, within the annite sector (Figure 2.2). The garnet is an almandine, with a large grossular and smaller pyrope and spessartine component ($Alm_{75-79}Spess_5Py_{4-5}Gross_{11-16}$). Marginal zonation is developed with the margins depleted in iron and magnesium, and enriched in calcium and manganese ($Alm_{75}Spess_{5-9}Py_{2-4}Gross_{14-16}$), suggesting garnet growth with falling temperatures (Allan and Clarke 1981). The plagioclase is an albite.

2.3 THE MGENI BATHOLITH

The various granites identified within the Mgeni batholith have been grouped into three distinct suites (Kerr and Milne 1994):

1) the megacrystic biotite granites, the Ximba Suite, which forms the major portion of the complex. These occur as a single body, with a finer grained mafic margin, also present as veins in the Nagle Dam Formation, grading into a biotite granite and finally a core of biotite garnet granite (Figure 2.1);
2) the hornblende granites, the Mlahlanja Suite, which occur as a series of mineralogically distinct lens shaped plutons within the Ximba Suite (Figure 2.1). All are megacrystic, with a mafic mineralogy of hornblende + biotite ± orthopyroxene ± clinopyroxene ± garnet; and
3) a coarse-grained leucogranite, the Nqwadolo Suite, present in the core of the complex (Figure 2.1).

2.3.1 XIMBA SUITE

The fresh granites are grey in colour with a red discoloration adjacent to shear zones. They consist essentially of megacrystic feldspars set in a matrix of feldspar, quartz and biotite, locally with garnet (Figure 2.5) and hornblende. The megacrysts vary considerably in size, averaging 4cm by 1.5cm, and shape with rectangular, ellipsoidal and circular megacrysts found. Prominent Carlsbad twins and rapakivi textures are common features of the K-feldspar. The preferred orientation of the long axes of the feldspar megacrysts and the biotite define a crude foliation, considered to be a deformed magmatic fabric (Milne 1986) with a general east - west orientation. The marginal granite and granite veins are characterised by the presence of fewer and smaller feldspar megacrysts but a higher mafic content than the normal biotite granite. Small gneissic enclaves are common in the marginal granite, while large bodies of gneiss are enclosed within the granite veins. Deformation ultimately results in the production of a gneissose rock (the biotite hornblende gneiss of Kuyper 1979). Similarly, local deformation of the biotite granite adjacent to a large hornblende granite - charnockite pluton has produced an augen gneiss (Kuyper 1979).

Estimation of the modal content of these granites is hindered by the extremely large size of the megacrysts. The concentration of the various minerals present are therefore estimated, from both thin sections and hand specimens (Appendix 1).

Megacrysts comprise on average 60 percent of the granites (Kuyper 1979), the majority being K-feldspar, either orthoclase or microcline, frequently perthitic, with fewer plagioclase (c.An_{28}) and quartz megacrysts. The groundmass consists of quartz and feldspar plus the mafic minerals, primarily biotite, locally garnet and rarely hornblende. Allanite, apatite, zircon, ilmenite and titanite occur in accessory amounts, with secondary prehnite, chlorite, sericite and clay minerals. These are coarse porphyritic granites, with an extremely heterogranular texture. The megacrystic feldspars are euhedral - subhedral while the groundmass consists of interlocking minerals displaying lobate or amoeboid crystal faces. Deformation is recorded in the bent plagioclase twins and biotite laths, the undulose extinction of the quartz crystals and the mortar texture around many of the megacrysts.

Three samples of the Ximba Suite were selected for microprobe analysis, one from the biotite granite (UND 40) and two from the biotite garnet granite (XS 4, UND 90) (Appendix 2).

The plagioclase is typically an oligoclase (c.An_{26-30}), with the albite content increasing slightly from the biotite garnet granite to the biotite granite. Normal chemical zonation patterns, with marginal sodium enrichment, are present. The K-feldspar is typically potassic (14-15.6%), but with a substantial sodium content (0.5-1.7%). Variations in the degree of perthitic unmixing result in a heterogeneous range of compositions.

Biotite analytical totals are commonly low, and in particular those from the biotite garnet granite, through potassium loss. Intrasection variability may therefore be extreme. Unaltered analyses display extreme iron enrichment (Fe/Fe+Mg = 0.84-0.85), at levels comparable with biotite from rapakivi and A-type granites (Barker *et al.* 1975; Czamanske *et*

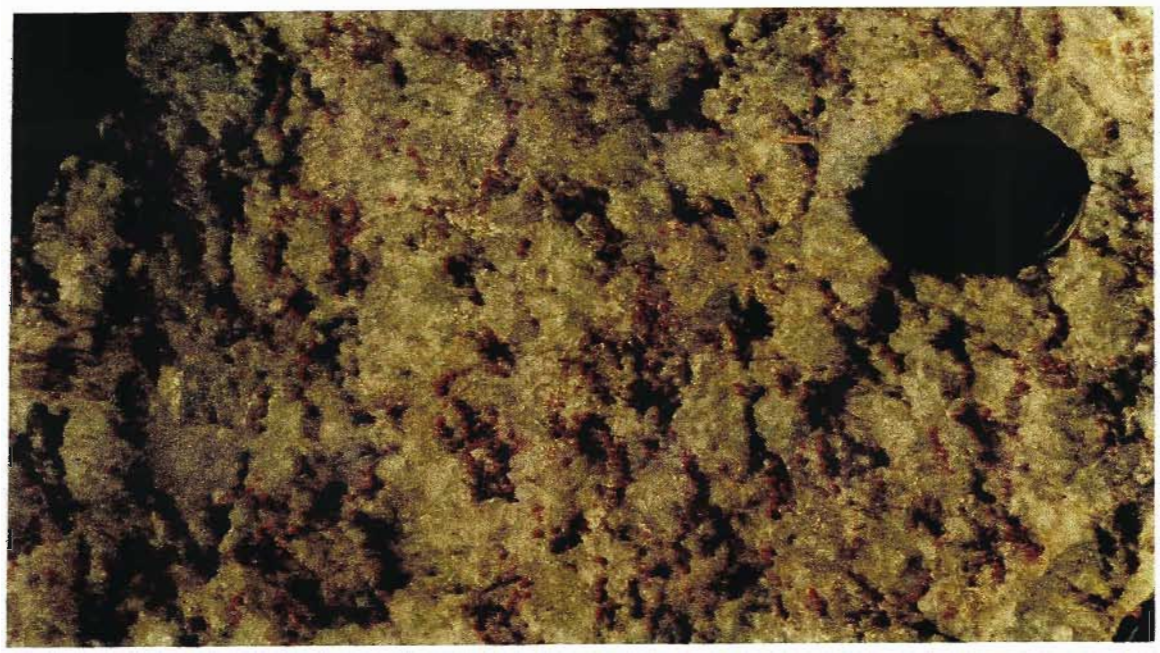

Figure 2.5. Biotite garnet granite of the Ximba Suite.

al. 1977; Haapala 1977; Kinnaird *et al.* 1985; Anderson and Bender 1989; Abdel-Rahman 1994) rather than the calc-alkaline granites (Dodge *et al.* 1969; de Albuquerque 1973; Mason 1978; Noyes *et al.* 1983; Pitcher *et al.* 1985). All analyses plot in the biotite field of the ideal biotite plane, within the annite sector (Figure 2.2).

The garnet is an almandine (0.72-0.79), with a large grossular (0.14-0.2) and smaller pyrope (0.03-0.04) and spessartine (0.03-0.05) component. Interslide variability is apparent, with the garnet of section XS 4 possessing lower iron and magnesium, but higher calcium and manganese contents than that from sample UND 90. These differ from the garnet of the granite enclaves, which has lower calcium levels. Zonation is developed with a marginal enrichment in manganese and calcium but depletion in iron and magnesium ($Alm_{72-74}Spess_5Py_{3-4}Gross_{18-20}$ —> $Alm_{71-74}Spess_{5-6}Py_3Gross_{18-22}$), comparable with the reverse zoning profile of Clarke (1981), and possibly the result of garnet growth with falling temperatures (Allan and Clarke 1981) or growth in an evolving magma (du Bray 1988).

2.3.2 MLAHLANJA SUITE

Several mineralogical varieties have been identified within the Mlahlanja Suite, all megacrystic:

1) dark green charnockite, forming prominent topographic highs;
2) light green hornblende granite - the subcharnockite of Kuyper (1979) - found surrounding the charnockite;
3) grey hornblende granite, which forms large depressions, characterised by extensive river meandering; and
4) grey garnet hornblende granite, found as pronounced topographic highs.

Individual plutons may be composite with an association of hornblende granite, subcharnockite and charnockite, such as the Sansikane pluton, or mineralogically simple, with either hornblende granite, the Enyoni pluton, or garnet hornblende granite, the Matata and Spitskop plutons (Figure 2.1).

Within suite contacts are diffuse. Kuyper (1979) noted a 'green porphyroblastic gneiss' (subcharnockite) which he believed was gradational between the charnockite and hornblende granite. No other within suite contact has been noted, nor has a contact with the Ximba Suite. The Nqwadolo Suite is, however, intrusive into the Mlahlanja Suite.

The extremely large grain size of these granites prohibits the determination of an accurate modal analysis. Modal analyses are therefore estimated,

from both hand specimen and thin sections (Appendix 1).

Feldspar megacrysts, typically an orthoclase or microcline perthite commonly with a rapakivi texture, comprise some 60 percent of these granites. More rarely, plagioclase (c. An_{25}), quartz and garnet megacrysts are observed. The groundmass consists of a mixture of quartz, feldspar and the mafic minerals, hornblende + biotite ± pyroxene ± garnet. Accessory amounts of apatite, ilmenite, zircon and allanite are present, with secondary prehnite, chlorite, sericite and clay minerals. The granites display an extremely heterogranular coarse porphyritic texture, with euhedral - subhedral feldspar megacrysts and an intergrown groundmass, with lobate or amoeboid crystal faces. Deformation is recorded in the bent plagioclase twins and biotite, the undulose extinction of the quartz crystals and the mortar texture around several of the megacrysts. The parallelism of the feldspar megacrysts helps define a crude fabric.

Four samples of the Mlahlanja Suite were selected for microprobe analysis, a charnockite from the Egugwini pluton (UND 74), a hornblende granite from the Sansikane pluton (UND 65) and two garnet hornblende granites from the Matata pluton (UND 6 and UND 9) (Appendix 2).

The plagioclase is an oligoclase or andesine (An_{22-34}). A progressive increase in anorthite content is found with the hornblende granite < charnockite < garnet hornblende granite. Intrasection variability may be large. Zonation has only been identified in the plagioclase from the garnet hornblende granite, with the development of an albite rim to the plagioclase. Varying degrees of perthite exsolution results in highly heterogeneous K-feldspar analyses, although the majority are potassic, but with a substantial sodium content (0.8-3%).

All the mafic minerals possess extreme iron enrichment (Fe/Fe+Mg c.0.8), typically with the charnockite < hornblende granite < garnet hornblende granite. These are comparable with mineral analyses from rapakivi granites and A-type granites (Barker *et al.* 1975; Haapala 1977; Czamanske *et al.* 1977; Kinnaird *et al.* 1985; Anderson and Bender 1989; Ramo 1991; Abdel-Rahman 1994), rather than the calc-alkaline granites (Dodge *et al.* 1968; 1969; de Albuquerque 1973; Mason 1978; Noyes *et al.* 1983; Pitcher *et al.* 1985; Hammarstrom and Zen 1986).

Many of the biotite analyses are low, apparently due to potassium loss, but unaltered analyses plot in the annite field on the ideal biotite plane (Figure 2.2). The amphibole possesses low titanium, but high total alkalis. Following the terminology of Leake (1997) it is a calcic amphibole ($(Ca+Na)_B>1$ and $Na_B<0.5$) and plots in the combined hastingsite and ferropargasite field (Figure 2.3) on the classification diagram of Leake (1997). Variations in the Fe^{3+}/Al^{VI} ratio suggest that the amphiboles from the hornblende granite and charnockite are hastingsite while that from the garnet hornblende granite is ferropargasite. These amphiboles are further distinguished by their variable alumina and magnesium contents, with:

1) the low alumina but high magnesium amphiboles of the charnockite and hornblende granite; and
2) the high alumina but low magnesium amphibole of the garnet hornblende granite.

Pyroxene data are limited to the orthopyroxene of the charnockite, and analytical totals are typically low. These analyses do indicate, however, the extreme iron enrichment (Fe/Fe+Mg = 0.82-0.83) and low nonquadrilateral component of this pyroxene. On the classification diagram of Morimoto (1988) it plots in the ferrosillite field.

2.3.3 NQWADOLO SUITE

The granite of the Nqwadolo Suite consists principally of quartz and feldspar, a microcline perthite and a plagioclase (c. An_{30}), with minor amounts of biotite and rare garnet (Appendix 1). Allanite, opaque oxides and zircon occur in accessory quantities. It has an almost isogranular coarse texture. Elongate quartz crystals and the long axes of the biotite laths define the foliation that strikes east - west, swinging to northeast - southwest in the western extremity of the body. Both Kuyper (1979) and Du Toit (1979) noted an increase in grain size towards the core of the complex and slight colour changes. Sampling of the tailings from the water pipeline constructed through Nqwadolo Mountain indicates, however, that the granite is internally complex. Individual samples display a wide range of colours, most notably green, white and red, and grain sizes, from medium grained to pegmatitic. The coarse grained texture of the Nqwadolo Suite allows simple discrimination from the megacrystic Ximba and Mlahlanja Suites, which it intrudes.

One section of the Nqwadolo Suite was selected for microprobe analysis (UND 19), with one additional sample (UND 22) from a late granite vein

(Appendix 2), initially identified as a quartzo-feldspathic gneiss (Kuyper 1979), and a possible feeder to the Nqwadolo Suite (but see Section 4.4.3).

The plagioclase from sample UND 19 is an oligoclase (c.An_{14-17}), while that from sample UND 22 is an albite (c.An_{3-8}). Normal zonation patterns are found in sample UND 19, with the development of an albite margin to the oligioclase cores. The K-feldspar is typically highly potassic, but exhibits extreme variability, due to differing degrees of perthite unmixing, with sodium contents to a maximum of 4 percent.

The garnets are almandines, but that from sample UND 19 possesses a small grossular and insignificant pyrope and spessartine solid solution, while the garnet from sample UND 22 is spessartine rich ($Alm_{64-66}Spess_{24}Py_3Gross_8$), with a marginal zone marked with slight manganese enrichment. These latter are comparable to medium to high manganese garnet analyses from high level granites (Hall 1965; Joyce 1973; Harris 1974; Nevia 1975; Deer *et al.* 1982). The lack of solid solution in the garnet from sample UND 19, however, distinguishes it from the analyses of Deer *et al.* (1982).

CHAPTER 3

PRESSURE - TEMPERATURE EVOLUTION OF THE VALLEY OF A THOUSAND HILLS

3.1 INTRODUCTION

This chapter attempts to define the evolution of the temperature and pressure conditions prevailing during the metamorphism of the Mapumulo Group and the intrusion of the Mgeni batholith through an analysis of the metamorphic mineral assemblages in the Mapumulo Group and the use of various geothermobarometers. Several authors have analysed the conditions of metamorphism within the study area (for example Bulley 1981), but these tended to be generalised estimates based on the presence or absence of specific mineral phases. Quantification of the pressure and temperature conditions prevalent within the Valley of a Thousand Hills has not been undertaken.

The metamorphic conditions within the central portion of the Natal Province were summarised by Cain (1975) and Thomas (1989a), who identified a regional upper amphibolite facies event (600-700°C and 5-6 kb (Cain 1975)). Localised metamorphism to the granulite facies was noted, typically associated with the megacrystic granites, and at Nagle Dam Cain described a granulitic mélange, believed to represent a portion of the basement to the Mapumulo Group. Kerr (1984), however, suggested a minimum metamorphic temperature of 700-800°C at pressures of 4-6.5 kb for the gneisses within the Valley of a Thousand Hills.

3.2 METAMORPHISM OF THE VALLEY OF A THOUSAND HILLS

3.2.1 PREVIOUS WORK

The conditions of metamorphism of the Nagle Dam and Valley Trust Formations were summarised by Bulley (1981) and Kuyper (1979) respectively.

Bulley (1981) noted that diagnostic minerals are generally lacking in the Nagle Dam Formation, hindering the determination of metamorphic conditions. Several features, however, and in particular the widespread partial melting of the gneisses, led Bulley to propose metamorphism within the granulite facies, with temperature estimates of 700-780°C at 4-5 kb.

Within the Valley Trust Formation, Kuyper (1979) noted the localised occurrence of hypersthene bearing lithologies (the amphibolite and fine grained granulite). Other lithologies, and in particular the pelitic gneiss, were found to possess assemblages common to the granulite facies, such as:

K-feldspar + cordierite + sillimanite + biotite + quartz + garnet.

Limited results from a garnet-cordierite geothermobarometry study of the pelitic enclaves indicated temperatures of 730-790°C at 4-6 kb.

The conditions of intrusion of the Mgeni batholith have been little studied. Kuyper (1979) believed that the granites had been metamorphosed, the charnockites representing a localised thermal spike, with their mineralogy reflecting this event. Pressure estimates for the granites were obtained, however, from the Q-Ab-An plot, which suggested low-intermediate pressures of crystallisation, 2-5 kb, for the majority of the granites, but increasing for the charnockite. Bulley (1981) proposed that the Mgeni batholith was a catazonal intrusive.

In summarising the metamorphic evolution of the Valley of a Thousand Hills, Kuyper (1979), Du Toit (1979) and Bulley (1981) identified two metamorphic events, which could, however, comprise a linked prograde and retrograde phase. Du Toit believed that this progressed as a smooth P-T-t path, although Kuyper noted a more erratic variation in temperatures, with the production of local metamorphic highs associated with the development of the charnockites and granulite facies metamorphism within the Valley Trust Formation.

3.2.2 PRESENT STUDY

As noted by Bulley (1981) there is a general lack of diagnostic minerals to define the P-T conditions prevailing during the metamorphism of the Nagle Dam Formation. The identification of localised occurrences of hypersthene bearing lithologies within the Nagle Dam Formation tends, however, to support the high grade of metamorphism proposed by Bulley for this unit.

Thin section analysis of the various lithologies within the Valley Trust Formation indicates the existence of a variety of assemblages indicative of granulite facies metamorphism, and in particular the presence of hypersthene in the amphibolite and the fine grained granulite. This phase of granulite

facies metamorphism Kuyper (1979) considered to be restricted to the vicinity of the charnockite within the core of the batholith, beyond which the peak of metamorphism was believed to be within the amphibolite facies. This conclusion was not confirmed during the present study, however, and granulite facies metamorphism is judged to be conspicuously more widespread than proposed by Kuyper (1979).

For the majority of the lithologies studied, thin section analysis indicates only post-peak metamorphic reactions, including the breakdown of pyroxene to hornblende, and late stage retrograde reactions, such as the development of chlorite. Specific mineralogical evidence for high grade metamorphic evolution can, however, be identified within three units:

1) the pelitic gneiss;
2) the pelitic fine grained granulite; and
3) the fine grained amphibolitic granulite;

with a developing metamorphic texture and mineral assemblage.

Within the fine grained amphibolitic granulite, however, this takes the form of the transformation of an original igneous assemblage of:

$$Plagioclase_1 + clinopyroxene_1 + orthopyroxene_1,$$

to a metamorphic assemblage of:

$$Plagioclase_2 + clinopyroxene_2 + orthopyroxene_2 + hornblende + quartz + ore (\pm garnet),$$

suggesting that the reaction largely involved the recrystallisation of the igneous mineral phases, with associated hydration to produce hornblende. Occasional occurrences of garnet, with abundant pyroxene and hornblende inclusions, may have formed through:

Orthopyroxene + anorthite —>
clinopyroxene + almandine + quartz, or

Orthopyroxene + anorthite —>
hornblende + almandine + quartz
(De Waard 1965).

Garnet 'veins' may have originated as an extreme example of the garnetiferous shear zones of Buddington (1963).

a) Pelitic Gneiss

The pelitic gneiss comprises a series of mineralogically distinct domains:

1) biotite + sillimanite + cordierite gneiss;
2) garnetiferous leucosome; and
3) biotite + sillimanite folia;

with the interrelationships between these differing assemblages indicating an evolving metamorphic and deformation history.

The presence of rare rounded inclusions of remnant biotite and sillimanite within the quartzo-feldspathic portion of the leucosome, suggest that the leucosome may represent a localised concentrated partial melt product of the gneiss, derived through the reaction:

Biotite + sillimanite + quartz —>
garnet $\pm$ K-feldspar $\pm$ melt (Tracy 1978).

Marginal dissolution of the garnet porphyroblasts and the removal of the associated quartzo-feldspathic material with the generation of the biotite + sillimanite folia suggest that the latter is a relatively late assemblage, originating through the development of a high-strain domain (Bell 1981; 1985). Variations in the orientation of this texture within individual thin sections indicate that these represent an evolving stress field pattern.

Cordierite occurs in a variety of settings. Within the biotite + sillimanite + cordierite domain it typically possesses a polygonal habit, although it is frequently found enclosing sillimanite and occasionally K-feldspar, perhaps formed through:

Biotite + sillimanite + quartz —>
cordierite + K-feldspar + melt
(Harley and Fitzsimons 1991).

Within the less deformed portions of the biotite-sillimanite folia cordierite is associated with biotite and may be included with the biotite and sillimanite as marginal inclusions within the garnet overgrowth of certain of these zones, indicating:

Quartz + sillimanite + biotite —>
K-feldspar + cordierite + garnet + melt
(Grant 1985).

A partial cordierite mantle to garnet in association with biotite and between garnet and ore in association with sillimanite is also present, suggesting the late growth of cordierite to mantle

the peak assemblage (Stuwe and Powell 1989) through:

Garnet + sillimanite + quartz —>
cordierite (Harley and Fitzsimons 1991).

The occasional occurrence of spinel as inclusions in individual garnets, suggests the additional possible reaction:

Sillimanite + biotite —>
Garnet + spinel + cordierite + magnetite
(Stuwe and Powell 1989).

b) Pelitic Fine Grained Granulite

Within the fine grained granulite an early orthopyroxene assemblage appears to be overprinted by a garnet + biotite assemblage. In the nonbanded granulite this is marked by the presence of orthopyroxene inclusions in the garnet and the occurrence of an orthopyroxene free - quartz rich zone surrounding the garnet, suggesting the generation of the garnet through:

Orthopyroxene + plagioclase —>
garnet + quartz
(Harley and Fitzsimons 1991);

which progressed until the garnet replaced the orthopyroxene.

Generation of the biotite may have similarly occurred with the breakdown of orthopyroxene:

Orthopyroxene + K-feldspar + vapour —>
biotite + quartz (Harley *et al.* 1990).

Rare secondary orthopyroxene may occur marginal to individual garnets, as noted by Harley *et al.* (1990), derived from:

Biotite + quartz ± plagioclase —>
orthopyroxene + cordierite + K-feldspar
+ vapour/melt; or

Garnet + K-feldspar + Vapour —>
orthopyroxene + cordierite + biotite
(Harley and Fitzsimons 1991).

Evidence from individual thin sections suggests that the fine grained granulite may have been affected by a series of fabric forming events. In the well banded granulite this is marked by the presence of biotite specific zones, possibly generated in a high-strain domain (Bell 1985), with subsequent overgrowth by garnet, to form the garnet banded gneiss. Similarly, in poorly banded granulite, a multideformed biotite + orthopyroxene fabric may be overgrown by garnet, with the preservation of the biotite to define the original fabric. Evidence of garnet growth zoning is found in individual garnets with a quartz inclusion rich core surrounded by an inclusion poor margin.

An additional biotite bearing fabric is present, associated with the development of cordierite, and transgressing the biotite + garnet bands. Extension of this fabric into the predominately quartzo-feldspathic bands is evidenced by the presence of a cordierite lineation. Cordierite may also be associated with the garnet overgrowth of the biotite + orthopyroxene assemblage noted above, and, in the orthopyroxene free zones, enclosing sillimanite, possibly through the reaction:

Garnet + sillimanite + quartz —>
cordierite (Harley and Fitzsimons 1991).

3.3 GEOTHERMOBAROMETRY

An overview of the mineralogical composition of the various lithologies within the Proterozoic basement of the Valley of a Thousand Hills reveals the presence of numerous potential geothermometers and geobarometers, several of which can be utilised using the available microprobe data. Where possible a number of different barometers and thermometers were applied simultaneously to individual rock types, to provide an audit of the derived results. A complete integrated quantitative study of the pressure and temperature conditions prevalent in these rocks is not, however, possible, with the available microprobe data (Appendix 2).

The Fe^{3+}/Fe^{2+} ratio is an unknown factor in this study, as all mineral analyses were undertaken using an electron microprobe. Estimation of Fe^{3+} is possible for several of the minerals analysed, including pyroxene, amphibole and garnet, through the assumption of ideal stoichiometry. For the micas, however, this is not possible (Schumacher 1991). Calculations by several authors including Harley (1985), Guidotti and Dyar (1991) and Schumacher (1991) have suggested that consideration of total iron as Fe^{2+} will result in varying degrees of error when utilising individual geothermobarometers. Harley (1985), for example, found that disregarding Fe^{3+} produces pressure and temperature minima for the garnet-orthopyroxene geothermobarometers, with temperatures of 20-50°C and pressures of 0.7 kb below the figures obtained with Fe^{3+}. Similarly, Guidotti and Dyar

(1991) and Rathmell *et al.* (1999) determined that for the garnet-biotite geothermometer, ignoring Fe^{3+} may result in an overestimation of temperatures to 45°C or 30°C respectively. In several cases, however, Schumacher (1991) found that the assumption of $Fe^{2+}=Fe_{TOT}$ had no effect on the derived pressure or temperature, and is preferable to the estimation of Fe^{3+} in only one of the components of a geothermobarometer, a situation which may result in larger errors than ignoring Fe^{3+} and accepting $Fe^{2+}=Fe_{TOT}$. For the garnet-orthopyroxene geothermobarometers of Harley (1984a; 1984b) Carson and Powell (1997) recommended the use of high Al-orthopyroxenes (>5% Al_2O_3), which minimise the effects of Fe^{3+}.

Within this study Fe^{3+} has been calculated for several of the mineral phases, and with the exception of hornblende, has been found to be low or negligible. Total iron will therefore be taken as Fe^{2+} for the various geothermobarometers, with the exception of those formulations which utilise hornblende.

3.3.1 GEOTHERMOMETRY

A wide variety of geothermometers have been proposed in the literature (Essene 1982; 1989). The mineralogy of the various lithologies present and the availability of accurate microprobe data, however, limits the applicability of these thermometers and only seven are considered suitable for consideration:

1) the two-pyroxene thermometer;
2) the garnet-orthopyroxene thermometer;
3) the biotite-garnet thermometer;
4) the two feldspar thermometer;
5) the pyroxene-hornblende thermometer;
6) the plagioclase-amphibole thermometer; and
7) the hornblende thermometer.

Essene (1982) has reviewed several of these geothermometers, the majority of which he did not consider provided accurate temperature estimates for the granulite facies. The garnet-biotite thermometer he believed to be unsuitable due to the increasing inclusion of additional elements such as Ti and F. Similarly, the two feldspar thermometer suffers from the need to reintegrate exsolved phases, although Essene (1989) noted that subsequent formulations can record granulite grade temperatures when exsolved K-feldspars are reintegrated correctly. The two-pyroxene thermometer was considered by Essene (1982) to provide low temperatures for metamorphic rocks due to Ca-Mg-Fe exchange during cooling. The majority of these geothermometers are, however, the standard means of quantifying temperatures within the granulite facies (for example Daly *et al.* 1989). Several of these thermometers have also been applied successfully to granitic rocks (Anderson 1996), including the two feldspar, amphibole-plagioclase and two-pyroxene thermometers, although they are primarily calibrated for metamorphic conditions (JL Anderson, 1989, pers. comm.[1]).

a) Two-pyroxene Geothermometry

For the purpose of this study, two of the thermometers recommended by Lindsley (1983) were utilised : the graphic thermometers of Lindsley (as amended by Nabelek *et al.* 1987); and the thermometers of Kretz (1982), together with the graphic thermometers of Saxena *et al.* (1986). These were applied to the amphibolite of the Valley Trust Formation while single pyroxene thermometry through the graphic thermometer of Lindsley (1983) was utilised for the charnockite of the Mgeni batholith (orthopyroxene), the fine grained granulite (orthopyroxene) and the amphibolite of the Nagle Dam Formation (clinopyroxene).

Single pyroxene thermometry yields temperatures below that normally considered characteristic of the granulite grade for all the lithologies appraised - c. 600°C for the charnockite and Nagle Dam Formation amphibolite, and c.500°C for the fine grained granulite of the Valley Trust Formation. This may have resulted from the requilibration of the pyroxene during retrogression in these lithologies.

Application of the various two-pyroxene geothermometers to the average orthoproxene and clinopyroxene core analyses (Appendix 2) of the amphibolite of the Valley Trust Formation derive temperatures of c.700°C. For the thermometers of Kretz (1982) temperatures of 690-740°C are obtained, with the exchange reaction thermometer constantly 50-60°C higher than the transfer reaction thermometer (as found by Ellis and Green 1985). This latter is equivalent to temperatures derived from the graphic thermometer of Lindsley (1983). Higher temperatures of 790°C are obtained from the thermometer of Saxena *et al.* (1986). Errors in the thermometer of Saxena *et al.* were estimated to be a maximum of 50°C.

[1]Prof JL Anderson, USC, Los Angeles, USA

b) Garnet-orthopyroxene Geothermometry

Available analyses of coexisting garnet and orthopyroxene are limited to the fine grained granulite of the Valley Trust Formation. Utilisation of these analyses with several of the garnet-orthopyroxene thermometers (Dahl 1980; Sen and Bhattacharya 1984; Harley 1984b; Perchuk *et al.* 1985; Lee and Ganguly 1988; Bhattacharya *et al.* 1991; Lal 1993) generate a range of temperatures from 700-860°C (NDF 67a) and 740-900°C (NDF70) for average garnet core-orthopyroxene analyses (Appendix 2). A similar spread of temperatures was obtained by Bhattacharya *et al.* (1991), who found that the various geothermometers generated a range of temperatures of c.100°C, with the thermometer of Harley (1984b) providing the lowest temperatures (also Lee and Ganguly 1988), and that of Lee and Ganguly (1988) the highest. Rock composition may also influence the results of these geothermometers, and for aluminous granulites Lal (1993) noted that the thermometer of Sen and Bhattacharya (1984) produced high results.

Core-core temperatures in excess of 700°C, and frequently in excess of 800°C are, however, indicated, while temperatures calculated using the garnet margins range from 660-790°C (NDF 67a) and 760-945°C (NDF 70). Compositional variation within the mineral phases generate a range of results to a maximum of 300°C in sample NDF 67a.

c) Biotite-garnet Geothermometry

This thermometer has a wide range of potential applicability within the Valley of a Thousand Hills, with coexisting biotite and garnet present in several members of the Mgeni batholith and the Mapumulo Group. Reliable data are available from the pelitic gneisses of the Nagle Dam and Valley Trust Formations and the fine grained granulite. Data are not, however, available for the biotite coexisting with garnet within the Mgeni batholith, with the exception of the granitic enclaves found in the Ximba Suite.

Regional analyses of the garnet-biotite geothermometers (Chipera and Perkins 1988; Dasgupta *et al.* 1991) suggest that the majority of these thermometers poorly define peak temperatures within the granulite facies. Similarly, the present study derives an extreme range of temperatures, to a maximum of 260°C within a single sample. In particular the thermometer of Ferry and Spear (1978) yields high temperatures, while the results from the thermometers of Perchuk *et al.* (1985) and Indares and Martignole (1985) are low. Dasgupta *et al.* (1991) noted, however, that their geothermometer produced results comparable with other temperature estimates within the granulite facies, with uncertainties considered to average 50°C. Subsequently it was utilised by Neogi *et al.* (1998) to identify granulite grade peak temperatures. This was applied to the pelitic gneisses, for core-core analyses (Appendix 2), as temperatures derived from garnet and biotite margins within the granulite facies are generally low (Indares and Martignole 1985).

A wide range of results are derived: 770°C from the Nagle Dam Formation; 665°C from the pelitic gneiss of the Valley Trust Formation and 700-830°C from the individual samples of the fine grained granulite. Variable Fe-Mg ratios generate a range of temperatures to a maximum of 200°C in the fine grained granulite. Recalculation to take account of potential Fe^{3+} (Guidotti and Dyar 1991; Holdaway *et al.* 1997; Rathmell *et al.* 1999) results in a decline in the temperatures calculated by c.20°C.

Results from the garnet-biotite geothermometers are also available for a sample of the granitic enclaves within the Ximba Suite. The majority of the thermometers record core-core temperatures of c.600°C, but the thermometer of Ferry and Spear (1978), which Anderson (1996) considered provided the best temperature estimates for granites with low-Mn garnets, yields temperatures of c.650°C$\pm$30°C. Temperatures calculated from the biotite and garnet margins provide lower temperatures, c.500°C, possibly due to marginal requilibration at lower temperatures.

d) Two Feldspar Geothermometry

The two feldspar thermometer is potentially applicable to almost all the identified lithologies within the Valley of a Thousand Hills, and in particular the granites of the Mgeni batholith. Analysis of the available data from the Mapumulo Group and Mgeni batholith, however, provide consistently low results, typically approximating 400°C, presumably due to the effect of the extensive perthite exsolution which is widely observed in these rocks. Utilisation of available perthite analyses provide higher temperature estimates, generally within the range 600-800°C, but the limited data set and the lack of internally consistent chemical trends within the perthite analyses does not allow a high degree of confidence in these results.

e) Pyroxene-hornblende Geothermometry

Available coexisting pyroxene-amphibolite analyses are restricted to the amphibolites of the Mapumulo Group. These display varying K_D of 1.49 and 1.32 (assuming $Fe^{2+} = Fe_{TOT}$) from the amphibolites of the Valley Trust and Nagle Dam Formations, respectively, which on the graphic thermometer of Kretz and Jen (1978) correspond to temperatures of approximately 725°C and 785°C. Consideration of Fe^{3+} results in a minor change in these temperatures.

Similarly, Perchuk *et al.* (1985) proposed a graphic amphibole-orthopyroxene and amphibole-clinopyroxene thermometer. These provide temperature estimates of 670-680°C and 750°C for the amphibolites of the Valley Trust and Nagle Dam Formation, respectively. Anderson (1996) noted, however, that this thermometer is untested, and advised caution in its use.

f) Plagioclase-amphibole Geothermometry

The plagioclase-amphibole thermometer was applied to the various hornblende bearing granites of the Mgeni batholith and the amphibolites of both the Nagle Dam and Valley Trust Formations.

The Spear thermometers provide low temperatures. On the graphical thermometer of Spear (1980) the analyses plot between Spear's 490°C and 530°C isotherms, but clustering towards the low temperature side of this field. Slightly higher temperatures, up to 550°C for the charnockite, are calculated using the formulation of Spear (1981a).

The thermometer of Blundy and Holland (1990), however, provides much higher temperatures, 760°C-790°C from the average plagioclase and amphibole core analyses of the various granites (Appendix 2). Individual amphibole analyses (Appendix 2), with the relevant average plagioclase composition from the granite, generate a range of temperatures to a maximum of 20°C within an individual granite. These high temperatures may represent near solidus temperatures, and the lack of markedly lower temperatures suggest little subsolidus reequilibration. Holland and Blundy (1994) and Anderson (1996) noted that the thermometer of Blundy and Holland may give high results for granites with high Al-hornblendes. The present results do not, however, provide the extreme temperatures derived by Anderson (1996), and calculation of the preferred (Anderson 1996) edenite-richterite thermometer of Holland and Blundy (1994), provides comparable, but typically slightly lower (20-60°C) results for the hornblende and garnet hornblende granites, at equivalent pressure estimates.

The amphibolite of the Nagle Dam Formation provides temperatures comparable to those determined from the granites, c. 760°C, but those of the Valley Trust Formation provide considerably higher temperatures, c. 830°C for either of these calibrations using average core analyses (Appendix 2). Mineral heterogeneity generates a minor spread of results, typically c.20°C.

g) Hornblende Geothermometry

The hornblende-melt geothermometer (Helz 1979) has limited potential applicability within the Valley of a Thousand Hills and was employed only for the granites of the Mlahlanja Suite. Calculations reveal average temperatures of 817°C for the charnockite and 902-916°C for the garnet hornblende granite. These temperatures are not, however, considered highly accurate, in particular as no data are available regarding the cell volumes of the hornblendes analysed.

3.3.2 GEOBAROMETRY

Numerous geobarometers have been calibrated for use in the granulite facies (Essene 1989). Of these, however, the appropriate mineralogy and analytical data are only available for the garnet-plagioclase-aluminum silicate-quartz (GASP) barometer. The garnet-orthopyroxene barometer has also been considered, but, as noted by Essene (1989), this may be inaccurate at crustal pressures, although it has been used by several authors (including Harley 1985) to determine the pressures of metamorphism.

The geobarometry of granites has been less well researched, but several barometers are available (for example Anderson *et al.* 1988; Anderson 1996). The mineralogy of the Mgeni batholith, however, and in particular the absence of muscovite and the lack of appropriate data from specific mineral phases, limits the applicability of many of these barometers, and data are only available for the hornblende barometer (Hammarstrom and Zen 1986; Hollister *et al.* 1987; Johnson and Rutherford 1989; Schmidt 1992; Anderson and Smith 1995).

a) Garnet-orthopyroxene Geobarometer

Available analyses of coexisting garnet and orthopyroxene are limited to the fine grained granulite of the Valley Trust Formation, for which

the analytical totals of the orthopyroxenes are typically slightly low, 97-100 percent.

Numerous formulations of the garnet-orthopyroxene geobarometer are available, including Boyd (1973), MacGregor (1974), Wood (1974), Wood and Banno (1973), Harley and Green (1982) and Harley (1984a). The majority of these were not considered in the present study as they were originated primarily for mantle derived garnet peridotites, with extrapolation to granulites criticised by Harley (1984a). For the purpose of this study, therefore, only the geobarometers of Harley and Green (1982) and Harley (1984a) were considered. Bhattacharya and Sen (1986) found that the latter provides results comparable with those of Newton and Perkins (1981), with the wide spread of pressures derived in other studies the result of not correcting for Fe^{3+}.

Calculation of these geobarometers, however, derive highly variable and frequently extremely low results, suggesting alumina reequilibration following the peak of metamorphism. This is contrary to the findings of several authors, including Aranovich and Berman (1997), who considered Fe-Mg exchange to be more sensitive to reequilibration.

b) Garnet-Plagioclase-Aluminum Silicate-Quartz (GASP) Geobarometer

Within the Valley of a Thousand Hills use of this barometer is restricted to the aluminosilicate bearing pelitic gneiss of the Valley Trust Formation. Pressures of 5-6 kb are suggested by the barometers of Ghent *et al.* (1979) and Powell and Holland (1988), for average garnet and plagioclase core analyses (Appendix 2). The derived pressure estimates are, however, strongly controlled by the temperature utilised, and for Ghent *et al.* (1979), a range of pressures from 4.47-6.4 kb are calculated using the temperatures derived from the garnet-biotite (pelitic gneiss) and amphibolite-plagioclase (from the adjacent amphibolite) thermometers, respectively.

The accuracy of the various GASP geobarometers has been evaluated by several authors, including Hodges and Crowley (1985), Powell and Holland (1985; 1988), McKenna and Hodges (1988) and Kohn and Spear (1991a; 1991b). McKenna and Hodges (1988) calculated potential error at 2.5 kb but noted that the GASP barometer was the '*best-calibrated thermobarometric reaction available*'. A similar assessment was given by Kohn and Spear (1991b) who summarised the various potential sources of error, and estimated total pressure uncertainties within the range 1560-2350 bars. This increases for samples with low grossular and anorthite contents, and, although the present analyses are within the range of acceptable data, this generates an estimated uncertainty of c.1100 bars (Todd 1998). Pressure variations of c.2kb are derived from the heterogeneity of the mineral phases.

c) Hornblende Geobarometer

Within the Mgeni batholith hornblende has been reported in all three identified granite suites (Kuyper 1979), although not noted in the Nqwadolo granite during the present study. Microprobe analyses are, however, limited to the Mlahlanja Suite, where samples from all the major granite subtypes were analysed. In each case the hornblende exhibits the igneous characteristics of Hammarstrom and Zen (1986), and displays the features of late crystallising minerals, as indicated by the presence of abundant inclusions and its formation through pyroxene breakdown in the charnockite. Although all these rocks are silica saturated, only the hornblende granite possesses the mineral assemblage defined by Hammarstrom and Zen (1986). Within the charnockite the presence of pyroxene is unlikely to affect the alumina content of the hornblende, as it is largely enclosed within the hornblende (and see Hammarstrom and Zen 1986). The presence of garnet, however, although sporadic within several of the granites and not present in the analysed probe sections, could, as an alumina buffer, have a serious influence on the hornblende geobarometer.

The various geobarometers (Hammarstrom and Zen 1986; Hollister *et al.* 1987; Johnson and Rutherford 1989; Schmidt 1992) suggest pressures in excess of 5 kb, and typically 6 kb, with the variable Al_{TOT} content of the granites allowing the identification of a lower pressure group, consisting of the hornblende granite and the charnockite, and the higher pressure garnet hornblende granite. As noted by Cosca *et al.* (1991) the various microprobe normalisation models can result in slight differences in the calculation of the hornblende formula. As proposed by these authors the available hornblende analyses were recalculated using the 13 cation model. This results in a slight reduction in the estimated pressures, typically less than 0.1 kb. Variable Al_{TOT} within the individual granites results in a spread of pressures to a maximum of 0.5 kb.

Potentially, this barometer may also apply to the

hornblende bearing assemblages of the Mapumulo Group (Hammarstrom and Zen 1986). Available hornblende analyses are restricted to the amphibolites and these suggest pressures of c. 5 and 5.5 kb for the amphibolites of the Nagle Dam and the Valley Trust Formations, respectively.

Blundy and Holland (1990) criticised the various hornblende geobarometers, suggesting that Al^{IV} is distinctly temperature dependent and that the hornblende geobarometer is consistent with pressure estimates at a fixed temperature, approximating the granite solidus. Anderson and Smith (1995) also noted the temperature dependence of the hornblende geobarometer, and proposed a temperature correction factor for the barometer. This provides highly variable results, of 4.5 kb for the charnockite to 6.3 kb for the garnet hornblende granite utilising the temperatures derived from the Holland and Blundy (1994) thermometer and average mineral compositions.

3.4 P-T EVOLUTION OF THE VALLEY OF A THOUSAND HILLS

Regional studies of the Natal Province have suggested a metamorphic history dominated by a single event (Thomas 1988a; 1988b), which may be devisable into a series of prograde and retrograde stages (for example Grantham 1983; Evans 1984), and locally affected by the intrusion of the granite batholiths of the Oribi Gorge Suite (Thomas 1988a; Cornell *et al.* 1996). P-T-t models for the Natal Province are, however, generally lacking and no metamorphic model has been advanced for the central portion of the belt.

Within the Valley of a Thousand Hills mineralogical evidence indicative of a high grade evolutionary P-T-t trend is limited to the pelitic phases of the Valley Trust Formation, within which metamorphism can be summarised into a series of distinct phases:

a) for the fine grained granulite:

1) development of an orthopyroxene bearing assemblage;
2) breakdown of orthopyroxene to form garnet + sillimanite + biotite; and
3) formation of cordierite;

b) for the pelitic gneiss:

1) development of a biotite + sillimanite assemblage;
2) partial melting to produce a garnetiferous partial melt;
3) development of biotite-sillimanite folia; and
4) formation of cordierite.

Vernon (1996) noted the difficulty in identifying different assemblages formed within an evolving system at approximately similar grades of metamorphism. In particular Vernon questioned the identification of distinct phases of metamorphism from the interpretation of pophyroblast-matrix and mineral replacement relationships. Within the present study two distinct examples of these reactions have been observed - the presence of biotite - sillimanite folia that wrap around the garnet porphyroblasts and the occurrence of cordierite as polygonal aggregates in the biotite + sillimanite matrix and moulding garnet, biotite and sillimanite. Various interpretations are possible, including that of Vernon who suggested that this may represent a single metamorphic assemblage with the different textural relationships the result of deformation. The biotite-sillimanite folia wrapping around garnet and cordierite porphyroblasts have, however, also been interpreted as a M2 assemblage (Hand *et al.* 1992).

Within the present study the apparent crosscutting of garnet porphyroblasts by the biotite-sillimanite folia and subsequent overgrowth of the folia by a secondary garnet, with cordierite, favours the interpretation of Vernon, with the mineral assemblages evolving in varying deformation and growth phases during a single metamorphic event. The apparent relationship between the garnet and a partial melt product, however, indicates that the garnet was derived through an evolving P-T system, while the presence of a cordierite mantle to garnet + sillimanite + ore and the possible existence of a minor partial melt phase in association with the cordierite suggest that cordierite was a late phase within the pelitic gneiss, rather than a component in a biotite + sillimanite + cordierite assemblage.

The evolving assemblages within the different series do not form parallel paths. The fine grained granulite is distinguished by a retrograde path from the orthopyroxene bearing assemblage to that of the garnet + sillimanite + biotite assemblages. The pelitic gneiss, however, displays a prograde path with the development of a garnet bearing partial melt derived from the dehydration melting of a biotite + sillimanite assemblage.

Subsequent reactions indicate a comparable decompression event, resulting in the formation of cordierite. The coincident trend for this later phase

of metamorphism suggests that the fine grained granulite and the pelitic gneiss were evolving as a single system, possibly within the regional structure resultant on the intrusion of the Mgeni batholith. The evidence for the interaction of the pelitic gneiss and its melt phase with the associated megacrystic granite suggests that at least from phase 2 of the metamorphism of the pelitic gneiss this unit was a part of the larger P-T system.

A possible P-T-t evolution loop for the Valley of a Thousand Hills is summarised on Figure 3.1. Although data are lacking to define the initial phase of the metamorphic evolution of this area, available data from the Nagle Dam Formation suggest a metamorphic peak of c.770°C (Figure 3.1a), with a minimum pressure estimate of 6 kb extrapolated from the Mgeni batholith and Valley Trust Formation. Peak temperatures from the Valley Trust Formation are higher, c.850°C (Figure 3.1b), with temperatures to a possible maxima of 900°C (Figure 3.1c) from the Mgeni batholith, the latter higher temperatures comparable with the range of temperatures derived from the M-Zr plot of Watson and Harrison (1984), as determined by Thomas *et al.* (1993). These temperature variations suggest an influx of heat from the Mgeni batholith, which may have generated the orthopyroxene bearing lithologies within the Nagle Dam Formation, as suggested by Thomas (1988a) from the Ntimbankulu batholith. Corroboration of the higher temperature estimates are provided by the biotite dehydration reactions observed in the pelitic gneiss for which temperatures of c.750°C at 6 kb for a biotite of c.$Mg_{0.5}$ were proposed by Le Breton and Thompson (1988), and c.850°C by Vielzeuf and Holloway (1988). These latter may represent a superior estimation of peak metamorphic temperatures than the Fe-Mg exchange thermometers, as the tendency for the garnet-biotite thermometers to record relatively low temperatures (Burgess *et al.* 1995), with Perchuk and Lavrent'eva (1983) as the representative thermometer, suggest an underestimation of temperatures (Greenfield *et al.* 1998).

Subsequently, temperatures declined, with a marked clustering of results from the Valley Trust Formation at 700°C, while the pressure remained almost constant, as evidenced by the consistent pressures obtained from the granites and the pelitic gneiss and the generation of garnet after orthopyroxene in the fine grained amphibolitic granulite (Harley 1989). A later decline in pressure is indicated by the formation of cordierite bearing assemblages in the pelitic gneiss and fine grained granulite of the Valley Trust Formation and the presence of high manganese, low pressure, garnet in late granitic veins (Green 1977). Assuming garnet crystallisation above the minimum melt solidus this suggests an almost isothermal decline in pressure.

This pattern differs markedly from the simple isothermal and isobaric P-T paths described by Harley (1989). Although a general near isothermal decompression model is indicated for the Valley of a Thousand Hills area, superimposed on this is a near isobaric heating and cooling phase. The similarity of the temperatures derived from the metamorphosed lithologies and the Mgeni batholith suggest a relationship, possibly a local overprinting of the original PT characteristics of the Mapumulo Group through the influence of the granites. The range of temperatures obtained from the Mapumulo Group may, therefore, reflect the cooling history of the Mgeni batholith, superimposed on variations in the reaction rate of the various mineral assemblages present in the Mapumulo Group. Specifically, the high temperatures of the garnet-orthopyroxene thermometer may define a lower limit to the intrusion temperature of the granite, with the temperatures derived from the plagioclase-amphibole thermometer reflecting a stage in the cooling history of the granite, as suggested by Blundy and Holland (1990). The majority of mineralogical reactions identified within the Valley Trust Formation can therefore be interpreted as resultant on either of the processes identified. In particular the production of a partial melt phase in the pelitic gneiss may be the result of an increase in temperature, generated by the intrusion of the Mgeni batholith, rather than decompression as suggested by Harley (1989). This is comparable with the model of isobaric cooling associated with granite intrusion described by Sandiford *et al.* (1991), and mirrors the intrusion related thermal spikes of Williams and Karlstrom (1996), but in the Valley of a Thousand Hills forms only a phase in the isothermal decompression of the region. Sequential production of garnet and cordierite melts during heating and extensional decompression was noted by Escuder Viruete *et al.* (1997).

Quantification of the time span of the various metamorphic events identified is hindered by the lack of geochronological data from the Valley of a Thousand Hills. In particular, no data are available for the initial metamorphism of the Mapumulo Group, although Cornell *et al.* (1996) proposed a c.1100 Ma collision event within the Mzumbe Terrane. Lead isotopic data, however, suggest a 1030 ±20 Ma intrusion age for the Mgeni batholith

Figure 3.1. P-T evolution of the Valley of a Thousand Hills.
a) Temperature ranges within the Nagle Dam Formation.
b) P-T conditions within the Valley Trust Formation.
c) P-T conditions within the Mgeni batholith.
d) Summary of P-T evolution within the Valley of a Thousand Hills.
Symbol within P-T range represents the average P-T of the sample.

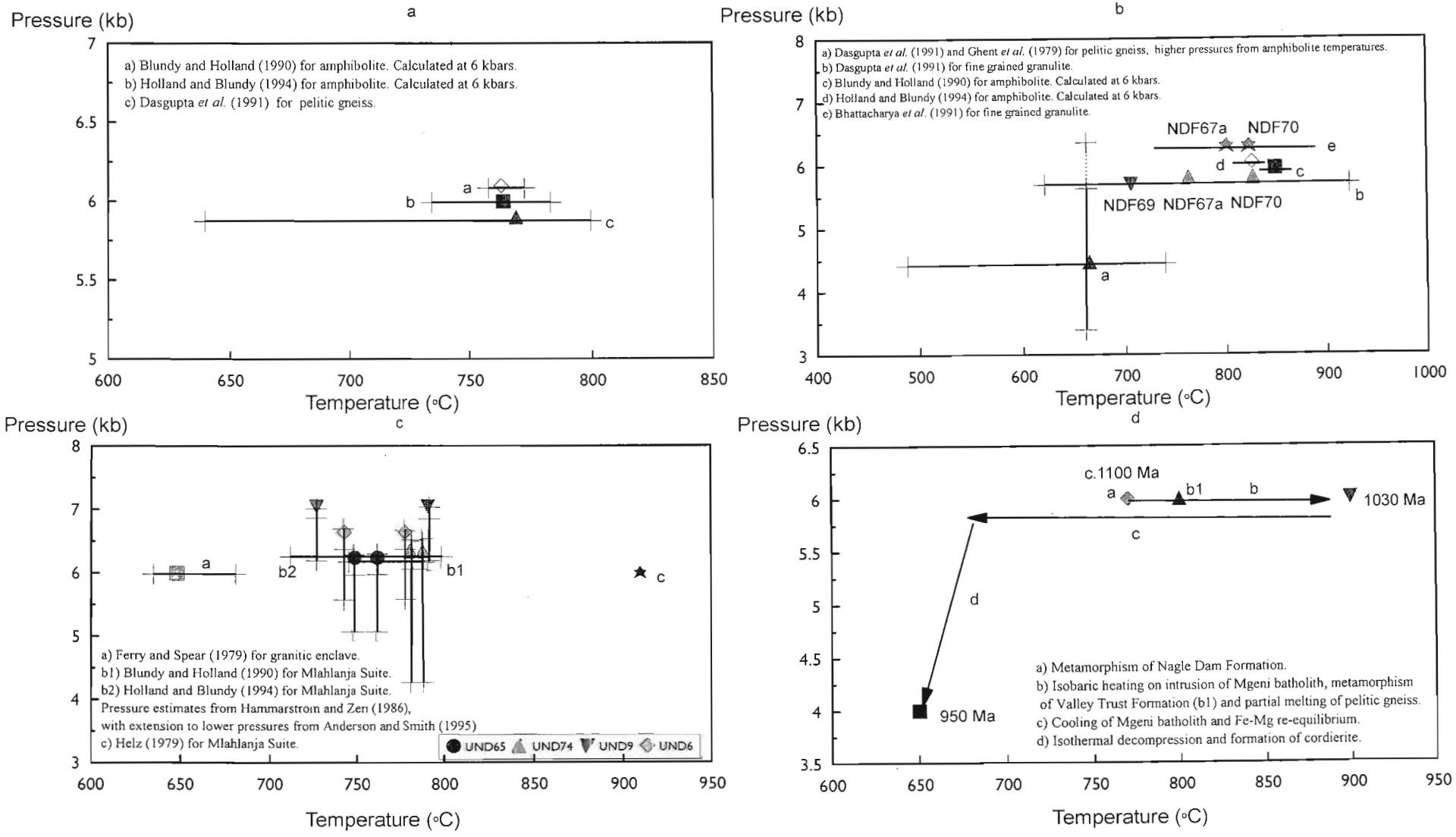

(Eglington *et al.* 1989b), which may date the isobaric heating and cooling event, including the partial melting of the pelitic gneiss. Late intrusions into the Natal Province have been dated at 1026±3Ma, with the tectono-metamorphic evolution of the Natal Province believed to have ended c.950 Ma (Thomas *et al.* 1993). These dates can be utilised to constrain the late stage granitic intrusions within the Valley of a Thousand Hills.

3.5 DISCUSSION - RAPAKIVI GRANITE INTRUSION LEVELS

Typically, the rapakivi granites display a range of physical features suggestive of a high level of intrusion. In particular are their sharp intrusive contacts, the local presence of volcanic or subvolcanic members, roof pendants and roof breccia outcrops (Haapala and Ramo 1990). This is supported by several lines of experimental data, including granite crystallisation modelling (Barker *et al.* 1975; Anderson and Cullers 1978; Anderson 1980), geothermobarometry of the country rocks (Anderson and Bender 1989; Brown *et al.* 1991) and fluid and mineral inclusion studies (Sonyushkin *et al.* 1991). The Proterozoic rapakivi granites of Natal differ from these typical rapakivi granites, however, in not displaying any physical evidence of a high level of intrusion. Rather, they are intrusive into high grade metamorphics (Thomas 1988a).

Various intrusion depths have been proposed for these granites. Introductory studies of the Mgeni batholith by Kuyper (1979) indicated intrusion into an intermediate pressure regime of 2-5 kb. Mineral assemblage analysis and cordierite-garnet geobarometry of enclaves within the granites undertaken by Kuyper corroborated this, indicating metamorphism at pressures of 4-6 kb. The presence of hypersthene in semi-pelitic rocks in the contact zone of the Ntimbankulu batholith, however, led Thomas (1988a, after Winkler 1979) to suggest a maximum intrusion level of 7 km for this member of the Oribi Gorge Suite.

Estimates of the depth of emplacement of the Mgeni batholith gained during the present study (Milne and Kerr 1995) support the view of Kuyper (1979) that these granites developed at a moderate pressure rather than the high level favoured by Thomas (1988a). Available hornblende geobarometer data suggest depths of intrusion of 16.5-23 km from the pressure estimates of Anderson and Smith (1995).

This depth estimate is, however, dependant on the accuracy of the hornblende geobarometer which has been questioned by Blundy and Holland (1990), who proposed a temperature dependence on the Al^{IV} content of hornblende. Further, the use of the hornblende geobarometer for high iron hornblendes was queried by Anderson and Bender (1989), who found that the various hornblende barometers gave geologically unreasonable results for A-type granites in the southwestern United States. Anderson and Smith (1995) noted the lack of correspondence between the pressures derived for granites with a high Fe/Fe+Mg mineralogy using the hornblende barometer and the associated metamorphic rocks. Vyhnal *et al.* (1991) also noted an Fe/Fe+Mg-pressure relationship from the amphiboles of the southern Appalachian granitoids. This is supported by experimental evidence (Mysen and Boettcher 1975; Allen and Boettcher 1978), and may be the result of Fe/Fe+Mg-Al coupling (Robinson *et al.* 1982).

The hornblende geobarometers have, however, derived geologically consistent results from a number of studies, including Anderson *et al.* (1988), Vyhnal and McSween (1990), Vyhnal *et al.* (1991) and Dawes and Evans (1991). Hammarstrom and Zen (1986), moreover, did not consider that the concentration of iron had an influence on the hornblende geobarometer and used hornblendes with high iron contents (18-19%) in determining the high pressure portion of their barometer. Similarly, Johnson and Rutherford (1989) used hornblendes with iron contents to a maximum of 22 percent in their calibration of the hornblende geobarometer. The hornblende of the San Isabel batholith is equally iron rich (Cullers *et al.* 1992), with the high pressures obtained from the hornblende geobarometers being supported by the presence of magmatic epidote (although the high pressure origin of magmatic epidote has been questioned by several authors including Tulloch 1986; Moench 1986; Vyhnal *et al.* 1991; but not Schmidt and Thompson 1996). Vyhnal *et al.* (1991) also determined geologically consistent and comparable results from high (26%) and low iron hornblendes. Vyhnal *et al.* found that although a crude relationship exists between $Fe^{2+}/Fe^{2+}+Mg$ and pressure, this did not hold for highly iron enriched hornblende. Anderson and Smith (1995), emphasised the importance of the Fe/Fe+Mg ratio, noting that the hornblende barometer provides acceptable pressures for iron rich hornblende if their ratio was c.0.6, as for the San Isabel batholith.

Studies of amphibole developed under high pressure metamorphic conditions have tended to support the positive correlation between alumina in

amphibole and pressure (Leake 1965a; 1965b; Kostyuk and Sobolev 1969; Raase 1974; Robinson *et al.* 1982; Selverstone *et al.* 1984). This is confirmed by experimental studies (Spear 1981b; Plyusnina 1982; Cao *et al.* 1986; Jenkins 1988; 1989; but not Cho and Ernst 1991 or Leger and Ferry 1991). These latter studies found that the associated mineral assemblage strongly controls the alumina content of amphibole. Leger and Ferry (1991) in particular noted the control imposed by the combination of P, T and mineral assemblage, with declining alumina as pressure increases for specific mineral assemblages.

The hornblendes of the Mgeni batholith possess high iron contents with high Fe/Fe+Mg ratios (Section 2.3.2). The high pressures of crystallisation indicated by the various hornblende geobarometers may therefore be extreme, and lower pressures, more typical of the rapakivi granites, may be more realistic. Unlike the majority of the rapakivi granites, however, evidence does exist for high pressures of metamorphism within the Valley of a Thousand Hills, with minimum pressure estimates of 4.5 kb derived from the GASP barometer. In addition further evidence for high pressures of crystallisation are supplied by the garnets found within the Mgeni batholith and in melts produced by partial melting of the pelitic enclaves within the granites. These are characterised by low manganese and high calcium contents, indicating pressures of c.7 kb (Green 1977). The amphibole-plagioclase geothermometer of Holland and Blundy (1994) indicates that all these granites crystallised over a narrow temperature range, 720-790°C, with temperature inversely related to pressure. It seems unlikely, therefore, that temperature alone could have controlled the hornblende geobarometer, as suggested by Blundy and Holland (1990).

Comparable emplacement depths for A-type granites, although rare, have been determined for other granites. In particular emplacement depths of 17 to 23 km (5-7 kb) were proposed by Cullers *et al.* (1992) for the San Isabel batholith. Although the granites of the Mgeni batholith lack the epidote found in the San Isabel batholith, it appears that they may have formed at a similar mid-crustal depth.

The high iron hornblendes of the Mgeni batholith therefore appear to provide tolerable estimates of the intrusion depth of these granites, and so the problems associated with the use of the hornblende geobarometer in estimating the intrusion levels of rapakivi granites must be revaluated. In particular Leake and Cobbing (1993) questioned whether this barometer indicates the depth of emplacement or the depth of crystallisation of the granites.

CHAPTER 4

GEOCHEMISTRY

4.1 INTRODUCTION

Limited geochemical data are available from the Proterozoic rocks within the Valley of a Thousand Hills. Kuyper (1979) and Du Toit (1979) reported some 46 analyses, predominately from the biotite granites of the Ximba Suite, the Nqwadolo Suite and the amphibolite and quartzo-feldspathic gneiss of the Valley Trust Formation. Additional samples of the Ximba Suite and Nagle Dam Formation were collected by Bulley, but the analyses were never reported.

To establish a data base sufficient to undertake a preliminary regional geochemical investigation of the various lithologies identified within the Proterozoic basement of the Valley of a Thousand Hills, an extensive sampling programme was initiated (Appendix 3). This targeted previously unsampled lithologies, including the pelitic gneiss of the Valley Trust Formation, and localities within formerly sampled lithologies which would assist with establishing a petrogenetic model, such as the core zone of the Nqwadolo Suite.

This chapter will describe the chemical characteristics of the various units identified in the Valley of a Thousand Hills, identify possible correlates and, in the case of the metamorphosed lithologies, determine the nature of their original protolith. Sample data are given in Appendix 3, with the sample localities on the attached plan. Correlation coefficients, elemental ranges and means of the sample data set are presented in Appendix 4.

4.2 ANALYSIS OF THE DATA SET

The samples collected during this study were approximately 50kg in mass. This large sample size was chosen to compensate for the megacrystic nature of the granites and the heterogeneous character of the gneisses. To test the appropriateness of the selected sample size, the analyses of three adjacent, visually homogeneous specimens of the biotite garnet granite are compared in Table 4.1. These are almost identical, with minor standard deviation, suggesting that the selected sample size is sufficient to obtain representative chemical analyses of these granites.

Three geochemical data sets are available:

1) older data collected by Kuyper (1979), Du Toit (1979) and Bulley (unpubl);
2) data collected during the present study and analysed at the Geological Survey, Pretoria; and
3) data collected during the present study and analysed at the Department of Geology, University of Natal, Pietermaritzburg.

The generation of geochemical data from a variety of sources allows the possibility of discrete bias within the individual data sets. Insufficient data are available to undertake a relevant statistical analysis of these data and so determine the relative degree of any potential bias, which is further complexed by the geographical spread of individual sampling phases and the nonrandom selection of specific samples. For example, six garnet hornblende granite samples were collected from the Matata pluton, four by Kuyper (1979) and Du Toit (1979), and two during the present study. These latter are, on average, more siliceous than the former, but this is due to the deliberate selection of a less mafic sample, UND 81, to investigate the degree of fractionation present within the pluton. Similarly, when comparing the available data from the hornblende granite and charnockite of the Mlahlanja Suite distinct differences are apparent between the different data sets, with the original analyses typically enriched in specific elements, and in particular Zr, although individual granites do not necessary reveal these distinctions. Analysis of the data from the hornblende granite of the Sansikane pluton, from which Kuyper (1979) collected a single sample with nine additional samples collected during the present study, reveals a slight increase in the standard deviation and decline in the degree of correlation between the elements and silica if the original sample is included with those collected during the present study, but comparable differences are derived if individual samples from the control set are excluded from the calculations. Calculation of the sum of the squares of the residuals of a model UND 26 analysis, derived through extrapolation from the adjacent samples with silica as a constant, is comparable with that calculated between analyses from the hornblende granite control data set. Differences are also apparent between the biotite garnet granite sample UND 36 (Kuyper 1979; Du Toit 1979) and samples UND 90-92, which were collected from adjacent sites. In particular, Al_2O_3, MgO, Na_2O and Y levels are high, while SiO_2 concentrations are low in sample UND 36. Comparison with those biotite garnet granites contaminated by inclusion of pelitic material, however, suggests that sample UND 36 may represent a contaminated biotite garnet

Table 4.1. Comparison of adjacent biotite garnet granite analyses, Ximba Suite.

	NDF90	NDF91	NDF92	SD
SiO_2(wt%)	69.25	69.59	69.31	0.181
TiO_2	0.37	0.36	0.37	0.003
Al_2O_3	15.79	15.61	15.55	0.125
Fe_2O_3	3.45	3.34	3.5	0.082
MnO	0.04	0.05	0.05	0.006
MgO	0.34	0.34	0.34	0
CaO	2.3	2.2	2.25	0.05
Na_2O	2.91	2.8	2.65	0.131
K_2O	5.27	5.42	5.15	0.135
P_2O_5	0.11	0.11	0.11	0
Trace elements in ppm				
Ba	2062	2098	2049	25.384
Rb	137	141	136	2.73
Sr	227	226	226	0.611
Zr	321	348	368	23.672
Pb	37	35	37	1.155
Nb	17	17	18	0.7
Y	27	31	28	1.823
La	64	62	71	4.726
Ga	24	24	25	0.577
Zn	71	71	71	0.4

granite (Section 6.4.2).

Several samples were analysed at both the Geological Survey and the Department of Geology, Pietermaritzburg, during the present study, although insufficient to undertake a statistical analysis of potential bias. Comparison of the various analyses of the charnockitic samples UND 74 and UND 71 and the marginal granite UND 72 may suggest a tenancy for the analyses from the Geological Survey to be higher in SiO_2, but lower in Al_2O_3, MgO and Zr than those from the Department of Geology, Pietermaritzburg, but not for UND 317, which, with those samples analysed earlier at the Geological Survey, rather indicates a tenancy towards higher Y concentrations. Comparison with the charnockite analyses, however, reveals no particular variation in the concentrations of Y from the different laboratories.

With the exception of the high SiO_2 but low Al_2O_3 content of UND 71A the observed elemental abundances within the duplicate samples are within the range of chemistries derived from the other samples. The range of data from the individual sample sites, however, exceeds the standard deviation of the biotite garnet granite samples UND 90-92, suggesting a possible bias in one of the data sets. Comparison of the duplicate charnockite analyses with a control set from the same pluton, the latter all analysed at the Geological Survey, suggests that the inclusion of those analyses done at the University of Natal results in the smaller standard deviation and better correlation between the elements and silica than the inclusion of those analyses done at the Geological Survey, although the inclusion of either of the data sets typically results in an increase in the standard deviation and a decline in the correlation coefficient. This suggests that the analytical difference between laboratories may be less than that between runs from a single laboratory.

Within the amphibolite of the Valley Trust Formation, two distinct series can be distinguished by their immobile trace element ratios, Zr/Y and Zr/Nb (Figure 4.5b), of which all the high Zr/Y amphibolite samples were collected by Du Toit (1979), while the low Zr/Y amphibolite was collected during the present study. Comparison of the data from the gneisses of the Nagle Dam Formation suggest that the samples of Bulley, which were analysed at the laboratory of the Geological Survey at the same time as those of Du Toit, may have higher Nb concentrations than the samples collected during the present study, but no differences are apparent between the Zr and Y concentrations from the different sample sets. A portion of the range in Zr/Nb ratios identified may therefore have originated from analytical variability, but this will not explain the distinct Zr/Y ratios. Individual elemental abundances may also vary between the series, with the high Zr/Y series characterised by higher TiO_2, but lower MgO concentrations than the low Zr/Y series. Fractionation trends also differ, while variations in the possible influence of crustal interaction with the melt are apparent (Figure 6.5c). This suggests that the amphibolitic groups identified through variations in the trace element ratios may reflect original heterogeneous basalt chemistries and evolutionary histories within the study area.

Insufficient data exist to identify a constant bias between the different data sets available and inspection of the spread of data points on the Harker diagrams typically demonstrates an overlap between the data sets. For the purpose of this study, therefore, the available data will be taken to indicate the existence of real differences between the samples. In individual cases, however, apparent trends which may be related to variations in laboratory results will be noted and in particular the possible variation in chemistry identified in the amphibolite of the Valley Trust Formation.

4.3 NAGLE DAM FORMATION

4.3.1 INTRODUCTION

Twenty samples (one duplicated, one divided into three portions) of the Nagle Dam Formation were collected for analysis (Appendix 3), sixteen during the present study and the remainder by Bulley (unpubl. report). The sample of biotite hornblende gneiss analysed by Kuyper (1979) has subsequently been shown to form a portion of the marginal phase of the Mgeni batholith (Section 4.3.3).

4.3.2 NATURE OF THE PROTOLITH

Zircon morphology and mineralogical characteristics led Davies (1964), Kuyper (1979) and Bulley (1981) to identify the Nagle Dam Formation as a predominately metasedimentary succession. The available geochemical data, however, plot parallel to the igneous trend lines (Figure 4.1) on the various diagrams devised to distinguish between para- and orthogneisses (Leake 1964; de la Roche 1966; van de Kamp 1968; Leake and Singh 1986), suggesting an igneous protolith for the Nagle Dam Formation, excluding the unsampled pelitic gneiss. Further, on discrimination diagrams such as the Cr-mg diagram

Figure 4.1. Niggli norm protolith discrimination diagrams for the Nagle Dam and Valley Trust Formations.
a) c-mg (Leake 1964).
b) Cr-mg (Leake 1964), for amphibolites and pelitic gneisses.
c) al-alk - c (van de Kamp 1968; Leake and Singh 1986).
d) si-mg (Leake and Singh 1986).

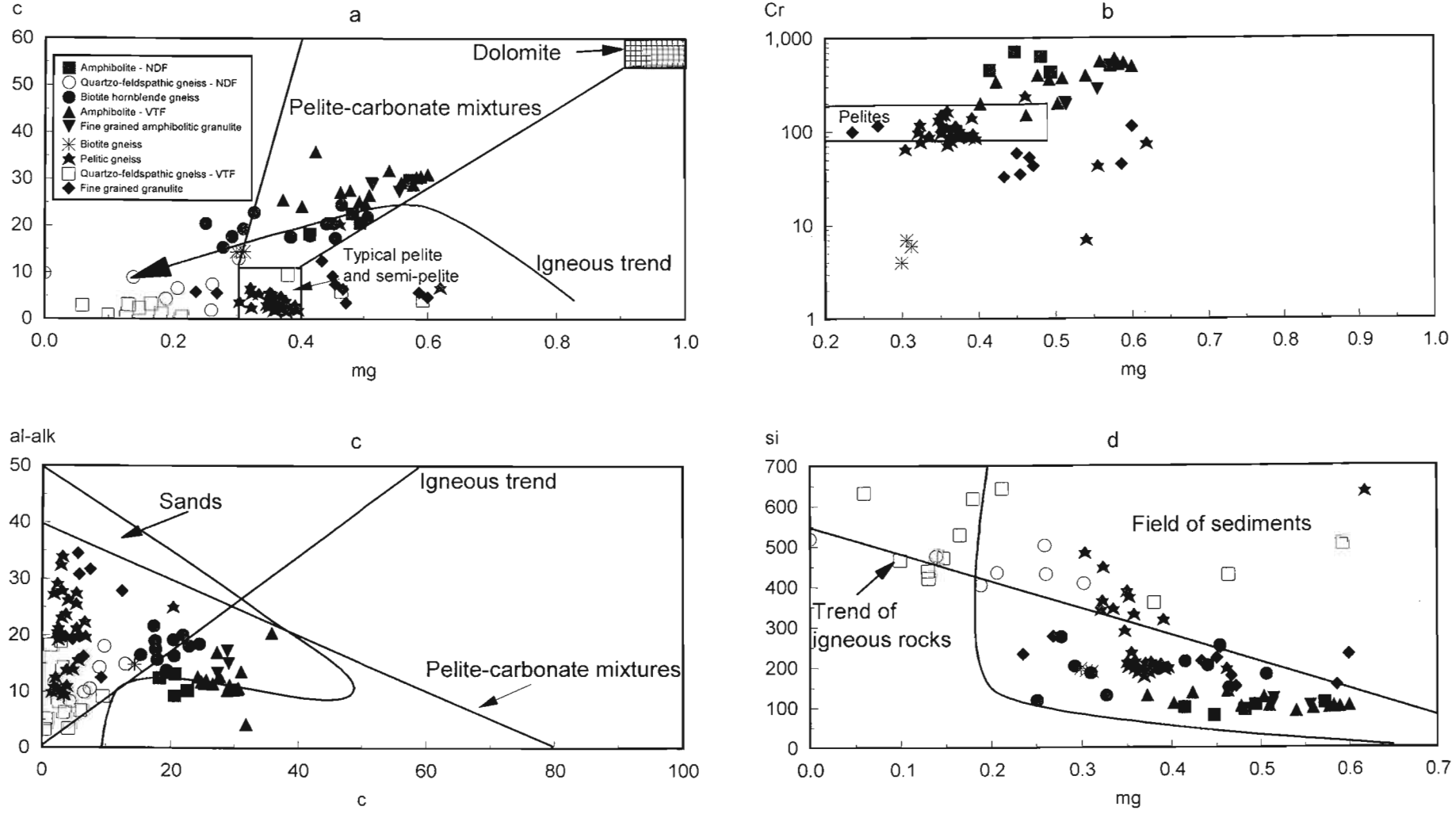

(Figure 4.1b) the amphibolite plots outside the pelitic field. The quartzo-feldspathic gneiss may display a degree of overlap with the field of sands, but on the si-mg diagram (Figure 4.1d) extends beyond this field, paralleling the igneous trend.

4.3.3 REGIONAL CORRELATION

Previous studies of the Nagle Dam Formation (for example Bulley 1981) have suggested that it comprises a series of related, but distinct, lithologies. Milne (1988), however, using the unpublished analyses of Bulley, identified two distinct chemical subtypes within the Nagle Dam Formation, characterised predominately by marked variations in their Zr content. Additional sampling of the Nagle Dam Formation and the marginal portion of the Mgeni batholith indicates a close chemical similarity between the high Zr member of the Nagle Dam Formation, found immediately adjacent to the Mgeni batholith, and the marginal phase of the Ximba Suite (Figure 4.2a). Comparison of the average major element concentrations of the biotite hornblende gneiss and the marginal phase of the Mgeni batholith reveal distinct differences in CaO, MnO, MgO, K_2O and P_2O_5 concentrations, while the granite is relatively enriched in Zr, Pb and Ba. Field mapping supports the contention that at least a portion of Milne's high Zr member of the Nagle Dam Formation, including the biotite hornblende gneiss of Kuyper (1979), may represent a finer grained, foliated marginal segment of the Mgeni batholith, or veins of the granite in the Nagle Dam Formation.

Kuyper (1979) correlated the gneisses of the Nagle Dam Formation with the enclaves of the Valley Trust Formation. Similarly, Kerr and Milne (1991b) proposed, on limited geochemical data, a possible relationship between the amphibolites of the Nagle Dam Formation and the Valley Trust Formation. Bulley (1981), however, considered only those enclaves adjacent to the margin of the Mgeni batholith (c.200m from the margin) to have been derived from the Nagle Dam Formation. Other enclaves found within the batholith he believed to be restite material.

The gross chemical characteristics of these two units do not support the proposed correlation, and in particular is the unimodal silica distribution pattern found in the Nagle Dam Formation relative to the bimodal pattern of the Valley Trust Formation. Similarly, analysis of the individual members of the Nagle Dam and Valley Trust Formations reveal distinct chemical differences, particularly marked for K_2O, MnO, TiO_2, P_2O_5, Cr and Ni (Figure 4.2b) in the amphibolites, which does not support the correlation of Kerr and Milne (1991b), and Al_2O_3, TiO_2, MnO, CaO, Na_2O, P_2O_5, Zr, Sr and Ba for the quartzo-feldspathic gneisses.

4.3.4 CHEMICAL CHARACTERISATION

The Nagle Dam Formation displays a range in silica concentrations from 47 - 78 percent SiO_2. Minor gaps exist within this sequence, for example between 55.5 and 60.5 percent SiO_2, but this is considered to represent a sampling phenomenon. The Harker diagrams display simple trends over the entire sequence (Figure 4.3), with the concentration of the majority of the elements - TiO_2, Al_2O_3, FeO, MgO, MnO, CaO, P_2O_5, Zr, Zn, Ni, Y and Cr - declining with increasing silica, while that of K_2O, Rb, Ba and Pb rises. The concentrations of Na_2O, Sr and Nb remain constant with silica variation. Calculation of the correlation coefficient for the entire available range of silica values (Appendix 4) reveals significant correlation at the one percent level between silica and TiO_2, FeO_{TOT}, MgO and CaO. The correlation between silica and Al_2O_3, K_2O and P_2O_5 is less well defined, while Na_2O possesses almost no correlation with silica. The majority of the trace elements display a moderate degree of correlation with silica.

These trends are broadly analogous with those of the typical calc-alkaline analyses of Gribble (1969), although the lack of continuation between the amphibolite and the biotite hornblende gneiss limits this comparison. Some variation is found, however, and in particular is the decline in Zr and Y concentrations with increasing silica. Nb concentrations are typically low, while their trend does not display the enrichment at high silica levels found by Gribble.

4.3.5 INTRAFORMATIONAL CORRELATION

Variable chemical characteristics distinguish the individual members of the Nagle Dam Formation (Figure 4.3) and in particular the amphibolite may plot as a separate grouping.

The amphibolite and the biotite hornblende gneiss are distinguished by distinct MgO concentrations precluding their derivation from a common magma through fractionation (Figure 4.3), while the quartzo-feldspathic and biotite hornblende gneisses display markedly different alkali concentrations (Figure 4.2c). The main series of the Nagle Dam Formation therefore appears to consist of a number of sequences, not related through a simple fractionation model. These are distinguished on the

Figure 4.2. Correlation diagrams, Nagle Dam Formation.

a) MgO-Zr discrimination of the marginal granite - Ximba Suite and the Nagle Dam Formation.

b) Ni-TiO_2 discrimination of the Nagle Dam and Valley Trust Formation amphibolites.

c) $Na_2O+K_2O-Al_2O_3$ discrimination of the quartzo-feldspathic and biotite hornblende gneisses of the Nagle Dam Formation.

d) Zr/Y-Zr immobile trace element correlation plot for the Nagle Dam Formation.

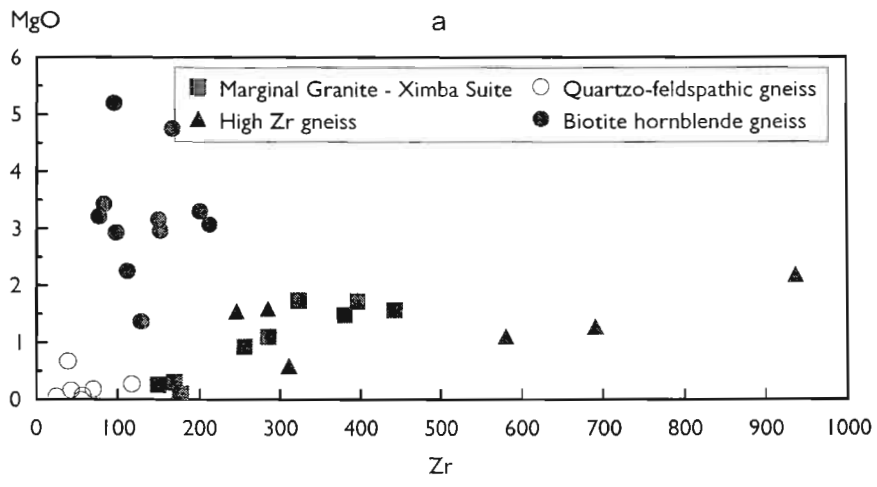

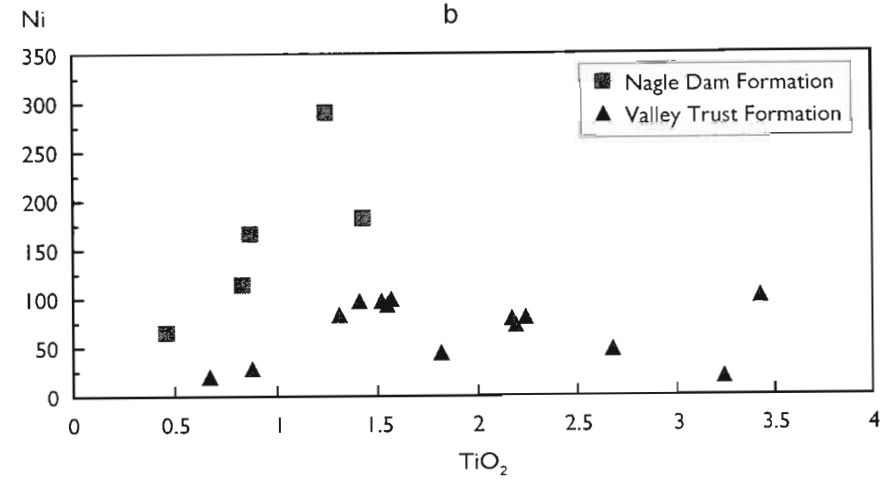

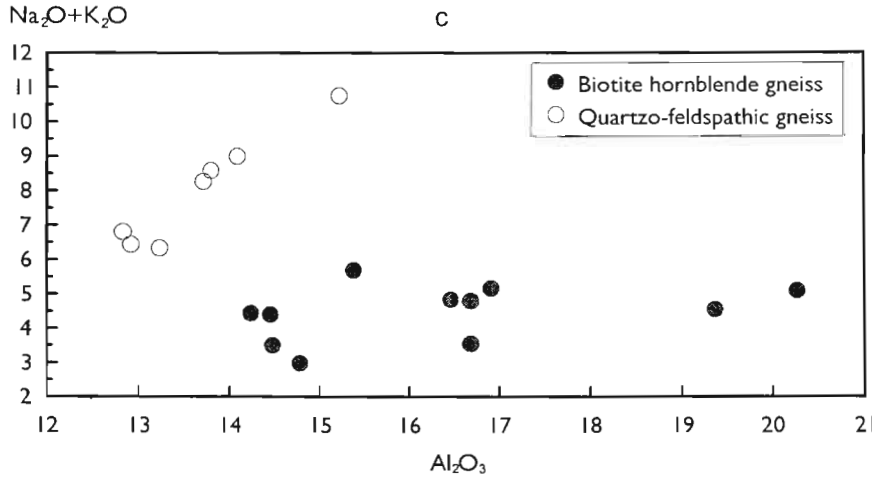

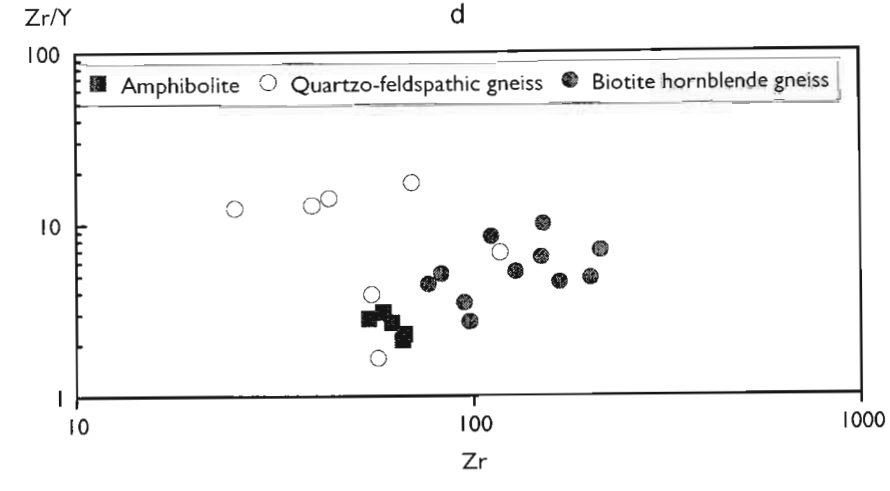

Figure 4.3. Element-silica variation diagrams, Nagle Dam Formation.
a) Major elements.
Potential fractionation trends are displayed on the Al_2O_3-SiO_2 plot. Fields on the MgO-SiO_2 plot after Smith *et al.* (1997).

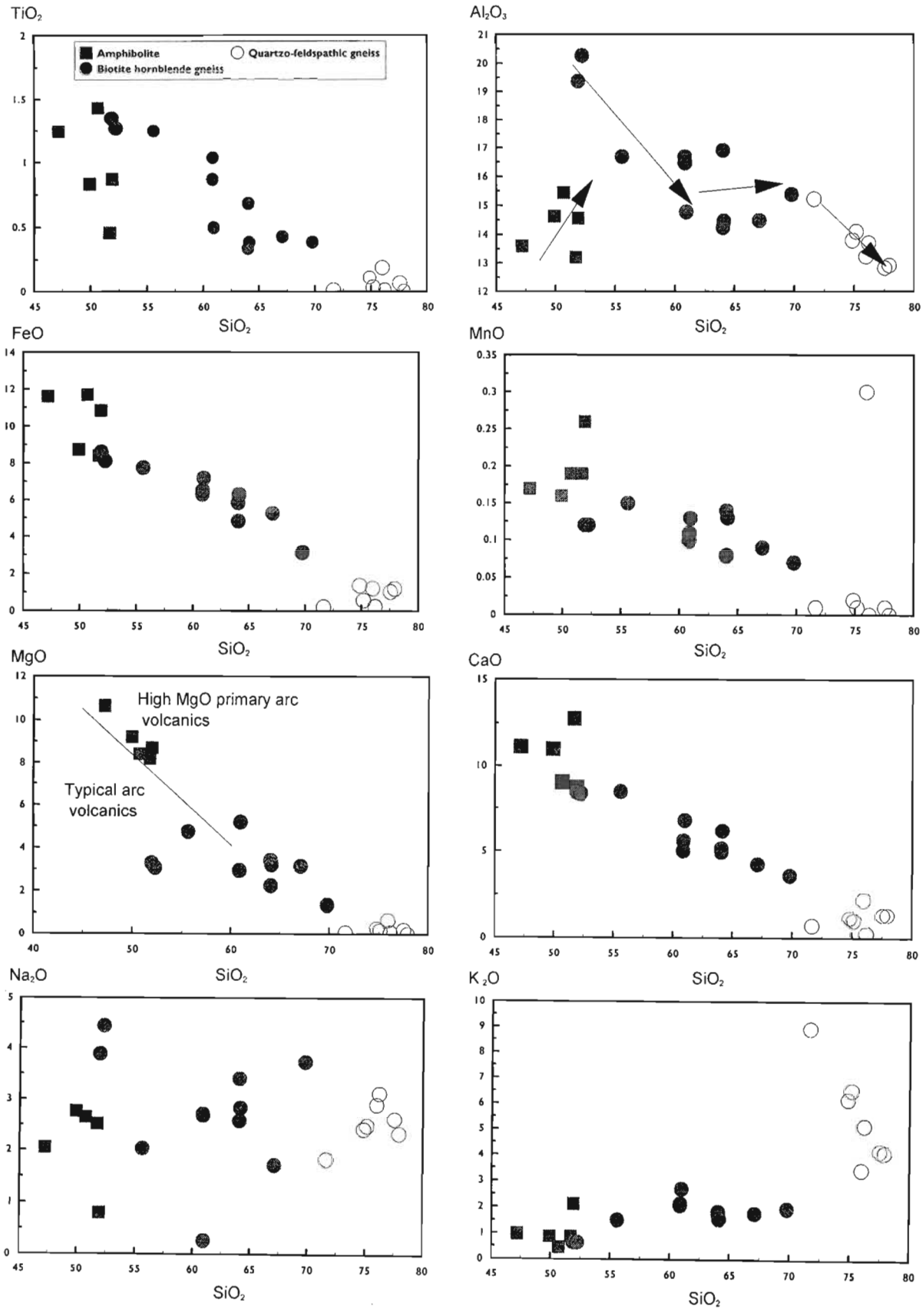

b) Trace elements.
(Quartzo-feldspathic gneiss analyses below 1 ppm not shown).

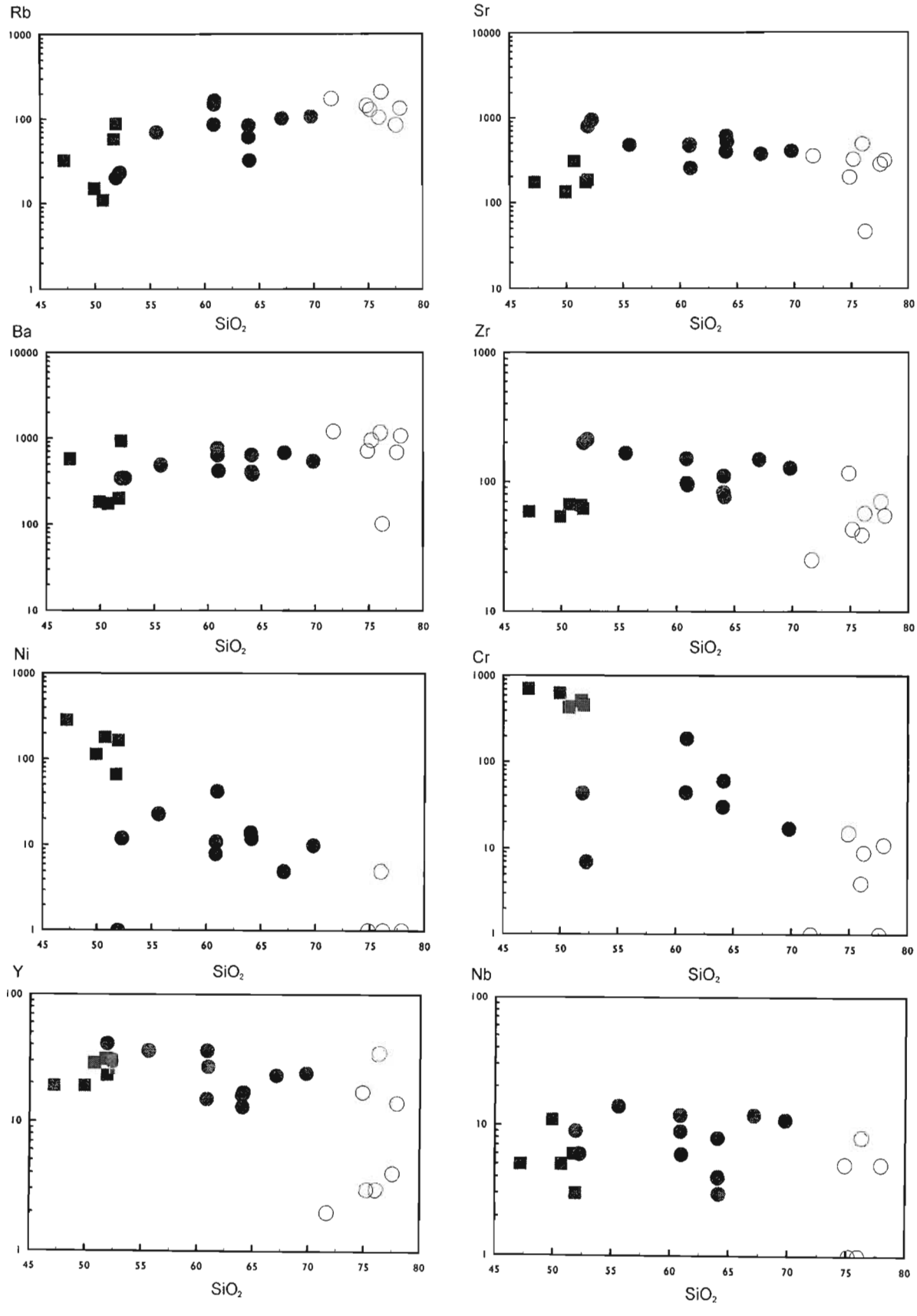

Al_2O_3-SiO_2 diagram (Figure 4.3).

Although the range of elemental abundances observed within the biotite hornblende gneiss is comparable with a typical arc batholith (Pitcher *et al.* 1985), the most basic samples exhibit distinct Al_2O_3 and Na_2O enrichment and MgO depletion relative to the other members of the series. Analysis of the trace element fractionation trends suggest the existence of two separate groups with distinct fractionation vectors, one originating with the low silica sample UND 317 and comprising the mafic portion of the gneiss, with silica concentrations less than 61 percent, the other originating with the group of samples with 64 percent silica, and including all the more siliceous gneiss. This precludes a simple fractionation process generating the biotite hornblende gneiss as a single unit.

Potentially immobile trace element data (Cann 1970; Hart *et al.* 1974; Winchester and Floyd 1976; Weaver and Tarney 1981 but not Kuznetsov 1971; Smith and Smith 1976; Hynes 1980), suggest a distinct quartzo-feldspathic unit (Sevigny and Brown 1989; Crow and Condie 1990; Winchester *et al.* 1995; 1998) distinguished by a markedly higher Zr/Y ratio than the majority of the Nagle Dam Formation (Figure 4.2d). The remainder of the succession displays a relatively narrow range of Zr/Y ratios, comparable to that developed within a fractionating calc-alkaline pluton (Janser 1994) or batholith (Pitcher *et al.* 1985), suggesting that the majority of the Nagle Dam Formation may represent the product of a evolving magma series. Possible groupings may, however, exist evolving from Zr/Y ratios of c.3 and c.5 (Figure 4.2d) for the biotite hornblende gneiss.

These correspond with the series identified by their variable trace element content, with the lower silica series possessing a higher Zr content at a lower Zr/Y ratio than the higher silica group, although the range of Zr/Y is comparable between the series (Figure 4.2d). One sample, UND 52, does not plot with either of these groupings, possibly indicating an additional series within the Nagle Dam Formation. This sample has therefore not been included in the petrogenetic modelling of the Nagle Dam Formation (Section 6.2.3).

4.3.6 NOMENCLATURE AND CLASSIFICATION

None of the lithologies comprising the Nagle Dam Formation possess any relict mineralogy or textures which may be used to identify the original lithology. Nomenclature and classification must therefore be based on the chemical characteristics of these rocks.

On the total alkali versus silica (TAS) diagram the Nagle Dam Formation plots across a spectrum of fields, from basalt (amphibolite) to rhyolite (quartzo-feldspathic gneiss) (Figure 4.4a). It is predominately subalkalic with medium to high K_2O concentrations, a moderate FeO/FeO+MgO ratio (Figure 4.4b) and a calc-alkaline trend of initial moderate iron enrichment, followed by a marked increase in total alkalis with MgO and FeO depletion on the AFM diagram. A best fit line through the entire sequence indicates a Peacock Index of 61.5, within the calcic field (Figure 4.4c). The quartzo-feldspathic gneiss does not, however, plot with the other members of the Nagle Dam Formation on this diagram. If it is therefore excluded then a best fit line indicates a Peacock Index of 66 (calcic), although actual CaO = Na_2O+K_2O intersection occurs at 64 percent SiO_2. The Nagle Dam Formation is classified as metaluminous on the A-B diagram of Debon and Le Fort (1982), with extension into the peraluminous field at high silica levels. The trend of these analyses on this diagram is comparable to that of the calc-alkaline series.

The amphibolite is metaluminous, with normative analyses indicating that it is a tholeiitic basalt with minor olivine or quartz in its norm. Individual samples may, however, have abundant olivine in their norm and in one case nepheline. The biotite hornblende gneiss may be either peraluminous or metaluminous. The quartzo-feldspathic gneiss displays a highly variable range of alumina saturation, with individual samples possessing peraluminous, metaluminous and peralkaline characteristics. All contain minor amounts of corundum in their norm.

The low HFS element content of the biotite hornblende and quartzo-feldspathic gneisses separate them from the A-type granites (Whalen *et al.* 1987). The relatively high Na_2O, CaO and Sr but low K_2O and Ni content of the biotite hornblende gneiss rather suggest a similarity to the I-type granites of Chappell and White (1974) (Figure 4.4d), although Cr is high and several samples are peraluminous. The high K_2O concentration of the quartzo-feldspathic gneiss approximates that of the S-type granites (Figure 4.4d), although only occasional samples are peraluminous, suggesting comparison with the I-type granites. The low concentrations of all the

Figure 4.4. Nomenclature plots - Nagle Dam Formation.

a) TAS plot (Le Maitre 1989).

b) SiO_2-FeO/FeO+MgO (after Miyashiro 1974).

c) Log(CaO/Na_2O+K_2O)-SiO_2 (Brown 1982).

d) Na_2O-K_2O (after White and Chappell 1983). Lower silica gneiss and amphibolite excluded from plot.

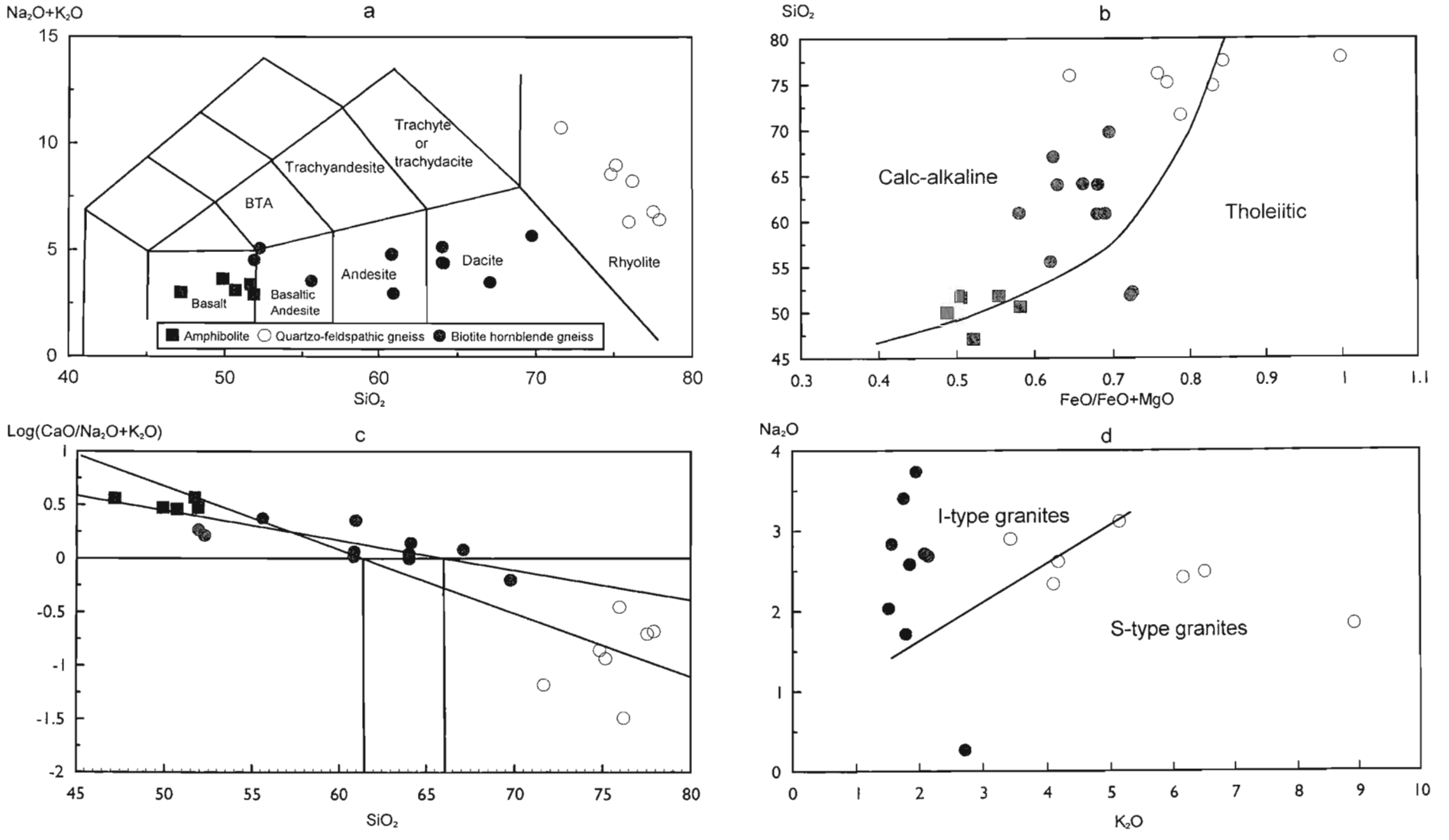

major elements, with the exception of SiO_2 and K_2O, is analogous to the minimum melt granite of White and Chappell (1977).

4.4 VALLEY TRUST FORMATION

4.4.1 INTRODUCTION

Eleven samples of the Valley Trust Formation were previously analysed, six from the amphibolite (Du Toit 1979) and five from the quartzo-feldspathic gneiss (Kuyper 1979, Du Toit 1979). In addition, Bulley (unpubl. report) collected one sample of the quartzo-feldspathic gneiss for analysis. During the present study an additional 63 samples were collected, primarily from the pelitic gneiss (Appendix 3).

4.4.2 NATURE OF THE PROTOLITH

Mineralogical characteristics of the various lithologies and limited chemical data from the amphibolite led Kuyper (1979) and Du Toit (1979) to suggest that the Valley Trust Formation represented a mixed volcanosedimentary succession, comprising the metasedimentary pelitic gneiss and fine grained granulite and the orthoamphibolites. The quartzo-feldspathic gneiss was considered to form a portion of the Mgeni batholith and its potential protolith derivation was therefore not investigated, although Bulley (1981) concluded that it constituted a series of metasedimentary enclaves within the granites.

The model of Kuyper (1979) and Du Toit (1979) for the amphibolite and pelitic gneiss is supported by the additional geochemical data, with the amphibolite exhibiting igneous characteristics, while the pelitic gneiss plots predominately within the pelite or sedimentary fields on a variety of diagrams (Figure 4.1a,b) including those of Bard and Moine (1979) and Winchester and Max (1984).

The available geochemical evidence suggests that the quartzo-feldspathic gneiss possesses predominately igneous characteristics. For example on the si-mg diagram of Leake and Singh (1986), the gneiss parallels the trend of igneous rocks (Figure 4.1d), plotting well below the field of river sands. Bulley (1981) suggested that their high silica content precluded an igneous origin, but igneous rocks with silica contents of c.80 percent have been reported in the literature (for example Bickford *et al.* 1981; Tarney *et al.* 1982; Wybron *et al.* 1987). In addition, the megacrystic feldspars found in certain of the samples occasionally display concentrically arranged inclusions, a structure believed to be indicative of an igneous origin (Vernon 1986). Relict feldspar phenocrysts have been previously described from high grade quartzo-feldspathic gneisses (Pepper and Ashley 1998).

The fine grained granulite displays a mixture of igneous and sedimentary characteristics on the various chemical protolith discrimination diagrams, with mg contents in excess of the typical pelite (Figure 4.1a,b), although al-alk and c variations parallel the sedimentary trend (Figure 4.1c), suggesting an origin as a mixture of clay minerals and quartz. Both the pelitic gneiss and the fine grained granulite possess low Ni contents, which tends to result in their plotting in the field of igneous rocks on the Ni-TiO_2 diagram of van de Kamp (1969) and Winchester and Max (1984), although shales with low Ni contents have been reported in the literature (Vine and Tourtelot 1970) and where the fine grained granulite contains an appreciable Ni content, it plots in or adjacent to the sedimentary fields on the various diagrams. The accumulated chemical and mineralogical evidence suggest that this sequence had a sedimentary protolith.

The relict igneous mineralogy and textures of the incompletely metamorphosed portion of the fine grained amphibolitic granulite indicate their igneous derivation. This is supported by the limited available chemical data (Figure 4.1).

4.4.3 CORRELATION

a) Orthogneisses

Immobile trace element variations suggest the possible existence of three dissimilar groups within the quartzo-feldspathic gneiss (Figure 4.5a). These are further discriminated by distinct Rb/Sr, K/Rb and Na_2O/K_2O ratios. Of these, however, one sample identified by Kuyper (1979) as a quartzo-feldspathic gneiss displays an extreme Zr/Y ratio and possesses igneous type garnets suggesting that it may be a late intrusion. It is therefore not correlated with the quartzo-feldspathic gneiss, and is not considered further here. The different Zr/Y ratios of the amphibolite and the quartzo-feldspathic gneiss (Figure 4.5a), and the lack of Zr enrichment in the acidic gneiss suggest that they are not related through simple fractionation processes (Garland *et al.* 1995).

Mineralogical variability within the amphibolites of the Valley Trust Formation suggests the existence

Figure 4.5. Correlation diagrams, Valley Trust Formation.

a) Zr/Y-Zr immobile trace element diagram.

b) Zr/Y-Zr/Nb immobile trace element ratio diagram for the amphibolite of the Valley Trust Formation.

c) Y-P_2O_5 sedimentary discriminant diagram.

d) R1-R2 diagram (de la Roche *et al.* 1980) for the paragneisses.

R1 = 4Si - 11(Na+K) 1 2(Fe+Ti).

R2 = 6Ca + 2Mg + Al.

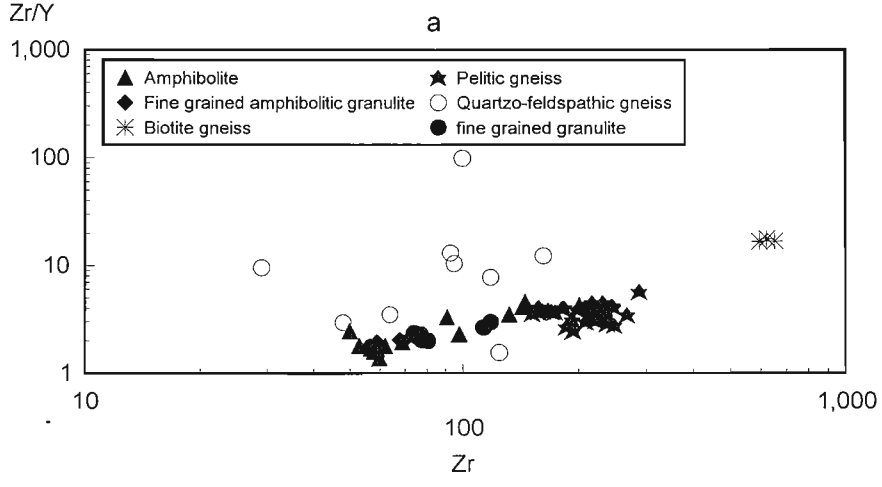

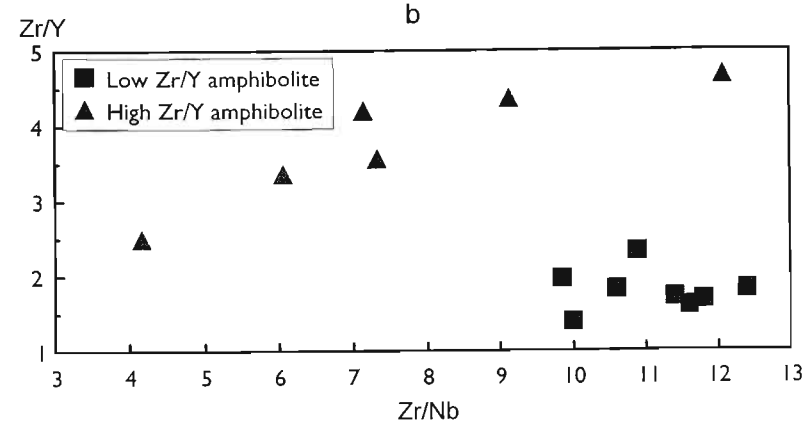

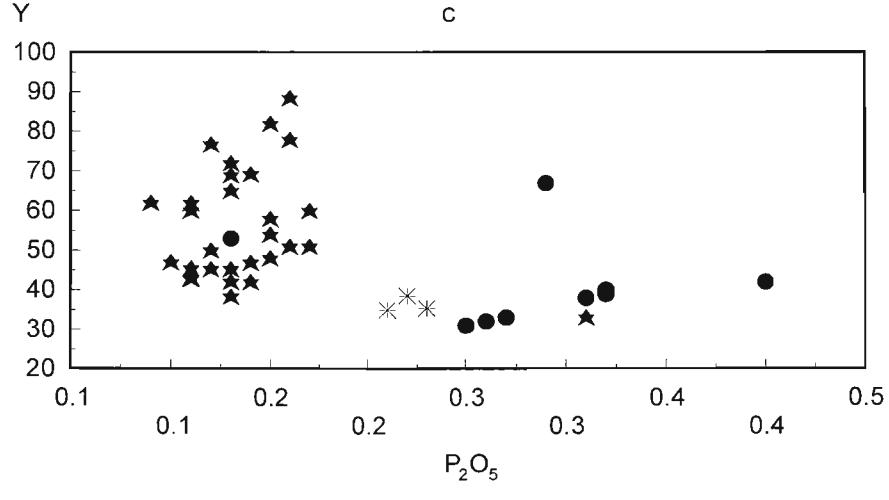

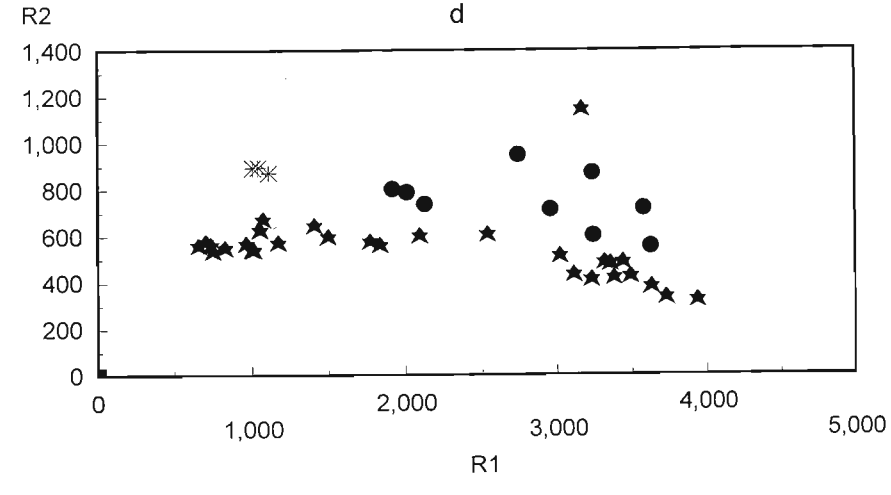

of several distinct subgroups within the association. This is supported by variations in the Cr/Ni and MgO/TiO_2 content of the fine grained amphibolitic granulite and medium grained amphibolite. The former consequently appears to represent a distinct unit, not related to the medium grained amphibolite. Variation in Zr/Y-Zr/Nb (Figure 4.5b) similarly suggests that the medium grained amphibolite may also comprise distinct series.

b) Paragneisses

Two paragneiss sequences are found within the Valley Trust Formation: the pelitic gneiss and the fine grained granulite. These were discriminated initially on variations in grain size, but this is confirmed by their distinct chemical characteristics as displayed on the Harker diagrams (Figure 4.6) and immobile trace element variation diagrams (Figure 4.5a). They are further distinguished within the chemical parameters utilised by Lambert *et al.* (1981) to identify sedimentary sequences (Figure 4.5c) and the de la Roche *et al.* (1980) diagram (Figure 4.5d).

The pelitic gneiss displays well developed fractionation trends (Figure 4.5, 4.6) suggesting that it forms a related sequence. An exception to this is the chemically distinct biotite gneiss. These differences may, however, be related to the processes involved in its development (Section 6.3.5) rather than a distinct protolith.

The more siliceous pelitic gneiss possesses silica concentrations comparable with the quartzo-feldspathic gneiss. These are distinguished, however, both mineralogically, by the presence of sillimanite in the more felsic component of the pelitic gneiss, and chemically through their distinct Zr/Y-Zr characteristics (Figure 4.5a). In addition, the higher alkali content of the quartzo-feldspathic gneiss and its lower FeO_{TOT}, MgO, Zr, Zn and Y levels are distinctive.

The fine grained granulite forms a highly heterogeneous sequence, correlated initially on its textural similarity, and in particular fine grain size. Some intragroup chemical variability is noted on the Harker diagrams (Figure 4.6) but its coherent Zr/Y-Zr fractionation trend (Figure 4.5a), suggests that it originated from a distinct initial lithology. Given its highly variable mineralogy and fine lithological banding, chemical variability may be a sampling phenomena.

4.4.4 CHEMICAL CHARACTERISATION

a) Amphibolite

The amphibolite is basic in composition, with silica concentrations varying from 45-54 percent. On Harker diagrams it plots within well constrained fields (Figure 4.6), but with occasional anomalous analyses on individual diagrams. Calculation of the correlation coefficient (Appendix 4) demonstrates significant correlation at the five percent level between silica and all the major elements, with the exception of Na_2O and CaO, but is less well defined with the trace elements. With increasing silica TiO_2, FeO, MnO, MgO, CaO, Ni, Cr, Zr, Y and Nb decline in concentration, while Al_2O_3, Na_2O, K_2O, P_2O_5, Ba, Rb, Sr and Pb contents increase. Comparable trends are found if MgO is used as the index of fractionation, although individual elements, such as TiO_2 and FeO may display considerable scatter.

b) Quartzo-feldspathic Gneiss

The quartzo-feldspathic gneiss is highly silicic, with silica concentrations of 72 - 81 percent. It plots within well constrained fields, occasionally with minor scatter, and typically with discernible trends on the Harker diagrams (Figure 4.6). With increasing silica, all the major and trace elements, with the exception of Pb and Y, decline in concentration. Calculation of the correlation coefficient (Appendix 4) demonstrates significant correlation at the five percent level between silica and Al_2O_3 but the correlation with the majority of the major elements is poorly defined. Correlation with the trace elements is more pronounced, and especially Sr and Ba.

c) Pelitic Gneiss

The pelitic gneiss is highly heterogeneous with a range of silica concentrations from 56-79 percent, but, with the exclusion of a distinct subgroup - the biotite gneiss - plots within well defined fields on the Harker diagrams. The majority of elements display a distinct negative correlation with silica (Figure 4.6). Individual elements, and in particular K_2O, Na_2O and Y may, however, display extreme variability, inhibiting the identification of simple trends, while P_2O_5, Sr and Zr increase in concentration with increasing silica. Calculation of the correlation coefficient for the entire available range of silica values (Appendix 4) demonstrates significant correlation at the one percent level between silica and the major elements, with the exception of TiO_2, MnO, CaO and P_2O_5 (which

Figure 4.6. Element-silica variation diagrams, Valley Trust Formation.
a) Major elements.

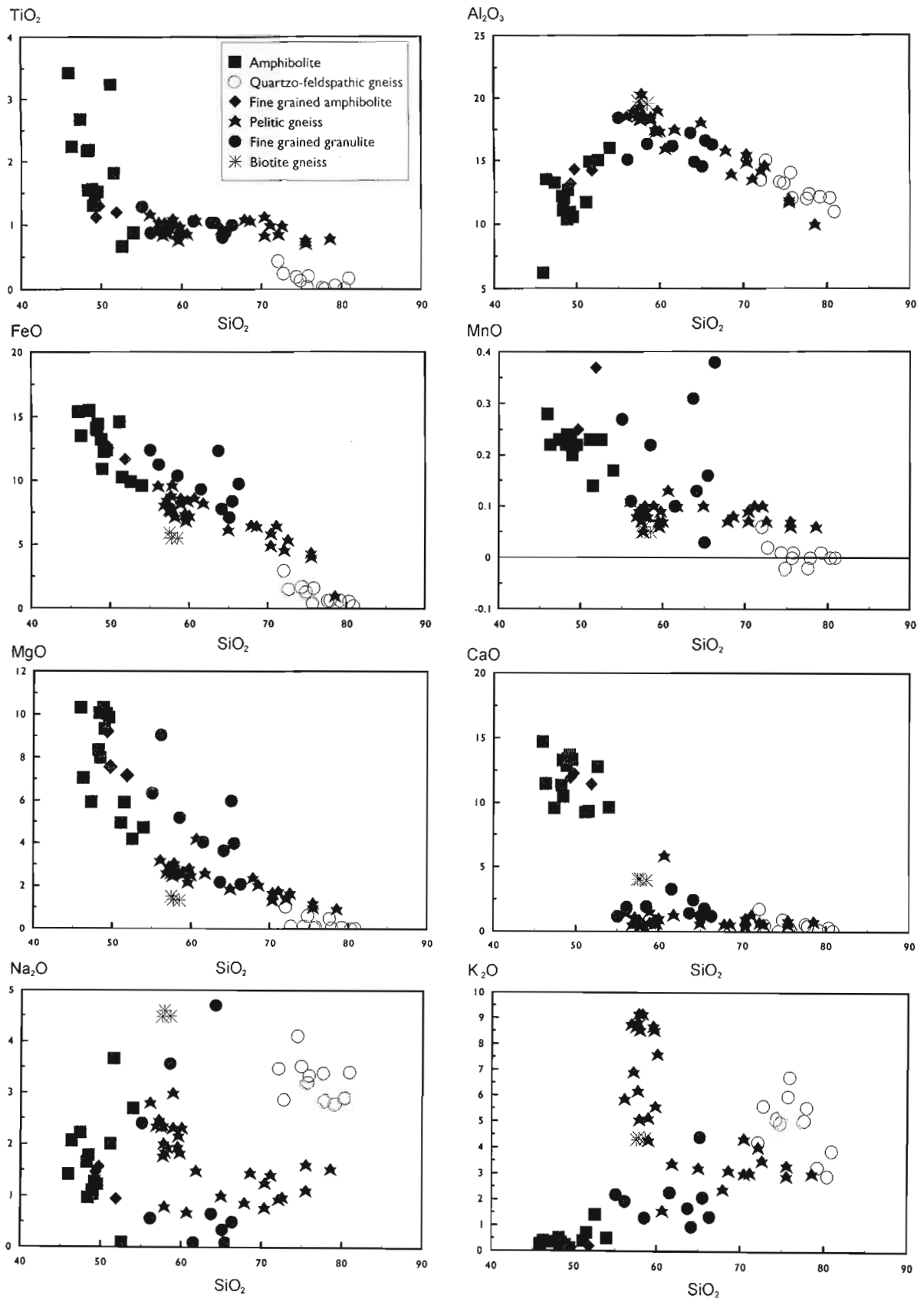

b) Trace elements.

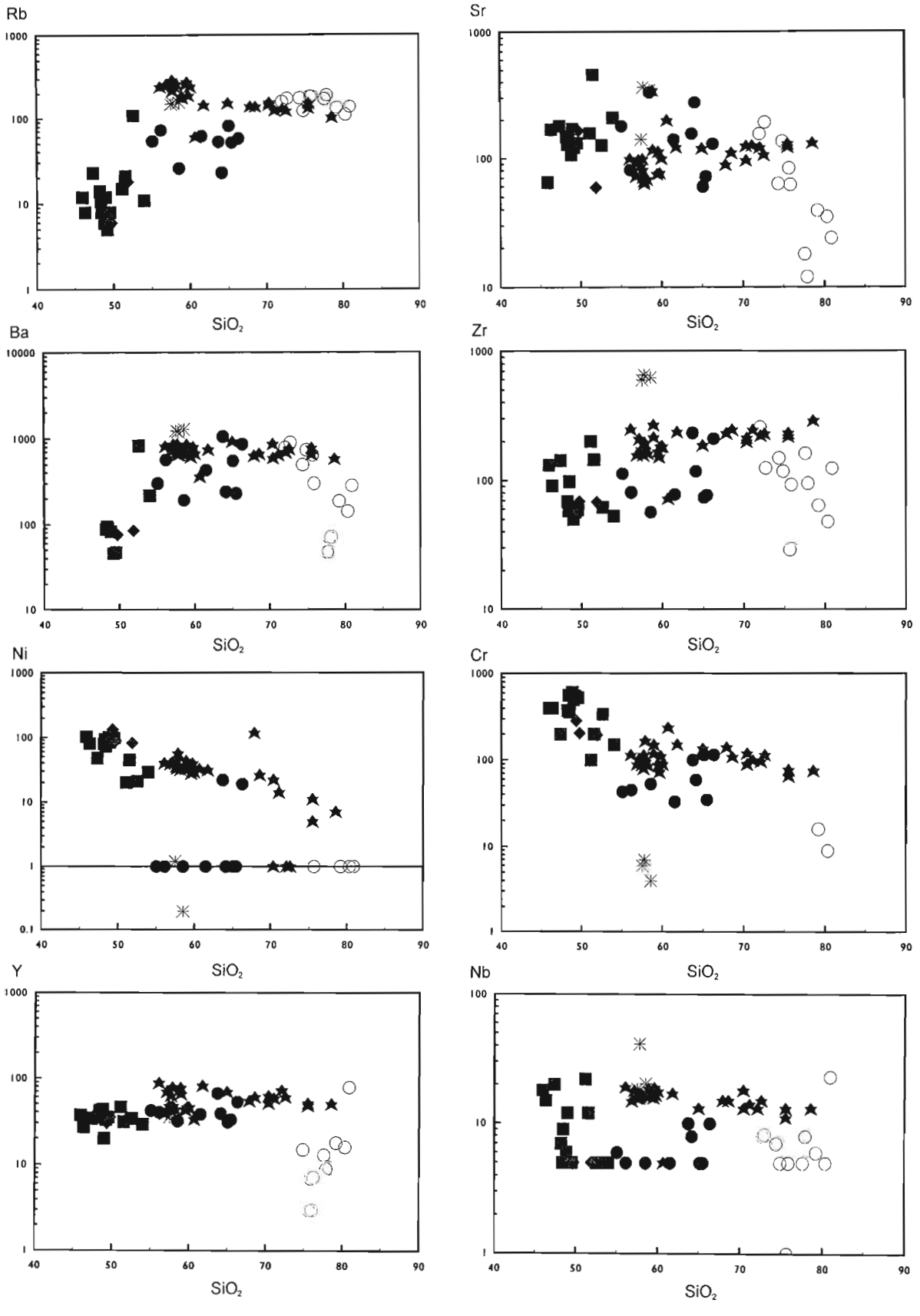

possess almost no correlation with silica). This correlation is particularly marked for Al_2O_3 and FeO_{TOT}. Correlation with the trace elements is poorly defined.

The majority of the samples were collected from a single large pelitic enclave, with the available data revealing marked chemical differences between individual sample sites (Appendix 3). Most notable is the high K_2O content of the samples collected from the core of the enclave, and their low Al_2O_3, FeO_{TOT}, Zr, Ba and Cr concentrations relative to those samples collected from the margin of the enclave. Relative to the pelite samples collected away from this site, the samples from the large enclave possess higher K_2O and Y and lower FeO concentrations.

d) Fine Grained Granulite

The majority of the fine grained granulite samples collected are from the heterogeneous sillimanite $\pm$ orthopyroxene bearing variety, with the available data frequently exhibiting considerable scatter on the Harker diagrams (Figure 4.6). Calculation of the correlation coefficient for the pelitic fine grained granulite (Appendix 4) reveals little significant correlation between silica and the major elements, with the exception of MgO, but correlation with the trace elements is more pronounced. This hinders the identification of any trends on these diagrams. General tendencies, however, suggest declining Al_2O_3, TiO_2, FeO, MgO, P_2O_5 and Zn concentrations with increasing silica, while CaO, Pb, Ba, Zr, Cr, Y and Nb levels rise.

Three samples of the fine grained amphibolite are available. The limited number of samples collected and their narrow range of SiO_2 (49-52%) and MgO (7-9%) concentrations restricts any possible interpretation of elemental variation trends (Figure 4.6).

4.4.5 NOMENCLATURE AND CLASSIFICATION

a) Amphibolite

All the amphibolites plot across the basalt/basaltic andesite (gabbro or quartz gabbro) fields on the majority of the nomenclature diagrams (Figure 4.7a), although the ophitic or subophitic texture of the fine grained amphibolitic granulite suggests that it was originally a dolerite. On the diagrams of Winchester and Floyd (1977) they extend into the basalt and andesite fields.

Although their alumina : alkali ratio is variable, all the amphibolites are metaluminous. Their very low alkali contents (Figure 4.7a) and low Zr/TiO_2 and Nb/Y ratios (Winchester and Floyd 1977) indicate their subalkalic nature. The normative mineralogy demonstrates that the majority of the samples are tholeiitic, either slightly olivine normative, or quartz normative (Yoder and Tilley 1962).

On the AFM diagram the amphibolites display a distinct iron enrichment trend, within the tholeiitic field. They also plot in the tholeiitic field on the SiO_2-FeO/FeO + MgO diagram (Figure 4.7b) and the Jensen diagram, but with overlap into the komatiitic field on this latter. With the quartzo-feldspathic gneiss the complete series has a Peacock Index of c.60.

b) Quartzo-feldspathic Gneiss

The quartzo-feldspathic gneiss plots within the rhyolite or granite fields on the various nomenclature diagrams (Figure 4.7a), with extension into the comendite or pantellerite and trachyandesite fields on the Zr/TiO_2-Nb/Y diagram of Winchester and Floyd (1977). On the K_2O-Na_2O diagram of O'Connor (1965) it extends across the granite and adamellite fields.

The alumina : alkali ratio of the quartzo-feldspathic gneiss is highly variable. Samples with moderate silica levels are peralkaline or metaluminous, rarely peraluminous, while those with silica >79 percent are typically markedly peraluminous. Its variable alkali content and low Zr/TiO_2 and Nb/Y ratios indicate subalkalic characteristics, but occasional analyses may plot in the alkalic field. The majority of the samples contain normative corundum.

Its variable FeO/FeO + MgO values, 0.56 - 0.94, extend across the tholeiite and calc-alkaline boundary (Figure 4.7b). Typically, however, the majority of the analyses display tholeiitic characteristics. On the AFM diagram it plots close to the total alkali corner and no trend can be identified.

The low HFS element content of the gneiss distinguishes it from the A-type granites (Whalen *et al.* 1987), with its relatively high Na_2O, but low CaO and FeO contents and metaluminous character a feature of the I-type granites of Chappell and White (1974). Corundum is, however, present in its norm, while its variable K_2O content results in several samples plotting as S-type granites on the Na_2O-K_2O diagram (Figure 4.7d) of White and

Figure 4.7. Nomenclature diagrams - Valley Trust Formation.

a) TAS diagram (Le Maitre 1989) for orthogneisses.

b) SiO_2-FeO/FeO+MgO (after Miyashiro 1974) for orthogneisses.

c) SiO_2/Al_2O_3-K_2O/Na_2O sedimentary nomenclature diagram (Wimmenauer 1984).

d) Na_2O-K_2O (after White and Chappell 1983) for the quartzo-feldspathic gneiss and garnet granite.

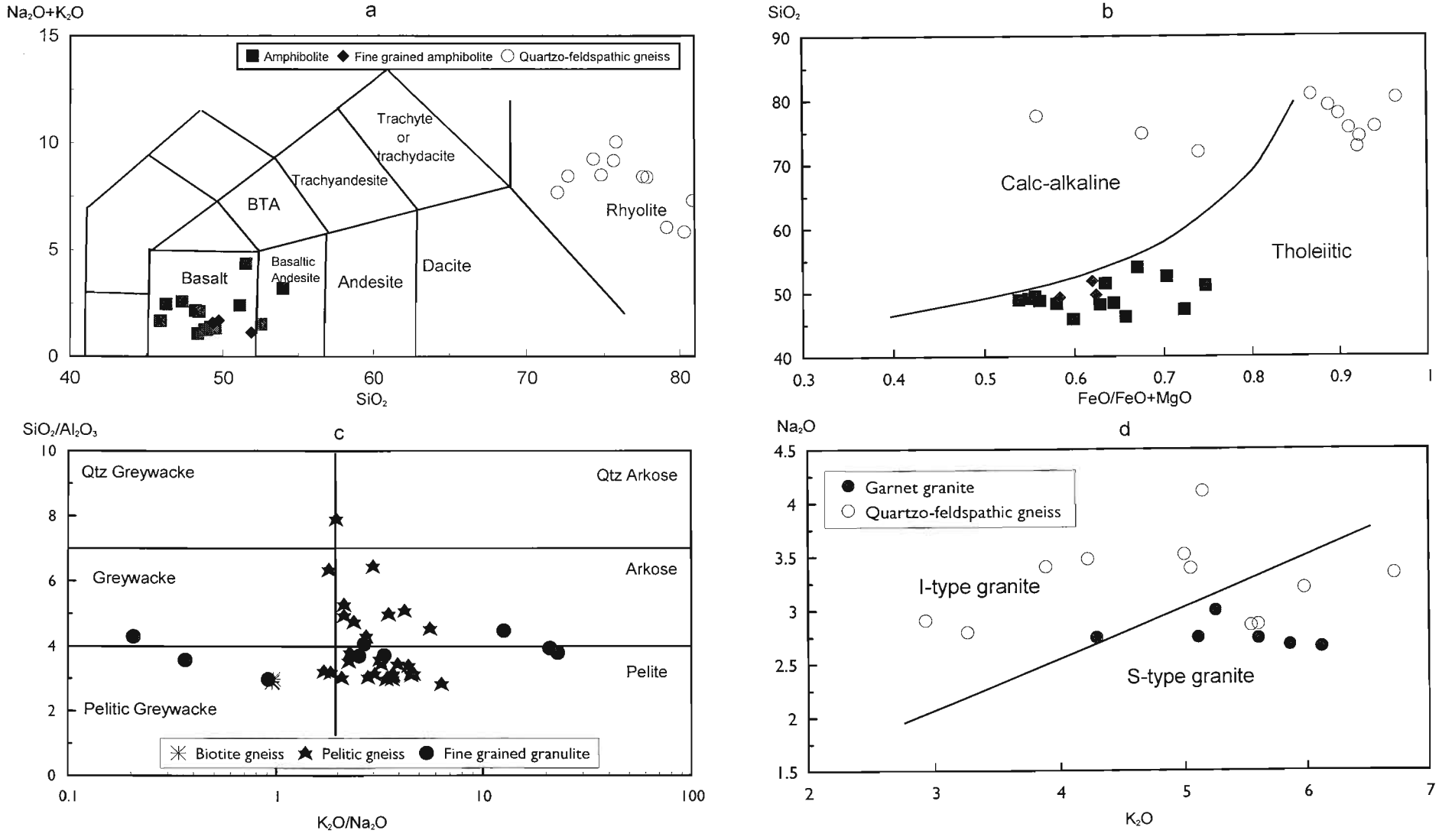

Chappell (1983). The high silica content of the quartzo-feldspathic gneiss and its gross elemental concentrations are comparable with the minimum melts of White and Chappell (1977).

c) Pelitic Gneiss

The sedimentary chemical classification system of Wimmenauer (1984, in Muller 1989) serves to subdivide the pelitic gneiss into a pelitic and psammitic (arkosic or quartz arkose) component, with the separation occurring at approximately 65 percent SiO_2 (Figure 4.7c). Further discrimination of the latter samples is possible with the Na_2O/K_2O-SiO_2/Al_2O_3 (Pettijohn *et al.* 1987) and Na_2O-Fe_2O_{3TOT}+MgO-K_2O (Winchester and Max 1989) classification diagrams for lithic sediments, which classify the relevant analyses as lithic arenite and arkose.

Relative to the average upper continental crust of Wedepohl (1995) the average pelitic gneiss possesses normal to slightly enriched (x2) elemental abundances, but with marked depletion in Nb and Sr. The relatively enriched LILE content of the pelitic gneiss contrasts with that of other metasedimentary granulites, such as those in the Bamble sector, southern Norway (Knudsen *et al.* 1997), although the pattern of enrichment or depletion observed for other elements is comparable, including depletion in Nb and Sr and enrichment in elements such as V and Cr. Low Sr is not, however, a characteristic of the proposed source material for the pelitic gneiss (Section 6.3.5), as Knudsen *et al.* suggested for the Bamble metasediments. Rather this may indicate a sedimentary leaching event, which possibly resulted in the relatively low levels of the other potential leachates, CaO and Na_2O (Harnois 1988), in the pelitic gneiss.

The average pelite displays the chemical characteristics of a Proterozoic shale (Taylor and McLennan 1985). Similarly, on the SiO_2/Al_2O_3-K_2O/Na_2O (Wronkiewicz and Condie 1987) and Cr-Ni (Taylor and McLennan 1985) diagrams it plots in the field of post-Archaean shales. This suggests a minimal Archaean input during its deposition. Rather a local source, within the Natal Province, is favoured, similar to the model of Eglington *et al.* (1989b).

The associated garnetiferous partial melt is peraluminous plotting in the S-type granite field on the Na_2O-K_2O diagram (Figure 4.7d) of White and Chappell (1983). Its high HFS element content, however, is comparable to the A-type granites (Whalen *et al.* 1987), with a high FeO/MgO ratio suggesting a tholeiitic character.

Evidence for partial melting of the pelitic gneiss with the production of a garnetiferous granite phase (Section 2.2.2b), demonstrates potential large scale element mobility within this lithology. Complete removal of this melt phase has not, however, typically occurred, and the garnet granite is found as fine segregations in the pelitic gneiss. As such elemental mobility is not to be expected (Greenfield *et al.* 1996). Some removal of melt is evidenced by the presence of a marginal rim of highly garnetiferous granite adjacent to individual pelitic enclaves, but the lack of a chemically distinct restitic phase and no evidence for K/Rb decoupling, with K/Rb ratios (pelitic gneiss 143-292, biotite gneiss 230-238) approximating average crustal levels (Taylor and McLennan 1985) and the undepleted samples of Tarney *et al.* (1972), suggest that the degree of elemental mobility in these gneisses is minor or localised. In addition large, 50kg, samples of the pelitic gneiss were collected for analysis so as to minimise the potential effect of localised melt migration and concentration.

d) Fine Grained Granulite

The fine grained granulite plots across a variety of fields on the sedimentary chemical classification scheme of Wimmenauer (1984), including the pelite, arkose, greywacke and pelitic greywacke fields (Figure 4.7c). The psammitic portion of this series is highly variable in composition, and on the various diagrams for lithic sediments, plot across the greywacke, lithic arenite and arkose fields.

4.5 THE MGENI BATHOLITH

4.5.1 INTRODUCTION

Eighty nine samples from the various granites of the Mgeni batholith were analysed for major and trace elements (3 duplicated), with individual samples selected for REE analysis (Appendix 3). Thirty three of these were reported by Kuyper (1979) and Du Toit (1979), and a further 8 were collected by Bulley (unpubl. chemical data). The remaining 48 samples were collected during the course of the present study.

4.5.2 CORRELATION

Kuyper (1979) believed that all the megacrystic granites of the Mgeni batholith were related through fractionation processes, with subsequent

metamorphic overprint, while the Nqwadolo Suite was considered to represent a possible partial melt of the megacrystic granites. This scheme was revised by Kerr (1985) who identified four granite suites on the basis of the available field, chemical and isotopic data. This was subsequently modified by Kerr and Milne (1994) who recognised three granitic families:

1) the biotite granites of the Ximba Suite;
2) the hornblende granites of the Mlahlanja Suite; and
3) the late leucogranite of the Nqwadolo Suite.

These correspond broadly with Suites II, I and III of Kerr (1985), respectively, but with the marginal granite of Kerr included with the Ximba Suite rather than the Mlahlanja Suite. Kerr's Suite IV is now considered to form a portion of the quartzo-feldspathic gneiss of the Valley Trust Formation.

Although a degree of overlap is apparent on the Harker diagrams (Figure 4.9), each suite displays a degree of chemical individuality, most particularly:

1) the high average TiO_2, CaO, Al_2O_3, FeO_{TOT}, MnO, P_2O_5, Zr, Sr and Zn concentrations of the Mlahlanja Suite; and
2) the high Pb, but low Sr, Zr, CaO and FeO_{TOT} abundances of the Nqwadolo Suite.

Significant chemical differences only exist, however, between the Nqwadolo Suite and the megacrystic granites, with disparities between the Ximba and Mlahlanja Suites restricted to MgO and P_2O_5. Separation of the megacrystic suites is not possible through the immobile trace elements (Figure 4.8a,b) or the cationic R1-R2 (de la Roche *et al.* 1980) and A-B (Debon and Le Fort 1982) diagrams although differences in trend are apparent and the Nqwadolo Suite is distinctly defined. Discrimination of the megacrystic granite suites is, however, obtained through the catonical variables devised by Ramsey *et al.* (1986) to identify the granite suites of the Arabian Shield (Figure 4.8c).

Further subdivision of these suites is suggested by variations in their trace element data. For the individual plutons of the Mlahlanja Suite distinct trends are apparent, radiating from an origin at Zr 700ppm - Y 40ppm and evolving along Zr/Y = 10, for the charnockite of the Egugwini pluton and the garnet hornblende granite of the Matata pluton, or with increasing Y but declining Zr concentrations towards lower Zr/Y ratios, for the granites of the Sansikane pluton (Figure 4.8a). The low Na_2O of the garnet hornblende granite when compared with the other members of the series suggests its characterisation as a subunit of the Mlahlanja Suite. Similarly, two distinct chemical types are evident in the Nqwadolo Suite through variations in Y-Zr, Zr/Y-Zr (Figure 4.8a,b) and Rb/Nb-Rb/Sr (McDermott *et al.* 1996). Chemical discrimination of distinct subunits within the Ximba Suite suggests that these may have evolved through petrogenetic processes (Section 6.4.2).

This chemical subdivision of the granites of the Mgeni batholith is supported by the isotopic data of Eglington *et al.* (1989b) which demonstrated distinct differences in Sr_I between the suites. Specifically, the Ximba Suite has an Sr_I of 0.7077±12, the Mlahlanja Suite 0.7042±28 (0.7053±8 (Eglington *et al.* 1989a)) and the Nqwadolo Suite 0.716±24.

4.5.3 CHEMICAL CHARACTERISATION

a) Ximba Suite

Forty seven samples of the Ximba Suite (one duplicated) were selected for analysis, 14 from the marginal granite, 17 from the biotite garnet granite and 16 from the biotite granite (Appendix 3). These were collected from sites throughout the Ximba pluton, with detailed sampling undertaken at selected localities, to assist in petrogenetic modelling (Section 6.4.2).

The Ximba Suite consists of a series of mineralogically distinct granites which together display a range of silica concentrations from 59-77 percent SiO_2. The average analysis of each member of the suite suggests an incremental increase in silica through the series: marginal granite - biotite garnet granite - biotite granite, but on the Harker diagrams considerable overlap is apparent between the individual granites.

As a group the analyses tend to display simple trends on the Harker diagrams (Figure 4.9), but frequently with a marked kink between the marginal granite and the biotite granite. As silica increases, TiO_2, Al_2O_3, FeO_{TOT}, MnO, MgO, CaO, Na_2O, P_2O_5, Ba, Sr, Zr, Nb, Zn and Y concentrations decline while those of K_2O, Rb, Pb and Th increase. Calculation of the correlation coefficient (Appendix 4) demonstrates significant correlation at the one percent level between silica and all the major elements, with the exception of K_2O, but is less well defined with the trace elements.

Figure 4.8. Correlation diagrams, Mgeni batholith.
a) Y-Zr (1 and 2 - Fractionation trends, Mlahlanja Suite) and b) Zr/Y-Zr immobile trace element diagrams.
c) CV2-CV1 Canonical variable discrimination diagram (Ramsey *et al.* 1986).
CV1 = - $0.5SiO_2$ + $0.54MgO$ - $0.313Na_2O$ - $2.828K_2O$ - $0.711FeO_T$ + 50.139.
CV2 = - $0.297SiO_2$ - $1.457MgO$ + $0.551Na_2O$ - $0.735K_2O$ + $2.091FeO_T$ - 25.009.

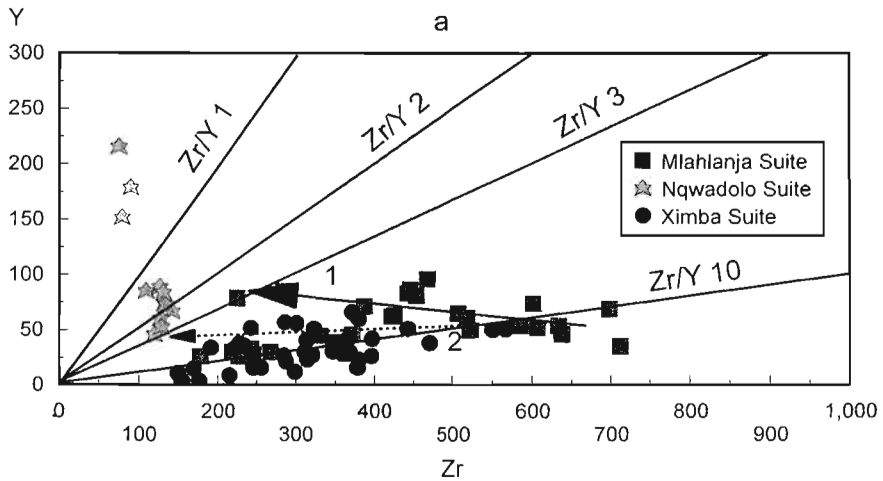

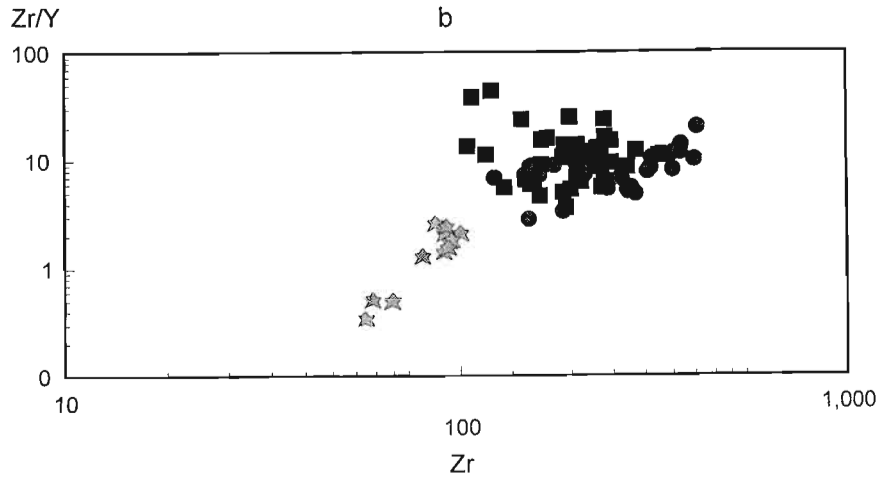

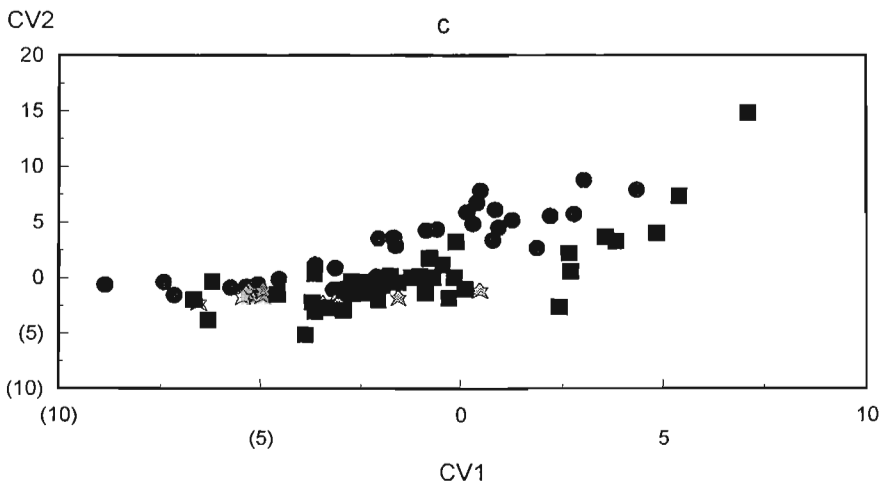

Figure 4.9. Element-silica variation diagrams, Mgeni batholith.
a) Major elements.

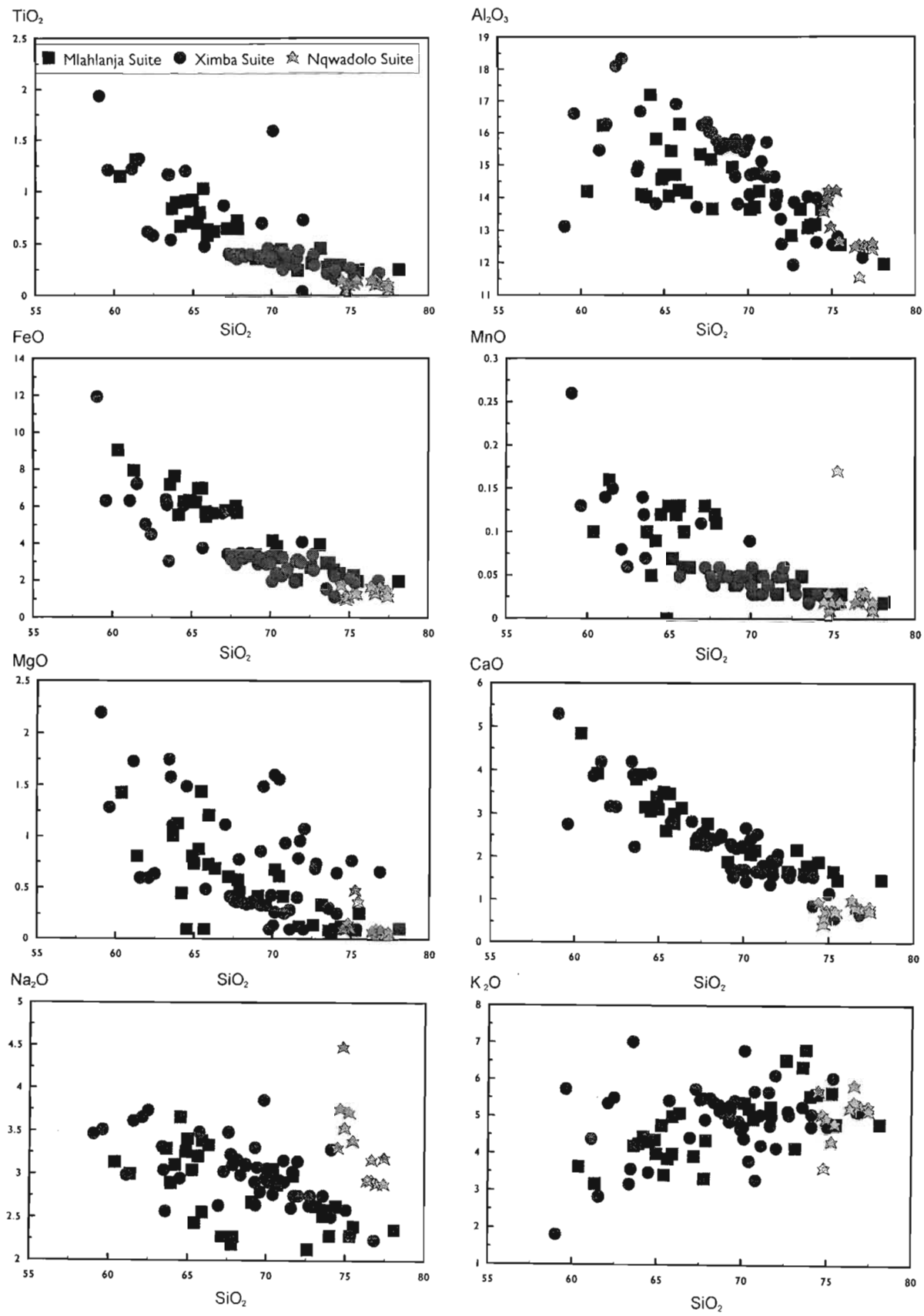

b) Trace elements.

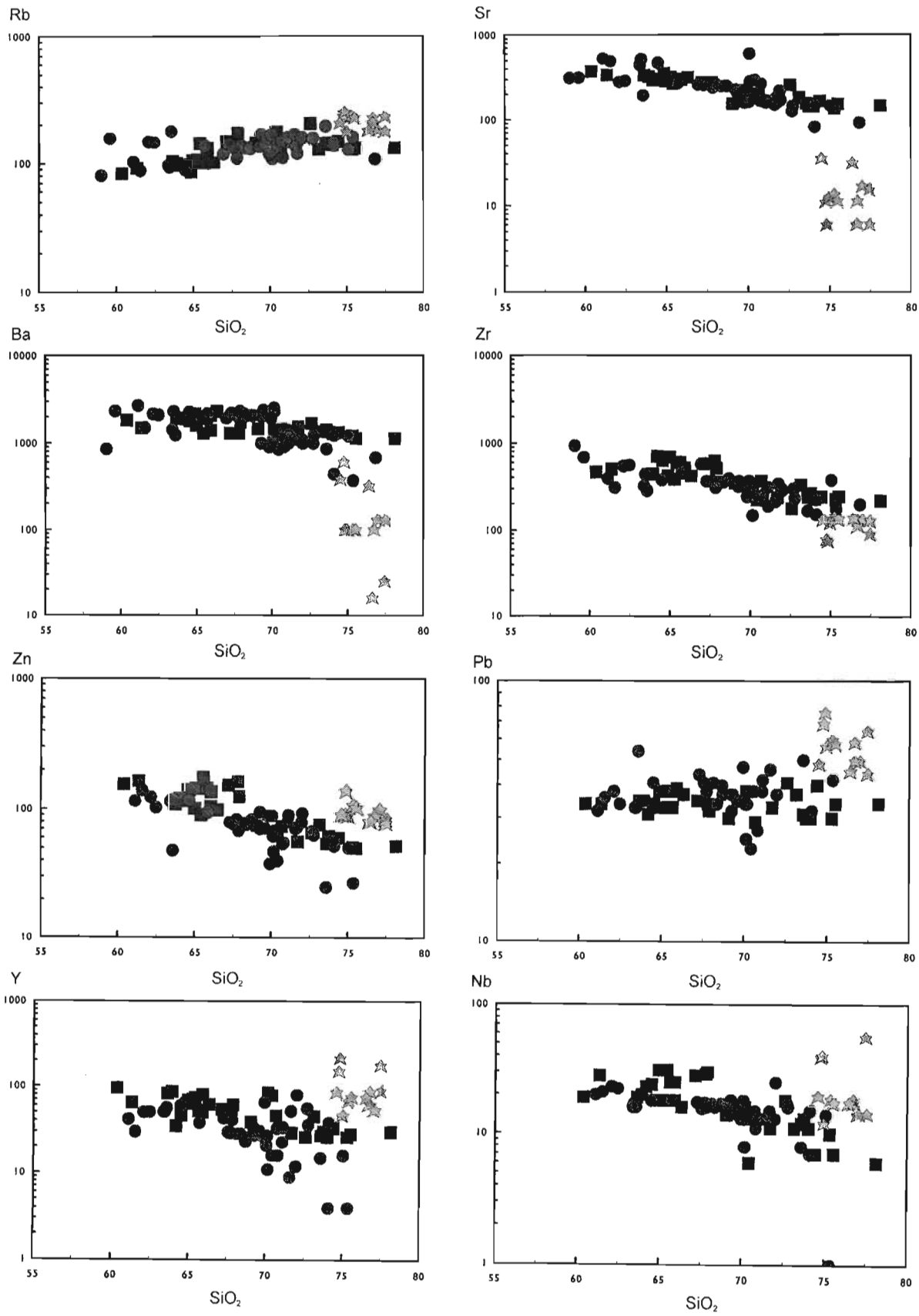

Normalised La/Lu ratios vary from 10.19-30.58, with almost parallel La/Sm and Gd/Lu trends (Figure 4.10) and a weak positive or negative Eu anomaly (Eu/Eu* 0.53-1.26). Within-suite REE variation may display a negative relationship between silica and REE abundance. A small negative epsilon Nd value, -0.2 at 1001±35 Ma, for the biotite granite was reported by Eglington *et al.* (1989b).

b) Mlahlanja Suite

Twenty nine samples (two duplicated) of the Mlahlanja Suite were selected for analysis, 13 from the charnockite and surrounding green hornblende granite (subcharnockite), 10 from the hornblende granite and 6 from the garnet hornblende granite. Sampling was concentrated in the Sansikane, Egugwini and Matata plutons, principally to aid in petrogenetic modelling (Section 6.4.3).

The Mlahlanja Suite displays a range of silica concentrations from 60-78 percent SiO_2. Within this series each member of the suite is chemically distinct, but no trend of simple progressive chemical change is apparent. Rather, they display an almost complete overlap within typically tightly constrained fields on the Harker diagrams. Chemical variations between the individual granites may, however, result in a broad spread of data, or in one of the mineralogical subtypes plotting separately. In particular, is the relatively siliceous nature of the charnockite and subcharnockite and their low HFSE content, and the low sodium content of the garnet hornblende granite.

With increasing silica TiO_2, Al_2O_3, FeO, MnO, CaO, MgO, Na_2O, P_2O_5, Ba, Zr, Sr, Zn, Nb and Y concentrations decline, while K_2O, Rb, Th and Pb increase (Figure 4.9). Calculation of the correlation coefficient (Appendix 4) demonstrates significant correlation at the one percent level between silica, all the major elements and the majority of the trace elements.

Normalised La/Lu ratios vary from 4.84-8.63, with La/Sm ratios of 2.08-3.11, Gd/Lu ratios of 1.08-2.20 (Figure 4.10) and a small positive or negative Eu anomaly (Eu/Eu* 0.57-1.28). No trend to the pattern of REE variation with silica concentration is apparent within the suite. The hornblende granite, however, displays a general decrease in REE concentration with increasing silica, while the charnockite exhibits a slight increase.

c) Nqwadolo Suite

Six samples of the Nqwadolo Suite and one late vein were originally selected for analysis (Kuyper 1979; Du Toit 1979), the former from the marginal portion of the granite. Six additional samples were collected from the core of the granite during the present study.

All the samples are siliceous (74-78% SiO_2). This narrow range in silica hinders the determination of well defined trends on Harker diagrams (Figure 4.9). Prevalent tendencies, however, indicate increasing concentrations of FeO, CaO, K_2O and Zr with rising silica, while TiO_2, Al_2O_3, MgO, Na_2O, P_2O_5, Sr, Zn, Rb, Ba, Y, Nb, Pb and Th levels fall. Calculation of the correlation coefficient (Appendix 4), however, reveals no significant correlation at the five percent level between silica, the major elements, with the exception of Al_2O_3, Na_2O and P_2O_5, and the trace elements.

No specific relationship exists between REE concentration and silica in this granite. La/Lu ratios vary from 4.79-8.65, with La/Sm ratios of 1.48-2.33, Gd/Lu ratios of 2.31-2.61 (Figure 4.10) and a large negative Eu anomaly (Eu/Eu* 0.11-0.03). One sample, the most siliceous of the Nqwadolo Suite, displays an anomalous 'cross-over' pattern, with LREE depletion and HREE enrichment, similar to that described by Dall'Agnol *et al.* (1991). A positive epsilon Nd value, 2.0 at 1033±18 Ma, was reported by Eglington *et al.* (1989b).

4.5.4 NOMENCLATURE AND CLASSIFICATION

The extremely large grain size of the megacrystic granites hinders the use of the Streckeisen (1976) diagram for nomenclature purposes, but estimated modal analyses of typical samples plot as quartz monzonite or granite (hypersthene granite or charnockite). Similar results are obtained with normative analyses, with the widespread occurrence of perthite resulting in a minor shift from the monzogranite or granodiorite fields to the syenogranite or monzogranite fields. Modal analyses of the Nqwadolo Suite plot as granites on the Streckeisen diagram.

The various members of the Mgeni batholith plot predominately as granites on the R1-R2 diagram of de la Roche *et al.* (1980), the TAS diagram (Le Bas *et al.* 1986; Le Maitre 1989) (Figure 4.11a), and the diagrams of Winchester and Floyd (1977). Individual samples plot in the alkalic fields. All the samples of the Nqwadolo Suite plot as granites.

Figure 4.10. Normalised REE abundances.

a) Biotite garnet granite, Ximba Suite; b) Biotite granite, Ximba Suite; c) Charnockite, Mlahlanja Suite;
d) Hornblende granite, Mlahlanja Suite; e) Garnet hornblende granite, Mlahlanja Suite; f) Nqwadolo Suite.
Chondrite normalising factor from Nakamura (1974).
La - 0.33, Ce - 0.865, Pr - 0.122, Nd - 0.63, Sm - 0.203, Eu - 0.077, Gd - 0.275, Dy - 0.342, Ho - 0.076, Er - 0.225, Yb - 0.22, Lu - 0.034.

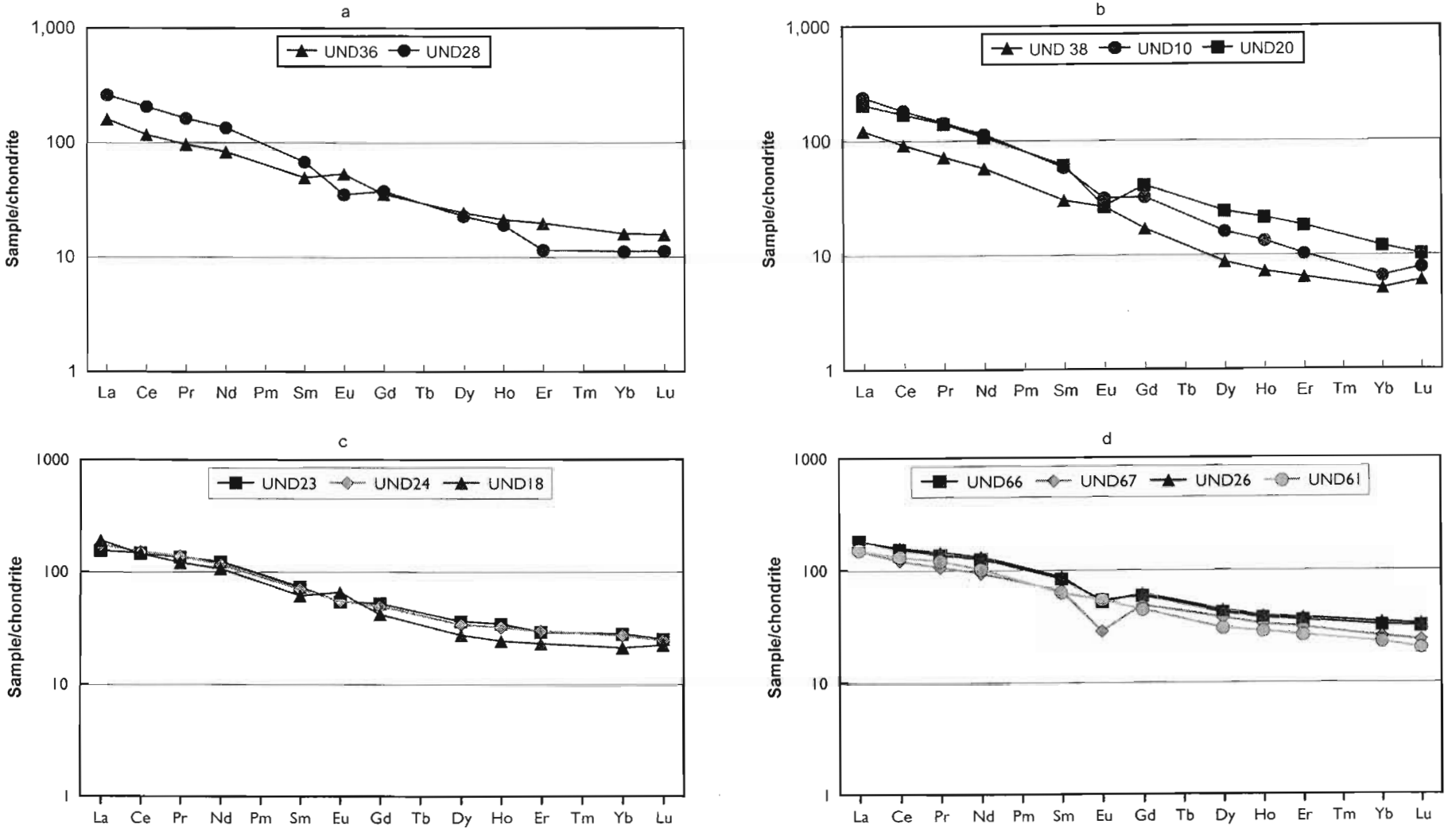

Figure 4.10. Normalised REE abundances - continued.

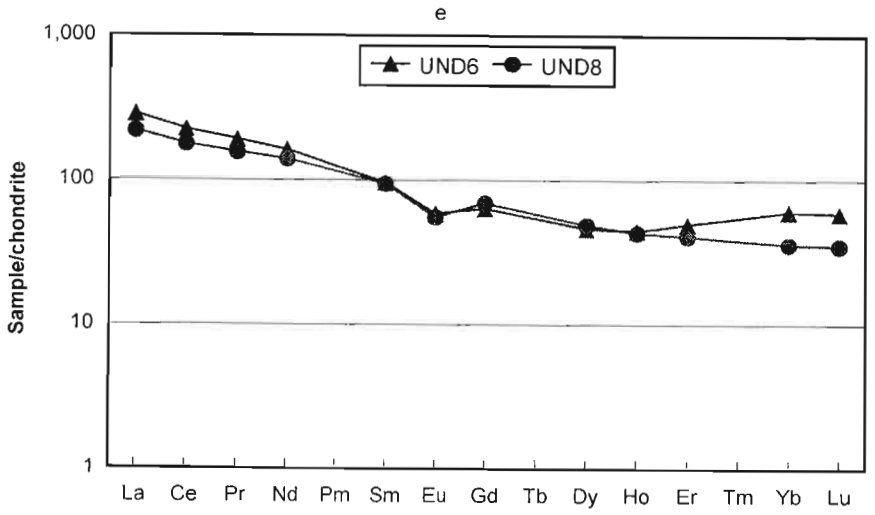

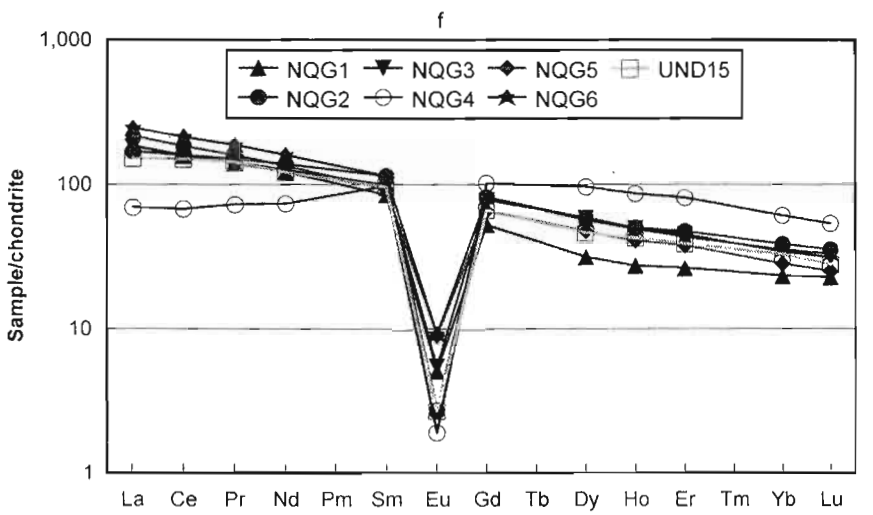

Figure 4.11. Nomenclature diagrams - Mgeni batholith.
a) TAS diagram (Le Maitre 1989).
b) SiO_2-FeO/FeO+MgO (after Miyashiro 1974).
c) Log(CaO/Na_2O+K_2O)-SiO_2 (Brown 1982).
d) FeO/MgO-Zr+Ce+Nb+Y (Whalen *et al.* 1987).

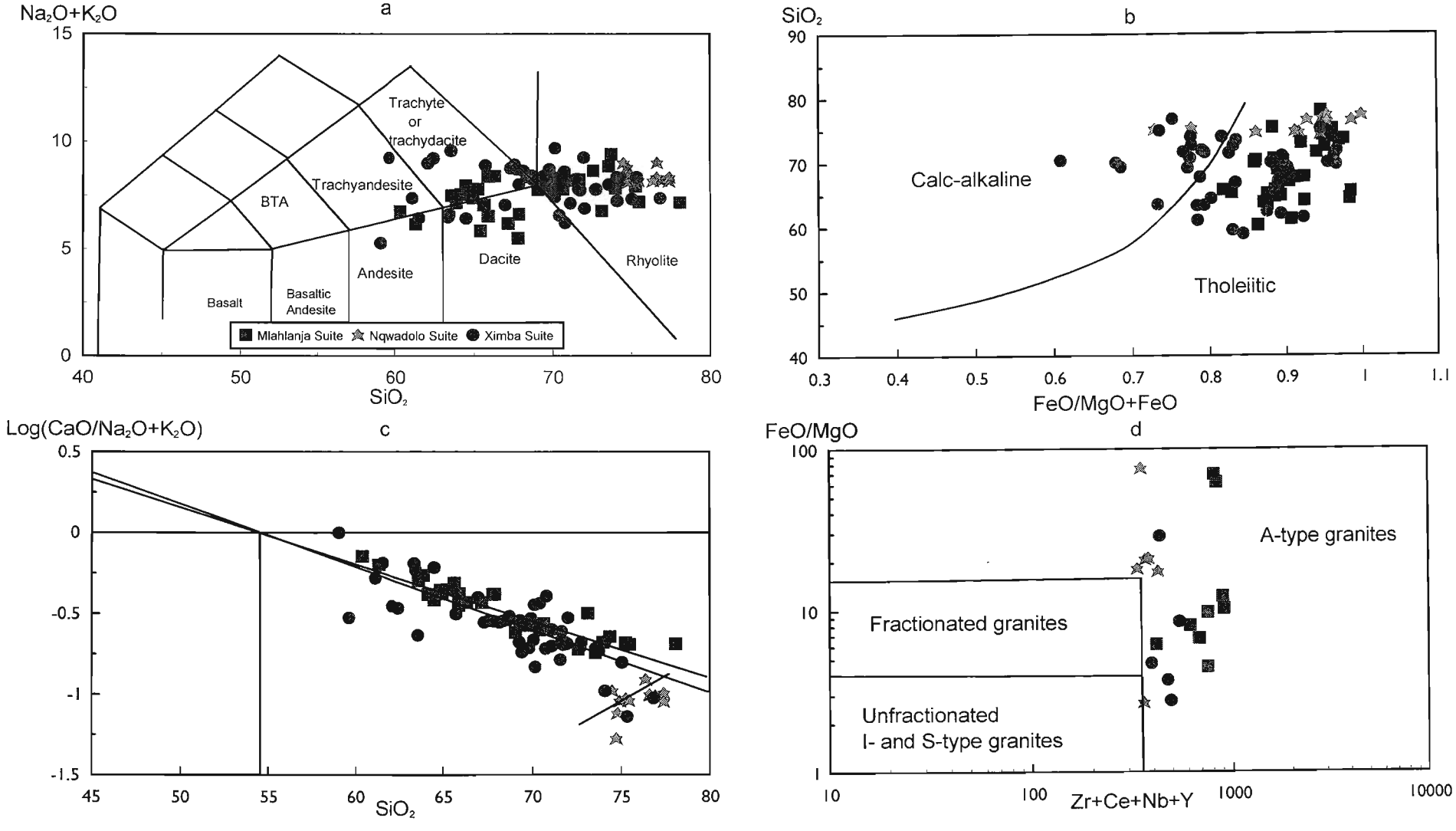

The average analyses of the various members of the Ximba and Mlahlanja Suites compare poorly with the average acidic analyses of Le Maitre (1976). Their high K_2O/Na_2O ratios (0.52-2.73 and 1.06-3.07 respectively) suggest comparison with Le Maitre's average granite or adamellite, but they display distinctive high K_2O and, in the Mlahlanja Suite, FeO, but low CaO (except in the marginal granite), MgO and Na_2O concentrations. The Nqwadolo Suite is comparable to the minimum melt of White and Chappell (1977). In particular its high SiO_2 and K_2O, but low Al_2O_3, FeO, MgO and CaO concentrations are distinctive.

The Ximba Suite displays a variable degree of alumina saturation, with individual samples possessing metaluminous, peraluminous and rarely peralkaline characteristics. The Nqwadolo Suite and the majority of the Mlahlanja Suite are metaluminous, but individual samples may be peraluminous and occasionally peralkaline. On the A-B diagram of Debon and Le Fort (1982) the Ximba Suite plots across all the delineated subdivisions of the peraluminous domain, including the muscovite > biotite field, but with extension into the metaluminous domain at low silica levels. The Mlahlanja Suite plots predominately in the metaluminous domain, with extension into the peraluminous field at high silica levels, but the garnet hornblende granite plots separately, within the peraluminous field. The Nqwadolo Suite exhibits an unusual vertical trend, within the peraluminous domain, similar to Debon and Le Fort's ALUM - quartz poor group. The hornblende granite is typically diopside normative, with the exception of the more siliceous analyses. The majority of the Ximba and Nqwadolo Suites, the charnockite and the garnet hornblende granite have corundum in their norms.

On the TAS diagram all the suites exhibit variable overlap between the alkaline and subalkaline fields, extending into the shoshonite field on the K_2O-SiO_2 diagram. Intermediate Nb/Y and Zr/TiO_2 ratios similarly result in occasional samples plotting in the alkalic portion of the diagrams of Winchester and Floyd (1977).

On the A-B diagram of Debon and Le Fort (1982) and the AFM diagram the Ximba Suite parallels the calc-alkaline trend, but with extension into the tholeiitic field on the SiO_2-FeO/FeO+MgO diagram (Figure 4.11b). The observed trend of the Mlahlanja Suite on the A-B diagram does not follow any of the typical styles illustrated by Debon and Le Fort (1982). The hornblende granite and charnockite parallel the calc-alkaline trend, but at lower B levels. The high FeO/MgO and FeO/FeO+MgO (0.82-0.99) ratios of the Mlahlanja Suite, however, indicate a tholeiitic character (Figure 4.11b), and on the AFM diagram the suite plots adjacent to the AF join, extending into the tholeiitic field. The Nqwadolo Suite plots at the A apex of the AFM diagram, and no trend can be distinguished, but its high FeO/MgO and FeO/FeO+MgO (0.73-1) ratios indicate a tholeiitic character (Figure 4.11b). The Ximba and Mlahlanja Suites have a Peacock Index of c.54 (Figure 4.11c), within the alkali-calcic field (Brown 1982). The limited range of silica hinders the identification of the Peacock Index of the Nqwadolo Suite (Figure 4.11c).

The high HFS element content of these granites, and in particular their high Zr concentration, classifies them as A-type granites (Whalen *et al.* 1987) (Figure 4.11d).

CHAPTER 5

TECTONIC RECONSTRUCTION

5.1 INTRODUCTION

Regional studies of the Proterozoic basement of KwaZulu Natal, and in particular by Matthews (1972) and Thomas (1989a), have resulted in the development of a collision model as a framework within which to explain the assemblage of the Natal Province. This model views the younger Natal Province as either a continental mass (Matthews 1972) or as a series of exotic terranes (Milne 1986; Thomas 1989a; Thomas *et al.* 1994; Jacobs and Thomas 1994), which collided with the older Kaapvaal Craton, producing a suture marked by ophiolite obduction. This resulted in the welding of the various terranes into a single tectonic unit, which served as a stable environment for the intrusion of the late- to post-orogenic granites of the Oribi Gorge Suite (Thomas 1989a).

These models, with the exception of Milne (1986), were primarily developed from studies based in northern (Matthews 1972) or southern (Thomas 1989a) KwaZulu Natal, with little attempt to specify the geotectonic setting of the metamorphic and igneous rocks of central KwaZulu Natal, including the Valley of a Thousand Hills, except through extrapolation. This chapter therefore attempts to develop a model to explain the evolution of the tectonic setting of the Valley of a Thousand Hills during the Proterozoic, through the chemical characterisation of the various units identified. To aid this the interpretation of the various tectonic discrimination diagrams will be reviewed.

5.2 GEOCHEMICAL TECTONIC DISCRIMINATION

5.2.1 NAGLE DAM FORMATION

The Nagle Dam Formation consists of a metamorphosed igneous series extending from basalt to rhyolite, with abundant intermediate members. Although the available chemical data suggest that the members of this series are not directly related (Section 4.3.5), their combined chemical characteristics indicate that they represent a unimodal suite in the sense of Martin and Piwinskii (1972), which typically forms within an orogenic setting. This identification is supported by a variety of chemical characteristics considered indicative of an orogenic series (Petro *et al.* 1979), including the high calc/alkali index of the Nagle Dam Formation and its calc-alkaline distribution pattern on the AFM diagram, together with its low Nb content (Pearce and Gale 1977).

Chemical discrimination of the intermediate and acidic gneisses suggest that they developed in a volcanic arc or collision environment (Figure 5.1, 5.2f). These environments are, however, discriminated by the Rb-Nb+Y diagram (Figure 5.1e), with the Nagle Dam Formation plotting essentially in the volcanic arc granite (VAG) field, with extension into the syn-collision granite (syn-COLG) field for the quartzo-feldspathic gneiss. Ocean ridge granite (ORG)-normalised spidergrams display a pattern of LILE enrichment and HFSE depletion (Figure 5.1f). This is comparable with the volcanic arc and collision granites, although the lack of an extreme Rb anomaly suggests an arc or post-collision environment. The relatively low HFSE concentration of the Nagle Dam Formation indicates an island arc rather than a continental margin setting. Division of the biotite hornblende and quartzo-feldspathic gneisses into their component series (Section 4.3.5) results in little change to this analysis (Figure 5.1g,h), although the high Zr/Y quartzo-feldspathic gneiss exhibits extreme Nb and Y depletion.

The amphibolite possesses both arc and mid-oceanic ridge basalt (MORB) characteristics (Figure 5.2a,c,f), although it plots predominately in the island arc basalt (IAB) field on the Ba-Nb diagram (Figure 5.2b). The discrimination of the amphibolite is hindered by the overlap of the fields on the majority of the tectonic discrimination diagrams but may also be a function of its primitive arc volcanic type character, these displaying both MORB and arc characteristics (Smith *et al.* 1997).

The MORB-normalised spidergram of Pearce (1982) (Figure 5.2g), displays a pattern of strong LILE enrichment, with depletion of Y, Zr and Ti and minor enrichment of the more compatible Cr. The lack of Y, Ti and Zr enrichment is suggestive of an arc rather than a mid-oceanic or within plate origin, although Nb is enriched. Similarly, on the primordial mantle normalised spidergram of Holm (1985) the pattern of declining HFS element concentrations indicate an arc origin (Figure 5.2h). The high LILE content of the amphibolite demonstrates considerable enrichment of these elements relative to the low-potassium tholeiite standard of Holm, but these are at levels comparable with the calc-alkaline and shoshonitic arc basalts (Pearce 1982).

Figure 5.1. Granitic tectonomagmatic discrimination diagrams (Pearce *et al.* 1984) for the biotite hornblende and quartzo-feldspathic gneisses of the Nagle Dam Formation, the quartzo-feldspathic gneiss of the Valley Trust Formation and the granites of the Mgeni Batholith.

a) Rb-SiO_2, b) Y-SiO_2, c) Nb-SiO_2, d) Nb-Y, e) Rb-Y+Nb, f-l) ORG normalised spidergrams (ORG normalising factors after Pearce *et al.* 1984), f) average biotite hornblende gneiss and quartzo-feldspathic gneiss - Nagle Dam Formation, g) individual quartzo-feldspathic gneiss series - Nagle Dam Formation, h) individual ,biotite hornblende gneiss series - Nagle Dam Formation, i) quartzo-feldspathic gneiss - Valley Trust Formation, j) Ximba Suite, k) Mlahlanja Suite, l) Nqwadolo Suite.

WPG - within plate granite; ORG - ocean ridge granite; VAG - volcanic arc granite; syn-COLG - syn-collision granite; COLG - collision granite.

ORG normalising factors - K_2O - 0.4; Rb - 4; Ba - 50; Th - 0.8; Ta - 0.7; Nb - 10; Ce - 35; Hf - 9; Zr - 340; Sm - 9; Y - 70; Yb - 8.

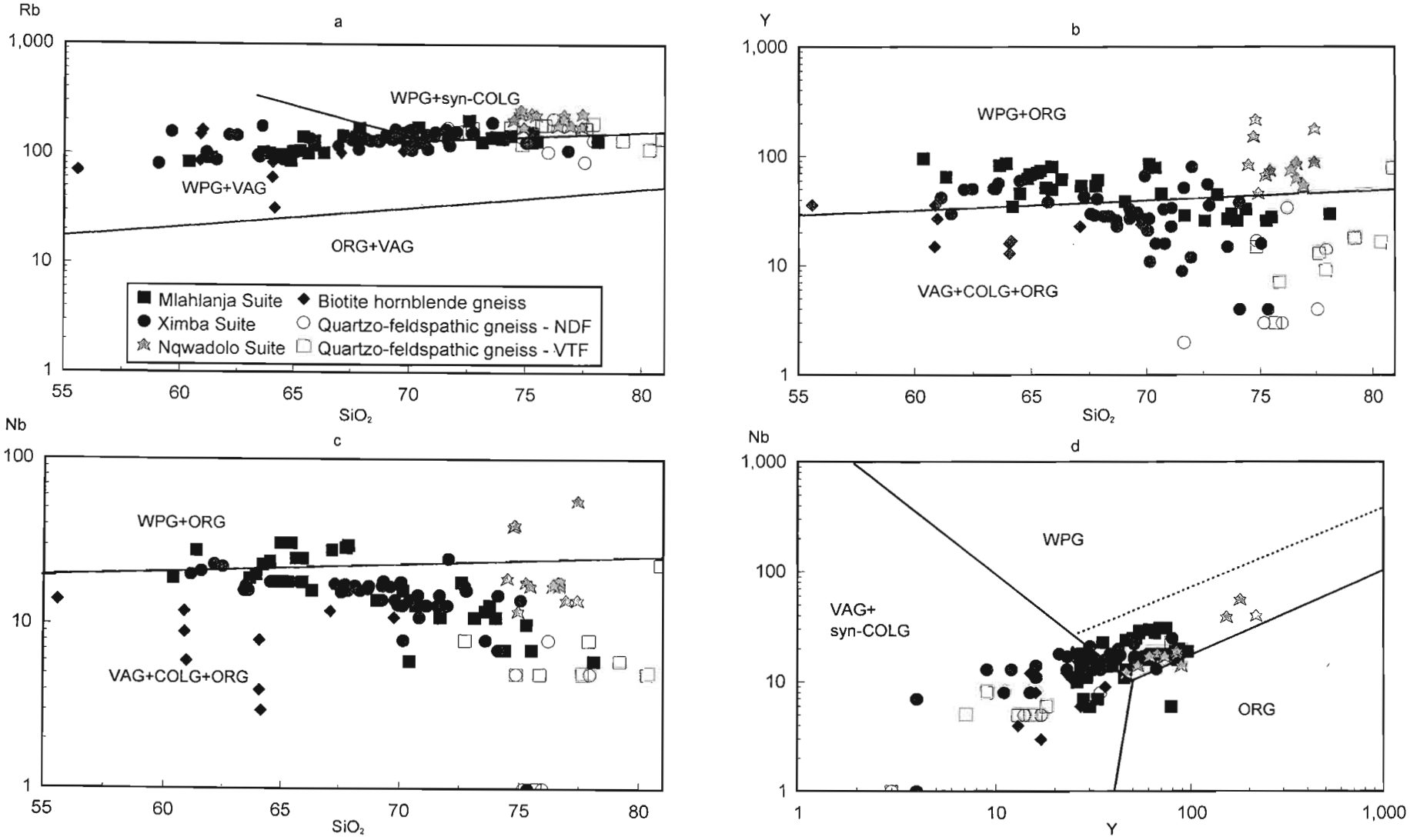

Figure 5.1. Granite tectonomagmatic discrimination diagrams - continued.

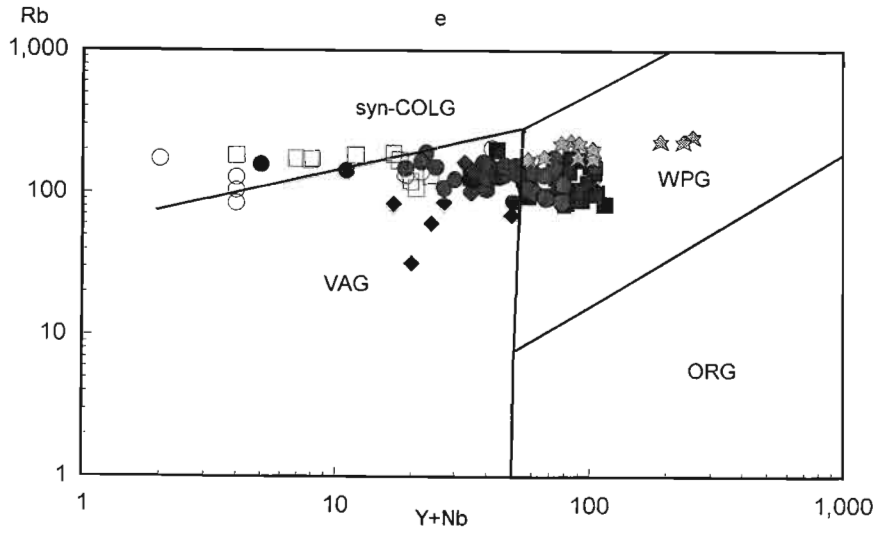

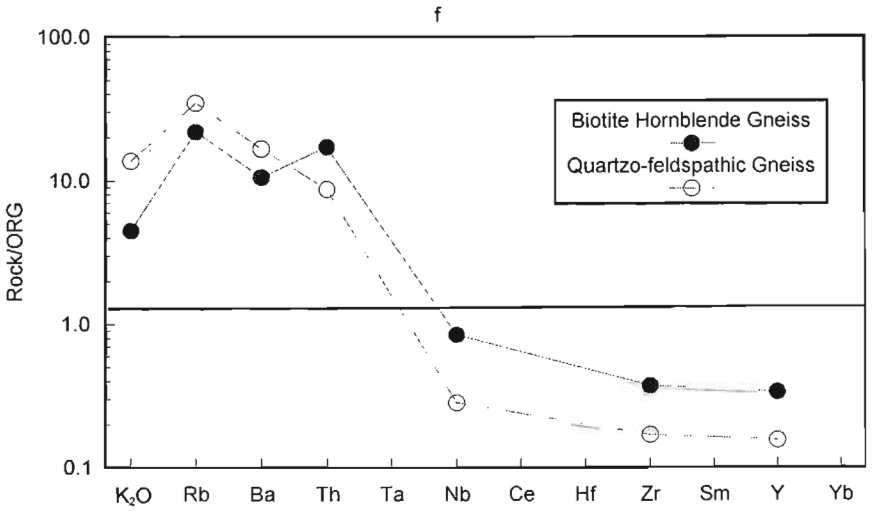

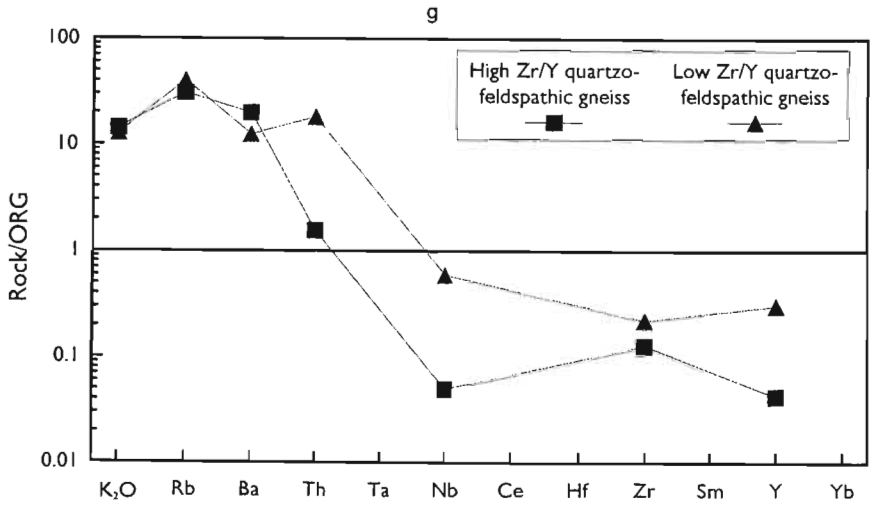

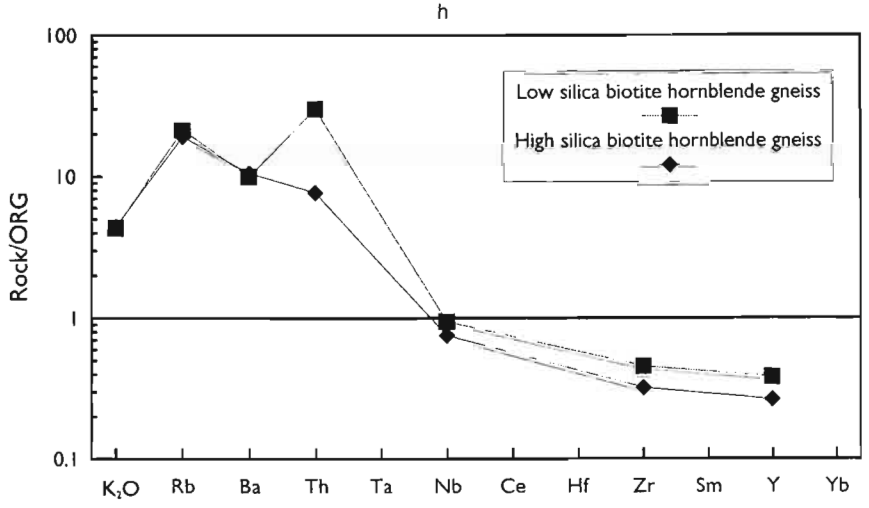

Figure 5.1. Granite tectonomagmatic discrimination diagrams - continued.

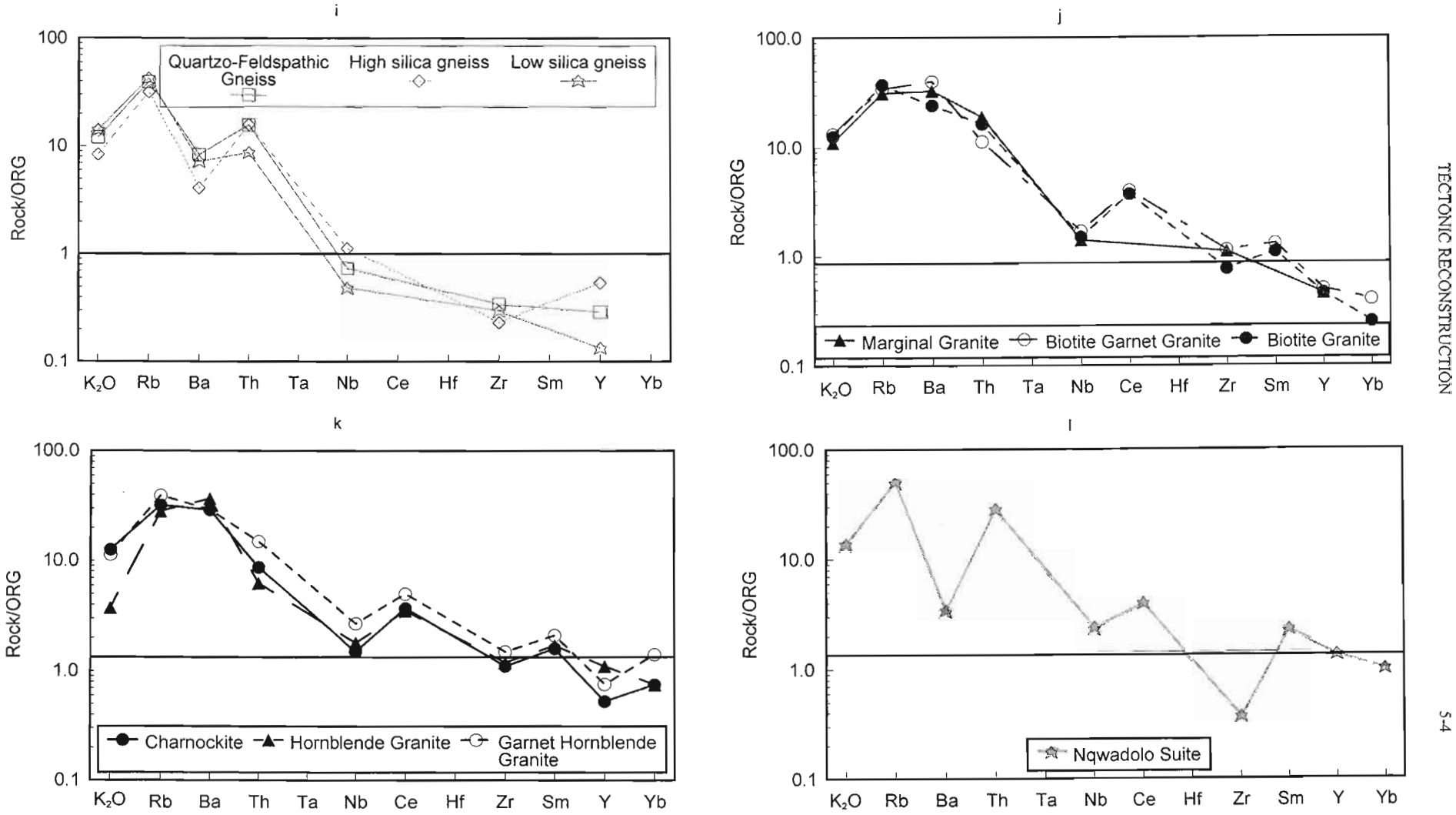

Figure 5.2. Basaltic tectonomagmatic discrimination diagrams for the amphibolites of the Nagle Dam and Valley Trust Formations.
a) Ti/Y-Nb/Y (Pearce 1982), b) Ba-Nb (Hawkesworth *et al.* 1991) for Nagle Dam Formation amphibolite, c) Zr/Y-Zr (Pearce and Norry 1979, Pearce 1983), d) Zr/Y-Ti/Y (Pearce and Gale 1977), e) Cr-Y (after Pearce 1982), f) Ti-Zr (after Pearce1982), g) MORB normalised spidergram for the amphibolite of the Nagle Dam Formation (Pearce 1982), g) Primordial mantle normalised spidergram for the amphibolite of the Valley Trust Formation (Holm 1985) (normalising factor (n) primordial mantle composition after Wood *et al.* 1979), i) MORB normalised spidergram for the amphibolite of the Valley Trust Formation (Pearce 1982), j) Primordial mantle normalised spidergram for the amphibolite of the Valley Trust Formation (Holm 1985) (normalising factor (n) primordial mantle composition after Wood *et al.* 1979).
WPB - within plate basalt; VAB - volcanic arc basalt; MORB - mid-oceanic arc basalt; IAB - island arc basalt.
Normalising factors for Pearce (1982) - Sr - 120; K_2O - 0.15; Rb - 2; Ba - 20; Th - 0.2; Ta - 0.18; Nb - 3.5; Ce - 10; P_2O_5 - 0.12; Zr - 90; Hf - 2.4; Sm - 3.3; TiO_2 - 1.5; Y - 30; Yb - 3.4; Sc - 40; Cr - 250.
Normalising factors for Holm (1985) - Rb - 0.86; Ba - 7.56; Th - 0.096; U - 0.027; K - 252; Nb - 0.62; La - 0.71; Ce - 1.9; Sr - 23; P - 90.4; Zr - 11; Sm - 0.385; Ti - 1527; Y - 4.87; Yb - 0.43.

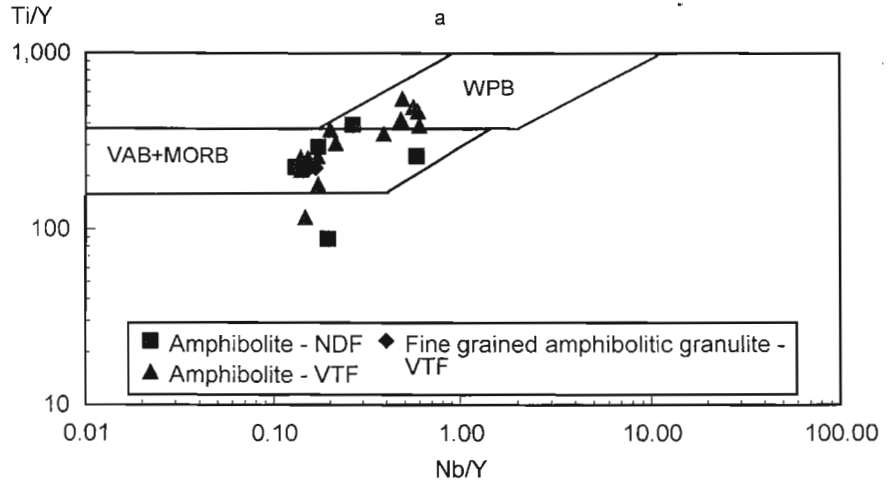

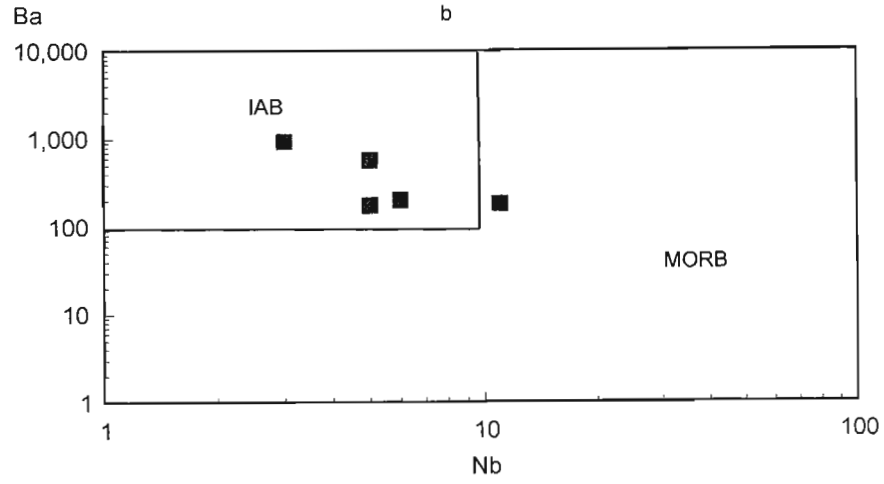

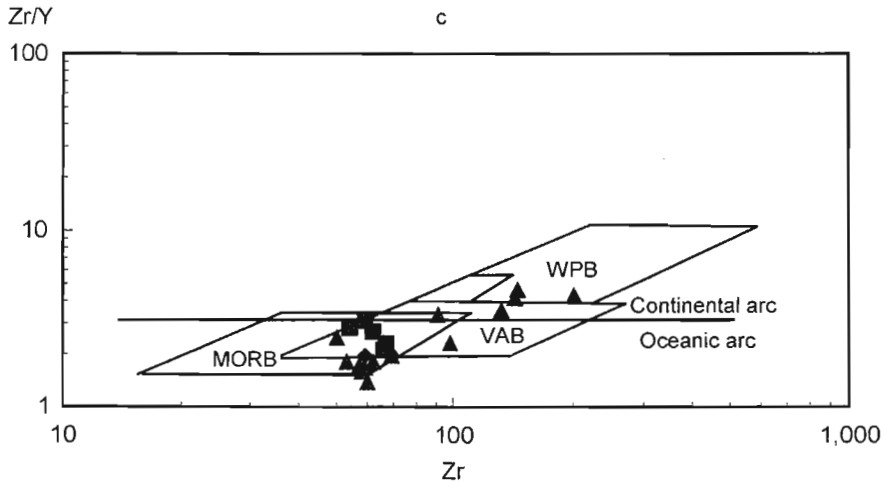

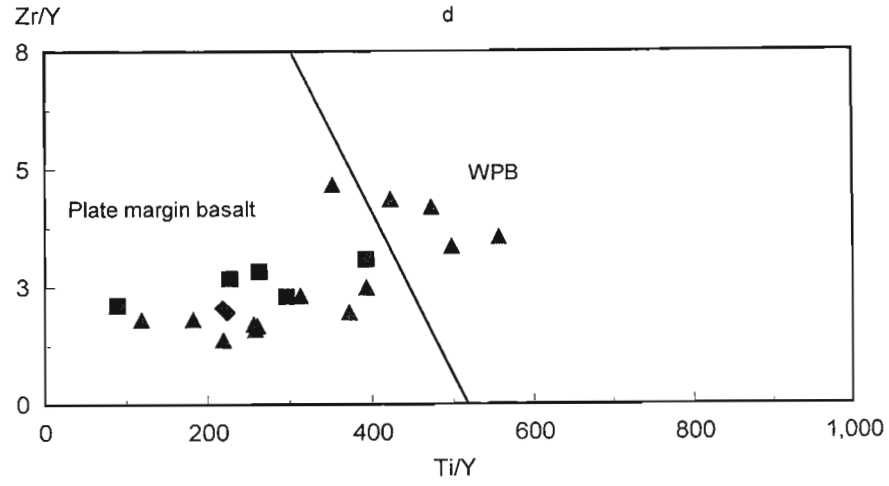

Figure 5.2. Basaltic tectonomagmatic discrimination diagrams - continued.

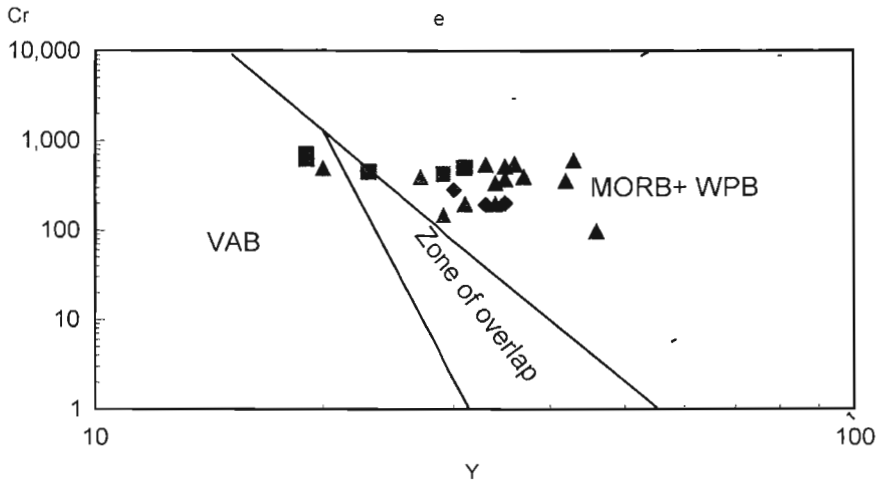

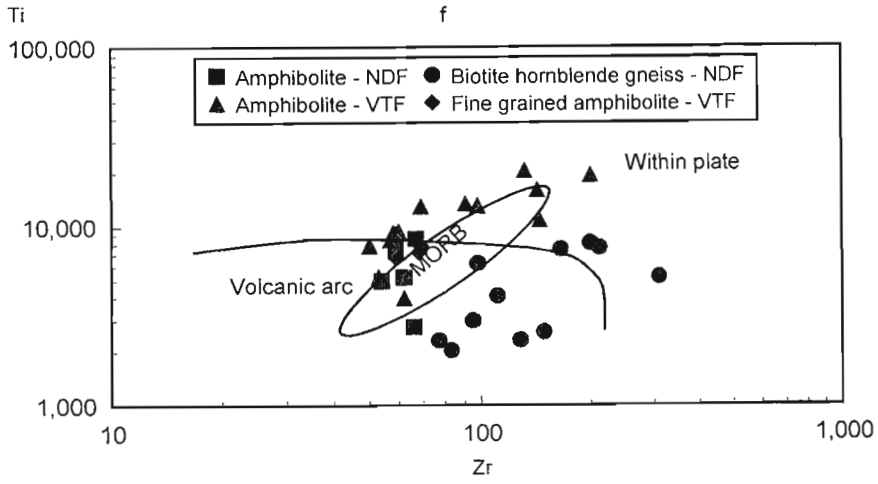

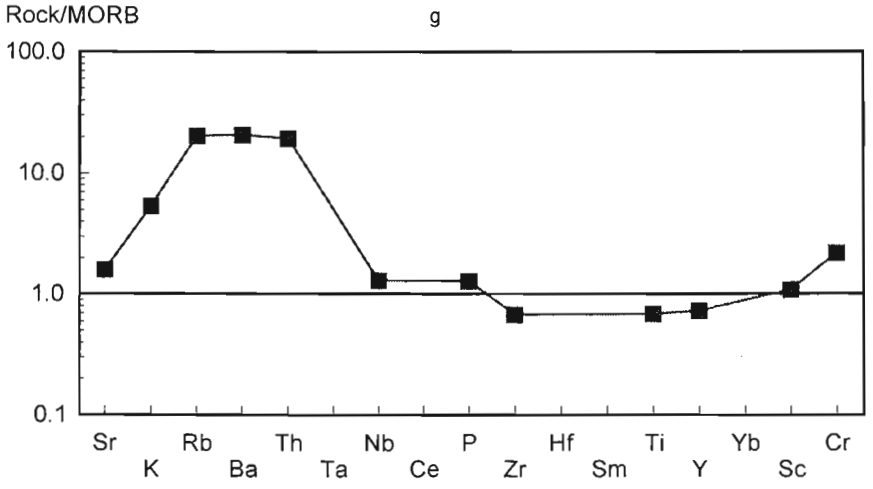

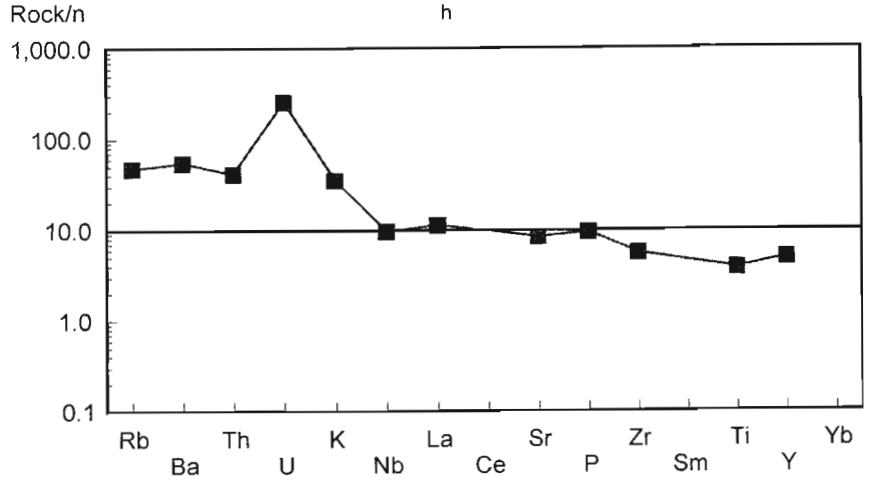

Figure 5.2. Basaltic tectonomagmatic discrimination diagrams - continued.

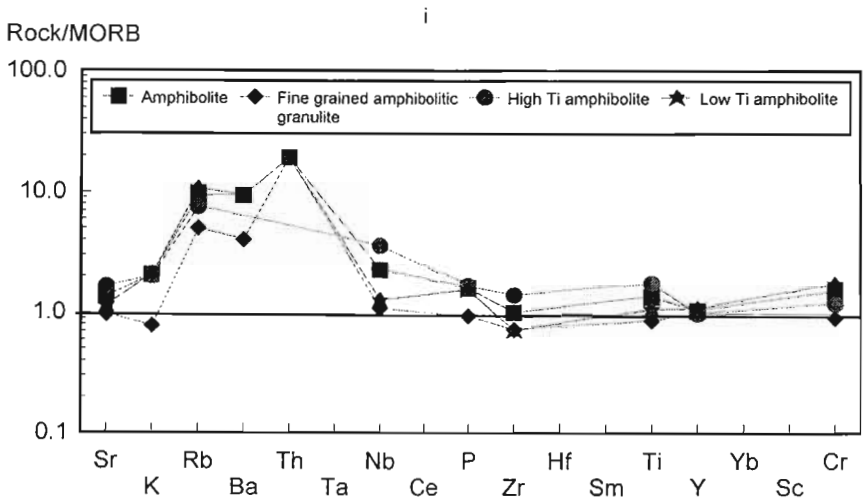

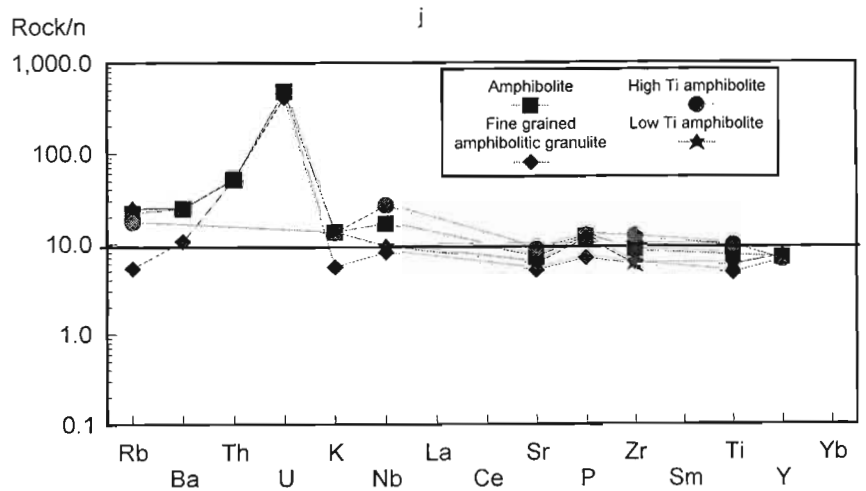

The isotopic analyses of Eglington (1987) and Eglington *et al.* (1989b) demonstrated the primary origin of the Natal Province with no Archaean crust involved in its derivation, suggesting an island arc, as opposed to a continental margin, setting for the Nagle Dam Formation. This is supported by its average composition (Brown 1982, after Mason and McDonald 1978) and element distribution patterns on the spidergram of Pearce *et al.* (1984), while the low Zr/Y ratio of the amphibolite is characteristic of the oceanic arcs (Figure 5.2c). The relatively high K_2O and Ba but low FeO/MgO ratio of the gneisses, are, however, analogous with those suites emplaced in cratonic crust (Coulon and Thorpe 1981; Brown 1982).

Evolutionary trends within arc volcanism have been recognised by numerous authors, including Gill (1970), Thorpe *et al.* (1981), Brown (1982) and Brown *et al.* (1984). In particular, Brown (1982) noted that constant chemical variations on the AFM and $\log(CaO/Na_2O+K_2O)$-SiO_2 diagrams are indicative of increasing maturity in a volcanic arc. Comparison with the data of Brown suggests that the Nagle Dam Formation was a fairly mature arc, plotting within the field of normal calc-alkaline rocks on the latter diagram. The trace element data, however, imply a more juvenile setting, with the Nagle Dam Formation displaying characteristics of primitive and normal arcs (Brown *et al.* 1984).

5.2.2 VALLEY TRUST FORMATION

a) Medium Grained Orthogneisses

The medium grained orthogneisses of the Valley Trust Formation represent a bimodal succession, comprising amphibolite and quartzo-feldspathic gneiss. Such sequences are typically developed in non-orogenic settings within tensional environments (Martin and Piwinskii 1972), although Pin and Paquette (1997) noted that bimodal suites may occur in a variety of environments, including an association with the compressional environment (also McBirney 1968; Brown *et al.* 1977; Notsu *et al.* 1987).

The lack of intermediate members within the Valley Trust Formation hinders its classification by the methods of Petro *et al.* (1979). The bimodal character of this unit, however, suggests that it formed in an extensional environment, with the abundant acidic material indicating a non-oceanic setting, although the low Nb content of the quartzo-feldspathic gneiss is comparable with the orogenic granites (Pearce and Gale 1977).

The basalt spidergrams of Pearce (1982) and Holm (1985) indicate that the amphibolite possesses chemical characteristics comparable with the within plate basalts. On the former (Figure 5.2i) all the elements display a degree of enrichment, markedly so for U, with the exception of Zr, which approaches unity. Particularly prominent is the enrichment of Ti and Nb, features not apparent in any environment other than the within plate setting. Similarly, on the Holm diagram (Figure 5.2j) the general decline in enrichment from Rb to Y suggests a within plate type rather than a MORB environment, while the high Nb content of the amphibolite serves to distinguish it from the arc basalts. The lack of a Nb anomaly suggests that the amphibolite was not emplaced in a back arc setting. Rather it is comparable to the continental tholeiites or initial rifting tholeiites, and particularly so if only the high TiO_2 amphibolite is considered.

Two disparate groupings are, however, apparent on several of the tectonic discrimination diagrams (Figure 5.2a,c), a low Ti group with primarily mid-oceanic ridge basalt characteristics and a higher Ti group, which plots in the within plate basalt field with some extension into the mid-oceanic ridge basalt field (corresponding with the low Zr/Y and high Zr/Y amphibolites identified in Section 4.4.3). Normalisation of these individual series with MORB (Pearce 1982) derives a pattern comparable with that of the entire series, but with the within plate characteristics of the average amphibolite emphasised for the high-Ti amphibolite. For the low-Ti amphibolite the pattern of normalised HFS element concentrations at unity is comparable with MORB (Figure 5.2i).

The quartzo-feldspathic gneiss exhibits both volcanic arc and collision granite characteristics (Figure 5.1). On the Rb-Y+Nb diagram, however, it plots across the syn-collision, volcanic arc and within plate granite fields (Figure 5.1e), a distribution pattern typical of the post-collision granites. Similarly, on the ORG-normalised spidergram, the quartzo-feldspathic gneiss displays a pattern of LILE enrichment and HFSE depletion (Figure 5.1i), comparable with the volcanic arc and collision granite patterns. The low Zr content of the quartzo-feldspathic gneiss contrasts with the typically high Zr content of rhyolites associated with bimodal suites and extensional environments (such as Cleverly *et al.* 1984), although low-Zr rhyolites have been reported in this environment and may be characteristic of specific portions of the succession (Ewart 1981; Hildreth 1981; Crecraft *et al.* 1981; Leat *et al.* 1986; Bellieni *et al.*

1986; Ryan *et al.* 1987; Vivallo and Claesson 1987; Garland *et al.* 1995).

b) Paragneisses

A variety of tectonic discrimination diagrams have been designed for clastic sediments, primarily for sandstones and greywackes, (Bhatia 1983; Bhatia and Crook 1986), but additional diagrams, such as that of Roser and Korsch (1986), are also considered suitable for pelitic sequences.

On the majority of the major element discrimination diagrams of Bhatia (1983), the psammitic portion of the medium grained paragneiss plots predominately within the active continental margin or oceanic/continental arc fields (Figure 5.3a,c,d). Trace element data (Bhatia and Crook 1986) similarly suggest a continental island arc or oceanic island arc setting. Limited data are available for the metasedimentary portion of the fine grained granulite, but the chemical characteristics of its psammitic portion suggest an oceanic island arc setting (Figure 5.3c,d). On the K_2O/Na_2O-SiO_2 diagram of Roser and Korsch (1986), however, both series plot across or beyond the various delineated fields (Figure 5.3b). This may be due to Na_2O loss during source rock weathering (Nesbitt and Young 1984; 1989; Condie *et al.* 1992; Nesbitt *et al.* 1996).

The available chemical data therefore suggest that the paragneisses were deposited in association with an arc environment. This may be related to the development of an extensional environment within which the bimodal volcanic sequence was deposited, with the arc material forming a prominent source

c) Fine grained amphibolitic granulite

The fine grained amphibolitic granulite displays arc or mid-ocean ridge basalt chemical characteristics (Figure 5.2). Similarly, on the spidergrams of Pearce (1982) and Holm (1985) the average fine grained amphibolitic granulite analysis exhibits many of the characteristics of the average ocean floor basalt, although its LILE, Th and U concentrations tend to be high (Figure 5.2i,j). The more incompatible elements approximate unity, discriminating these analyses from the within plate basalts. Equally, the lack of a negative Nb or a positive Sr anomaly distinguishes these analyses from the low-K tholeiites.

d) Summary

The chemical characteristics of the amphibolite are typical of the continental flood basalts, which display extremely variable incompatible element abundances both within an individual province and between differing provinces. In particular, the continental flood basalts tend not to plot within a specific field on the various tectonic discrimination diagrams (Morrison 1978; Holm 1982; Bertrand 1991; Wang and Glover 1992). This is partially due to the chemical complexity of individual flood basalt provinces in which distinct chemical types may be identified, such as the markedly bimodal TiO_2 and P_2O_5 distributions distinguished in the Karoo and Paraná Provinces (Mantovani *et al.* 1985; Cox 1988; Piccirillo *et al.* 1988).

The major continental flood basalt provinces are related to an extensional phase, frequently occurring as a precursor to continental rifting, such as the Karoo Province (Cox 1988), the Deccan Traps (Mahoney 1988) and the North Atlantic Tertiary Province (Dickin 1988). They may also, however, develop behind a previously active continental margin immediately after the cessation of calc-alkaline volcanism, such as the flood basalts of the Columbia River Province (Hooper 1988), coincidental with a change from compressional to extensional tectonics (Hooper 1988; Carlson and Hart 1988). These may not be distinct environments, as noted by Cox (1988) who proposed that the Karoo volcanics developed in an environment analogous to a back arc basin.

The relatively restricted distribution of the Valley Trust Formation is, however, distinctly different from the large continental flood basalt provinces. Rather, its local character suggests comparison with an extensional back-arc basin, or rifting associated with the development of a small sea, which acted as a loci for sedimentation. Bimodal volcanism is found within these environments (Myrow 1995; Wever *et al.* 1995; Keppie and Dostal 1998), with the basaltic member of the series displaying both MORB and OIB characteristics (Winchester *et al.* 1995; Worthing and Crawford 1996; Sharkov and Smolkin 1997; Schofield *et al.* 1998; Keppie and Dostal 1998).

5.2.3 MGENI BATHOLITH

Petro *et al.* (1979) recognised the difficulties inherent in distinguishing the environment of emplacement of an unimodal acidic suite, but noted that several chemical features appear to be characteristic of specific environments. In

Figure 5.3. Sedimentary tectonic discrimination diagrams for the pelitic gneiss and fine grained granulite of the Valley Trust Formation.
a) DF2-DF1 (Bhatia 1983), b) K_2O/Na_2O-SiO_2 (Roser and Korsch 1986), c) TiO_2-Fe_2O_3+MgO (Bhatia 1983), d) Al_2O_3/SiO_2-Fe_2O_3+MgO (Bhatia 1983).
a,c and d for sandstones; b for sandstones and mudstones. Sandstones identified using Figure 4.7c (Wimmenauer 1984) .
For 5.3a. $DF1 = -0.0447SiO_2 - 0.972TiO_2 + 0.008Al_2O_3 - 0.267Fe_2O_3 + 0.208FeO - 3.082MnO + 0.14MgO + 0.195CaO + 0.719Na_2O - 0.032K_2O + 7.51P_2O_5 + 0.303$.
$DF2 = -0.421SiO_2 + 1.988TiO_2 - 0.526Al_2O_3 - 0.551Fe_2O_3 - 1.610FeO + 2.72MnO + 0.881MgO - 0.907CaO - 0.177Na_2O - 1.840K_2O + 7.244P_2O_5 + 43.57$.

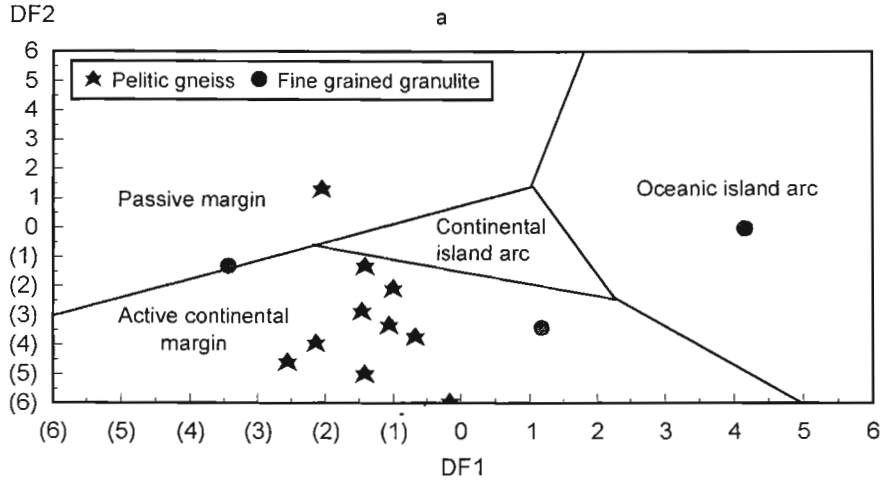

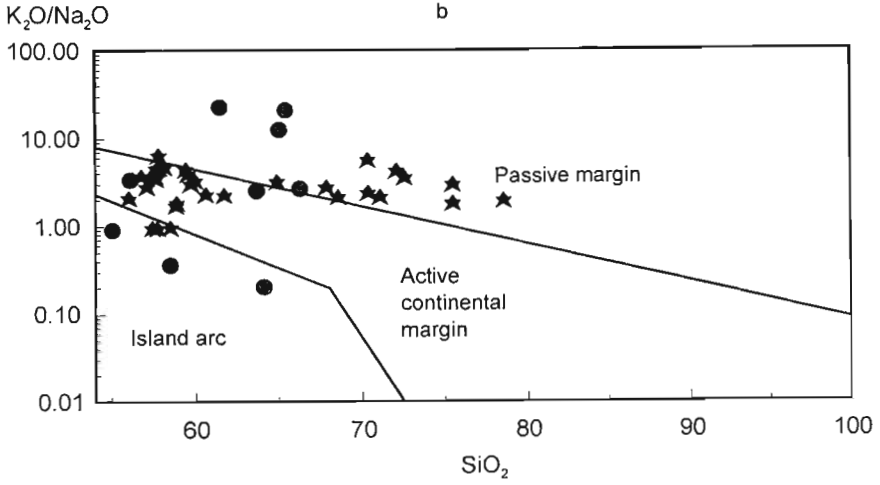

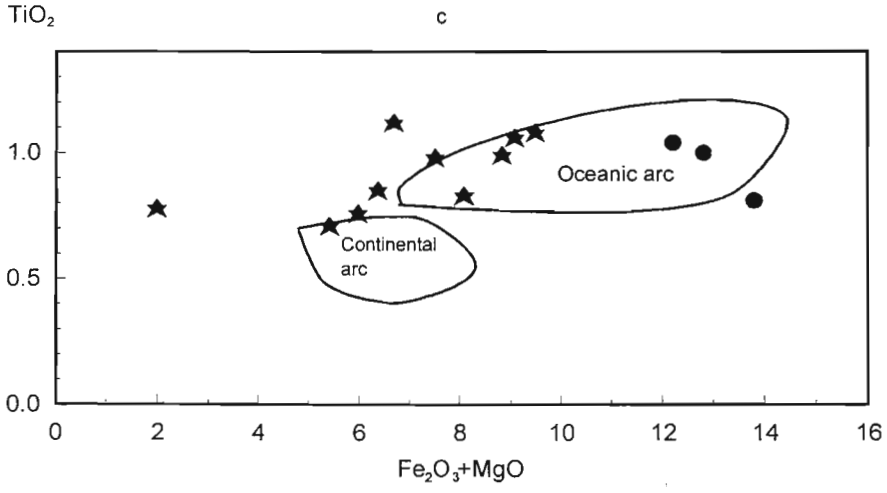

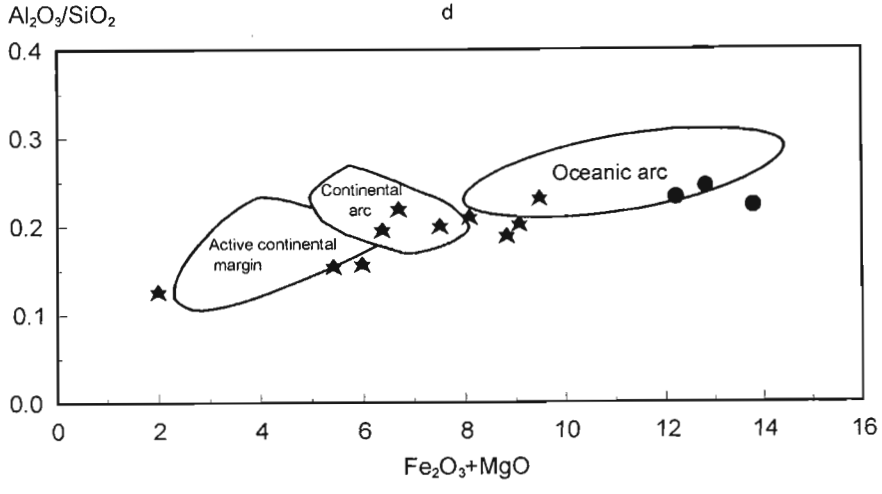

particular they found that the extensional suite granites possess lower CaO and CaO/Na_2O+K_2O but higher total alkalis and FeO/FeO+MgO than those granites developed in the compressional environment.

The chemical characteristics of the Mgeni batholith indicate features of both extensional - Mlahlanja Suite - and compressional - Ximba Suite - granitoids. This is particularly evident on the AFM diagram. Similar analysis of the Nqwadolo Suite is hindered by its limited range of silica, and no tectonic discrimination is possible using the methodology of Petro *et al.* (1979). The discriminant analysis of Agrawal (1995) generates a mixed signal, with individual granites within each of the megacrystic granite suites displaying orogenic and anorogenic characteristics. The Nqwadolo Suite possesses post-orogenic characteristics. On the log $CaO/Na_2O+K_2O-SiO_2$ diagram of Brown (1982), however, the granites plot in the extensional granite field. Equally, the presence of rare peralkaline granites in all the suites of the Mgeni batholith suggests an extensional environment (Petro *et al.* 1979).

Chemical discrimination of the Nqwadolo Suite suggests an origin as a within plate granite, but the Ximba and Mlahlanja Suites display mixed within plate and volcanic arc granite characteristics (Figure 5.1). On the R1-R2 diagram of Batchelor and Bowden (1985) the granites plot in the late orogenic and anorogenic fields.

On the ORG-normalised spidergram (Figure 5.1j,k,l), all the suites display enrichment in the LILE, discriminating them from the ocean ridge granites, but not the extreme enrichment of Rb found in the syn-collision granites. Particularly notable is the lack of a marked Ba anomaly for the Ximba and Mlahlanja Suites, suggesting development in a thin continental crust, with the negative Ba anomaly of the Nqwadolo Suite indicating growth of a thicker crust, while Nb concentrations are typically above unity. The other HFSE display variable degrees of enrichment or depletion but commonly Y is depleted, while Zr displays either slight enrichment or minor depletion. These features are characteristic of post-collision or within plate granites.

The high HFSE content of these granites is comparable to that of the A-type granites (Section 4.5.4), a series of distinct granites which intrude during the end phase of an orogenic cycle and in authentic anorogenic settings (Loiselle and Wones 1979; Collins *et al.* 1981; Pitcher 1983; Whalen *et al.* 1987; Sylvester 1989; Rogers and Greenberg 1990). These granites plot predominately as within plate granites on the diagrams of Pearce *et al.* (1984), but with overlap into the syn-collision and volcanic arc granite fields (Whalen *et al.* 1987), similar in distribution to the Mgeni batholith, but with less extension into the volcanic arc granite field.

A variety of broad chemical characteristics have been utilised to distinguish between the various A-type granite sub-groups (Rogers and Greenberg 1990). These, and in particular the high FeO, K_2O and Zr but low CaO content of the Ximba and Mlahlanja Suites, indicate an association with the anorogenic anorthosite and rapakivi granites. The low Y and Nb content of the Mgeni batholith suggest that it is late- to post-orogenic in character.

Emslie (1991) divided the A-type granites into the anorthosite-mangerite-charnockite-rapakivi granite (AMCG) suite and the late-orogenic-post-orogenic -anorogenic (LPA) suite. The presence of anorthosite was thought to distinguished the AMCG suite, but a variety of mineralogical, mineral chemical and bulk chemical data could also be used to separate these associations.

Although anorthosite has not been identified within the Natal Province, the abundant presence of charnockite suggests that the granites of the Mgeni batholith are related to the AMCG suite. This is supported by the high alkali content of these granites and the high FeO/FeO+MgO nature of their mafic mineral assemblage (Section 2.3). The relatively low FeO/FeO+MgO ratio of the Ximba Suite, however, overlaps with the LPA suite.

5.3 DISCUSSION

Identification of the tectonic setting of Precambrian aged high grade metamorphics and granites necessitates a comparison with data sets from known (Phanerozoic) locale, typically through the tectonic discrimination diagrams (for example Pharoah *et al.* 1987; Kalsbeek 1995; Mansfeld 1996). This process assumes that plate tectonic processes operated during the Proterozoic (Kerr 1985; Kröner 1991; Windley 1993; Passchier 1995; Hamilton 1998; de Wit, 1998) and that the chemical characteristics of individual rock types from the Proterozoic match those of the Phanerozoic (Pearce *et al.* 1984; Condie 1985; Taylor and McLennan 1985).

For high grade metamorphic rocks potential elemental mobility may influence the interpretation

of the tectonic discrimination diagrams. Although Winchester and Floyd (1976) suggested that the elements typically used for tectonic discrimination diagrams (Y, Ti, Zr) are immobile at amphibolite grades of metamorphism and possibly into the granulite facies (Fowler 1986; James *et al.* 1987; Winchester *et al.* 1998), *'Little is known about the stability of these elements'* beyond the amphibolite facies (Rollinson 1993). Evidence of immobile trace element mobility across the amphibolite/ granulite boundary is present in several studies (Figure 5.4), while mobility of these elements must be considered unequivocal for those granulites which have undergone a phase of partial melting. Dirks and Hand (1991), for example, noted the tenancy for zircon to dissolve when in contact with a melt, while Pidgeon and Aftalion (1978) and Williams *et al.* (1983) identified zircon entrainment within a melt. The tectonic discrimination diagrams have, however, been utilised for granulites (Winchester *et al.* 1998) and their capacity to identify the tectonic environment of these rocks must be considered if no evidence is available to suggest elemental mobility.

Within the Mapumulo Group, K/Rb ratios (88-492) comparable with crustal averages (Taylor and McLennan 1985), suggest that the possibility for misidentification of environments through elemental mobility is slight. Further, those discrimination plots which have been constructed using potentially mobile elements, such as the Zr-Ti-Sr plot of Pearce and Cann (1973), have not been considered for the high grade metamorphics of the Mapumulo Group.

An exception are the granitic tectonic discrimination plots of Pearce *et al.* (1984), which utilise the potentially mobile element Rb (criticised by Rollinson 1993). These have been applied to the quartzo-feldspathic gneisses, with potential misidentification of the tectonic environment of these units through Rb depletion from the higher levels common to the syn-collision granites to the lower levels of the volcanic arc granites during granulite grade metamorphism and partial melting. K/Rb ratios within the quartzo-feldspathic gneisses (202-426) do not, however, indicate any marked deviation from comparable unmetamorphosed lithologies (Taylor and McLennan 1985).

Rb mobility may also occur during low grade alteration of granites (Alderton *et al.* 1980; Petersson and Eliasson 1997). Evidence for elemental mobility within the granites of the Mgeni batholith is, however, lacking with the various suites displaying K/Rb ratios (121-421) comparable to typical crustal material (Taylor and McLennan 1985).

Any Rb mobility is therefore considered to have been minimal in extent, with limited potential for influencing the identification of the tectonic environment of the various units present within the Valley of a Thousand Hills.

The uncertainty regarding the specific relationship between rock chemistry and tectonic environment has resulted in criticism of the tectonic discrimination diagrams (Arculus 1987; Duncan 1987; Twist and Harmer 1987; Myers and Breitkopf 1989). The observed connection between certain rock types and tectonic environments, however, suggests a more than casual association and the possibility of geochemical characterisation of tectonic environments (Clarke 1992; Rollinson 1993; Förster *et al.* 1997). This may be related to an environmentally specific source or evolution process within an individual tectonic environment. Pearce *et al.* (1984), for example, noted that their tectonic discrimination plots for granites *'strictly reflect source regions (and melting and crystallizing histories) rather than tectonic regimes'*, while distinct sources for basalts from different environments have been proposed (Hedge and Peterman 1970; Hart 1971; Pearce 1982; Frey and Roden 1987; Hart and Zindler 1989). If such is the case then the tectonic discrimination diagrams may more properly be considered to identify the source material specific to a tectonic environment rather than the tectonic environment.

5.3.1 BASALTS

Initial attempts to discriminate the tectonic environment of basalts have focused on three primary environments:

1) within plate;
2) mid-oceanic ridge; and
3) arc.

Although numerous tectonic discrimination diagrams have been developed to distinguish these environments, a considerable degree of overlap is typically found between individual environments (Pearce 1982) hindering their identification. This may be partially due to the inclusion in these diagrams of data from the complete range of basalt mineralogical and chemical subtypes - tholeiitic, calc-alkaline and alkaline - which may have originated and evolved uniquely. To minimise this potential complexity in basalt tectonic discrimination, comparison should be limited to

Figure 5.4. Immobile elemental mobility across the amphibolite/granulite boundary.
a) Zr-Y, b) TiO_2-Zr (data from Raith and Srikantappa 1993), c) Zr-Y, d) TiO_2-Zr (data from Garde 1990).

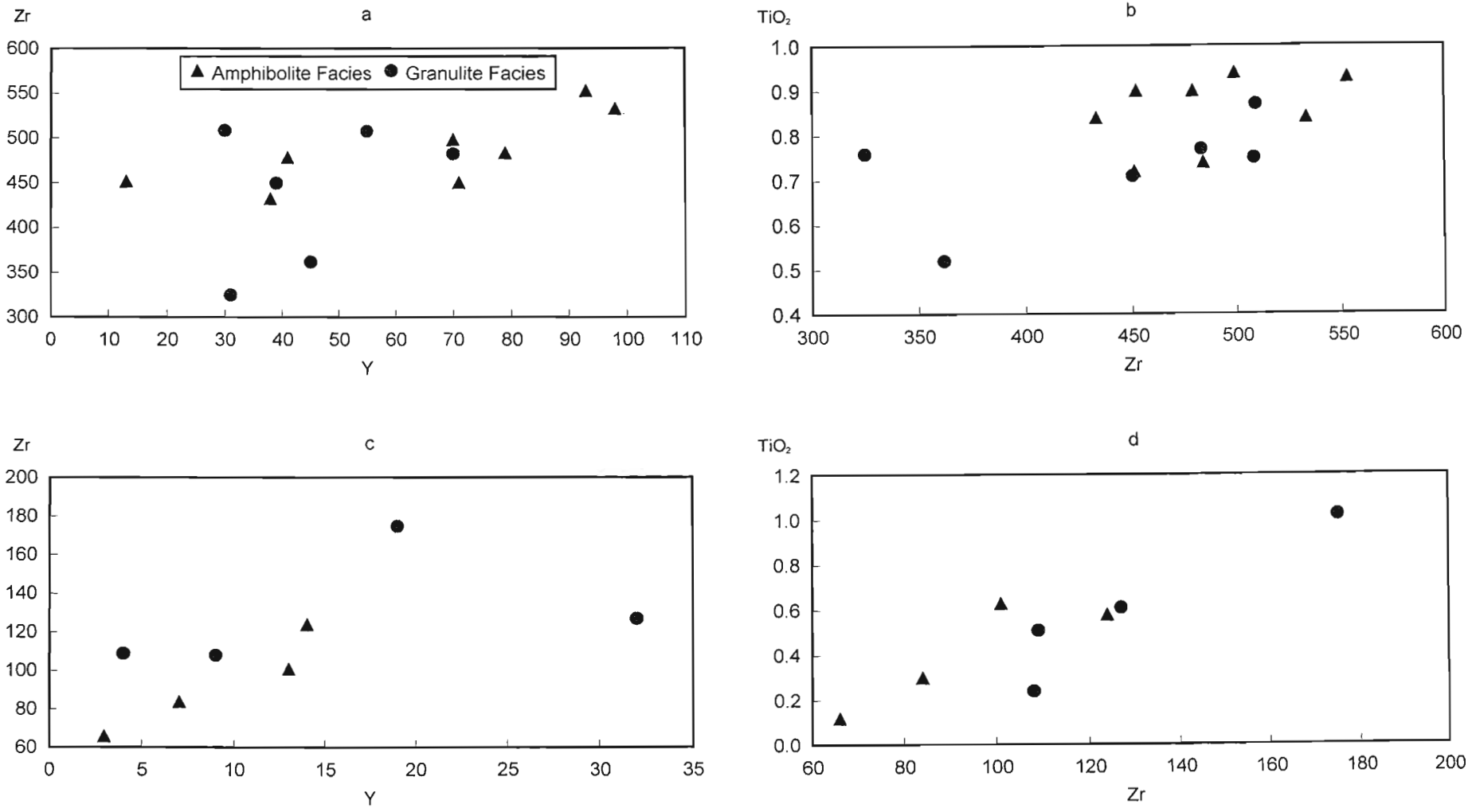

individual chemical types. This is illustrated in Figure 5.5a where data from tholeiitic basalts from a variety of sources are displayed on the Cr-Y diagram. No clear discrimination of the different tectonic environments is achieved at this level, but elimination of the more evolved members of the various series results in the separation of the arc volcanics from the ocean island tholeiites and mid-oceanic ridge basalts (Figure 5.5b), for which no division is possible, as noted by Pearce (1982). A similar scenario is illustrated on the TiO_2-Zr (Figure 5.5c) and Zr/Y-Zr (Figure 5.5e) diagrams, with no distinct discrimination of the individual environments if the full data sets are employed, while utilisation of only the less evolved members of the series allows a clearer division of the different environments (Figure 5.5d,f).

For the basaltic rocks the less evolved members of an individual series best specify the tectonic environment of the series. This is to be expected if the chemical characteristics which define the tectonic environment are inherited from the source material. A provisional reinterpretation of the basaltic tectonic discrimination diagrams is therefore undertaken based on this conclusion and utilising this data set. This provides highly variable results, indicating that the fields defined on the Cr-Y diagram by Pearce (1982) do not discriminate the various environments, with the MORB and WPB displaying considerable overlap with the arc basalt field. The fields defined on the TiO_2-Zr and Zr/Y-Zr diagrams, however, are similar to those of Pearce (1982; 1983), but with a clearer discrimination of the various environments, and in particular on the Zr/Y-Zr plot.

Classification of the Nagle Dam Formation amphibolite is complicated by its transitional tholeiitic/calc-alkaline nature (Figure 4.4b). On all the derived diagrams it plots with the mid-oceanic ridge basalts, suggesting a possible mid-oceanic ridge basalt source rather than an arc source. This contradicts the strong LILE enrichment of the amphibolite, a characteristic of the arc basalts through the interaction of slab and crustal sources and might reflect its non-tholeiitic character. As noted by Pearce (1982) the calc-alkaline arc basalts approach MORB levels of HFS element concentrations. Ramsey *et al.* (1984) also found MORB type HFS element concentrations in the primitive arc magmas.

The tholeiitic nature of the medium grained amphibolite of the Valley Trust Formation is compatible with the derived diagrams. The Cr-Y diagram (Figure 5.5b) demonstrates its non-arc character, and on the TiO_2-Zr and Zr/Y-Zr diagrams (Figure 5.5d,f) it plots predominately within the MORB field, but with extension parallel to the WPB to higher TiO_2 levels on the TiO_2-Zr diagram (Figure 5.5d).

The continental flood basalts were not included in the derivation of the revised tectonic discrimination diagrams, as they are considered to have been derived from a heterogeneous source with a complex evolutionary history including variable degrees of crustal assimilation (Carlson and Hart 1988) resulting in their nonclassification on a variety of tectonic discrimination plots (Holm 1982). Elimination of the more evolved members of individual continental flood basalt suites from consideration may, however, result in a minimisation of the effects of crustal assimilation, allowing greater specification of the original chemistry of the basaltic melt and the potential definition of a continental flood basalt field on the tectonic discrimination diagrams

Data from the Karoo Province are illustrated in Figure 5.6, with the development of distinct chemical subgroups on individual diagrams comparable with either the mid-oceanic ridge or within plate basalt data sets in Figure 5.5. This suggests an origin from a heterogeneous source zone, with both within plate basalt and mid-oceanic ridge basalt type source material. Detailed analysis of individual continental flood basalt provinces, however, have indicated that the low-Ti basalts may have originated at least partially from a lithospheric source (Peate and Hawkesworth 1996). On the derived diagrams these basalts plot in the field of mid-oceanic ridge basalts, suggesting that this may be a composite field, representing a variety of potential sources.

Comparison with the Valley Trust Formation amphibolite suggests a similarity to the low-Ti portion of the Karoo series but with the amphibolite originating from a lower Zr/Y source (Figure 5.6f). The Ti-Zr diagram (Figure 5.6d), however, discriminates between the amphibolite and the low-Ti Karoo basalts and indicates a trend for the amphibolite parallel to the Karoo series, but at a lower Zr concentration.

This suggests the derivation of the amphibolite from a heterogeneous source with both mid-oceanic ridge, lithospheric mantle and within plate basalt characteristics, differing considerably from that of the Karoo Province, and in particular with lower Zr concentrations. Comparison with the trace element data of Le Roux *et al.* (1983)

Figure 5.5. Evaluation of basaltic tectonomagmatic discrimination diagrams and comparision with the amphibolites of the Nagle Dam and Valley Trust Formations.
a , b and e - discrimination using full data sets. b, d and f - discrimination using unevolved data only.
Data from Dickey *et al.* (1977), Wood (1978), Bryan *et al.* (1981), Le Roex *et al.* (1981), Le Roex and Dick (1981), Le Roex and Erlank (1982), Le Roex *et al.* (1983), Bender *et al.* (1984), Le Roex (1985), Johnson *et al.* (1985), Weaver *et al.* (1987), Caroff *et al.* (1995):
MORB - Mid oceanic ridge basalt; OIB - Ocean island basalt; IAT - Island arc tholeiite.

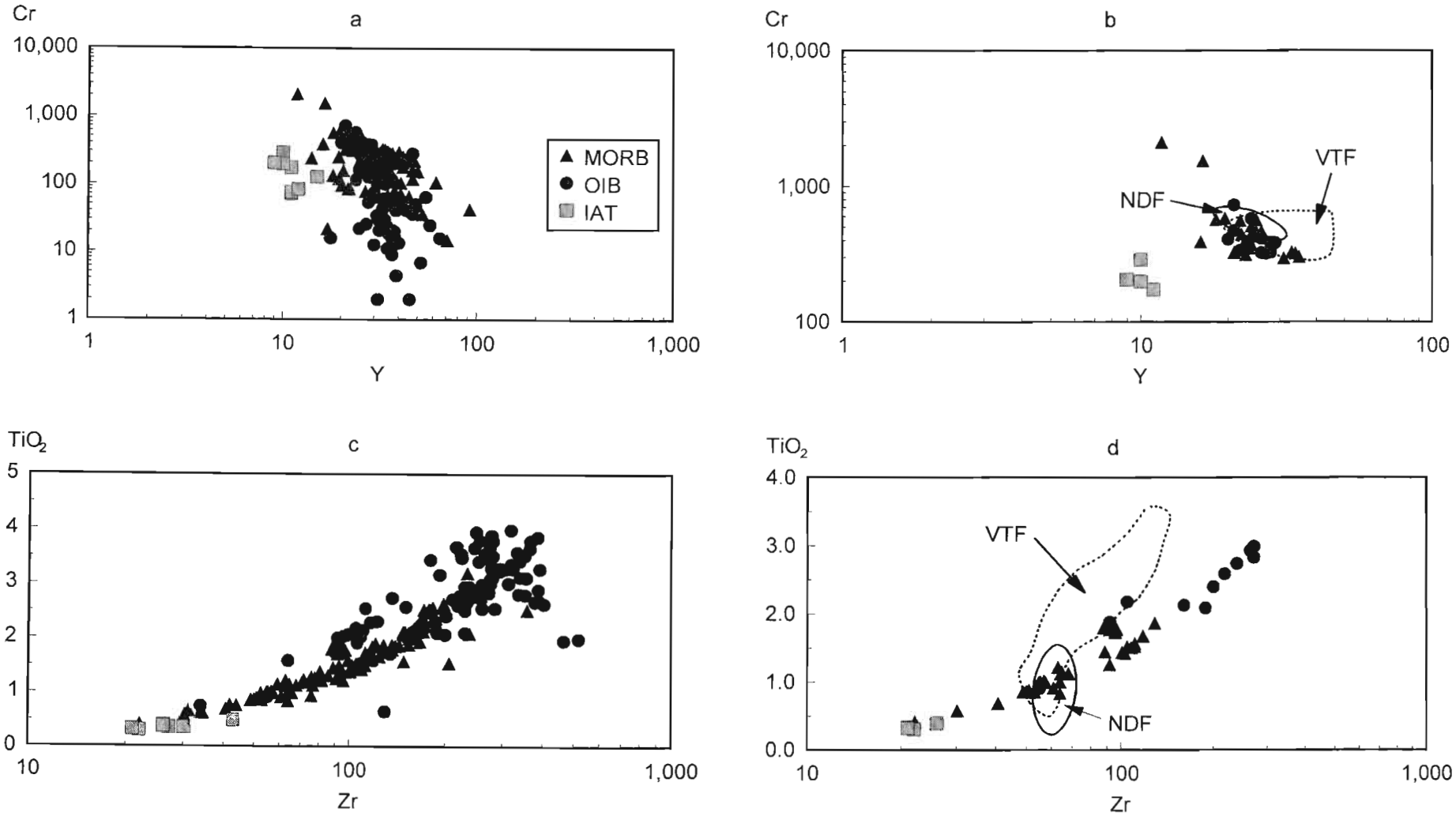

Figure 5.5. - continued.

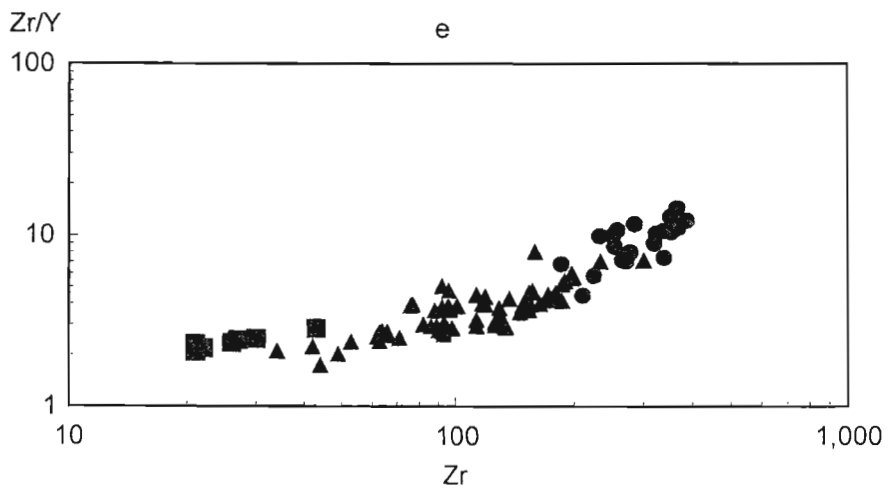

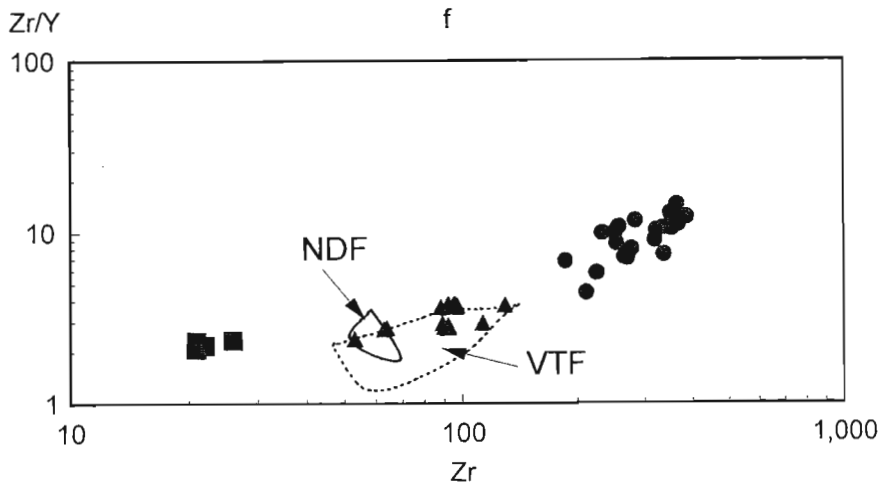

Figure 5.6. Evaluation of basaltic tectonomagmatic discrimination diagrams for the Karoo volcanics and comparision with the amphibolite of the Valley Trust Formation. Comparision of the amphibolite, Valley Trust Formation, and MORB subdivisions of Le Roux *et al.* (1983).
a , c and e - discrimination using full data sets. b , d and f - discrimination using unevolved data only. Data from Erlank (1984).
g and h - comparision with Le Roux *et al.* (1983). N-type MORB - normal MORB, P-type MORB - MORB with plume chemical characteristics , T-type MORB - transitional MORB, after Le Roux *et al.* (1983).

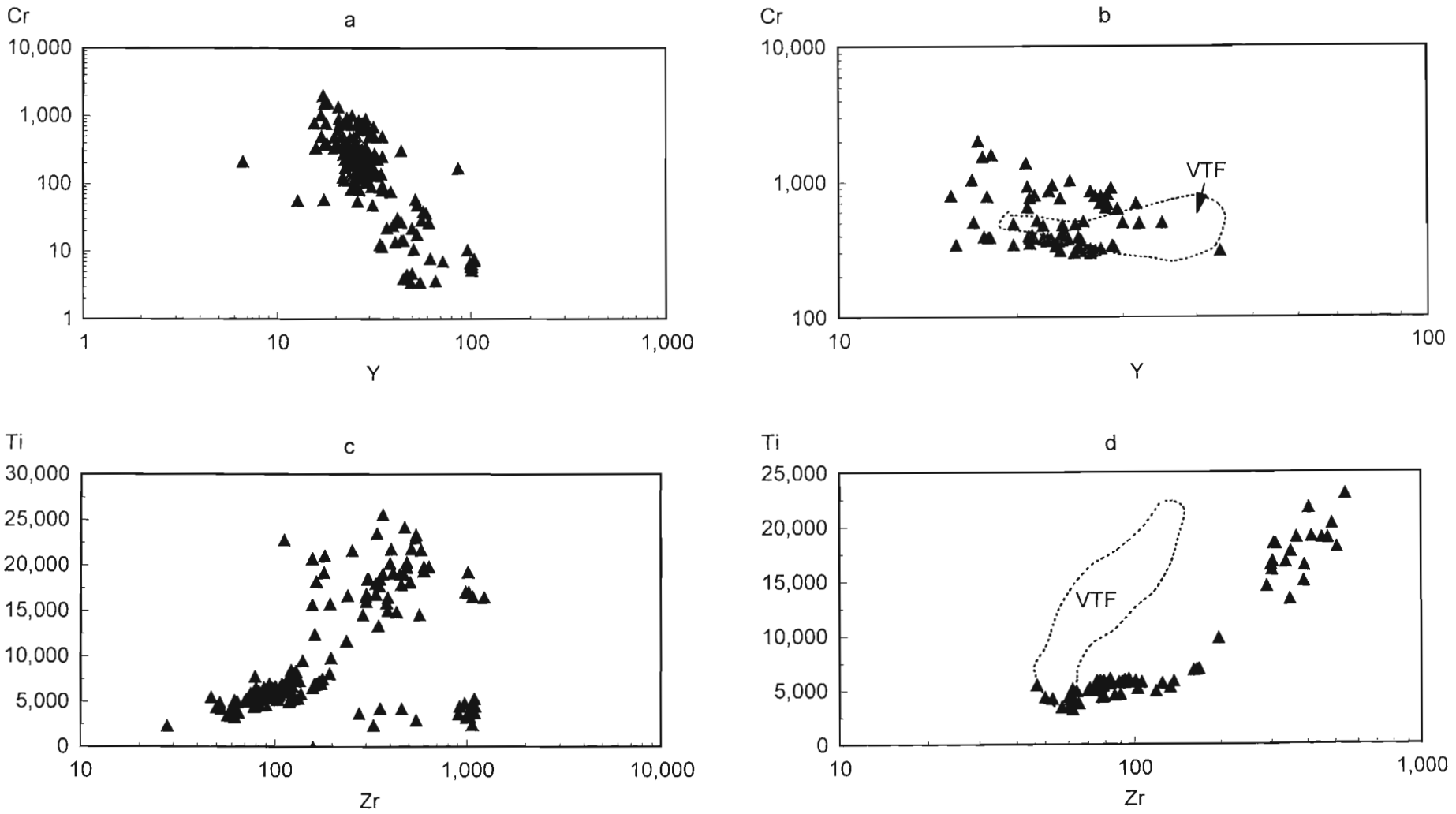

Figure 5.6. - Continued.

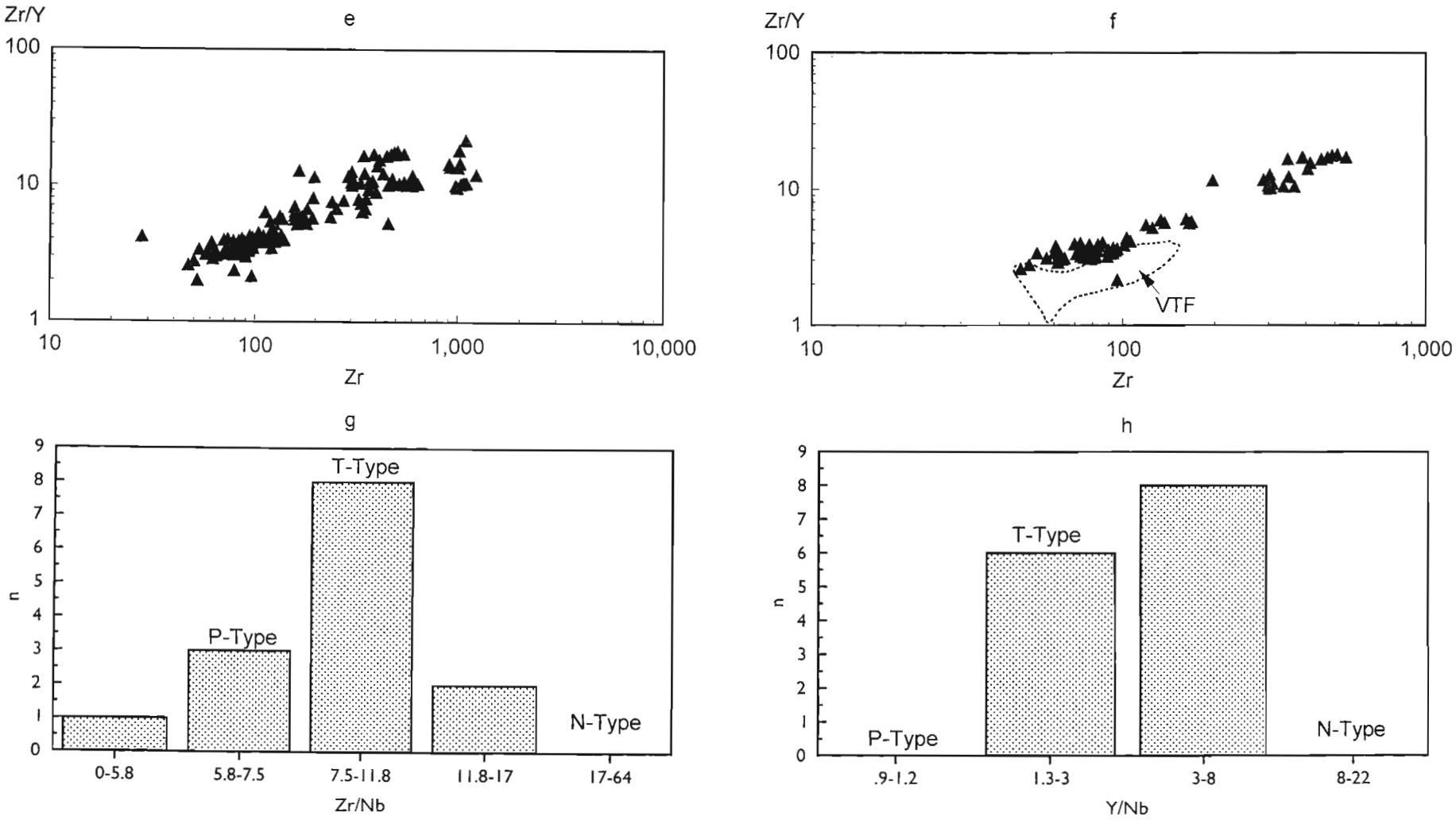

indicates that the amphibolite possesses a chemistry transitional between those of plume basalts and normal mid-oceanic ridge basalts, suggesting a variably enriched source zone (Figure 5.6g, h).

5.3.2 GRANITES

For the granites a more complex relationship exists between the environment and source, through the interaction with older crustal material. Attempts to identify distinct crustal sources for granites, such as Chappell and White (1974) and Chappell (1996a), have been hindered by the nature of the crust and the difficulty in discriminating the different potential sources (Collins 1996), although Pitcher (1983) proposed that a simple relationship exists between the source and the environment for granites. Given the complexity of the continental crust this model appears unlikely, but may have an influence within juvenile crust or for minimum melts.

Pearce *et al.* (1984) rationalised a petrogenetic basis for their granitic tectonic discrimination diagrams through variations in the mantle sources for the various granite types, implying a relationship between the source and tectonic environment for the granitic rocks similar to that for the basalts. Isotopic data, however, suggest a crustal component in the majority of granites (Clarke 1992), limiting the applicability of this model, but the MASH model for granite generation (Hildreth and Moorbath 1988), which proposes granite derivation through a complex process of interaction between basalt and the crust, may allow a system whereby mantle chemical signatures are transferred to granitic melts. Base level magmas generated through MASH processes may form the starting points for further chemical evolution in the way Pearce *et al.* (1984) utilised mantle source points in explaining the derivation of the tectonic discrimination diagrams.

Potential generation of the chemical characteristics of the volcanic arc granites through the fractionation and contamination of volcanic arc basalts was demonstrated by Hildreth and Moorbath (1988) and is compatible with the majority view that arc granites require distinct basalt and crustal sources (Clarke 1992). The majority of models for the derivation of the A-type granites, however, involve partial melting, typically of a lower crustal or depleted granulite source, or basalt fractionation, although the isotopic data suggest a degree of crustal interaction for the latter (Table 6.1). In Figure 5.7 the potential for crustal contaminated within plate basalts to serve as source points for AFC arrays to generate within plate granites is demonstrated. This model is discussed in more detail in Section 6.5.

Generation of granitic melts through interaction with a basaltic melt suggests that the more basic but noncumulate portion of the granite series would provide the best indicators of tectonic environment. As with the basaltic rocks evolution of the granitic melts through fractionation, contamination or a combination of processes would tend to remove the granitic magma from the unique chemical characteristics of the tectonic environment, as suggested by Förster *et al.* (1997). This is particularly true for the effects of contamination as the potential contaminant may possess a variety of chemical characteristics.

Following the proposed model the within plate granites should comprise a series related through variable degrees of fractionation of granitic magma generated by the interaction of continental material with an enriched basalt, each component contributing to a different degree in individual granites. Further, the mantle input may be primary or secondary, through partial melting of flood basalts (Cleverly *et al.* 1984; Garland *et al.* 1995). Additional acidic material may be derived through crustal melting with no chemical input from the mantle melt (Cleverly *et al.* 1984).

No simple chemical signature therefore defines the within plate granites, rather their chemistry is related to a combination of the process and source rock. This complicates any interpretation of the tectonic environment of the granites. Certain generalities can, however, be proposed and in particular that either the mantle input or the crustal component controls the chemical signature of the granites, with the within plate chemical characteristics suggesting the addition of enriched mantle material into the crust either as a primary melt or as a secondary source. A variety of chemical characteristics can, however, develop within the extensional environment, including arc type granites derived through partial melting of an arc source material with a minor enriched mantle contribution (Encarnación and Mukasa 1997). Interpretation of these features may allow the analysis of both the tectonic history of an area and the various controls on granite generation.

Three distinct granite subgroups may therefore be distinguished:

1) granites derived directly from mantle source

Figure 5.7. Contaminated within plate basalts as a potential source for within plate granites. Granitic tectonomagmatic discrimination diagrams (Pearce *et al.* 1984) with fields extended to lower silica levels.
A-type granite data from Ramo (1991), Tack *et al.* (1994), Duchesne and Wilmart (1997); basalt analyses from Hooper (1988).

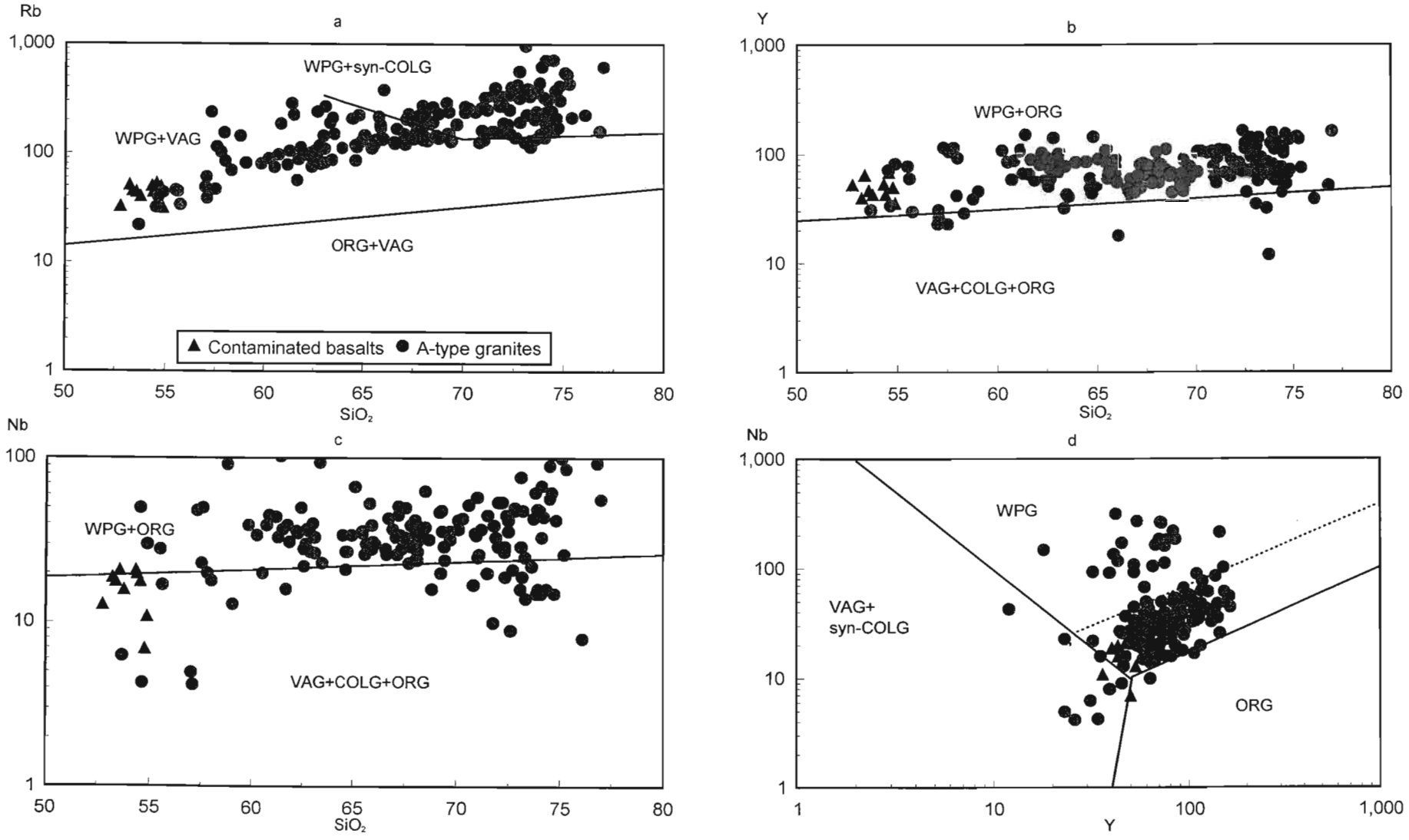

material;
2) granites with a crustal source; and
3) granites with a mixed source;

corresponding to the cafemic, aluminous and alumino-cafemic associations of Debon and Le Fort (1982). Of these groupings those with direct mantle input should provide chemical evidence of the tectonic environment within which they originated. Those granites which are derived directly from a crustal source with no chemical input from mantle material, however, will not, but rather provide data concerning the nature of the crustal source material (Twist and Harmer 1987). These granites will be generated primarily, but not exclusively, within the post-collision environment through overthickening of the crust (England and Thompson 1984; 1986), and should therefore be excluded from the tectonic discrimination diagrams, where they overlap several of the delineated fields (Pearce *et al.* 1984) and are considered to form a distinct tectonic subgroup (Harris *et al.* 1986b).

Recognition of the tectonic environment of an individual granite is complicated by these complexities, and in particular simple interpretations using trace element abundances may be erroneous. Rather the gross chemical and mineralogical characteristics of the granite and its relationship with associated rock types must be considered, with the trace element data from the more primitive members of the series. In the case of the Ximba Suite, for example, its overall chemical and mineralogical characteristics suggest an A-type granite while its more basic portions possess the HFS element enrichment of a within plate granite, but its general trace element data indicate an origin within a volcanic arc (Figure 5.1). This might result from the contamination of the melt with a arc type material masking the enriched mantle input or through the accumulation of felsic material. A similar model might apply to the quartzo-feldspathic gneiss of the Valley Trust Formation. The more distinct within plate granite chemical signature of the Mlahlanja Suite, however, implies a larger enriched mantle input, as does its low Sr_I.

On the A-B diagram of Debon and Le Fort (1982) the various units identified within the Valley of a Thousand Hills are compared with those of typical crustal sourced granites and the Peruvian batholith, the latter as an example of a granite potentially derived through MASH processes (Figure 5.8). For the Nagle Dam Formation and the megacrystic granites of the Mgeni batholith their distinct fractionation profiles, paralleling that of the Peruvian batholith, indicate their mixed crustal and mantle origin. The limited data range of the quartzo-feldspathic gneiss of the Valley Trust Formation and the Nqwadolo Suite hinder this comparison, but the trend of these units appears to mimic the fractionation path of certain crustal melts, which for the Nqwadolo Suite, with its high Sr_I, strongly implies a predominately crustal origin. The high HFSE content of the Nqwadolo Suite, however, suggests an enriched component in its source material, indicating an origin through partial melting of crustal material and the addition of an enriched basalt component. The quartzo-feldspathic gneiss of the Valley Trust Formation is not enriched, suggesting that it represents a pure crustal melt. No tectonic discrimination can therefore be undertaken for this unit.

5.4 CONCLUSIONS

Tectonic discrimination analysis indicates that during the Proterozoic the Valley of a Thousand Hills evolved through a variety of mantle and mantle+crustal melt inputs. Initially a volcanic arc mantle source, perhaps associated with an intraoceanic subduction process, was tapped to derive the Nagle Dam Formation. Subsequently an extensional phase developed with basaltic volcanism generated from a heterogeneous source but with an enriched mantle component, and acidic magmas, largely crustal sourced. Sedimentation resulted from the weathering of arc material.

Following arc collision and the associated high grade metamorphism which terminated the initial phase of crustal development in the Valley of a Thousand Hills, the megacrystic granites of the Mgeni batholith intruded the gneisses. These contain an enriched mantle component, but appear to be predominately crustal sourced or to contain a primary crustal component.

This simplified model for the tectonic evolution of the Valley of a Thousand Hills is illustrated in Figure 5.9. This will be refined and expanded for Central KwaZulu Natal in Chapter 7.

Figure 5.8. Comparision of the fractionation trends of the Mgeni batholith, Nagle Dam Formation (excluding amphibolite) and quartzo-feldspathic gneiss of the Valley Trust Formation, with the calc-alkaline Peruvian batholith (Pitcher *et al.* 1985) and aluminous association of Debon and Le Fort (1982).
A=Al-(K+Na+2Ca), B=Fe+Mg+Ti, expressed as gram-atoms x10^3 of each element in 100g rock (Debon and Le Fort 1982).

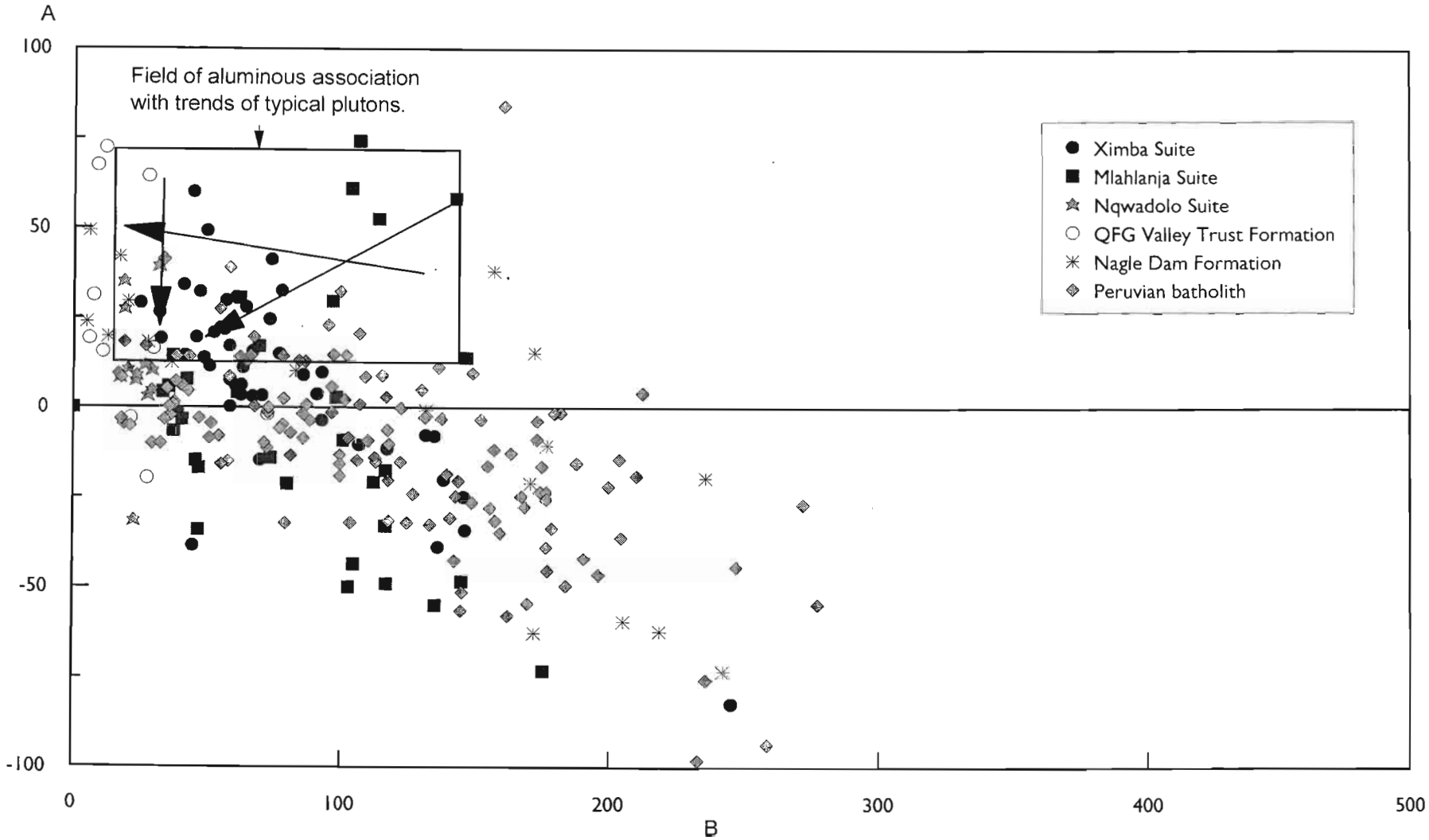

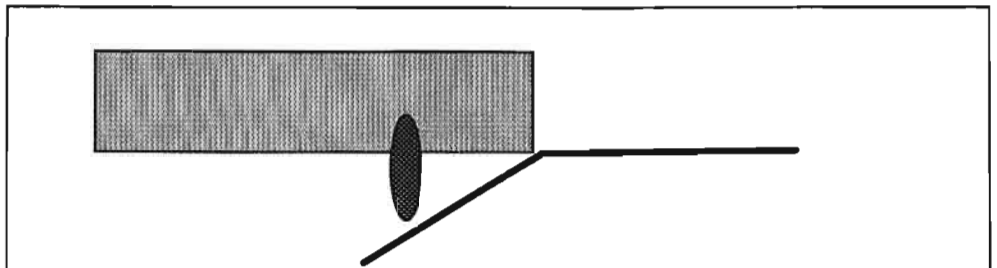

a. Formation of the Mgeni arc - Nagle Dam Formation - above a subduction zone.

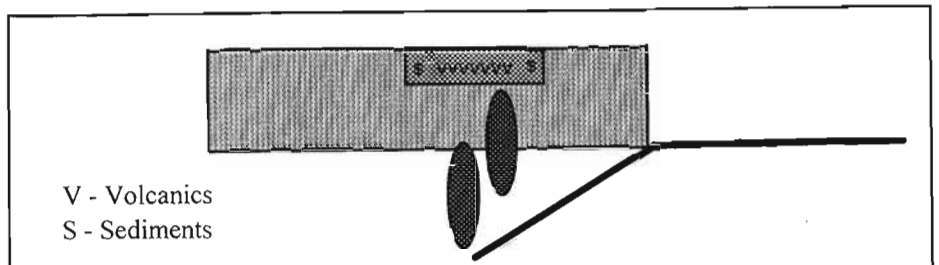

b. Interarc rifting with intrusion of primitive arc magmas (amphibolite) and deposition of sediments (pelitic gneiss).

c. Rifting and intrusion of Valley Trust Formation amphibolite. Crustal partial melting - quartzo-feldspathic gneiss. Sedimentation.

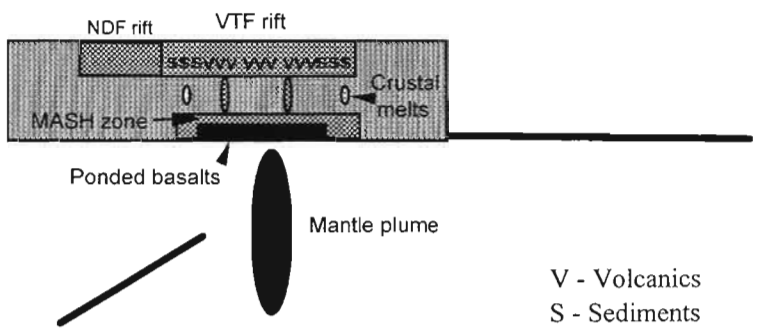

d. Arc collision and metamorphism.

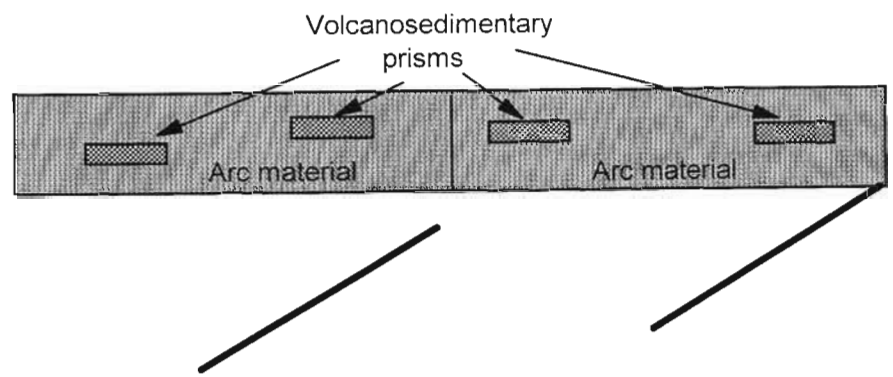

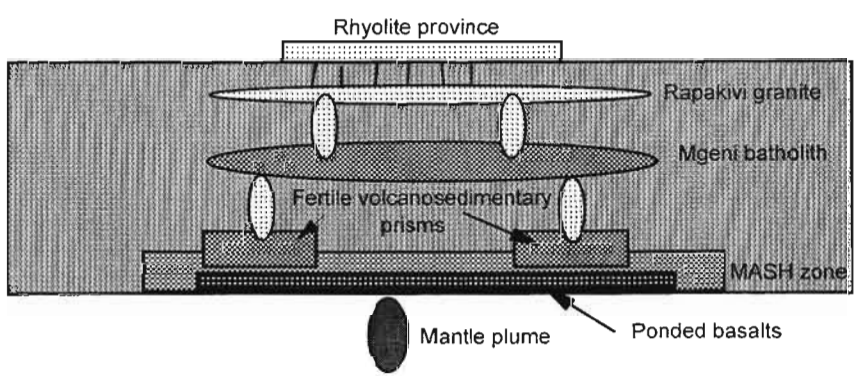

Figure 5. 9. Tectonic evolution of the Valley of a Thousand Hills during the Proterozoic.

CHAPTER 6

PETROGENESIS

6.1 INTRODUCTION

No petrogenetic models are available for the Nagle Dam and Valley Trust Formations. Analysis of the geochemical and isotopic data from the megacrystic phases of the Mgeni Batholith, however, has resulted in the development of a number of petrogenetic models to explain their interrelationship, including:

1) fractionation of a single magma pulse (Kuyper 1979);
2) multiple magma pulses (Kerr 1985); and
3) country rock contamination of an initial Ximba Suite magma (Eglington 1987; Kerr *et al.* 1987; Eglington *et al.* 1989a; Kerr and Milne 1991a).

These models were reviewed by Kerr and Milne (1994), who concluded that none were capable of explaining all the observed features of the granites, for which evidence exists for the operation of a variety of concurrent processes, including assimilation of country rocks and mixing with melts derived from the partial melting of pelitic enclaves. Similarly, a number of petrogenetic models have been proposed for the Nqwadolo Suite, which was believed to have originated through either the differentiation (Du Toit 1979) or the partial melting (Kuyper 1979) of the megacrystic granites. The distinct isotopic composition of the Nqwadolo Suite (Eglington 1987), however, led Kerr (1985) to propose its derivation from a discrete magma pulse. The various members of the Mgeni Batholith and the Oribi Gorge Suite are considered to have originated through the partial melting of a juvenile crustal source (Kerr *et al.* 1987; Eglington *et al.* 1989b), possibly depleted from an earlier melting event (Thomas 1988a).

This chapter therefore attempts to develop petrogenetic models for the various metamorphosed sequences within the Valley of a Thousand Hills, including the identification of potential source materials for certain of the ortho and paragneisses. A petrogenetic model for the individual granite series within the Mgeni batholith will also be proposed, and extended to include the granites of the Oribi Gorge Suite. In addition, a model for the generation of the A-type granites will be derived.

6.2 NAGLE DAM FORMATION

6.2.1 INTRODUCTION

Chemical variability within the Nagle Dam Formation suggests that it comprises a series of distinct units (Section 4.3.5):

1) amphibolite;
2) biotite hornblende gneiss; and
3) quartzo-feldspathic gneiss;

with further subdivision of the gneisses possible from the available chemical data (Section 4.3.5).

No previous petrogenetic model has been presented for these series.

6.2.2 AMPHIBOLITE

The majority of the amphibolite samples plot adjacent to the 1 atm. plag-ol-cpx+liq cotectic of Thompson *et al.* (1983), suggesting that the original basaltic magma last equilibrated in a low pressure environment, although individual samples display evidence for crystallisation at higher pressures. Declining compatible element concentrations with fractionation, including Ni (Figure 6.1a), Cr and CaO; FeO enrichment; and constant Sr and Al_2O_3 indicate that the original magma may have evolved through low pressure fractionation of olivine + clinopyroxene + plagioclase (Cox 1980; Cox and Hawkesworth 1985). Major element fractionation modelling is, however, unable to derive the range of compositions present in the amphibolite, and in particular its variable K_2O/Na_2O ratios. This has not been improved by the elimination of those analyses that produce the majority of the scatter observed on the X-MgO fractionation diagrams, although this revision eliminates the necessity for significant plagioclase fractionation. The low Cr and Ni content of the amphibolite (comparable with the upper intrusives of DeBari 1997) suggests a minimum role for cumulate accumulation, with cumulate modelling generating a silica deficient evolved composition.

The high MgO content of the amphibolite suggests comparison with the primary arc magmas (Figure 4.3) of Smith *et al.* (1997), but in contrast with these basalts (Ramsey *et al.* 1984; Eggins 1993) the amphibolite displays a minor degree of intragroup fractionation, as defined by MgO (Figure 6.1a), while FeO and CaO concentrations vary considerably. Similarly, the Y-Zr and Zr/Y-Zr fractionation trends of the amphibolite do not

Figure 6.1. Petrogenesis of the Nagle Dam Formation amphibolite.
a) Ni-MgO, b) Zr/Y-Zr (comparision with typical high MgO basalts, data from Ramsey *et al.* (1984) and Eggins (1993)),
c) K_2O/P_2O_5-MgO/MgO+FeO (fractionation and ACF trends after Carlson and Hart 1988), d) Rb/Zr-Zr (fractionation, assimilation and metasomatic trends after Smith *et al.* 1997).

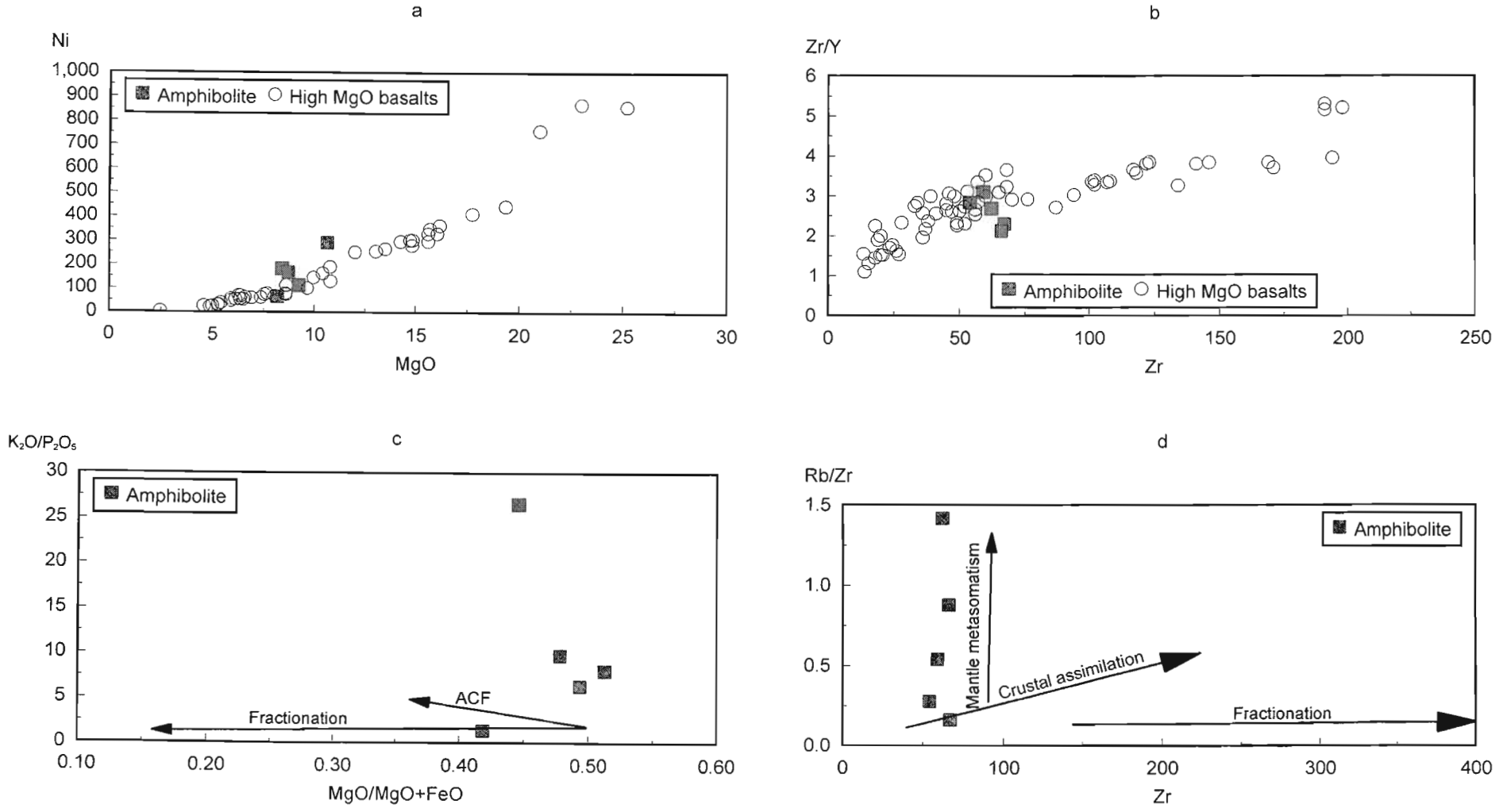

match those of the high MgO basalts (Figure 6.1b).

The highly variable trace element data do not suggest that the amphibolite developed from a single fractionating series. In particular, divergence in the Rb/Zr-Zr relationship and the lack of Zr enrichment within the series (Figure 6.1d) are inconsistent with a model of fractionation from a single magma. This is supported by the scatter on the X-MgO fractionation diagrams, the poorly defined fractionation trends and differences in incompatible element ratios, such as Rb/Zr-MgO and Ba/Zr-MgO. The amphibolite similarly does not follow the mixing lines of Johnson *et al.* (1985). The trend of increasing K_2O/P_2O_5 ratios with fractionation parallels the ACF trend of Carlson and Hart (1988), but at higher levels (Figure 6.1c), suggesting that the chemical character of the amphibolite was not derived through crustal assimilation.

Variable Y with declining Cr (Figure 5.2e) indicates a derivation through either differing degrees of partial melting of a common source with fractionation or partial melting of distinct sources with fractionation (Pearce 1982). The latter is supported by variations in the Ti/Y-Nb/Y ratio, which, although predominately comparable with arc basalts, also displays characteristics typical of an origin from an alkaline source, indicating possible mantle heterogeneity. Similarly, the highly variable Rb/Zr ratio at constant Zr (Figure 6.1d) is consistent with derivation from a chemically heterogeneous source (Smith *et al.* 1997).

Comparison with the average arc basalts reveals a highly enriched LIL element content, with relative enrichment of Nb, P, Zr and Cr (Pearce 1982). This pattern is similar to that of the transitional arc basalts of Pearce (1982), which were considered to have resulted from mantle enrichment, including a potential within plate component.

6.2.3 BIOTITE HORNBLENDE GNEISS

Within the biotite hornblende gneiss, elemental distribution patterns (Figure 4.3) suggest the fractionation of a Fe-Mg phase, probably hornblende, plagioclase, Fe-Ti oxides and zircon, with a minor role for K-feldspar and biotite fractionation (Tindle and Pearce 1981; Atherton and Sanderson, in Pitcher *et al.* 1985; McDermott *et al.* 1996), and the possible presence of a cumulate phase indicated by occasional high Sr concentrations (Rapela and Pankhurst 1996). These trends do not, however, appear related to simple variations in silica, and assist in the definition of the distinct series identified within the biotite hornblende gneiss (Section 4.3.5).

a) Low Silica Series

Elemental variations in the low silica series suggest the fractionation of plagioclase, a mafic phase, probably hornblende, zircon and Fe-Ti oxides (Tindle and Pearce 1981; Atherton and Sanderson, in Pitcher *et al.* 1985; Rapela and Pankhurst 1996; McDermott *et al.* 1996). Major element fractionation modelling, however, does not produce an acceptable model, with the primary fractionation of plagioclase incompatible with the increasing silica content of the melt during fractionation. Major element cumulate modelling (Appendix 5.1), utilising as an initial melt composition the average of the available analyses and sample UND 327 (lowest Na_2O, Sr, Zr concentrations and highest Rb content) as the evolved melt, provides a model, for which the sum of the squares of the residuals (SSR) is 0.06, for a cumulate assemblage of:

hornblende + plagioclase + magnetite + ilmenite + apatite.

Trace element modelling generates the required range of elemental compositions, with the cumulate phase high in Sr but low in Ba and Rb, and evolving towards lower Sr but higher Ba and Rb. The potential cumulate does not, however, plot with the model cumulate, while the more evolved portion of the series displays a degree of scatter around the model melt trend (Figure 6.2). These features may indicate incomplete melt/cumulate separation.

b) High Silica Series

The high silica series displays elemental variations compatible with the fractionation of a mafic phase, probably hornblende, and plagioclase (Tindle and Pearce 1981; Atherton and Sanderson, in Pitcher *et al.* 1985; Rapela and Pankhurst 1996; McDermott *et al.* 1996). Major element fractionation modelling (Appendix 5.2), with sample UND 315 taken to represent the initial melt (highest FeO and CaO but lowest K_2O, Rb and Ba), the most siliceous sample, UND 300, as the evolved melt composition and a fractionating assemblage of:

hornblende + biotite + plagioclase + K-feldspar + clinopyroxene + orthopyroxene + magnetite + apatite + quartz,

yields a model, SSR 0.16, for the series. Rb-Ba

Figure 6.2. Cumulate model for the low silica series of the biotite hornblende gneiss, Nagle Dam Formation.
Individual symbols along the evolutionary paths represent 10% fractionation. Model data from Appendix 5.1.

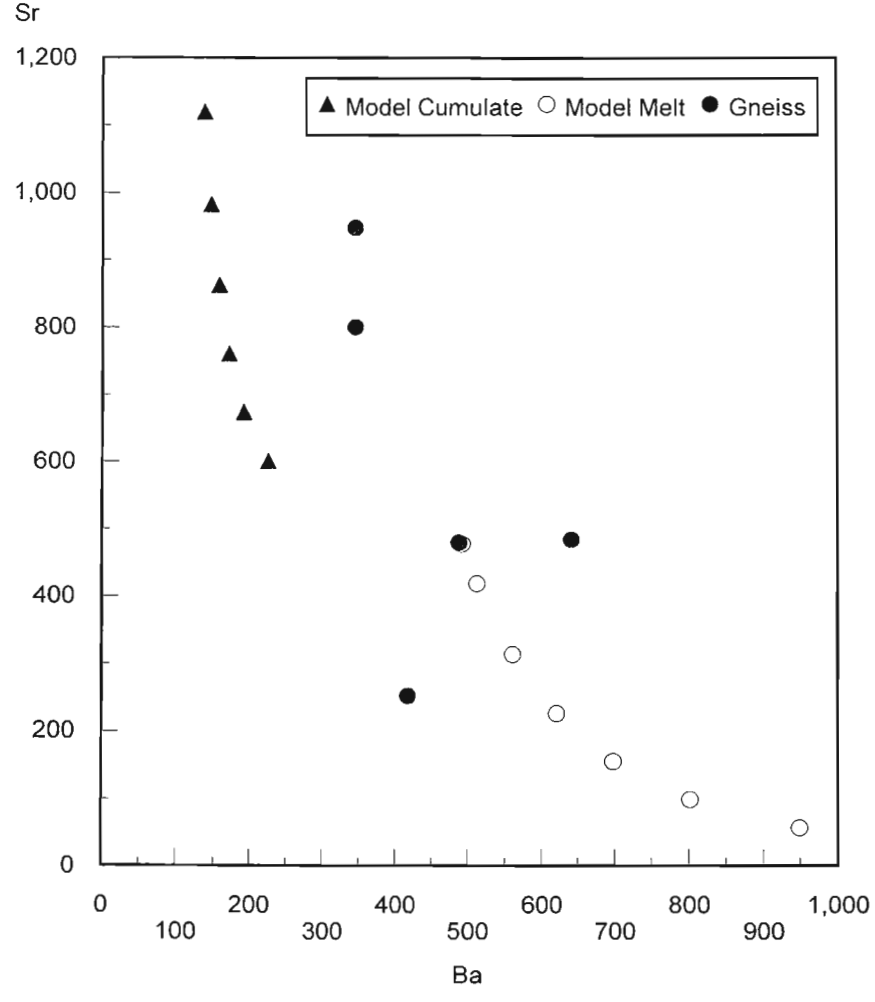

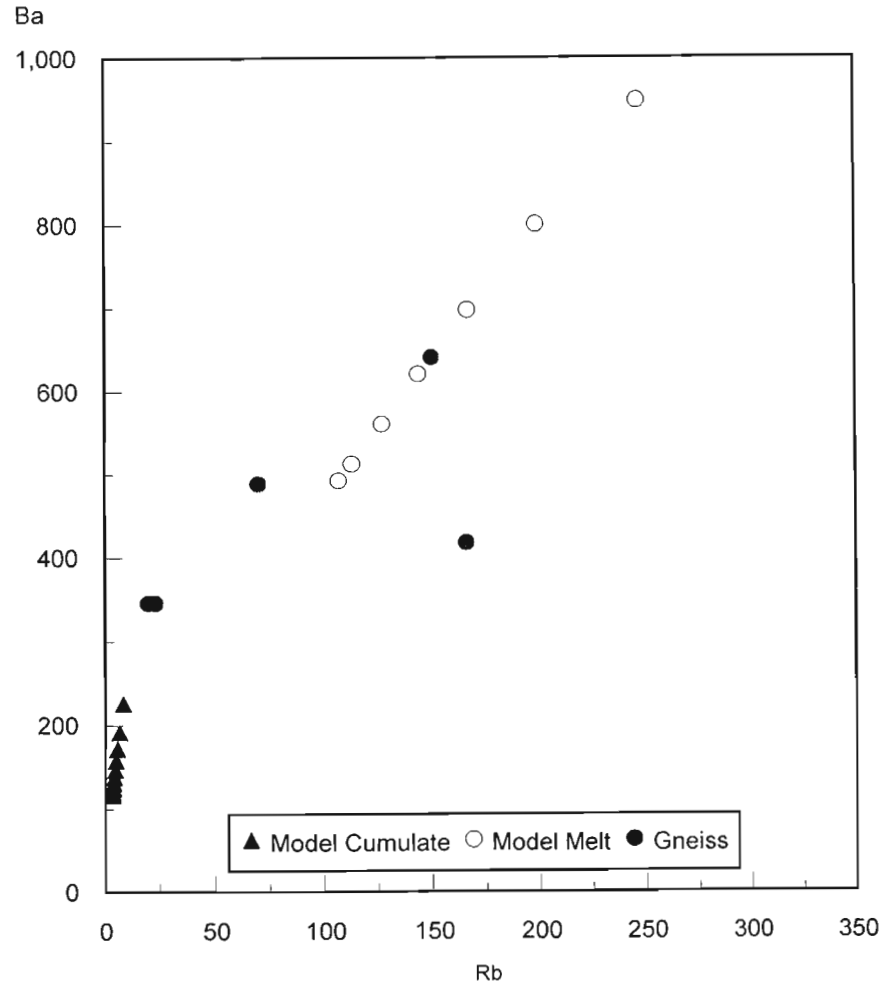

trace element modelling approximates the observed evolutionary trend of the series, but modelling of the Sr-Ba fractionation is less successful, with the available data trending away from the model trend (Figure 6.3a,b).

Cumulate modelling (Appendix 5.3), utilising the average of the available analyses as the initial magma, generates a model, SSR 0.26, for a cumulate assemblage of:

hornblende + biotite + plagioclase + K-feldspar + magnetite + quartz.

As with the fractionation model, the Ba-Rb trace element model provides a satisfactory approximation of the observed evolutionary trend, but the Sr-Ba data display a degree of scatter around the model, which does, however, describe the general fractionation trend (Figure 6.3c,d). This scatter is due primarily to a single sample, UND 312, which also displays extreme TiO_2, Al_2O_3, FeO_{TOT}, MgO and Na_2O concentrations. These features may have resulted from preferential concentration of specific phases in this sample.

c) Source Characteristics

Although both of the series which comprise the biotite hornblende gneiss are relatively sodic, with Na>K, their chemical characteristics distinguish them from the sodic, slab derived, adakites, and in particular is their relatively low Sr, Sr/Y and Zr/Y, but high Y and Sc (Drummond *et al.* 1996). The moderately enriched LIL character of the biotite hornblende gneiss, together with its low HFS elements, and in particular Zr and Y, suggest comparison with the typical volcanic arc granites, and an origin in the subcontinental mantle, enriched through fluxing from the descending slab (Saunders and Tarney 1979; Pearce 1982). The low Rb/Sr and Ba/Sr of individual samples indicate a mantle or lower crustal source (Kay and Gordillo 1994), with an increase in these ratios, and a highly variable K/Rb ratio, suggesting greater upper crustal involvement. Relatively low concentrations of potentially crustally derived elements, and in particular K_2O and Zr (Hildreth and Moorbath 1988), however, and a constant Rb/Zr ratio of 1-2 in the high silica series (Wever *et al.* 1995) imply relatively little crustal involvement in the generation of the series. The wide range of Rb/Zr ratios, 0.5-10, in the low silica series may reflect the influence of a heterogeneous crustal segment, or the effect of a zircon cumulate phase. Given the extreme variability of the Rb/Zr ratio, comparable to that of the Peruvian batholith (Pitcher *et al.* 1985), the latter model is preferred.

6.2.4 QUARTZO-FELDSPATHIC GNEISS

Variations in the Zr/Y ratio allow the division of the quartzo-feldspathic gneiss into two distinct series (Section 4.3.5). Two samples of the high Zr/Y quartzo-feldspathic gneiss were collected, one of which was subdivided to test the effects of metamorphic segregation, with analyses from the quartzo-feldspathic and mafic portions of the gneiss and the undivided sample. Insufficient data are therefore available to undertake a petrogenetic analysis of this series. The nature of the observed chemical variations within the individual sections of the gneiss, however, and in particular the concentration of Rb, Sr, Ba, Al_2O_3 and K_2O in the mafic portion of the gneiss and of Zr, TiO_2, FeO, MgO, CaO and Na_2O in the quartzo-feldspathic portion of the gneiss, suggest the effect of preferential K-feldspar and biotite concentration in the former, while zircon, Fe-Ti oxides, plagioclase and quartz accumulated in the latter.

For the low Zr/Y gneiss only three samples were collected and insufficient data exist to undertake a petrogenetic analysis of this series. Distinct fractionation patterns are, however, apparent for TiO_2, Al_2O_3, FeO_{TOT}, MgO, K_2O, Zr and Sr, which decline with increasing SiO_2. These trends are not comparable with the metamorphic differentiation pattern identified from the high Zr/Y quartzo-feldspathic gneiss, and in particular these will not produce the low MgO and Zr concentrations of the more acidic low Zr/Y sample.

The lack of lower silica correlates mitigate against potential derivation of the low Zr/Y quartzo-feldspathic gneiss through fractionation, suggesting that it originated through the partial melting of a distinct source. Comparison with alumina concentrations derived from partial melting experiments on a variety of potential source materials indicate that the quartzo-feldspathic gneiss does not possess the high alumina content of melts derived from water saturated basalts or metapelites (Helz 1976; Vielzeuf and Holloway 1988). Rather its alumina content approximates that produced by the partial melting of metasediments or tonalitic gneisses (Patiño Douce and Johnston 1991; Skjerlie and Johnston 1993) with extension to higher silica levels. On the Na_2O-K_2O source discrimination diagram of White and Chappell (1983) it plots predominately in the S-type granite field (Figure 4.4d), suggesting derivation from a sedimentary protolith. The quartzo-feldspathic gneiss is, however,

Figure 6.3. Petrogenesis of the high silica series of the biotite hornblende gneiss, Nagle Dam Formation.
Fractionation modelling - a) Sr-Ba, b) Ba-Rb. Model data from Appendix 5.2.
Cumulate modelling - c) Sr-Ba, d) Ba-Rb. Model data from Appendix 5.3.
Individual symbols along the evolutionary paths represent 10% fractionation.

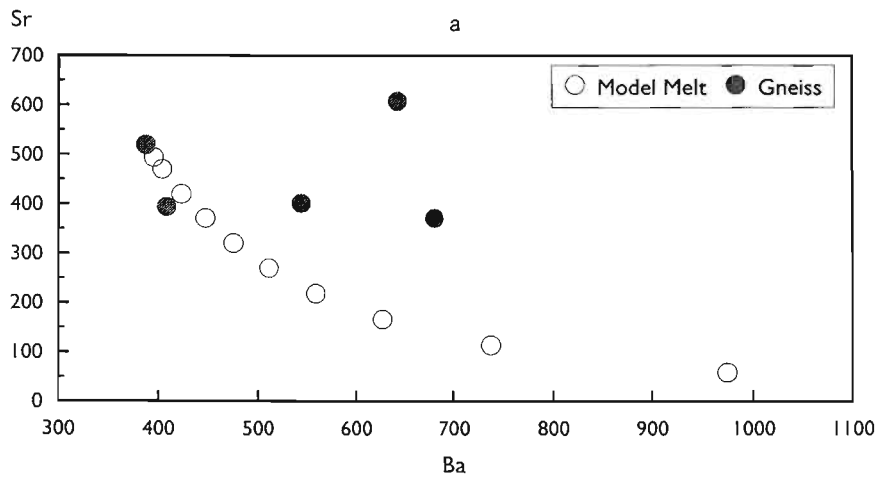

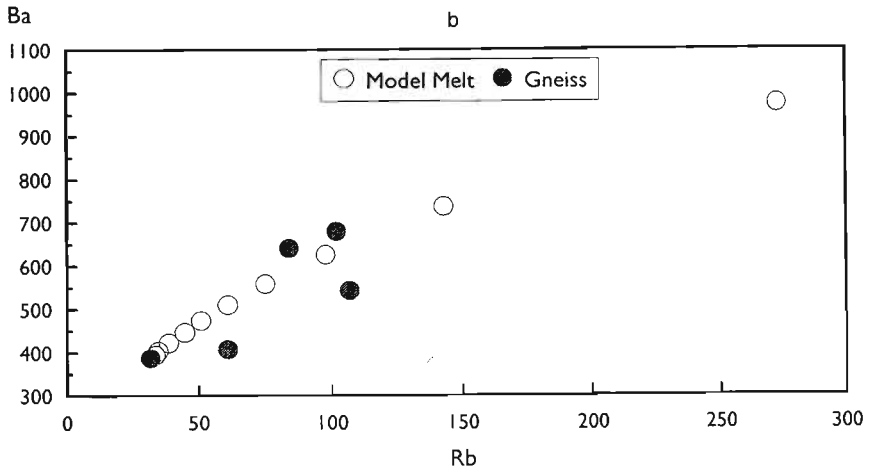

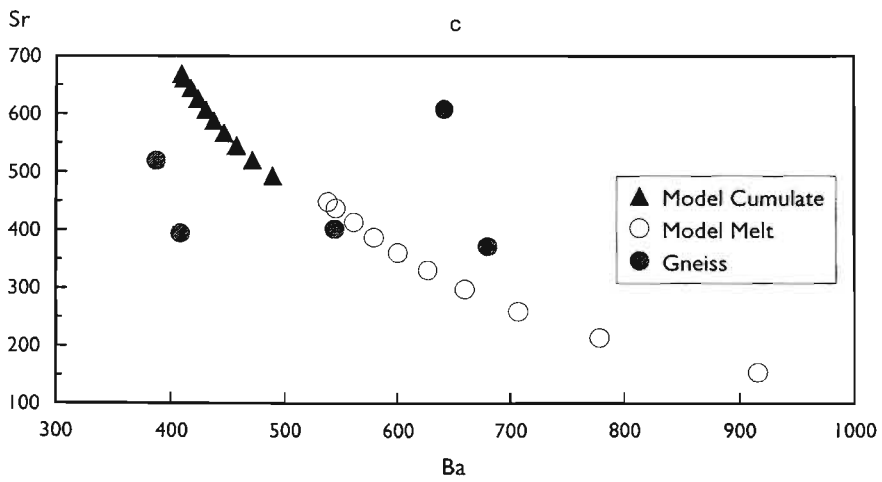

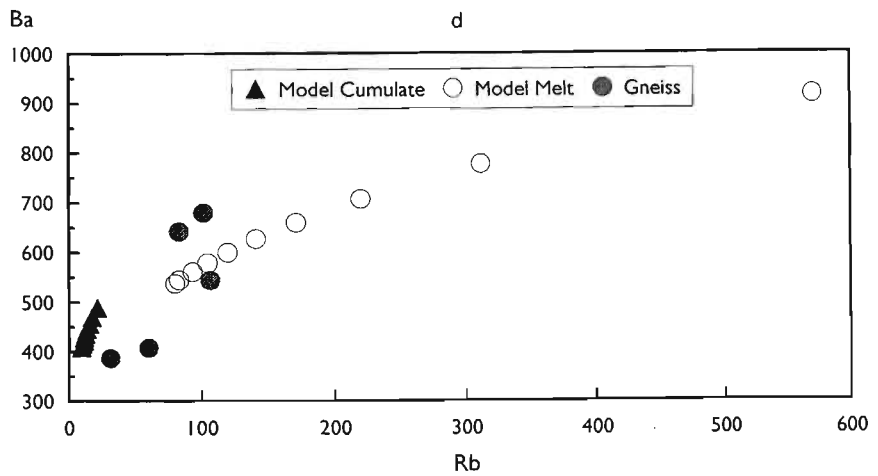

metaluminous to weakly peraluminous rather than strongly peraluminous as expected from a sedimentary sourced melt (Stevens *et al.* 1997a). This suggests a metaluminous source (Conrad *et al.* 1988; Clarke 1992) from which potassic melts may be derived (Skjerlie and Johnston 1993; Singh and Johannes 1996).

Trace element modelling of the partial melting systematics is complexed by potential fractionation processes that may have acted within the quartzo-feldspathic gneiss, masking its original chemical characteristics. Modelling of possible igneous source materials, however, suggest derivation from a tonalite or granodiorite, although the low Ba and Sr content of potential tonalite sources within Natal (Thomas 1989b), do not generate reasonable approximations of the available data. Similarly, utilising the acidic portion of the biotite hornblende gneiss as a potential source provides a poor fit with the observed chemical composition of the quartzo-feldspathic gneiss.

The low Y and high Sr/Y ratio of the high Zr/Y quartzo-feldspathic gneiss is similar to that of the adakite series (Drummond *et al.* 1996). These are believed to have been derived by limited melting of subducting young slab material (Saunders *et al.* 1987; Defant and Drummond 1990; Kay *et al.* 1993; Drummond *et al.* 1996; Stern and Kilian 1996), underplated basalts (Atherton and Petford 1993; Muir *et al.* 1995), or basaltic magma (Feeley and Hacker 1995; Wareham *et al.* 1997) with varying inputs from mantle and crustal material. These melts typically have an ASI of 1, but moderately peraluminous variants are found (Drummond *et al.* 1996). Relative to the average adakite of Drummond *et al.* (1996) the quartzo-feldspathic gneiss is silicic, although high silica adakites have been reported (Atherton and Petford 1993; Wareham *et al.* 1997; Pankhurst *et al.* 1998), and enriched in K_2O, Rb and Ba, possibly due to the inclusion of crustal material (Stern and Kilian 1996), while Sr is low.

6.3 VALLEY TRUST FORMATION

6.3.1 INTRODUCTION

Three distinct units have been identified within the Valley Trust Formation:

1) a bimodal igneous association comprising the amphibolite and quartzo-feldspathic gneiss;
2) metasedimentary pelitic gneiss; and
3) metasedimentary fine grained granulite.

No previous petrogenetic model has been presented for these series.

6.3.2 QUARTZO-FELDSPATHIC GNEISS

The low Zr/Y series of the quartzo-feldspathic gneiss includes all the more siliceous members of the unit, with 79-80 percent SiO_2. Only three samples of this series were collected, however, insufficient to undertake a petrogenetic analysis.

The high Zr/Y series clusters between 75-78 percent SiO_2. Additional analyses, all from Kuyper (1979), have reported Y concentrations below the detection level and cannot be categorised using the Zr/Y ratio (other analyses from Kuyper possess Zr/Y ratios within the high Zr/Y series). Several chemical characteristics of these analyses and in particular their high K_2O, Rb and Ba contents suggest that they are members of the high Zr/Y series. These samples will not, however, be utilised for the petrogenetic analysis of this group.

Elemental variation trends within the high Zr/Y gneiss (Figure 4.6) may have resulted from the fractionation of plagioclase, Fe-Ti oxides, apatite and zircon, possibly with K-feldspar (Tindle and Pearce 1981; McDermott *et al.* 1996; Rapela and Pankhurst 1996). The increasing Rb/Ba ratio with fractionation suggests K-feldspar fractionation in preference to biotite, although this is not supported by an increasing K/Rb ratio.

Major element fractionation modelling, with sample UND 34 (lowest silica) as the assumed initial magma, sample UND 302 (highest silica) as the evolved magma and utilising high Fe/Mg minerals from a typical A-type granite (Ramo 1991), yields a model, SSR 0.84, for a fractionating assemblage of:

hornblende + plagioclase + apatite.

Comparable results are obtained for a fractionating assemblage with biotite $\pm$ hornblende. This poor fit results primarily from the relatively low SiO_2 and high MgO of the model melt. Utilisation, however, of minerals from a calc-alkaline granite (Pitcher *et al.* 1985), generates a model (Appendix 5.4), SSR 0.03, for a fractionating assemblage of:

hornblende + biotite + plagioclase + oxide + apatite.

This model deteriorates slightly if biotite or hornblende is used as the sole mafic phase.

Trace element modelling, however, generates a model markedly dissimilar from the observed trace element fractionation pattern. In particular it indicates a marked increase in Rb with fractionation, and a slight decline in Ba, while the available data shows a marked decline in Ba concentration and a slight increase in Rb (Figure 6.4a,b).

Major element cumulate modelling (Appendix 5.5), utilising the average quartzo-feldspathic gneiss as the initial melt composition, UND 302 as the evolved composition and either A-type or calc-alkaline mineral chemistries, generates a model, SSR 0.16 and 0.05 respectively, for a fractionating assemblage of:

biotite + plagioclase + K-feldspar; and
biotite + plagioclase + K-feldspar + quartz.

Trace element modelling, utilising the latter assemblage, approximates the fractionation trends observed in the quartzo-feldspathic gneiss (Figure 6.4c,d).

6.3.3 AMPHIBOLITE

The amphibolite plots adjacent to the 1 atm. plag-ol-cpx+liq cotectic of Thompson *et al.* (1983), suggesting that the original basaltic magma last equilibrated in a low pressure environment. Elemental variations (Figure 4.6, 6.5a) indicate a general fractionation process controlled by low pressure olivine + clinopyroxene + plagioclase fractionation (Cox 1980; Cox and Hawkesworth 1985). Trends on the Harker diagrams suggest a common fractionation history for the amphibolite, although a degree of scatter is frequently apparent (Figure 4.6).

Trace element ratios, however, suggest that the amphibolite consists of two distinct series, defined by Zr/Y and Zr/Nb ratios (Figure 4.5b). Differences in these ratios imply a variable mantle source, as has been identified from spatially related chemically distinct basalt series in several locations, including the Columbia River Province (Hooper 1988), the Paraná Basin (Peate and Hawkesworth 1996) and the Tertiary basalts of Greenland (Fram and Lesher 1997).

The wide range of Y concentrations within the amphibolite indicate that the individual series were derived through differing degrees of partial melting, or mantle heterogeneity. The enrichment of the incompatible elements with fractionation and the distinct fractionation pattern of declining Cr with constant Y present in the low Zr/Y amphibolite, however, suggest that contrasts in partial melting or source heterogeneity did not generate the observed range in chemical composition of the amphibolite. An increasing Zr/Y ratio with Zr within the individual amphibolite series also implies fractionation. The high Zr/Y but low Zr/Nb and Y/Nb ratios indicate a possible enriched mantle input (Le Roux *et al.* 1983), while evolving Ti/Y-Nb/Y ratios follow the within plate enrichment trend identified by Pearce (1982). Variations in Zr and Nb generate a trend (Figure 6.5d) that parallels the primitive mantle ratio (Sun and McDonough 1989) for both series, with the low Zr/Y amphibolite approximating the primitive mantle ratio. These features may have originated through varying degrees of MORB and OIB mixing (Peltonen *et al.* 1996). Divergence from the MORB-OIB mixing line indicates the action of partial melting and fractionation.

The two amphibolite series identified within the Valley Trust Formation appear to have undergone comparable fractionation processes, distinguished by minor differences in plagioclase fractionation. Variations in FeO with fractionation suggest that this was a complex process, with increasing FeO followed by a sharp decline in FeO concentrations at approximately consistent MgO (Figure 6.5b).

Major element fractionation modelling (Appendix 5.6 and 5.7) for the low Zr/Y amphibolite suggests the initial fractionation of:

plagioclase + Mg-clinopyroxene + Mg-olivine + apatite,

with the subsequent fractionation of:

plagioclase + Fe-clinopyroxene + Fe-olivine + magnetite + ilmenite + apatite,

to generate the fractionation pattern observed in the amphibolite, with SSR 0.42 and 0.67 respectively (Figure 6.5b).

For the high Zr/Y amphibolite, the fractionation modelling has excluded the least evolved sample, which the chemical data suggest may represent an accumulation of specific phases. The subsequent apparent fractionation trend indicates a multiphase process (Appendix 5.8, 5.9 and 5.10), with the initial Fe-Ti enrichment phase modelled through the fractionation of:

plagioclase + Mg-clinopyroxene + Mg-olivine,

Figure 6.4. Petrogenesis of the high Zr/Y quartzo-feldspathic gneiss, Valley Trust Formation.
Fractionation modelling - a) Sr-Ba, b) Ba-Rb. Model data from Appendix 5.4.
Cumulate modelling - c) Sr-Ba, d) Ba-Rb. Model data from Appendix 5.5.
Individual symbols along the evolutionary paths represent 10% fractionation.

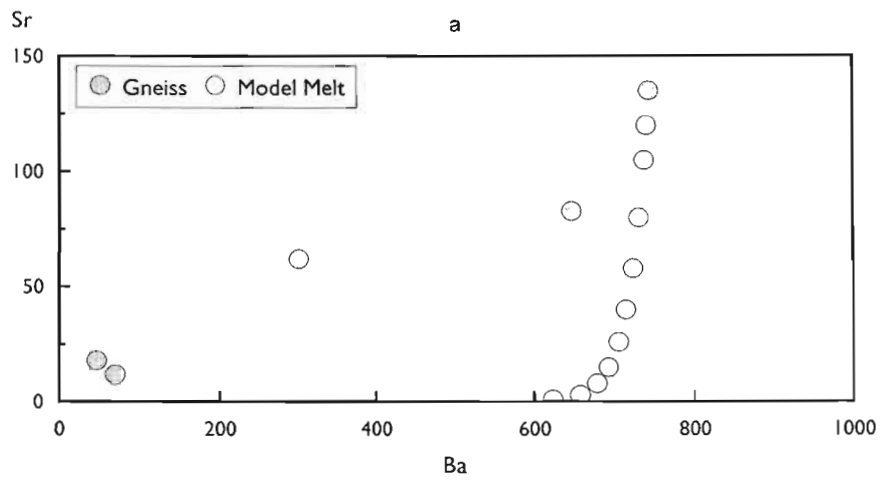

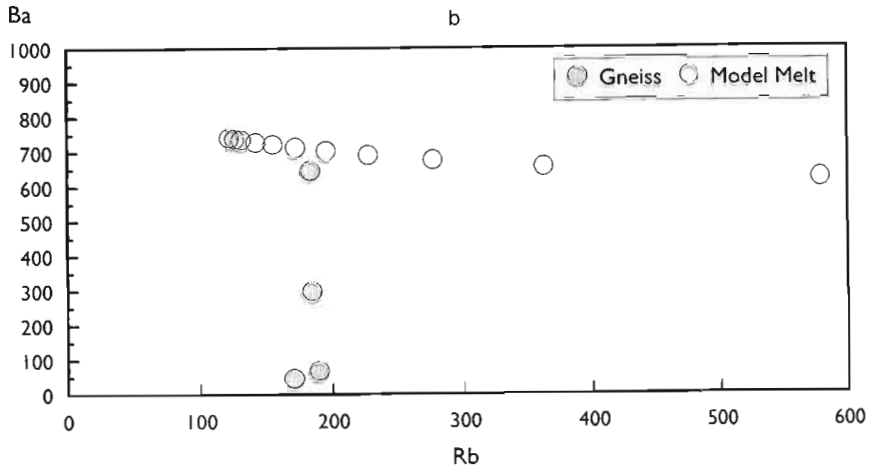

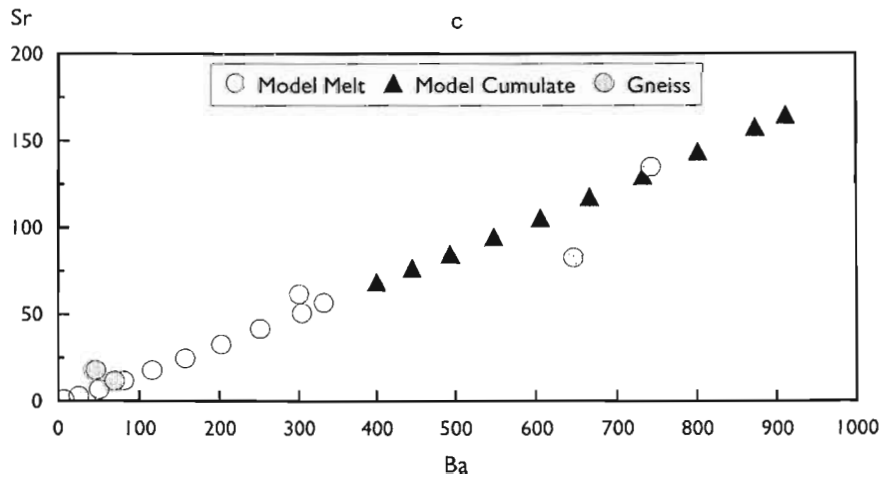

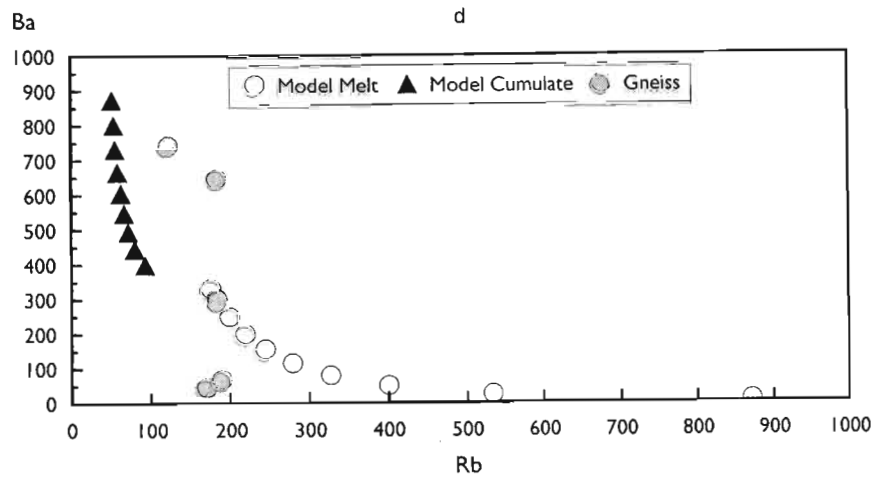

Figure 6.5. Petrogenesis of the amphibolite, Valley Trust Formation.

a) Ni-MgO, b) FeO-MgO (with apparent fractionation vector trends), c) K_2O/P_2O_5-MgO/MgO+FeO (fractionation and ACF trends after Carlson and Hart (1988)), d) Zr-Nb (with fractionation and enrichment trends after Peltonen *et al.* (1996). OIB and MORB after Sun and McDonough (1989)).

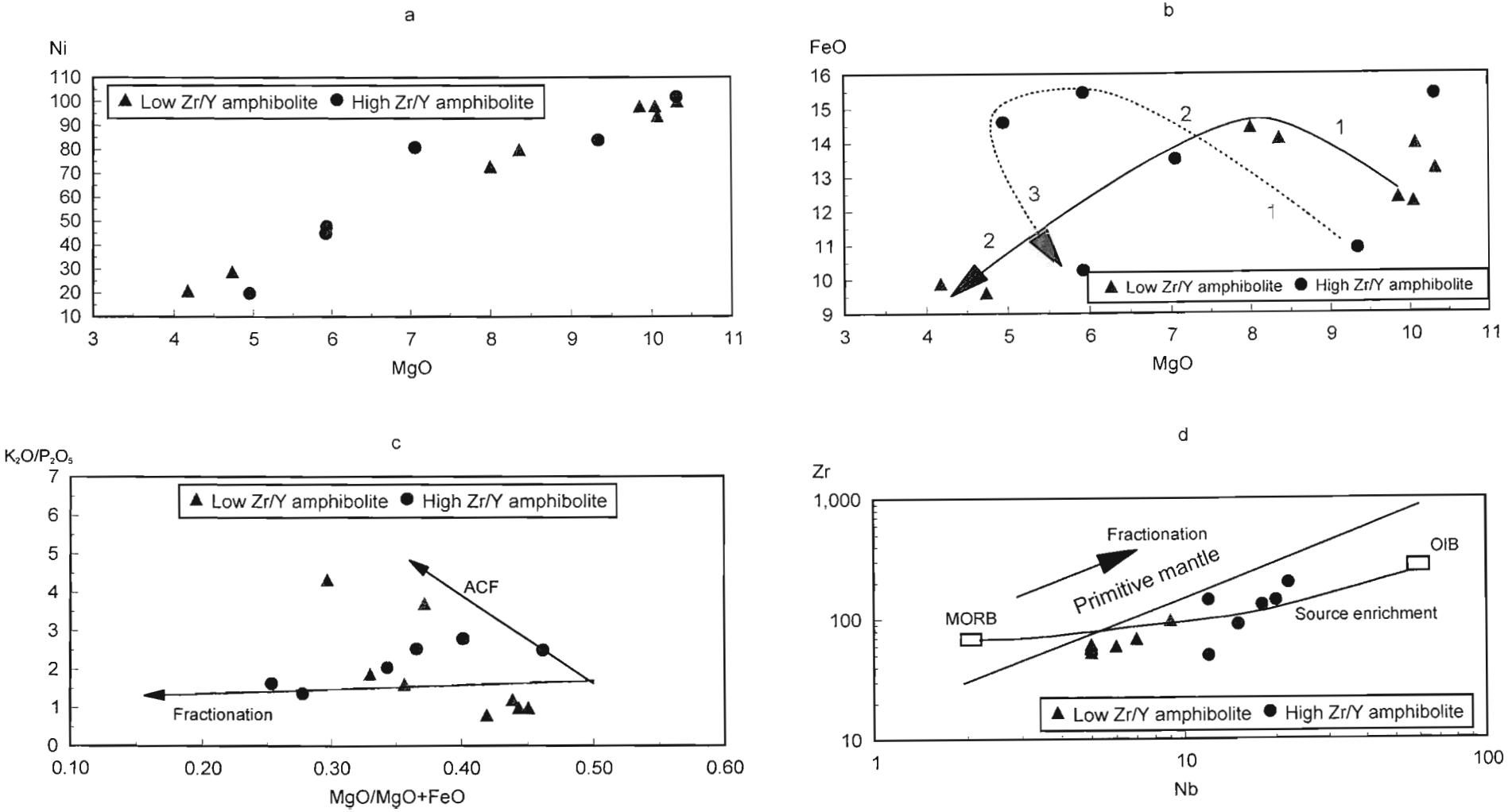

and:

plagioclase + Mg-clinopyroxene + Mg-olivine + magnetite + apatite,

to generate the extreme iron and titanium enrichment found in the amphibolite (Figure 6.5b). Subsequent fractionation to lower iron concentrations is modelled from the intermediate Fe amphibolite, to parallel the fractionation of the low Zr/Y amphibolite, through the fractionation of:

plagioclase + Fe-clinopyroxene + Fe-olivine + magnetite + apatite.

Highly variable silica contents within the high Zr/Y amphibolite hinder the statistical evaluation of this fractionation model, SSR >5, but with the error concentrated in the silica. The entire iron enrichment phase has been modelled for one stage fractionation, with a lower SSR, but without yielding the observed high TiO_2 content of the series.

A comparable range of chemical variations were, however, observed by Fram and Lesher (1997) who proposed that they represented the effect of different parental magmas, fractionation and crustal contamination. Following this the Fe enrichment trends advanced for the amphibolite may represent differences in the parental magma, while the low MgO samples were possibly formed through crustal contamination.

The high silica and Ba concentrations present in the amphibolite are indicative of a degree of crustal contamination (Piccirillo and Cox 1988). This is supported by the increasing ratio of potential crustal components with fractionation and the degree of correlation between LIL/HFS ratios with fractionation, including large variations in the Ba/Zr and K/Y ratios. Similarly, the low Mg' of the amphibolite (54-27) implies that it was not in equilibrium with the mantle. The Zr/Ti contamination index of Fram and Lesher (1997), however, indicates a minimum role for contamination, although two of the samples plot in the field of contaminated basalts. Trend variations on the K_2O/P_2O_5-MgO/MgO+FeO diagram demonstrate that the amphibolite series may have evolved along distinct contamination vectors, with the high Zr/Y series displaying minimal evidence for contamination while the low Zr/Y series parallels the ACF evolution curve of Carlson and Hart (1988), suggesting a possible role for crustal contamination in its evolution (Figure 6.5c).

6.3.4 AMPHIBOLITE - QUARTZO-FELDSPATHIC GNEISS RELATIONSHIP

The occurrence of associated basic and acidic magmas has been explained as the result of fractionation, partial melting of basement crust and the partial melting of the earlier basaltic component of the series (Mahoney 1988). Although the former model was supported by Ewart (1985), with associated side wall melting and assimilation, and Garland *et al.* (1995) for specific rhyolites of the Paraná Province, perhaps more studies have favoured the partial melting model, and in particular the partial melting of a basaltic source (Cleverly *et al.* 1984; Piccirillo *et al.* 1988; Garland *et al.* 1995). The importance of basaltic melt intrusions as heat sources for the production of acidic melts was emphasised by Hildreth (1981).

No apparent chemical continuation exists between the amphibolite and quartzo-feldspathic gneiss on potential fractionation plots such as Zr-SiO_2 (Figure 4.6), suggesting that the quartzo-feldspathic gneiss did not develop from the amphibolite through fractionation processes. Partial melting modelling of the amphibolite indicates its potential as a source for the quartzo-feldspathic gneiss, but the distinct immobile trace element content of the amphibolite and quartzo-feldspathic gneiss, and in particular their comparable Zr content, mitigates against the derivation of the quartzo-feldspathic gneiss through partial melting of the amphibolite. Similarly, the quartzo-feldspathic gneiss does not possess the high HFSE content common to the melts derived through partial melting of within plate basalts (Cleverly *et al.* 1984; Garland *et al.* 1995), or their high Sr concentrations (Garland *et al.* 1995). The quartzo-feldspathic gneiss may therefore have developed from the melting of crustal material through the introduction of basaltic melts as a heat source.

Given the high crystallisation temperatures calculated for the bimodal association, Garland *et al.* (1995) noted that any upper crustal source material with hydrous phases would suffer complete melting and therefore preferred lower crustal metasediments and granulites or underplated basalts as sources for individual rhyolites. Comparison with alumina concentrations derived from partial melting experiments indicate that the quartzo-feldspathic gneiss does not possess the high alumina content produced by the partial melting of water saturated basalts or metapelites (Helz 1976; Vielzeuf and Holloway 1988), while water undersaturated melting of basalt produces

low silica melts (Spulber and Rutherford 1983). Rather, their alumina content approximates that produced by the partial melting of metasediments or tonalite gneisses (Patiño Douce and Johnston 1991; Skjerlie and Johnston 1993), with extension to higher silica levels.

Variations in the alumina saturation of the different quartzo-feldspathic gneiss series, highly peraluminous low Zr/Y gneiss and metaluminous high Zr/Y gneiss, implies derivation from distinct sources. The peraluminous nature of the low Zr/Y gneiss suggests that it was generated through partial melting of a metasedimentary source material (Chappell and White 1974; Puziewicz and Johannes 1988; McDermott *et al.* 1996; Stevens *et al.* 1997a), although the predominately sodic nature of the gneiss results in the majority of the samples plotting in the I-type granite field (Figure 4.7d) of White and Chappell (1983). This high Na_2O/K_2O ratio may result from a source with a relatively sodic plagioclase, An<15 (McDermott *et al.* 1996), or a melting assemblage with a high plagioclase/ biotite ratio through biotite dehydration melting in a sillimanite deficient source (Vielzeuf and Montel 1994). Equally it could have been generated through the partial melting of a greywacke type source (Skjerlie and Johnston 1996). The extremely low Fe_2O_3+MgO and CaO of the gneiss, however, mitigates against biotite partial melting (McDermott *et al.* 1996). Rather muscovite dehydration melting is suggested, with an average Rb/Sr of c.4 indicating vapour absent melting (Harris and Inger 1992).

The metaluminous nature of the high Zr/Y gneiss indicates an origin from a metaluminous source (Clarke 1992). Partial melting modelling of potential igneous sources suggest that the quartzo-feldspathic gneiss may have originated through melting of a granodioritic or tonalitic source.

6.3.5 PELITIC GNEISS

Moderate to high SiO_2/Al_2O_3 (2.84-7.91) and K_2O/Na_2O (1.81-6.40) ratios suggest that the protolith of the pelitic gneiss has undergone a variable degree of weathering. Calculation of the Chemical Index of Alteration (CIA) (Nesbitt and Young 1982) for the average pelitic gneiss derives a CIA of 58, comparable to relatively unweathered material. This low CIA results from the very low CIA of the samples from the large enclave site and individual analyses may display a CIA of more weathered rock (CIA c.70). Such a low CIA is comparable to that of glacial sediments (CIA±65). No indication of the effects of sorting can be determine for this unit through variations in A-CN-K (Nesbitt *et al.* 1996), with the majority of the samples plotting on the weathering trend line between the potential source material, as defined by the sample with the lowest CIA, and illite. Possible addition of potassium is, however, indicated by the samples from the large enclave which diverge from the weathering trend line towards the K apex (Fedo *et al.* 1995; 1997), although Yang *et al.* (1998) suggested that this trend, without extension to the A-K join, may result from the erosion of a K-rich source.

The CIA model was criticised by Harnois (1988), specifically because of the incorporation of K into the equation, as K enrichment may occur during weathering and is a common feature of the Precambrian (Retallack 1986). Fedo *et al.* (1995), however, proposed a correction factor for potassium metasomatism, which indicates an original CIA of 60-70 for the K-enriched pelitic gneiss. Fedo *et al.* also noted that the Chemical Index of Weathering (CIW) devised by Harnois does not account for Al_2O_3 associated with alkali feldspar and is therefore potentially inaccurate.

Calculation of the Niggli norms (al, alk, si, ti, c, k, fm and mg) allows the identification of sedimentary fractionation trends. Variation is noted in the fractionation trends of the psammitic and pelitic portions of the pelitic gneiss, and in particular through divergent trends in SiO_2-al-alk (Figure 6.6a). The psammites display the effect of quartz dilution, with the majority of the elements and al-alk declining in concentration with increasing silica, while large variations in elemental concentration and al-alk at almost constant SiO_2 are noted in the pelites, indicating the influence of mineral phases other than quartz. Analysis of the Niggli normative mineralogy of the pelitic gneiss suggests that it originally comprised a mixture of illite and chlorite-montmorillonite (Leake 1996). No major limestone or dolomite component is identified.

Senior and Leake (1978) noted that al-alk reflects the clay and mica content of the original sediment. Variations in al-alk can therefore be used to determine the influence that the clay and mica minerals had on the chemistry of the sediment. Condie *et al.* (1992) used Al_2O_3 in a similar fashion, but alumina is not restricted to the clay and mica minerals, occurring in other phases, such as detrital feldspar. Within the psammitic gneiss Al_2O_3, MgO, Ba, Rb and Y increase in concentration with al-alk (Figure 6.6c,d), indicating

Figure 6.6. Sedimentary fractionation trends within the pelitic gneiss, Valley Trust Formation.
a) SiO_2 - al-alk, b) K_2O - al-alk, c) MgO - al-alk, d) Y - al-alk.

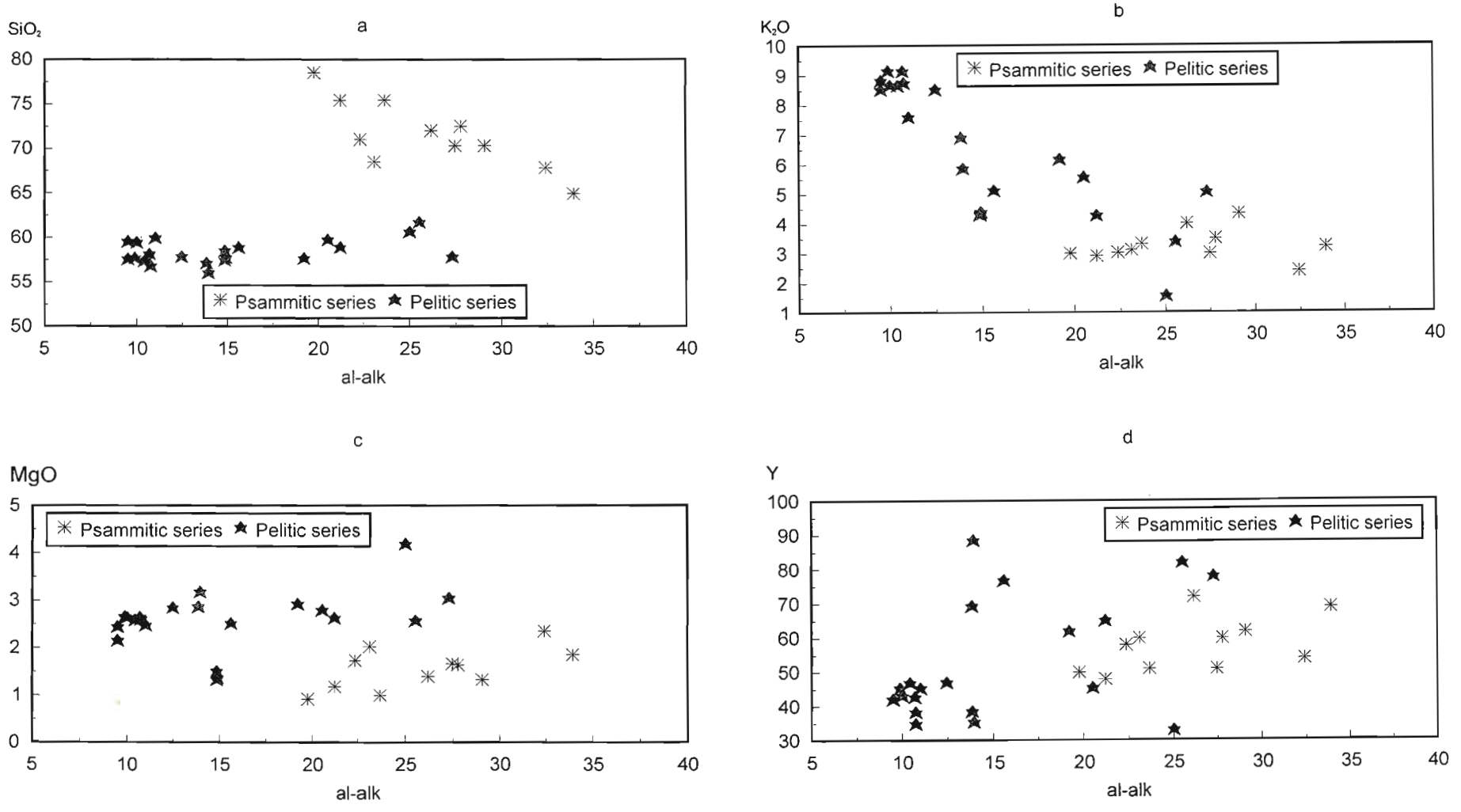

that these elements were possibly added to the sediment through the clay and mica minerals. FeO and V possess a similar trend, but the link between FeO-V and FeO-TiO_2 fractionation suggest the possible existence of an Fe-Ti oxide phase. Declining P_2O_5, CaO, Na_2O and Sr with increasing al-alk implies the presence of apatite and possibly plagioclase.

Within the pelitic portion of the gneiss, increasing Al_2O_3, SiO_2, FeO, MgO, P_2O_5, Zr, Y, Ni, V and Sr with al-alk is found (Figure 6.6a,c,d), suggesting the inclusion of these elements in the clay and mica phases. Zr, Y, CaO and P_2O_5 concentrations vary considerably with al-alk, however, implying the existence of an independent zircon and apatite phase, but without the high Zr/Sc ratios indicative of zircon accumulation (Yang *et al.* 1998). Similarly, the increase in V and TiO_2 with FeO suggest the presence of an oxide phase. The declining K_2O (Figure 6.6b), Na_2O and Rb with increasing al-alk, but constant Ba, and the high K_2O/Al_2O_3 ratio of the gneiss, indicate that these elements may have been incorporated into a separate potassic phase, possibly a K-feldspar (Okonkwo 1989; Cox *et al.* 1995), although the low Ba/Rb ratio of the pelitic gneiss does not suggest a high K-feldspar content.

Although a variety of sedimentary processes may influence the chemical characteristics of pelites, including the grain size, diagenesis and chemical weathering (Wronkiewicz and Condie 1987), the source area may be imaged by elements such as the REE and HFSE (Taylor and McLennan 1985). Elements typically associated with basic source areas, such as FeO, MgO, Cr, Ni and Co (Garver *et al.* 1996; McCaffrey and Kneller 1996), are variably enriched in the pelitic gneiss, with high FeO but low MgO. Cr overlaps with the lower range of Garner *et al.* but TiO_2 and Ni are low, suggesting an acidic source (McCann 1998). Intermediate La/Sc, Th/Sc and Co/Th ratios (Yang *et al.* 1998) and variations in La-Th-Sc (Taylor and McLennan 1985, amended by Wronkiewicz and Condie 1987) support this assertion, and indicate a mixed source area for the pelitic gneiss.

The sedimentary provenance discrimination diagrams of Roser and Korsch (1988) suggest that the pelitic gneiss was derived from either a felsic -intermediate igneous provenance or a quartzose sedimentary provenance (Figure 6.7a,b). No potential source comparable with the latter is known from the Valley of a Thousand Hills or surrounding areas, but the Nagle Dam Formation represents a possible source of felsic or intermediate material.

Trace element ratio diagrams designed to model potential source mixing (Cullers *et al.* 1988; Condie *et al.* 1992) suggest that the pelitic gneiss may have been derived from a source representing a mixture of the amphibolite and quartzo-feldspathic gneiss of the Nagle Dam Formation or derived primarily from the intermediate biotite hornblende gneiss. On the La-Th-Sc diagram the pelitic gneiss is almost intermediate between the biotite hornblende gneiss and the quartzo-feldspathic gneiss of the Nagle Dam Formation, suggesting that the pelitic gneiss may represent a mixture of these units. The biotite hornblende gneiss, however, may form a source point for the pelitic gneiss fractionation array (Figure 6.7c,d), while a variety of trace element ratios, including Zr/Y, indicate a similarity between the biotite hornblende gneiss and the pelitic gneiss. The lack of Sc analyses from the Valley Trust Formation inhibits any attempt to assess its potential role in the derivation of the pelitic gneiss.

Partial melting of the pelitic gneiss is evidenced by the production of a garnetiferous melt phase, found as thin veins within the gneiss. Associated with these veins is a distinct garnetiferous phase present as a marginal mantle to several of the enclaves, possibly representing the crystal mush melt sheet of McLeod and Sparks (1998), with the rare concentration of the melt phase as garnetiferous granite veins.

The biotite gneiss has been identified as a detached and possibly restitic portion of the pelitic gneiss produced through the physical dismemberment of the gneiss and the removal of a granitic melt phase. If Al_2O_3 or TiO_2 are taken to be immobile (the biotite gneiss possesses higher Al_2O_3 but comparable TiO_2 to the pelitic gneiss) FeO, MgO, K_2O, Rb, Ni, Cr, Sc and V appear to have been lost from the biotite gneiss while CaO, Na_2O, Sr, Ba, La, Zr, U and Th have been enriched. This indicates the preferential accumulation of zircon and feldspar in the biotite gneiss, while biotite was lost, perhaps due to a biotite dehydration melt producing reaction. The chemical characteristics of the biotite gneiss do not suggest, however, that it was associated with a granitic melt generating event, with the apparent enrichment/depletion pattern found inconsistent with that identified by Ahmed-Said and Leake (1990) or Barbey (1991) for a restite produced through the partial melting of a metasediment. In particular the depletion of elements not commonly associated with the generation of granitic melts, such as MgO, FeO_{TOT},

Figure 6.7. Provenance analysis of the pelitic gneiss and fine grained granulite of the Valley Trust Formation.
a) and b) DF2-DF1 major element discriminant function diagrams (Roser and Korsch 1988), c) Cr-Zr, d) Sc-La.
For 6.7a. DF1 = $-1.773TiO_2 + 0.607Al_2O_3 + 0.76Fe_2O_{3(TOTAL)} - 1.5MgO + 0.616CaO + 0.505Na_2O - 1.224K_2O - 9.09$.
DF2 = $0.445TiO_2 + 0.07Al_2O_3 - 0.25Fe_2O_{3(TOTAL)} - 1.142MgO + 0.438CaO + 1.475Na_2O + 1.426K_2O - 6.861$.
For 6.7b. DF1 = $30.638TiO_2/Al_2O_3 - 12.541Fe_2O_{3(TOTAL)}/Al_2O_3 + 7.329MgO/Al_2O_3 + 12.031Na_2O/Al_2O_3 + 35.402K_2O/Al_2O_3 - 6.382$.
DF2 = $56.5TiO_2/Al_2O_3 - 10.879Fe_2O_{3(TOTAL)}/Al_2O_3 + 30.875MgO/Al_2O_3 - 5.404Na_2O/Al_2O_3 + 11.112K_2O/Al_2O_3 - 3.89$.

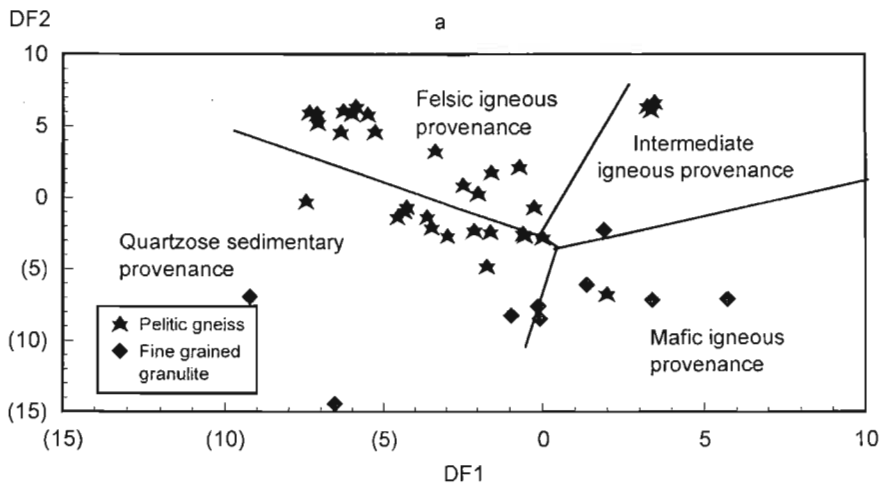

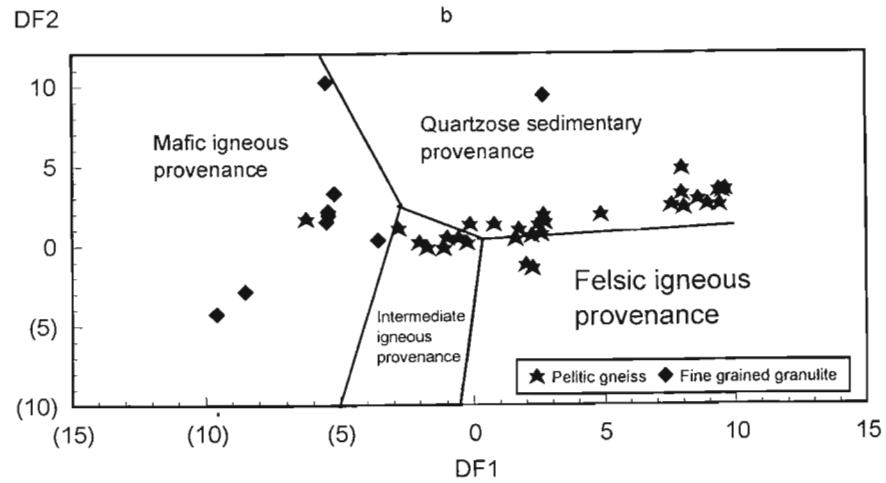

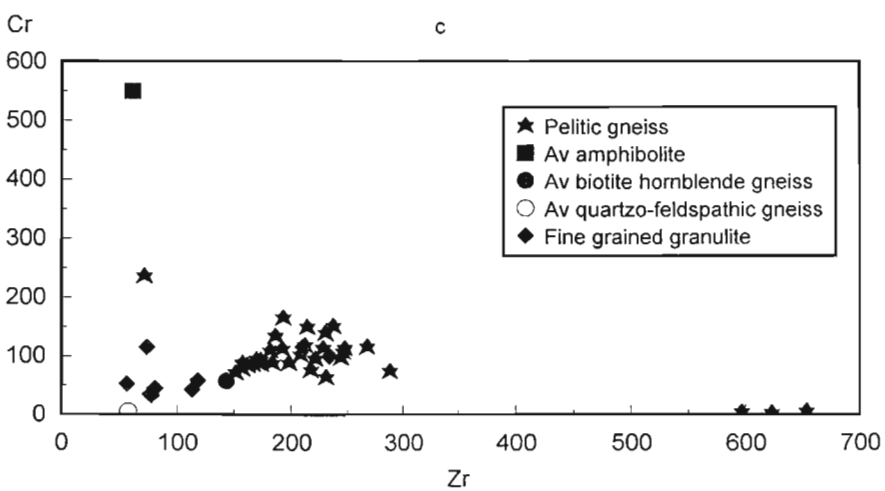

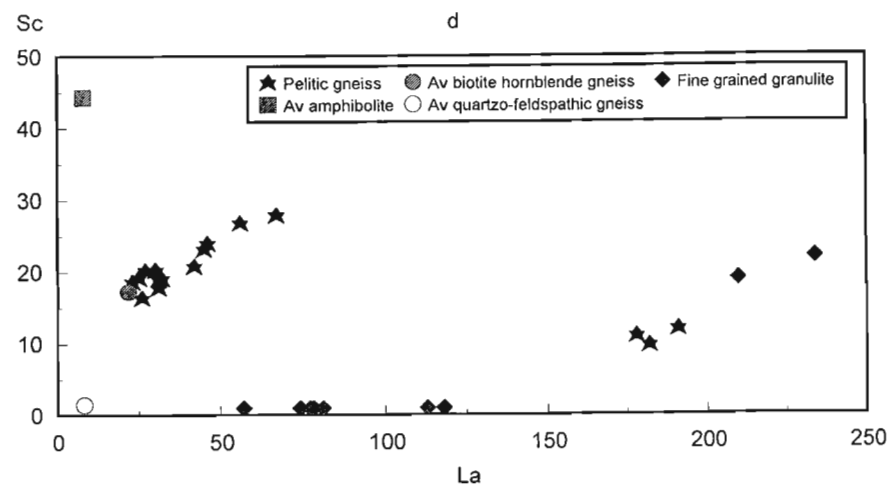

Cr, Ni and V, does not suggest the removal of a granitic phase. Similarly, the K/Rb ratio of the biotite gneiss (230-238) is analogous to crustal averages, although its enrichment in specific elements such as Zr, U and Th is comparable with that identified by Barbey in typical restites. These chemical characteristics may, however, reflect the distinct chemical character of the resultant melt phase, and in particular the presence of abundant garnet in the melt, into which FeO, MgO, Ni, Cr, Sc, V and Y may have partitioned.

6.3.6 FINE GRAINED GRANULITE

Variations in al-alk, c, mg and si suggest that the protolith of the fine grained granulite consisted primarily of a clay mineral and a siliceous phase, with minor carbonate. Extension of the unit beyond the typical pelitic fields indicates an additional input from a mg rich phase (Figure 4.1). The available chemical data indicate the effect of increasing quartz dilution on the majority of the major elements, Zr, Pb and Nb (Figure 4.6). K_2O, however, increases in concentration with increasing silica, while Na_2O possesses an extreme range of concentrations, with the possible division of the unit into distinct groupings based on sodium fractionation trends. The majority of the trace elements display no distinct correlation with silica and a wide scatter of concentrations.

Identification of potential clay fractionation profiles is hindered by the presence of occasional chemically distinct samples characterised by anomalous concentrations of individual elements, including K_2O, MgO and FeO_{TOT}. Elimination of this sample on the respective plots allows the identification of sedimentary fractionation trends in the fine grained granulite. Al_2O_3, FeO, Rb, Y and K_2O concentrations remain constant or display no particular trend (Figure 6.8a,b,d) with variation in al-alk, while Ba, MgO, Cr, Zr and TiO_2 decline with increasing al-alk, suggesting that a clay or mica phase played a minor role in defining the chemical character of the granulite. The increase in MgO and TiO_2 with FeO_{TOT}, but not MgO with TiO_2, implies the existence of both an Fe-Mg and an Fe-Ti mineral phase. The general increase in Rb, Ba and K_2O with FeO (Figure 6.8c) suggest that these may have been contained within an Fe-Mg mineral phase, possibly biotite.

The sedimentary provenance diagrams of Roser and Korsch (1988) and the relatively high MgO content of the granulite suggest that the fine grained granulite was derived from a mafic igneous source (Figure 6.7a,b), similar to the model for Mg-pelites of Sheraton (1980) and Harley *et al.* (1990). The low Cr and Sr content of the fine grained granulite does not, however, support this model. The Cr and Zr data rather suggest an origin through mixing of the biotite and quartzo-feldspathic gneisses of the Nagle Dam Formation, although this is not supported by the low Sc of the fine grained granulite, which might indicate a dominant role for the quartzo-feldspathic gneiss (Figure 6.7c,d).

6.4 MGENI BATHOLITH

6.4.1 INTRODUCTION

With a relatively large geochemical data base, the granites grouped by Thomas (1988a) into the Oribi Gorge Suite are perhaps the most amenable component of the Natal Province for an analysis of their petrogenetic development. Initially, the various studies of the Mgeni batholith (Kuyper 1979; Du Toit 1979) and of those members of the Oribi Gorge Suite from southern KwaZulu Natal (Thomas 1988a) suggested that the megacrystic granites of the individual batholiths were related through fractionation processes. Within this system the Nqwadolo Suite was viewed as either the end phase of the megacrystic granite fractionation process (Du Toit 1979) or as a partial melt of the megacrystic granites (Kuyper 1979). Subsequent isotopic analysis of the Mgeni batholith (Eglington 1987), however, led Kerr (1985) to propose the existence of three distinct granitic suites within the Mgeni batholith:

1) biotite granite;
2) hornblende granite and charnockite; and
3) Nqwadolo granite;

distinguished on mineralogical, chemical and isotopic grounds (Kerr 1985; Kerr and Milne 1994). These correspond with the Ximba, Mlahlanja and Nqwadolo Suites, respectively (Kerr and Milne 1991a).

Eglington (1987) interpreted the chemical similarity of the marginal granite of the Ximba Suite and the Mlahlanja Suite as the product of the contamination of a common initial magma, the biotite granite of the Ximba Suite, with the Nagle Dam Formation. A similar model was proposed by Kerr *et al.* (1987), Eglington *et al.* (1989a) and Kerr and Milne (1991a). Kerr and Milne (1994), however, reviewed the various models for the petrogenesis of the Mgeni batholith and concluded, from a larger data base, that the preexisting models could not explain all the observed features of the

Figure 6.8. Sedimentary fractionation trends within the fine grained granulite, Valley Trust Formation.
a) FeO - al-alk, b) K_2O - al-alk, c) FeO-K_2O, d) Y- al-alk.

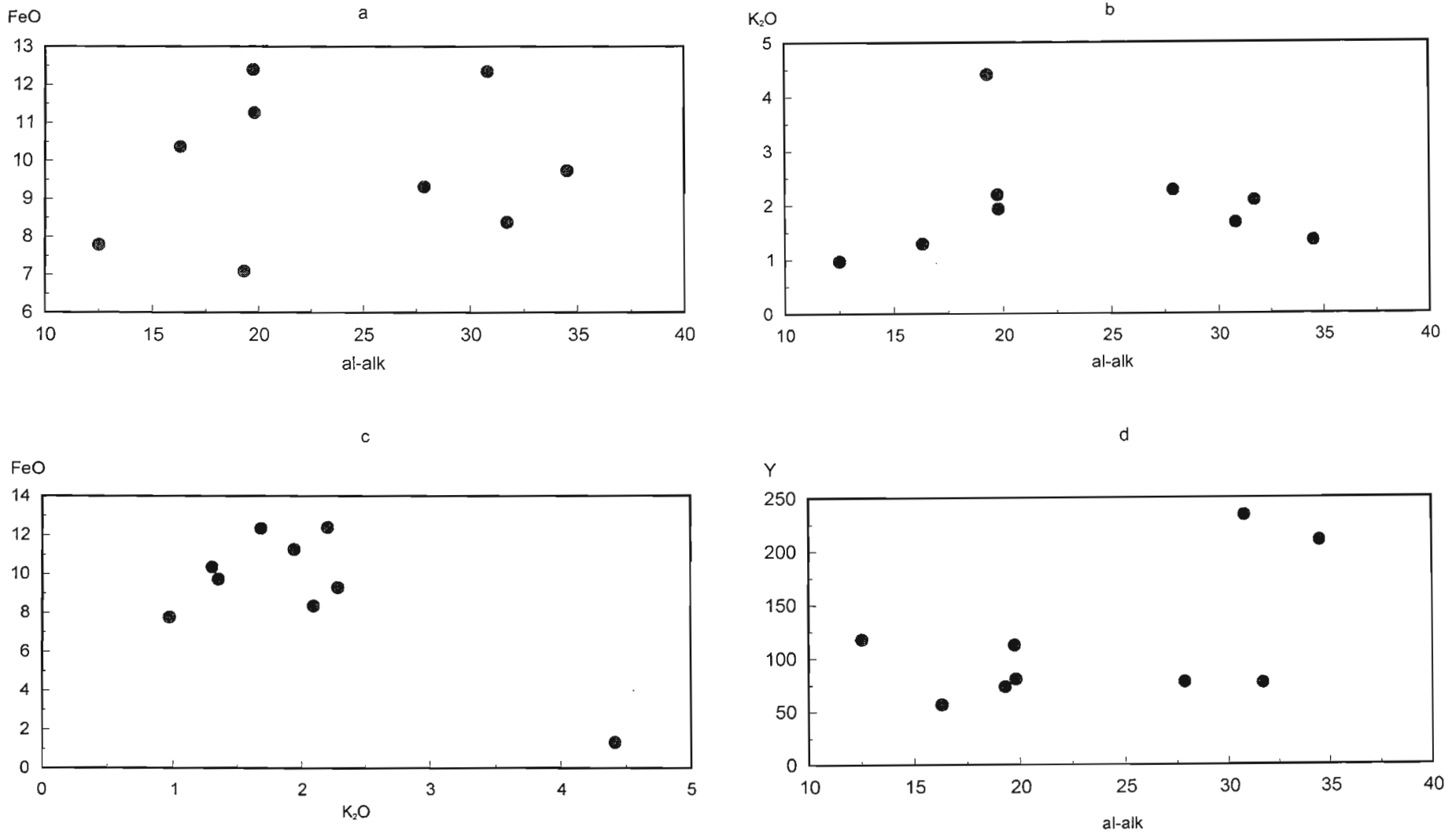

granites. Although these authors did not offer a general model for the development of the Mgeni batholith, they noted that evidence existed for the potential operation of a variety of concurrent processes during the crystallisation of the megacrystic granites.

The distinct isotopic character of the individual suites within the Mgeni batholith identified by Eglington (1987) precludes the fractionation model of Du Toit (1979), Kuyper (1979) and Thomas (1988a). Such isotopic, chemical and mineralogical zonation within a single granite may be generated only by contamination or melting of a vertically zoned source (Halliday 1983), but these models produce an internally consistent Sr_I and trace element content within the component members of the resultant granite, features not identified within the Mgeni batholith. Equally, field work has demonstrated that the proposed country rock contaminant of Eglington *et al.* (1989a) is a marginal member of the Ximba Suite. Utilisation of the extended data base for the Nagle Dam Formation collected during the present study suggests that the trace element content of the Nagle Dam Formation, and in particular its low Ba, Zr, Nb and La content, is not conducive to a possible role in generating the high Zr Mlahlanja Suite through mixing with the low Zr Ximba Suite (Figure 6.9).

Isotopes, trace element ratios and major element discrimination analysis (Figure 4.8) suggest that the suites of the Mgeni batholith may represent distinct units. Interpretation of the petrogenetic development of the Mgeni batholith will therefore be undertaken through an analysis of the individual suites.

6.4.2 XIMBA SUITE

The Ximba Suite consists predominately of a series of megacrystic biotite granites. In the core of the pluton these may contain garnet, while adjacent to the contact with the Nagle Dam Formation they become darker and finer grained, with fewer megacrysts and a mafic assemblage of hornblende + biotite. Three granitic variants are therefore apparent in the field:

1) a highly heterogeneous, but typically low silica, marginal phase;
2) a relatively acidic inner biotite granite; and
3) a core of intermediate biotite garnet granite (Figure 2.1);

providing a distribution pattern with elements of both normal and reverse zonation (Halliday 1983; Nabelek *et al.* 1986). Although contacts are diffuse, available chemical data suggest a degree of internal gradation between the marginal granite and the biotite granite, which form a coherent differentiation trend on the Harker diagrams, possibly due to the action of crystal-liquid fractionation processes. The biotite garnet granite, however, plots away from this trend, with field evidence indicating that this may be related to the assimilation of pelitic material. The marginal granite - biotite granite and biotite garnet granite series will therefore be discussed separately.

a) Marginal Granite - Biotite Granite

The marginal and biotite granites form a completely overlapping series on the Harker diagrams. Although a contamination model for the Ximba Suite has been proposed by Eglington (1987) and is supported in the field by the presence of abundant xenoliths within the marginal granite, the nonlinear relationships evident on the Harker diagrams do not suggest a simple contamination model, but rather the effects of fractionation. Further, the derivation of the marginal granite through contamination of the biotite granite by the Nagle Dam Formation is not supported by the available trace element data (Section 6.4.1 and Figure 6.9).

Petrographic observations suggest a fractionating sequence similar to that found in other rapakivi granites - early feldspar and quartz megacrysts with later mafics partially mantling the megacrysts and a finer grained quartzo-feldspathic groundmass. Coeval growth of the various components of the granite is suggested, however, with inclusions of the mafics and fine grained quartzo-feldspathic groundmass within the megacrysts. Similar textural relationships are common in the rapakivi granites, with the late growth of mafic phases attributed to the low water content of the rapakivi granite melt (Anderson 1980).

The mafic assemblage evolves through the series. Biotite, with lesser hornblende, occur together in the more basic marginal granite, while biotite is the principal, and typically only mafic phase in the more evolved biotite granite. Both K-feldspar and plagioclase megacrysts occur throughout the series, although the latter is more common in the marginal granite than the biotite granite, where quartz megacrysts may become abundant.

Variations in the elemental distribution patterns suggest the fractionation of feldspar, biotite and or

Figure 6.9. Contamination model for the Mgeni batholith, with the biotite granite of the Ximba Suite as the initial magma, the Nagle Dam Formation as the contaminant and the marginal granite of the Ximba Suite and the Mlahlanja Suite as the product, with potential mixing lines, demonstrating the lack of extension of the marginal granite and Mlahlanja Suite along the mixing lines.

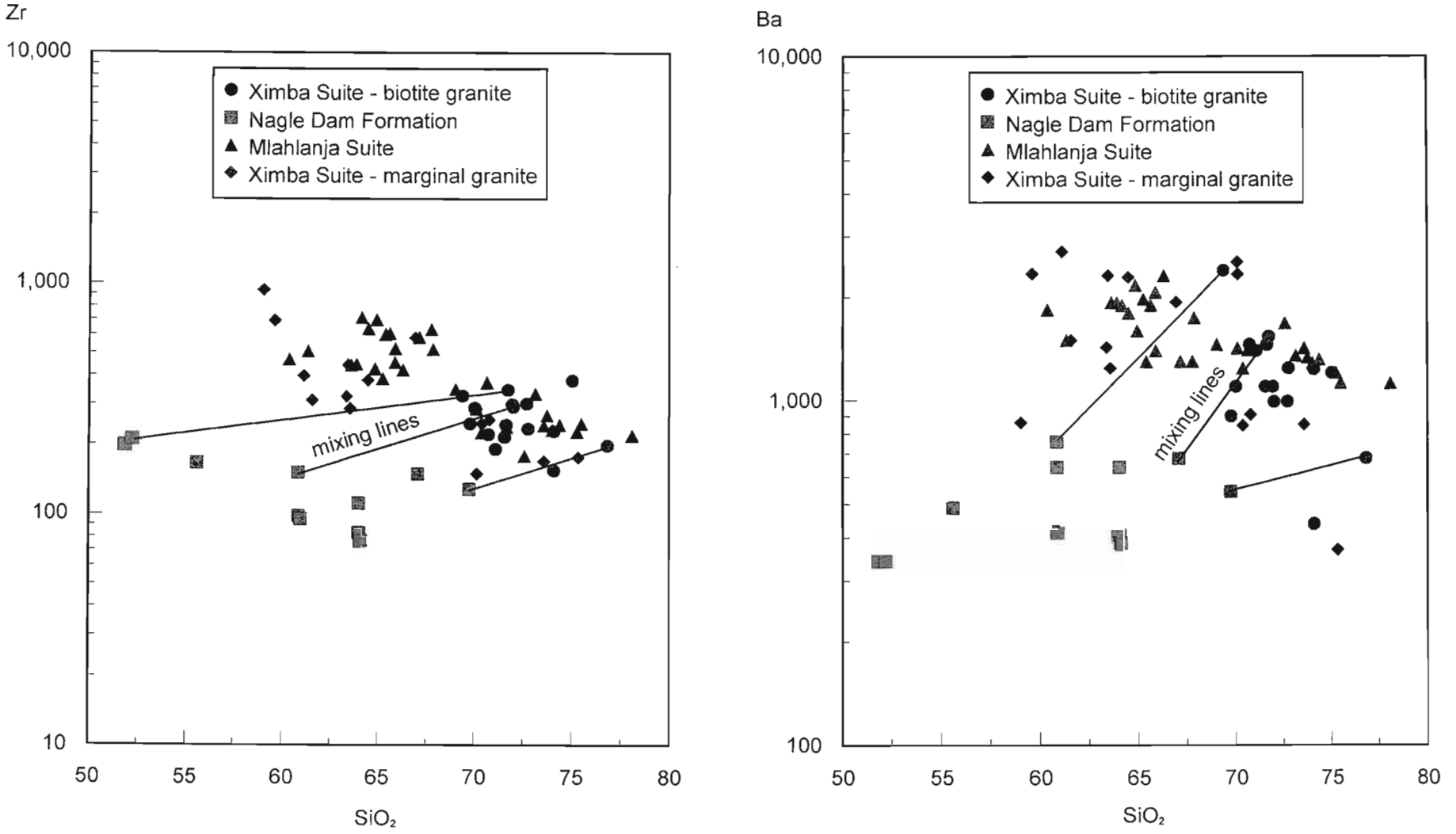

hornblende, Fe-Ti oxides, apatite and zircon (Tindle and Pearce 1981; Atherton and Sanderson, in Pitcher *et al.* 1985; Rapela and Pankhurst 1996). The increasing Rb/Ba ratio indicates the predominance of K-feldspar fractionation over biotite but the K/Rb ratio remains constant (with minor scatter) through the fractionation sequence, suggesting that K and Rb did not become decoupled during fractionation.

Fractionation modelling, however, does not produce an acceptable model for the generation of the more acidic biotite granite from an initial melt with the chemical composition of the marginal granite through the removal of the observed mineral phases. A two phase model of marginal granite - biotite granite - evolved biotite granite similarly fails to generate a model for the complete evolution of the series, although a reasonable model for the evolution of the biotite granite is obtained. Trace element modelling utilising an estimated model fractionation assemblage reproduces the declining Sr and Ba contents observed in the biotite granite, but not the slight increase in Rb content. Rather the model suggests a marked increase in Rb with fractionation, possibly due to the low biotite content in the model mineral assemblage. Equally, the available REE data do not support a fractionation model, with the decreasing Eu anomaly with increasing silica inconsistent with a fractionation model primarily controlled by feldspar fractionation, or REE enriched phases such as allanite (Miller and Mittlefehldt 1982).

Major element cumulate modelling (Appendix 5.11-5.14) of the marginal granite - biotite granite series utilising a variety of mineral assemblages, initial melt compositions (average marginal and biotite granite samples with silica concentrations between 69-71%; and average marginal and biotite granite samples with silica >69%, including and excluding the more basic samples (UND 41, 49 and 76) with possible cumulate components) and UND 2 as the evolved magma (lowest Sr and Ba), produces a model, with SSR varying from 0.18-0.36. Trace element modelling reproduces the trend of declining Ba and Sr, but fails to derive the observed slight increase in Rb concentrations found within the series (Figure 6.10). The decreasing Eu anomaly with increasing silica (Figure 4.10) may indicate progressive feldspar accumulation, while the higher REE levels for the lower silica samples is possibly due to a higher concentration of biotite and hornblende, with the increased spread in HREE the result of the accumulation of a HREE enriched phase, such as zircon (Fujimaki 1986).

b) Biotite Garnet Granite

The biotite garnet and biotite granites form a series with minimal overlap on the Harker diagrams, with the biotite garnet granite displaying a well defined straight line trend intersecting the biotite granite at approximately 70 percent SiO_2 (Figure 4.9) and projecting towards the chemically distinct biotite gneiss associated with the pelitic gneiss of the Valley Trust Formation, suggesting the formation of the biotite garnet granite through progressive mixing of the biotite granite magma with the biotite gneiss. This is evidenced in the field by the formation of a 'black granite' along strike from the biotite gneiss, grading through a darker coloured granite phase into the normal light coloured biotite garnet granite, corresponding with the progressive evolution in chemistries noted. Specific chemical evidence for this process is the almost straight line relationship between the biotite garnet granite and the biotite gneiss for the majority of the elements, particularly marked for FeO_{TOT}-SiO_2, Al_2O_3-SiO_2, Sr-SiO_2 and Zr-SiO_2 (Figure 6.11a).

Marked enrichment in specific elements, when compared with the biotite granite, such as Ba and Y, indicate an additional mixing component, which the available chemical data suggest may have been the garnet granite. This is illustrated on the Y-Zr and Zr/Y-Zr diagrams (Figure 6.11c,d) with the biotite garnet granite trending from a potential point source biotite granite towards the biotite gneiss and the garnet granite. This pattern is similar to that illustrated on the Ba-SiO_2 diagram (Figure 6.11b).

For several elements a deviation from straight line mixing is apparent on the Harker diagrams, and in particular the CaO-SiO_2, K_2O-SiO_2, Ba-SiO_2 (Figure 6.11b) and Y-SiO_2 diagrams. Decoupling of phases such as K_2O and Ba from enclave - granite mixing lines is possibly due to the crystallisation of K-feldspar or biotite in the granite (Di Vincenzo *et al.* 1996; Bellieni *et al.* 1996), or melt infiltration through magma mushes (D'Lemos 1996).

6.4.3 MLAHLANJA SUITE

The Mlahlanja Suite comprises a series of hornblende granite, subcharnockite (green hornblende granite termed subcharnockite by Kuyper 1979), charnockite and garnet hornblende granite. These occur within plutons of variable mineralogical complexity, with individual plutons of: hornblende granite; hornblende granite - subcharnockite - charnockite; charnockite -

Figure 6.10. Cumulate modelling of the marginal granite - biotite granite series, Ximba Suite.
Model 1 - a) Sr-Ba, b) Ba-Rb. Model data from Appendix 5.11.
Model 2 - c) Sr-Ba, d) Ba-Rb. Model data from Appendix 5.12.
Model 3 - e) Sr-Ba, f) Ba-Rb. Model data from Appendix 5.13.
Model 4 - g) Sr-Ba, h) Ba-Rb. Model data from Appendix 5.14.
Individual symbols along the evolutionary paths represent 10% fractionation. Extreme model melt values not used.

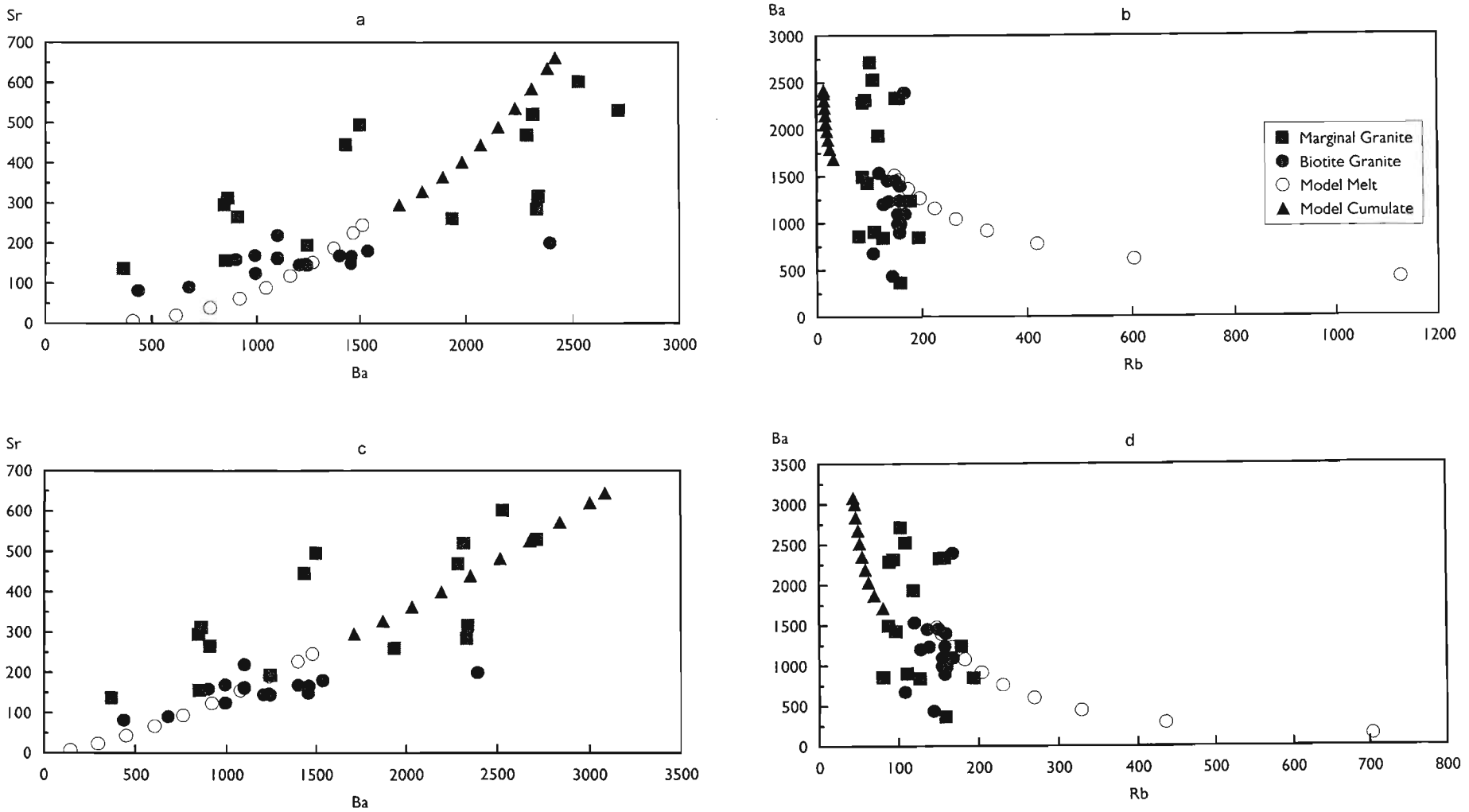

Figure 6.10. Cumulate modelling of the marginal granite - biotite granite series, Ximba Suite - continued.

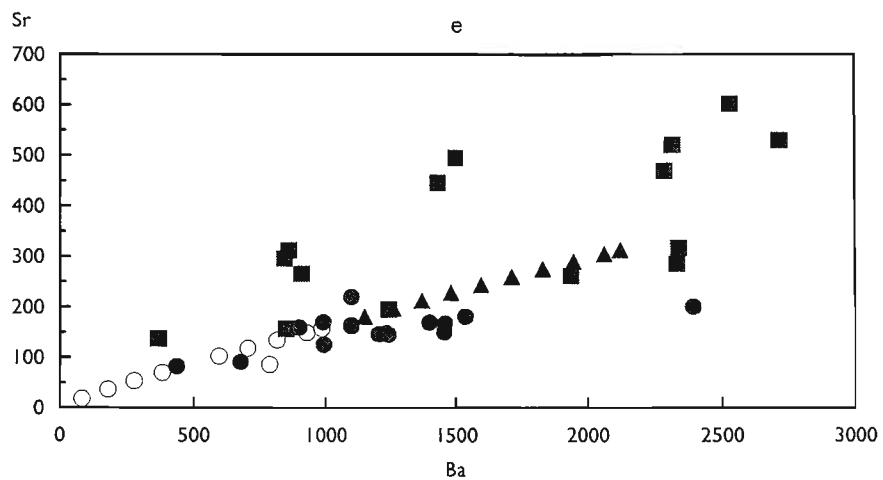

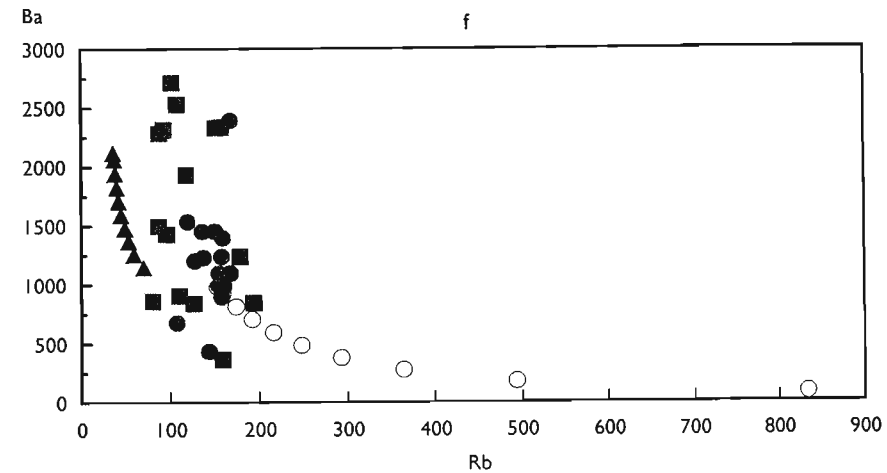

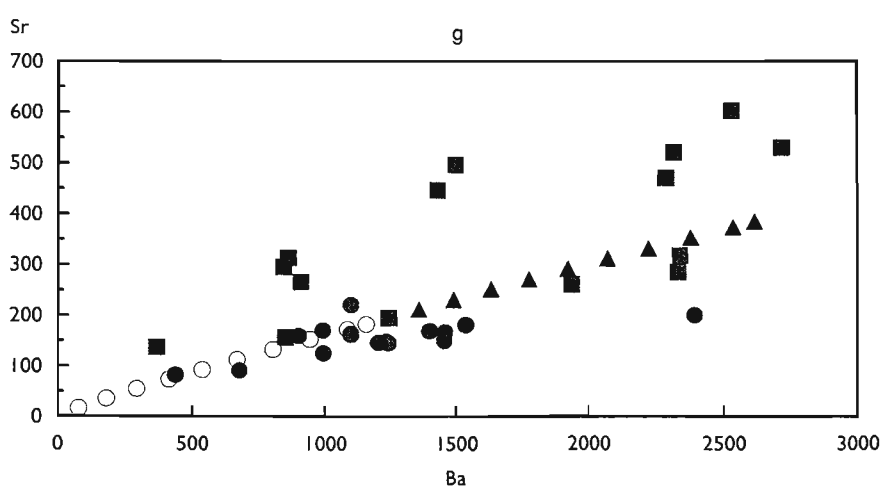

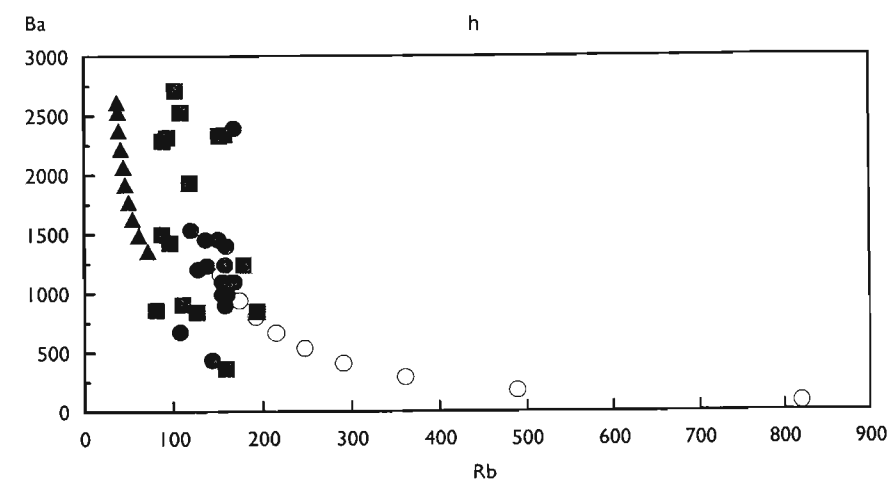

Figure 6.11. Petrogenesis of the biotite garnet granite - Ximba Suite.
a) Zr-SiO_2, b) Ba-SiO_2, c) Y-Zr, d) Zr/Y-Zr.

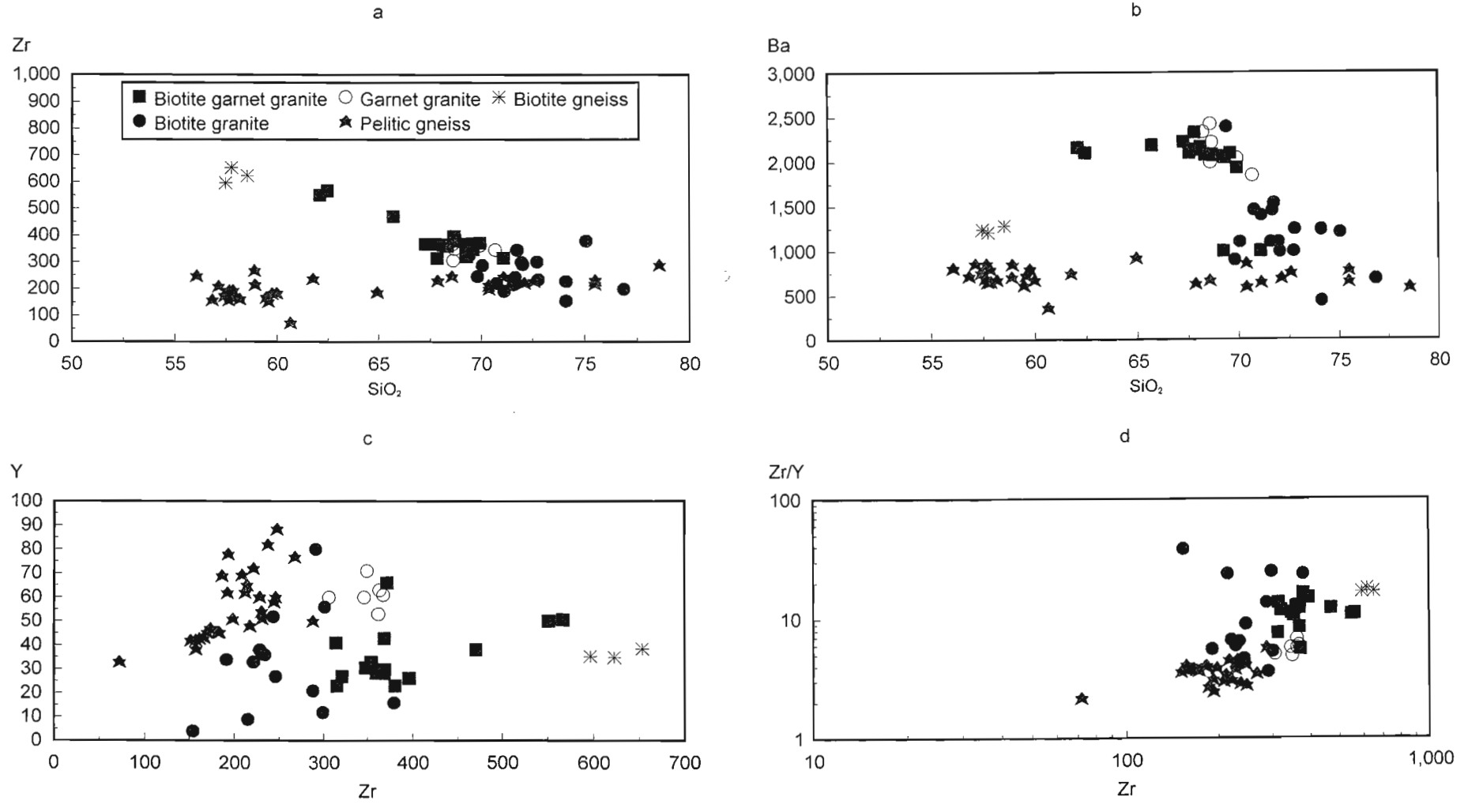

subcharnockite; and garnet hornblende granite identified. Three of these were sampled:

1) the Matata pluton - garnet hornblende granite;
2) the Sansikane pluton - hornblende granite - subcharnockite - charnockite (previously termed the Msunduzi pluton by Milne and Kerr 1990); and
3) the Egugwini pluton - subcharnockite - charnockite (Figure 2.1).

Although the various members of the series have broadly comparable chemical characteristics, with a major element-silica correlation coefficient of 0.62-0.95 for the entire series, analysis of the data from individual plutons reveals that each possesses unique fractionation features (Section 4.5.2).

Petrographic observations suggest a fractionating sequence similar to that identified in the Ximba Suite - early feldspar and quartz megacrysts with later mafics which may mantle the megacrysts, and a finer grained quartzo-feldspathic groundmass partially enclosed within the megacrysts, indicating a degree of overlap in their growth histories. Through the charnockite - subcharnockite - hornblende granite series a variation in the mafic assemblage is found, with an apparent fractionation history of pyroxene —> hornblende, biotite the dominant mafic in the more acidic granites and rare garnet in the subcharnockite. In the garnet hornblende granite the garnet occurs with the hornblende in the more basic phase of the granite, while biotite is the dominant mafic in the felsic portion. K-feldspar, plagioclase and quartz megacrysts occur throughout the series.

Although pyroxene is observed breaking down to form hornblende in the charnockite no indication exists that the charnockite forms the more basic portion of the hornblende granite - charnockite series, as found in several rapakivi granite batholiths (Anderson and Cullers 1978; Petersen 1980; Emslie 1991; Creaser 1996), or that the field evidence for charnockite mantled by hornblende granite represents a simple pyroxene —> hornblende fractionation series. Rather the hornblende granite and charnockite of the Sansikane pluton display a degree of overlap on the Harker diagrams, but with distinct differences for individual elements, such as Zr which is relatively enriched in the charnockite. A pyroxene —> hornblende fractionation series may, however, exist for the charnockite - subcharnockite of the Egugwini pluton, although the available chemical data do not indicate a simple zonation pattern, with the charnockite chemically comparable with the subcharnockite.

Available chemical data suggest that the Egugwini and Sansikane plutons display a broad reverse zonation pattern, with a relatively basic core, consisting of either charnockite or hornblende granite, surrounded by more acidic material. This is not, however, related to the mineralogical zonation of the plutons, with the most basic member of the Sansikane pluton being a hornblende granite rather than a charnockite. Milne and Kerr (1990) proposed that this resulted from mineral accumulation and subsequent autointrusion in a model similar to that of Nabelek *et al.* (1986) for the Notch Peak Granite.

A marked inflection in the chemical data at c.69 percent SiO_2 within the hornblende granite suggests that the hornblende granite - subcharnockite - charnockite association may consist of two distinct series:

1) a basic series (60-69% SiO_2), comprising the majority of the hornblende granite; and
2) an acidic series (+69% SiO_2), comprising the majority of the subcharnockite;

with the acidic series relatively enriched in Rb, but depleted in Sr, Zr and Ba.

The two series display similar fractionation trends, possibly the result of the fractionation of plagioclase, apatite, Fe-Ti oxides, zircon and a mafic phase, which the increasing K_2O and Rb levels suggest was probably not biotite (Tindle and Pearce 1981; Atherton and Sanderson, in Pitcher *et al.* 1985; Rapela and Pankhurst 1996).

Major element fractionation modelling was attempted for the general fractionation trends of the Mlahlanja Suite as defined by the hornblende granite for the basic portion of the series and the subcharnockite for the acidic portion of the series and UND 63 as the initial magma composition. Major element modelling of the basic portion of the series (Appendix 5.15) provides a model, SSR 0.91, for a fractionating assemblage of:

hornblende + biotite + plagioclase + K-feldspar + clinopyroxene + orthopyroxene + oxide + apatite.

For the acidic portion of the series (Appendix 5.16) a model, SSR 0.06, is generated for a fractionating assemblage of:

hornblende + biotite + plagioclase + K-feldspar + apatite.

Trace element modelling of the hornblende granite,

however, does not derive the trace element characteristics of the subcharnockite, and in particular its low Ba content (Figure 6.12a,b). Modelling of the subcharnockite fractionation trend approximates that observed, but with the subcharnockite exhibiting little extension along the fractionation path.

Major element cumulate modelling of the series (Appendix 5.17), utilising as a model initial magma an average of the analyses with silica concentrations c.70 percent, yields a model, SSR 0.11, for an assemblage of:

hornblende + biotite + plagioclase + K-feldspar + clinopyroxene + orthopyroxene + apatite + quartz.

Trace element modelling defines the general trend of the series, although the modelled Ba is high and Sr low, but the available data display little of the modelled trace element variability, and in particular a limited range of Rb concentrations (Figure 6.12c,d).

The narrow range of REE concentrations suggest limited total REE fractionation (Figure 4.10). This is incompatible with the proposed fractionation of zircon and apatite, the latter of which was emphasised by Zhao *et al.* (1997) and Duchesne and Wilmart (1997) in defining the REE fractionation patterns in charnockites and monzonites. Hughes *et al.* (1997), however, noted that the constant range of REE within charnockites is inconsistent with fractionation of apatite and zircon, suggesting rather that the range of REE within charnockites is inherited.

6.4.4 THE MEGACRYSTIC GRANITES

Modelling of the various megacrystic granites of the Mgeni batholith poorly constrains their observed trace element variability. In particular the variations in the Rb content of the megacrystic granites are not derived through the modelling, with an apparent lack of an evolved fractionation phase within the available data set. This suggests that the megacrystic granites do not represent an evolving liquid composition generated through simple fractionation, or cumulate-melt unmixing, but rather, the observed chemical characteristics may have resulted from the Mgeni batholith representing only a portion of a complete melt differentiation process. Several features, including the increasing K/Rb ratio (Creaser 1996) and the marked variation in specific elements, and in particular Zr, suggest that this may represent a cumulate assemblage.

Petrographic evidence suggests that the individual suites evolved through a simple variation in mineralogy, for the Ximba Suite:

Plagioclase + biotite + K-feldspar + quartz + hornblende *(Marginal granite)*
—>
K-feldspar + quartz + plagioclase + biotite *(Biotite granite),*

and the Mlahlanja Suite:

Hornblende + plagioclase + K-feldspar + quartz + biotite (± orthopyroxene ± clinopyroxene) *(Hornblende granite+Charnockite)*
——>
K-feldspar + quartz + plagioclase + biotite *(Evolved hornblende granite).*

Analysis of the major element concentrations within the granites suggest that these can be modelled through variations in the observed mineral phases, with the mineralogical differences between the end members of the individual series being compatible with the trace element differentiation trend. In particular the increasing Rb content in the fractionating biotite granite of the Ximba Suite and the hornblende granite of the Mlahlanja Suite results from the growing biotite content of the granites, with a decline in Rb in the more siliceous granites as increasing quartz and feldspar dilutes the biotite concentration. This cannot be related to simple fractionation, as the typical modelled fractionation trends indicate a marked increase in Rb concentrations within the melt with continued fractionation. Rather it suggests that the megacrystic granites represent an accumulation of cumulate mineral phases. Modelling of this proposed process is hindered by the uncertainty regarding the initial chemistry of the melt, and for the basic portion of the hornblende granite of the Mlahlanja Suite was undertaken with an average initial granite composition from Creaser (1996), and a variety of modeled cumulate assemblages for the hornblende granite. This provides a close approximation to the observed trace element variations within the basic portion of the hornblende granite (Figure 6.13), although slight Sr enrichment is apparent for individual samples, possibly indicating preferential plagioclase accumulation. The plotting of the subcharnockite and acidic hornblende granite adjacent to this cumulate evolution trend suggests that the chemical differences identified between these and the hornblende granite may represent differences in their cumulate assemblage. Similarly, the general trend of the evolution of the

Figure 6.12. Petrogenesis of the Mlahlanja Suite.
Fractionation modelling - a) Sr-Ba, b) Ba-Rb. Model data from Appendix 5.15 and 5.16.
Cumulate modelling - c) Sr-Ba, d) Ba-Rb Model data from Appendix 5.17.
Individual symbols along the evolutionary paths represent 10% fractionation.

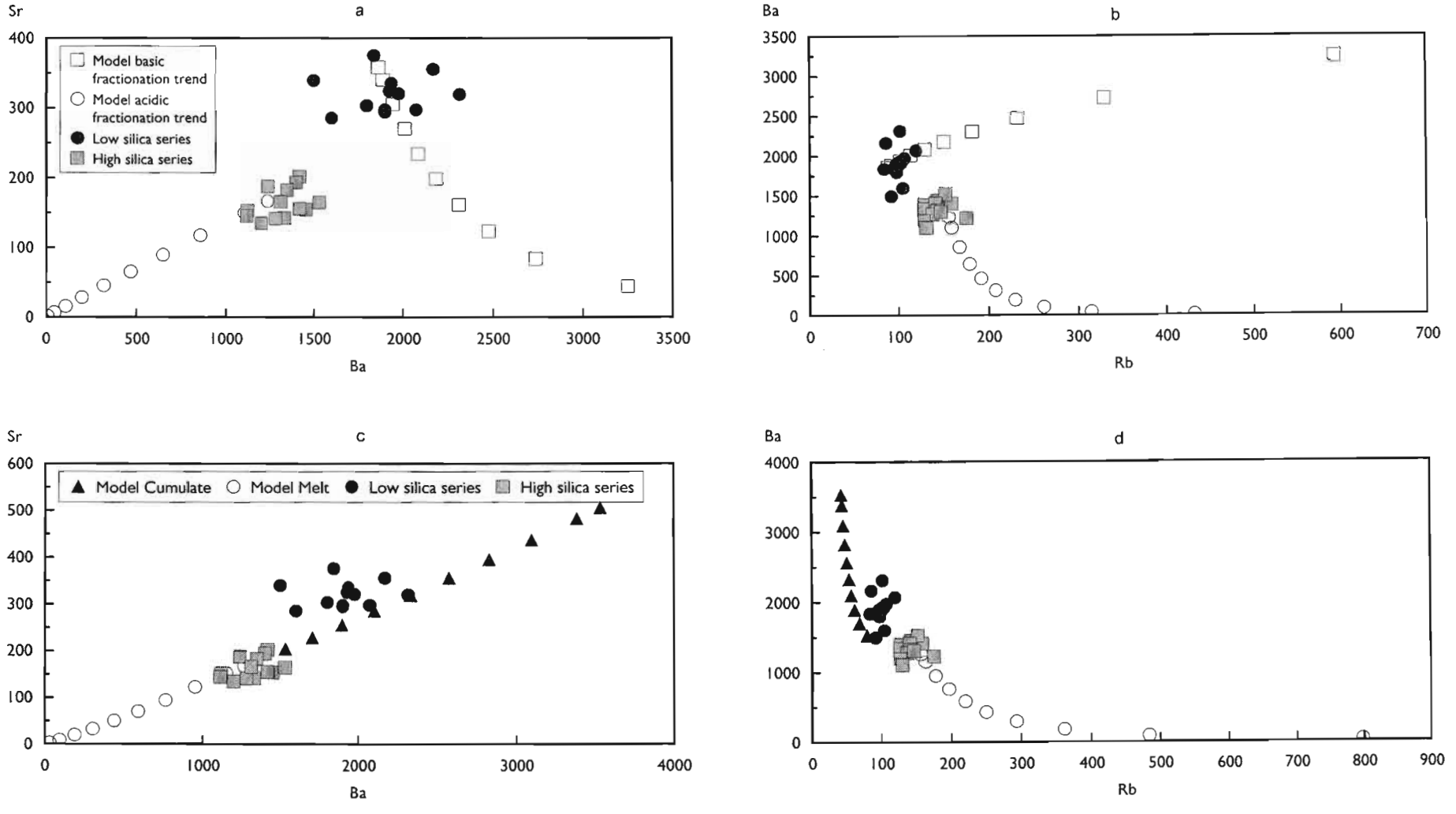

Figure 6.13. Cumulate model for the hornblende granite and subcharnockite, using the initial melt of Creaser (1996) as the reference initial melt. Individual symbols along the evolutionary paths represent 10% fractionation.

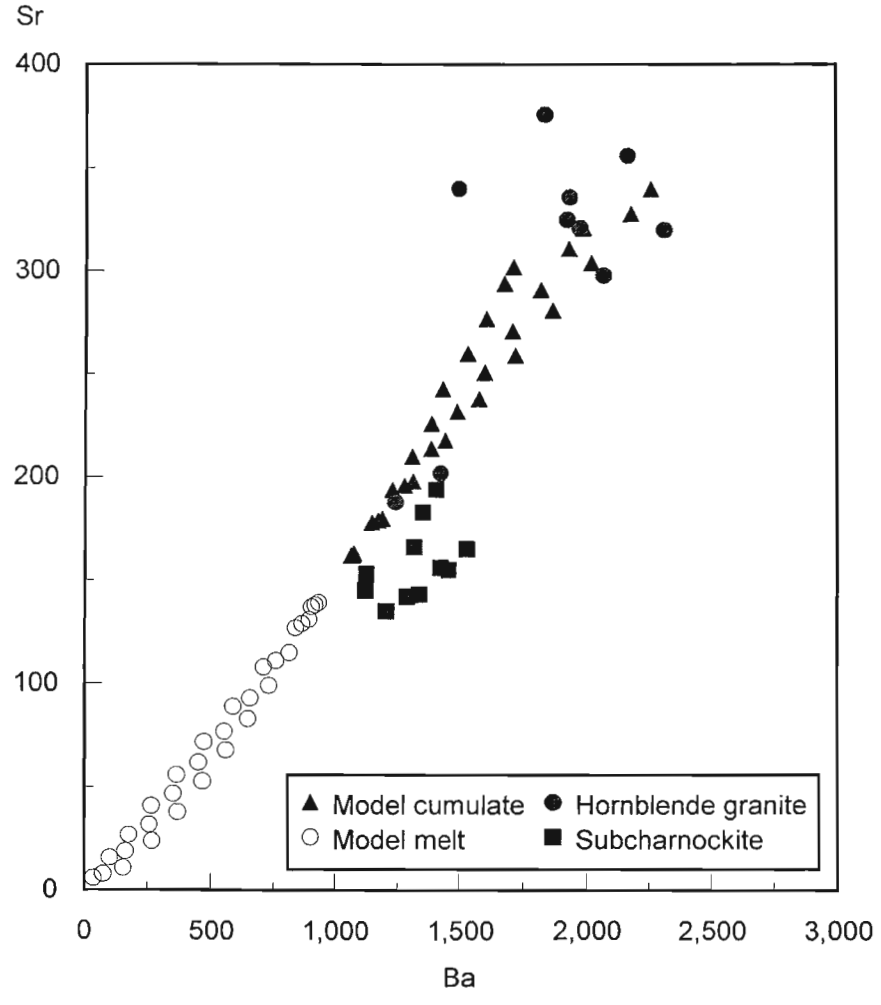

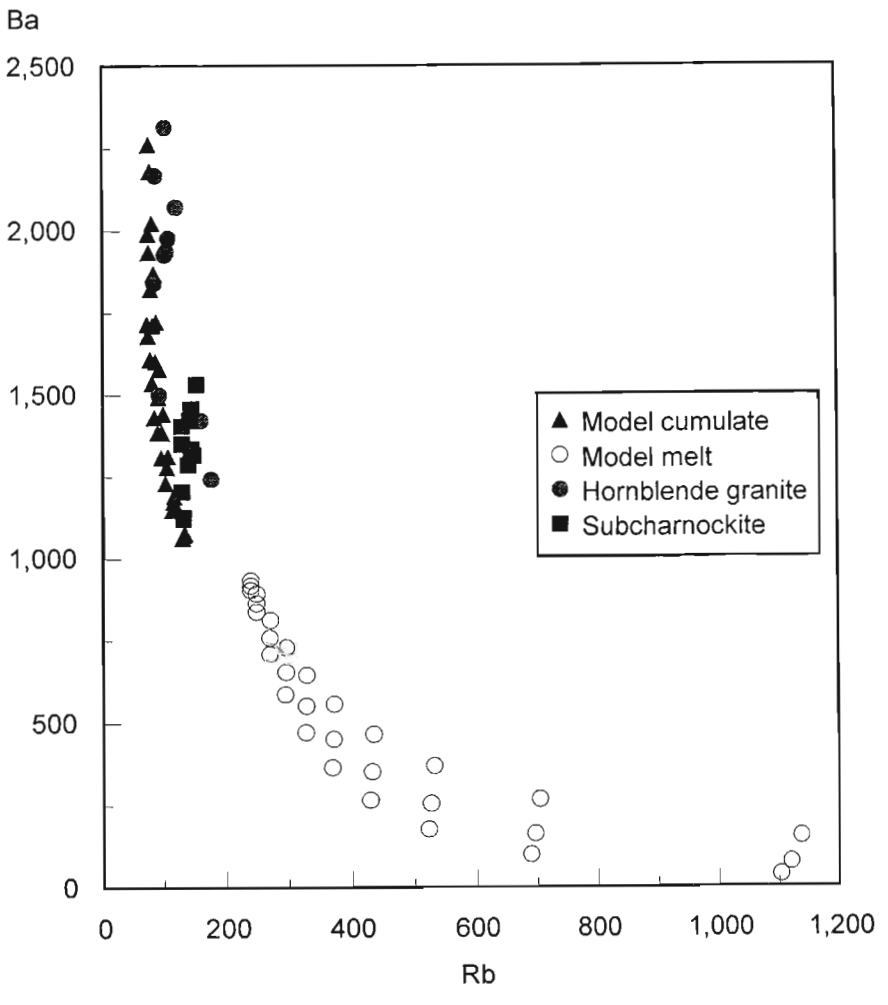

marginal granite - biotite granite is generated through this data, although not the more extreme Sr enriched members of the marginal granite, which again may indicate the preferential concentration of plagioclase.

The majority of rapakivi and A-type granites are considered to have evolved through crystal fractionation processes (Nedelec *et al.* 1995; Han *et al.* 1997; Zhao *et al.* 1997; Hassanen 1997), but various studies of the rapakivi granites have suggested that they may contain a variable cumulate-liquid fractionation component (Anderson and Cullers 1978; Ramo 1991; Cullers *et al.* 1992; Tack *et al.* 1994; Creaser 1996), with the cumulate typically considered to form the relatively basic phase of the individual intrusions, and in particular the charnockitic portion of the rapakivi association (Hubbard 1989; Emslie 1991; Creaser 1996). Comparison of the megacrystic granites of the Mgeni batholith with the cumulates identified by Ramo (1991) in the granites of the Suomenniemi batholith, reveals a similar trend in chemical evolution, with little extension along the liquid evolution curve (Figure 6.14). In particular is the almost constant Rb content of the cumulates and the Mgeni batholith with highly variable but declining Sr. The fractionation pattern for Ba is more complex, but the concentration range for the Mgeni batholith is similar to that of the cumulates of Ramo. The trace element data from the Mgeni batholith, however, extends to higher levels of Sr and Ba than observed by Ramo, with the cumulates of Ramo corresponding to the more evolved biotite granite and subcharnockite, for a comparable range of silica. Modelling of the hornblende granite utilising the initial melt of Ramo with the modelled cumulate assemblage derives its general trace element variation trend, but does not give the observed high concentrations of Ba and Sr found in the less siliceous hornblende granite. This results from the relatively low levels of these elements in the initial melt of Ramo.

Several authors have proposed that the rapakivi granites are predominately an upper crustal phenomenon (Barker *et al.* 1975; Vorma 1976; Anderson and Cullers 1978; Anderson 1983; Haapala and Ramo 1990) forming shallow level granitic batholiths and rhyolites. Cullers *et al.* (1992) and Milne and Kerr (1995), however, identified individual rapakivi granite batholiths that may have originated as midcrustal intrusives. Cullers *et al.* in deriving a model for the San Isabel batholith proposed a primary fractionation model, although it was noted that the generation and separation of cumulate phases controlled the development of at least a portion of the batholith, with the possibility that the chemical variability observed within this batholith was due to the separation of cumulate phases.

Hubbard (1989), however, modelled the evolution of the rapakivi granites through the production of a cumulate phase, which could, if the conditions were favourable, become separated from the granitic liquid phase of the intrusion. In the case of the Varberg granite complex, Hubbard noted that the granites remained in contact with their associated cumulates only through a major thrust fault which acted as a barrier to their upward accent. The midcrustal rapakivi granites may represent such a cumulate assemblage, coeval with the upper level granitic activity (Cullers *et al.* 1992). This suggests the possible occurrence of a depth related rapakivi evolution trend, with:

1) a midcrustal accumulation of rapakivi granite related cumulate material;
2) upper crustal cumulate and melt related rapakivi granites; and
3) an extrusive rhyolite series.

It is uncertain from the present data if the mid- to upper crustal series represents an evolutionary progression or if this is the result of distinct fractionation processes within similar magmas trapped at different levels. If these do, however, represent stages in the formation of a rapakivi granite series, then the possibility exists for the presence in the midcrust of an abundance of rapakivi granite cumulate bodies beneath the upper crustal and extrusive rapakivi granite - rhyolite province.

Thomas (1988a) has proposed that the granites of the Oribi Gorge Suite formed at high levels, suggesting that these may form a portion of an upper crustal rapakivi granite province in southern KwaZulu Natal. These granites, however, display chemical characteristics comparable to the Mgeni batholith (Figure 6.14), indicating that they may also have originated as cumulates beneath higher level rapakivi granite-rhyolite activity derived from the extraction of the melt phase from the cumulates. The occurrence of similar rapakivi granites throughout the Natal Province indicates that a major rapakivi granite-rhyolite province may have extended across the Natal Province in the Proterozoic, similar to that identified in North America (Bickford *et al.* 1986), but subsequently removed by erosion.

Figure 6.14. Comparision of the Ximba and Mlahlanja Suites with the rapakivi granite evolutionary trend of Ramo (1991).
The Ximba Suite - a) Sr-Ba; b) Ba-Rb.
The Mlahlanja Suite, with the Oribi Gorge Suite (Thomas 1988a) - c) Sr-Ba; d) Ba-Rb .

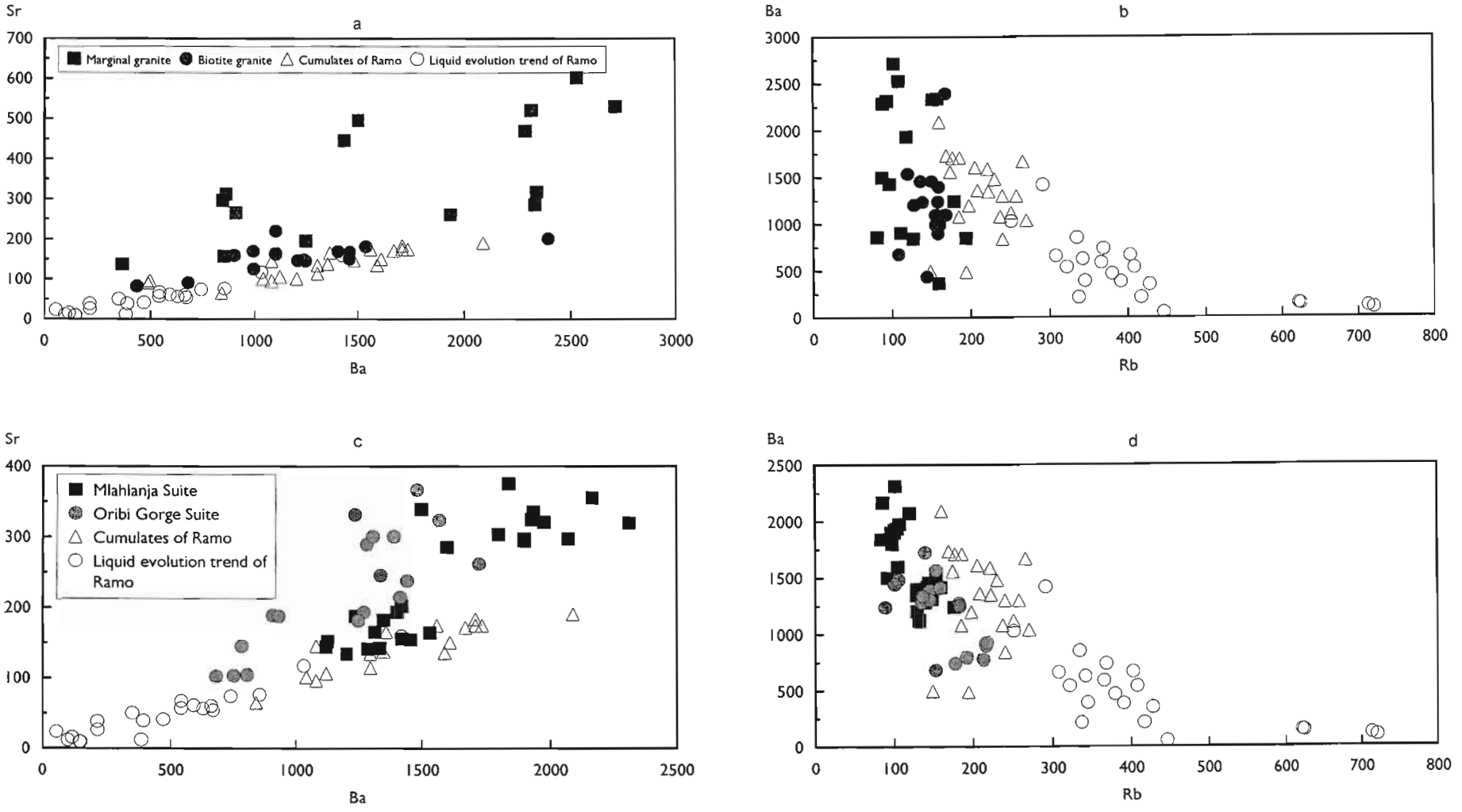

6.4.5 NQWADOLO SUITE

Only three analyses of the low Zr/Y granite are available, insufficient for a petrogenetic analysis, which will therefore concentrate on the high Zr/Y granite.

Removal of the low Zr/Y granite samples from consideration considerably reduces the spread of data within the Nqwadolo Suite, and only Al_2O_3, Na_2O, K_2O, Rb, Sr, Ba, Zn and Pb display any consistent large variation in concentration, all, with the exception of K_2O, declining in concentration with increasing silica. The almost constant concentrations of FeO, TiO_2, MgO and Zr with increasing silica while Ba declines, suggest minor fractionation of biotite and zircon. The more variable Al_2O_3, Na_2O, K_2O and Sr concentrations imply more extensive feldspar fractionation, which the declining Na_2O but increasing K_2O concentrations indicate was primarily a plagioclase. An increasing Rb/Ba ratio with fractionation is suggestive of K-feldspar rather than biotite fractionation, although this is not supported by an increasing K/Rb ratio. Ba-Sr and Ba-Rb fractionation vector trends indicate K-feldspar fractionation (Tindle and Pearce 1981). The sharply increasing Rb/Sr ratio (McDermott *et al.* 1996), and increasing TiO_2, Y and Rb concentrations with increasing Zr (Atherton and Sanderson, in Pitcher *et al.* 1985), however, imply plagioclase fractionation.

Major element fractionation modelling (Appendix 5.18), utilising an average of the two lowest silica granites as the initial melt and NQG 3 as the evolved melt composition, provides a reasonable model for all the elements, SSR 0.96, with the exception of silica, (SSR SiO_2 = 0.95), for a fractionating assemblage of:

biotite + plagioclase + K-feldspar + apatite.

Trace element modelling, however, is unable to derive the high Sr and Ba concentrations found in individual samples, although the general fractionation trend parallels that observed in the series (Figure 6.15a,b).

Major element cumulate modelling (Appendix 5.19), utilising an average of the available data as the initial magma composition, yields a model, SSR 0.148, for an assemblage of:

biotite + plagioclase + K-feldspar + ilmenite + apatite.

Trace element modelling closely follows the observed trace element concentrations found in the granite, and in particular the high Ba and Sr content of individual samples (Figure 6.15c,d). Deviations from the model trends may indicate preferential accumulations of specific mineral phases or incomplete cumulate/melt unmixing.

The Nqwadolo Suite is predominately metaluminous in nature, with occasional slightly peraluminous or peralkaline samples possibly the result of preferential concentration of individual mineral phases. It is also enriched in the HFS elements, demonstrating an A-type character. The metaluminous nature of the granite indicates derivation through the partial melting of a metaluminous source (Conrad *et al.* 1988; Clarke 1992), possibly an I-type tonalite or granodiorite (Cullers *et al.* 1981; Anderson 1983; Sylvester 1989; Creaser *et al.* 1991 and supported by the experimental data of Skjerlie and Johnston 1993; 1994; Patiño Douce 1997), although Rutter and Wyllie (1988) and Chappell and Stevens (1988) proposed that the partial melting of a tonalite would result in the production of a granodioritic melt, rather than an A-type granite.

Simple batch melting of the tonalite of Cullers *et al.* (1981) and potential local tonalite sources, however, indicate that these are unlikely sources for the granite, with low LREE contents and a high feldspar component resulting in a high Sr and Ba content in the melt. In addition, this model is not supported by the available isotopic data, with the relatively high Sr_I of the Nqwadolo Suite implying a crustal source for the melt. Potential modelling of the Nqwadolo Suite through the partial melting of basaltic material (Garland *et al.* 1995) is similarly inconsistent with the high Sr_I of the granite, without considerable crustal contamination. Such a model would, moreover, result in the production of a Sr enriched melt, as identified by Garland *et al.* in their modelling of the partial melting of the Pitanga basalts to derive the Chapeco rhyolites, with a model Sr content of 585ppm.

Halliday *et al.* (1991) determined that extremely high Rb/Sr ratios in granite could not be formed through partial melting. Rather they proposed a fractionation model to generate high Rb/Sr ratios, indicating that the chemical variations in the Nqwadolo Suite do not represent primary variations in a partial melt.

The relatively low Sr_I of the majority of the early orthogneisses from the Natal Province (Eglington

Figure 6.15. Petrogenesis of the Nqwadolo Suite.
Fractionation modelling - a) Sr-Ba, b) Ba-Rb. Model data from Appendix 5.18.
Cumulate modelling - c) Sr-Ba, d) Ba-Rb. Model data from Appendix 5.19.
Individual symbols along the evolutionary paths represent 10% fractionation.

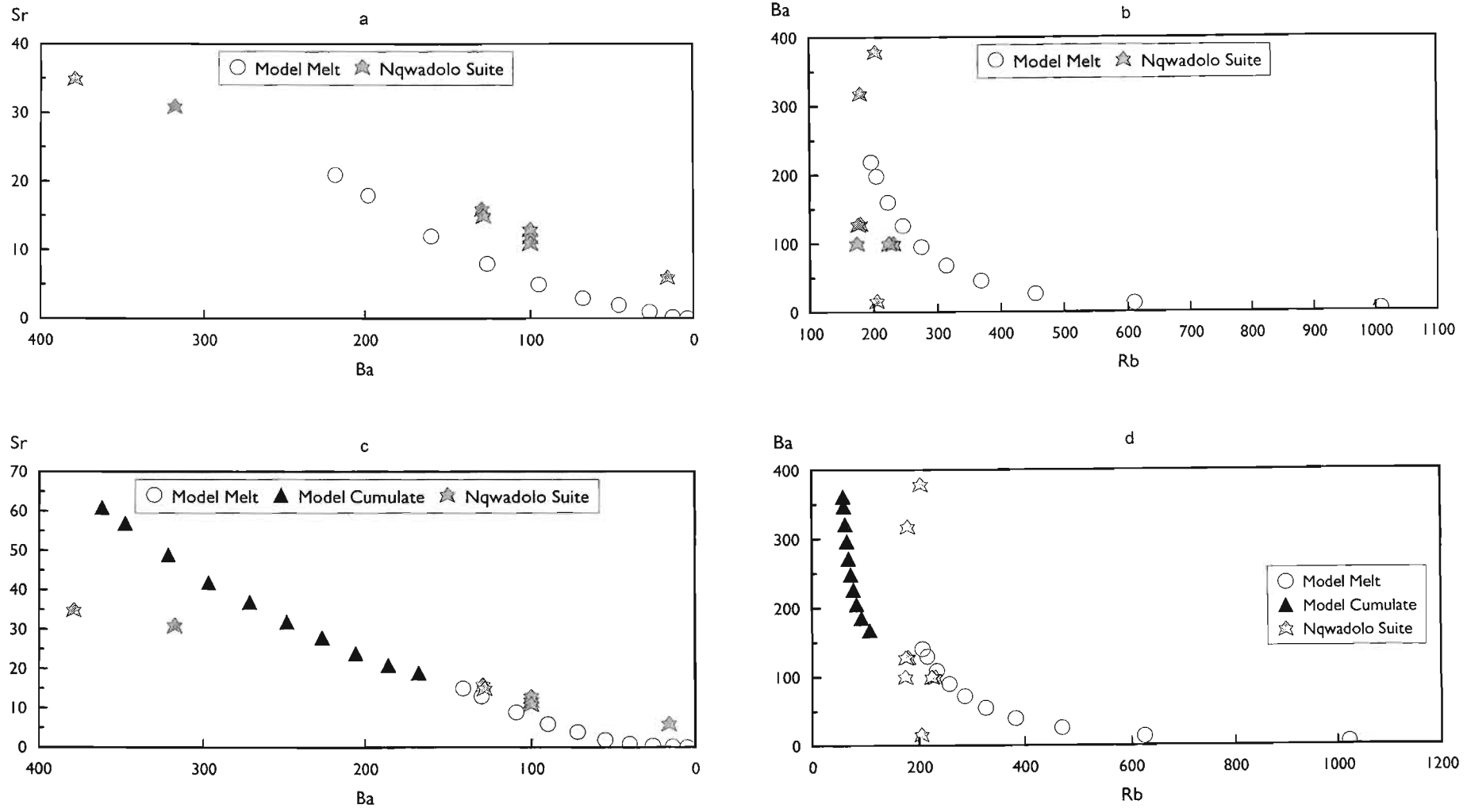

et al. 1989b), and the limited time range over which the province developed precludes the isotopic evolution of a potential source to allow the simple derivation of the isotopic character of the Nqwadolo Suite through partial melting. The high Sr_I of the Nqwadolo Suite and other granites within the Natal Province Eglington *et al.* suggested originated through *'rapid growth within a high Rb/Sr environment, rather than evolution over an extended period of time'*. Thomas *et al.* (1990), however, considered that the microgranite dykes from Margate, with a Sr_I of 0.716, were *'derived from melting of a pre-existing radiogenic crust'*, which could have provided a source for the Nqwadolo Suite.

6.5 MODEL FOR THE ORIGIN OF THE A-TYPE GRANITES

The A-type granite series comprise an association of granites which intrude during the closing stages of an orogenic cycle or during an anorogenic phase. They are chemically distinct from the orogenic calc-alkaline granites, with marked enrichment in total alkalis, FeO/MgO, F, Zr, Nb, Ga, Y and REE, but with low CaO and Sr (Collins *et al.* 1982; Whalen *et al.* 1987). Within the Proterozoic the anorogenic series consists of regionally specific rapakivi granites with a related extrusive rhyolite component, and anorthosites (Windley 1995).

Several models have been proposed to explain the origin of the A-type granites (Table 6.1), but typically they are considered to be the product of:

1) partial melting of previously depleted granulites;
2) partial melting of lower crustal material; or
3) fractionation of basaltic material.

The majority of these models have, however, been criticised as unlikely to generate A-type granites.

Creaser *et al.* (1991), for example, in discussing the depleted granulite model noted the low incompatible/compatible element ratios formed in residual granulites through the initial melt extraction event (Rudnick and Presper 1990; Ahmed-Said and Leake 1990), rendering these an unlikely source for granitic melt. Similarly, melting experiments by Dooley and Patiño Douce (1996) suggest that partial melting of F-rich sources generate peraluminous granites, rather than A-type granites. This finding also impacts on the lower crustal melting model, where the majority of studies explained the characteristic trace element content of the A-type granites as a function of the influence of a high F content or high temperatures (Collins *et al.* 1982; Whalen *et al.* 1987).

Melting experiments of lower crustal material have generated a variety of results. Skjerlie and Johnston (1993; 1994) and Patiño Douce (1997) derived a melt product with the major element characteristics of an A-type granite through partial melting of a tonalitic source, while Rutter and Wyllie (1988) and Chappell and Stephens (1988) suggested that tonalite melting would produce a melt with a granodioritic composition rather than an A-type melt. The experiments of Singh and Johannes (1996) derived A-type granite chemistries for specific starting compositions. Patiño Douce (1997) noted, however, that in his experiments A-type granite melt was only generated under low pressures. Hence this cannot explain the existence of deeper level A-type granites (Cullers *et al.* 1992).

As noted by Turner *et al.* (1992) the majority of the A-type granites possess low Sr_I, typically 0.702-0.707, suggesting a primary mantle component through their derivation from extended fractionation of basaltic melts (Turner *et al.* 1992), or the partial melting of basaltic material (Garland *et al.* 1995), although Anderson (1983) argued that this indicated derivation from an unradiogenic Proterozoic source material rather than the mantle. The former model is, however, supported by the generation of A-type granites within the oceanic islands (Rasmussen *et al.* 1988; Geist *et al.* 1995), but cannot explain the origin of A-type granites with high Sr_I (Turner *et al.* Table I). These latter are typically considered to result from a degree of crustal mixing in their origin (Eby 1990).

In Section 5.3.2 a model whereby granites reflect their source or initiator was proposed, within which the A-type granites are considered to have evolved from a continental flood basalt, through fractionation and assimilation of continental material, similar to the MASH (melting, assimilation, storage and homogenisation) model of Hildreth and Moorbath (1988) for arc magmas.

The chemical characteristics of several of the A-type granites suggest derivation from ocean island basalts (Eby 1990) and within plate type basalts are frequently found associated with A-type granites and rhyolites, in the bimodal association common to the extensional environment (Piccirillo *et al.* 1988; Clarke 1992; Garland *et al.* 1995). Evidence for widespread contamination of basaltic material within the extensional environment is found in the contaminated basalts commonly

Table 6.1. Models proposed for the generation of the A-type granites.

	Model	References
1	Fractionation of basaltic magma, possibly alkaline	Loiselle and Wones 1979, Eby 1990, Turner *et al.* 1992, Tack *et al.* 1994, Geist *et al.* 1995, Garland *et al.* 1995
2	Melting of lower crustal material under fluxing of mantle derived volatiles	Bailey 1978
3	Melting of previously depleted granulites	Collins *et al.* 1982, Clemens *et al.* 1986, Whalen *et al.* 1987
4	Melting of a tonalitic I- type granite	Anderson and Cullers 1978, Cullers *et al.* 1981, Anderson 1983, Sylvester 1989, Ramo 1991, Creaser *et al.* 1991, Skjerlie and Johnston 1993, Patiño Douce 1997, King *et al.* 1997
5	Partial melting of a depleted mafic-intermediate lower crust	Landenberger and Collins 1996
6	Magma mixing	Barker *et al.* 1975, Eby 1990, Neymark *et al.* 1991, Stimac and Wark 1991, Foland and Allen 1991, Kerr and Freyer 1993, Poitrasson *et al.* 1995, Frost and Frost, 1997, Han *et al.* 1997
7	Partial melting of metamorphosed amphibolite bearing K_2O rich mafic cumulates	Poitrasson *et al.* 1994
8	Melting of a granodioritic crustal protolith	Nedelec *et al.* 1995
9	Metasomatic alteration	Harris *et al.* 1986a, Taylor *et al.* 1981
10	Partial melting of suprasubduction zone lithospheric mantle	Whalen *et al.* 1996
11	Partial melting of underplated ferrodiorite	Frost *et al.* 1999

present in continental flood basalt provinces (Hooper 1988), the more evolved members of which can plot in the within plate granite field (Figure 5.7) on the tectonic discrimination diagrams of Pearce *et al.* (1984).

The HFS element enriched chemistry of the continental flood basalts (Pearce 1982) serves as a potential HFSE source for the A-type granites, while the MASH process would generate a homogeneous base chemistry, which would assist in the production of the fundamental A-type granite chemical characteristics of the melt. Harris (1995) and Wickham *et al.* (1996) have adopted such a model for the generation of the homogeneous oxygen isotopic characteristics of several A-type granites.

Kerr and Freyer (1993) utilised the MASH model of Hildreth and Moorbath (1988) to explain the derivation of the A-type granites of Labrador, for which isotopic data indicate mixing of basaltic melt and the country rocks. In formulating this model, an initial Mg-rich basaltic component was proposed. This could not, however, provide the high HFSE content of the A-type granites, as noted by Kerr and Freyer, who suggested that the primary source for HFSE in the A-type granites was the breakdown of accessory phases in lower crustal rocks.

In the proposed model within plate basalts pond at the base of the crust, evolving and developing through the MASH process, with the chemistry of the base level A-type granite magmas determined by the degree of interaction of the primary MASH processes - basalt fractionation, contamination with country rocks and mixing with partial melts of the country rocks. This is illustrated in Figure 6.16, with crude estimates of the relative proportion of each component defined by the Sr_I of the derived melt. Low Sr_I granites would result from a melt generated predominately through basalt fractionation, basalt partial melting or through contamination of the system with low Sr_I country rocks. Higher Sr_I within these granites indicates greater degrees of magma mixing and contamination.

It is envisaged that at lower crustal levels the primary result of these processes is the development of a melt with chemical and isotopic characteristics comparable with the evolved continental flood basalts (Hooper 1988), which display evidence for contamination with crustal material. Further fractionation would increase the concentration of elements such as Y in the magma (Pearce 1982), by an estimated 1.5-2 times during the fractionation of the Imnaha Basalt (Hooper 1988). The formation of a feldspar dominant cumulate could further concentrate the HFSE in the melt (Pearce *et al.* 1984). Fractionation modelling of an evolved continental flood basalt, using the proposed fractionation assemblage of Pearce *et al.* (1984), indicates the general potential for the generation of A-type granites through this process. In particular, the typical high HFSE contents present in the A-type granites are obtained from such a model.

A high silica end member to this series would result from the mixing of a primary basalt sourced A-type granite with a crustal minimum melt. This would yield a high silica granite with a variably evolved isotopic character and variable HFSE enrichment, such as the Nqwadolo Suite. Simple major and trace element mixing models for average A-type granites, derived through fractionation of basaltic material, and typical S-type granite melts (data from Turner *et al.* 1992) suggest the potential for individual A-type granites to develop through the mixing of distinct granitic melts. The extreme values for the HFSE found in the fractionated basalt derived A-type granites allows the derivation of A-type granites through the small scale addition of the primary A-type granite to the crustal sourced melt.

Detailed modelling of these processes is complicated by the wide range of potential components, as noted by Hildreth and Moorbath (1988). Evidence exists, however, for the generation of A-type granites through the direct mixing of basalts and granite melts in the upper crust (Wiebe 1996). The identification of such upper crustal MASH processes suggest the potential for the operation of MASH type processes in the lower crust, which Cruden *et al.* (1995) and Wiebe (1996) considered was a more favourable environment for magma mixing.

A wide range of potential products can be generated depending on the degree of mixing between the basalt fractionation product and the country rocks. Those members of bimodal suites which do not possess A-type granite characteristics may be taken to represent crustal partial melts, in which the basalts acted primarily as a heat source, while those granites with chemical characteristics intermediate between the highly enriched granites produced by basalt fractionation and the crustal granites indicate a varying degree of mixing. Within individual regions this can result in the generation of granites and rhyolites with a wide

Figure 6.16. Proposed model for the generation of the A-type granites.

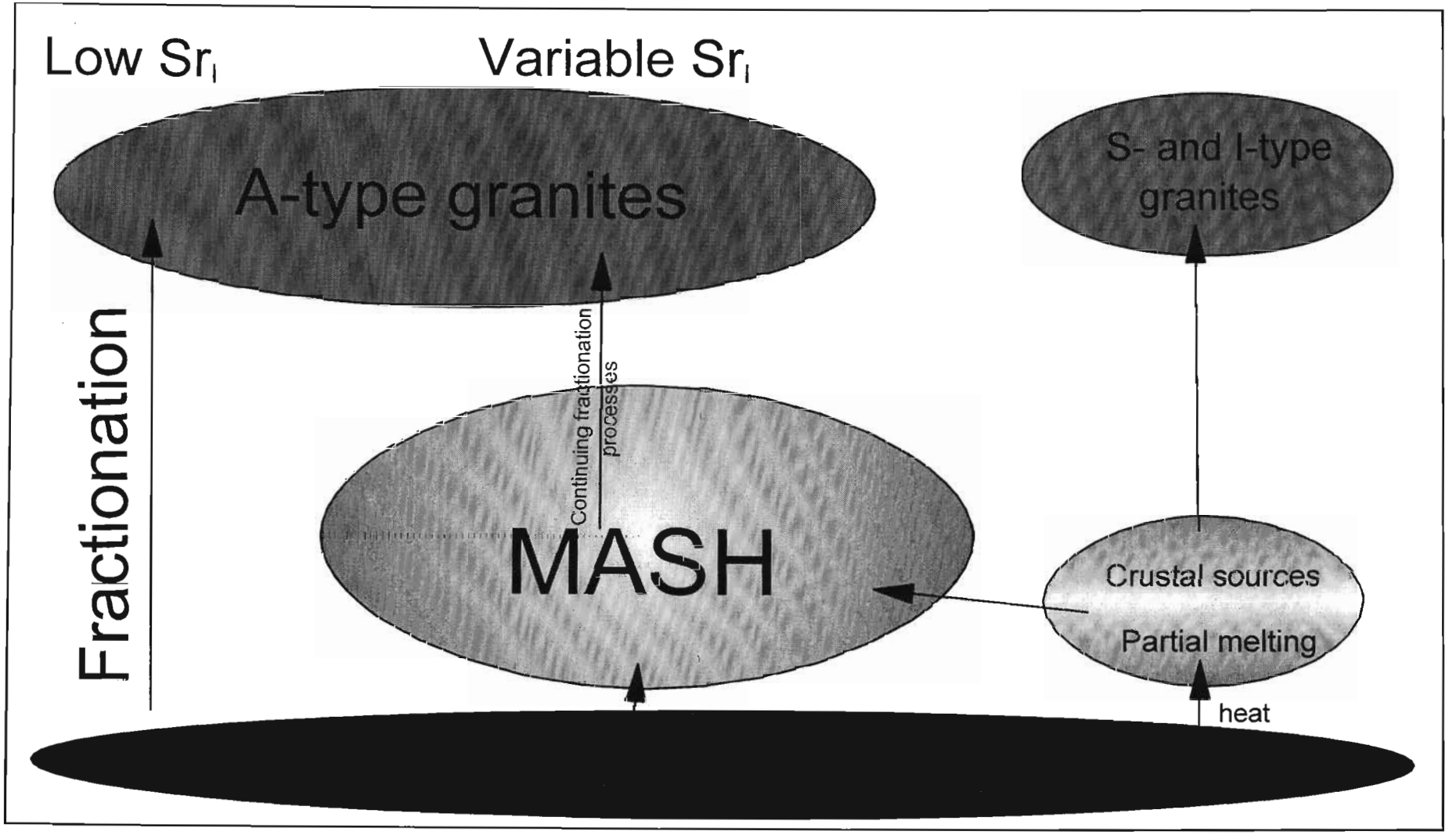

range of chemical characteristics. Leat *et al.* (1986), for example, noted a transitional chemistry from arc to within plate character for the rhyolitic members of the bimodal series in the Southern Caledonides, which may have resulted from variable interaction between within plate basalts and arc crustal material. Similarly, the peraluminous granites of Palmer Land, Antarctic, were considered by Wever *et al.* (1995) to have been derived through mixing of an enriched basalt and crustal melt. Analysis of their trace element data reveals a variable degree of HFSE enrichment, which overlaps with the within plate granites on the Rb-Y+Nb diagram of Pearce *et al.* (1984).

Within the Valley of a Thousand Hills no melt generation model can be derived for the megacrystic phases of the Mgeni batholith, as the original chemical characteristics of these melts are uncertain, with only the cumulates available for study. Isotopic data are available for two potential lower crustal source materials, granulite xenoliths in kimberlites (Rogers and Hawkesworth 1982) and metapelites (Eglington *et al.* 1989b), which could serve as potential crustal components in the derivation of the Oribi Gorge Suite. Comparison with the isotopic data from the Oribi Gorge Suite (Eglington *et al.* 1989b) indicate that the megacrystic granites of the Natal Province possess isotopic characteristics comparable with the lower crustal material, but stretched towards depleted mantle levels (Figure 6.17). This may suggest the origin of the granites through mixing of depleted mantle material and a lower crust with isotopic characteristics comparable with the model potential sources.

The low HFSE content of the Ximba Suite is possibly the result of greater feldspar accumulation, as suggested by Pearce *et al.* (1984), but differentiation cannot explain the increasing Sr_I through the series Mlahlanja —> Ximba Suite. Rather this suggests an increasing crustal involvement in the generation of these magmas, with the relatively higher HFSE content of the Mlahlanja Suite when compared with the Ximba Suite possibly the result of a greater incorporation of HFS enriched basaltic material into this magma. The relatively high Sr_I of the Nqwadolo Suite indicates that it consists, to a large degree, of crustal material, with its high HFSE and limited silica content suggesting it may have developed through the mixing of a fractionated primary A-type granite melt with a secondary minimum melt of crustal origin.

Isotopic data are lacking for the quartzo-feldspathic gneiss of the Valley Trust Formation, but its limited range of silica concentrations and typically low HFSE contents suggest that it may have originated as a primary crustal melt.

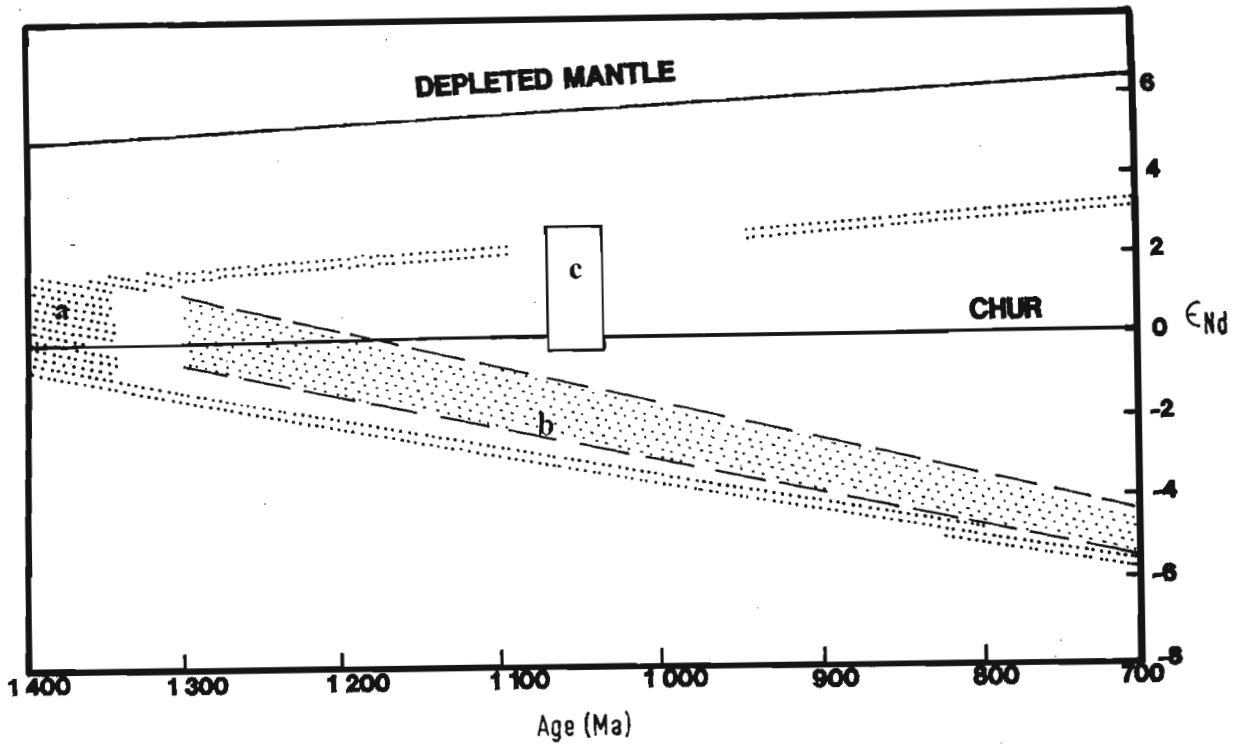

Figure 6.17. ϵ_{Nd}-age diagram for the Oribi Gorge Suite. Depleted mantle curve after Ben Othman *et al.* (1984). Field a - mafic lower crustal xenoliths of Rogers and Hawkesworth (1982). Field b - metapelites. (Fields a and b from Eglington *et al.* 1989b). Field c - Oribi Gorge Suite (Thomas *et al.* 1993).

CHAPTER 7

CRUSTAL EVOLUTION OF THE NATAL PROVINCE

7.1 INTRODUCTION

Thomas (1989a) and Jacobs and Thomas (1994) in their analysis of the Natal Province, identified three, possibly four, distinct tectonic terranes (Figure 1.1) which assembled during a series of collision events c.1100 Ma, ultimately welding onto the Archaean Kaapvaal Craton. From the north these terranes are:

1) the Tugela Terrane, a remnant of the Tugela Ocean, present as a series of thrust sheets obducted onto the craton margin;
2) the granitoid dominant arc related Mzumbe Terrane;
3) the arc related Margate Terrane, with a distinctive associated metasedimentary series; and
4) the Transkei Terrane of uncertain origin.

Boundaries between these terranes are marked by structural discontinuities, with evidence for thrust tectonics (Jacobs and Thomas 1994), but their primary recognition was based on the identification of terrane specific lithological units (Thomas 1989a). This analysis was undertaken, however, principally in southern KwaZulu Natal, and was poorly constrained by a geochronological data set which predominantly reflects metamorphic cooling ages (Thomas *et al.* 1993) and limited geochemical data. Extension into central KwaZulu Natal was conducted on the basis of general lithological similarity and the available geochemical data base of Kuyper (1979) and Du Toit (1979) (in Kerr 1985). Within southern KwaZulu Natal reinterpretation of the relationship between specific units has been initiated with the growth of the geochemical data base (Thomas *et al.* 1990).

In this chapter the existing crustal evolution model for the Natal Province will be revised. This will be undertaken through a re-examination of the regional lithological correlations proposed by Thomas (1989a) and Cornell *et al.* (1996) to allow the identification of distinct tectonic terranes within central KwaZulu Natal. From each terrane specific units, for which a geochemical data base is available, will be targeted to define their tectonic environment of origin, and allow the development of a model for the evolution of each terrane. Further, the accepted age and intrusion model for the Oribi Gorge Suite will be reviewed. This will be incorporated into a dynamic tectonic model for the Natal Province.

7.2 REGIONAL GEOCHEMICAL CORRELATION

Several authors have noted that the granites within orogenic belts may be divided into a series of mineralogically, texturally and chemically similar units. This was first observed by Larsen (1948), and has subsequently been rediscovered by White and Chappell in the Lachlan Fold Belt (White and Chappell 1983) and Pitcher in the Peruvian Coastal Batholith (Pitcher *et al.* 1985), who termed these fundamental units suites or superunits respectively. White and Chappell extended this concept to propose that the suites originated from simple variations in source material. More complex modelling by Collins (1996) suggests that the suites of the Lachlan Fold Belt result from unique parent magma compositions produced by complex mixing of a series of potential source components. Similar analyses have been undertaken for basaltic (Hooper 1988) and sedimentary (Winchester and Max 1996) sequences and utilisation of this technique has allowed the correlation of units, including the granite suites of the Lachlan Fold Belt of Australia (Chappell 1996b), over hundreds of kilometres. A degree of chemical similarity should therefore be apparent between the various correlates from different localities within the individual terranes of the Natal Province.

Thomas (1989a) proposed the regional correlation of the metamorphosed sequences of the Mzumbe Terrane - the Mapumulo Group - within which Thomas (1992) recognised the Quha and Ndonyane Formations. The Quha Formation was described as a series of biotite hornblende gneiss and migmatite, with abundant associated amphibolite and lesser marble and quartzite. Available geochemical data from the type Quha River area (Cornell *et al.* 1996), however, suggest that the orthogneiss of the Quha Formation is predominately basic in composition, with the more acidic portion of the series considered to be locally derived paragneiss. The Ndonyane Formation consists of siliceous quartzo-feldspathic gneiss, believed to represent a sheared portion of the S-type Mzimlilo granite (Thomas and Gain 1989).

Thomas (1989a) identified a number of granite series which intrude these gneisses. The most prominent of these is the Mzumbe Gneiss Suite (Thomas 1989b), a diorite-tonalite-trondhjemite-granodiorite series with a calc-alkaline evolution trend, dated at 1207±10 Ma (Thomas and

Eglington 1990) and a group of post-orogenic megacrystic granite batholiths - the Oribi Gorge Suite (Thomas 1988a, 1989a), which intruded between 1068±2 Ma (Oribi Gorge batholith) and 1029±10 Ma (Fafa batholith) (Thomas *et al.* 1993). The subsequent dating of the Quha Formation, 1163±12 Ma (Cornell *et al.* 1996), however, suggests that the Mzumbe Suite is older than the Mapumulo Group, with the arc intrusives associated with the Quha Formation representing later arc activity.

Within the Valley of a Thousand Hills the majority of the supercrustal gneisses of the Nagle Dam and Valley Trust Formations were correlated with the Quha Formation (Cornell *et al.* 1996). A potential correlation was, however, also suggested between the Mzumbe Gneiss Suite and the Nagle Dam Formation (Thomas 1989b). Similarly, the multiple batholiths of the Oribi Gorge Suite were taken to represent a single related magmatic suite, of which the Mgeni batholith was considered to be a member (Thomas 1988a; Thomas *et al.* 1993).

To date chemical data to support the identification of these predominately lithologically defined suites has been limited, and typically obtained only from southern KwaZulu Natal. In the case of the Oribi Gorge Suite the geochemical data base was derived predominately from the Oribi Gorge batholith, with the remaining batholiths being assigned to the suite on mineralogical similarity, broad chemical characteristics and comparable post-tectonic intrusion age. The existence of these suites will be re-examined from a broader data base, with the inclusion of data from the Valley of a Thousand Hills.

7.2.1 MAPUMULO GROUP

The amphibolite of the Quha Formation is more highly evolved, with markedly lower Cr, Ni and MgO concentrations but higher Zr, than that of the Nagle Dam Formation (Figure 7.1a,c). In particular the low MgO of the Quha Formation distinguishes it from the high MgO primitive arc type Nagle Dam amphibolite (Figure 7.1b). Fractionation trends are distinct between these units (Figure 7.1a), with the Zr/Y-Zr fractionation pattern (Figure 7.1d) indicating that the Quha amphibolite is not an evolved member of the Nagle Dam amphibolite.

Similarly, the low TiO_2 concentration, constant V content and distinct fractionation trends (Figure 7.1a). found in the Quha Formation allow distinction to be made with the Valley Trust Formation amphibolite. The Quha amphibolite plots on the Zr/Y-Zr fractionation trend of the Valley Trust amphibolite (Figure 7.1d), but intermediate between the different groups distinguished in the amphibolite (Section 4.4.3).

A more acidic series intrudes the amphibolite of the Quha Formation. Variations in Zr/Y ratios suggest that this series may comprise two distinct units, with the low silica samples forming a separate group. Insufficient data hinders a comparison with the biotite hornblende gneiss of the Nagle Dam Formation and in particular is the lack of more evolved members within the Quha gneisses. Distinct elemental abundances (Figure 7.2a) and fractionation trends, however, serve to separate these series, including a trend towards higher Zr and Y concentrations in the Quha Formation.

The Ndonyane Formation typically possesses higher Zr, Ga and Y, but lower Na_2O and Sr concentrations than the quartzo-feldspathic gneisses of the Nagle Dam and Valley Trust Formations (Figure 7.2b). These features allow the separation of these units.

The Quha Formation paragneiss sequence (Cornell *et al.* 1996) is less siliceous than the pelitic gneiss of the Valley Trust Formation with distinct Rb and K_2O enrichment in the pelitic gneiss, low Sr and CaO (Figure 7.2c), and constant P_2O_5 concentrations. Discrimination of the fine grained granulite is apparent through its lower Zr content (Figure 7.2d).

The available data therefore indicate that the various units of the Nagle Dam and Valley Trust Formation are chemically dissimilar to the orthogneisses of the Mapumulo Group in southern KwaZulu Natal and cannot be considered to form chemically unique suites, in the sense of White and Chappell (1983). Potential correlation of the metasedimentary units provides similar results, although the fine grained granulite and the paragneiss of the Quha Formation possess several similarities.

7.2.2 MZUMBE GNEISS SUITE

Thomas (1989b) suggested a possible correlation between the Mzumbe Gneiss Suite and the Nagle Dam Formation. Available data, however, suggest that the Mzumbe Gneiss Suite is chemically distinct from the Nagle Dam Formation, with higher Na_2O, but lower Ba concentrations and higher Zr/Y ratios (Figure 7.3a,b), indicating that

Figure 7.1. Comparision of the chemical characteristics of the amphibolites of the Nagle Dam, Valley Trust and Quha Formations (Cornell *et al.* 1996). Fields in 7.1b after Smith *et al.* (1997) for Nagle Dam and Quha Formations.

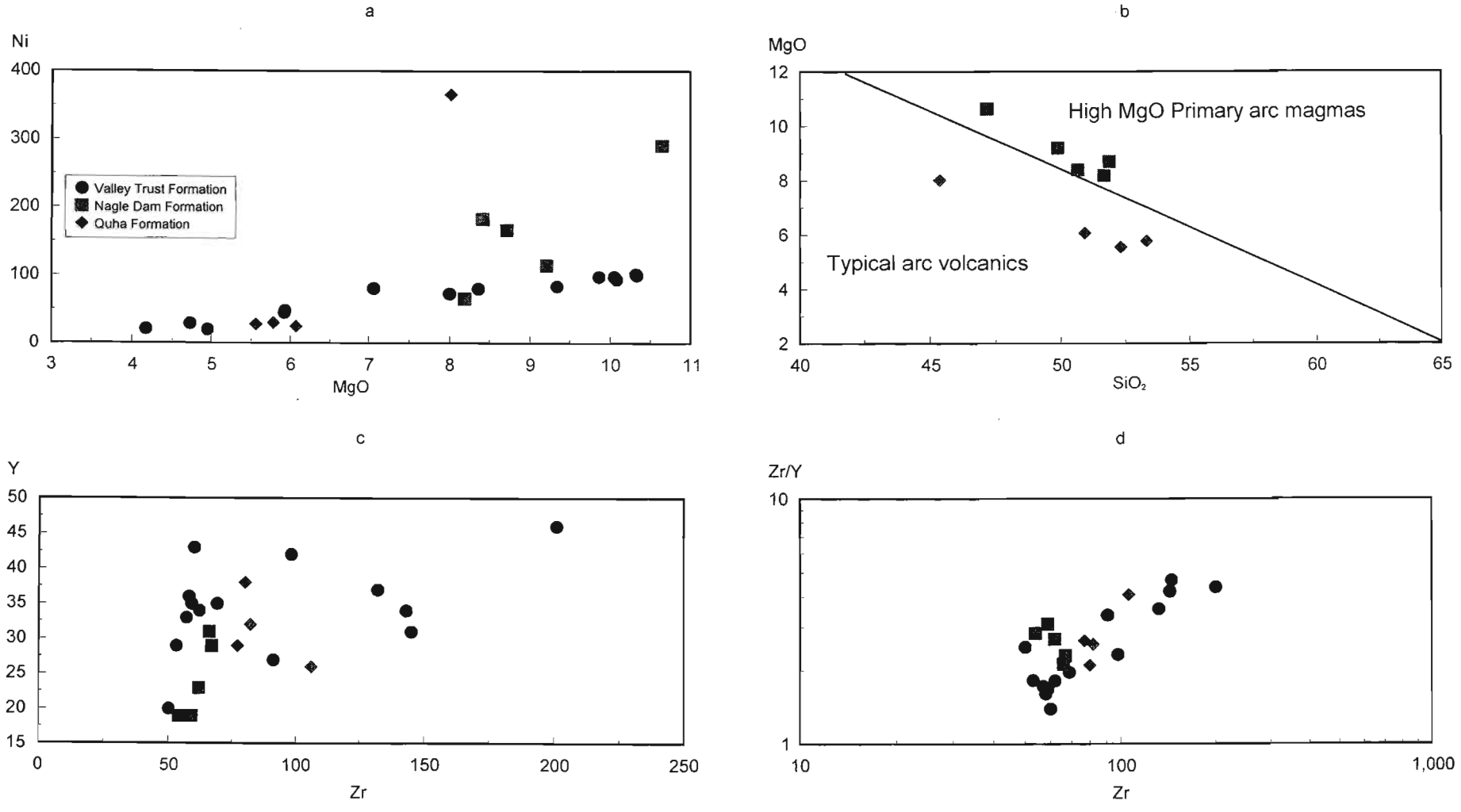

Figure 7.2. Comparision of the chemical characteristics of the intermediate, acidic and paragneiss members of the Quha, Ndonyane, Nagle Dam and Valley Trust Formations.
a) Sr-Rb. Biotite hornblende gneiss of the Nagle Dam Formation and the intermediate intrusives into the Quha Formation (Cornell *et al.* 1996).
b) Y-Zr. Quartzo-feldspathic gneisses of the Nagle Dam, Valley Trust and Ndonyane Formations (Thomas and Gain 1989).
c) CaO-Y, d) Zr/Y-Zr. Pelitic gneiss and fine grained granulite of the Valley Trust Formation and the peraluminous intermediate gneiss of the Quha Formation (Cornell *et al.* 1996).

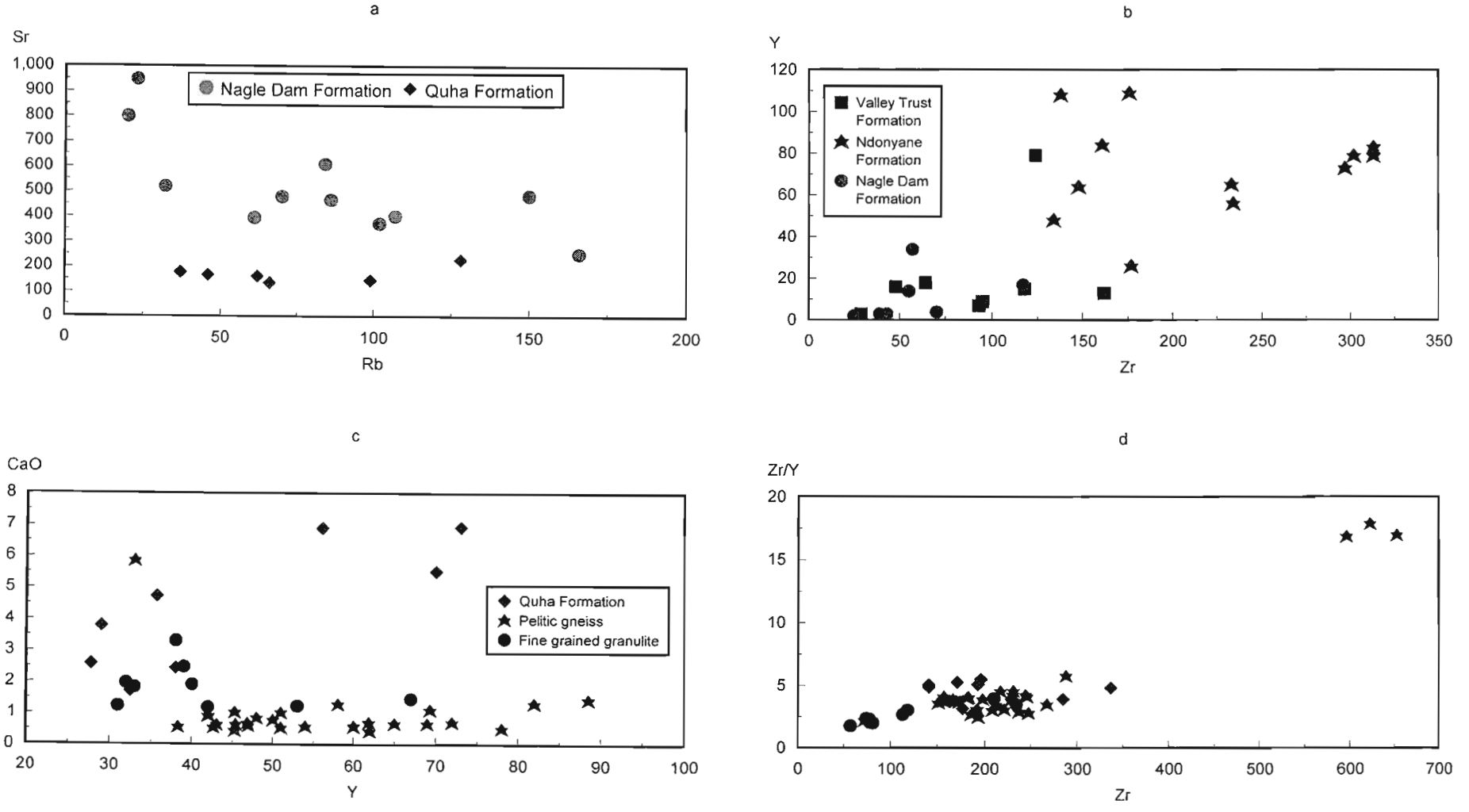

they form separate series.

7.2.3 EQUEEFA METABASITE SUITE

The Equeefa Suite was described by Thomas *et al.* (1992) from various localities in southern KwaZulu Natal. It consists of a variety of mafic and ultramafic rocks, partially to completely metamorphosed to the upper amphibolite facies. It intrudes the Quha Formation and the Mzumbe Suite; and is in turn intruded by the various syn- and late-tectonic granitoids, including the Oribi Gorge Suite. Available Rb-Sr age dates, 1024±32 Ma (Eglington *et al.* 1989b), are comparable with those from the Oribi Gorge Suite, and Thomas *et al.* suggested that the Equeefa Suite is a high level expression of a mafic underplating event, the heat pulse which generated the syn- and late-tectonic granitoids of KwaZulu Natal.

The Equeefa Metabasite Suite may be potentially correlated with the amphibolite of the Valley Trust Formation. The former, however, is relatively unevolved, with high MgO, Sr and Al_2O_3 but low FeO and Y, when compared to the Valley Trust Formation amphibolite, and displays distinct fractionation trends (Figure 7.3c,d). A degree of overlap is apparent, however, possibly suggesting a similar source type, but the chemical differences apparent between these amphibolite groups indicate that they are not directly related.

7.2.4 CORRELATION OF ORIBI GORGE SUITE BATHOLITHS

Consideration of the data presented by Thomas (1988a) reveal chemical differences between the different granites grouped into the Oribi Gorge Suite. In particular, the data from the Mvenyane pluton suggest that it is a high silica granite without the intermediate members present in the Oribi Gorge batholith. Specific elemental abundances also differ between the two batholiths, with relatively low K_2O, P_2O_5 and Ba concentrations in the Mvenyane pluton, while Na_2O is high. The Mvenyane pluton and the Oribi Gorge batholith may not, therefore, have derived from a common magma. Insufficient data are available in Thomas from the Fafa and KwaLembe batholiths to distinguish them from the Oribi Gorge batholith.

In analysing the possible chemical correlation of the megacrystic batholiths of KwaZulu Natal, comparison is made between the Mgeni, Fafa and Oribi Gorge batholiths, the former two batholiths being emplaced in the Mzumbe Terrane, and the latter in the Margate Terrane, as defined by Thomas (1989a). All are megacrystic in nature, with a prominent charnockite component and A-type granite chemical characteristics, including high FeO/MgO and a high HFS element content. The individual batholiths can, however, be distinguished through their distinct chemical characteristics and fractionation trends. The Mgeni batholith, for example, displays declining Y levels with increasing silica, while in the other batholiths Y concentrations increase with fractionation (Figure 7.4a). Similarly, the Oribi Gorge batholith possesses higher Rb concentrations than the Fafa and Mgeni batholiths from 64 to 69 percent silica, due to its distinct fractionation trend (Figure 7.4b). Batholith specific Y-Zr and Zr/Y-SiO_2 fractionation trends are also apparent (Figure 7.4c,d), while variations in the Zr/Y ratio suggest a progressive increase in Zr/Y, with Fafa<Oribi Gorge<Mgeni.

The distinct chemical characteristics of individual batholiths suggest that they are not members of a single suite. This is supported by the range of age dates obtained from the megacrystic granites, although previously interpreted as demonstrating a single intrusion event, which indicate an intrusion age of 1068±2 Ma for the Oribi Gorge batholith and c.1030 Ma for the Fafa and Mgeni batholiths (1029±10 Ma and 1030±20 Ma respectively) (Thomas *et al.* 1993).

7.3 REINTERPRETATION OF THE TECTONIC ENVIRONMENT OF SELECTED UNITS WITHIN THE NATAL PROVINCE

Crucial to the development of a tectonic model for the Natal Province is the identification of the tectonic environment of origin of the various units within the province, which must then be integrated with the available geochronological data base to provide a model of the evolution of the province. To this end seven units from southern KwaZulu Natal, for which chemical data are available, were selected for an analysis of their origins through the utilisation of the standard tectonic discrimination plots. Interpretation of such plots is complex, as noted in Chapter 5, and in many cases insufficient data are available to provide a reasonable result. In several cases therefore the identification of any tectonic environment must be viewed as provisional, to be revaluated when additional data becomes available.

Seven units were selected for analysis -

1) the Quha Formation, which comprises an amphibolite with a MORB character and an

Figure 7.3. Comparision of the chemical characteristics of the Nagle Dam Formation and Mzumbe Gneiss Suite (Thomas 1989b) and the amphibolite of the Valley Trust Formation and Equeefa Metabasite Suite (Thomas *et al.* 1992).
a) Na_2O-SiO_2, b) Y-Zr. Nagle Dam Formation and Mzumbe Gneiss Suite .
c) Al_2O_3-MgO, d) Zr/Y-Zr. Valley Trust Formation and Equeefa Metabasite Suite.

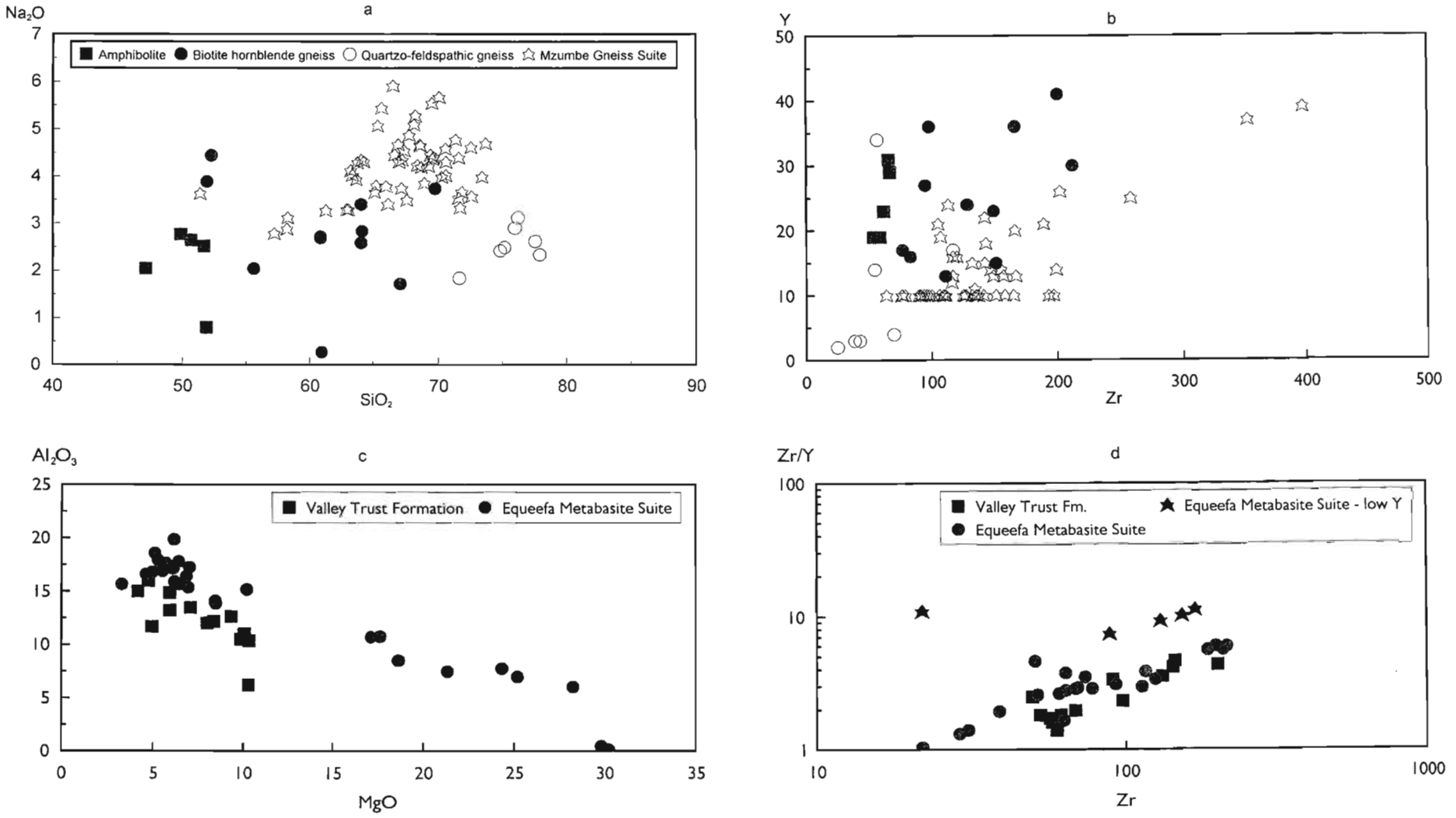

Figure 7.4. Comparision of the chemical characteristics of the granites of the Fafa (Eglington 1987), Oribi Gorge (Thomas 1988a) and Mgeni batholiths.

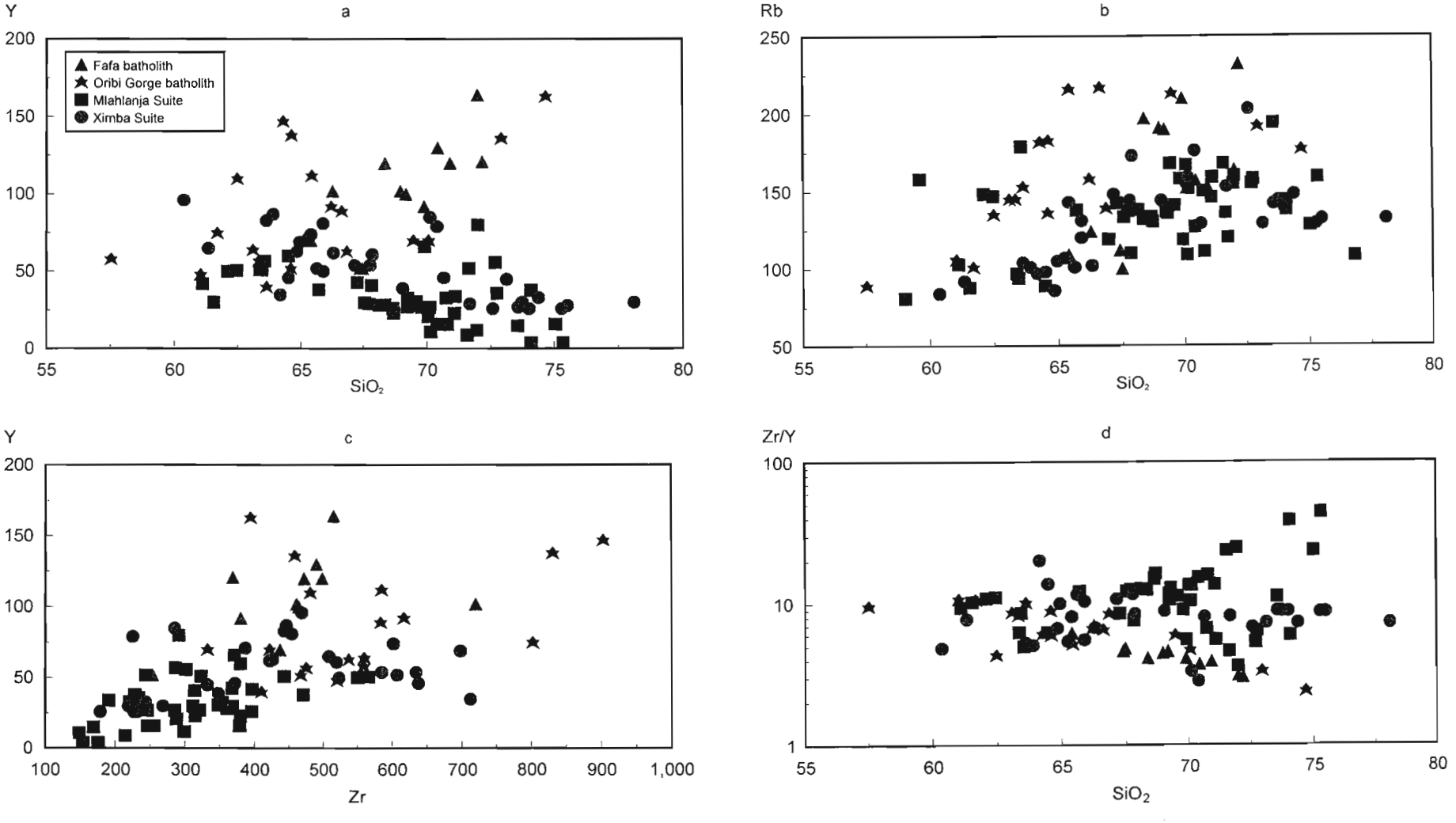

intermediate member with calc-alkaline arc chemical characteristics (Cornell *et al.* 1996);
2) the S-type Ndonyane Formation (Thomas and Gain 1989);
3) the Equeefa Metabasite Suite, heterogeneous but predominately a within plate basalt (Thomas *et al.* 1992);
4) the mafic to intermediate Munster Suite with calc-alkaline affinities (Mendonidis and Grantham 1989);
5) the S-type Sikombe Granite (Thomas and Mawson 1989);
6) the I-type Mzumbe Gneiss Suite (Thomas 1989b); and
7) the I-type Banana Beach Tonalite (Thomas 1989a).

7.3.1 THE BASIC SERIES

The high TiO_2, Zr and Y concentrations found in the Munster Suite suggest a degree of enrichment in its chemistry and an origin as a within plate basalt (Figure 7.5b,c), although its relative over enrichment in Y results in an overlap with the arc+MORB basalts (Figure 7.5a) and plate margin basalts (Figure 7.5d). The chemical characteristics of the amphibolites of the Quha Formation and the Equeefa Metabasite Suite do not allow a similar simple identification of their tectonic environment. Rather they plot across the defined fields on the various tectonic discrimination diagrams (Figure 7.5). In general, however, the Quha Formation does not display evidence for within plate basalt enrichment nor the low Y concentrations common to the arc basalts, suggesting a MORB origin, and on the Ti-Zr diagram it plots in the MORB field. The Equeefa Metabasite Suite does not possess the high V common to the arc tholeiites (Figure 7.5b), although its Y and TiO_2 are low, but with extension to levels found in the WPB. Typically, however, the majority of the samples from the Equeefa Metabasite Suite display MORB+WPB chemical characteristics, suggesting an origin for at least a portion of the Equeefa Metabasite Suite in an extensional environment (Figure 7.5b).

7.3.2 THE ACIDIC SERIES

The Mzumbe Gneiss Suite and the higher silica Quha gneiss plot predominately as volcanic arc granites, with minor extension into the within plate granite field for the former on the Nb-SiO_2 diagram (Figure 7.6). The single sample from the northern exposure of the Mzumbe Gneiss Suite plots with the Mzumbe Gneiss Suite on the tectonic discrimination diagrams, but approaches the within plate granite field on the Nb-Y and Rb-Y+Nb diagrams.

The lack of Ga and Ce analyses inhibits the construction of the A-type granite discrimination diagrams of Whalen *et al.* (1987), but the low Zr, Y and Nb concentrations of the Mzumbe Gneiss Suite are comparable with I- and S-type granites rather than the A-type granites. Similarly, its high CaO and relatively sodic nature suggest an I-type granite character.

The Banana Beach tonalite displays variable chemical characteristics, plotting across the within plate and volcanic arc granite fields on the tectonic discrimination diagrams of Pearce *et al.* (1984) (Figure 7.6). Equally, the high Zr levels of the tonalite is within the range of the A-type granites, rather than the I- and S-type granites. Its total alkali content is low, however, with high MgO and CaO concentrations, features not characteristic of the A-type granites (Whalen *et al.* 1987). The Banana Beach tonalite may, therefore, represent an I-type granite with a degree of enrichment in its source.

The remainder of the acidic series display within plate granite chemical characteristics (Figure 7.6d), with variably enriched Y and Nb (Figure 7.6b,c), while their high Zr+Y+Nb content may exceed the Zr+Y+Nb+Ce content required to characterise the A-type granites (Whalen *et al.* 1987). These granites do not, however, typically display the major element ratios identified by Whalen *et al.* as representative of the A-type granites. In particular is the low FeO/MgO ratio of the Sikombe Granite and the low silica member of the Quha Formation, while the Ndonyane Formation possesses a low total alkali content. This combination of chemical characteristics suggest that these granites may represent crustal melts with an enriched component.

7.4 IDENTIFICATION OF TECTONIC TERRANES

Thomas (1989a) identified the Mzumbe Terrane as a discrete component of the Natal Province, separated from the Margate Terrane to the south by the Melville Thrust and distinguished by dissimilar lithological associations. In particular Thomas noted the abundant amphibolite grade migmatite and pelitic gneiss of the Mapumulo Group, the presence of the Equeefa Metabasite Suite and the tonalite-trondhjemite Mzumbe Gneiss Suite within the Mzumbe Terrane. In contrast the Margate Terrane was characterised by a granulite grade metacarbonate series, rare pelitic gneiss, the Munster Metabasite Suite and the tonalite of the

Figure 7.5. Basaltic tectonomagmatic discrimination diagrams for the Equeefa Suite (Thomas *et al.* 1992), Munster Suite (Mendonidis and Grantham 1989) and Quha Formation (Cornell *et al.* 1996).
a) Ti/Y-Nb/Y (Pearce 1982), b) V- Ti/1000 (Shervais 1982), c) Zr/Y-Zr (Pearce and Norry 1979; Pearce 1983), d) Zr/Y-Ti/Y (Pearce and Gale 1977).
WPB - Within plate basalt; VAB - Volcanic arc basalt; MORB - Mid-oceanic ridge basalt; BAB - Back arc basalt; CFB - Continental flood basalt; OIB - Oceanic island basalt; AB - Alkali basalt.

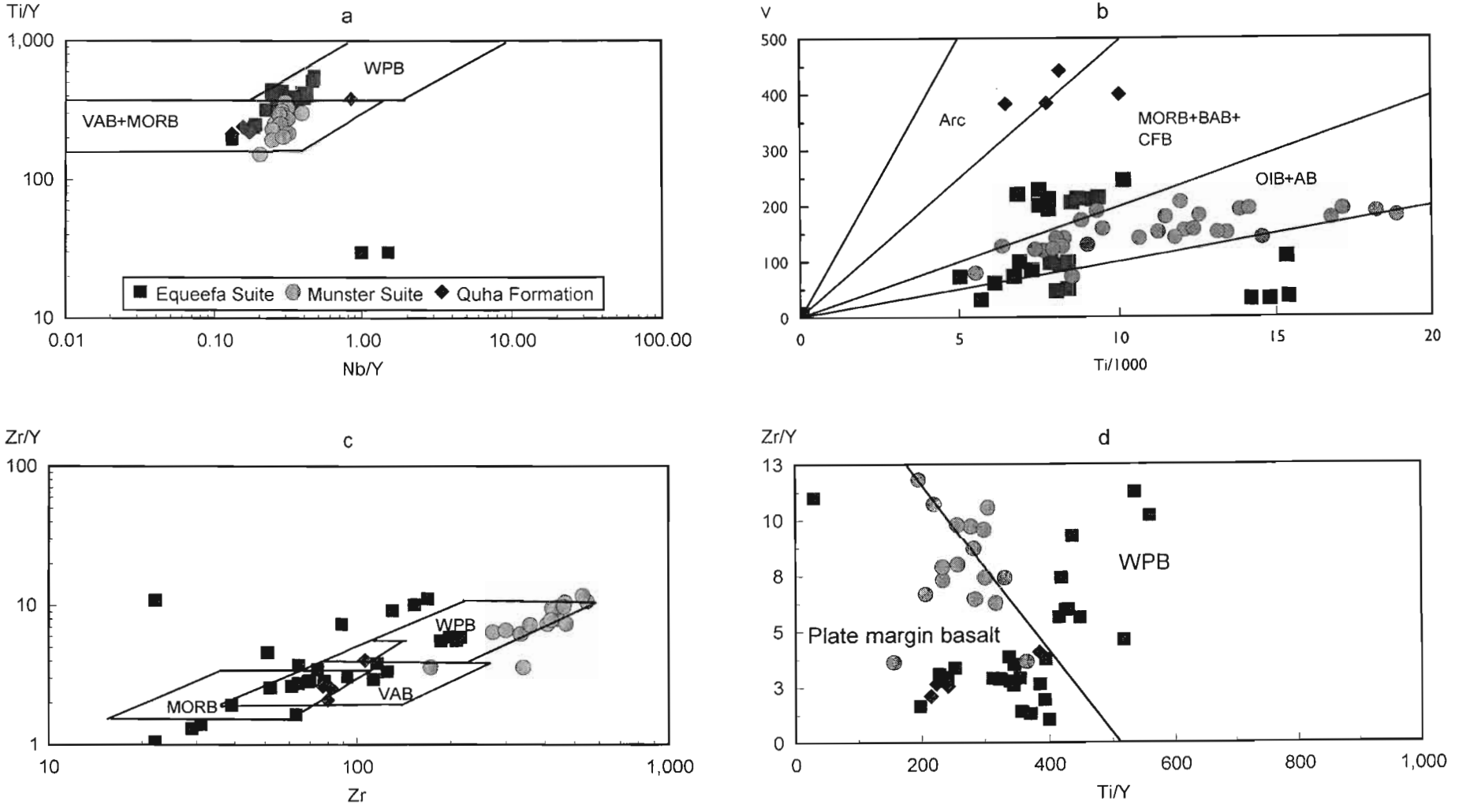

Figure 7.6. Granitic tectonomagmatic discrimination diagrams (Pearce *et al.* 1984) for the Sikombe granite (Thomas and Mawson 1989), Munster Suite (Mendonidis and Grantham 1989), Mzumbe Gneiss Suite (Thomas 1989b), Quha Formation (Cornell *et al.* 1996) and Ndonyane Formation (Thomas and Gain 1989).
a) Rb-SiO_2, b) Y-SiO_2, c) Nb-SiO_2, d) Nb-Y.
ORG - ocean ridge granite, VAG - volcanic arc granite, COLG - collision granite, WPG - within plate granite.

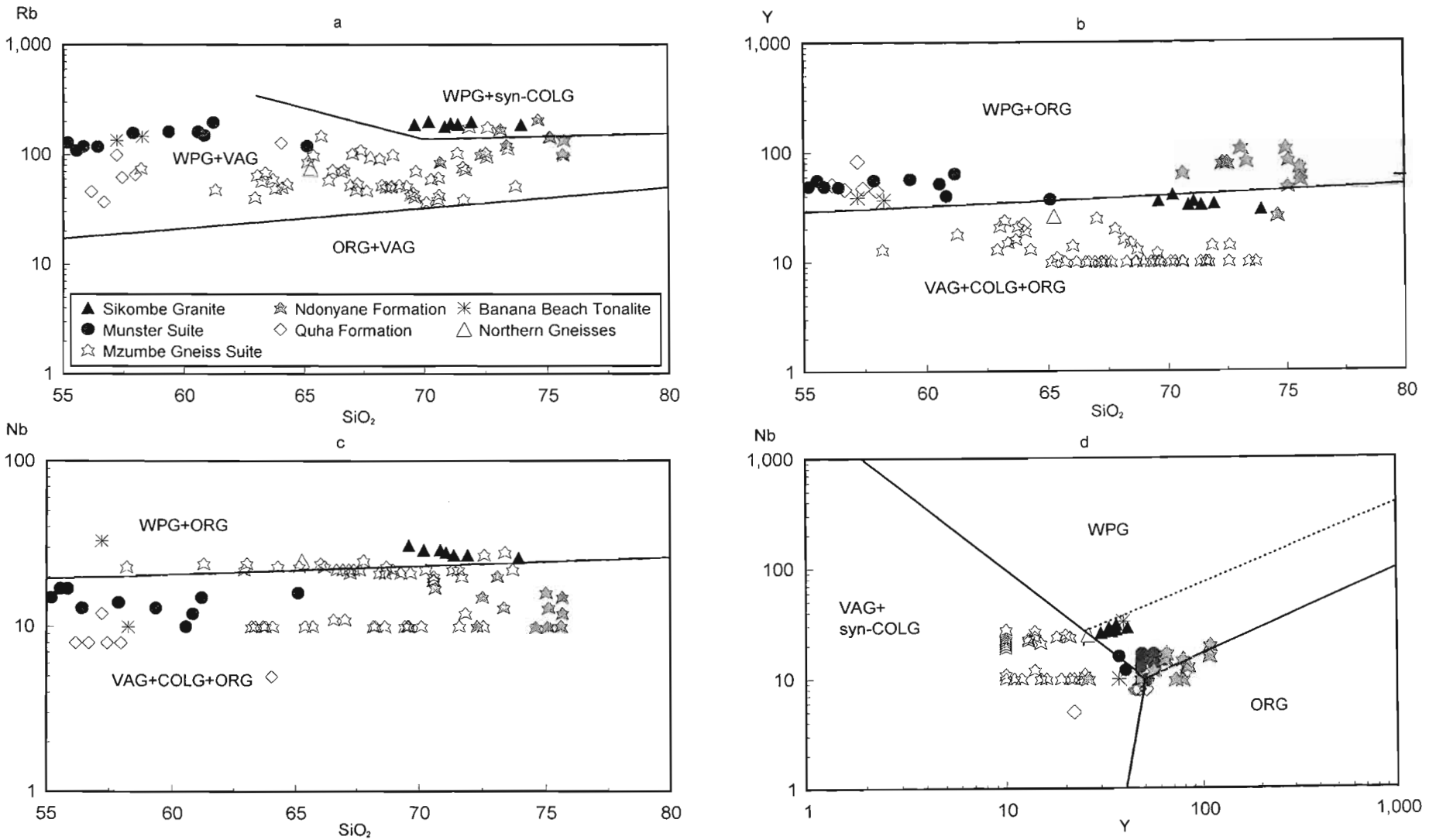

Banana Beach area. Distinct pre- and syn-tectonic granitoid series were also identified by Thomas in both terranes, with the Margate Complex and the Glenmore granite in the Margate Terrane and the Mkomazi, Mzimlilo and Mahlongwa Suites in the Mzumbe Terrane.

Analysis of the distribution of the various units within the southern portion of the Mzumbe Terrane indicates that individual units tend to occur marginal to the Mzumbe Gneiss Suite. Identification of the tectonic environment of several of these units, including the Quha Formation, suggests that they developed in environments distinct from the Mzumbe arc. The proposed back arc environment of the Quha Formation (Cornell *et al.* 1996), which divides the outcrop pattern of the Mzumbe Gneiss of Thomas (1989b), may suggest that the Mzumbe Gneiss Suite, as defined by Thomas, actually consists of two distinct units. Thomas noted that the northern portion of the Mzumbe Gneiss differed conspicuously from the main exposure to the south, but chemical data are unavailable to confirm this contention as Thomas (1989b) reported only one analysis from the former. This, however, displays higher Ba, Zr and Y concentrations, but lower Sr than the typical Mzumbe Gneiss. In addition, Thomas *et al.* (1992) established that the Equeefa Metabasite Suite is not present within this unit. The northern portion of the Mzumbe Gneiss Suite may, therefore, represent a separate arc segment.

This suggests that the southern portion of the Mzumbe Terrane as defined by Thomas (1989a) may not form a single integral unit, but rather consists of a variety of distinct terranes. The definition of terranes within this zone is, however, hindered by the possible origin of the Quha Formation during an extension event that split the Mzumbe arc. This shall therefore be termed the Quha sub-terrane, a northern portion of the Mzumbe Terrane. Intrusive into this zone is the Humberdale and Sezela granites and the main body of the Equeefa Metabasite Suite (Thomas 1988b).

Within this area three potential zones are therefore identified (Figure 7.7):

1) the Mzumbe arc to the south comprising essentially of the Mzumbe Gneiss Suite - the Mzumbe Terrane;
2) the Quha basin - the Quha sub-terrane - developed in a back arc spreading centre; and
3) the northern 'Mzumbe Gneisses' - the Mgangeni Terrane - possibly developed in an arc environment.

Beyond the Mgangeni Terrane the area is dominated by the S-type Mkomazi Gneiss Suite, associated with the gneisses of the Mpambanyoni Formation. The lack of arc type material, as found in the Mgangeni Terrane, suggests a fundamental division between this area, provisionally termed the Mkomazi Terrane, and the Mgangeni Terrane. The northern extent of this terrane is uncertain, being covered by Phanerozoic sediments, with the occasional inliers of basement gneiss correlated with the Nagle Dam Formation. This may indicate the presence of an arc fragment in this area.

Within the Valley of a Thousand Hills the Proterozoic basement can be divided into the extension related Valley Trust Formation and the composite arc sequence of the Nagle Dam Formation. The presence of high MgO amphibolite in the Nagle Dam Formation, possibly generated during extension within the arc (Smith *et al.* 1997), suggests that the Valley Trust Formation may have originated through the splitting of the Nagle Dam arc, with the southern extension of the arc located within the basement inliers to the north of the Mkomazi Terrane. This area will be provisionally termed the Mgeni Terrane, with the Valley Trust and Nagle Dam Formations forming distinct zones within this unit.

To the north of the Valley of a Thousand Hills, geochemical data are lacking. The discrimination of the environment in which the various units formed or the identification of any terrane is therefore not possible. The relationship between this area and the Mgeni Terrane is uncertain, and the area will be provisionally separated from the Mgeni Terrane as the Mapumulo Terrane. This zone terminates at the Lilani-Matigula Shear Zone beyond which is the Tugela Terrane.

7.5 TECTONIC MODEL FOR THE NATAL PROVINCE

Several models have been proposed to explain the development of the Natal Province (Matthews 1972; Milne 1986; Thomas 1989a; Thomas *et al.* 1994; Jacobs and Thomas 1994). Typically, however, these involve the formation of at least one volcanic arc with subsequent accretion onto the Kaapvaal Craton, and late intrusion of rapakivi like granites (the Oribi Gorge Suite of Thomas 1988a). The present study, however, suggests a more elaborate origin for the Natal Province, and in particular the recognition of a number of discrete terranes, each marked by a specific lithological association which originated in a distinct tectonic environment, with the redefinition of the Natal

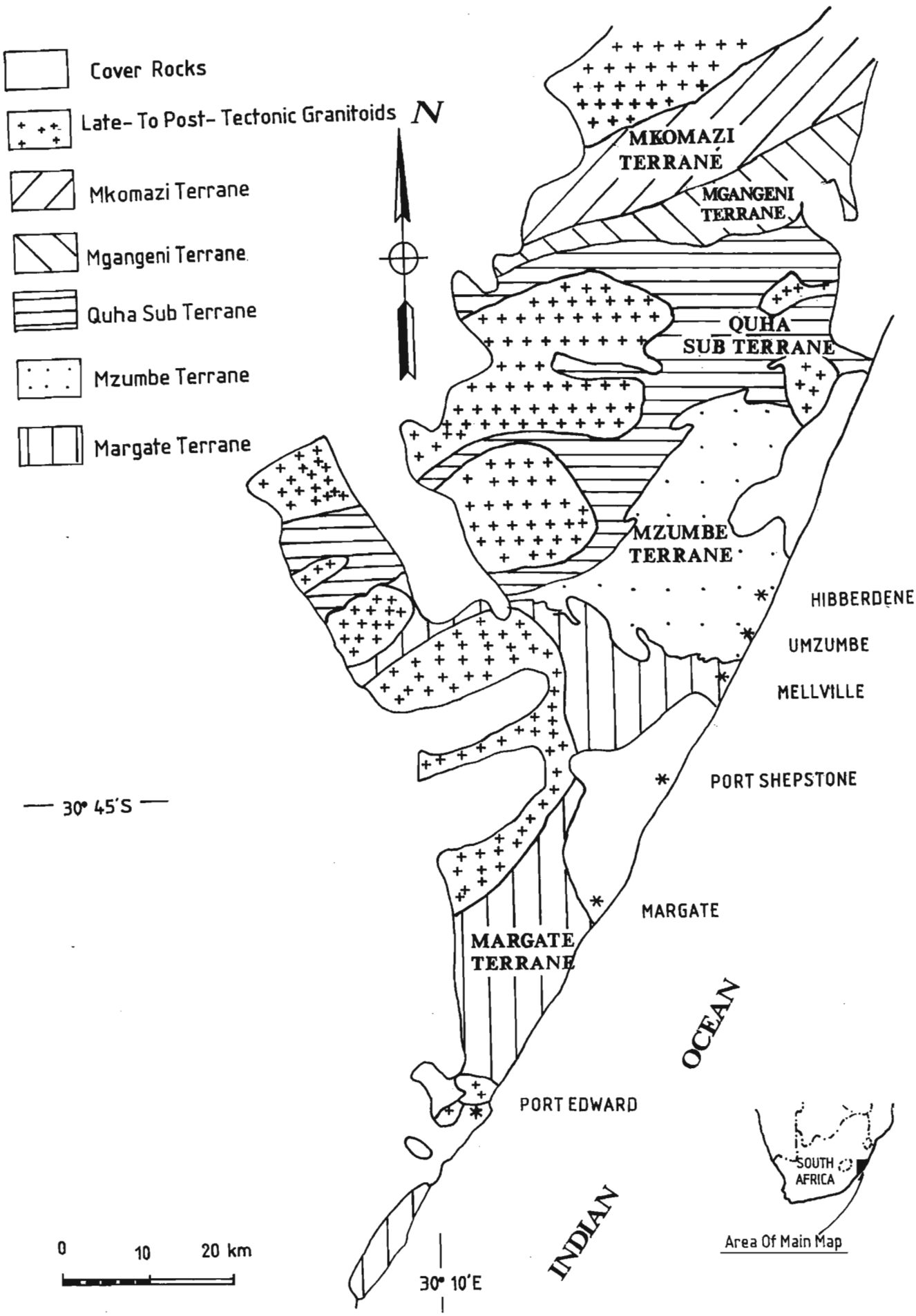

Figure 7.7. Revised tectonic subdivision of the southern portion of the Natal Province.

Province as a complex multiterrane zone (Figure 7.7).

The initial phase of the development of the Natal Province was marked by the generation of a series of volcanic arcs (Figure 7.8a), represented now by the Mzumbe Gneiss Suite of the Mzumbe Terrane, the 'northern Mzumbe Gneisses' of the Mgangeni Terrane and the Nagle Dam Formation of the Mgeni Terrane. Subsequently these accreted, ultimately to the Kaapvaal Craton, in an unknown sequence of collision events (Figure 7.8c). Potentially this involved the progressive amalgamation of the smaller arcs into composite structures or the sequential collision of individual arcs. Age dates are limited for this period but a lead isotopic age of 1207±10 Ma for the Mzumbe Gneiss Suite is considered to represent the crystallisation age of the original granitoid (Thomas and Eglington 1990).

Associated with these arc cores, frequently marginal to the arcs, are a series of zones, including the Margate Terrane and Quha sub-terrane, characterised by the presence of extension related orthogneiss, occasionally in a bimodal association with an enriched HFS element chemistry, profuse sediments and a late arc related intrusion event. Subsequent melting of the metasediments resulted in the production of S-type granites. The timing of the development of these sequences is uncertain, although a lead age of 1163±12 Ma was obtained for the Quha Formation (Cornell *et al.* 1996), demonstrating that they are younger than the arc cores. The presence of abundant acidic gneiss associated with these series indicates that they do not represent accreted oceanic islands, but rather comparison may be made with the bimodal series developed in a back-arc basin or local rifting setting (Winchester *et al.* 1995; Schofield *et al.* 1998), formed through the splitting of the arc margin. Subsequent arc volcanism, represented by the acidic Quha gneiss (Figure 7.8b), may explain the ambivalent field relationships noted by Cornell *et al.* between the Quha Formation and the Mzumbe Gneiss Suite.

Information regarding the evolution of the individual terranes is generally lacking, as insufficient data are available to allow the subdivision of the prominent lithological units identified, and so trace their tectonic development. Within the redefined Mzumbe Terrane, however, the data suggest a history of :

1) initial arc formation;
2) possible marginal splitting to form the Quha back-arc basin, with associated sedimentary deposition;
3) secondary arc volcanism;
4) intrusion of the Equeefa Metabasite Suite, possibly related to a rifting event; and
5) syn-tectonic to post-collision granite intrusion.

The ages of the collision events which amalgamated these various terranes are uncertain, and where age dates are available from the various units identified these tend to indicate metamorphic cooling ages rather than intrusion ages (Thomas *et al.* 1993). In the case of the Equeefa Metabasite Suite, for example, the derived age of 1024±32 Ma suggests a late collision between the Margate and Mzumbe Terranes. This is not, however, compatible with the 1068±2 Ma age of the Oribi Gorge batholith, which cuts across the Equeefa dykes, or the 1055±60 Ma age of the Belmont Suite, which occurs across the boundary of the Margate and Mzumbe Terranes. Relative ages can, however, be determined from the presence of granitic and basaltic series that transcend terrane boundaries. The possible occurrence of the Margate Complex, including the reassigned Belmont Suite, dated at 1055±60 Ma (Thomas *et al.* 1990), in the Transkei, Margate and Mzumbe Terranes demonstrates that these terranes must have collided prior to its intrusion. Similarly the Equeefa Metabasite (Rb-Sr age of 1024±32 Ma (Eglington *et al.* 1989b)) is found in the Mzumbe Terrane and the Quha sub-terrane, but not the Mgangeni, Mkomazi and Margate Terranes, indicating that the collision event(s) which fused these terranes occurred after the intrusion of the Equeefa Metabasite Suite.

Several regional correlations have not been considered here, such as that of the Mahongwa Suite, which the 1:250000 Geological Survey Sheet (Thomas 1988b) places in the Margate Terrane and Quha sub-terrane, but not in the Mzumbe Terrane. This suggests that an essentially analogous series of granitoids were derived from a similar source, but their absence from the intervening Mzumbe Terrane indicates that this was not related to a regional magmatic episode, but rather represented a local event. Correlation of these granitoids awaits a regional geochemical study.

The multiple collision events, ending with the accretion of the Natal Province to the Kaapvaal Craton, resulted in regional high grade metamorphism, to the granulite facies, and multiple deformation events within the various terranes. Available P-T-t data from individual terranes suggest an initial isothermal decompression event,

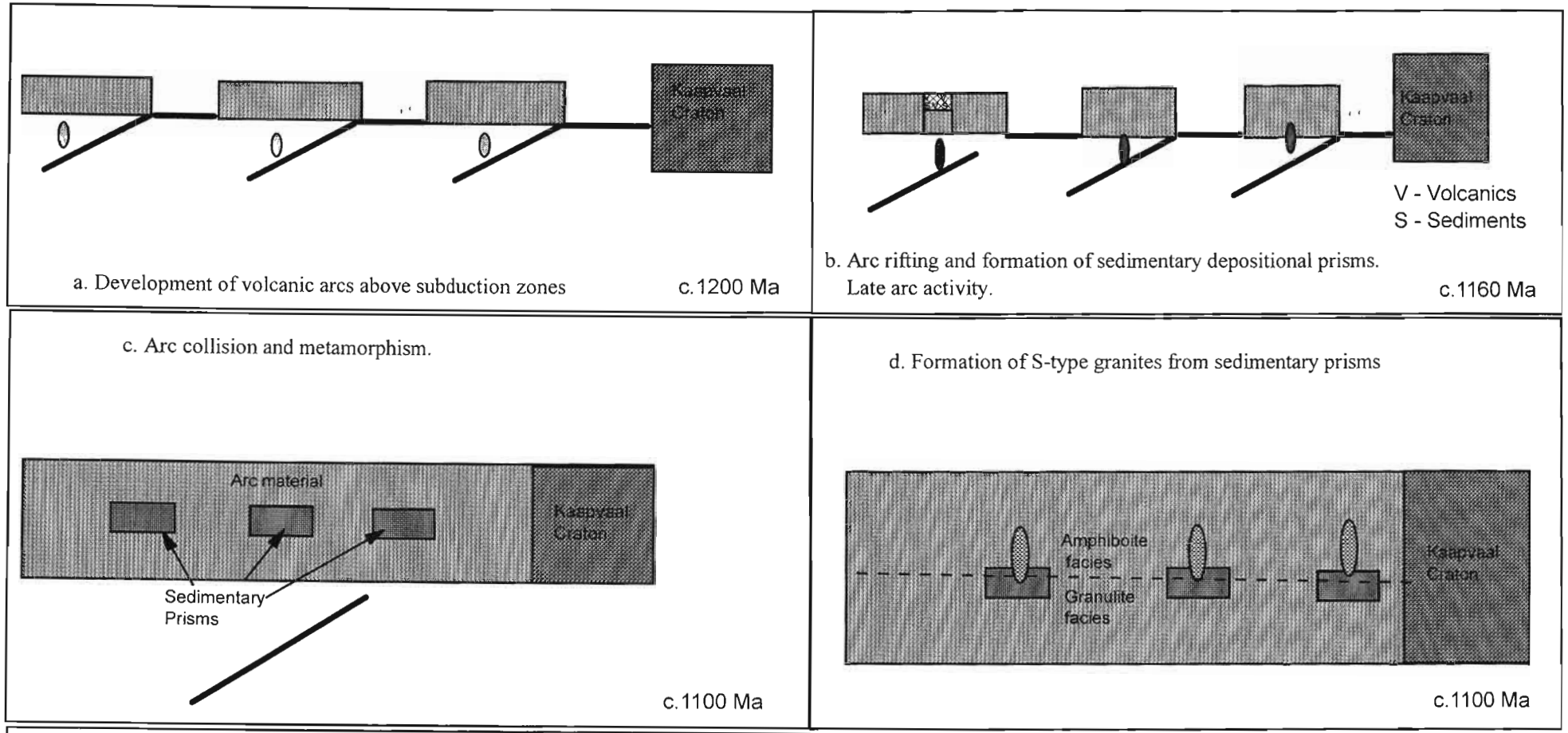

Figure 7.8. Tectonic evolution of the Natal Province during the Proterozoic.

which may have been followed by an isobaric cooling event (Evans 1984). This model differs from that identified within the Valley of a Thousand Hills, in the timing of the isobaric cooling event, but both identify a metamorphic event with elements of isothermal decompression and isobaric cooling. Isothermal decompression is typically considered to reflect the effect of crustal thickening, followed by uplift (Harley 1989), while isobaric cooling is thought to result from magma accretion (Wells 1980; Bohlen 1987). Combined decompression and isobaric cooling models were discussed by Harley (1989) as the possible effect of the extension of thickened crust, and are associated with the occurrence of syn-collision S-type granites and syn-extension bimodal magmatism. These may be represented by the abundant S-type granites and in particular the Margate Complex and Mkomazi Gneiss Suite, locally derived from the sedimentary prisms of the extensional belts (Figure 7.8d), and the various megacrystic granite batholiths.

Following the peak of metamorphism a series of granites, including the megacrystic granites originally grouped in the Oribi Gorge Suite, intruded (Figure 7.8e). Available age dates demonstrate the younging of the megacrystic granite intrusion ages towards the north, with two distinct age groupings identified. Anorogenic granite intrusions with substantially similar ages to the northern megacrystic granites (1026±3 Ma (U-Pb)) are, however, present in southern KwaZulu Natal (Thomas *et al.* 1993) and may constitute components of a single event, which possibly includes the Sezela quartz monzonite, with an Rb-Sr age of 951±15Ma (Eglington and Kerr 1989). These may represent the final phase of the evolution of the Natal Province.

The presence of two post-orogenic magmatic events in the Natal Province, separated by c.40 My, with no apparent variation in the loci of intrusion is indicated. This suggests that these granites were not generated through thermal relaxation following thrusting (Windley 1991) or interaction with an isolated mantle hot spot. Rather comparison can be made with the Proterozoic North American Craton where a number of anorogenic intrusion events occurred almost synchronously within a restricted area (Anderson 1983) as a result of crustal melting through interaction with a number of mantle plumes (Anderson and Bender 1989).

CONCLUSIONS

During the present study three primary series have been identified within the Proterozoic rocks of the Valley of a Thousand Hills:

1) the gneisses of the Nagle Dam Formation;
2) the megacrystic granites of the Mgeni batholith; and
3) the gneisses of the Valley Trust Formation.

The Nagle Dam Formation occurs as a series of orthogneisses, ranging in chemistry from basalt to rhyolite but predominately intermediate in character, with lesser paragneiss. The orthogneisses possess the chemical characteristics of a typical arc type batholith, plotting in the arc fields on the various chemical tectonic discrimination diagrams. Distinct fractionation trends on the Harker diagrams and trace element data, however, suggest that it may consist of a series of units, with a limited range of compositions, which originated within an evolving tectonic environment from distinct source zones. The high MgO content of the amphibolite of the Nagle Dam Formation indicates that it is a member of a primitive arc series, with the distinct variations in major and trace element data incompatible with simple fractionation processes. Rather derivation from a chemically heterogeneous source with possible crustal assimilation is suggested. Analysis of the individual units within the biotite hornblende gneiss demonstrate a degree of cumulate accumulation in their evolution, although the available data are limited. The distinct high Sr/Y ratio found within a specific series of the quartzo-feldspathic gneiss suggests comparison with the adakites. The remainder of the quartzo-feldspathic gneiss may have been derived through partial melting of a tonalitic or granodioritic source material. The biotite hornblende gneiss is characterised by a high sodium content, but does not possess the chemical characteristics of the adakites. Available geothermometry suggests metamorphism at temperatures of c. 750°C.

The Valley Trust Formation occurs as a series of enclaves within the Mgeni batholith. Its primarily bimodal metavolcanic character with abundant paragneiss distinguishes it from the Nagle Dam Formation, a separation supported by the distinct chemical character of the orthogneiss relative to the Nagle Dam Formation. The orthogneiss comprises a series of amphibolite and quartzo-feldspathic gneiss, with no sampled intermediate member. Available data suggest that these did not form through fractionation from a single magma, but rather they occur as a series of chemically distinct units which originated from discrete sources. On the chemical tectonic discrimination diagrams the orthogneisses of the Valley Trust Formation plot in a variety of fields, with the amphibolite plotting across the within plate basalt and MORB fields, while the quartzo-feldspathic gneiss plots predominately in the arc field. Revaluation of the tectonic discrimination diagrams for the basaltic rocks suggests that for the amphibolite this may indicate a heterogeneous source with MORB and within plate components. Various fractionation models were attempted for the amphibolite of the Valley Trust Formation, but failed to derive its high silica content. Rather a model of distinct parental magmas with fractionation and variable crustal contamination is favoured. The peraluminous quartzo-feldspathic gneiss is believed to have resulted from the partial melting of a metasediment, although its high sodium content results in it plotting in the I-type granite field on the plots of White and Chappell (1983). This may have resulted from the melting of a source with a distinct mineralogical composition, possibly through a muscovite dehydration event. The metaluminous quartzo-feldspathic gneiss may have been derived from the partial melting of a tonalitic or granodioritic source. Modelling of the quartzo-feldspathic gneiss suggests that it contains a cumulate component.

The paragneiss comprises two distinct series - the pelitic gneiss and the fine grained granulite, distinguished initially on mineralogy and subsequently on the basis of distinct chemical characteristics. The pelitic gneiss appears to comprise an evolving series ranging from pelitic to psammitic in composition. These possess dissimilar fractionation trends, with the psammite fractionation controlled by increasing quartz dilution, while the pelite displays major variations in elemental abundance at constant silica levels. The chemical composition of the fine grained granulite is controlled by increasing quartz dilution. Provenance analysis suggests that these units were derived from an igenous source, with trace element data indicating the Nagle Dam Formation as a possible source for both of these series. Geothermobarometry suggests metamorphism to 850°C and 6 kb.

The Mgeni batholith is a composite batholith comprising granite and charnockite characterised by megacrystic feldspars. Mineralogical, chemical and isotopic data allow the subdivision of the Mgeni batholith into three distinct suites:

1) the Ximba Suite - a series of megacrystic biotite bearing granites, comprising a relatively basic hornblende bearing margin grading into an acidic biotite granite with an inner core of garnetiferous biotite granite;
2) the Mlahlanja Suite - a series of megacrystic hornblende granites and charnockite, which occur as a series of lensoid plutons within the Ximba Suite, each distinguished by distinct mineralogical and chemical characteristics; and
3) the Nqwadolo Suite - a coarse grained leucogranite, which may be divided into two distinct series on chemical grounds.

As a group the Mgeni batholith displays the chemical and mineralogical characteristics of the A-type granites and on the granitic tectonic discrimination diagrams plot across the within plate granite and volcanic arc fields. Petrogenetic modelling of the megacrystic granites of the Mgeni batholith suggests that they did not evolve through contamination of a single parental magma with the Nagle Dam Formation as proposed by Eglington *et al.* (1989a), and in particular the latter does not possess the necessary trace element content to derive the HFS element enriched Mlahlanja Suite from the relatively depleted Ximba Suite. Rather a model in which each suite represents the differentiation product of a distinct parental magma is proposed. Modelling of the Ximba and Mlahlanja Suites suggests that these principally represent accumulations of cumulate material. Similarly, modelling of the Nqwadolo Suite indicates that it contains a cumulate component. Within the biotite granite, however, local assimilation of pelitic material generates the chemically distinct biotite garnet granite. Analysis of the A-type granite association suggests that they may have originated from within plate basalt interaction with the crust through MASH type processes. Geothermometry of the Mgeni batholith predominately derives subsolidus temperatures, although potential magmatic temperatures of c.760°C are generated by the amphibole-plagioclase thermometer, but with higher temperatures, c.900°C, suggested by the hornblende-melt thermometer and the M-Zr diagram. Pressure estimates of c.5 kb are derived by the hornblende barometer, and are supported by the low Mn content of the garnet present in the granites. The increase in peak metamorphic temperatures from the Nagle Dam to the Valley Trust Formation suggest a degree of thermal input from the Mgeni batholith, which the comparable pressure estimates from the Valley Trust Formation and the Mgeni batholith indicate was an essentially isobaric event. High Mn garnet, suggesting crystallisation at lower pressures, is present in late veins within the batholith, indicating a phase of isothermal decompression.

The diverse chemical characteristics of the various units found within the Valley of a Thousand Hills together with its apparent metamorphic P-T-t path suggest a complex tectonomagmatic evolution for this section of the Natal Province during the Proterozoic. This involved:

1) the development of an island arc system, the Nagle Dam Formation;
2) subsequent rifting and the development of the bimodal Valley Trust Formation, with associated sedimentation into the rift from the erosion of the Nagle Dam Formation;
3) metamorphism, possibly associated with an arc-arc collision and crustal thickening;
4) intrusion of the Mgeni batholith, providing a thermal pulse to reheat the gneisses;
5) uplift and intrusion of late, high level granitic veins.

This model was extended to southern KwaZulu Natal, with an analysis of the available chemical data from this area together with that from the Valley of a Thousand Hillls to allow the identification of possible lithological correlates, and hence any potential discontinuities within the basement. This suggests that several of the lithological correlations proposed in the literature are not compatible with the chemical data, and that the basement contains a more complex lithological association than previously suspected. Provisional identification of the tectonic environment of origin of several of these units with the available geochronological data allows the development of a model for the evolution of this portion of the Natal Province. This appears to involve the collision of a number of arcs with associated backarcs, which served as loci for sedimentation. Subsequent to the individual arc-arc collision events S-type granites developed in response to isothermal decompression of the terrane. Following the metamorphic peak a number of post-orogenic granites intruded the area in a series of pulses. These are typically members of the rapakivi granite association, and in particular the megacrystic granites of the Oribi Gorge Suite.

REFERENCES

Abdel-Rahman, A.-F.M. (1994). Nature of biotites from alkaline, calc-alkaline, and peraluminous magmas. *J. Petrol.*, **35**, 525-541.

Agrawal, S. (1995). Discrimination between late-orogenic, post-orogenic, and anorogenic granites by major element compositions. *J. Geol.*, **103**, 529-537.

Ahmed-Said, Y. and Leake, B.E. (1990). S-type granite formation in the Dalradian rocks of Connemara, W. Ireland. *Mineralog. Mag.*, **54**, 1-22.

Alderton, D.H.A., Pearce, J.A. and Potts, J.A. (1980). Rare earth element mobility during granite alteration: evidence from south-west England. *Earth Planet. Sci. Lett.*, **40**, 149-165.

Allan, B.D. and Clarke, D.B. (1981). Occurrence and origin of garnets in the South Mountain Batholith, Nova Scotia. *Can. Miner.*, **19**, 19-24.

Allen, J.C. and Boettcher, A.L. (1978). Amphiboles in andesite and basalts: II. Stability as a function of P-t-f_{H2O}-f_{O2}. *Am. Miner.*, **63**, 1074-1087.

Anderson, J.L. (1980). Mineral equilibria and crystallization conditions in the late Precambrian Wolf River rapakivi massif, Wisconsin. *Am. J. Sci.*, **280**, 289-332.

Anderson, J.L. (1983). Proterozoic anorogenic granite plutonism of North America. *In*: Medaris, L.C., Byers, C.W., Mickelson, D.M. and Shanks, W.C. (Eds.). *Proterozoic Geology*. Geol. Soc. Am. Mem., **161**, 133-154.

Anderson, J.L. (1996). Status of thermobarometry in granite batholiths. *Trans. Roy. Soc. Edin.*, **87**, 125-138.

Anderson, J.L. and Cullers, R.L. (1978). Geochemistry and evolution of the Wolf River batholith, a late Precambrian rapakivi massif in North Wisconsin, USA. *Precambrian Res.*, **7**, 287-324.

Anderson, J.L., Barth, A.P. and Young, E.D. (1988). Mid-crustal Cretaceous roots to Cordilleran metamorphic core complexes. *Geology*, **16**, 366-369.

Anderson, J.L. and Bender, E.E. (1989). Nature and origin of Proterozoic A-type magmatism in the southwestern United States of America. *Lithos*, **23**, 19-52.

Anderson, J.L. and Smith, D.R. (1995). The effect of temperature and oxygen fugacity on the Al-in-hornblende barometer. *Am. Miner.*, **80**, 549-559.

Anderson, W. (1902). Report on the geology of the Lower Tugela District, Victoria County, Natal. *A. Rep. Geol. Surv. Natal Zululand*, **1**, 77-95.

Aranovich, L.Y. and Berman, R.G. (1997). A new garnet-orthopyroxene thermometer based on reversed Al_2O_3 solubility in FeO-Al_2O_3-SiO_2 orthopyroxene. *Am. Miner.*, **82**, 345-353.

Arculus, R.J. (1987). The significance of source versus process in the tectonic controls of magma genesis. *J. Volc. Geotherm. Res.*, **32**, 1-12.

Arnett, O.J.L. (1953). *The geology of the Groenberg district, Natal.* M.Sc. thesis (unpubl.), Univ. Natal, Durban, 18 pp.

Arth, J.C. (1976). Behavior of trace elements during magmatic processes - a summary of theoretical models and their applications. *U.S. Geol. Surv. J. Res.*, **4**, 41-47.

Atherton, M.P. and Sanderson, L.M. (1985). The chemical variation and evolution of the superunits of the segmented Coastal Batholith. *In*: Pitcher, W.S., Atherton, M.P., Cobbing, E.J. and Beckinsale, R.D. (Eds.). *Magmatism at a plate edge*. Blackie, London, 208-227.

Atherton, M.P. and Petford, N. (1993). Generation of sodium-rich magmas from newly underplated basaltic crust. *Nature*, **362**, 144-146.

Bailey, D.K. (1978). Continental rifting and mantle degassing. *In*: Neumann, E.-R. and Ramberg, I.B. (Eds.). *Petrology and geochemistry of continental rifts*. Reidel, Dordrecht, 1-13.

Barbey, P. (1991). Restites in migmatites and autochthonous granites: their main features and their genesis. *In*: Didier, J. and Barbarin, B. (Eds.). *Enclaves and Granite Petrology*. Developments in Petrology, Elsevier, Amsterdam, 479-492.

Bard, J.P. and Moine, B. (1979). Acebuches amphibolites in the Aracena Hercynian metamorphic belt (southwest Spain): geochemical

variations and basaltic affinities. *Lithos*, **12**, 271-282.

Barker, F., Wones, D.R., Sharp, W.N. and Desborough, G.A. (1975). The Pikes Peak batholith, Colorado Front Range, and a model for the origin of the gabbro-anorthosite-syenite-potassic granite suite. *Precambrian Res.*, **2**, 97-160.

Batchelor, R.A. and Bowden, P. (1985). Petrogenetic interpretation of granitoid rock series using multicationic parameters. *Chem. Geol.*, **48**, 43-55.

Bell, T.H. (1981). Foliation development - the contribution, geometry and significance of progressive bulk inhomogeneous shortening. *Tectonophysics*, **75**, 273-296.

Bell, T.H. (1985). Deformation partitioning and porphyroblast rotation in metamorphic rocks: a radical reinterpretation. *J. metamorphic Geol.*, **3**, 109-118.

Bellieni, G., Comin-Chiaramonti, P., Marques, L.S., Melfi, A.J., Nardy, A.J.R., Papatrechas, C., Piccirillo, E.M., Roisenberg, A. and Stolfa, D. (1986). Petrogenetic aspects of acid and basaltic lavas from the Paraná Plateau (Brazil): geological, mineralogical and petrochemical relationships. *J. Petrol.*, **27**, 915-944.

Bellieni, G., Cavazzini, G., Fioretti, A.M., Peccerillo, A. and Zantedeschi, P. (1996). The Cima di Vila (Zinsnock) Intrusion, Eastern Alps: evidence for crustal melting, acid-mafic magma mingling and wall-rock fluid effects. *Miner. Pet.*, **56**, 125-146.

Ben Othman, D., Polve, M. and Allegre, C.J. (1984). Nd-Sr isotopic composition of granulites and constraints on the evolution of the lower continental crust. *Nature*, **307**, 510-515.

Bence, A.E. and Albee, A.L. (1968). Empirical correction factors for the electron microanalysis of silicates and oxides. *J. Geol.*, **76**, 382-403.

Bender, J.F., Langmuir, C.H. and Hanson, G.N. (1984). Petrogenesis of basalt glasses from the Tamayo Region, East Pacific Rise. *J. Petrol.*, **25**, 213-254.

Betrand, H. (1991). The Mesozoic tholeiitic province of northwest Africa: a volcanotectonic record of the early opening of Central Atlantic. *In*: Kaampunzu, A.B. and Lubala, R.T. (Eds.). *Magmatism in extensional structural settings - the Phanerozoic African Plate*. Springer-Verlag, Berlin, 147-188.

Bhatia, M.R. (1983). Plate tectonics and geochemical composition of sandstones. *J. Geol.*, **91**, 611-627.

Bhatia, M.R. and Crook, K.A.W. (1986). Trace element characteristics of greywackes and tectonic setting discrimination of sedimentary basins. *Contrib. Miner. Petrol.*, **92**, 181-193.

Bhattacharya, A. and Sen, S.K. (1986). Granulite metamorphism, fluid buffering, and dehydration melting in the Madras charnockites and metapelites. *J. Petrol.*, **27**, 1119-1141.

Bhattacharya, A., Krishnakumar, K.R., Raith, M. and Sen, S.K. (1991). An improved set of a-X parameters for Fe-Mg-Ca garnets and refinement of the orthopyroxene-garnet thermometer and the orthopyroxene - garnet - plagioclase - quartz barometer. *J. Petrol.*, **32**, 629-656.

Bickford, M.E., Sides, J.R. and Cullers, R.L. (1981). Chemical evolution of magmas in the Proterozoic terrane of the St. Francois Mountains, southeastern Missouri. 1. Field, petrographic, and major element data. *J. Geophys. Res.*, **86**, 10365-10386.

Bickford, M.E., Van Schmus, W.R. and Zietz, I. (1986). Proterozoic history of the midcontinent region of North America. *Geology*, **14**, 492-496.

Blundy, J.D. and Holland, T.J.B. (1990). Calcic amphibole equilibria and a new amphibole-plagioclase geothermometer. *Contrib. Miner. Petrol.*, **104**, 208-224.

Bohlen, S.R. (1987). Pressure-temperature-time paths and a tectonic model for the evolution of granulites. *J. Geol.*, **95**, 617-632.

Boyd, F.R. (1973). A pyroxene geotherm. *Geochim. Cosmochim. Acta*, **37**, 2533-2546.

Brown, G.C. (1982). Calc-alkaline intrusive rocks: their diversity, evolution and relation to volcanic arcs. *In*: Thorpe, R.S. (Ed.). *Andesites*. Wiley, Chichester, 437-461.

Brown, G.C., Thorpe, R.S. and Webb, P.C. (1984). The geochemical characteristics of granitoids in contrasting arcs and comments on magma sources.

J. geol. Soc. Lond., **141**, 413-426.

Brown, G.M., Holland, J.G., Sigurdsson, H., Tomblin, J.F. and Arculus, R.J. (1977). Geochemistry of the Lesser Antilles volcanic arc. *Geochim. Cosmochim. Acta*, **41**, 785-801.

Brown, P.E., Dempster, T.J. and Hutton, D.H.W. (1991). The rapakivi intrusions of south Greenland. *In*: Haapala, I. and Ramo, O.T. (Eds.). *Symposium on rapakivi granites and related rocks.* Geol. Surv. Finl., **34**, 10.

Bryan, W.B., Thompson, G. and Ludden, J.N. (1981). Compositional variation in normal MORB from 22°-25°N: Mid-Atlantic Ridge and Kane Fracture Zone. *J. Geophys. Res.*, **86**, 11815-11836.

Buddington, A.F. (1963). Isograds and the role of H_2O in metamorphic facies of orthogneisses of the northwest Adirondack area, New York. *Geol. Soc. Am. Bull.*, **74**, 1155-1182.

Bulley, B.G. (1981). *Geology of the Tafamasi area, Natal.* M.Sc. thesis (unpubl.), Univ. Natal, Durban, 126pp.

Burgess, J.L., Brown, M., Dallmeyer, R.D. and Van Staal, C.R. (1995). Microstructure, metamorphism, thermochronology and P-T-t-deformation history of the Port aux Basques gneisses, south-west Newfoundland, Canada. *J. metamorphic Geol.*, **13**, 751-776.

Butler, B.C.M. (1965). A chemical study of some rocks of the Moine Series of Scotland. *J. geol. Soc. Lond.*, **121**, 163-208.

Cain, A.C. (1975). A preliminary review of the stratigraphic relationships and distribution of metamorphism in the northern part of the Natal-Namaquarides, South Africa. *Geol. Rundsch.*, **64**, 192-216.

Cann, J.R. (1970). Rb, Sr, Y, Zr and Nb in some ocean floor basaltic rocks. *Earth Planet. Sci. Lett.*, **10**, 7-11.

Cao, R.L., Ross, C. and Ernst, W.G. (1986). Experimental studies to 10 kb of the bulk composition $tremolite_{50}$ - $tschermakite_{50}$ + excess H_2O. *Contrib. Miner. Petrol.*, **93**, 160-170.

Carlson, R.W. and Hart, W.K. (1988). Flood basalt volcanism in the northwestern United States. *In*: Macdougall, J.D. (Ed.). *Continental Flood Basalts.* Kluwer Academic Publishers, Hingham, Mass., 35-61.

Caroff, M., Maury, R.C., Vidal, P., Guille, G., Dupuy, C., Cotten, J., Guillou, H. and Gillot, P.-Y. (1995). Rapid temporal changes in ocean island basalt composition: evidence from an 800m deep drill hole in Eiao Shield (Marquesas). *J. Petrol.*, **36**, 1333-1365.

Carson, C.J. and Powell, R. (1997). Garnet-orthopyroxene geothermometry and geobarometry: error propagation and equilibration effects. *J. metamorphic Geol.*, **15**, 679-686.

Chappell, B.W. (1996a). Compositional variation within granite suites of the Lachlan Fold Belt: its causes and implications for the physical state of granite magma. *Trans. Roy. Soc. Edin.*, **87**, 159-170.

Chappell, B.W. (1996b). Magma mixing and the production of compositional variations within granite suites: evidence from the granites of southeastern Australia. *J. Petrol.*, **37**, 449-470.

Chappell, B.W. and White, A.J.R. (1974). Two contrasting granite types. *Pacific Geol.*, **8**, 173-174.

Chappell, B.W. and Stephens, W.E. (1988). Origin of infracrustal (I-type) granite magmas. *Trans. R. Soc. Edin.*, **79**, 71-86.

Cherry, D.W. (1946). *The geology of the Umgeni Dam and surrounding country, Valley of a Thousand Hills, Natal.* M.Sc. thesis (unpubl.), Univ. Natal, Durban, 88 pp.

Chipera, S.J. and Perkins, D. (1988). Evaluation of biotite-garnet geothermometers: application to the English River subprovince, Ontario. *Contrib. Miner. Petrol.*, **98**, 40-48.

Cho, M. and Ernst, W.G. (1991). An experimental determination of calcic amphibole solid solution along the join tremolite - tschermakite. *Am. Miner.*, **76**, 985-1001.

Clarke, D.B. (1981). The mineralogy of peraluminous granites: a review. *Can. Miner.*, **19**, 3-17.

Clarke, D.B. (1992). *Granitoid Rocks.* Chapman Hall, London, 283pp.

Clemens, J.D., Holloway, J.R. and White, A.J.R. (1986). Origin of an A-type granite: experimental constraints. *Am. Miner.*, **71**, 317-324.

Cleverly, R.W., Betton, P.J. and Bristow, J.W. (1984). Geochemistry and petrogenesis of the Lebombo rhyolites. *In*: Erlank, A.J. (Ed.). *Petrogenesis of the volcanic rocks of the Karoo Province.* Spec. Publ. geol. Soc. S. Afr., **13**, 171-194.

Collins, W.J. (1996). Lachlan Fold Belt granitoids: products of three-component mixing. *Trans. Roy. Soc. Edin.*, **87**, 171-181.

Collins, W.J., Beams, S.D., White, A.J.R. and Chappell, B.W. (1982). Nature and origin of A-type granites with particular reference to southeastern Australia. *Contrib. Miner. Petrol.*, **80**, 189-200.

Condie, K.C. (1985). Secular variation in the composition of basalts: an index to mantle evolution. *J. Petrol.*, **26**, 545-563.

Condie, K.C., Noll, P.D. and Conway, C.M. (1992). Geochemical and detrital mode evidence for two sources of Early Proterozoic sedimentary rocks from the Tonto Basin Supergroup, central Arizona. *Sedi. Geol.*, 77, 51-76.

Conrad, W.K., Nicholls, I.A. and Wall, V.J. (1988). Water-saturated and -undersaturated melting of metaluminous and peraluminous crustal compositions at 10 kb: evidence for the origin of silicic magmas in the Taupo Volcanic Zone, New Zealand, and other occurrences. *J. Petrol.*, **29**, 765-803.

Cornell, D.H., Thomas, R.J., Bowring, S.A., Armstrong, R.A. and Grantham, G.H. (1996). Protolith interpretation in metamorphic terranes: a back-arc environment with Besshi-type base metal potential for the Quha Formation, Natal Province, South Africa. *Precambrian Res.*, 77, 243-271.

Cosca, S.J., Essene, E.J. and Bowman, J.R. (1991). Complete chemical analyses of metamorphic hornblendes: implications for normalizations, calculated H_2O activities, and thermobarometry. *Contrib. Miner. Petrol.*, **108**, 472-484.

Coulon, C. and Thorpe, R.S. (1981). Role of continental crust in petrogenesis of orogenic volcanic associations. *Tectonophysics*, 77, 79-93.

Cox, K.G. (1980). A model for flood basalt volcanism. *J. Petrol.*, **21**, 629-650.

Cox, K.G. (1988). The Karoo Province. *In*: Macdougall, J.D. (Ed.). *Continental Flood Basalts.* Kluwer Academic Publishers, Hingham, Mass., 239-271.

Cox, K.G. and Hawkesworth, C.J. (1985). Geochemical stratigraphy of the Deccan Traps at Mahabaleshwar, western Ghats, India, with implications for open system magmatic processes. *J. Petrol.*, **26**, 355-377.

Cox, R., Lowe, D.R. and Cullers, R.L. (1995). The influence of sediment recycling and basement composition on evolution of mudrock chemistry in the southwestern United States. *Geochim. Cosmochim. Acta*, **59**, 2919-2940.

Creaser, R.A. (1996). Petrogenesis of a Mesoproterozoic quartz latite-granitoid suite from the Roxby Downs area, South Australia. *Precambrian Res.*, **79**, 371-394.

Creaser, R.A., Price, R.C. and Wormald, R.J. (1991). A-type granites revisited: assessment of a residual-source model. *Geology*, **19**, 163-166.

Crecraft, H.R., Nash, W.P. and Evans, S.H. (1981). Late Cenozoic volcanism at Twin Peaks, Utah: geology and petrology. *J. Geophys. Res.*, **86**, 10303-10320.

Crow, C. and Condie, K.C. (1990). Geochemistry and origin of early Proterozoic volcanic rocks of the Transvaal and Soutpansberg successions, South Africa. *Precambrian Res.*, **47**, 17-26.

Cruden, A.R., Koyi, H. and Schmeling, H. (1995). Diapiric basal entrainment of mafic into felsic magma. *Earth Planet. Sci. Lett.*, **131**, 321-340.

Cullers, R.L., Koch, R.J. and Bickford, M.E. (1981). Chemical evolution of magmas in the Proterozoic Terrane of the St Francois Mountains, Southeastern Missouri. 2. Trace elements. *J. Geophys. Res.*, **86**, 10388-10401.

Cullers, R.L., Basu, A. and Suttner, L.J. (1988). Geochemical signature of provenance in sand-size material in soils and stream sediments near the Tobacco Root Batholith, Montana, U.S.A. *Chem. Geol.*, **70**, 335-348.

Cullers, R.L., Griffin, T., Bickford, M.E. and Anderson, J.L. (1992). Origin and chemical evolution of the 1360 Ma San Isabel Batholith,

Wet Mountains, Colorado: a mid-crustal granite of anorogenic affinities. *Geol. Soc. Am. Bull.*, **104**, 316-328.

Czamanske, G.K., Wones, D.R. and Eichelberger, J.C. (1977). Mineralogy and petrology of the intrusive complex, Pliny Range, New Hampshire. *Am. J. Sci.*, **277**, 1073-1123.

Dahl, P.S. (1980). The thermal-compositional dependence of Fe^{2+}-Mg distributions between coexisting garnet and pyroxene: applications to geothermometry. *Am. Miner.*, **65**, 854-866.

Dall'Agnol, R., Macambira, M. and Lafon, J.-M. (1991). Petrological and geochemical characteristics of the lower and middle Proterozoic anorogenic granites of the central Amazonian Province, Amazonian Craton. *In*: Haapala, I. and Ramo, O.T. (Eds.). *Symposium on rapakivi granites and related rocks.* Geol. Surv. Finl., **34**, 12-13.

Daly, J.S., Cliff, R.A. and Yardley, B.W.D. (1989). *Evolution of Metamorphic Belts*. Geol. Soc. Spec. Publ., **43**, 566pp.

Dasgupta, S., Sengupta, P., Guha, D. and Fukuoka, M. (1991). A refined garnet-biotite Fe-Mg exchange thermometer and its application in amphibolites and granulites. *Contrib. Miner. Petrol.*, **109**, 130-137.

Davies, R.D. (1964). *The geology of the area north-west of Table Mountain, Natal.* M.Sc. thesis (unpubl.), Univ. Natal, Durban, 110 pp.

Dawes, R.L. and Evans, B.W. (1991). Mineralogy and geothermobarometry of magmatic epidote-bearing dikes, Front Range, Colorado. *Geol. Soc. Am. Bull.*, **103**, 1017-1031.

De Albuquerque, C.A.R. (1973). Geochemistry of biotites from granitic rocks, northern Portugal. *Geochim. Cosmochim. Acta*, **37**, 1779-1802.

De Beer, J.H., Van Zijl, J.S.V. and Gough, D.I. (1982). The Southern Cape Conductivity Belt: its composition, origin and tectonic significance. *Tectonophysics*, **83**, 205-225.

De Beer, J.H. and Meyer, R. (1983). Geoelectrical and gravitational characteristics of the Namaqua-Natal mobile belt and its boundaries. *In*: Botha, B.J.V. (Ed.). *Namaqualand Metamorphic Complex*. Spec. Publ. geol. Soc. S. Afr., **10**, 91-100.

De la Roche, H. (1966). Sur l'existance de plusieurs facies geochimiques dans les schistes paleozoiques des Pyrenees Luchonnaises. *Geol. Rundsch.*, **55**, 274-301.

De la Roche, H., Leterrier, J., Grand Claude, P. and Marchal, M. (1980). A classification of volcanic and plutonic rocks using R1-R2 diagrams and major element analyses - its relationships with current nomenclature. *Chem. Geol.*, **29**, 183-210.

De Waard, D. (1965). The occurrence of garnet in the granulite-facies terrane of the Adirondack Highlands. *J. Petrol.*, **6**, 165-191.

De Wit, M.J. (1998). On Archean granites, greenstones, cratons and tectonics: does the evidence demand a verdict? *Precambrian Res.*, **91**, 181-226.

DeBari, S.M. (1997). Evolution of magmas in continental and oceanic arcs: the role of the lower crust. *Can. Miner.*, **35**, 501-519.

Debon, F. and Le Fort, P. (1982). A chemical-mineralogical classification of common plutonic rocks and associations. *Trans. Roy. Soc. Edin.*, **73**, 135-149.

Deer, W.A., Howie, R.A. and Zussman, J. (1971). *Rock Forming Minerals, Vol.3: Sheet silicates.* Longman, London, 270pp.

Deer, W.A., Howie, R.A. and Zussman, J. (1982). *Rock Forming Minerals, Vol.1A : Orthosilicates.* Longman, London, 919pp.

Defant, M.J. and Drummond, M.S. (1990). Derivation of some modern arc magmas by melting of young subducted lithosphere. *Nature*, **347**, 662-665.

Di Vincenzo, G., Andriessen, P.A.M. and Ghezzo, C. (1996). Evidence of two different components in a Hercynian peraluminous cordierite-bearing granite: the San Basilio intrusion (Central Sardinia, Italy). *J. Petrol.*, **37**, 1175-1206.

Dickey, J.S., Frey, F.A., Hart, S.R. and Watson, E.B. (1977). Geochemistry and petrology of dredged basalts from the Bouvet triple junction, South Atlantic. *Geochim. Cosmochim. Acta*, **41**, 1105-1118.

Dickin, A.P. (1988). The North Atlantic Tertiary Province. *In*: Macdougall, J.D. (Ed.). *Continental Flood Basalts*. Kluwer Academic Publishers,

Hingham, Mass., 111-149.

Didier, J. and Barbarin, B. (1991). The different types of enclaves in granites - Nomenclature. *In*: Didier, J. and Barbarin, B. (Eds.). *Enclaves and Granite Petrology*. Developments in Petrology, Elsevier, Amsterdam, 19-24.

Dirks, P. and Hand, M. (1991). Structural and metamorphic controls on the distribution of zircon in an evolving quartzofeldspathic migmatite: an example from the Reynolds Range, central Australia. *J. metamorphic Geol.*, **9**, 191-201.

D'Lemos, R.S. (1996). Mixing between granitic and dioritic crystal mushes, Guernsey, Channel Islands, UK. *Lithos*, **38**, 233-257.

Dodge, F.C.W, Papike, J.J. and Mays, R.E. (1968). Hornblendes from granitic rocks of the central Sierra Nevada Batholith, California. *J. Petrol.*, **9**, 378-410.

Dodge, F.C.W., Smith, V.C. and Mays, R.E. (1969). Biotites from granitic rocks of the central Sierra Nevada batholith, California. *J. Petrol.*, **10**, 250-271.

Dodson, R.G. (1950). *Geology of the Shongweni district, Natal.* MSc thesis (unpubl.), University of Natal, Durban, 18 pp.

Dooley, D.F. and Patiño Douce, A.E. (1996). Fluid-absent melting of F-rich phlogopite + rutile + quartz. *Am. Miner.*, **81**, 202-212.

Drummond, M.S., Defant, M.J. and Kepezhinskas, P.K. (1996). Petrogenesis of slab-derived trondhjemite - tonalite - dacite/adakite magmas. *Trans. Roy. Soc. Edin.*, **87**, 205-215.

Du Bray, E.A. (1988). Garnet compositions and their use as indicators of peraluminous granitoid petrogenesis - southeastern Arabian Shield. *Contrib. Miner. Petrol.*, **100**, 205-212.

Du Toit, A.L. (1954). *The geology of South Africa.* Oliver and Boyd, London, 611 pp.

Du Toit, P. (1979). *Geology of the Nanda area, Natal.* M.Sc. thesis (unpubl.), Univ. Natal, Durban, 132pp.

Duchesne, J.-C. and Wilmart, E. (1997). Igneous charnockites and related rocks from the Bjerkreim-Sokndal layered intrusion (Southwest Norway): a jotunite (hypersthene monzodiorite)-derived A-type granitoid suite. *J. Petrol.*, **38**, 337-369.

Duncan, A.R. (1987). The Karoo igneous province - a problem area for inferring tectonic setting from basalt geochemistry. *J. Volc. Geotherm. Res.*, **32**, 13-34.

Duncan, A.R., Erlank, A.J. and Betton, P.J. (1984). Analytical techniques and database descriptions. *In*: Erlank, A.J. (Ed.). *Petrogenesis of the volcanic rocks of the Karoo Province.* Spec. Publ. geol. Soc. S. Afr., **13**, 389-395.

Eby, G.N. (1990). The A-type granitoids: a review of their occurrence and chemical characteristics and speculations on their petrogenesis. *Lithos*, **26**, 115-134.

Eggins, S.M. (1993). Origin and differentiation of picritic arc magmas, Ambae (Aoba), Vanuatu. *Contrib. Miner. Petrol.*, **114**, 79-100.

Eglington, B.M. (1987). *Field, geochemical and isotopic studies of selected areas of Proterozoic crust in south-central Natal.* Ph.D. thesis (unpubl.), Univ. Natal, Durban, 373pp.

Eglington, B.M., Harmer, R.E. and Kerr, A. (1989a). Rb-Sr isotopic constraints on the age of the Mgeni and Nqwadolo granites, Valley of a Thousand Hills, Natal. *S. Afr. J. Geol.*, **92**, 393-399.

Eglington, B.M., Harmer, R.E. and Kerr, A. (1989b). Isotopic and geochemical constraints on Proterozoic crustal evolution in south-eastern Africa. *Precambrian Res.*, **45**, 159-174.

Eglington, B.M. and Kerr, A. (1989). Rb-Sr and Pb-Pb geochronology of Proterozoic intrusives from the Scottburgh area of southern Natal. *S. Afr. J. Geol.*, **92**, 400-409.

Ellis, D.J. and Green, D.H. (1985). Garnet-forming reactions in mafic granulites from Enderby Land, Antarctica - implications for geothermometry and geobarometry. *J. Petrol.*, **26**, 633-662.

Emslie, R.F. (1991). Granitoids of rapakivi granite - anorthosite and related associations. *Precambrian Res.*, **51**, 173-192.

Encarnación, J. and Mukasa, S.B. (1997). Age and geochemistry of an 'anorogenic' crustal melt and implications for I-type granite petrogenesis. *Lithos*, **42**, 1-13.

England, P.C. and Thompson, A.B. (1984). Pressure-temperature-time paths of regional metamorphism. I. Heat transfer during the evolution of regions of thickened continental crust. *J. Petrol.*, **25**, 894-928.

England, P.C. and Thompson, A.B. (1986). Some thermal and tectonic models for crustal melting in continental collision zones. *In*: Coward, M.P. and Ries, A.C. (Eds.). *Collision Tectonics*. Geol. Soc. Specl. Publ., **19**, 83-94.

Erlank, A.J. (1984). *Petrogenesis of the volcanic rocks of the Karoo Province.* Spec. Publ. geol. Soc. S. Afr., **13**, 395pp.

Escuder Viruete, J., Indares, A. and Arenas, R. (1997). P-T path determinations in the Tormes Gneissic Dome, NW Iberian Massif, Spain. *J. metamorphic Geol.*, **15**, 645-663.

Essene, E.J. (1982). Geologic thermometry and barometry. *In*: Ferry, J.M. (Ed.). *Characterization of metamorphism through mineral equilibria*. Min. Soc. Am. Rev. Min., **10**, 153-206.

Essene, E.J. (1989). The current status of thermobarometry in metamorphic rocks. *In*: Daly, J.S., Cliff, R.A. and Yardley, B.W.D. (Eds.). *Evolution of metamorphic belts*. Spec. Publ. Geol. Soc. Lond., **43**, 1-44.

Evans, M.J. (1984). *Precambrian geology west of Scottburgh, Natal.* M.Sc. thesis (unpubl.), Univ. Natal, Durban, 173pp.

Ewart, A. (1981). The mineralogy and chemistry of the anorogenic silicic volcanics of S.E. Queensland and N.E. New South Wales, Australia. *J. Geophys. Res.*, **86**, 10242-10256.

Ewart, A. (1985). Aspects of the mineralogy and chemistry of the intermediate - silicic Cainozoic volcanic rocks of eastern Australia. Mineralogy and petrogenesis. *Aust. J. Earth Sci.*, **32**, 383- 413.

Fedo, C.M., Nesbitt, H.W. and Young, G.M. (1995). Unraveling the effects of potassium metasomatism in sedimentary rocks and paleosols, with implications for paleoweathering conditions and provenance. *Geology*, **23**, 921-924.

Fedo, C.M., Young, G.M., Nesbitt, H.W. and Hanchar, J.M. (1997). Potassic and sodic metasomatism in the Southern Province of the Canadian Shield: evidence from the Paleoproterozoic Serpent Formation, Hurian Supergroup, Canada. *Precambrian Res.*, **84**, 17-36.

Feeley, T.C. and Hacker, M.D. (1995). Intracrustal derivation of Na-rich andesitic and dacitic magmas: an example from Volcan Ollague, Andean Central Volcanic Zone. *J. Geol.*, **103**, 213- 225.

Ferry, J.M. and Spear, F.S. (1978). Experimental calibration of the partitioning of Fe and Mg between biotite and garnet. *Contrib. Miner. Petrol.*, **66**, 113-117.

Foland, K.A. and Allen, J.C. (1991). Magma sources for Mesozoic anorogenic granites of the White Mountain magma series, New England, USA. *Contrib. Miner. Petrol.*, **109**, 195-211.

Förster, H.-J., Tischendorf, G. and Trumbull, R.B. (1997). An evaluation of the Rb vs. (Y+Nb) discrimination diagram to infer tectonic setting of silicic igneous rocks. *Lithos*, **40**, 261-293.

Fowler, M.B. (1986). Large-ion lithophile element characteristics of an amphibolite facies to granulite facies transition at Gruinard Bay, north-west Scotland. *J. metamorphic Geol.*, **4**, 345- 359.

Fram, M.S. and Lesher, C.E. (1997). Generation and polybaric differentiation of East Greenland Early Tertiary flood basalts. *J. Petrol.*, **38**, 231-275.

Frey, F.A. and Roden, M.F. (1987). The mantle source for the Hawaiian Islands: constraints from the lavas and the ultramafic inclusions. *In*: Menzies, M.A. and Hawkesworth, C.J. (Eds.). *Mantle Metasomatism*. Academic Press, London, 423-463.

Frick, C. and Walraven, F. (1985). The petrology and geochemistry of the pre-Karoo Elandskraal volcano, South Africa. *Trans. geol. Soc. S. Afr.*, **88**, 225-243.

Frost, C.D. and Frost, B.R. (1997). Reduced rapakivi-type granites: the tholeiitic connection. *Geology*, **25**, 647-650.

Frost, C.D., Frost, B.R., Chamberlain, K.R. and Edwards, B.R. (1999). Petrogenesis of the 1.43 Ga Sherman Batholith, SE Wyoming, USA: a reduced, rapakivi-type anorogenic granite. *J. Petrol.*, **40**, 1771-1802.

Fujimaki, H. (1986). Partition coefficients of Hf,

Zr, and REE between zircon, apatite, and liquid. *Contrib. Miner. Petrol.*, **94**, 42-45.

Garde, A.A. (1990). Thermal granulite-facies metamorphism with diffuse retrogression in Archaean orthogneisses, Fiskefjord, southern west Greenland. *J. metamorphic Geol.*, **8**, 663-687.

Garland, F., Hawkesworth, C.J. and Mantovani, M.S.M. (1995). Description and petrogenesis of the Paraná rhyolites, southern Brazil. *J. Petrol.*, **36**, 1193-1227.

Garver, J.I., Royce, P.R. and Smick, T.A. (1996). Chromium and nickel in shale of the Taconic foreland: a case study for the provenance of fine-grained sediments with an ultramafic source. *J. sedim. Res.*, **66**, 100-106.

Geist, D., Howard, K.A. and Larson, P. (1995). The generation of oceanic rhyolites by crystal fractionation: the basalt-rhyolite association at Volcan Alcedo, Galapagos Archipelago. *J. Petrol.*, **36**, 965-982.

Ghent, E.D., Robbins, D.B. and Stout, M.Z. (1979). Geothermometry, geobarometry, and fluid compositions of metamorphosed calc-silicates and pelites, Mica Creek, British Columbia. *Am. Miner.*, **64**, 874-885.

Gill, J.B. (1970). Geochemistry of Viti Levu, Fiji, and its evolution as an island arc. *Contrib. Miner. Petrol.*, **27**, 179-203.

Gold, D. (1957). *The geology of the area around Pinetown and Hillcrest, Natal.* M.Sc. thesis (unpubl.), Univ. Natal, Durban, 41 pp.

Goodwin, A.M. (1991). *Precambrian Geology.* Academic Press, London, 666 pp.

Grant, J.A. (1985). Phase equilibria in partial melting of pelitic rocks. *In*: Ashworth, J.R. (Ed.). *Migmatites*. Blackie, London, 86-144.

Grantham, G.H. (1983). *The tectonic, metamorphic and intrusive history of the Natal mobile belt between Glenmore and Port Edward, Natal.* M.Sc. thesis (unpubl.), Univ. Natal, Pietermaritzburg, 243pp.

Green, T.H. (1977). Garnet in silicic liquid and its possible use as a P-T indicator. *Contrib. Miner. Petrol.*, **65**, 59-68.

Greenfield, J.E., Clarke, G.L., Bland, M. and Clark, D.J. (1996). In-situ migmatite and hybrid diatexite at Mt Stafford, central Australia. *J. metamorphic Geol.*, **14**, 413- 426.

Greenfield, J.E., Clarke, G.L. and White, R.W. (1998). A sequence of partial melting reactions at Mt Stafford, central Australia. *J. metamorphic Geol.*, **16**, 363-378.

Gribble, C.D. (1969). Distribution of elements in igneous rocks of the normal calc-alkaline sequence. *Scott. J. Geol.*, **5**, 322-327.

Griesbach, C.L. (1871). On the geology of Natal, in South Africa. *Quart. J. geol. Soc. Lond.*, **27**, 53-72.

Groenewald, P.B., Grantham, G.H. and Watkeys, M.K. (1991). Geological evidence for a Proterozoic to Mesozoic link between southeastern Africa and Droning Maud Land, Antarctica. *J. geol. Soc. Lond.*, **148**, 1115-1124.

Guidotti, C.V. (1984). Micas in metamorphic rocks. *In*: Bailey, S.W. (Ed.). *Micas*. Min. Soc. Am. Rev. Min., **13**, 357-467.

Guidotti, C.V. and Dyar, M.D. (1991). Ferric iron in metamorphic biotite and its petrologic and crystallochemical implications. *Am. Miner.*, **76**, 161-175.

Guy, J.E. (1974). *The geology of an area to the northwest of Mandini, Zululand.* M.Sc. thesis (unpubl.), Univ. Natal, Durban, 228 pp.

Haapala, I. (1977). Petrography and geochemistry of the Eurajoki Stock, a rapakivi-granite complex with greisen-type mineralization in southwestern Finland. *Bull. Geol. Surv. Finl.*, **286**, 128pp.

Haapala, I.J. and Ramo, O.T. (1990). Petrogenesis of the Proterozoic rapakivi granites of Finland. *In*: Stein, H.J. and Hannah, J.L. (Eds.). *Ore-bearing granite systems: Petrogenesis and mineralizing processes*. Geol. Soc. Am. Spec. Pap., **246**, 275-286.

Hall, A. (1965). The origin of accessory garnet in the Donegal granite. *Mineralog. Mag.*, **35**, 628-633.

Halliday, A.N. (1983). Crustal melting and the genesis of isotopically and chemically zoned plutons in the Southern Uplands of Scotland. *In:*

Atherton, M.P. and Gribble, C.D. (Eds.). *Migmatites, melting and metamorphism*. Shiva, Nantwich, 54-61.

Halliday, A.N., Davidson, J.P., Hildreth, W. and Holden, P. (1991). Modelling the petrogenesis of high Rb/Sr silicic magmas. *Chem. Geol.*, **92**, 107-114.

Hamilton, W.B. (1998). Archean magmatism and deformation were not products of plate tectonics. *Precambrian Res.*, **91**, 143-179.

Hammarstrom, J.M. and Zen, E-an. (1986). Aluminium in hornblende: an empirical igneous geobarometer. *Am. Miner.*, **71**, 1297-1313.

Han, B., Wang, S., Jahn, B., Hong, D., Kagami, H. and Sun, Y. (1997). Depleted-mantle source for the Ulungur River A-type granites from North Xinjiang, China: geochemistry and Nd-Sr isotopic evidence, and implications for Proterozoic crustal growth. *Chem. Geol.*, **138**, 135-159.

Hand, M., Dirks, P.H.G.M., Powell, R. and Buick, I.S. (1992). How well established is isobaric cooling in Proterozoic orogenic belts? An example from the Arunta Inlier, central Australia. *Geology*, **20**, 649-652.

Hargraves, R.B. (1952). *The geology of the area north of Botha's Hill, Natal.* M.Sc. thesis (unpubl.), Univ. Natal, Durban, 41 pp.

Harley, S.L. (1984a). The solubility of alumina in orthopyroxene coexisting with garnet in FeO-MgO-Al_2O_3-SiO_2 and CaO-FeO-MgO-Al_2O_3-SiO_2. *J. Petrol.*, **25**, 665-696.

Harley, S.L. (1984b). An experimental study of the partitioning of Fe and Mg between garnet and orthopyroxene. *Contrib. Miner. Petrol.*, **86**, 359-373.

Harley, S.L. (1985). Garnet-orthopyroxene bearing granulites from Enderby Land, Antarctica: metamorphic Pressure - Temperature - Time evolution of the Archaean Napier Complex. *J. Petrol.*, **26**, 819-856.

Harley, S.L. (1989). The origins of granulites: a metamorphic perspective. *Geol. Mag.*, **126**, 215-247.

Harley, S.L. and Green, D.H. (1982). Garnet-orthopyroxene barometry for granulites and peridotites. *Nature*, **300**, 697-701.

Harley, S.L., Hensen, B.J. and Sheraton, J.W. (1990). Two-stage decompression in orthopyroxene-sillimanite granulites from Forefinger Point, Enderby Land, Antarctica: implications for the evolution of the Archaean Napier Complex. *J. metamorphic Geol.*, **8**, 591-613.

Harley, S.L. and Fitzsimons, I.C.W. (1991). Pressure-temperature evolution of metapelitic granulites in a polymetamorphic terrane: the Rauer Group, east Antarctica. *J. metamorphic Geol.*, **9**, 231-243.

Harnois, L. (1988). The CIW index: a new chemical index of weathering. *Sedi Geol.*, **55**, 319-322.

Harris, C. (1995). Oxygen isotope geochemistry of the Mesozoic anorogenic complexes of Damaraland, northwest Namibia: evidence for crustal contamination and its effect on silica saturation. *Contrib. Miner. Petrol.*, **122**, 308-321.

Harris, N.B.W. (1974). The petrology and petrogenesis of some muscovite granite sills from the Barousse Massif, Central Pyrenees. *Contrib. Miner. Petrol.*, **45**, 215-230.

Harris, N.B.W., Marzouki, F.M.H. and Ali, S. (1986a). The Jabel Sayid Complex, Arabian Shield: geochemical constraints on the origin of peralkaline and related granites. *J. geol. Soc. Lond.*, **143**, 287-295.

Harris, N.B.W., Pearce, J.A. and Tindle, A.G. (1986b). Geochemical characteristics of collision-zone magmatism. *In*: Coward, M.P. and Ries, A.C. (Eds.). *Collision Tectonics*. Geol. Soc. Specl. Publ., **19**, 67-82.

Harris, N.B.W. and Inger, S. (1992). Trace element modelling of pelite-derived granites. *Contrib. Miner. Petrol.*, **110**, 46-56.

Hart, S. and Zindler, A. (1989). Constraints on the nature and development of chemical heterogeneities in the mantle. *In*: Peltier, W.R. (Ed.). *Mantle Convection, Plate Tectonics and Global Dynamics*. The Fluid Mechanics of Astrophysics and Geophysics, **4**, 261-387.

Hart, S.R. (1971). K, Rb, Sc, Sr and Ba contents and Sr isotope ratios of ocean floor basalts. *Phil. Trans. Roy. Soc. Lond. A*, **26**, 573-587.

Hart, S.R., Erlank, A.J. and Kable, E.J.D. (1974).

Sea floor basalt alteration: some chemical and Sr isotopic effects. *Contrib. Miner. Petrol.*, **44**, 219-230.

Hassanen, M.A. (1997). Post-collision, A-type granites of Homrit Waggat Complex, Egypt: petrological and geochemical constraints on its origin. *Precambrian Res.*, **82**, 211-236.

Haughton, S.H. (1969). *The geological history of Southern Africa.* Geol. Soc. S. Afr., Cape Town, 535 pp.

Hawkesworth, C.J., Hergt, J.M., McDermott, F. and Ellam, R.M. (1991). Destructive margin magmatism and the contributions from the mantle wedge and subducted crust. *Aust. J. Earth Sci.*, **38**, 577-594.

Hedge, C.E. and Peterman, Z.E. (1970). The strontium isotope composition of basalts from the Gordo and Juan de Fuca Rises, Northeastern Pacific Ocean. *Contrib. Miner. Petrol.*, **27**, 114-120.

Helz, R.T. (1976) Phase relations of basalts in their melting ranges at P_{H2O}=5 kb. Melt compositions. *J. Petrol.*, **17**, 139-193.

Helz, R.T. (1979). Alkali exchange between hornblende and melt: a temperature-sensitive reaction. *Am. Miner.*, **64**, 953-965.

Hildreth, W. (1981). Gradients in silicic magma chambers: implications for lithospheric magmatism. *J. Geophys. Res.*, **86**, 10153-10192.

Hildreth, W. and Moorbath, S. (1988). Crustal contributions to arc magmatism in the Andes of central Chile. *Contrib. Miner. Petrol.*, **98**, 455-489.

Hodges, K.V. and Crowley, P.D. (1985). Error estimation and empirical geothermobarometry for pelitic systems. *Am. Miner.*, **70**, 702-709.

Holdaway, M.J., Mukhopadhyay, B., Dyar, M.D., Guidotti, C.V. and Dutrow, B.L. (1997). Garnet-biotite geothermometry revised: new Margules parameters and a natural specimen data set from Maine. *Am. Miner.*, **82**, 582-595.

Holland, T. and Blundy, J. (1994). Non-ideal interactions in calcic amphiboles and their bearing on amphibole-plagioclase thermometry. *Contrib. Miner. Petrol.*, **116**, 433-447.

Hollister, L.S. (1977). .The reaction forming cordierite from garnet, the Khtada Lake metamorphic complex, British Columbia. *Can. Mineral.*, **15**, 217-229.

Hollister, L.S., Grissom, G.C., Peters, E.K., Stowell, H.H. and Sisson, V.B. (1987). Confirmation of the empirical correlation of Al in hornblende with pressure of solidification of calc-alkaline plutons. *Am. Mineral.*, **72**, 231-239.

Holm, P.E. (1982). Non-recognition of continental tholeiites using the Ti-Y-Zr diagram. *Contrib. Miner. Petrol.*, **79**, 308-310.

Holm, P.E. (1985). The geochemical fingerprints of different tectonomagmatic environments using hygromagmatophile element abundances of tholeiitic basalts and basaltic andesites. *Chem. Geol.*, **51**, 303-323.

Hooper, P.R. (1988). The Columbia River Basalt. *In*: Macdougall, J.D. (Ed.). *Continental Flood Basalts*. Kluwer Academic Publishers, Hingham, Mass., 1-33.

Hubbard, F.H. (1989). The geochemistry of Proterozoic lower-crustal depletion in southwest Sweden. *Lithos*, **23**, 101-113.

Hughes, S.S., Lewis, S.E., Bartholomew, M.J., Sinha, A.K., Hudson, T.A. and Herz, N. (1997). Chemical diversity and origin of Precambrian charnockitic rocks of the central Pedlar massif, Grenvillian Blue Ridge Terrane, Virginia. *Precambrian Res.*, **84**, 37-62.

Hynes, A. (1980). Carbonatization and mobility of Ti, Y, and Zr in Ascot Formation metabasalts, SE. Quebec. *Contrib. Miner. Petrol.*, **75**, 79-87.

Indares, A. and Martignole, J. (1985). Biotite-garnet geothermometry in the granulite facies: the influence of Ti and Al in biotite. *Am. Miner.*, **70**, 272-278.

Jacobs, J., Thomas, R.J. and Weber, K. (1993). Accretion and indentation tectonics at the southern margin of the Kaapvaal Craton during the Kibaran (Grenville) Orogeny. *Geology*, **21**, 203-206.

Jacobs, J. and Thomas, R.J. (1994). Oblique collision at about 1.1 Ga along the southern margin of the Kaapvaal continent, south-east Africa. *Geol. Rundsch.*, **83**, 322-333.

James, S.D., Pearce, J.A. and Oliver, R.A. (1987). The geochemistry of the lower Proterozoic Willyama Complex volcanics, Broken Hill Block, New South Wales. *In*: Pharaoh, T.C., Beckinsale, R.D. and Rickard, D. (Eds.). *Geochemistry and mineralization of Proterozoic volcanic suites*. Geol. Soc. Spec. Publ., **33**, 395-408.

Janser, B.W. (1994). The Star Lake Pluton, La Ronge Domain, northern Saskatchewan: petrogenesis of a Proterozoic island-arc pluton. *Precambrian Res.*, **70**, 145-164.

Jenkins, D.M. (1988). Experimental study of the join tremolite - tschermakite: a reinvestigation. *Contrib. Miner. Petrol.*, **99**, 392-400.

Jenkins, D.M. (1989). Experimental reversal of the Al content of tremolitic amphiboles coexisting with diopside, anorthite and quartz. *Geol. Soc. Am. Abstracts*, **21**, A157.

Johnson, M.C. and Rutherford, M.J. (1989). Experimental calibration of the aluminium-in-hornblende geobarometer with application to Long Valley Caldera (California) volcanic rocks. *Geology*, **17**, 837-841.

Johnson, R.W., Jaques, A.L., Hickey, R.L., McKee, C.O. and Chappell, B.W. (1985). Manam Island, Papua New Guinea: petrology and geochemistry of a low TiO_2 basaltic island-arc volcano. *J. Petrol.*, **26**, 283-323.

Joyce, A.S. (1973). Chemistry of the minerals of the granitic Murrumbidgee Batholith, Australian Capital Territory. *Chem. Geol.*, **11**, 271-296.

Kalsbeek, F. (1995). Geochemistry, tectonic setting, and poly-orogenic history of Palaeoproterozoic basement rocks from the Caledonian fold belt of North-East Greenland. *Precambrian Res.*, **72**, 301-315.

Kay, S.M., Ramos, V.A. and Marques, M. (1993). Evidence in Cerro Pampa volcanic rocks for slab-melting prior to ridge-trench collision in southern South America. *J. Geol.*, **101**, 703-714.

Kay, S.M. and Gordillo, C.E. (1994). Pocho volcanic rocks and the melting of depleted continental lithosphere above a shallowly dipping subduction zone in the central Andes. *Contrib. Miner. Petrol.*, **117**, 25-44.

Kent, L.E. (1938). The geology of a portion of Victoria County, Natal. *Trans. geol. Soc. S. Afr.*, **41**, 1-36.

Keppie, J.D. and Dostal, J. (1998). Birth of the Avalon arc in Nova Scotia, Canada: geochemical evidence for ~700-630 Ma back-arc rift volcanism off Gondwana. *Geol. Mag.*, **135**, 171-181.

Kerr, A. and Freyer, B.J. (1993). Nd isotope evidence for crust-mantle interaction in the generation of A-type granitoid suites in Labrador, Canada. *Chem. Geol.*, **104**, 39-60.

Kerr, A. (1984). *A report on the Proterozoic rocks in the Valley of a Thousand Hills area, Natal.* Rep. Geol. Surv. S. Afr. (unpubl.).

Kerr, A. (1985). Characterization of the granitic rocks from the Valley of a Thousand Hills area, Natal. *S. Afr. J. Sci.*, **81**, 475-479.

Kerr, A., Eglington, B.M. and Milne, G.C. (1987). Geological, geochemical and isotopic studies on Proterozoic granites from Natal, South Africa. *Ricerca. Sci. Educ. Perm., Univ. Milano*, **59a**, 112-117.

Kerr, A. and Milne, G.C. (1991a). The Mgeni Granite: an example of the megacrystic rapakivi granite - charnockite intrusives in southeastern Africa. *In*: Haapala, I. and Ramo, O.T. (Eds.). *Symposium on rapakivi granites and related rocks*. Geol. Surv. Finl., **34**, 35-36.

Kerr, A. and Milne, G.C. (1991b). Geochemical fingerprints of some amphibolites from the Mapumulo Group and their implications for possible tectonomagmatic environments in pre-Mgeni megacrystic granite times. *Petros*, **14**, 54-69.

Kerr, A. and Milne, G.C. (1994). The Mgeni Granite: an example of the megacrystic mantled-feldspar granite-charnockite intrusives in southeastern Africa. *Miner. Pet.*, **50**, 139-155.

Kerr, R.A. (1985). Plate tectonics goes back 2 billion years. *Science*, **230**, 1364-1367.

King, P.L., White, A.J.R., Chappell, B.W. and Allen, C.M. (1997). Characterization and origin of aluminous A-type granites from the Lachlan Fold Belt, Southeastern Australia. *J. Petrol.*, **38**, 371-391.

Kinnaird, J.A., Bowden, P., Ixer, R.A. and Odling, N.W.A. (1985). Mineralogy, geochemistry and mineralization of the Ririwai Complex, northern Nigeria. *J. Afr. Earth Sci.*, **3**, 185-222.

Knudsen, T.-L., Andersen, T., Maijer, C. and Verschure, R.H. (1997). Trace-element characteristics and Pb isotopic evolution of metasediments and associated Proterozoic rocks from the amphibolite- to granulite-facies Bamble sector, southern Norway. *Chem. Geol.*, **143**, 145-169.

Kohn, M.J. and Spear, F.S. (1991a). Error propagation for barometers. 1. Accuracy and precision of experimentally located end-member reactions. *Am. Miner.*, **76**, 128-137.

Kohn, M.J. and Spear, F.S. (1991b). Error propagation for barometers. 2. Application to rocks. *Am. Miner.*, **76**, 138-147.

Kostyuk, E.A. and Sobolev, V.S. (1969). Paragenetic types of calciferous amphiboles and metamorphic rocks. *Lithos*, **2**, 67-81.

Kretz, R. (1982). Transfer and exchange equilibria in a portion of the pyroxene quadrilateral as deduced from natural and experimental data. *Geochim. Cosmochim. Acta*, **46**, 411-422.

Kretz, R. and Jen, L.S. (1978). Effect of temperature on the distribution of Mg and Fe^{2+} between calcic pyroxene and hornblende. *Can. Miner.*, **16**, 533-537.

Krige, L.J. (1935). The geology of Durban. *Trans. geol. Soc. S. Afr.*, **35**, 37-67.

Kröner, A. (1991). Tectonic evolution in the Archaean and Proterozoic. *Tectonophysics*, **187**, 393-410.

Krynauw, J.R. (1986). *The petrology and geochemistry of intrusions at selected nunataks in the Ahlmannryggen and Giaeverryggen, Western Dronning Maud Land, Antarctica.* Ph.D. thesis (unpubl.), Univ. Natal, Pietermaritzburg, 370pp.

Kuyper, J.L. (1979). *Geology of an area south-east of Nagle Dam, Natal.* M.Sc. thesis (unpubl.), Univ. Natal, Durban, 166pp.

Kuznetsov, V.A. (1971). Transfers of titanium, zirconium and hafnium in high-temperature solutions. *Inter. Geol. Rev.*, **13**, 1795-1797.

Lachize, M., Lorand, J.P. and Juteau, T. (1996). Calc-alkaline differentiation trend in the plutonic sequence of the Wadi Haymiliyah section, Haylayan massif, Semail ophiolite, Oman. *Lithos*, **38**, 207-232.

Lal, R.K. (1993). Internally consistent recalibrations of mineral equilibria for geothermobarometry involving garnet-orthopyroxene-plagioclase-quartz assemblages and their application to the South Indian granulites. *J. metamorphic Geol.*, **11**, 855-866.

Lambert, J.F. (1954). *The geology of a portion of the Valley of a Thousand Hills.* M.Sc. thesis (unpubl.), Univ. Natal, Durban, 60 pp.

Lambert, R.St.J., Winchester, J.A. and Holland, J.G. (1981). Comparative geochemistry of pelites from the Moinian and the Appin Group (Dalradian) of Scotland. *Geol. Mag.*, **118**, 477-490.

Landenberger, B. and Collins, W.J. (1996). Derivation of A-type granites from a dehydrated charnockitic lower crust: evidence from the Chaelundi Complex, eastern Australia. *J. Petrol.*, **37**, 145-170.

Larsen, E.S. (1948). Batholiths and associated rocks of Corona, Elsinore, and San Luis Rey quadrangles, Southern California. *Geol. Soc. Am. Mem.*, **29**, 182pp.

Le Bas, M.J., Le Maitre, R.W., Streckeisen, A. and Zanettin, B. (1986). A chemical classification of volcanic rocks based on the total alkali-silica diagram. *J. Petrol.*, **27**, 745-750.

Le Breton, N. and Thompson, A.B. (1988). Fluid-absent (dehydration) melting of biotite in metapelites in the early stages of crustal anatexis. *Contrib. Miner. Petrol.*, **99**, 226-237.

Le Maitre, R.W. (1976). The chemical variability of some common igneous rocks. *J. Petrol.*, **17**, 589-637.

Le Maitre, R.W. (1989). *A classification of igneous rocks and glossary terms.* Recommendations of the International Union of Geological Sciences Subcommission on the Systematics of Igneous Rocks. Blackwell Scientific Publications, Oxford, 201pp.

Le Roex, A.P. (1985). Geochemistry, mineralogy and magmatic evolution of the basaltic and

trachytic lavas from Gough Island, South Atlantic. *J. Petrol.*, **26**, 149-186.

Le Roex, A.P. and Dick, H.J.B. (1981). Petrography and geochemistry of basaltic rocks from the Conrad fracture zone on the America-Antarctica Ridge. *Earth Planet. Sci. Lett.*, **54**, 117-138.

Le Roex, A.P., Erlank, A.J. and Needham, H.D. (1981). Geochemical and mineralogical evidence for the occurrence of at least three distinct magma types in the 'Famous" region. *Contrib. Miner. Petrol.*, **77**, 24-37.

Le Roex, A.P. and Erlank, A.J. (1982). Quantitative evaluation of fractional crystallization in Bouvet Island lavas. *J. Volcano. Geotherm. Res.*, **13**, 309-338.

Le Roex, A.P., Dick, H.J.B., Erlank, A.J., Reid, A.M., Frey, F.A. and Hart, S.R. (1983). Geochemistry, mineralogy and petrogenesis of lavas erupted along the southwest Indian Ridge between the Bouvet triple junction and 11 degrees east. *J. Petrol.*, **24**, 267-318.

Leake, B.E. (1964). The chemical distinction between ortho- and para-amphibolites. *J. Petrol.*, **5**, 238-254.

Leake, B.E. (1965a). The relationship between tetrahedral aluminum and the maximum possible octahedral aluminum in natural calciferous and subcalciferous amphiboles. *Am. Miner.*, **50**, 843-851.

Leake, B.E. (1965b). The relationship between composition of calciferous amphibole and grade of metamorphism. *In*: Pitcher, W.S. and Flinn, G.W. (Eds.). *Controls of Metamorphism*. Willey, New York, 299-318.

Leake, B.E. (1996). Geochemically unravelling the sedimentary components of Archaean metasediments from western Australia. *J. geol. Soc. Lond.*, **153**, 637-651.

Leake, B.E. (1997). Nomenclature of amphiboles: report of the subcommittee on amphiboles of the international mineralogical association commission on new minerals and mineral names. *Mineralog. Mag.*, **61**, 295-321.

Leake, B.E. and Singh, D. (1986). The Delaney Dome Formation, Connemara, W. Ireland, and the geochemical distinction of ortho- and para-quartzofeldspathic rocks. *Mineralog. Mag.*, **50**, 205-215.

Leake, B.E. and Cobbing, J. (1993). Transient and long-term correspondence of erosion level and the tops of granite plutons. *Scott. J. Geol.*, **29**, 177-182.

Leat, P.T., Jackson, S.E., Thorpe, R.S. and Stillman, C.J. (1986). Geochemistry of bimodal basalt-subalkaline/peralkaline rhyolite provinces within the Southern British Caledonides. *J. geol. Soc. Lond.*, **143**, 259-273.

Lee, H. and Ganguly, J. (1988). Equilibrium compositions of coexisting garnet and orthopyroxene: experimental determinations in the system FeO-MgO-Al_2O_3-SiO_2 and applications. *J. Petrol.*, **29**, 93-114.

Leger, A. and Ferry, J.M. (1991). Highly aluminous hornblende from low-pressure metacarbonates and a preliminary thermodynamic model for the Al content of calcic amphibole. *Am. Miner.*, **76**, 1002-1017.

Lindsley, D.H. (1983). Pyroxene thermometry. *Am. Miner.*, **68**, 477-493.

Loiselle, M.C. and Wones, D.R. (1979). Characteristics and origin of anorogenic granites. *Geol. Soc. Am. Bull. Abstr. Prog.*, **92**, 468.

MacGregor, I.D. (1974). The system MgO-Al_2O_3-SiO_2: solubility of Al_2O_3 in enstatite for spinel and garnet peridotite compositions. *Am. Miner.*, **59**, 110-119.

Mahoney, J.J. (1988). Deccan Traps. *In*: Macdougall, J.D. (Ed.). *Continental Flood Basalts*. Kluwer Academic Publishers, Hingham, Mass., 151-194.

Mansfeld, J. (1996). Geological, geochemical and geochronological evidence for a new Palaeoproterozoic terrane in southeastern Sweden. *Precambrian Res.*, **77**, 91-103.

Mantovani, M.S.M., Marques, L.S., De Sousa, M.A., Civetta, L., Atalla, L. and Innocenti, F. (1985). Trace element and strontium isotope constraints on the origin and evolution of Paraná continental flood basalts of Santa Catarina State (Southern Brazil). *J. Petrol.*, **26**, 187-209.

Martin, R.F. and Piwinskii, A.J. (1972). Magmatism and tectonic settings. *J. Geophys. Res.*,

77, 4966-4975.

Mason, D.R. (1978). Compositional variations in ferromagnesian minerals from porphyry copper - generating and barren intrusions of the Western Highlands, Papua, New Guinea. *Econ. Geol.*, **73**, 878-890.

Mason, D.R. and McDonald, J.A. (1978). Intrusive rocks and porphyry copper occurrences of the Papua-New Guinea-Solomon Islands region: a reconnaissance study. *Econ. Geol.*, **73**, 857- 877.

Matthews, P.E. (1952). *A contribution to the geology of the Valley of a Thousand Hills, Natal.* M.Sc. thesis (unpubl.), Univ. Natal, Durban, 49 pp.

Matthews, P.E. (1972). Possible Precambrian obduction and plate tectonics in southeastern Africa. *Nature*, **240**, 37-39.

Matthews, P.E. (1981a). Eastern or Natal sector of the Namaqua-Natal Mobile Belt in southern Africa. *In*: Hunter, D.R. (Ed.). *Precambrian of the Southern Hemisphere.* Elsevier, Amsterdam, 705-715.

Matthews, P.E. (1981b). A new tectonic model for the northern region of the Namaqua-Natal Belt in Natal (Natal Belt). *South African Geodynamics Symposium, 19th Earth Science Congr. of the Geol. Soc. S. Afr.*, 150-151.

McBirney, A.R. (1968). Petrochemistry of the Cascade andesite volcanoes. *In*: Dole. H.M. (Ed.). *Andesite conference guidebook.* Oregon Dept. of Geol. and Min. Indust. Bull., **62**, 101-107.

McCaffrey, W.D. and Kneller, B.C. (1996). Silurian turbidite provenance on the northern Avalonian margin. *J. geol. Soc. Lond.*, **153**, 437-450.

McCann, T. (1998). Sandstone composition and provenance of the Rotliegend of the NE German Basin. *Sedi. Geol.*, **116**, 177-198.

McDermott, F., Harris, N.B.W. and Hawkesworth, C.J. (1996). Geochemical constraints on crustal anatexis: a case study from the Pan-African Damara granitoids of Namibia. *Contrib. Miner. Petrol.*, **123**, 406-423.

McKenna, L.W. and Hodges, K.V. (1988). Accuracy versus precision in locating reaction boundaries: implications for the garnet - plagioclase - aluminium silicate - quartz geobarometer. *Am. Miner.*, **73**, 1205-1208.

McLeod, P. and Sparks, R.S.J. (1998). The dynamics of xenolith assimilation. *Contrib. Miner. Petrol.*, **132**, 21-33.

Mendonidis, P. and Grantham, G.H. (1989). The distribution, petrology and geochemistry of the Munster Suite, South Coast, Natal. *S. Afr. J. Geol.*, **92**, 377-388.

Miller, C.F. and Mittlefehldt, D.W. (1982). Depletion of light rare-earth elements in felsic magmas. *Geology*, **10**, 129-133.

Milne, G.C. (1986). Geology and geochemistry of the Valley of a Thousand Hills. *Talk delivered at research symposium*, Univ. Natal, Durban.

Milne, G.C. (1988). *The geology and geochemistry of the Proterozoic rocks of the Valley of a Thousand Hills.* University of Natal, Internal Report, 75pp.

Milne, G.C. and Kerr, A. (1990). The Msunduzi pluton - a reversely zoned charnockitic intrusion within the Mgeni Granite. *23rd Earth Science Congr. of the Geol. Soc. S. Afr.*, Cape Town, 706-707.

Milne, G.C. and Kerr, A. (1995). Midcrustal post orogenic granite intrusion levels as revealed by hornblende geobarometry. *Petrology*, **3**, 278-290.

Miyashiro, A. (1974). Volcanic rock series in island arcs and active continental margins. *Am. J. Sci.*, **274**, 321-355.

Moench, R.H. (1986). Comments and reply on "Implications of magmatic epidote-bearing plutons on crustal evolution in the accreted terranes of northwestern North America" and "Magmatic epidote and its petrologic significance". *Geology*, **14**, 187-188.

Morimoto, N. (1988). Nomenclature of pyroxenes. *Mineralog. Mag.*, **52**, 535-550.

Morrison, M.A. (1978). The use of "immobile" trace elements to distinguish the paleotectonic affinities of metabasalts: applications to the Palaeocene basalts of Mull and Skye, northwest Scotland. *Earth Planet. Sci. Lett.*, **39**, 407-416.

Muir, R.J., Weaver, S.D., Bradshaw, J.D., Eby,

G.N. and Evans, J.A. (1995). The Cretaceous Separation Point batholith, New Zealand: granitoid magmas formed by melting of mafic lithosphere. *J. geol. Soc. Lond.*, **152**, 689-701.

Muller, H.D. (1989). Geochemistry of metasediments in the Hercynian and pre-Hercynian crust of the Schwarzwald, the Vosges and northern Switzerland. *Tectonophysics*, **157**, 97-108.

Myers, R.E. and Breitkopf, J.H. (1989). Basalt geochemistry and tectonic settings: a new approach to relate tectonic and magmatic processes. *Lithos*, **23**, 53-62.

Myrow, P.M. (1995). Neoproterozoic rocks of the Newfoundland Avalon Zone. *Precambrian Res.*, **73**, 123-136.

Mysen, B.O. and Boettcher, A.L. (1975). Melting of a hydrous mantle: II Geochemistry of crystals and liquids formed by anatexis of mantle peridotite at high pressures and high temperatures as a function of controlled activities of water, hydrogen and carbon dioxide. *J. Petrol.*, **16**, 549-593.

Nabelek, P.I., Papike, J.J. and Laul, J.C. (1986). The Notch Peak granitic stock, Utah: origin of reverse zoning and petrogenesis. *J. Petrol.*, **27**, 1035-1069.

Nabelek, P.I., Lindsley, D.H. and Bohlen, S.R. (1987). Experimental examination of two-pyroxene graphical thermometers using natural pyroxenes with applications to metaigneous pyroxenes from the Adirondack Mountains, New York. *Contrib. Miner. Petrol.*, **97**, 66-71.

Nakamura, N. (1974). Determination of REE, Ba, Fe, Mg, Na and K in carbonaceous and ordinary chrondrites. *Geochim. Cosmochim. Acta*, **38**, 757-775.

Nedelec, A., Stephens, W.E. and Fallick, A.E. (1995). The PanAfrican stratoid granites of Madagascar: alkaline magmatism in a post-collisional extensional setting. *J. Petrol.*, **36**, 1367- 1391.

Neogi, S., Dasgupta, S. and Fukuoka, M. (1998). High P-T polymetamorphism, dehydration melting, and generation of migmatites and granites in the Higher Himalayan Crystalline Complex, Sikkim, India. *J. Petrol.*, **39**, 61-99.

Nesbitt, H.W. and Young, G.M. (1982). Early Proterozoic climates and plate motions inferred from major element chemistries of lutites. *Nature*, **299**, 715-717.

Nesbitt, H.W. and Young, G.M. (1984). Prediction of some weathering trends of plutonic and volcanic rocks based on thermodynamic and kinetic considerations. *Geochim. Cosmochim. Acta*, **48**, 1523-1534.

Nesbitt, H.W. and Young, G.M. (1989). Formation and diagenesis of weathering profiles. *J. Geol.*, **97**, 129-147.

Nesbitt, H.W., Young, G.M., McLennan, S.M. and Keays, R.R. (1996). Effects of chemical weathering and sorting on the petrogenesis of siliciclastic sediments, with implications for provenance studies. *J. Geol.*, **104**, 525-542.

Nevia, A.M.R. (1975). Geochemistry of coexisting aplites and pegmatites and of their minerals from central northern Portugal. *Chem. Geol.*, **16**, 153-177.

Newton, R.C. and Perkins, D. (1981). Thermodynamic calibration of geobarometers based on the assemblages garnet - plagioclase - orthopyroxene (clinopyroxene) - quartz. *Am. Miner.*, **67**, 203-222.

Neymark, L.A., Amelin, J.V., Larin, A.M. and Yakovleva, S.Z. (1991). Geochronology and isotope geochemistry of the 1.54-1.57 Ga old Salmi anorthosite - rapakivi granite batholith (North Ladoga region, Soviet Karelia). *In*: Haapala, I. and Ramo, O.T. (Eds.). *Symposium on rapakivi granites and related rocks*. Geol. Surv. Finl., **34**, 36.

Nicolaysen, L.O. and Burger, A.J. (1965). Note on an extensive zone of 1 000 million-year old metamorphic and igneous rocks in southern Africa. *Sci. Terres*, **10**, 497-518.

Notsu, K., Ono, K. and Soya, T. (1987). Strontium isotopic relations of bimodal volcanic rocks at Kikai volcano in the Ryukyu arc, Japan. *Geology*, **15**, 345-348.

Noyes, H.J., Wones, D.R. and Frey, F.A. (1983). A tale of two plutons: petrographic and mineralogical constraints on the petrogenesis of the Red Lake and Eagle Peak plutons, central Sierra Nevada, California. *J. Geol.*, **91**, 353-379.

O'Connor, J.T. (1965). A classification for quartz-rich igneous rock based on feldspar ratios.

U.S. Geol. Surv. Prof. Paper, **525B**, B79-B84.

Okonkwo, C.T. (1989). Geochemistry and sedimentology of Grampian Group metasedimentary rocks, Upper Strathspey. *Scott. J. Geol.*, **25**, 239-248.

Pankhurst, R.J., Leat, P.T., Sruoga, P., Rapela, C.W., Marquez, M., Story, B.C. and Riley, T.R. (1998). The Chon Aike province of Patagonia and related rocks in west Antarctica: a silicic large igneous province. *J. Volcano. Geotherm. Res.*, **81**, 113-136.

Passchier, C.W. (1995). Precambrian orogenesis: was it really different? *Geologie en Mijnbouw*, **74**, 141-150.

Patiño Douce, A.E. (1997). Generation of metaluminous A-type granites by low-pressure melting of calc-alkaline granitoids. *Geology*, **25**, 743-746.

Patiño Douce, A.E. and Johnston, A.D. (1991). Phase equilibria and melt productivity in the pelitic system: implications for the origin of peraluminous granitoids and aluminous granulites. *Contrib. Miner. Petrol.*, **107**, 202-218.

Pearce, J.A. (1982). Trace element characteristics of lavas from destructive plate boundaries. *In*: Thorpe, R.S. (Ed.). *Andesites*. Wiley, Chichester, 525-548.

Pearce, J.A. (1983). Role of sub-continental lithosphere in magma genesis at active continental margins. *In*: Hawkesworth, C.J. and Norry, M.J. (Eds.) *Continental basalts and mantle xenoliths*. Shiva, Cheshire, 230-249.

Pearce, J.A. and Cann, J.R. (1973). Tectonic setting of basic volcanic rocks determined using trace element analyses. *Earth Planet. Sci. Lett.*, **19**, 290-300.

Pearce, J.A. and Gale, G.H. (1977). Identification of ore-deposition environment from trace element geochemistry of associated igneous host rocks. *Geol. Soc. Spec. Publ.*, **7**, 14-24.

Pearce, J.A. and Norry, M.J. (1979). Petrogenetic implications of Ti, Zr, Y and Nb variations in volcanic rocks. *Contrib. Miner. Petrol.*, **69**, 33-47.

Pearce, J.A., Harris, N.B.W. and Tindle, A.G. (1984). Trace element discrimination diagrams for the tectonic interpretation of granitic rocks. *J. Petrol.*, **25**, 956-983.

Peate, D.W. and Hawkesworth, C.J. (1996). Lithospheric to asthenospheric transition in low-Ti flood basalts from southern Paraná, Brazil. *Chem. Geol.*, **127**, 1-24.

Peltonen, P., Kontinen, A. and Huhma, H. (1996). Petrology and geochemistry of metabasalts from the 1.95 Ga Jormua ophiolite, northeastern Finland. *J. Petrol.*, **37**, 1359-1383.

Pepper, M.A. and Ashley, P.M. (1998). Volcanic textures in quartzo-feldspathic gneiss of the Willyama Supergroup, Olary Domain, South Australia. *Aust. J. Earth Sci.*, **45**, 971-978.

Perchuk, L.L. and Lavrent'eva, I.V. (1983). Experimental investigation of exchange equilibria in the system cordierite-garnet-biotite. *In*: Saxena, S.K. (Ed.). *Kinetics and equilibrium in mineral systems.* Springer Verlag, New York, 199-239.

Perchuk, L.L., Aranovich, L.Y., Podlesskii, K.K., Lavrent'eva, I.V., Gerasimov, V.Y., Fed'kin, V.V., Kitsul, V.I., Karsakov, L.P. and Berdnikov, N.V. (1985). Precambrian granulites of the Aldan shield, eastern Siberia, USSR. *J. metamorphic Geol.*, **3**, 265-310.

Petersen, J.S. (1980). The zoned Kleivan Granite - an end member of the anorthosite suite in southwest Norway. *Lithos*, **13**, 79-95.

Petersson, J. and Eliasson, T. (1997). Mineral evolution and element mobility during episyenitization (dequartzification) and albitization in the postkinematic Bohus granite, southwest Sweden. *Lithos*, **42**, 123-146.

Petro, W.L., Vogel, T.A. and Wilband, J.T. (1979). Major-element chemistry of plutonic rock suites from compressional and extensional plate boundaries. *Chem. Geol.*, **26**, 217-235.

Pettyjohn, F.J., Potter, P.E. and Siever, R. (1987). *Sand and Sandstone*. Springer-Verlag, New York, 553 pp.

Pharaoh, T.C., Beckinsale, R.D. and Rickard, D. (1987). *Geochemistry and mineralization of Proterozoic volcanic suites*. Geol. Soc. Spec. Publ., **33**, 575pp.

Piccirillo, E.M. and Cox, K.G. (1988). Origins of

variation in the mafic rocks of the S. Paraná Basin. *Int. Conf. on Geochemical Evolution of the Continental Crust*, Pocos de Caldas, 83-89.

Piccirillo, E.M., Melfi, A.J., Comin-Chiaramonti, P., Bellieni, G., Ernesto, M., Marques, L.S., Nardy, A.J.R., Pacca, I.G., Roisenberg, A. and Stolfa, D. (1988). Continental flood volcanism from the Paraná Basin (Brazil). *In*: Macdougall, J.D. (Ed.). *Continental Flood Basalts*. Kluwer Academic Publishers, Hingham, Mass., 195-238.

Pidgeon, R.T. and Aftalion, M. (1978). Cogenetic and inherited zircon U-Pb systems in Palaeozoic granites from Scotland and adjacent regions. *In*: Bowes, D.R. and Leake, B.E. (Eds.). *Crustal evolution in northwestern Britain and adjacent regions*. Geol. J. Spec. Issue, **10**, 183- 220.

Pin, C. and Paquette, J.-L. (1997). A mantle-derived bimodal suite in the Hercynian Belt: Nd isotope and trace element evidence for a subduction-related rift origin of the Late Devonian Brevenne metavolcanics, Massif Central (France). *Contrib. Miner. Petrol.*, **129**, 222-238.

Piper, J.D.A. (1974). Proterozoic crustal distribution, mobile belts and apparent polar movements. *Nature*, **251**, 381-384.

Pitcher, W.S. (1983). Granite type and tectonic environment. *In*: Hsu, K. (Ed.). *Mountain Building Processes*. Academic Press, London, 19-40.

Pitcher, W.S., Atherton, M.P., Cobbing, E.J. and Beckinsale, R.D. (1985). *Magmatism at a plate edge*. Blackie, London, 328 pp.

Plyusnina, L.P. (1982). Geothermometry and geobarometry of plagioclase-hornblende bearing assemblages. *Contrib. Miner. Petrol.*, **80**, 140-146.

Poitrasson, F., Pin, C., Duthou, J.-L. and Platevoet, B. (1994). Aluminous subsolvus anorogenic granite genesis in the light of Nd isotopic heterogeneity. *Chem. Geol.*, **112**, 199-219.

Poitrasson, F., Duthou, J.-L. and Pin, C. (1995). The relationship between petrology and Nd isotopes as evidence for contrasting anorogenic granite genesis: example of the Corsican Province (SE France). *J. Petrol.*, **36**, 1251-1274.

Powell, R. and Downes, J. (1990). Garnet porphyroblast-bearing leucosomes in metapelites: mechanisms, phase diagrams and an example from Broken Hill, Australia. *In*: Ashworth, J.R. and Brown, M. (Eds.). *High-Temperature Metamorphism and Crustal Anatexis*. The Mineralogical Society Series, **2**, 105-123.

Powell, R.E. and Holland, T.J.B. (1985). An internally consistent dataset with uncertainties and correlations: 1. Methods and a worked example. *J. metamorphic Geol.*, **3**, 327-342.

Powell, R.E. and Holland, T.J.B. (1988). An internally consistent dataset with uncertainties and correlations: 3. Applications to geobarometry, worked examples and a computer program. *J. metamorphic Geol.*, **6**, 173-204.

Puziewicz, J. and Johannes, W. (1988). Phase equilibria and compositions of Fe-Mg-Al minerals and melts in water-saturated peraluminous granitic systems. *Contrib. Miner. Petrol.*, **100**, 156-168.

Raase, P. (1974). Al and Ti contents of hornblende, indicators of pressure and temperature of regional metamorphism. *Contrib. Miner. Petrol.*, **45**, 231-236.

Raith, M. and Srikantappa, C. (1993). Arrested charnockite formation at Kottavattam, Southern India. *J. metamorphic Geol.*, **11**, 815-832.

Ramo, O.T. (1991). Petrogenesis of the Proterozoic rapakivi granites and related basic rocks of southeastern Fennoscandia: Nd, and Pb isotopic and general geochemical constraints. *Bull. Geol. Surv. Fin.*, **355**, 161pp.

Ramsey, C.R., Odell, J. and Drysdall, A.R. (1986). Felsic plutonic rocks of the Midyan Region, Kingdom of Saudi Arabia - II. Pilot study in chemical classification of Arabian granitoids. *J. Afr. Earth Sci.*, **4**, 79-85.

Ramsey, W.R.H., Crawford, A.J. and Foden, J.D. (1984). Field setting, mineralogy, chemistry, and genesis of arc picrites, New Georgia, Solomon Islands. *Contrib. Miner. Petrol.*, **88**, 386-402.

Rapela, C.W. and Pankhurst, R.J. (1996). Monzonite suites, the innermost Cordilleran plutonism of Patagonia. *Trans. Roy. Soc. Edin.*, **87**, 193-203.

Rasmussen, E., Neumann, E.-R., Andersen, T., Sundvoll, B., Fjerkingstad, V. and Stabel, A. (1988). Petrogenetic processes associated with intermediate and silicic magmatism in the Oslo Rift, southeast Norway. *Mineralog. Mag.*, **52**, 293-307.

Rathmell, M.A., Streepey, M.M., Essene, E.J. and van der Pluijm, B.A. (1999). Comparision of garnet-biotite, calcite-graphite, and calcite-dolomite thermometry in the Grenville Orogen; Ontario, Canada. *Contrib. Miner. Petrol.*, **134**, 217-231.

Retallack, G.J. (1986). The fossil record of soils. *In*: Wright, V.P. (Ed.). *Paleosols, their recognition and interpretation*. Blackwell, London, 1-57.

Robinson, P., Spear, F.S., Schumacher, J.C., Laird, J., Klein, C., Evans, B.W. and Doolan, B.L. (1982). Phase relations of metamorphic amphiboles: natural occurrence and theory. *In:* Vablen, D.R. and Ribbe, P.H. (Eds.). *Amphiboles*. Min. Soc. Am. Rev. Min., **9B**, 1-227.

Rogers, J.J.W. and Greenberg, J.K. (1990). Late-orogenic, post-orogenic, and anorogenic granites: distinction by major-element and trace element chemistry and possible origins. *J. Geol.*, **98**, 291-309.

Rogers, N.W. and Hawkesworth, C.J. (1982). Proterozoic age and cumulate origin for granulite xenoliths, Lesotho. *Nature*, **299**, 409-413.

Rollinson, H. (1993). *Using geochemical data: evaluation, presentation, interpretation*. Longman, Singapore, 352pp.

Roser, B.P. and Korsch, R.J. (1986). Determination of tectonic setting of sandstone/mudstone suites using SiO_2 content and K_2O/Na_2O ratio. *J. Geol.*, **94**, 635-650.

Roser, B.P. and Korsch, R.J. (1988). Provenance signatures of sandstone-mudstone suites determined using discriminant function analysis of major-element data. *Chem. Geol.*, **67**, 119-139.

Rudnick, R.L. and Presper, T. (1990). Geochemistry of intermediate/high-pressure granulites. *In:* Vielzeuf, D. and Vidal, P. (Eds.). *Granulites and crustal evolution.* NATO ASI series **c 311**. Kluwer Academic Publishers, Dordrecht, 523-550.

Rutter, M.J. and Wyllie, P.J. (1988). Melting of vapour-absent tonalite at 10 kbar to simulate dehydration-melting in the deep crust. *Nature*, **311**, 159-160.

Ryan, A.B., Baragar, R.A. and Kontak, D.J. (1987). Geochemistry, tectonic setting, and mineralization of high-potassium middle Proterozoic rocks in central Labrador, Canada. *In*: Pharaoh, T.C., Beckinsale, R.D. and Rickard, D. (Eds.). *Geochemistry and mineralization of Proterozoic volcanic suites*. Geol. Soc. Spec. Publ., **33**, 241-254.

SACS (South African Commission for Stratigraphy) (1980). Stratigraphy of South Africa, Part 1. (Comp. Kent, L.E.), Lithostratigraphy of the Republic of South Africa, South West Africa/Namibia, and the Republics of Bophuthatswana, Transkei and Venda. *Handbk. geol. Surv. S. Afr.*, **8**, 690pp.

Sandiford, M., Martin, N., Zhou, S. and Fraser, G. (1991). Mechanical consequences of granite emplacement during high-T, low-P metamorphism and the origin of "anticlockwise" PT paths. *Earth Planet. Sci. Lett.*, **107**, 164-172.

Saunders, A.D. and Tarney, J. (1979). The geochemistry of basalts from a back-arc spreading centre in the East Scotia Sea. *Geochim. Cosmochim. Acta*, **43**, 555-572.

Saunders, A.D., Rogers, G., Marriner, G.F., Terrell, D.J. and Verma, S.P. (1987). Geochemistry of Cenozoic volcanic rocks, Baja California, Mexico: implications for the petrogenesis of post-subduction magmas. *J. Volcanol. Geotherm. Res.*, **32**, 223-245.

Saxena, S.K., Sykes, J. and Eriksson, G. (1986). Phase equilibria in the pyroxene quadrilateral. *J. Petrol.*, **27**, 843-852.

Scheepers, A.I.H. (1952). *The geology of the Ndwedwe-Inanda Native Reserve, Natal.* M.Sc. thesis (unpubl.), Univ. Natal, Durban, 53 pp.

Schmidt, M.W. (1992). Amphibole composition in tonalite as a function of pressure: an experimental calibration of the Al-in-hornblende barometer. *Contrib. Miner. Petrol.*, **110**, 304-310.

Schmidt, M.W. and Thompson, A.B. (1996). Epidote in calc-alkaline magmas: an experimental study of stability, phase relationships, and the role of epidote in magmatic evolution. *Am. Miner.*, 81, 462-474.

Schofield, D.I., van Staal, C.R. and Winchester, J.A. (1998). Tectonic setting and regional significance of the 'Port aux Basques Gneiss', SW Newfoundland. *J. geol. Soc. Lond.*, **155**, 323-334.

Schumacher, R. (1991). Compositions and phase

relations of calcic amphiboles in epidote - and clinopyroxene - bearing rocks of the amphibolite and lower granulite facies, central Massachusetts, USA. *Contrib. Miner. Petrol.*, **108**, 196-211.

Selverstone, J., Spear, F.S., Franz, G. and Morteani, G. (1984). High pressure metamorphism in the SW Tauern window, Austria: P-T paths from hornblende-kyanite-staurolite schists. *J. Petrol.*, **25**, 501-531.

Sen, S.K. and Bhattacharya, A. (1984). An orthopyroxene-garnet thermometer and its application to the Madras charnockites. *Contrib. Miner. Petrol.*, **88**, 64-71.

Senior, A. and Leake, B.E. (1978). Regional metasomatism and the geochemistry of the Dalradian metasediments of Connemara, western Ireland. *J. Petrol.*, **19**, 585-625.

Sevigny, J.H. and Brown, E.H. (1989). Geochemistry and tectonic interpretation of some metavolcanic rock units of the western North Cascades, Washington. *Geol. Soc. Am. Bull.*, **101**, 391-400.

Sharkov, E.V. and Smolkin, V.F. (1997). The early Proterozoic Pechenga-Varzuga Belt: a case of Precambrian back arc spreading. *Precambrian Res.*, **82**, 133-151.

Sheraton, J.W. (1980). Geochemistry of Precambrian metapelites from East Antarctica: secular and metamorphic variations. *BMR J. Aust. Geol. Geophys.*, **5**, 279-288.

Shervais, J.W. (1982). Ti-V plots and the petrogenesis of modern and ophiolitic lavas. *Earth Planet. Sci. Lett.*, **59**, 101-118.

Singh, J. and Johannes, W. (1996). Dehydration melting of tonalites. Part II. Composition of melts and solids. *Contrib. Miner. Petrol.*, **125**, 26-44.

Skjerlie, K.P. and Johnston, A.D. (1993). Fluid-absent melting behaviour of an F-rich tonalitic gneiss at mid-crustal pressures: implications for the generation of anorogenic granite. *J. Petrol.*, **34**, 785-815.

Skjerlie, K.P. and Johnston, A.D. (1994). Vapour-absent melting at 10 kbar of a biotite- and amphibole-bearing tonalitic gneiss: implications for the generation of A-type granites. *Geology*, **20**, 263-266.

Skjerlie, K.P. and Johnston, A.D. (1996). Vapour-absent melting from 10 to 20 kbar of crustal rocks that contain multiple hydrous phases: implications for anatexis in the deep to very deep continental crust and active continental margins. *J. Petrol.*, **37**, 661-691.

Smith, A.G. and Hallam, A. (1970). The fit of the southern continents. *Nature*, **225**, 139-144.

Smith, I.E.M., Worthington, T.J., Price, R.C. and Gamble, J.A. (1997). Primitive magmas in arc-type volcanic associations: examples from the southwest Pacific. *Can. Miner.*, **35**, 257-273.

Smith, R.E. and Smith, S.E. (1976). Comments on the use of Ti, Zr, Y, Sr, K, P and Nb in classification of basaltic magmas. *Earth Planet. Sci. Lett.*, **32**, 114-120.

Sonyushkin, V.E., Sukhorukov, Y.T. and Tcherbakova, T.F. (1991). P-T environment of crystallization of quartz in granites of the Salmi rapakivi batholith in Karelia, USSR. *In*: Haapala, I. and Ramo, O.T. (Eds.). *Symposium on rapakivi granites and related rocks*. Geol. Surv. Finl., **34**, 47.

Spear, F.S. (1980). NaSi=CaAl exchange equilibrium between plagioclase and amphibole, an empirical model. *Contrib. Miner. Petrol.*, **72**, 33-41.

Spear, F.S. (1981a). Amphibole-plagioclase equilibria: an empirical model for the reaction albite+tremolite=edenite+4 quartz. *Contrib. Miner. Petrol.*, **77**, 355-364.

Spear, F.S. (1981b). An experimental study of hornblende stability and compositional variability in amphibolite. *Am. J. Sci.*, **281**, 697-734.

Spulber, S.D. and Rutherford, M.J. (1983). The origin of rhyolite and plagiogranite in oceanic crust: an experimental study. *J. Petrol.*, **24**, 1-25.

Stern, C.R. and Kilian, R. (1996). Role of the subducted slab, mantle wedge and continental crust in the generation of adakites from the Andean Austral Volcanic Zone. *Contrib. Miner. Petrol.*, **123**, 263-281.

Stevens, G., Clemens, J.D. and Droop, G.T.R. (1997a). Melt production during granulite-facies anatexis: experimental data from "primitive" metasedimentary protoliths. *Contrib. Miner. Petrol.*, **128**, 352-370.

Stimac, J.A. and Wark, D.A. (1991). The origin and implications of plagioclase mantles on sanidine in silicic volcanic rocks, Clear Lake, California. *In*: Haapala, I. and Ramo, O.T. (Eds.). *Symposium on rapakivi granites and related rocks*. Geol. Surv. Finl., **34**, 49.

Streckeisen, A. (1976). To each plutonic rock its proper name. *Earth Sci. Rev.*, **12**, 1-33.

Stuwe, K. and Powell, R. (1989). Low-pressure granulite facies metamorphism in the Larsemann Hills area, East Antarctica; petrology and tectonic implications for the evolution of the Prydz Bay area. *J. metamorphic Geol.*, **7**, 465-483.

Sun, S.-S. and McDonough, W.F. (1989). Chemical and isotopic systematics of oceanic basalts: implications for mantle composition and processes. *In*: Saunders, A.D. and Norry, M.J. (Eds.). *Magmatism in the ocean basins*. Geol. Soc. Spec. Publ., **42**, 313-345.

Sutherland, P.C. (1855). Notes on the geology of Natal, South Africa. *Quart. J. geol. Soc. Lond.*, **11**, 465-468.

Sylvester, P.J. (1989). Post-collisional alkaline granites. *J. Geol.*, **97**, 261-280.

Tack, L., Liegeois, J.P., Deblond, A. and Duchesne, J.C. (1994). Kibaran A-type granitoids and mafic rocks generated by two mantle sources in a late orogenic setting (Burundi). *Precambrian Res.*, **68**, 323-356.

Tankard, A.J., Jackson, M.P.A., Eriksson, K.A., Hobday, D.K., Hunter, D.R. and Minter, W.E.L. (1982). *Crustal evolution of Southern Africa: 3.8 billion years of Earth history*. Springer-Verlag, New York, 523pp.

Tarney, J., Skinner, A.C. and Sheraton, J.W. (1972). A geochemical comparison of major Archaean gneiss units from northwest Scotland and east Greenland. *24th Int. Geol. Congr.*, Montreal, **Sect 1**, 162-174.

Tarney, J., Weaver, S.D., Saunders, A.D., Pankhurst, R.J. and Barker, P.F. (1982). Volcanic evolution of the northern Antarctic Peninsula and the Scotia arc. *In:* Thorpe, R.S. (Ed.). *Andesites*. Wiley, Chichester, 371-400.

Taylor, R.P., Strong, D.F. and Fryer, B.J. (1981). Volatile control of contrasting trace element distributions in peralkaline granitic and volcanic rocks. *Contrib. Miner. Petrol.*, **77**, 267-271.

Taylor, S.R. and McLennan, S.M. (1985). *The continental crust: Its composition and evolution*. Blackwell, Oxford, 312pp.

Thomas, R.J. (1988a). The petrography of the Oribi Gorge Suite: Kibaran charnockitic granitoids from southern Natal. *S. Afr. J. Geol.*, **91**, 275-291.

Thomas, R.J. (1988b). *The geology of the Port Shepstone area*. Explan. sheet 3030 (Port Shepstone), Geol. Surv. S. Afr., 136pp.

Thomas, R.J. (1989a). A tale of two tectonic terranes. *S. Afr. J. Geol.*, **92**, 306-321.

Thomas, R.J. (1989b). The petrogenesis of the Mzumbe Gneiss Suite, a tonalite-trondhjemite orthogneiss suite from the southern part of the Natal Structural and Metamorphic Province. *S. Afr. J. Geol.*, **92**, 322-338.

Thomas, R.J. (1992). Mapumulo Group. *In*: Johnson, M.R. (Ed.). *Catalogue of South African Lithostratigraphic Units*. S. Afr. Comm. Stratigr., **4**, 11-14.

Thomas, R.J. and Mawson, S.A. (1989). Newly discovered outcrops of Proterozoic basement rocks in northeastern Transkei. *S. Afr. J. Geol.*, **92**, 369-376.

Thomas, R.J. and Gain, S.B. (1989). The geological setting of gold mineralization at Dumisa, Natal. *S. Afr. J. Geol.*, **92**, 410-419.

Thomas, R.J. and Eglington, B.M. (1990). A Rb-Sr, Sm-Nd and U-Pb zircon isotopic study of the Mzumbe Suite, the oldest intrusive granitoid in southern Natal, South Africa. *S. Afr. J. Geol.*, **93**, 761-765.

Thomas, R.J., Eglington, B.M. and Kerr, A. (1990). The geology and geochronology of the Belmont pluton and microgranite dykes from the Margate area - the search for Pan-African magmatism in southern Natal. *S. Afr. J. Geol.*, **93**, 766-775.

Thomas, R.J., Eglington, B.M., Evans, M.J. and Kerr, A. (1992). The petrology of the Proterozoic Equeefa Suite, southern Natal, South Africa. *S. Afr. J. Geol.*, **95**, 116-130.

Thomas, R.J., Eglington, B.M., Bowring, S.A., Retief, E.A. and Walraven, F. (1993). New isotopic data from a Neoproterozoic porphyritic granitoid-charnockite suite from Natal, South Africa. *Precambrian Res.*, **62**, 83-101.

Thomas, R.J., Agenbacht, A.L.D., Cornell, D.H. and Moore, J.M. (1994). The Kibaran of southern Africa: tectonic evolution and metallogeny. *Ore Geol. Rev.*, **9**, 131-160.

Thompson, H.G. (1955). *The geology of the area about Tafamasi, Inanda, Natal.* M.Sc. thesis (unpubl.), Univ. Natal, Durban, 41 pp.

Thompson, R.N., Morrison, M.A., Dickin, A.P. and Hendry, G.L. (1983). Continental flood basalts...Arachnids rule OK? *In*: Hawkesworth, C.J. and Norry, M.J. (Eds.). *Continental Basalts and Mantle Xenoliths*. Shiva, Cheshire, 158-185.

Thorpe, R.S., Francis, P.W. and Harmon, R.S. (1981). Andesites in crustal evolution. *Phil. Trans. R. Soc. Lond.*, **301**, 305-320.

Tindle, A.G. and Pearce, J.A. (1981). Petrogenetic modelling of in situ fractional crystallization in the zoned Loch Doon pluton, Scotland. *Contrib. Miner. Petrol.*, **78**, 196-207.

Todd, C.S. (1998). Limits to the precision of geobarometry at low grossular and anorthite content. *Am. Miner.*, **83**, 1161-1167.

Tracy, R.J. (1978). High grade metamorphic reactions and partial melting in pelitic schists, west-central Massachusetts. *Am. J. Sci.*, **278**, 150-178.

Tracy, R.J. (1982). Compositional zoning and inclusions in metamorphic minerals. *In*: Ferry, J.M. (Ed.). *Characterization of metamorphism through mineral equilibria*. Min. Soc. Am. Rev. Min., **10**, 355-397.

Tracy, R.J., Robinson, P. and Thompson, A.B. (1976). Garnet composition and zoning in the determination of temperature and pressure of metamorphism, central Massachusetts. *Am. Miner.*, **61**, 762-775.

Tulloch, A.J. (1986). Comments and reply on "Implications of magmatic epidote-bearing plutons on crustal evolution in the accreted terranes of northwestern North America" and "Magmatic epidote and its petrologic significance". *Geology*, **14**, 186-187.

Turner, S.P., Foden, J.D. and Morrison, R.S. (1992). Derivation of some A-type magmas by fractionation of basaltic magma: an example from the Padthaway Ridge, South Australia. *Lithos*, **28**, 151-179.

Twist, D. and Harmer, R.E.J. (1987). Geochemistry of contrasting siliceous magmatic suites in the Bushveld Complex: genetic aspects and implications for tectonic discrimination diagrams. *J. Volc. Geotherm. Res.*, **32**, 83-98.

Van de Kamp, P.C. (1968). Geochemistry and the origin of metasediments in the Haliburton-Madoc area, southeastern Ontario. *Can. J. Earth Sci.*, **5**, 1337-1372.

Van de Kamp, P.C. (1969). Origin of amphibolites in the Beartooth Mountains, Wyoming Montana: new data and interpretation. *Geol. Soc. Am. Bull.*, **81**, 1127-1136.

Van Straten, O.J. (1952). *Geology of the uMlazi area, Natal.* M.Sc. thesis (unpubl.), Univ. Natal, Durban, 31 pp.

Vernon, R.H. (1986). K-feldspar megacrysts in granites - phenocrysts, not porphyroblasts. *Earth Sci. Rev.*, **23**, 1-63.

Vernon, R.H. (1996). Problems with inferring P-T-t paths in low-P granulite facies rocks. *J. metamorphic Geol.*, **14**, 143-153.

Vielzeuf, D. and Holloway, J.R. (1988). Experimental determination of the fluid-absent melting relations in the pelitic system. *Contrib. Miner. Petrol.*, **98**, 257-276.

Vielzeuf, D. and Montel, J.M. (1994). Partial melting of metagreywackes. I Fluid absent experiments and phase relationships. *Contrib. Miner. Petrol.*, **117**, 375-393.

Vine, J.D. and Tourtelot, E.B. (1970). Geochemistry of black shale deposits - a summary report. *Econ. Geol.*, **65**, 253-272.

Vivallo, W. and Claesson, L.-A. (1987). Intra-arc rifting and massive sulphide mineralization in an early Proterozoic volcanic arc, Skellefte district, northern Sweden. *In*: Pharaoh, T.C., Beckinsale, R.D. and Rickard, D. (Eds.). *Geochemistry and mineralization of Proterozoic volcanic suites.* Geol. Soc. Spec. Publ., **33**, 69-79.

Vorma, A. (1976). On the petrochemistry of

rapakivi granites with special reference to the Laitila massif, southeastern Finland. *Geol. Surv. Fin. Bull*, **272**, 98pp.

Vyhnal, C.R. and McSween, H.Y. (1990). Constraints on Alleghanian vertical crustal displacements in the southern Appalachians, based on aluminum-hornblende barometry. *Geology*, **18**, 938-941.

Vyhnal, C.R., McSween, H.Y. and Speer, J.A. (1991). Hornblende chemistry in southern Appalachian granitoids: implications for aluminum hornblende thermobarometry and magmatic epidote stability. *Am. Miner.*, **76**, 176-188.

Walsh, J.N., Buckley, F. and Barker, J. (1981). The simultaneous determination of the rare-earth elements in rocks using inductively coupled plasma source spectrometry. *Chem. Geol.*, **33**, 141-153.

Wang, P. and Glover, L. (1992). A tectonics test of the most commonly used geochemical discriminant diagrams and patterns. *Earth Sci. Rev.*, **33**, 111-131.

Wareham, C.D., Millar, I.L. and Vaughan, A.P.M. (1997). The generation of sodic granite magmas, western Palmer Land, Antarctic Peninsula. *Contrib. Miner. Petrol.*, **128**, 81-96.

Watson, E.B. and Harrison, M. (1984). Accessory minerals and the geochemical evolution of crustal magmatic systems: a summary and prospectus of experimental approaches. *Phys. E. Plan. Inter.*, **35**, 19-30.

Weaver, B.L. and Tarney, J. (1981). Chemical changes during dyke metamorphism in high-grade basement terrains. *Nature*, **289**, 47-49.

Weaver, B.L., Wood, D.A., Tarney, J. and Joron, J.L. (1987). Geochemistry of ocean island basalts from the South Atlantic: Ascension, Bouvet, St. Helens, Gough and Tristan da Cunha. *In*: Fitton, J.G. and Upton, B.G.J. (Eds.). *Alkaline Igneous Rocks*. Geol. Soc. Specl. Publ., **30**, 253-267.

Wedepohl, K.H. (1995). The composition of the continental crust. *Geochim. Cosmochim. Acta*, **59**, 1217-1232.

Wells, P.R.A. (1980). Thermal models for the magmatic accretion and subsequent metamorphism of continental crust. *Earth Planet. Sci. Lett.*, **46**, 253-265.

Wever, H.E., Storey, B.C. and Leat, P. (1995). Peraluminous granites in NE Palmer Land, Antarctic Peninsula: early Mesozoic crustal melting in a magmatic arc. *J. geol. Soc. Lond.*, **152**, 85-96.

Whalen, J.B., Currie, L.C. and Chappell, B.W. (1987). A-type granites: geochemical characteristics, discrimination and petrogenesis. *Contrib. Miner. Petrol.*, **95**, 407-419.

Whalen, J.B., Jenner, G.A., Longstaffe, F.J., Robert, F. and Gariepy, C. (1996). Geochemical and isotopic (O, Nd, Pb and Sr) constraints on A-type granite petrogenesis based on the Topsails Igneous Suite, Newfoundland Appalachians. *J. Petrol.*, **37**, 1463-1489.

White, A.J.R. and Chappell, B.W. (1977). Ultrametamorphism and granitoid genesis. *Tectonophysics*, **43**, 7-22.

White, A.J.R. and Chappell, B.W. (1983). Granitoid types and their distribution in the Lachlan Fold Belt, southeastern Australia. *Geol. Soc. Am. Mem.*, **159**, 21-34.

Wickham, S.M., Alberts, A.D., Zanvilevich, A.N., Litvinovsky, B.A., Bindeman, I.N. and Schauble, E.A. (1996). A stable isotope study of anorogenic magmatism in east Central Asia. *J. Petrol.*, **37**, 1063-1095.

Wiebe, R.A. (1996). Mafic-silicic layered intrusions: the role of basaltic injections on magmatic processes and the evolution of silicic magma chambers. *Trans. Roy. Soc. Edin.*, **87**, 125-138.

Williams, I.S., Compston, W. and Chappell, B.W. (1983). Zircon and monazite U-Pb systems and the histories of I-type magmas, Berridale Batholith, Australia. *J. Petrol.*, **24**, 76-97.

Williams, M.L. and Karlstrom, K.E. (1996). Looping P-T paths and high-T, low-P middle crustal metamorphism: Proterozoic evolution of the southwestern United States. *Geology*, **24**, 1119-1122.

Wimmenauer, W. (1984). Das pravariskische Kristallin im Schwarzwald. *Fortschr. Miner., Beih.*, **62**, 69-86.

Winchester, J.A. and Floyd, P.A. (1976). Geochemical magma type discrimination: application to altered and metamorphosed basic

igneous rocks. *Earth Planet. Sci. Lett.*, **28**, 459-469.

Winchester, J.A. and Floyd, P.A. (1977). Geochemical discrimination of different magma series and their differentiation products using immobile elements. *Chem. Geol.*, **20**, 325-343.

Winchester, J.A. and Max, M.D. (1984). Geochemistry and origins of the Annagh Division of the Precambrian Erris Complex, N.W. County Mayo, Ireland. *Precambrian Res.*, **25**, 397-414.

Winchester, J.A. and Max, M.D. (1989). Tectonic setting discrimination in clastic sequences: an example from the late Proterozoic Erris group, NW Ireland. *Precambrian Res.*, **45**, 191-201.

Winchester, J.A., Floyd, P.A., Chocyk, M., Horbowy, K. and Kozdroj, W. (1995). Geochemistry and tectonic environment of Ordovician meta-igneous rocks in the Rudawy Janowickie Complex, SW Poland. *J. geol. Soc. Lond.*, **152**, 105-115.

Winchester, J.A. and Max, M.D. (1996). Chemostratigraphic correlation, structure and sedimentary environments in the Dalradian of the NW Co. Mayo inlier, NW Ireland. *J. geol. Soc. Lond.*, **153**, 779-801.

Winchester, J.A., Floyd, P.A., Awdankiewicz, M., Piasecki, M.A.J., Awdankiewicz, H., Gunia, P. and Gliwicz, T. (1998). Geochemistry and tectonic significance of metabasic suites in the Gory Sowie Block, SW Poland. *J. geol. Soc. Lond.*, **155**, 155-164.

Windley, B.F. (1991). Early Proterozoic collision tectonics, and rapakivi granites as intrusions in an extensional thrust-thickened crust: the Ketilidian orogen, South Greenland. *Tectonophysics*, **195**, 1-10.

Windley, B.F. (1993). Uniformitarianism today: plate tectonics is the key to the past. *J. geol. Soc. Lond.*, **150**, 7-19.

Windley, B.F. (1995). *The evolving continents*. Wiley, Chichester, 526 pp.

Winkler, H.G.F. (1979). *Petrogenesis of Metamorphic Rocks*. Springer, New York, 348 pp.

Wood, B.J. (1974). The solubility of alumina in orthopyroxene co-existing with garnet. *Contrib. Miner. Petrol.*, **46**, 1-15.

Wood, B.J. and Banno, S. (1973). Garnet-orthopyroxene and orthopyroxene-clinopyroxene relationships in simple and complex systems. *Contrib. Miner. Petrol.*, **42**, 109-127.

Wood, D.A. (1978). Major and trace element variations in the Tertiary lavas of Eastern Iceland and their significance with respect to the Iceland geochemical anomaly. *J. Petrol.*, **19**, 393-436.

Wood, D.A., Joron, J.L., Treuil, M., Norry, M. and Tarney, J. (1979). Elemental and Sr-isotope variations in basic lavas from Iceland and the surrounding ocean floor. *Contrib. Miner. Petrol.*, **70**, 319-339.

Worthing, M.A. and Crawford, A.J. (1996). The igneous geochemistry and tectonic setting of metabasites from the Emo Metamorphics, Papua New Guinea; a record of the evolution and destruction of a backarc basin. *Miner. Pet.*, **58**, 79-100.

Wronkiewicz, D.J. and Condie, K.C. (1987). Geochemistry of Archean shales from the Witwatersrand Supergroup, South Africa: source-area weathering and provenance. *Geochim. Cosmochim. Acta*, **51**, 2401-2416.

Wyborn, L.A.I., Page, R.W. and Parker, A.T. (1987). Geochemical and geochronological signatures in Australian Proterozoic igneous rocks. *In*: Pharaoh, T.C., Beckinsale, R.D. and Rickard, D. (Eds.). *Geochemistry and mineralization of Proterozoic volcanic suites*. Geol. Soc. Spec. Publ., **33**, 377-394.

Yang, H., Kyser, K. and Ansdell, K. (1998). Geochemical and Nd isotopic compositions of the metasedimentary rocks in the La Ronge Domain, Trans-Hudson Orogen, Canada: implications for evolution of the domain. *Precambrian Res.*, **92**, 37-64.

Yoder, H.S. and Tilley, C.E. (1962). Origin of basalt magmas: an experimental study of natural and synthetic rock systems. *J. Petrol.*, **3**, 342-532.

Zhao, J., Ellis, D.J., Kilpatrick, J.A. and McCulloch, M.T. (1997). Geochemical and Sr-Nd isotopic study of charnockites and related rocks in the northern Prince Charles Mountains, East Antarctica: implications for charnockite petrogenesis and Proterozoic crustal evolution. *Precambrian Res.*, **81**, 37-66.

APPENDIX 1

MODAL ANALYSES

Modal analyses of the majority of the lithologies were determined from 500-1000 point counts, dependent on the mineralogy, texture and mineral size distribution of an individual section. Jump spacings were determined from the largest mineral phase present in the individual thin section, with the exception of those sections with porphyroblastic phases, where the point counter was set to maximum. For the mineralogical bands of the fine grained granulites 100 point counts were used. For the megacrystic granites estimates based on hand specimens and microscopic analysis were used.

+ = Present in trace amounts
- = Absent

1. Modal analyses of the biotite hornblende gneiss - Nagle Dam Formation.

	NDF 9	UND 300	NDF 26	UND 312	UND 315	UND 45	UND 50	UND 52	UND 53	UDF 325
Quartz	30	38	34	17	18	16	43	34	26	17
Plagioclase	11	31	34	35	41	35	29	29	39	39
K-feldspar	38	13	24	13	15	8	2	12	12	5
Hornblende	-	-	-	11	16	24	-	3	18	7
Biotite	20	17	8	21	8	15	24	20	4	28
Ore	1	1	+	3	2	2	2	1	1	3
Apatite	-	-	-	+	-	-	-	1	+	-
Sphene	-	-	-	-	-	-	-	-	-	1
Zircon	+	+	+	+	+	+	+	+	+	+
Carbonate*	-	-	-	-	-	-	-	-	-	+
TOTAL	100	100	100	100	100	100	100	100	100	100

* Secondary

2. Modal analyses of the quartzo-feldspathic gneiss - Nagle Dam Formation.

	NDF 3	UND 309	UND 311	UND 311a	UND 318	UND 319
K-feldspar	29	49	36	9	36	13
Plagioclase	36	16	29	64	26	43
Quartz	27	33	32	27	36	38
Biotite	8	2	3	-	2	6
Ore	+	-	+	-	-	-
Apatite	+	+	+	+	+	+
Zircon	+	+	+	+	+	+
TOTAL	100	100	100	100	100	100

3. Modal analyses of the amphibolite - Nagle Dam Formation.

	UND 307	UND 308	UND 308	UND 308	UND 314	UND 320
Hornblende	56	65	70	80	64	36
Plagioclase	34	30	29	17	25	39
Quartz	+	1	-	2	9	-
Clinopyroxene	10	-	-	-	-	25
Ore	+	-	1	1	2	-
Biotite*	-	4	-	-	-	-
TOTAL	100	100	100	100	100	100

* Secondary

4. Modal analyses of the pelitic gneiss - Nagle Dam Formation.

	NDF8	NDF60
Quartz	31	27
Plagioclase	37	49
Biotite	23	23
Garnet	4	+
K-feldspar	4	+
Apatite	+	+
Zircon	+	+
Ore	1	1
Carbonate*	+	-
Muscovite*	+	-
TOTAL	100	100

*Secondary

5. Modal analyses of the amphibolite - Valley Trust Formation.

	UND 334	UND 334	2a/3	UND 347	UND 348	UND 349	UND 350	UND 357		UND 358
Plagioclase	45	33	22	25	24	21	16	35	33	38
Hornblende	50	60	60	40	55	56	56	49	46	36
Clinopyroxene	-	4	11	20	15	12	17	6	9	18
Orthopyroxene	-	-	4	13	4	6	8	3	6	7
Quartz	4	+	-	+	-	3	2	2	-	+
Biotite*	1	1	-	-	-	-	-	-	3	-
Ore	+	2	3	2	2	2	1	5	3	1
TOTAL	100	100	100	100	100	100	100	100	100	100

*Secondary

6. Modal analyses of the pelitic gneiss - Valley Trust Formation.

a) Pelites collected away from the main pelitic gneiss enclave.

	UND 336	UND 353	UND 354	UND 355
Plagioclase	8	1	8	15
Quartz	20	35	26	30
K-feldspar	44	45	38	24
Biotite	11	8	9	12
Sillimanite	8	7	7	8
Cordierite	5	3	11	7
Garnet	3	1	+	4
Ore	1	+	1	+
TOTAL	100	100	100	100

b) Biotite gneiss detached from main pelitic gneiss enclave.

	UND379	UND380	UND381
Plagioclase	61	57	44
Quartz	7	7	12
K-feldspar	8	23	24
Biotite	24	13	20
Ore	+	+	+
Allanite	+	-	+
Apatite	+	+	+
TOTAL	100	100	100

c) Pelitic gneisses from the main enclave.

	NDF56	UND328	UND364	UND367	UND376	UND378	UND342	UND343	UND344	UND345	UND346
Plagioclase	+	15	30	2	8	10	1	6	9	3	11
Quartz	9	17	39	5	8	6	7	12	21	28	38
K-feldspar	32	31	-	57	49	49	41	36	37	32	37
Biotite	12	19	9	33	14	20	23	15	10	11	9
Sillimanite	8	10	-	-	4	2	10	6	2	-	-
Cordierite	9	2	7	-	4	+	6	12	9	11	1
Garnet	18	5	11	1	8	11	12	12	11	14	4
Ore	12	1	4	2	5	2	+	1	1	1	+
TOTAL	100	100	100	100	100	100	100	100	100	100	100

7. Modal analyses of the quartzo-feldspathic gneiss - Valley Trust Formation.

	UND1	UND3	UND4	UND34	UND42	UND302	UND305	UND306
K-feldspar	42	48	42	47	53	54	35	26
Plagioclase	26	15	27	21	21	14	37	21
Quartz	31	29	28	28	18	30	25	51
Biotite	-	8	-	2	7	1	1	-
Ore	1	+	3	+	1	1	+	1
Hornblende	-	-	-	2	-	-	-	-
Muscovite*	-	-	-	-	-	-	2	1
Sphene*	-	-	-	+	+	-	-	-
Apatite	-	+	+	+	+	+	+	+
Zircon	+	+	+	+	+	+	+	+
Allanite	-	+	-	+	-	-	-	-
TOTAL	100	100	100	100	100	100	100	100

* Secondary

8. Modal analyses of the fine grained granulite - Valley Trust Formation.

a) Fine grained granutite from the vicinity of the large pelitic enclave.

	UND359			UND360			UND361	UND362	UND363	NDF89
	a	b	c	a	b	c				
Quartz+feldspar	41	78	77	56	54	73	72	68	57	40
Garnet	52	2	3	25	29	3	21	10	28	35
Biotite	2	-	-	-	-	-	-	+	5	4
Pyroxene	1	16	19	18	16	22	+	21	8	20
Ore	2	2	1	1	1	2	1	1	2	+
Cordierite	-	1	-	-	-	-	-	-	-	-
Sillimanite	-	-	-	-	-	-	4	-	-	-
Tourmaline*	2	1	-	-	-	-	2	-	+	1
TOTAL	100	100	100	100	100	100	100	100	100	100

NDF84 a) Garnet rich band
b) Pyroxene rich band
c) Pyroxene rich band
NDF85 a) Garnet rich band
b) Garnet rich band
c) Garnet poor band

*Secondary

b) Fine grained pyroxene granulite collected away from the large pelitic enclave.

	NDF67					NDF69				NDF70		UND329
	a	b	c	d	e	a	b	c	d	a	b	
Quartz+feldspar	59	39	55	62	34	88	77	18	68	56	54	65
Garnet	-	-	-	2	11	-	-	48	10	-	-	-
Biotite	-	20	-	7	19	12	17	27	15	31	36	15
Pyroxene	39	40	28	25	29	-	-	-	-	13	10	20
Ore	2	1	2	1	1	+	+	+	+	+	+	+
Cordierite	-	-	15	3	6	-	6	7	7	-	-	-
Sillimanite	-	-	-	-	-	-	-	-	-	-	-	-
Tourmaline*	-	-	-	-	-	-	-	-	-	+	+	-
TOTAL	100	100	100	100	100	100	100	100	100	100	100	100

NDF67 a) Pyroxene rich layer
b) Pyroxene and biotite rich layer
c) Pyroxene and cordierite rich layer
d) Traverse at 90° to banding
e) Traverse at 90° to banding

NDF69 a) Mafic poor layer
b) Mafic poor layer
c) Garnet rich band
d)Traverse at 90° to banding

NDF70 a+b Random traverses

*Secondary

c) Fine grained sillimanite granulite collected away from the large pelitic enclave.

	1/6	2b4	UND 339		2/9		2a/1	2a/2	2b/3
			a	b	a	b			
Quartz+feldspar	62	62	61	68	63	27	85	80	47
Garnet	10	17	17	16	7	32	12	7	49
Biotite	8	15	6	2	20	19	-	+	2
Pyroxene	-	-	-	-	-	-	-	-	-
Ore	2	1	2	1	2	3	1	3	1
Cordierite	-	-	-	-	2	3	-	-	-
Sillimanite	18	5	14	13	6	16	2	10	-
Tourmaline*	-	-	+	-	+	+	-	+	1
TOTAL	100	100	100	100	100	100	100	100	100

UND339 a) Random traverse
b) Random traverse
2/9 a) Random traverse
b) Garnet rich band

*Secondary

d) Fine grained amphibolitic granulite.

	2b/1	UND338	UND340
Plagioclase	56	41	33
Pyroxene	40	31	41
Hornblende	-	24	25
Ore	4	3	1
Quartz	-	1	-
Tourmaline*	+	-	+
TOTAL	100	100	100

*Secondary

9. Modal analyses of the biotite-hornblende gneiss - Valley Trust Formation.

	NDF78	NDF81
Plagioclase	40	46
Quartz	17	17
K-feldspar	14	4
Biotite	15	32
Hornblende	13	1
Ore	1	+
Zircon	+	+
Apatite	+	+
TOTAL	100	100

10. Modal analyses of the granitic enclaves - Valley Trust Formation.

	UND330	UND330	UND330
Plagioclase	24	35	26
K-feldspar	41	36	39
Quartz	16	22	30
Biotite	14	6	4
Apatite	+	+	+
Zircon	+	+	+
Allanite	+	+	+
Garnet	5	1	1
Ore	-	+	-
TOTAL	100	100	100

11. Estimated modal analyses for the megacrystic granites - Mgeni batholith.

	Biotite granite	Hornblende granite	Charnockite
K-feldspar	50	45	40
Plagioclase	25	25	25
Quartz	20	15	20
Biotite	5	5	3
Hornblende	+	10	7
Pyroxene	-	-	5
TOTAL	100	100	100

12. Modal analyses of the Nqwadolo Suite.

	UND 14	UND 15	UND 16	UND 19	UND 29	NQ 1	NQ 2	NQ 3	NQ 4	NQ 5	NQ 6
K-feldspar	47	38	40	42	31	38	41	40	41	40	42
Plagioclase	16	24	21	22	33	23	21	20	21	19	21
Quartz	34	36	37	34	35	37	36	38	37	40	34
Biotite	3	2	2	1	1	2	2	2	1	1	3
Garnet	-	-	-	1	-	-	-	-	-	-	-
Zircon	+	+	+	+	+	+	+	+	+	+	+
Apatite	+	+	+	+	+	+	+	+	+	+	+
Ore	+	+	+	+	+	+	+	+	+	+	+
TOTAL	100	100	100	100	100	100	100	100	100	100	100

APPENDIX 2

MICROPROBE ANALYSES

Major element microprobe analyses were undertaken on carbon coated polished thin-sections at Rhodes University following the techniques described by Duncan *et al.* (1984) with natural standards. Matrix effects were corrected using Bence and Albee (1968). Precision is estimated at an absolute 0.1-0.16% for individual elements. Mafic mineral cation calculations performed using MINFILE 9-89, written by Afifi and Essene.

C = core
M = margin

Plagioclase Feldspar

NDF2 - Biotite hornblende gneiss, Nagle Dam Formation.

	1 C	2 C	3* C	4 C	5 C	Average
SiO_2	59.29	59.63	58.85	59.10	60.05	59.52
Al_2O_3	25.43	25.00	24.58	24.79	24.50	24.93
FeO	0.16	0.13	0.12	0.10	0.16	0.14
CaO	6.93	7.06	7.13	7.16	7.34	7.12
Na_2O	7.59	7.60	7.18	7.67	6.81	7.42
K_2O	0.24	0.25	0.17	0.20	0.42	0.28
TOTAL	99.64	99.67	98.03	99.02	99.28	99.41
Formula per 32 oxygens						
Si	10.62	10.68	10.70	10.66	10.78	10.69
Al	5.37	5.28	5.27	5.27	5.18	5.28
Fe	0.02	0.02	0.02	0.02	0.02	0.02
Ca	1.33	1.35	1.39	1.38	1.41	1.37
Na	2.64	2.64	2.53	2.68	2.37	2.58
K	0.05	0.06	0.04	0.05	0.10	0.06
An	0.331	0.334	0.351	0.337	0.364	0.341
Ab	0.655	0.652	0.639	0.652	0.611	0.643
Or	0.014	0.014	0.010	0.011	0.025	0.016

* Excluded from average

UND 309 - Quartzo-feldspathic gneiss, Nagle Dam Formation.

	1 C	2 C	3 M	4 Albite exsol.	5 M	6 Albite exsol.	7 C	8 M	9 C	10 C	11 M	12 C	13 M	14 C	15 C	Av	Av Core	Av Albite margin
SiO_2	68.50	61.58	62.07	68.79	68.16	68.28	61.00	68.15	61.52	60.80	61.62	61.56	60.47	60.39	60.55	62.80	61.99	68.16
Al_2O_3	19.87	24.22	24.35	19.85	20.03	20.12	24.71	20.21	24.84	24.79	24.80	24.72	24.54	24.61	24.68	23.57	24.06	20.12
FeO	0.01	0.00	0.03	0.01	0.02	0.04	0.10	0.02	0.00	0.05	0.01	0.02	0.00	0.00	0.00	0.02	0.02	0.02
CaO	0.94	5.55	5.27	0.21	0.39	0.20	5.50	0.46	5.58	5.73	5.52	5.52	5.44	5.41	5.58	4.38	4.98	0.43
Na_2O	11.18	8.77	8.93	12.06	11.65	11.70	8.56	11.58	8.48	8.52	8.58	8.55	8.78	8.66	8.66	9.30	8.92	11.62
K_2O	0.06	0.14	0.10	0.09	0.07	0.16	0.13	0.22	0.14	0.16	0.08	0.08	0.12	0.12	0.12	0.12	0.12	0.15
TOTAL	100.56	100.26	100.75	101.01	100.32	100.50	100.00	100.64	100.56	100.05	100.61	100.45	99.35	99.19	99.59	100.19	100.09	100.50
Formula per 32 oxygens																		
Si	11.91	10.92	10.94	11.92	11.89	11.89	10.84	11.86	10.86	10.81	10.87	10.88	10.83	10.82	10.81	11.09	10.98	11.87
Al	4.07	5.06	5.06	4.05	4.12	4.13	5.18	4.14	5.17	5.20	5.16	5.15	5.18	5.20	5.19	4.90	5.02	4.13
Fe	0.00	0.00	0.00	0.00	0.00	0.01	0.01	0.00	0.00	0.01	0.00	0.00	0.00	0.00	0.00	0.00	0.00	0.00
Ca	0.18	1.05	1.00	0.04	0.07	0.04	1.05	0.09	1.06	1.09	1.04	1.05	1.04	1.04	1.07	0.83	0.95	0.08
Na	3.77	3.01	3.05	4.05	3.94	3.95	2.95	3.91	2.90	2.94	2.94	2.93	3.05	3.01	3.00	3.19	3.06	3.92
K	0.01	0.03	0.02	0.02	0.02	0.04	0.03	0.05	0.03	0.04	0.02	0.02	0.03	0.03	0.03	0.03	0.03	0.03
An	0.044	0.257	0.244	0.009	0.018	0.009	0.260	0.021	0.265	0.268	0.261	0.262	0.253	0.255	0.261	0.205	0.234	0.020
Ab	0.953	0.735	0.750	0.986	0.978	0.982	0.733	0.967	0.727	0.723	0.734	0.734	0.740	0.738	0.732	0.788	0.759	0.972
Or	0.003	0.008	0.006	0.005	0.004	0.009	0.007	0.012	0.008	0.009	0.005	0.004	0.007	0.007	0.007	0.007	0.007	0.008

UND 320 - Amphibolite, Nagle Dam Formation.

	1 C	2 C	3 C Inclusion in diopside	4 C	5 C Adjacent to hornblende	6 C* Adjacent to diopside	Average
SiO_2	57.38	56.66	56.63	56.95	55.35	60.40	56.59
Al_2O_3	27.39	27.77	27.69	27.93	25.68	26.39	27.29
FeO	0.14	0.13	0.22	0.22	2.25	0.11	0.59
CaO	8.92	9.33	9.24	9.19	9.68	1.63	9.27
Na_2O	6.48	6.10	6.22	6.34	5.59	7.63	6.15
K_2O	0.38	0.41	0.39	0.34	0.46	3.05	0.40
TOTAL	100.69	100.40	100.39	100.97	99.01	99.21	100.29
Formula per 32 oxygens							
Si	10.24	10.15	10.15	10.14	10.18	10.82	10.17
Al	5.76	5.86	5.85	5.86	5.56	5.57	5.78
Fe	0.02	0.02	0.03	0.03	0.35	0.02	0.09
Ca	1.70	1.79	1.77	1.75	1.91	0.31	1.78
Na	2.24	2.12	2.16	2.19	1.99	2.65	2.14
K	0.09	0.09	0.09	0.08	0.11	0.70	0.09
An	0.423	0.447	0.441	0.436	0.476	0.086	0.444
Ab	0.556	0.529	0.537	0.545	0.497	0.724	0.533
Or	0.021	0.024	0.022	0.019	0.027	0.190	0.023

* Excluded from average

NDF 60 - Pelitic gneiss, Nagle Dam Formation.

	1 C	2 C	3 C	4 C	5 C	6 C	7 C	8 C	9 C	10 C	11 C	Average
SiO_2	59.64	59.29	59.32	60.00	60.10	59.18	59.48	59.33	58.80	59.18	59.02	59.39
Al_2O_3	26.08	25.82	26.43	26.06	25.97	25.79	26.06	25.65	25.70	25.80	25.80	25.92
FeO	0.07	0.00	0.10	0.06	0.04	0.08	0.07	0.06	0.11	0.12	0.06	0.07
CaO	7.09	7.07	6.66	7.14	6.97	7.00	7.05	7.00	7.05	6.51	7.02	6.96
Na_2O	7.59	7.51	7.35	7.37	7.28	7.22	7.46	7.37	7.50	7.45	7.33	7.40
K_2O	0.22	0.28	0.58	0.20	0.37	0.32	0.25	0.26	0.33	0.50	0.23	0.32
TOTAL	100.69	99.97	100.44	100.83	100.73	99.59	100.37	99.67	99.49	99.56	99.46	100.06
Formula per 32 oxygens												
Si	10.57	10.58	10.54	10.61	10.63	10.60	10.57	10.61	10.56	10.60	10.58	10.59
Al	5.45	5.43	5.54	5.43	5.41	5.44	5.46	5.41	5.44	5.45	5.45	5.45
Fe	0.01	0.00	0.01	0.01	0.01	0.01	0.01	0.01	0.02	0.02	0.01	0.01
Ca	1.35	1.35	1.27	1.35	1.32	1.34	1.34	1.34	1.36	1.25	1.35	1.33
Na	2.61	2.60	2.53	2.53	2.50	2.51	2.57	2.56	2.61	2.59	2.55	2.56
K	0.05	0.06	0.13	0.05	0.08	0.07	0.06	0.06	0.08	0.11	0.05	0.07
An	0.336	0.337	0.323	0.345	0.339	0.342	0.338	0.339	0.335	0.316	0.342	0.336
Ab	0.651	0.647	0.644	0.644	0.640	0.639	0.648	0.646	0.646	0.655	0.645	0.646
Or	0.013	0.016	0.033	0.011	0.021	0.019	0.014	0.015	0.019	0.029	0.013	0.018

NDF 8 - Pelitic gneiss, Nagle Dam Formation.

	1 C	2 C	3 C	4 C Assoc. with garnet	5 C	6 M Assoc. with biotite	7 C	8 C	9 M	10 C	11 C	12 M	Average	Average Core	Average Margin
SiO_2	59.16	59.94	59.93	59.51	59.01	58.93	58.95	59.34	59.23	58.80	58.81	58.77	59.20	59.27	58.98
Al_2O_3	26.08	25.60	26.04	25.82	26.02	26.01	25.86	26.07	26.23	26.01	26.09	26.03	25.99	25.96	26.09
FeO	0.04	0.05	0.13	0.10	0.05	0.23	0.11	0.03	0.04	0.04	0.03	0.01	0.07	0.06	0.09
CaO	8.31	7.60	7.29	7.25	7.58	7.48	7.28	7.58	7.65	7.72	7.61	7.73	7.59	7.58	7.62
Na_2O	6.91	7.12	7.44	7.50	7.25	7.44	7.34	7.30	7.11	7.16	7.25	7.22	7.25	7.25	7.26
K_2O	0.24	0.22	0.14	0.16	0.19	0.14	0.16	0.20	0.13	0.15	0.20	0.13	0.17	0.18	0.13
TOTAL	100.74	100.53	100.97	100.34	100.10	100.23	99.70	100.52	100.39	99.88	99.99	99.89	100.27	100.30	100.17
Formula per 32 oxygens															
Si	10.50	10.63	10.59	10.59	10.53	10.51	10.55	10.54	10.53	10.52	10.51	10.51	10.54	10.55	10.52
Al	5.46	5.35	5.42	5.41	5.47	5.47	5.46	5.46	5.49	5.48	5.49	5.49	5.46	5.45	5.48
Fe	0.01	0.01	0.02	0.01	0.01	0.03	0.02	0.00	0.01	0.01	0.00	0.00	0.01	0.01	0.01
Ca	1.58	1.44	1.38	1.38	1.45	1.43	1.40	1.44	1.46	1.48	1.46	1.48	1.45	1.45	1.46
Na	2.38	2.45	2.55	2.59	2.51	2.57	2.55	2.51	2.45	2.48	2.51	2.50	2.50	2.50	2.51
K	0.05	0.05	0.03	0.04	0.04	0.03	0.04	0.05	0.03	0.03	0.05	0.03	0.04	0.04	0.03
An	0.394	0.366	0.348	0.345	0.362	0.354	0.351	0.361	0.370	0.370	0.363	0.369	0.363	0.363	0.364
Ab	0.593	0.621	0.644	0.646	0.627	0.638	0.640	0.628	0.622	0.621	0.626	0.624	0.627	0.627	0.628
Or	0.013	0.013	0.008	0.009	0.011	0.008	0.009	0.011	0.008	0.009	0.011	0.007	0.010	0.010	0.008

UND 357 - Amphibolite, Valley Trust Formation.

	1 C	2 C	3 M	4 C	5 C	6 C	7 C	8 C	9 M	10 C	11 C	12 M	Average	Average Core	Average Margin
SiO_2	52.79	52.74	52.78	52.47	52.96	52.76	52.87	52.25	52.45	52.64	52.57	51.20	52.54	52.67	52.14
Al_2O_3	30.76	30.97	30.80	30.53	29.43	29.46	29.64	29.40	29.45	29.22	29.16	30.22	29.92	29.84	30.16
FeO	0.07	0.09	0.30	0.24	0.07	0.25	0.05	0.13	0.32	0.14	0.22	0.37	0.19	0.14	0.33
CaO	12.67	12.73	12.33	12.31	12.46	12.61	12.91	12.94	12.95	12.57	12.80	13.87	12.76	12.67	13.05
Na_2O	4.44	4.32	4.46	4.55	4.55	4.59	4.39	4.23	4.38	4.42	4.44	3.84	4.38	4.44	4.23
K_2O	0.15	0.07	0.05	0.09	0.15	0.12	0.16	0.13	0.11	0.14	0.10	0.06	0.11	0.12	0.07
TOTAL	100.88	100.92	100.72	100.19	99.62	99.79	100.02	99.08	99.66	99.13	99.29	99.56	99.90	99.88	99.98
Formula per 32 oxygens															
Si	9.49	9.47	9.50	9.50	9.64	9.60	9.59	9.57	9.57	9.63	9.62	9.38	9.55	9.57	9.47
Al	6.52	6.56	6.53	6.51	6.31	6.32	6.34	6.35	6.33	6.30	6.29	6.52	6.41	6.39	6.46
Fe	0.01	0.01	0.05	0.04	0.01	0.04	0.01	0.02	0.05	0.02	0.03	0.06	0.03	0.02	0.05
Ca	2.44	2.45	2.38	2.39	2.43	2.46	2.51	2.54	2.53	2.46	2.51	2.72	2.48	2.47	2.54
Na	1.55	1.50	1.56	1.60	1.61	1.62	1.54	1.50	1.55	1.57	1.57	1.36	1.54	1.56	1.49
K	0.03	0.02	0.01	0.02	0.03	0.03	0.04	0.03	0.03	0.03	0.02	0.01	0.03	0.03	0.02
An	0.607	0.617	0.603	0.596	0.597	0.599	0.613	0.624	0.617	0.606	0.611	0.664	0.613	0.608	0.628
Ab	0.385	0.379	0.394	0.399	0.394	0.394	0.378	0.369	0.377	0.386	0.383	0.333	0.381	0.385	0.368
Or	0.008	0.004	0.003	0.005	0.009	0.007	0.009	0.007	0.006	0.008	0.006	0.003	0.006	0.007	0.004

NDF 56 - Pelitic gneiss, Valley Trust Formation.

	1 C	2 C	3 C	4 M	5 M	6 C	Average	Average Core	Average Margin
SiO_2	62.36	61.40	62.64	62.89	63.31	63.17	62.63	62.39	63.10
Al_2O_3	23.38	23.69	23.82	23.54	23.69	23.09	23.54	23.50	23.62
FeO	0.02	0.00	0.05	0.12	0.38	0.03	0.10	0.03	0.25
CaO	5.36	5.78	5.33	4.86	4.95	4.60	5.15	5.27	4.91
Na_2O	8.42	8.16	8.41	8.17	8.21	8.74	8.35	8.43	8.19
K_2O	0.14	0.12	0.12	0.11	0.12	0.21	0.14	0.15	0.12
TOTAL	99.68	99.15	100.37	99.69	100.66	99.84	99.91	99.77	100.19
Formula per 32 oxygens									
Si	11.08	10.99	11.05	11.14	11.12	11.19	11.10	11.08	11.13
Al	4.90	4.99	4.95	4.91	4.90	4.82	4.91	4.92	4.91
Fe	0.00	0.00	0.01	0.02	0.06	0.00	0.01	0.00	0.04
Ca	1.02	1.11	1.01	0.92	0.93	0.87	0.98	1.00	0.93
Na	2.90	2.83	2.88	2.81	2.80	3.00	2.87	2.90	2.80
K	0.03	0.03	0.03	0.02	0.03	0.05	0.03	0.03	0.02
An	0.258	0.279	0.258	0.246	0.248	0.223	0.252	0.255	0.247
Ab	0.734	0.714	0.735	0.747	0.745	0.765	0.740	0.737	0.746
Or	0.008	0.007	0.007	0.007	0.007	0.012	0.008	0.009	0.007

UND 42 - Quartzo-feldspathic gneiss, Valley Trust Formation.

	1 M Adjacent to K-feldspar megacryst	2 M Adjacent to K-feldspar megacryst	3 C Inclusion in K-feldspar megacryst	4 C Adjacent to K-feldspar megacryst	5 C Adjacent to K-feldspar megacryst	Average
SiO_2	67.53	67.11	68.39	68.27	69.14	68.09
Al_2O_3	19.75	19.88	19.37	19.52	19.80	19.66
FeO	0.03	0.00	0.05	0.00	0.06	0.03
CaO	0.17	0.32	0.35	0.47	0.24	0.31
Na_2O	11.59	11.22	11.79	11.33	11.52	11.49
K_2O	0.15	0.61	0.12	0.52	0.07	0.29
TOTAL	99.22	99.14	100.07	100.11	100.83	99.87
Formula per 32 oxygens						
Si	11.91	11.87	11.96	11.95	11.97	11.93
Al	4.10	4.14	3.99	4.03	4.04	4.06
Fe	0.00	0.00	0.01	0.00	0.01	0.00
Ca	0.03	0.06	0.07	0.09	0.04	0.06
Na	3.96	3.85	4.00	3.84	3.87	3.90
K	0.03	0.14	0.03	0.12	0.02	0.06
An	0.008	0.015	0.016	0.022	0.011	0.015
Ab	0.984	0.951	0.977	0.950	0.985	0.969
Or	0.008	0.034	0.007	0.028	0.004	0.016

UND 302 - Quartzo-feldspathic gneiss, Valley Trust Formation.

	1 C	2 C	3 M	4 M	5 C	6 M	7 M	8 C	9 M	10 C	11 M	12 C	13 M	14 C	15 M	16 C	Average	Average Core	Average Margin
SiO_2	66.99	64.53	64.42	64.45	64.54	64.75	64.09	63.88	64.68	64.51	64.81	64.28	64.43	64.30	65.48	64.13	64.64	64.65	64.64
Al_2O_3	21.24	22.54	21.66	22.55	22.52	22.59	22.74	22.85	22.32	22.77	22.66	22.41	22.39	22.66	21.83	22.38	22.38	22.42	22.34
FeO	0.07	0.01	0.03	0.03	0.08	0.01	0.04	0.07	0.05	0.00	0.13	0.11	0.00	0.00	0.00	0.01	0.04	0.04	0.04
CaO	1.45	3.00	2.36	3.10	3.02	2.91	2.56	3.21	2.55	3.12	2.98	3.08	2.83	3.07	2.28	2.78	2.77	2.84	2.70
NaO_2	11.03	10.24	10.86	10.15	10.11	10.05	10.01	9.85	10.52	9.93	10.00	9.76	9.51	9.39	9.98	9.66	10.07	10.00	10.14
K_2O	0.10	0.07	0.10	0.09	0.15	0.07	0.34	0.11	0.14	0.08	0.16	0.17	0.08	0.11	0.07	0.08	0.12	0.11	0.13
TOTAL	100.88	100.39	99.43	100.37	100.42	100.38	99.78	99.97	100.26	100.41	100.74	99.81	99.24	99.53	99.64	99.04	100.02	100.06	99.99
Formula per 32 oxygens																			
Si	11.66	11.34	11.43	11.33	11.34	11.36	11.33	11.28	11.38	11.32	11.35	11.36	11.41	11.36	11.53	11.39	11.38	11.38	11.39
Al	4.36	4.67	4.53	4.67	4.66	4.67	4.74	4.75	4.63	4.71	4.68	4.67	4.67	4.72	4.53	4.68	4.65	4.65	4.64
Fe	0.01	0.00	0.00	0.00	0.01	0.00	0.01	0.01	0.01	0.00	0.02	0.02	0.00	0.00	0.00	0.00	0.01	0.01	0.01
Ca	0.27	0.56	0.45	0.58	0.57	0.55	0.49	0.61	0.48	0.59	0.56	0.58	0.54	0.58	0.43	0.53	0.52	0.54	0.51
Na	3.72	3.49	3.74	3.46	3.44	3.42	3.43	3.37	3.59	3.38	3.39	3.34	3.26	3.22	3.41	3.33	3.44	3.41	3.46
K	0.02	0.02	0.02	0.02	0.03	0.02	0.08	0.02	0.03	0.02	0.04	0.04	0.02	0.02	0.02	0.02	0.03	0.02	0.03
An	0.067	0.139	0.107	0.144	0.141	0.137	0.121	0.152	0.117	0.147	0.140	0.147	0.140	0.152	0.112	0.136	0.131	0.135	0.127
Ab	0.927	0.857	0.888	0.851	0.851	0.857	0.860	0.842	0.875	0.848	0.851	0.843	0.855	0.841	0.884	0.859	0.862	0.859	0.866
Or	0.006	0.004	0.005	0.005	0.008	0.004	0.019	0.006	0.008	0.005	0.009	0.010	0.005	0.007	0.004	0.005	0.007	0.006	0.007

UND 330 - Granitic enclave.

	1 C
SiO_2	67.69
Al_2O_3	19.33
FeO	0.04
CaO	0.34
Na_2O	11.64
K_2O	0.07
TOTAL	99.11
Formula per 32 oxygens	
Si	11.95
Al	4.02
Fe	0.01
Ca	0.06
Na	3.98
K	0.02
An	0.016
Ab	0.98
Or	0.004

UND 40 - Biotite granite, Ximba Suite.

	1 M	2 C	3 C	4 C	5 M	6 C Myrmekite	7 M	8 C	9 M	10 C	11 C
SiO_2	68.64	61.63	62.10	62.08	67.32	68.34	68.96	62.20	68.29	61.68	61.35
Al_2O_3	19.20	24.10	24.27	23.93	19.82	20.01	19.46	24.11	19.77	23.86	23.88
FeO	0.00	0.03	0.02	0.03	0.13	0.00	0.02	0.02	0.00	0.03	0.07
CaO	0.33	5.49	5.48	5.42	0.76	2.27	0.22	5.49	0.62	5.64	5.66
Na_2O	11.19	8.28	8.26	8.34	11.01	9.47	11.12	8.17	11.03	8.12	7.79
K_2O	0.08	0.14	0.16	0.18	0.08	0.05	0.09	0.17	0.08	0.12	0.26
TOTAL	99.44	99.67	100.29	99.98	99.12	100.14	99.87	100.16	99.79	99.45	99.01
Formula per 32 oxygens											
Si	12.04	10.96	10.97	11.01	11.88	11.90	12.03	11.00	11.95	10.99	10.98
Al	3.96	5.05	5.05	5.00	4.12	4.11	4.00	5.03	4.08	5.01	5.04
Fe	0.00	0.00	0.00	0.00	0.02	0.00	0.00	0.00	0.00	0.00	0.01
Ca	0.06	1.05	1.04	1.03	0.14	0.42	0.04	1.04	0.12	1.08	1.09
Na	3.80	2.86	2.83	2.87	3.77	3.20	3.76	2.80	3.74	2.81	2.70
K	0.02	0.03	0.04	0.04	0.02	0.01	0.02	0.04	0.02	0.03	0.06
An	0.016	0.266	0.266	0.262	0.036	0.117	0.011	0.268	0.030	0.275	0.282
Ab	0.979	0.726	0.725	0.728	0.959	0.880	0.984	0.722	0.965	0.718	0.703
Or	0.005	0.008	0.009	0.010	0.005	0.003	0.005	0.010	0.005	0.007	0.015

Table continued.

12 M	13 C	Average	Average Core	Average Margin
67.95	62.15	64.82	61.88	68.23
19.64	24.33	22.03	24.07	19.58
0.02	0.09	0.04	0.04	0.03
0.32	5.33	3.31	5.50	0.45
11.22	8.24	9.40	8.17	11.11
0.07	0.18	0.13	0.17	0.08
99.22	100.32	99.73	99.83	99.48
11.95	10.98	11.44	10.98	11.97
4.07	5.06	4.58	5.04	4.05
0.00	0.01	0.01	0.01	0.00
0.06	1.01	0.63	1.05	0.08
3.83	2.82	3.22	2.81	3.78
0.02	0.04	0.03	0.04	0.02
0.015	0.261	0.162	0.268	0.022
0.981	0.729	0.831	0.722	0.973
0.004	0.001	0.007	0.010	0.005

XS 4 - Biotite garnet granite, Ximba Suite.

	1 M	2 C	3 C	4 C	Average
SiO_2	60.82	61.74	60.30	60.89	60.94
Al_2O_3	25.25	24.70	24.36	24.52	24.71
FeO	0.09	0.12	0.08	0.06	0.09
CaO	5.38	6.19	6.12	6.33	6.01
Na_2O	7.67	7.92	8.07	7.86	7.88
K_2O	0.92	0.30	0.18	0.26	0.42
TOTAL	100.13	100.97	99.11	99.92	100.05
Formula per 32 oxygens					
Si	10.80	10.87	10.83	10.84	10.84
Al	5.29	5.13	5.15	5.14	5.18
Fe	0.01	0.02	0.01	0.01	0.01
Ca	1.02	1.17	1.18	1.21	1.14
Na	2.64	2.70	2.81	2.71	2.72
K	0.21	0.07	0.04	0.06	0.10
An	0.264	0.297	0.292	0.303	0.289
Ab	0.682	0.686	0.698	0.682	0.687
Or	0.054	0.017	0.010	0.015	0.024

UND 65 - Hornblende granite, Mlahlanja Suite.

	1 C	2 M	3 C	4 M	5 M	6 C	7 C	8 M	9 C Assoc. with perthite	10 C	11 M	Average	Average Core	Average Margin
SiO_2	62.28	64.48	62.34	63.33	63.53	63.07	62.42	63.08	62.88	62.69	62.89	63.00	62.61	63.46
Al_2O_3	23.40	22.85	23.47	23.70	23.58	23.78	23.41	23.64	22.96	23.38	23.45	23.42	23.40	23.44
FeO	0.05	0.02	0.10	0.11	0.06	0.07	0.13	0.12	0.12	0.08	0.14	0.09	0.09	0.09
CaO	4.81	3.92	5.00	4.78	4.61	4.95	4.57	4.78	4.53	4.66	4.83	4.68	4.75	4.58
Na_2O	8.90	9.20	8.43	8.70	8.84	8.56	8.72	8.72	8.70	8.73	8.78	8.75	8.67	8.85
K_2O	0.12	0.10	0.30	0.15	0.14	0.22	0.18	0.15	0.13	0.15	0.15	0.16	0.18	0.14
TOTAL	99.56	100.57	99.64	100.77	100.76	100.65	99.43	100.49	99.32	99.69	100.24	100.10	99.70	100.56
Formula per 32 oxygens														
Si	11.08	11.30	11.08	11.12	11.15	11.09	11.11	11.11	11.19	11.12	11.11	11.13	11.11	11.16
Al	4.91	4.72	4.92	4.90	4.88	4.93	4.91	4.91	4.82	4.89	4.88	4.88	4.90	4.86
Fe	0.01	0.00	0.02	0.02	0.01	0.01	0.02	0.02	0.02	0.01	0.02	0.01	0.01	0.01
Ca	0.92	0.74	0.95	0.90	0.87	0.93	0.87	0.90	0.86	0.89	0.91	0.88	0.90	0.86
Na	3.07	3.13	2.91	2.96	3.01	2.92	3.01	2.98	3.00	3.00	3.01	3.00	2.98	3.02
K	0.03	0.02	0.07	0.03	0.03	0.05	0.04	0.03	0.03	0.03	0.03	0.04	0.04	0.03
An	0.228	0.189	0.243	0.231	0.222	0.239	0.222	0.230	0.222	0.226	0.231	0.226	0.230	0.221
Ab	0.765	0.805	0.740	0.760	0.770	0.748	0.767	0.761	0.771	0.765	0.760	0.765	0.760	0.771
Or	0.007	0.006	0.017	0.009	0.008	0.013	0.011	0.009	0.007	0.009	0.009	0.009	0.010	0.008

UND 74 - Charnockite, Mlahlanja Suite.

	1 M Adjacent to perthite	2 C	3 C	4 M Adjacent to perthite	Average Core	Average Margin
SiO_2	61.36	61.25	61.95	62.58	61.60	61.97
Al_2O_3	24.00	24.29	24.21	24.12	24.25	24.06
FeO	0.13	0.09	0.07	0.11	0.08	0.12
CaO	5.65	5.90	5.44	5.14	5.67	5.40
Na_2O	8.16	7.93	8.09	8.15	8.01	8.16
K_2O	0.19	0.30	0.15	0.22	0.22	0.21
TOTAL	99.49	99.76	99.91	100.32	99.83	99.92
Formula per 32 oxygens						
Si	10.95	10.91	10.98	11.04	10.94	10.99
Al	5.05	5.10	5.06	5.01	5.08	5.03
Fe	0.02	0.01	0.01	0.02	0.01	0.02
Ca	1.08	1.13	1.03	0.97	1.08	1.03
Na	2.82	2.74	2.78	2.79	2.76	2.81
K	0.04	0.07	0.03	0.05	0.05	0.05
An	0.274	0.286	0.269	0.255	0.277	0.265
Ab	0.715	0.696	0.722	0.732	0.710	0.723
Or	0.011	0.017	0.009	0.013	0.013	0.012

UND 9 - Garnet hornblende granite, Mlahlanja Suite.

	1 C
SiO_2	61.83
Al_2O_3	24.26
FeO	0.05
CaO	6.52
Na_2O	7.03
K_2O	0.17
TOTAL	99.86
Formula per 32 oxygens	
Si	10.96
Al	5.07
Fe	0.01
Ca	1.24
Na	2.42
K	0.04
An	0.335
Ab	0.654
Or	0.011

UND 6 - Garnet hornblende granite, Malhlanja Suite.

	1 C	2 M	3 C	4 C	5 C	6 C	7 C	8 C	Average Core
SiO_2	60.79	68.25	60.85	60.35	60.85	61.43	60.49	60.98	60.82
Al_2O_3	24.60	19.70	24.45	24.32	24.45	24.53	24.53	24.69	24.51
FeO	0.10	0.01	0.08	0.09	0.04	0.04	0.11	0.06	0.07
CaO	6.11	0.44	6.10	6.15	6.04	6.32	6.25	6.38	6.19
Na_2O	7.91	11.29	7.88	7.85	7.62	7.51	7.64	7.78	7.74
K_2O	0.24	0.08	0.17	0.30	0.17	0.17	0.28	0.18	0.22
TOTAL	99.75	99.77	99.53	99.06	99.17	100.00	99.30	100.07	99.55
Formula per 32 oxygens									
Si	10.84	11.95	10.86	10.84	10.88	10.90	10.83	10.83	10.85
Al	5.17	4.06	5.14	5.15	5.15	5.13	5.18	5.17	5.16
Fe	0.02	0.00	0.01	0.01	0.01	0.01	0.02	0.01	0.01
Ca	1.17	0.08	1.17	1.18	1.16	1.20	1.20	1.21	1.19
Na	2.73	3.83	2.73	2.73	2.64	2.58	2.65	2.68	2.68
K	0.05	0.02	0.04	0.07	0.04	0.04	0.06	0.04	0.05
An	0.295	0.021	0.297	0.297	0.302	0.314	0.306	0.309	0.302
Ab	0.691	0.974	0.693	0.686	0.688	0.676	0.677	0.681	0.685
Or	0.014	0.005	0.010	0.017	0.010	0.010	0.016	0.010	0.013

UND 19 - Nqwadolo Suite.

	1 C Assoc with K-feld	2 M	3 C	4 M	5 C	6 C	7 C	8 C	9 M	10 Exsol. in perthite	11 M Inclusion in K-feld
SiO_2	64.43	68.99	65.64	67.77	64.78	64.97	64.46	64.64	67.38	66.32	64.69
Al_2O_3	22.51	19.86	22.45	20.60	22.55	22.23	22.52	22.38	20.28	20.42	22.50
FeO	0.01	0.00	0.00	0.00	0.06	0.00	0.02	0.03	0.00	0.00	0.03
CaO	3.38	0.30	3.26	1.15	3.57	3.13	3.55	3.11	0.51	0.89	3.22
Na_2O	9.87	10.99	9.46	11.03	9.54	9.86	9.56	9.99	11.38	10.12	9.89
K_2O	0.13	0.06	0.12	0.13	0.18	0.10	0.21	0.20	0.06	1.74	0.13
TOTAL	100.33	100.20	100.93	100.68	100.68	100.29	100.32	100.35	99.61	99.49	100.46
Formula per 32 oxygens											
Si	11.33	11.99	11.43	11.79	11.35	11.41	11.34	11.36	11.83	11.75	11.36
Al	4.67	4.07	4.61	4.22	4.66	4.60	4.67	4.64	4.20	4.26	4.65
Fe	0.00	0.00	0.00	0.00	0.01	0.00	0.00	0.00	0.00	0.00	0.00
Ca	0.64	0.06	0.61	0.21	0.67	0.59	0.67	0.59	0.10	0.17	0.61
Na	3.37	3.70	3.19	3.72	3.24	3.36	3.26	3.41	3.87	3.48	3.37
K	0.03	0.01	0.03	0.03	0.04	0.02	0.05	0.04	0.01	0.39	0.03
An	0.158	0.015	0.159	0.054	0.170	0.148	0.168	0.145	0.024	0.042	0.151
Ab	0.835	0.982	0.834	0.939	0.820	0.846	0.820	0.844	0.973	0.861	0.841
Or	0.007	0.003	0.007	0.007	0.010	0.006	0.012	0.011	0.003	0.097	0.007

Excluded from average

Table continued.

12# C	13 C	14 M	15 C	16 M	17 Albite exsol in K-feld	18# C	19 M	20 C	21 M	22 C	Average Core	Average Margin
67.51	63.97	68.35	64.51	68.86	65.38	67.10	67.04	64.48	68.25	64.50	64.64	68.09
19.57	22.61	19.89	22.78	20.01	22.28	20.69	20.77	22.62	19.85	22.54	22.52	20.18
0.00	0.03	0.00	0.01	0.01	0.00	0.00	0.00	0.00	0.00	0.01	0.02	0.00
0.18	3.29	0.28	3.58	0.29	2.81	1.12	1.26	3.27	0.15	3.04	3.32	0.56
11.73	9.83	11.67	9.43	11.49	9.81	11.20	10.86	9.62	11.73	9.83	9.71	11.31
0.06	0.03	0.06	0.20	0.06	0.43	0.09	0.10	0.13	0.07	0.12	0.14	0.08
99.05	99.76	100.25	100.51	100.72	100.71	100.20	100.03	100.12	100.05	100.04	100.35	100.22
11.92	11.31	11.92	11.32	11.94	11.44	11.74	11.74	11.35	11.92	11.36	11.35	11.88
4.07	4.71	4.09	4.71	4.09	4.59	4.27	4.29	4.69	4.09	4.68	4.66	4.15
0.00	0.00	0.00	0.00	0.00	0.00	0.00	0.00	0.00	0.00	0.00	0.00	0.00
0.03	0.62	0.05	0.67	0.05	0.53	0.21	0.24	0.62	0.03	0.57	0.62	0.10
4.02	3.37	3.95	3.21	3.86	3.33	3.80	3.69	3.28	3.97	3.36	3.31	3.82
0.01	0.01	0.01	0.04	0.01	0.10	0.02	0.02	0.03	0.02	0.03	0.03	0.02
0.009	0.156	0.013	0.172	0.014	0.133	0.052	0.060	0.157	0.007	0.145	0.158	0.027
0.988	0.842	0.984	0.817	0.983	0.843	0.943	0.934	0.836	0.989	0.848	0.834	0.969
0.003	0.002	0.003	0.011	0.003	0.024	0.005	0.006	0.007	0.004	0.007	0.008	0.004

UND 22 - Granite vein.

	1 M	2 M	3 M	4 C	5 M	6 C	7 M	8 C	9 M	10* Albite exsol in perthite	11* Albite exsol in perthite	12 M
SiO_2	66.23	67.60	67.75	66.57	68.45	67.30	68.09	67.41	68.57	66.74	66.97	68.40
Al_2O_3	19.99	19.90	19.94	21.54	20.40	20.97	20.39	20.80	20.34	21.33	20.92	20.44
FeO	0.17	0.05	0.10	0.08	0.02	0.03	0.00	0.09	0.03	0.05	0.07	0.06
CaO	0.72	0.31	0.06	1.63	0.30	1.06	0.30	0.66	0.24	1.45	0.99	0.49
Na_2O	11.90	12.05	12.41	10.93	11.60	11.51	11.80	11.53	11.72	11.22	11.40	11.34
K_2O	0.09	0.06	0.08	0.15	0.13	0.07	0.10	0.12	0.09	0.11	0.09	0.09
TOTAL	99.10	99.97	100.34	100.90	100.90	100.94	100.68	100.61	100.99	100.90	100.44	100.82
Formula per 32 oxygens												
Si	11.75	11.85	11.85	11.59	11.86	11.70	11.84	11.75	11.87	11.62	11.70	11.86
Al	4.18	4.11	4.11	4.42	4.17	4.30	4.18	4.27	4.15	4.38	4.31	4.18
Fe	0.03	0.01	0.01	0.01	0.00	0.00	0.00	0.01	0.00	0.01	0.01	0.01
Ca	0.14	0.06	0.01	0.30	0.06	0.20	0.06	0.12	0.04	0.27	0.19	0.09
Na	4.09	4.10	4.21	3.69	3.90	3.88	3.98	3.90	3.93	3.79	3.86	3.81
K	0.02	0.01	0.02	0.03	0.03	0.02	0.02	0.03	0.02	0.02	0.02	0.02
An	0.032	0.014	0.003	0.076	0.014	0.048	0.014	0.030	0.011	0.066	0.046	0.023
Ab	0.963	0.983	0.993	0.916	0.979	0.948	0.981	0.963	0.984	0.928	0.949	0.972
Or	0.005	0.003	0.004	0.008	0.007	0.004	0.005	0.007	0.005	0.006	0.005	0.005

Table continued.

13 M	14 C	15* C	16 C	Average	Average Core	Average Margin
68.32	66.40	65.19	66.13	67.48	66.76	67.93
19.92	21.23	22.34	20.79	20.51	21.07	20.17
0.05	0.06	0.09	0.08	0.06	0.07	0.06
0.21	1.53	0.56	1.55	0.70	1.29	0.33
12.04	11.25	10.56	11.36	11.65	11.32	11.86
0.11	0.09	1.05	0.12	0.10	0.11	0.09
100.65	100.56	99.79	100.03	100.50	100.62	100.44
Formula per 32 oxygens						
11.89	11.61	11.50	11.64	11.78	11.66	11.85
4.09	4.38	4.64	4.31	4.22	4.34	4.15
0.01	0.01	0.01	0.01	0.01	0.01	0.01
0.04	0.29	0.11	0.29	0.13	0.24	0.06
4.06	3.81	3.61	3.88	3.94	3.83	4.01
0.02	0.02	0.24	0.03	0.02	0.02	0.02
0.009	0.069	0.027	0.070	0.032	0.059	0.015
0.985	0.926	0.913	0.924	0.963	0.935	0.980
0.006	0.005	0.060	0.006	0.005	0.006	0.005

* Not included in average

K-feldspar

UND 309 - Quartzo-feldspathic gneiss, Nagle Dam Formation.

	1 C	2 C	3 C	4 C	5 C	6 C Assoc. with plag.	7* Albite exsol in K-feld.	8 C	9 Perthite core	10 Perthite core	11 M	12 C	13 C	14 Pethite core	15 C	16* Albite exsol in K-feld.	Average	Average Core
SiO_2	64.60	64.54	64.70	64.87	64.48	65.09	67.39	64.76	64.49	65.13	64.53	65.25	65.33	64.26	64.51	65.41	64.75	64.77
Al_2O_3	18.54	18.71	18.61	18.73	18.57	18.72	19.57	18.74	18.61	18.73	18.55	18.82	18.77	18.69	18.82	19.12	18.69	18.70
FeO	0.03	0.04	0.04	0.00	0.04	0.01	0.09	0.04	0.04	0.03	0.02	0.04	0.02	0.03	0.03	0.03	0.03	0.03
CaO	0.03	0.02	0.01	0.00	0.00	0.00	0.20	0.06	0.00	0.02	0.03	0.06	0.02	0.03	0.03	0.03	0.02	0.02
Na_2O	0.66	0.68	0.63	0.79	0.77	0.61	9.11	0.72	0.42	0.60	0.55	0.94	0.02	0.03	0.04	0.14	0.53	0.53
K_2O	15.59	15.65	15.62	15.43	15.18	15.52	4.24	15.54	15.86	15.56	15.44	15.20	15.48	15.76	15.23	9.05	15.50	15.51
TOTAL	99.45	99.64	99.61	99.82	99.04	99.95	100.60	99.86	99.42	100.07	99.12	100.31	99.64	98.80	98.66	93.78	99.52	99.56
Formula per 32 oxygens																		
Si	11.98	11.95	11.97	11.97	11.98	11.99	11.90	11.95	11.97	11.98	11.99	11.97	12.03	11.98	11.99	12.27	11.98	11.98
Al	4.05	4.08	4.06	4.07	4.07	4.06	4.07	4.08	4.07	4.06	4.06	4.07	4.07	4.11	4.12	4.23	4.08	4.08
Fe	0.00	0.01	0.01	0.00	0.01	0.00	0.01	0.01	0.01	0.00	0.00	0.01	0.00	0.00	0.00	0.00	0.00	0.00
Ca	0.01	0.00	0.00	0.00	0.00	0.00	0.04	0.01	0.00	0.00	0.01	0.01	0.00	0.01	0.01	0.01	0.00	0.00
Na	0.24	0.24	0.23	0.28	0.28	0.22	3.12	0.26	0.15	0.21	0.20	0.33	0.01	0.01	0.01	0.05	0.19	0.19
K	3.69	3.70	3.69	3.63	3.60	3.65	0.96	3.66	3.75	3.65	3.66	3.56	3.64	3.75	3.61	2.17	3.66	3.66
An	0.002	0.001	0.000	0.000	0.000	0.000	0.009	0.003	0.000	0.001	0.002	0.003	0.001	0.002	0.002	0.003	0.001	0.001
Ab	0.060	0.062	0.058	0.072	0.072	0.056	0.759	0.066	0.039	0.055	0.051	0.086	0.002	0.003	0.004	0.023	0.049	0.049
Or	0.938	0.937	0.942	0.928	0.928	0.944	0.232	0.931	0.961	0.944	0.947	0.911	0.997	0.995	0.994	0.974	0.950	0.950

* Not included in average

NDF 56 - Pelitic gneiss, Valley Trust Formation.

	1 M	2 C	3 C	4 M	5 C	6 C	7 C	8 C	9 C	10 C	11* Albite Exsol. in K-feld	12 C	Average	Average Core	Average Margin
SiO_2	66.91	66.90	65.88	66.36	66.18	66.78	66.29	65.82	65.86	66.28	67.32	65.94	66.29	66.21	66.64
Al_2O_3	18.65	18.79	18.66	18.68	18.55	18.58	18.55	18.53	18.50	18.42	18.95	18.43	18.58	18.56	18.67
FeO	0.08	0.14	0.06	0.08	0.00	0.00	0.00	0.08	0.04	0.01	0.06	0.03	0.05	0.04	0.08
CaO	0.03	0.04	0.03	0.03	0.12	0.07	0.08	0.05	0.07	0.09	0.14	0.07	0.06	0.07	0.03
Na_2O	1.61	1.41	1.47	1.13	3.27	3.90	2.61	1.64	1.84	2.14	5.62	2.41	2.13	2.30	1.37
K_2O	13.07	13.25	13.40	13.72	12.18	11.26	12.95	14.17	14.11	13.63	8.57	13.22	13.18	13.13	13.40
TOTAL	100.35	100.53	99.50	100.00	100.30	100.59	100.48	100.29	100.42	100.57	100.66	100.10	100.29	100.31	100.19
Formula per 32 oxygens															
Si	12.11	12.10	12.06	12.09	12.02	12.04	12.04	12.03	12.02	12.05	12.02	12.03	12.05	12.04	12.10
Al	3.99	4.00	4.03	4.01	3.97	3.95	3.97	3.99	3.98	3.95	3.99	3.96	3.98	3.98	3.99
Fe	0.01	0.02	0.01	0.01	0.00	0.00	0.00	0.01	0.01	0.00	0.01	0.00	0.01	0.01	0.01
Ca	0.01	0.01	0.01	0.01	0.02	0.01	0.02	0.01	0.01	0.02	0.03	0.01	0.01	0.01	0.01
Na	0.57	0.49	0.52	0.40	1.15	1.36	0.92	0.58	0.65	0.75	1.95	0.85	0.75	0.81	0.48
K	3.02	3.06	3.13	3.19	2.82	2.59	3.00	3.30	3.29	3.16	1.95	3.08	3.06	3.05	3.10
An	0.002	0.002	0.001	0.002	0.006	0.003	0.004	0.003	0.003	0.004	0.007	0.004	0.003	0.004	0.002
Ab	0.157	0.139	0.143	0.111	0.288	0.344	0.234	0.149	0.165	0.192	0.496	0.216	0.197	0.209	0.134
Or	0.841	0.859	0.856	0.887	0.706	0.653	0.762	0.848	0.832	0.804	0.497	0.780	0.800	0.787	0.864

* Not included in average

UND42 - Quartzo-feldspathic gneiss, Valley Trust Formation.

	1 C Megacryst	2 C Megacryst	3 C Megacryst	4 C Megacryst	5 C Megacryst	6 C Megacryst	Average
SiO_2	64.13	63.75	64.23	64.53	64.04	64.55	64.21
Al_2O_3	18.57	18.55	18.54	18.70	18.34	18.67	18.56
FeO	0.07	0.03	0.03	0.06	0.05	0.04	0.05
CaO	0.01	0.00	0.03	0.01	0.01	0.01	0.01
Na_2O	0.98	0.68	1.16	1.42	0.77	1.10	1.02
K_2O	15.32	16.12	15.25	14.88	15.84	15.03	15.41
TOTAL	99.08	99.13	99.24	99.60	99.05	99.40	99.26
Formula per 32 oxygens							
Si	11.94	11.91	11.94	11.93	11.96	11.95	11.94
Al	4.07	4.09	4.06	4.08	4.04	4.07	4.07
Fe	0.01	0.00	0.00	0.01	0.01	0.01	0.01
Ca	0.00	0.00	0.01	0.00	0.00	0.00	0.00
Na	0.35	0.25	0.42	0.51	0.28	0.39	0.37
K	3.64	3.84	3.62	3.51	3.77	3.55	3.66
An	0.000	0.000	0.002	0.000	0.000	0.001	0.001
Ab	0.089	0.060	0.103	0.127	0.069	0.100	0.091
Or	0.911	0.940	0.895	0.873	0.931	0.899	0.908

UND 302 - Quartzo-feldspathic gneiss, Valley Trust Formation.

	1 C	2 C	3 C	4 C Perthite	5 M Perthite	6 M Perthite	7 C Perthite	8 C	9 C Perthite	10 M	11 C	12 C	13 C Perthite	14 C	15 C Perthite	16 M Perthite	17 C	18 M	19 C	Average	Average Core	Average Margin
SiO_2	64.93	64.53	64.81	64.84	64.67	64.90	64.17	65.14	64.76	64.34	64.14	64.54	64.61	64.51	64.51	64.50	64.56	64.41	64.37	64.59	64.62	64.42
Al_2O_3	18.90	18.77	18.92	18.75	18.71	18.71	18.51	18.75	18.74	18.76	18.65	18.76	18.94	18.68	18.75	18.65	18.72	18.79	18.76	18.75	18.75	18.73
FeO	0.01	0.02	0.00	0.06	0.03	0.05	0.04	0.05	0.01	0.07	0.07	0.02	0.08	0.04	0.05	0.05	0.03	0.02	0.00	0.04	0.07	0.05
CaO	0.01	0.00	0.00	0.00	0.00	0.01	0.74	0.03	0.01	0.01	0.02	0.00	0.00	0.01	0.00	0.00	0.00	0.00	0.00	0.04	0.05	0.03
Na_2O	1.03	0.50	0.39	0.27	0.40	0.36	0.54	1.59	0.34	0.48	0.63	0.46	0.61	0.56	0.32	0.26	0.49	0.28	0.65	0.53	0.57	0.34
K_2O	15.39	15.90	16.13	16.01	16.00	16.00	15.73	14.39	15.99	15.95	15.75	15.95	15.89	15.84	16.25	16.20	15.55	15.98	15.40	15.81	15.76	16.04
TOTAL	100.27	99.72	100.25	99.93	99.81	100.03	99.73	99.95	99.85	99.61	99.26	99.73	100.13	99.64	99.88	99.66	99.35	99.48	99.18	99.76	99.82	99.61
Formula per 32 oxygens																						
Si	11.93	11.94	11.94	11.97	11.96	11.97	11.91	11.96	11.97	11.93	11.93	11.95	11.92	11.95	11.94	11.96	11.97	11.95	11.95	11.95	11.95	11.94
Al	4.09	4.09	4.11	4.08	4.08	4.07	4.05	4.06	4.08	4.10	4.09	4.09	4.12	4.08	4.09	4.08	4.09	4.11	4.10	4.09	4.09	4.09
Fe	0.00	0.00	0.00	0.01	0.00	0.01	0.01	0.01	0.00	0.01	0.01	0.00	0.01	0.01	0.01	0.01	0.00	0.00	0.00	0.01	0.01	0.01
Ca	0.00	0.00	0.00	0.00	0.00	0.00	0.15	0.01	0.00	0.00	0.00	0.00	0.00	0.00	0.00	0.00	0.00	0.00	0.00	0.01	0.01	0.01
Na	0.37	0.18	0.14	0.10	0.14	0.13	0.19	0.57	0.12	0.17	0.23	0.17	0.22	0.20	0.11	0.09	0.18	0.10	0.23	0.19	0.20	0.12
K	3.61	3.75	3.79	3.77	3.77	3.76	3.72	3.37	3.77	3.77	3.74	3.77	3.74	3.74	3.84	3.83	3.68	3.78	3.65	3.73	3.72	3.79
An	0.001	0.000	0.000	0.000	0.000	0.001	0.036	0.001	0.001	0.000	0.001	0.000	0.000	0.000	0.000	0.000	0.000	0.000	0.000	0.002	0.003	0.002
Ab	0.092	0.046	0.035	0.025	0.037	0.033	0.048	0.144	0.031	0.044	0.057	0.042	0.055	0.051	0.029	0.024	0.046	0.026	0.060	0.048	0.052	0.031
Or	0.907	0.954	0.965	0.975	0.963	0.966	0.916	0.855	0.968	0.956	0.942	0.958	0.945	0.949	0.971	0.976	0.954	0.974	0.940	0.950	0.945	0.967

UND 40 - Biotite granite, Ximba Suite.

	1 C	2 C	3 M	4 C	5 C	6 C	7 C	Average	Average Core
SiO_2	64.74	64.98	64.81	64.66	65.16	65.08	64.81	64.89	64.91
Al_2O_3	18.51	18.56	18.37	18.38	18.42	18.51	18.46	18.46	18.47
FeO	0.00	0.06	0.02	0.00	0.01	0.02	0.05	0.02	0.02
CaO	0.05	0.02	0.00	0.02	0.04	0.07	0.05	0.04	0.04
Na_2O	0.97	0.66	0.37	0.53	1.16	1.66	0.84	0.88	0.97
K_2O	15.08	15.18	15.54	15.60	14.63	13.94	14.99	14.99	14.90
TOTAL	99.35	99.46	99.11	99.19	99.42	99.28	99.20	99.28	99.31
Formula per 32 oxygens									
Si	11.99	12.01	12.03	12.01	12.03	12.00	12.01	12.01	12.01
Al	4.04	4.04	4.02	4.02	4.01	4.02	4.03	4.03	4.03
Fe	0.00	0.01	0.00	0.00	0.00	0.00	0.01	0.00	0.00
Ca	0.01	0.00	0.00	0.00	0.01	0.01	0.01	0.01	0.01
Na	0.35	0.24	0.13	0.19	0.42	0.59	0.30	0.32	0.35
K	3.56	3.58	3.68	3.70	3.44	3.28	3.54	3.54	3.52
An	0.002	0.001	0.000	0.001	0.002	0.003	0.003	0.002	0.002
Ab	0.089	0.062	0.035	0.049	0.107	0.153	0.078	0.082	0.090
Or	0.909	0.937	0.965	0.950	0.891	0.844	0.919	0.916	0.908

XS 4 - Biotite garnet granite, Ximba Suite.

	1 C	2 M	3* Albite exsol in K-feld	4 C	Average
SiO_2	65.73	65.48	66.08	64.60	65.27
Al_2O_3	18.79	18.64	19.50	18.70	18.71
FeO	0.02	0.07	0.02	0.00	0.03
CaO	0.08	0.06	0.74	0.11	0.08
Na_2O	1.23	2.16	7.55	1.71	1.70
K_2O	14.67	13.72	5.42	14.03	14.14
TOTAL	100.52	100.13	99.31	99.15	99.93
Formula per 32 oxygens					
Si	12.00	11.98	11.86	11.95	11.98
Al	4.04	4.02	4.13	4.08	4.05
Fe	0.00	0.01	0.00	0.00	0.00
Ca	0.02	0.01	0.14	0.02	0.02
Na	0.44	0.77	2.63	0.61	0.60
K	3.42	3.20	1.24	3.31	3.31
An	0.004	0.003	0.035	0.006	0.004
Ab	0.113	0.192	0.655	0.155	0.154
Or	0.883	0.805	0.310	0.839	0.842

* Not included in average.

UND 65 - Hornblende granite, Mlahlanja Suite.

	1* Albite exsol in K-feld	2 C Perthite	3 C Perthite	4 M	5* Albite exsol in K-feld	6 C	7 M	8 C	9 C	10 C Perthite	11* Albite exsol in K-feld	12* Albite exsol in K-feld	13 C Perthite	Average	Average Core	Average Margin
SiO_2	64.04	65.01	64.63	64.61	63.83	65.02	64.66	64.75	65.68	64.82	66.57	64.64	64.73	64.88	64.95	64.64
Al_2O_3	21.35	18.67	18.43	18.54	22.05	18.62	18.55	18.58	18.75	18.34	18.99	21.06	18.29	18.53	18.52	18.55
FeO	0.07	0.02	0.04	0.03	0.07	0.03	0.02	0.05	0.03	0.05	0.03	0.08	0.04	0.03	0.04	0.02
CaO	2.43	0.05	0.03	0.01	3.64	0.07	0.01	0.03	0.11	0.03	0.27	2.50	0.03	0.04	0.05	0.01
Na_2O	6.83	2.23	1.16	0.80	7.33	2.20	0.94	1.11	2.94	0.89	5.53	6.50	0.83	1.46	1.62	0.87
K_2O	4.39	13.36	14.79	15.15	3.21	13.33	15.17	14.81	12.30	15.16	8.53	5.20	15.17	14.36	14.13	15.16
TOTAL	99.11	99.34	99.08	99.14	100.13	99.27	99.35	99.33	99.81	99.29	99.92	99.98	99.09	99.30	99.31	99.25
Formula per 32 oxygens																
Si	11.51	11.97	11.99	11.99	11.36	11.98	11.97	11.98	11.99	12.01	11.98	11.56	12.02	11.99	11.99	11.98
Al	4.53	4.05	4.03	4.05	4.63	4.04	4.05	4.05	4.03	4.01	4.03	4.44	4.00	4.04	4.03	4.05
Fe	0.01	0.00	0.01	0.00	0.01	0.00	0.00	0.01	0.00	0.01	0.00	0.01	0.01	0.00	0.01	0.00
Ca	0.47	0.01	0.01	0.00	0.69	0.01	0.00	0.01	0.02	0.01	0.05	0.48	0.01	0.01	0.01	0.00
Na	2.38	0.80	0.42	0.29	2.53	0.79	0.34	0.40	1.04	0.32	1.93	2.25	0.30	0.52	0.58	0.31
K	1.01	3.14	3.50	3.59	0.73	3.13	3.59	3.50	2.86	3.58	1.96	1.19	3.59	3.39	3.33	3.59
An	0.121	0.002	0.002	0.001	0.176	0.003	0.001	0.002	0.005	0.001	0.013	0.122	0.001	0.002	0.003	0.001
Ab	0.618	0.202	0.106	0.074	0.640	0.200	0.086	0.102	0.265	0.082	0.490	0.575	0.077	0.134	0.148	0.080
Or	0.261	0.796	0.892	0.925	0.184	0.797	0.913	0.896	0.730	0.917	0.497	0.303	0.922	0.864	0.849	0.919

* Not included in average.

UND 74 - Charnockite, Mlahlanja Suite.

	1 C Perthite megacryst	2 C Perthite megacryst	3 C Perthite megacryst	4* Albite exsol in K-feld	5 C Perthite	6 C Perthite	7 M Perthite, adjacent to plag	8 C Perthite	9 C Perthite	10 C Perthite megacryst	11 C Perthite	12 C	Average Perthite Core
SiO_2	65.11	64.93	65.11	64.88	64.96	65.15	64.94	65.25	65.59	65.17	65.02	65.30	65.16
Al_2O_3	18.55	18.60	18.76	19.78	18.60	18.62	18.45	18.56	18.49	18.83	18.71	18.78	18.65
FeO	0.05	0.01	0.04	0.10	0.04	0.08	0.05	0.05	0.03	0.05	0.03	0.18	0.06
CaO	0.04	0.11	0.13	1.39	0.09	0.11	0.04	0.09	0.08	0.15	0.12	0.10	0.10
Na_2O	1.42	1.80	2.66	4.01	1.98	2.46	1.41	2.44	2.35	2.57	2.59	2.25	2.25
K_2O	14.36	13.76	12.42	9.42	13.52	12.63	14.36	12.98	12.92	12.60	12.56	12.95	13.07
TOTAL	99.53	99.21	99.12	99.58	99.19	99.05	99.25	99.37	99.46	99.37	99.03	99.56	99.29
Formula per 32 oxygens													
Si	12.00	11.98	11.97	11.78	11.98	11.99	12.00	11.99	12.03	11.96	11.97	11.97	11.99
Al	4.03	4.05	4.06	4.23	4.04	4.04	4.02	4.02	4.00	4.07	4.06	4.06	4.04
Fe	0.01	0.00	0.01	0.02	0.01	0.01	0.01	0.01	0.00	0.01	0.00	0.03	0.01
Ca	0.01	0.02	0.03	0.27	0.02	0.02	0.01	0.02	0.02	0.03	0.02	0.02	0.02
Na	0.51	0.64	0.95	1.41	0.71	0.88	0.51	0.87	0.84	0.91	0.92	0.80	0.80
K	3.38	3.24	2.91	2.18	3.18	2.97	3.39	3.04	3.02	2.95	2.95	3.03	3.07
An	0.002	0.006	0.007	0.070	0.005	0.006	0.002	0.005	0.004	0.008	0.006	0.005	0.005
Ab	0.130	0.165	0.244	0.365	0.181	0.227	0.130	0.221	0.216	0.235	0.237	0.208	0.206
Or	0.868	0.829	0.749	0.565	0.814	0.767	0.868	0.774	0.780	0.757	0.757	0.787	0.789

* Not included in average.

UND 6 - Garnet hornblende granite, Mlahlanja Suite.

	1 C	2 C	Average
SiO_2	66.67	64.52	65.60
Al_2O_3	18.53	18.52	18.53
FeO	0.00	0.00	0.00
CaO	0.08	0.01	0.05
Na_2O	1.09	1.05	1.07
K_2O	13.57	14.96	14.27
TOTAL	99.94	99.06	99.52
Formula per 32 oxygens			
Si	12.13	11.98	12.05
Al	3.97	4.05	4.01
Fe	0.00	0.00	0.00
Ca	0.02	0.00	0.01
Na	0.38	0.38	0.38
K	3.15	3.54	3.34
An	0.005	0.001	0.003
Ab	0.108	0.096	0.102
Or	0.887	0.903	0.895

UND 19 - Nqwadolo Suite.

	1 M	2 C	3 C	4 C Perthite	5 C Perthite	6 M	7 C	8 C	9 C	10 M	11 C	12 C	13* Albite exsol in K-feld	14 C	15 C	16 C Perthite
SiO_2	65.35	65.15	65.85	65.91	65.86	65.41	65.83	65.79	65.49	65.58	65.45	64.74	65.34	64.04	63.81	63.79
Al_2O_3	18.58	18.74	19.28	18.75	18.85	18.65	18.60	18.50	18.52	18.48	18.62	18.59	19.10	18.50	18.71	18.62
FeO	0.02	0.04	0.03	0.02	0.06	0.01	0.00	0.04	0.00	0.01	0.01	0.02	0.04	0.00	0.00	0.00
CaO	0.03	0.04	0.40	0.01	0.02	0.02	0.04	0.02	0.00	0.08	0.04	0.04	0.24	0.00	0.03	0.02
Na_2O	0.70	1.03	3.95	0.69	0.95	0.62	0.85	0.91	0.77	0.57	0.90	1.12	5.12	0.85	0.83	0.95
K_2O	15.64	14.93	10.84	15.52	14.98	16.17	15.63	15.51	15.79	15.71	15.68	15.20	9.92	15.86	15.77	15.72
TOTAL	100.32	99.93	100.35	100.90	100.72	100.88	100.95	100.77	100.57	100.43	100.70	99.71	99.76	99.25	99.15	99.10
Formula per 32 oxygens																
Si	12.00	11.98	11.91	12.01	12.00	11.98	12.01	12.02	12.01	12.03	11.99	11.96	11.88	11.93	11.90	11.90
Al	4.02	4.06	4.11	4.03	4.05	4.03	4.00	3.98	4.00	3.99	4.02	4.05	4.09	4.06	4.11	4.10
Fe	0.00	0.01	0.00	0.00	0.01	0.00	0.00	0.01	0.00	0.00	0.00	0.00	0.01	0.00	0.00	0.00
Ca	0.01	0.01	0.08	0.00	0.00	0.00	0.01	0.00	0.00	0.02	0.01	0.01	0.05	0.00	0.01	0.00
Na	0.25	0.37	1.38	0.24	0.34	0.22	0.30	0.32	0.27	0.20	0.32	0.40	1.80	0.31	0.30	0.34
K	3.66	3.50	2.50	3.61	3.48	3.78	3.64	3.62	3.69	3.68	3.66	3.58	2.30	3.77	3.75	3.74
An	0.001	0.002	0.020	0.001	0.001	0.001	0.002	0.001	0.000	0.004	0.002	0.002	0.011	0.000	0.001	0.001
Ab	0.064	0.095	0.349	0.063	0.088	0.055	0.076	0.082	0.069	0.052	0.080	0.101	0.435	0.075	0.074	0.084
Or	0.935	0.903	0.631	0.936	0.911	0.944	0.922	0.917	0.931	0.944	0.918	0.897	0.554	0.925	0.925	0.915

* Not included in average.

Table continued.

17 C Perthite	18 C By albite exsol.	19 C	20 M	21 C	22 M	23 C	24 C	25 M	26 C	27* Albite exsol in K-feld	28 C	29 C	30 C	Average Core	Average Margin
64.19	64.01	64.45	64.51	64.92	65.14	65.01	64.69	64.17	64.33	65.83	64.46	64.33	64.57	64.85	65.03
18.66	18.55	18.63	18.60	18.47	18.76	18.41	18.68	18.56	18.58	20.69	18.77	18.54	18.58	18.64	18.61
0.00	0.00	0.02	0.02	0.02	0.12	0.01	0.00	0.00	0.01	0.00	0.01	0.02	0.03	0.02	0.03
0.06	0.10	0.03	0.02	0.04	0.00	0.02	0.00	0.00	0.01	1.49	0.15	0.02	0.02	0.05	0.03
0.97	1.17	1.87	0.63	0.59	0.60	0.78	0.96	0.78	1.06	7.02	1.81	0.77	1.31	1.14	0.65
15.71	15.33	14.14	15.99	16.25	15.89	15.80	15.66	15.85	15.22	5.58	14.15	15.96	15.31	15.23	15.88
99.59	99.16	99.14	99.77	100.29	100.51	100.03	99.99	99.36	99.21	100.61	99.35	99.64	99.82	99.93	100.23
11.92	11.92	11.94	11.95	11.97	11.96	12.00	11.94	11.94	11.95	11.69	11.92	11.94	11.94	11.96	11.97
4.08	4.07	4.07	4.06	4.02	4.06	4.00	4.06	4.07	4.07	4.33	4.09	4.06	4.05	4.05	4.04
0.00	0.00	0.00	0.00	0.00	0.02	0.00	0.00	0.00	0.00	0.00	0.00	0.00	0.00	0.00	0.00
0.01	0.02	0.01	0.00	0.01	0.00	0.00	0.00	0.00	0.00	0.28	0.03	0.00	0.00	0.01	0.01
0.35	0.42	0.67	0.23	0.21	0.21	0.28	0.34	0.28	0.38	2.42	0.65	0.28	0.47	0.41	0.23
3.72	3.64	3.34	3.78	3.82	3.72	3.72	3.69	3.76	3.61	1.26	3.34	3.78	3.61	3.58	3.73
0.003	0.005	0.002	0.001	0.002	0.000	0.001	0.000	0.000	0.000	0.071	0.007	0.001	0.001	0.003	0.002
0.086	0.103	0.167	0.056	0.052	0.054	0.070	0.085	0.070	0.096	0.610	0.162	0.068	0.115	0.102	0.058
0.911	0.892	0.831	0.943	0.946	0.946	0.929	0.915	0.930	0.904	0.319	0.831	0.931	0.884	0.895	0.940

UND 22 - Granite vein.

	1 M	2 M	3 C	4 C Perthite	5 C Perthite	6 M Perthite	7 C	8 M	9 C	10 C Perthite	11 C Perthite
SiO_2	64.98	64.65	64.78	64.20	64.57	64.97	65.10	65.34	64.93	65.06	64.29
Al_2O_3	18.83	18.92	18.74	18.78	18.71	18.86	18.90	18.90	18.81	18.77	18.44
FeO	0.06	0.04	0.05	0.03	0.07	0.03	0.05	0.07	0.05	0.06	0.07
CaO	0.01	0.03	0.01	0.00	0.01	0.01	0.03	0.02	0.02	0.01	0.00
Na_2O	0.18	0.48	0.59	0.36	0.76	0.36	0.60	0.32	0.67	0.36	0.31
K_2O	16.17	15.85	15.67	16.04	15.50	15.83	15.55	15.86	15.25	15.68	16.38
TOTAL	100.23	99.97	99.84	99.41	99.62	100.06	100.23	100.51	99.73	99.94	99.49
Formula per 32 oxygens											
Si	11.96	11.93	11.96	11.93	11.95	11.96	11.96	11.98	11.97	11.98	11.96
Al	4.09	4.12	4.08	4.11	4.08	4.09	4.09	4.08	4.09	4.08	4.04
Fe	0.01	0.01	0.01	0.00	0.01	0.00	0.01	0.01	0.01	0.01	0.01
Ca	0.00	0.01	0.00	0.00	0.00	0.00	0.01	0.00	0.00	0.00	0.00
Na	0.06	0.17	0.21	0.13	0.27	0.13	0.21	0.11	0.24	0.13	0.11
K	3.80	3.73	3.69	3.80	3.66	3.72	3.64	3.71	3.59	3.68	3.89
An	0.000	0.001	0.001	0.000	0.001	0.001	0.002	0.001	0.001	0.000	0.000
Ab	0.017	0.044	0.054	0.033	0.069	0.033	0.055	0.030	0.063	0.034	0.028
Or	0.983	0.955	0.945	0.967	0.930	0.966	0.943	0.969	0.936	0.966	0.972

Table continued.

12 C Perthite	13 M	14 C	15 M	Average	Average Core	Average Margin
64.47	64.08	64.14	64.21	64.65	64.62	64.71
18.35	18.45	18.52	18.35	18.69	18.67	18.72
0.05	0.10	0.07	0.06	0.06	0.06	0.06
0.00	0.00	0.00	0.00	0.01	0.01	0.01
0.61	0.56	0.33	0.44	0.46	0.51	0.39
15.92	16.05	16.25	16.11	15.87	15.80	15.98
99.40	99.24	99.31	99.17	99.74	99.67	99.87
11.98	11.95	11.95	11.97	11.96	11.96	11.96
4.02	4.05	4.07	4.03	4.08	4.07	4.08
0.01	0.02	0.01	0.01	0.01	0.01	0.01
0.00	0.00	0.00	0.00	0.00	0.00	0.00
0.22	0.20	0.12	0.16	0.17	0.18	0.14
3.77	3.82	3.86	3.83	3.75	3.73	3.77
0.000	0.000	0.000	0.000	0.001	0.000	0.000
0.055	0.050	0.030	0.040	0.042	0.047	0.036
0.945	0.950	0.970	0.960	0.957	0.953	0.964

Biotite

NDF 2 - Biotite hornblende gneiss, Nagle Dam Formation.

	1 C	2 C	3 C	4 C	5 C	6 C	Average
SiO_2	37.57	36.89	37.15	37.02	37.57	36.80	37.17
TiO_2	5.21	4.96	4.70	4.90	3.87	5.38	4.84
Al_2O_3	14.55	14.16	14.23	13.97	14.57	14.54	14.34
Cr_2O_3	0.00	0.00	0.00	0.00	0.00	0.00	0.00
FeO	17.15	16.05	16.50	16.31	13.91	15.55	15.91
MnO	0.30	0.26	0.20	0.19	0.11	0.28	0.22
MgO	13.28	13.80	13.45	13.43	15.56	13.28	13.80
CaO	0.00	0.01	0.02	0.00	0.02	0.01	0.01
Na_2O	0.01	0.02	0.01	0.02	0.02	0.03	0.02
K_2O	9.34	9.63	9.85	9.69	9.52	9.55	9.60
H_2O	4.00	4.01	4.00	4.00	4.06	4.02	4.02
TOTAL	101.41	99.79	100.11	99.53	99.21	99.44	99.92
Formula per 22 oxygens							
Si	5.55	5.53	5.57	5.57	5.59	5.52	5.56
Al^{IV}	2.45	2.47	2.43	2.43	2.41	2.48	2.45
Al^{VI}	0.08	0.04	0.08	0.05	0.15	0.10	0.08
Ti	0.58	0.56	0.53	0.56	0.43	0.61	0.55
Fe	2.12	2.01	2.07	2.05	1.73	1.95	1.99
Mn	0.04	0.03	0.03	0.02	0.01	0.04	0.03
Mg	2.92	3.09	3.00	3.01	3.45	2.97	3.07
Na	0.00	0.00	0.00	0.01	0.01	0.01	0.01
K	1.76	1.84	1.88	1.86	1.81	1.83	1.83
Fe/Fe+Mg	0.42	0.39	0.41	0.41	0.33	0.40	0.39

NDF 24

	1 C	2 C	3 C	4 C	5 C
SiO_2	40.57	39.53	38.79	38.76	39.17
TiO_2	3.80	2.87	3.59	2.86	3.21
Al_2O_3	15.65	14.93	15.20	14.87	15.06
Cr_2O_3	0.00	0.00	0.00	0.00	0.00
FeO	18.76	17.02	16.53	16.38	15.94
MnO	0.39	0.33	0.30	0.31	0.33
MgO	11.64	11.72	11.21	12.29	11.86
CaO	0.14	0.38	0.18	0.44	0.40
Na_2O	0.18	0.39	0.53	0.45	0.24
K_2O	5.95	5.79	7.19	5.89	7.36
TOTAL	97.07	92.96	93.52	92.23	93.58

NDF 60 - Pelitic gneiss, Nagle Dam Formation.

	1 C	2 C	3 C	4 C	5 C	6 C	7 C	8 C	9 C	10 C	11 C	12 C	13 C	Average
SiO_2	35.13	35.12	34.79	35.38	35.21	36.11	35.68	35.81	35.26	35.21	35.43	35.01	34.62	35.29
TiO_2	3.75	3.85	3.82	3.38	3.67	3.79	3.62	3.60	3.58	3.77	3.82	3.84	3.78	3.71
Al_2O_3	18.38	18.38	18.57	18.58	18.43	19.16	18.85	18.69	18.50	18.98	18.29	18.32	18.34	18.57
Cr_2O_3	-	-	-	-	-	-	-	-	-	-	-	-	0.00	0.00
FeO	19.35	19.22	18.92	18.02	18.25	18.98	18.02	17.97	18.49	17.92	18.72	18.90	19.22	18.61
MnO	0.37	0.36	0.41	0.45	0.42	0.44	0.40	0.36	0.42	0.38	0.37	0.37	0.37	0.39
MgO	9.40	9.11	9.49	9.95	9.59	9.73	9.94	9.79	9.52	9.16	9.42	9.38	9.14	9.51
CaO	0.00	0.02	0.02	0.00	0.00	0.01	0.00	0.00	0.00	0.00	0.00	0.00	0.00	0.00
Na_2O	0.02	0.08	0.07	0.04	0.06	0.03	0.03	0.04	0.03	0.02	0.02	0.01	0.03	0.04
K_2O	9.54	9.82	9.49	9.46	9.81	9.40	9.93	9.71	9.88	9.88	9.81	9.85	9.61	9.71
H_2O	3.96	3.95	3.96	3.98	3.97	3.98	3.98	3.99	3.97	3.98	3.97	3.96	3.95	3.97
TOTAL	99.90	99.91	99.54	99.24	99.41	101.63	100.45	99.96	99.65	99.30	99.85	99.64	99.06	99.81
Formula per 22 oxygens														
Si	5.33	5.33	5.29	5.37	5.35	5.35	5.35	5.39	5.35	5.35	5.37	5.33	5.31	5.34
Al^{IV}	2.67	2.67	2.71	2.63	2.65	2.65	2.65	2.61	2.65	2.65	2.63	2.67	2.69	2.66
Al^{VI}	0.62	0.62	0.62	0.69	0.65	0.69	0.68	0.70	0.66	0.74	0.63	0.61	0.62	0.66
Ti	0.43	0.44	0.44	0.39	0.42	0.42	0.41	0.41	0.41	0.43	0.43	0.44	0.44	0.42
Fe	2.46	2.44	2.41	2.29	2.32	2.35	2.26	2.26	2.35	2.27	2.37	2.41	2.46	2.36
Mn	0.05	0.05	0.05	0.06	0.05	0.05	0.05	0.05	0.05	0.05	0.05	0.05	0.05	0.05
Mg	2.13	2.06	2.15	2.25	2.17	2.15	2.22	2.20	2.15	2.07	2.13	2.13	2.09	2.15
Na	0.01	0.02	0.02	0.01	0.02	0.01	0.01	0.01	0.01	0.01	0.01	0.00	0.01	0.01
K	1.85	1.90	1.84	1.83	1.90	1.78	1.90	1.86	1.91	1.91	1.90	1.91	1.88	1.88
Fe/Fe+Mg	0.54	0.54	0.53	0.50	0.52	0.52	0.50	0.51	0.52	0.52	0.53	0.53	0.54	0.52

NDF 8 - Pelitic gneiss, Nagle Dam Formation.

	1* M	2* C Inclusion in garnet	3 C Adjacent to garnet	4 C	5* M	6* C	7 C Adjacent to garnet	8* M Adjacent to garnet	9 C Adjacent to garnet	10 C	11 C Adjacent to garnet	Average
SiO_2	33.72	34.97	34.98	34.46	34.20	33.28	34.57	34.49	34.48	34.59	34.74	34.64
TiO_2	2.79	3.30	3.73	4.06	3.70	3.77	3.85	3.84	3.95	3.96	3.97	3.92
Al_2O_3	17.61	16.97	17.17	16.82	17.52	16.95	16.21	16.20	16.31	16.34	16.44	16.55
Cr_2O_3	0.00	0.00	0.00	0.00	0.00	0.00	0.00	0.00	0.00	0.00	0.00	0.00
FeO	21.44	20.58	20.93	21.44	21.68	22.45	21.71	21.50	21.67	21.90	21.33	21.50
MnO	0.17	0.09	0.11	0.12	0.16	0.17	0.13	0.19	0.09	0.13	0.14	0.12
MgO	9.85	9.58	9.18	8.89	7.34	9.43	9.21	9.20	9.19	9.16	9.18	9.14
CaO	0.02	0.00	0.00	0.00	0.02	0.03	0.00	0.00	0.00	0.00	0.00	0.00
Na_2O	0.11	0.08	0.08	0.08	0.12	0.10	0.06	0.08	0.06	0.07	0.10	0.08
K_2O	7.11	9.34	9.59	9.41	8.89	7.73	9.70	9.68	9.65	9.66	9.54	9.59
H_2O	3.95	3.93	3.92	3.91	3.91	3.91	3.89	3.89	3.89	3.89	3.91	3.90
TOTAL	96.77	98.84	99.69	99.19	97.54	97.82	99.33	99.07	99.29	99.70	99.35	99.43
Formula per 22 oxygen												
Si	5.29	5.40	5.37	5.33	5.38	5.22	5.36	5.36	5.35	5.35	5.37	5.36
Al^{iv}	2.71	2.60	2.63	2.67	2.62	2.78	2.64	2.64	2.65	2.65	2.63	2.65
Al^{vi}	0.55	0.49	0.47	0.40	0.62	0.36	0.33	0.33	0.33	0.32	0.36	0.37
Ti	0.33	0.38	0.43	0.47	0.44	0.44	0.45	0.45	0.46	0.46	0.46	0.46
Fe	2.81	2.66	2.68	2.78	2.85	2.95	2.82	2.80	2.81	2.83	2.76	2.78
Mn	0.02	0.01	0.01	0.02	0.02	0.02	0.02	0.02	0.01	0.02	0.02	0.02
Mg	2.30	2.21	2.10	2.05	1.72	2.21	2.13	2.13	2.13	2.11	2.12	2.11
Na	0.03	0.02	0.02	0.02	0.04	0.03	0.02	0.02	0.02	0.02	0.03	0.02
K	1.42	1.84	1.88	1.86	1.78	1.55	1.92	1.92	1.91	1.90	1.88	1.89
Fe/Fe+Mg	0.55	0.55	0.56	0.58	0.62	0.57	0.57	0.57	0.57	0.57	0.57	0.57

* Not included in average

NDF 56 - Pelitic gneiss, Valley Trust Formation.

	1 C Inclusion in garnet	2* C Inclusion in garnet	3* C	4 M Adjacent to garnet	5 C	6* C	7 C	8 C	9 C	10 C	11* C	Average	Average Core
SiO_2	34.97	34.78	35.34	37.79	35.94	35.11	35.70	36.03	35.84	35.76	33.91	35.56	35.71
TiO_2	5.21	5.18	3.90	5.52	5.99	4.97	5.30	5.10	4.86	4.66	4.43	5.01	5.19
Al_2O_3	17.65	17.70	18.49	18.59	17.56	17.04	17.15	17.82	17.39	17.66	18.36	17.76	17.54
Cr_2O_3	0.00	0.00	0.00	0.00	0.00	0.00	0.00	0.00	0.00	0.00	0.00	0.00	0.00
FeO	17.80	17.61	11.76	13.80	13.88	17.34	17.54	17.35	16.81	16.95	16.91	16.16	16.72
MnO	0.01	0.02	0.04	0.00	0.02	0.01	0.01	0.02	0.04	0.03	0.04	0.02	0.02
MgO	10.01	10.10	15.27	11.97	12.89	10.67	10.69	10.55	10.66	10.53	10.07	11.22	10.89
CaO	0.00	0.00	0.02	0.07	0.00	0.00	0.00	0.00	0.00	0.00	0.00	0.01	0.00
Na_2O	0.11	0.11	0.17	0.18	0.25	0.08	0.09	0.06	0.09	0.08	0.06	0.12	0.11
K_2O	9.35	9.30	8.66	8.12	9.53	9.46	9.95	9.35	9.42	9.58	9.27	9.27	9.53
H_2O	3.99	3.99	4.12	4.12	4.06	3.99	3.98	4.01	4.01	4.01	4.00	4.03	4.01
TOTAL	99.10	98.79	97.77	100.16	100.12	98.67	100.41	100.29	99.12	99.26	97.05	99.16	99.72
Formula per 22 oxygens													
Si	5.31	5.30	5.27	5.49	5.30	5.35	5.35	5.37	5.41	5.39	5.25	5.34	5.36
Al^{IV}	2.69	2.70	2.73	2.51	2.70	2.65	2.65	2.63	2.59	2.61	2.75	2.66	2.65
Al^{VI}	0.47	0.47	0.52	0.67	0.36	0.41	0.38	0.51	0.50	0.53	0.60	0.49	0.46
Ti	0.60	0.59	0.44	0.60	0.66	0.57	0.60	0.57	0.55	0.53	0.52	0.57	0.59
Fe	2.26	2.24	1.47	1.67	1.71	2.21	2.20	2.16	2.12	2.14	2.19	2.03	2.10
Mn	0.00	0.00	0.00	0.00	0.00	0.00	0.00	0.00	0.01	0.00	0.01	0.00	0.00
Mg	2.27	2.29	3.39	2.59	2.84	2.42	2.39	2.35	2.40	2.37	2.32	2.51	2.44
Ca	0.00	0.00	0.01	0.00	0.00	0.00	0.00	0.00	0.00	0.00	0.00	0.00	0.00
Na	0.03	0.03	0.05	0.05	0.07	0.02	0.03	0.02	0.03	0.02	0.02	0.03	0.03
K	1.81	1.81	1.65	1.50	1.79	1.84	1.90	1.78	1.81	1.84	1.83	1.78	1.82
Fe/Fe+Mg	0.50	0.49	0.30	0.39	0.38	0.48	0.48	0.48	0.47	0.47	0.49	0.45	0.46

*Excluded from average core

UND 42 - Quartzo-feldspathic gneiss, Valley Trust Formation.

	1 C	2* C	3* C	4* C	5* C	6 C	7 C	Average
SiO_2	35.94	33.99	35.54	29.94	35.38	36.08	36.43	36.15
TiO_2	4.26	3.19	2.92	1.46	3.87	4.07	4.13	4.15
Al_2O_3	13.96	14.64	14.61	16.04	14.16	14.28	13.99	14.08
Cr_2O_3	0.00	0.00	0.00	0.00	0.00	0.00	0.00	0.00
FeO	23.88	25.00	23.89	28.48	22.55	23.44	23.54	23.62
MnO	0.63	0.71	0.71	0.83	0.64	0.70	0.66	0.66
MgO	8.06	8.86	8.98	10.00	7.93	8.06	8.07	8.06
CaO	0.00	0.08	0.00	0.08	0.01	0.03	0.00	0.01
Na_2O	0.06	0.07	0.03	0.01	0.04	0.06	0.03	0.05
K_2O	9.42	7.58	8.05	2.84	8.70	8.61	9.30	9.11
H_2O	3.86	3.85	3.88	3.85	3.89	3.88	3.87	3.87
TOTAL	100.07	97.97	98.61	93.53	97.17	99.21	100.02	99.77
Formula per 22 oxygens								
Si	5.59	5.41	5.57	5.00	5.62	5.62	5.64	5.62
Al^{IV}	2.42	2.60	2.43	3.00	2.38	2.38	2.36	2.39
Al^{VI}	0.14	0.15	0.27	0.16	0.28	0.24	0.20	0.19
Ti	0.50	0.38	0.34	0.18	0.46	0.48	0.48	0.49
Fe	3.10	3.32	3.13	3.98	3.00	3.05	3.05	3.07
Mn	0.08	0.10	0.09	0.12	0.09	0.09	0.09	0.09
Mg	1.87	2.10	2.10	2.49	1.88	1.87	1.86	1.87
Ca	0.00	0.01	0.00	0.01	0.00	0.01	0.00	0.00
Na	0.02	0.02	0.01	0.00	0.01	0.02	0.01	0.02
K	1.87	1.54	1.61	0.61	1.76	1.71	1.84	1.81
Fe/Fe+Mg	0.62	0.61	0.60	0.62	0.61	0.62	0.62	0.62

*Excluded from average

NDF 70 - Fine grained granulite, Valley Trust Formation.

	1 C	2 C	3 C	4 C	5 C	6* C	7* C	8 C	9* C	10 C	Average
SiO_2	37.34	36.07	36.36	36.20	36.03	32.59	35.05	35.82	34.89	35.87	36.24
TiO_2	5.76	5.39	5.91	5.40	5.42	6.30	5.80	5.84	5.96	6.11	5.69
Al_2O_3	15.61	15.37	15.18	15.34	15.38	17.11	15.67	15.57	15.62	15.04	15.36
Cr_2O_3	0.00	0.00	0.00	0.00	0.00	0.00	0.00	0.00	0.00	0.00	0.00
FeO	16.60	15.77	15.29	16.04	15.81	15.35	14.62	15.51	14.43	14.92	15.71
MnO	0.02	0.04	0.05	0.04	0.03	0.04	0.05	0.05	0.06	0.03	0.04
MgO	12.62	12.45	12.69	12.56	12.31	11.02	12.49	12.33	12.53	12.70	12.52
CaO	0.01	0.00	0.01	0.00	0.00	0.03	0.07	0.00	0.01	0.00	0.00
Na_2O	0.07	0.08	0.08	0.06	0.07	0.10	0.09	0.04	0.06	0.04	0.06
K_2O	8.83	9.59	9.39	9.55	9.49	9.47	8.90	9.68	9.23	9.33	9.41
H_2O	4.03	4.01	4.03	4.01	4.02	3.99	4.04	4.02	4.03	4.03	4.02
TOTAL	100.89	98.78	98.99	99.20	98.56	96.00	96.78	98.86	96.82	98.07	99.05
Formula per 22 oxygens											
Si	5.50	5.46	5.47	5.46	5.46	5.11	5.38	5.41	5.36	5.44	5.46
Al^{IV}	2.50	2.54	2.53	2.54	2.54	2.89	2.62	2.59	2.64	2.56	2.54
Al^{VI}	0.21	0.20	0.16	0.18	0.21	0.27	0.22	0.19	0.19	0.13	0.18
Ti	0.64	0.61	0.67	0.61	0.62	0.74	0.67	0.66	0.69	0.70	0.64
Fe	2.04	2.00	1.92	2.02	2.00	2.01	1.88	1.96	1.86	1.89	1.98
Mn	0.00	0.01	0.01	0.01	0.00	0.01	0.01	0.01	0.01	0.00	0.01
Mg	2.77	2.81	2.85	2.82	2.78	2.58	2.86	2.78	2.87	2.87	2.81
Ca	0.00	0.00	0.00	0.00	0.00	0.01	0.01	0.00	0.00	0.00	0.00
Na	0.02	0.02	0.02	0.02	0.02	0.03	0.03	0.01	0.02	0.01	0.02
K	1.66	1.85	1.80	1.84	1.84	1.89	1.74	1.87	1.81	1.81	1.81
Fe/Fe+Mg	0.42	0.42	0.40	0.42	0.42	0.44	0.40	0.41	0.39	0.40	0.41

* Excluded from average

NDF 67 - Fine grained granulite, Valley Trust Formation.

	1 C	2 C	3 C	4 C	5 C	6 C	7 C	8 C	9 C	10 C	Average
SiO_2	37.09	35.99	36.33	36.13	35.90	36.64	36.20	36.26	35.87	36.30	36.27
TiO_2	3.58	3.55	3.50	4.88	3.71	4.11	3.90	3.03	4.25	4.08	3.86
Al_2O_3	16.77	15.76	15.87	15.15	15.67	16.28	16.16	16.48	16.06	15.55	15.97
Cr_2O_3	0.00	0.00	0.00	0.00	0.00	0.00	0.00	0.00	0.00	0.00	0.00
FeO	17.32	17.23	17.07	17.48	17.60	17.10	16.75	16.23	17.33	16.90	17.10
MnO	0.04	0.04	0.03	0.04	0.07	0.07	0.02	0.03	0.09	0.07	0.05
MgO	12.76	13.04	12.62	11.99	12.48	12.79	12.86	13.81	12.27	12.59	12.72
CaO	0.06	0.00	0.00	0.00	0.00	0.00	0.00	0.00	0.00	0.01	0.01
Na_2O	0.11	0.11	0.05	0.06	0.08	0.04	0.05	0.10	0.04	0.04	0.07
K_2O	8.18	9.48	9.46	9.57	9.48	9.44	9.72	9.06	9.80	9.80	9.40
H_2O	4.04	3.99	4.00	3.98	3.98	4.01	4.00	4.03	3.98	3.99	4.00
TOTAL	99.95	99.19	98.93	99.28	98.98	100.48	99.66	99.03	99.69	99.33	99.47
Formula per 22 oxygens											
Si	5.51	5.45	5.50	5.48	5.46	5.46	5.44	5.45	5.42	5.49	5.47
Al^{IV}	2.49	2.55	2.50	2.52	2.54	2.54	2.56	2.55	2.58	2.51	2.53
Al^{VI}	0.44	0.27	0.33	0.19	0.27	0.31	0.31	0.38	0.28	0.26	0.30
Ti	0.40	0.40	0.40	0.56	0.42	0.46	0.44	0.34	0.48	0.46	0.44
Fe	2.15	2.18	2.16	2.22	2.24	2.13	2.11	2.04	2.19	2.14	2.16
Mn	0.01	0.00	0.00	0.01	0.01	0.01	0.00	0.00	0.01	0.01	0.01
Mg	2.83	2.95	2.85	2.71	2.83	2.84	2.88	3.10	2.76	2.84	2.86
Ca	0.01	0.00	0.00	0.00	0.00	0.00	0.00	0.00	0.00	0.00	0.00
Na	0.03	0.03	0.01	0.02	0.02	0.01	0.01	0.03	0.01	0.01	0.02
K	1.55	1.83	1.86	1.85	1.84	1.79	1.87	1.74	1.89	1.89	1.81
Fe/Fe+Mg	0.43	0.42	0.43	0.45	0.44	0.43	0.42	0.40	0.44	0.43	0.43

NDF67a - Fine grained granulite, Valley Trust Formation.

	1* C In contact with garnet	2 C In contact with garnet	3 C In contact with garnet	4 C In contact with garnet	5 C In contact with garnet	6 C In contact with garnet	7 C In contact with garnet	8 C In contact with garnet	9 C From garnet rich area	10 C From garnet rich area	11* C From garnet rich zone	12* C Garnet free zone
SiO_2	38.33	37.71	37.72	38.01	37.43	38.03	37.48	36.40	37.09	37.18	38.86	37.92
TiO_2	4.53	3.54	4.04	3.98	4.35	4.20	4.64	4.59	4.08	4.64	4.22	3.92
Al_2O_3	16.70	16.46	15.82	16.04	15.76	16.03	16.27	16.34	16.09	15.80	16.94	17.03
Cr_2O_3	0.00	0.00	0.00	0.00	0.00	0.00	0.00	0.00	0.00	0.00	0.00	0.00
FeO	14.81	14.57	14.46	14.37	14.55	14.56	13.85	14.70	14.09	14.82	15.54	16.92
MnO	0.01	0.01	0.00	0.00	0.01	0.01	0.01	0.03	0.02	0.01	0.00	0.04
MgO	14.38	14.37	14.68	14.89	14.49	14.50	14.09	13.27	14.32	13.79	14.77	13.28
CaO	0.01	0.03	0.03	0.00	0.01	0.00	0.11	0.05	0.00	0.00	0.01	0.02
Na_2O	0.05	0.14	0.05	0.06	0.05	0.09	0.04	0.13	0.06	0.06	0.04	0.04
K_2O	9.08	9.41	9.57	9.80	9.70	9.75	9.80	9.55	9.40	9.72	8.75	8.85
H_2O	4.08	4.07	4.06	4.06	4.05	4.06	4.07	4.04	4.07	4.04	4.08	4.04
TOTAL	101.98	100.31	100.43	101.21	100.40	101.23	100.36	99.10	99.22	100.06	103.21	102.06
Formula per 22 oxygens												
Si	5.52	5.54	5.55	5.54	5.52	5.55	5.51	5.45	5.51	5.51	5.53	5.51
Al^{IV}	2.48	2.46	2.45	2.46	2.48	2.45	2.49	2.55	2.49	2.49	2.47	2.49
Al^{VI}	0.36	0.40	0.29	0.30	0.25	0.30	0.33	0.33	0.33	0.27	0.37	0.42
Ti	0.49	0.39	0.45	0.44	0.48	0.46	0.51	0.52	0.46	0.52	0.45	0.43
Fe	1.78	1.79	1.78	1.75	1.79	1.78	1.70	1.84	1.75	1.84	1.85	2.05
Mn	0.00	0.00	0.00	0.00	0.00	0.00	0.00	0.00	0.00	0.00	0.00	0.01
Mg	3.09	3.15	3.22	3.24	3.18	3.15	3.09	2.96	3.17	3.05	3.13	2.87
Ca	0.00	0.01	0.00	0.00	0.00	0.00	0.02	0.01	0.00	0.00	0.00	0.00
Na	0.01	0.04	0.02	0.02	0.01	0.02	0.01	0.04	0.02	0.02	0.01	0.01
K	1.67	1.77	1.79	1.82	1.82	1.81	1.84	1.82	1.78	1.84	1.59	1.64
Fe/Fe+Mg	0.37	0.36	0.36	0.35	0.36	0.36	0.35	0.38	0.36	0.38	0.37	0.42

* Excluded from average

Table continued.

13 C Garnet free zone	14 C Garnet free zone	Average biotite (in contact with garnet)	Average biotite (in garnet band but not in contact with garnet)	Average biotite (in garnet free area)
36.90	36.50	37.54	37.14	36.70
3.41	4.95	4.20	4.36	4.18
16.38	15.54	16.10	15.95	15.96
0.00	0.00	0.00	0.00	0.00
15.92	17.20	14.44	14.46	16.56
0.04	0.04	0.01	0.02	0.04
13.14	12.24	14.33	14.06	12.69
0.00	0.01	0.03	0.00	0.01
0.02	0.04	0.08	0.06	0.03
9.60	9.74	9.65	9.56	9.67
4.03	3.99	4.06	4.06	4.01
99.44	100.25	100.44	99.64	99.84
5.52	5.47	5.52	5.51	5.50
2.48	2.53	2.48	2.49	2.50
0.41	0.21	0.31	0.30	0.31
0.38	0.56	0.46	0.49	0.47
1.99	2.16	1.78	1.80	2.08
0.00	0.00	0.00	0.00	0.00
2.93	2.73	3.14	3.11	2.83
0.00	0.00	0.01	0.00	0.00
0.01	0.01	0.02	0.02	0.01
1.83	1.86	1.81	1.81	1.85
0.40	0.44	0.36	0.37	0.42

NDF69 - Fine grained granulite, Valley Trust Formation.

	1 C Garnet zone	2 C Garnet zone	3 C Garnet zone	4* C Garnet zone	5 C Garnet free zone	6 C Garnet free zone	7 C Garnet free zone	8 C Garnet free zone	9 C Garnet free zone	10 C Garnet free zone	11 C Garnet free zone	12 C Garnet free zone	13 C Garnet free zone	14 C Garnet free zone
SiO_2	36.54	36.31	36.35	34.99	36.43	36.68	36.19	36.39	37.38	36.60	37.30	37.29	36.54	36.42
TiO_2	5.14	5.11	5.05	5.04	5.46	5.31	5.03	5.41	5.58	5.34	5.22	5.47	5.21	5.14
Al_2O_3	15.57	16.09	15.87	15.31	16.03	15.80	15.69	15.97	16.60	16.29	15.96	16.36	16.18	16.07
Cr_2O_3	0.00	0.00	0.00	0.00	0.00	0.00	0.00	0.00	0.00	0.00	0.00	0.00	0.00	0.00
FeO	12.01	13.34	14.38	13.94	14.75	15.22	15.55	15.05	14.57	14.56	14.29	14.71	14.74	14.61
MnO	0.00	0.00	0.00	0.00	0.00	0.00	0.01	0.00	0.00	0.00	0.00	0.00	0.00	0.00
MgO	15.59	14.62	14.31	13.70	13.07	13.01	13.02	12.96	13.72	13.97	14.27	13.60	13.42	13.51
CaO	0.00	0.00	0.01	0.00	0.00	0.00	0.00	0.00	0.01	0.01	0.01	0.00	0.00	0.00
Na_2O	0.06	0.06	0.14	0.06	0.06	0.06	0.07	0.06	0.04	0.08	0.04	0.08	0.07	0.10
K_2O	10.11	9.83	9.48	9.73	9.76	9.67	9.80	9.55	9.36	9.90	10.08	9.51	9.64	9.56
H_2O	4.08	4.06	4.05	4.03	4.04	4.03	4.02	4.04	4.05	4.03	4.05	4.06	4.04	4.04
TOTAL	99.10	99.42	99.64	96.80	99.60	99.78	99.38	99.43	101.31	100.78	101.22	101.08	99.84	99 45
Formula per 22 oxygens														
Si	5.43	5.40	5.41	5.38	5.43	5.47	5.44	5.44	5.42	5.38	5.46	5.45	5.43	5.43
Al^{IV}	2.57	2.60	2.59	2.62	2.57	2.53	2.56	2.56	2.58	2.62	2.54	2.55	2.57	2.57
Al^{VI}	0.15	0.21	0.19	0.16	0.25	0.24	0.22	0.25	0.26	0.20	0.21	0.27	0.26	0.26
Ti	0.57	0.57	0.57	0.58	0.61	0.59	0.57	0.61	0.61	0.59	0.57	0.60	0.58	0.58
Fe^{3+}	0.00	0.00	0.00	0.00	0.00	0.00	0.00	0.00	0.08	0.05	0.00	0.00	0.00	0.00
Fe^{2+}	1.49	1.66	1.79	1.79	1.84	1.90	1.95	1.88	1.77	1.79	1.75	1.80	1.83	1.82
Mn	0.00	0.00	0.00	0.00	0.00	0.00	0.00	0.00	0.00	0.00	0.00	0.00	0.00	0.00
Mg	3.45	3.24	3.17	3.14	2.91	2.89	2.92	2.89	2.97	3.06	3.11	2.96	2.97	3.00
Ca	0.00	0.00	0.00	0.00	0.00	0.00	0.00	0.00	0.00	0.00	0.00	0.00	0.00	0.00
Na	0.02	0.02	0.04	0.02	0.02	0.02	0.02	0.02	0.01	0.02	0.01	0.02	0.02	0.03
K	1.91	1.86	1.80	1.91	1.86	1.84	1.88	1.82	1.73	1.85	1.88	1.77	1.83	1.82
Fe/Fe+Mg	0.30	0.34	0.36	0.36	0.39	0.40	0 40	0.39	0.38	0.38	0.36	0.38	0.38	0.38

* Not used in average

Table continued.

15 C Garnet free zone	16 C Garnet zone	17* C Garnet zone	18 C Garnet zone	19 C Garnet zone	20 C Garnet zone	21* C Garnet zone	22 C Garnet zone	23 C Garnet zone	24 C Garnet zone	Average	Average (Assoc. with garnet)	Average (In garnet free zone)
37.25	37.37	37.67	37.12	37.60	37.48	37.72	36.53	37.33	35.43	36.79	36.81	36.77
4.96	5.05	5.09	5.19	4.85	4.83	5.20	5.06	5.29	8.75	5.35	5.43	5.28
16.25	15.90	16.03	15.62	16.17	16.26	16.26	16.35	15.69	15.66	16.02	15.92	16.10
0.00	0.00	0.00	0.00	0.00	0.00	0.00	0.00	0.00	0.00	0.00	0.00	0.00
14.62	11.93	13.95	14.52	12.83	14.17	14.34	13.89	14.06	12.34	14.10	13.35	14.79
0.00	0.00	0.01	0.00	0.00	0.00	0.00	0.01	0.00	0.02	0.00	0.00	0.00
13.81	16.43	14.97	13.95	15.48	14.77	14.59	14.85	14.85	15.04	14.20	14.99	13.49
0.00	0.00	0.00	0.01	0.00	0.00	0.00	0.00	0.00	0.04	0.00	0.01	0.00
0.06	0.07	0.09	0.11	0.04	0.05	0.06	0.07	0.07	0.12	0.07	0.08	0.07
9.74	9.74	9.86	9.82	9.90	9.66	9.54	9.82	9.68	9.05	9.70	9.71	9.69
4.05	4.10	4.06	4.04	4.08	4.06	4.07	4.05	4.06	4.08	4.05	4.07	4.04
100.74	100.59	101.73	100.38	100.95	101.28	101.78	100.63	101.03	100.53	100.35	100.36	100.34
5.47	5.44	5.46	5.48	5.47	5.46	5.46	5.37	5.46	5.18	5.42	5.41	5.44
2.53	2.56	2.54	2.52	2.53	2.54	2.54	2.63	2.54	2.70	2.57	2.58	2.56
0.29	0.17	0.20	0.20	0.24	0.25	0.24	0.20	0.16	0.00	0.21	0.18	0.25
0.55	0.55	0.55	0.58	0.53	0.53	0.57	0.56	0.58	0.96	0.59	0.60	0.59
0.00	0.00	0.00	0.00	0.00	0.00	0.00	0.00	0.00	0.00	0.01	0.00	0.01
1.80	1.45	1.69	1.79	1.56	1.73	1.74	1.71	1.72	1.51	1.74	1.64	1.83
0.00	0.00	0.00	0.00	0.00	0.00	0.00	0.00	0.00	0.00	0.00	0.00	0.00
3.02	3.56	3.24	3.07	3.36	3.21	3.15	3.25	3.24	3.28	3.12	3.28	2.97
0.00	0.00	0.00	0.00	0.00	0.00	0.00	0.00	0.00	0.01	0.00	0.00	0.00
0.02	0.02	0.03	0.03	0.01	0.01	0.02	0.02	0.02	0.03	0.02	0.02	0.02
1.83	1.81	1.82	1.85	1.84	1.79	1.76	1.84	1.80	1.69	1.82	1.82	1.83
0.37	0.29	0.34	0.37	0.32	0.35	0.36	0.34	0.35	0.32	0.36	0.33	0.38

UND 330 - Granitic enclave.

	1 C	2 C	3 C	4 C	5 C	6 C	7 C	8 C	9 C	10 M	11 C	12 C	13 M	14 C	Average
SiO_2	34.72	34.21	33.79	34.70	34.80	34.60	34.04	34.58	34.78	34.04	34.70	34.12	33.71	34.21	34.36
TiO_2	4.24	4.13	3.58	4.30	4.05	4.14	4.45	4.07	3.78	4.29	3.89	3.58	4.29	4.43	4.09
Al_2O_3	15.54	15.90	16.33	15.41	15.88	15.32	15.27	15.73	16.09	15.78	15.83	15.92	15.64	15.35	15.71
Cr_2O_3	0.00	0.00	0.00	0.00	0.00	0.00	0.00	0.00	0.00	0.00	0.00	0.00	0.00	0.00	0.00
FeO	28.02	28.17	29.25	28.41	27.89	27.55	28.73	27.87	28.31	28.18	27.93	29.08	29.13	28.58	28.36
MnO	0.10	0.09	0.10	0.09	0.10	0.13	0.13	0.07	0.09	0.12	0.07	0.09	0.16	0.10	0.10
MgO	4.40	4.21	4.40	4.38	4.26	4.28	4.29	4.41	4.33	4.26	4.40	4.62	4.50	4.30	4.36
CaO	0.00	0.00	0.02	0.00	0.00	0.00	0.01	0.01	0.06	0.04	0.00	0.05	0.06	0.00	0.02
Na_2O	0.06	0.07	0.05	0.04	0.05	0.05	0.06	0.06	0.06	0.06	0.06	0.06	0.03	0.06	0.06
K_2O	9.29	9.10	8.32	9.37	9.23	9.31	8.94	9.19	8.56	8.88	9.06	8.22	7.13	8.96	8.83
H_2O	3.79	3.79	3.78	3.78	3.80	3.79	3.78	3.80	3.81	3.79	3.80	3.79	3.80	3.78	3.79
TOTAL	100.16	99.67	99.62	100.48	100.06	99.17	99.70	99.79	99.87	99.44	99.74	99.53	98.45	99.77	99.74
Formula per 22 oxygens															
Si	5.48	5.43	5.37	5.47	5.49	5.51	5.42	5.47	5.49	5.42	5.49	5.42	5.37	5.44	5.45
Al^{IV}	2.52	2.57	2.63	2.53	2.51	2.49	2.58	2.53	2.51	2.58	2.51	2.58	2.63	2.56	2.55
Al^{VI}	0.37	0.41	0.44	0.33	0.44	0.39	0.29	0.41	0.48	0.38	0.44	0.41	0.31	0.31	0.39
Ti	0.50	0.49	0.43	0.51	0.48	0.50	0.53	0.48	0.45	0.51	0.46	0.43	0.51	0.53	0.49
Fe^{3+}	0.00	0.00	0.00	0.03	0.00	0.00	0.00	0.00	0.00	0.00	0.00	0.00	0.00	0.00	0.00
Fe^{2+}	3.70	3.74	3.89	3.74	3.68	3.67	3.83	3.69	3.73	3.75	3.70	3.87	3.88	3.80	3.76
Mn	0.01	0.01	0.01	0.01	0.01	0.02	0.02	0.01	0.01	0.02	0.01	0.01	0.02	0.01	0.01
Mg	1.04	1.00	1.04	1.03	1.00	1.02	1.02	1.04	1.02	1.01	1.04	1.10	1.07	1.02	1.03
Ca	0.00	0.00	0.00	0.00	0.00	0.00	0.00	0.00	0.01	0.01	0.00	0.01	0.12	0.00	0.01
Na	0.02	0.02	0.01	0.01	0.01	0.02	0.02	0.02	0.02	0.01	0.02	0.02	0.01	0.02	0.02
K	1.87	1.84	1.69	1.88	1.86	1.89	1.82	1.86	1.72	1.80	1.83	1.67	1.45	1.82	1.79
Fe/Fe+Mg	0.78	0.79	0.79	0.79	0.79	0.78	0.79	0.78	0.79	0.79	0.78	0.78	0.78	0.79	0.78

UND 40 - Biotite granite, Ximba Suite.

	1 C	2 C	3 C	4 C	5 C	6 C	7 C	8 C	Average
SiO_2	34.55	34.71	34.60	34.99	34.13	34.27	34.74	34.12	34.51
TiO_2	4.33	4.03	4.33	3.96	4.09	3.80	3.25	3.76	3.94
Al_2O_3	14.22	15.15	15.64	15.50	15.06	15.86	16.56	14.30	15.29
Cr_2O_3	0.00	0.00	0.00	0.00	0.00	0.00	0.00	0.00	0.00
FeO	30.42	29.99	28.47	29.14	29.32	28.43	28.10	30.85	29.34
MnO	0.41	0.39	0.34	0.39	0.42	0.33	0.35	0.38	0.38
MgO	3.28	3.04	2.98	3.09	2.88	3.37	3.48	3.17	3.16
CaO	0.02	0.03	0.00	0.03	0.00	0.01	0.00	0.01	0.01
Na_2O	0.06	0.04	0.04	0.05	0.05	0.04	0.04	0.03	0.04
K_2O	8.91	8.92	9.30	9.08	9.24	9.27	9.36	8.98	9.13
H_2O	3.74	3.76	3.78	3.77	3.75	3.78	3.79	3.73	3.76
TOTAL	99.94	100.06	99.48	100.00	98.94	99.16	99.67	99.33	99.58
Formula per 22 oxygens									
Si	5.54	5.53	5.52	5.56	5.51	5.49	5.51	5.53	5.52
Al^{IV}	2.46	2.47	2.48	2.44	2.49	2.51	2.49	2.47	2.48
Al^{VI}	0.23	0.38	0.46	0.46	0.38	0.48	0.61	0.26	0.41
Ti	0.52	0.48	0.52	0.47	0.50	0.46	0.39	0.46	0.48
Fe	4.08	4.00	3.80	3.87	3.96	3.81	3.73	4.18	3.93
Mn	0.06	0.05	0.05	0.05	0.06	0.05	0.05	0.05	0.05
Mg	0.78	0.72	0.71	0.73	0.69	0.81	0.82	0.76	0.75
Ca	0.00	0.01	0.00	0.01	0.00	0.00	0.00	0.00	0.00
Na	0.02	0.01	0.01	0.02	0.02	0.01	0.01	0.01	0.01
K	1.82	1.82	1.89	1.84	1.91	1.89	1.90	1.86	1.87
Fe/Fe+Mg	0.84	0.85	0.84	0.84	0.85	0.82	0.82	0.85	0.84

XS 4 - Biotite garnet granite, Ximba Suite.

	1 C Adjacent to garnet	2 M Adjacent to garnet	3 M Adjacent to garnet
SiO_2	32.79	31.31	30.74
TiO_2	5.04	3.09	3.59
Al_2O_3	13.86	14.75	14.78
Cr_2O_3	0.00	0.00	0.00
FeO	29.35	31.85	32.63
MnO	0.14	0.19	0.15
MgO	3.68	4.23	4.65
CaO	0.51	0.07	0.00
Na_2O	0.05	0.03	0.04
K_2O	7.87	6.15	5.20
H_2O	3.75	3.73	3.74
TOTAL	97.04	95.40	95.52
Formula per 22 oxygens			
Si	5.41	5.28	5.16
Al^{IV}	2.59	2.72	2.84
Al^{VI}	0.10	0.21	0.09
Ti	0.62	0.39	0.45
Fe	4.05	4.49	4.59
Mn	0.02	0.03	0.02
Mg	0.91	1.06	1.17
Ca	0.09	0.01	0.00
Na	0.02	0.01	0.01
K	1.66	1.32	1.12
Fe/Fe+Mg	0.82	0.81	0.80

UND 65 - Hornblende granite, Mlahlanja Suite.

	1 C	2 C	3 C	4 C	5 C	6 C	7 C	8 C	9 C
SiO_2	26.85	31.77	29.27	33.33	30.14	30.49	31.91	34.45	30.02
TiO_2	3.21	4.60	4.76	4.02	3.68	3.16	5.51	5.00	5.46
Al_2O_3	14.61	14.15	13.84	13.78	13.90	14.53	13.90	13.91	13.80
Cr_2O_3	0.00	0.00	0.00	0.00	0.00	0.00	0.00	0.00	0.00
FeO	35.46	30.48	32.51	30.51	32.71	33.27	29.76	29.25	31.14
MnO	0.24	0.29	0.26	0.25	0.27	0.27	0.28	0.31	0.23
MgO	6.26	5.08	5.52	5.01	5.67	5.79	4.76	4.30	5.21
CaO	1.21	1.01	2.76	0.24	1.06	0.98	1.65	0.00	3.20
Na_2O	0.02	0.03	0.02	0.04	0.02	0.00	0.05	0.06	0.03
K_2O	0.86	6.37	2.89	7.69	3.85	4.08	6.32	8.96	3.55
TOTAL	88.72	93.78	91.83	94.87	91.30	92.57	94.14	96.24	92.64

UND 74 - Charnockite, Mlahlanja Suite.

	1 C	2 C	3 C	4 C	5 C	6 C	7 C	8 C	9 C	10 C	Average
SiO_2	34.97	35.17	35.31	35.02	34.66	34.29	34.80	34.72	34.62	34.42	34.80
TiO_2	5.59	5.36	5.41	5.75	5.49	5.32	5.05	5.48	4.80	5.42	5.37
Al_2O_3	12.68	12.84	13.04	13.20	13.09	13.16	13.26	13.32	13.00	13.18	13.08
Cr_2O_3	0.00	0.00	0.00	0.00	0.00	0.00	0.00	0.00	0.00	0.00	0.00
FeO	27.15	27.01	27.62	27.81	27.34	28.04	27.96	28.59	27.57	28.52	17.76
MnO	0.15	0.14	0.15	0.18	0.15	0.20	0.19	0.17	0.14	0.15	0.16
MgO	5.24	5.30	5.51	4.85	4.95	4.95	5.14	5.06	5.80	5.03	5.18
CaO	0.00	0.02	0.00	0.00	0.00	0.00	0.00	0.00	0.00	0.00	0.00
Na_2O	0.05	0.04	0.04	0.05	0.05	0.03	0.04	0.04	0.02	0.04	0.04
K_2O	9.19	9.00	9.44	9.32	9.02	9.26	9.28	9.28	9.24	9.34	9.23
H_2O	3.79	3.80	3.79	3.78	3.79	3.77	3.78	3.77	3.78	3.76	3.78
TOTAL	98.81	98.68	100.31	99.96	98.54	99.02	99.50	100.43	98.97	99.86	99.40
Formula per 22 oxygens											
Si	5.60	5.63	5.58	5.56	5.57	5.52	5.56	5.50	5.55	5.50	5.56
Al^{IV}	2.39	2.37	2.42	2.44	2.43	2.48	2.44	2.49	2.45	2.48	4.44
Al^{VI}	0.00	0.05	0.00	0.03	0.05	0.01	0.05	0.00	0.01	0.00	0.02
Ti	0.67	0.65	0.64	0.69	0.66	0.64	0.61	0.65	0.58	0.63	0.64
Fe	3.64	3.61	3.65	3.69	3.67	3.77	3.73	3.79	3.70	3.81	3.71
Mn	0.02	0.02	0.02	0.02	0.02	0.03	0.03	0.02	0.02	0.02	0.02
Mg	1.25	1.26	1.30	1.15	1.19	1.19	1.22	1.19	1.39	1.20	1.23
Ca	0.00	0.00	0.00	0.00	0.00	0.00	0.00	0.00	0.00	0.00	0.00
Na	0.02	0.01	0.01	0.02	0.01	0.01	0.01	0.01	0.01	0.01	0.01
K	1.88	1.84	1.90	1.89	1.85	1.90	1.89	1.88	1.89	1.90	1.88
Fe/Fe+Mg	0.74	0.74	0.74	0.76	0.76	0.76	0.75	0.76	0.73	0.76	0.75

UND 9 - Garnet hornblende granite, Mlahlanja Suite.

	1 C	2 C	3 C	4 C	5 C	6 C Associated with hornblende	7 C	8 C	Average
SiO_2	34.78	34.64	34.68	34.25	34.26	33.45	34.30	34.24	34.33
TiO_2	3.18	3.88	3.37	3.25	3.80	2.46	3.26	3.56	3.35
Al_2O_3	15.54	14.80	14.99	15.16	15.51	15.70	15.69	15.92	15.41
Cr_2O_3	0.00	0.00	0.00	0.00	0.00	0.00	0.00	0.00	0.00
FeO	29.97	30.11	30.16	30.40	30.07	30.52	29.00	29.03	29.91
MnO	0.21	0.27	0.25	0.24	0.24	0.34	0.21	0.25	0.25
MgO	3.50	3.37	3.49	3.51	2.91	3.63	3.46	3.16	3.38
CaO	0.00	0.00	0.00	0.00	0.00	0.01	0.00	0.00	0.00
Na_2O	0.02	0.04	0.05	0.03	0.05	0.04	0.04	0.04	0.04
K_2O	9.19	9.02	8.95	8.97	9.22	9.06	9.15	9.27	9.10
H_2O	3.76	3.75	3.75	3.75	3.75	3.73	3.77	3.77	3.75
TOTAL	100.15	99.88	99.69	99.56	99.81	98.94	98.87	99.23	99.52
Formula per 22 oxygens									
Si	5.54	5.54	5.56	5.51	5.49	5.44	5.52	5.49	5.51
Al^{IV}	2.46	2.46	2.44	2.49	2.51	2.56	2.48	2.51	2.49
Al^{VI}	0.46	0.33	0.39	0.38	0.42	0.44	0.50	0.50	0.43
Ti	0.38	0.47	0.41	0.39	0.46	0.30	0.39	0.43	0.40
Fe	3.99	4.03	4.04	4.09	4.03	4.15	3.90	3.89	4.02
Mn	0.03	0.04	0.03	0.03	0.03	0.05	0.03	0.03	0.03
Mg	0.83	0.80	0.83	0.84	0.70	0.88	0.83	0.76	0.81
Na	0.01	0.01	0.02	0.01	0.01	0.01	0.01	0.01	0.01
K	1.87	1.84	1.83	1.84	1.89	1.88	1.88	1.90	1.87
Fe/Fe+Mg	0.83	0.83	0.83	0.83	0.85	0.83	0.82	0.84	0.83

UND 6 - Garnet hornblende granite, Mlahlanja Suite.

	1 C	2 C	3 C	4 C	5 C	6 C	7 C	8 C	9 C	10 C	11 C	12 C
SiO_2	39.44	26.76	26.66	26.03	24.63	25.17	43.94	27.44	41.99	26.20	24.61	25.58
TiO_2	1.06	1.09	3.17	2.44	0.34	0.51	0.27	0.24	0.44	0.89	0.20	0.51
Al_2O_3	19.80	16.96	15.55	15.93	16.57	16.81	19.88	16.86	19.97	16.14	16.69	16.45
Cr_2O_3	0.00	0.00	0.00	0.00	0.00	0.00	0.00	0.00	0.00	0.00	0.00	0.00
FeO	25.74	38.35	36.34	38.04	41.19	40.70	19.00	36.72	20.78	38.02	40.50	41.02
MnO	0.31	0.48	0.51	0.48	0.55	0.56	0.14	0.53	0.16	0.54	0.52	0.52
MgO	3.58	5.24	4.92	4.87	4.79	5.38	3.07	5.48	3.08	5.12	4.94	4.84
CaO	0.76	0.78	2.69	2.15	0.22	0.44	0.05	0.03	0.06	0.46	0.07	0.45
Na_2O	0.00	0.00	0.03	0.02	0.00	0.01	0.01	0.02	0.02	0.02	0.00	0.01
K_2O	4.10	0.47	0.31	0.00	0.00	0.00	7.28	0.46	7.01	0.18	0.00	0.00
TOTAL	94.79	90.13	90.18	89.96	88.29	89.58	93.64	87.78	93.51	87.57	87.53	89.38

Amphibole

UND 320 - Amphibolite, Nagle Dam Formation.

	1 C	2 C	3 C	4 C Enclosed in diopside	5 C	6 C	7 C	8 C	9 M Adjacent to diopside	10 C	11 M Adjacent to diopside	12 C	Average
SiO_2	44.18	44.53	44.60	44.55	44.69	44.34	44.07	43.83	44.79	44.69	44.67	44.53	44.46
TiO_2	1.09	1.11	1.09	1.12	1.15	1.16	1.24	1.19	1.11	1.15	1.14	1.18	1.14
Al_2O_3	9.69	9.57	9.69	9.52	9.98	9.89	10.22	9.98	9.67	9.98	9.98	10.16	9.86
Cr_2O_3	0.00	0.00	0.00	0.00	0.00	0.00	0.00	0.00	0.00	0.00	0.00	0.00	0.00
FeO	14.65	14.82	14.45	14.83	14.39	14.99	14.78	14.96	14.13	14.39	14.27	14.38	14.59
MnO	0.23	0.21	0.22	0.24	0.25	0.23	0.22	0.27	0.25	0.25	0.24	0.23	0.24
MgO	12.71	12.74	12.77	12.71	12.50	12.41	12.40	12.33	12.42	12.50	12.37	12.29	12.51
CaO	12.01	11.94	11.85	12.00	11.82	11.92	11.79	11.75	12.06	11.82	11.83	11.80	11.88
Na_2O	1.32	1.23	1.30	1.23	1.23	1.26	1.20	1.19	1.15	1.23	1.22	1.20	1.23
K_2O	1.05	1.03	1.03	1.01	1.08	1.03	1.01	1.00	1.01	1.08	1.01	1.04	1.03
H_2O	2.00	2.01	2.01	2.01	2.01	2.01	2.00	1.99	2.00	2.01	2.01	2.01	2.01
TOTAL	98.93	99.19	99.01	99.22	99.10	99.24	98.93	98.49	98.59	99.10	98.74	98.82	98.94
Formula per 24 oxygens													
Si	6.63	6.66	6.66	6.66	6.67	6.63	6.60	6.61	6.71	6.67	6.68	6.66	6.65
Al^{IV}	1.37	1.34	1.34	1.34	1.33	1.37	1.40	1.39	1.29	1.33	1.32	1.34	1.35
Al^{VI}	0.34	0.34	0.37	0.34	0.42	0.37	0.41	0.38	0.42	0.42	0.44	0.45	0.39
Ti	0.12	0.13	0.12	0.13	0.13	0.13	0.14	0.14	0.13	0.13	0.13	0.13	0.13
Mg	2.84	2.84	2.85	2.83	2.78	2.77	2.72	2.77	2.77	2.78	2.56	2.74	2.77
Fe	1.70	1.69	1.66	1.71	1.67	1.73	1.69	1.72	1.69	1.67	1.67	1.68	1.69
Fe	0.14	0.16	0.15	0.15	0.13	0.15	0.17	0.17	0.08	0.13	0.11	0.12	0.14
Mn	0.03	0.03	0.03	0.03	0.03	0.03	0.03	0.03	0.03	0.03	0.03	0.03	0.03
Ca	1.83	1.81	1.83	1.82	1.84	1.82	1.81	1.80	1.89	1.84	1.86	1.85	1.83
Ca	0.10	0.10	0.07	0.10	0.05	0.09	0.09	0.10	0.05	0.05	0.04	0.04	0.07
Na	0.38	0.36	0.38	0.36	0.36	0.37	0.35	0.35	0.33	0.36	0.35	0.35	0.36
K	0.20	0.20	0.20	0.19	0.21	0.20	0.19	0.19	0.19	0.21	0.19	0.20	0.20
Fe/Fe+Mg	0.39	0.39	0.39	0.40	0.39	0.40	0.41	0.41	0.39	0.39	0.41	0.40	0.40

UND 357 - Amphibolite, Valley Trust Formation.

	1 C	2 C	3 C	4 C	5 M	6 C	7 M	8 C	9 M	10 C	Average	Average Core	Average Margin
SiO_2	43.66	44.33	43.45	43.39	43.49	43.33	43.22	43.36	43.21	43.39	43.48	43.56	43.31
TiO_2	1.89	1.82	1.88	1.87	1.97	1.81	1.80	1.91	1.89	1.88	1.87	1.87	1.89
Al_2O_3	10.53	10.16	10.49	10.74	10.47	10.49	10.37	10.62	10.44	10.47	10.48	10.50	10.42
Cr_2O_3	0.00	0.00	0.00	0.00	0.00	0.00	0.00	0.00	0.00	0.00	0.00	0.00	0.00
FeO	19.47	19.49	19.34	18.80	18.59	19.40	18.70	19.25	18.80	18.86	19.07	19.23	18.70
MnO	0.20	0.18	0.19	0.15	0.15	0.14	0.19	0.19	0.16	0.15	0.17	0.17	0.17
MgO	8.76	9.26	8.92	8.84	8.97	9.06	9.05	8.95	8.91	8.95	8.97	8.96	8.98
CaO	11.48	11.49	11.51	11.54	11.52	11.01	11.35	11.42	11.43	11.50	11.43	11.42	11.43
Na_2O	1.40	1.39	1.39	1.38	1.32	1.24	1.35	1.37	1.33	1.23	1.34	1.34	1.33
K_2O	0.96	0.86	0.96	0.97	1.01	0.93	1.00	0.93	0.95	1.00	0.96	0.94	0.99
H_2O	1.99	2.01	1.98	1.98	1.98	1.97	1.97	1.98	1.97	1.98	1.98	1.98	1.97
TOTAL	100.35	100.99	100.12	99.67	99.46	99.39	99.00	99.99	99.08	99.41	99.75	99.99	99.18
Formula per 24 oxygens													
Si	6.58	6.63	6.57	6.57	6.59	6.58	6.59	6.56	6.58	6.59	6.58	6.58	6.59
Al^{IV}	1.42	1.37	1.43	1.43	1.41	1.42	1.41	1.44	1.42	1.41	1.42	1.42	1.41
Al^{VI}	0.45	0.42	0.43	0.49	0.46	0.46	0.45	0.45	0.46	0.46	0.45	0.45	0.46
Ti	0.21	0.20	0.21	0.21	0.22	0.21	0.21	0.22	0.22	0.21	0.21	0.21	0.22
Mg	1.97	2.06	2.01	2.00	2.03	2.05	2.06	2.02	2.02	2.03	2.03	2.02	2.04
Fe	2.36	2.31	2.34	2.31	2.29	2.28	2.29	2.32	2.30	2.30	2.31	2.32	2.29
Fe(M4)	0.09	0.12	0.10	0.07	0.07	0.19	0.10	0.12	0.09	0.09	0.10	0.11	0.09
Mn(M4)	0.03	0.02	0.02	0.02	0.02	0.02	0.03	0.02	0.02	0.02	0.02	0.02	0.02
Ca(M4)	1.85	1.84	1.86	1.87	1.87	1.79	1.85	1.85	1.86	1.87	1.85	1.85	1.86
Na(M4)	0.03	0.01	0.01	0.04	0.04	0.00	0.02	0.01	0.02	0.02	0.02	0.02	0.03
Na(A)	0.38	0.39	0.40	0.37	0.35	0.36	0.38	0.39	0.37	0.35	0.37	0.38	0.37
K(A)	0.18	0.16	0.19	0.19	0.20	0.18	0.19	0.18	0.18	0.19	0.18	0.18	0.19
Fe/Fe+Mg	0.55	0.54	0.55	0.54	0.54	0.55	0.54	0.55	0.54	0.54	0.54	0.55	0.54

UND 65 - Hornblende granite, Mlahlanja Suite.

	1 C	2 C	3 C	4 C	5 C Associated with biotite	6 C Associated with biotite	7 C	8 C	9 C	10 C	11 M Adjacent to plagioclase	12 C	13 C	14 C	Average
SiO_2	39.26	39.51	39.52	39.81	39.46	39.30	39.16	39.75	39.88	39.70	39.57	39.88	39.72	39.49	39.57
TiO_2	1.83	1.90	1.92	1.91	1.77	2.12	1.90	1.88	1.80	1.83	2.44	1.92	1.83	2.08	1.94
Al_2O_3	10.56	10.63	10.92	10.70	10.88	10.85	10.77	10.68	10.54	10.65	10.57	10.86	10.82	10.65	10.72
Cr_2O_3	0.00	0.00	0.00	0.00	0.00	0.00	0.00	0.00	0.00	0.00	0.00	0.00	0.00	0.00	0.00
FeO	27.34	27.44	27.46	27.24	27.45	27.20	26.98	27.33	27.13	27.43	26.70	27.01	27.24	27.01	27.21
MnO	0.64	0.66	0.68	0.66	0.63	0.63	0.64	0.68	0.68	0.65	0.63	0.68	0.65	0.67	0.66
MgO	3.72	3.78	3.77	3.71	3.56	3.54	3.67	3.82	3.80	3.83	3.60	3.78	3.73	3.68	3.71
CaO	10.88	10.84	10.92	10.69	10.97	10.85	10.81	10.75	10.73	10.81	11.20	10.78	10.91	10.84	10.86
Na_2O	1.49	1.55	1.78	1.75	1.67	1.71	1.68	1.70	1.70	1.71	1.50	1.76	1.76	1.65	1.67
K_2O	1.23	1.29	1.30	1.31	1.32	1.31	1.36	1.34	1.34	1.29	1.17	1.36	1.37	1.28	1.30
H_2O	1.86	1.87	1.89	1.88	1.87	1.87	1.86	1.88	1.88	1.88	1.88	1.89	1.88	1.87	1.88
TOTAL	98.81	99.47	100.16	99.66	99.58	99.38	98.83	99.81	99.48	99.78	99.26	99.92	99.91	99.22	99.52
Formula per 24 oxygens															
Si	6.33	6.32	6.28	6.35	6.31	6.29	6.30	6.33	6.37	6.33	6.32	6.34	6.32	6.32	6.32
Al^{IV}	1.67	1.68	1.72	1.65	1.69	1.71	1.70	1.67	1.63	1.67	1.68	1.66	1.68	1.68	1.68
Al^{VI}	0.33	0.33	0.33	0.36	0.36	0.34	0.35	0.34	0.35	0.33	0.31	0.37	0.35	0.33	0.34
Ti	0.22	0.23	0.23	0.23	0.21	0.26	0.23	0.23	0.22	0.22	0.29	0.23	0.22	0.25	0.23
Mg	0.89	0.90	0.89	0.88	0.85	0.84	0.88	0.91	0.91	0.91	0.86	0.89	0.88	0.88	0.88
Fe	3.56	3.54	3.55	3.53	3.58	3.56	3.54	3.53	3.53	3.54	3.54	3.51	3.54	3.54	3.54
Fe(M4)	0.13	0.13	0.11	0.10	0.09	0.08	0.09	0.11	0.10	0.12	0.03	0.08	0.08	0.08	0.10
Mn	0.09	0.09	0.09	0.09	0.09	0.09	0.09	0.09	0.09	0.09	0.09	0.09	0.09	0.09	0.09
Ca	1.79	1.78	1.80	1.81	1.82	1.83	1.82	1.80	1.81	1.79	1.88	1.83	1.83	1.83	1.82
Ca(A)	0.09	0.08	0.06	0.02	0.06	0.03	0.04	0.04	0.02	0.05	0.04	0.01	0.03	0.03	0.04
Na(A)	0.46	0.48	0.55	0.54	0.52	0.53	0.52	0.53	0.53	0.53	0.46	0.54	0.54	0.51	0.52
K(A)	0.25	0.26	0.26	0.27	0.27	0.27	0.28	0.27	0.27	0.26	0.24	0.28	0.28	0.26	0.27
Fe/Fe+Mg	0.81	0.80	0.80	0.80	0.81	0.81	0.80	0.80	0.80	0.80	0.81	0.80	0.80	0.80	0.81

UND 74 - Charnockite, Mlahlanja Suite.

	1 C	2 C	3 C	4 C	5 C	6 C	7 C	8 C	9 C	Average
SiO_2	39.04	39.17	39.31	38.39	38.95	39.24	38.85	38.87	39.12	38.99
TiO_2	1.85	1.72	1.80	1.55	1.87	1.87	1.88	1.70	1.88	1.79
Al_2O_3	10.67	10.71	10.60	10.95	10.71	10.57	10.71	11.00	10.65	10.73
Cr_2O_3	0.00	0.00	0.00	0.00	0.00	0.00	0.00	0.00	0.00	0.00
FeO	27.57	27.88	27.63	27.81	27.30	27.10	27.35	27.36	27.29	27.48
MnO	0.40	0.40	0.41	0.34	0.41	0.42	0.38	0.37	0.39	0.39
MgO	3.83	3.81	3.87	3.76	4.02	3.87	3.77	3.71	3.85	3.83
CaO	10.61	10.70	10.80	10.64	10.56	10.62	10.41	10.52	10.65	10.61
Na_2O	1.71	1.60	1.61	1.54	1.69	1.79	1.65	1.50	1.71	1.64
K_2O	1.46	1.43	1.47	1.46	1.45	1.48	1.46	1.43	1.43	1.45
H_2O	1.86	1.87	1.87	1.84	1.86	1.86	1.85	1.85	1.86	1.86
TOTAL	99.00	99.29	99.37	98.28	98.82	98.82	98.31	98.31	98.83	98.78
Formula per 24 oxygens										
Si	6.29	6.29	6.31	6.24	6.28	6.32	6.30	6.29	6.30	6.29
Al^{IV}	1.71	1.71	1.69	1.76	1.72	1.68	1.70	1.71	1.70	1.71
Al^{VI}	0.31	0.32	0.31	0.34	0.31	0.33	0.34	0.39	0.32	0.33
Ti	0.22	0.21	0.22	0.19	0.23	0.23	0.23	0.21	0.23	0.22
Mg	0.92	0.91	0.93	0.91	0.97	0.93	0.91	0.90	0.92	0.92
Fe	3.54	3.56	3.55	3.56	3.49	3.52	3.52	3.51	3.52	3.53
Fe	0.17	0.19	0.16	0.22	0.19	0.13	0.19	0.19	0.15	0.18
Mn	0.05	0.05	0.06	0.05	0.06	0.06	0.05	0.05	0.05	0.05
Ca	1.77	1.76	1.78	1.73	1.76	1.81	1.76	1.75	1.79	1.77
Ca	0.06	0.09	0.07	0.12	0.07	0.02	0.04	0.07	0.04	0.06
Na	0.53	0.50	0.50	0.49	0.53	0.56	0.52	0.47	0.53	0.51
K	0.30	0.29	0.30	0.30	0.30	0.30	0.30	0.30	0.29	0.30
Fe/Fe+Mg	0.80	0.80	0.80	0.81	0.79	0.80	0.80	0.80	0.80	0.80

UND 9 - Garnet hornblende granite - Mlahlanja Suite.

	1 C	2 C	3 C	4 C	5 C	6 C	7 C	Average
SiO_2	39.46	39.32	39.78	39.81	39.92	39.85	39.57	39.67
TiO_2	1.59	1.70	1.72	1.49	1.67	1.73	1.83	1.68
Al_2O_3	11.59	11.37	11.52	11.68	11.58	11.59	11.59	11.56
Cr_2O_3	0.00	0.00	0.00	0.00	0.00	0.00	0.00	0.00
FeO	27.34	27.92	27.55	27.75	27.73	27.60	27.53	27.63
MnO	0.42	0.49	0.46	0.50	0.49	0.46	0.51	0.48
MgO	2.83	2.65	2.71	2.67	2.77	2.63	2.69	2.71
CaO	11.05	11.08	11.02	11.29	11.22	11.04	10.95	11.09
Na_2O	1.45	1.36	1.48	1.33	1.36	1.48	1.38	1.41
K_2O	1.54	1.58	1.57	1.59	1.52	1.40	1.39	1.51
H_2O	1.87	1.87	1.88	1.88	1.89	1.88	1.87	1.88
TOTAL	99.14	99.34	99.69	99.99	100.15	99.66	99.31	99.62
Formula per 24 oxygens								
Si	6.33	6.31	6.34	6.34	6.34	6.35	6.33	6.33
Al^{IV}	1.67	1.69	1.66	1.66	1.66	1.65	1.67	1.67
Al^{VI}	0.52	0.47	0.51	0.53	0.50	0.53	0.51	0.51
Ti	0.19	0.20	0.21	0.18	0.20	0.21	0.22	0.20
Mg	0.68	0.64	0.64	0.63	0.66	0.63	0.64	0.65
Fe	3.62	3.69	3.64	3.66	3.64	3.64	3.63	3.65
Fe(M4)	0.05	0.06	0.03	0.03	0.04	0.04	0.06	0.04
Mn	0.06	0.07	0.06	0.07	0.07	0.06	0.07	0.07
Ca	1.89	1.88	1.88	1.90	1.89	1.89	1.87	1.89
Na	0.00	0.00	0.02	0.00	0.00	0.02	0.00	0.00
Ca(A)	0.00	0.03	0.00	0.02	0.02	0.00	0.00	0.01
Na(A)	0.45	0.42	0.44	0.41	0.42	0.44	0.43	0.43
K(A)	0.31	0.32	0.32	0.32	0.31	0.28	0.28	0.31
Fe/Fe+Mg	0.84	0.85	0.85	0.85	0.85	0.85	0.85	0.85

UND 6 - Garnet hornblende granite, Mlahlanja Suite.

	1 C	2 C	3 C	Average
SiO_2	39.47	39.39	39.74	39.53
TiO_2	1.89	1.94	1.95	1.93
Al_2O_3	11.22	11.12	10.89	11.08
Cr_2O_3	0.00	0.00	0.00	0.00
FeO	27.44	27.48	27.88	27.60
MnO	0.47	0.47	0.44	0.46
MgO	2.66	2.72	2.85	2.74
CaO	10.80	10.72	10.82	10.78
Na_2O	1.52	1.52	1.58	1.54
K_2O	1.55	1.52	1.47	1.51
H_2O	1.86	1.86	1.87	1.86
TOTAL	98.88	98.74	99.49	99.04
Formula per 24 oxygens				
Si	6.35	6.35	6.36	6.35
Al^{IV}	1.65	1.65	1.64	1.65
Al^{VI}	0.48	0.46	0.42	0.45
Ti	0.23	0.23	0.23	0.23
Mg	0.64	0.65	0.68	0.66
Fe	3.66	3.65	3.67	3.66
Fe(M4)	0.04	0.05	0.06	0.05
Mn	0.06	0.06	0.06	0.06
Ca	1.86	1.85	1.86	1.86
Na	0.04	0.03	0.02	0.03
Na(A)	0.44	0.44	0.47	0.45
K(A)	0.32	0.31	0.30	0.31
Fe/Fe+Mg	0.85	0.85	0.85	0.85

Pyroxene

UND 320 - Amphibolite, Nagle Dam Formation.

	1 C	2 C Adjacent to hornblende	Average
SiO_2	51.21	51.70	51.46
TiO_2	0.11	0.11	0.11
Al_2O_3	1.63	1.54	1.59
Cr_2O_3	0.07	0.01	0.04
FeO	9.91	9.44	9.68
MnO	0.35	0.41	0.38
MgO	13.54	13.53	13.54
CaO	21.78	22.13	21.96
Na_2O	0.40	0.39	0.40
K_2O	0.00	0.00	0.00
TOTAL	99.00	99.26	99.14
Formula per 6 oxygens			
Si	1.94	1.95	1.95
Al^{iv}	0.06	0.05	0.06
Al^{vi}	0.02	0.02	0.02
Fe	0.31	0.30	0.31
Mn	0.01	0.01	0.01
Mg	0.77	0.76	0.77
Ca	0.89	0.90	0.90
Na	0.03	0.03	0.03
Fe/Fe+Mg	0.29	0.28	0.29

UND 357 - Amphibolite, Valley Trust Formation.

	1 C	2 C	3 M	4 C	5 C	6 C	7 C	Average	Average Core
SiO_2	50.25	51.18	51.45	50.92	50.76	50.40	50.77	50.82	50.71
TiO_2	0.10	0.09	0.09	0.15	0.09	0.14	0.12	0.11	0.12
Al_2O_3	1.13	1.08	1.02	1.10	0.89	1.12	1.03	1.05	1.06
Cr_2O_3	0.00	0.00	0.00	0.00	0.00	0.01	0.00	0.00	0.00
FeO	13.86	14.14	14.33	14.03	14.29	14.36	14.20	14.17	14.15
MnO	0.24	0.28	0.31	0.32	0.31	0.30	0.30	0.29	0.29
NiO	0.02	0.02	0.03	0.00	0.00	0.02	0.00	0.01	0.01
MgO	10.88	10.88	10.87	10.87	10.90	10.65	10.75	10.83	10.82
CaO	21.60	21.71	21.69	21.77	21.81	21.71	21.90	21.74	21.75
Na_2O	0.22	0.24	0.24	0.25	0.21	0.24	0.24	0.23	0.23
K_2O	0.00	0.00	0.00	0.00	0.00	0.00	0.00	0.00	0.00
TOTAL	98.30	99.62	100.03	99.41	99.26	98.95	99.31	99.27	99.15
Formula per 6 oxygens									
Si	1.96	1.97	1.97	1.96	1.96	1.96	1.96	1.96	1.96
Al^{IV}	0.04	0.03	0.03	0.04	0.04	0.04	0.04	0.04	0.04
Al^{VI}	0.01	0.01	0.02	0.01	0.00	0.01	0.01	0.01	0.01
Fe	0.45	0.45	0.46	0.45	0.46	0.47	0.46	0.46	0.46
Mn	0.01	0.01	0.01	0.01	0.01	0.01	0.01	0.01	0.01
Mg	0.63	0.62	0.62	0.62	0.63	0.62	0.62	0.62	0.62
Ca	0.90	0.89	0.89	0.90	0.90	0.90	0.91	0.90	0.90
Na	0.02	0.02	0.02	0.02	0.02	0.02	0.02	0.02	0.02
Fe/Fe+Mg	0.42	0.42	0.43	0.42	0.42	0.43	0.43	0.43	0.43

UND 357 - Amphibolite, Valley Trust Formation.

	1 C	2 C	3 C	4 C	5 C	6 M	7 C	8 C	9 C	10 M	11 M	12 C	13 C	14 C	15 C	16 C	17 C	18 C Adjacent to cpx	19 C	20 M Adjacent to cpx	Av
SiO_2	50.37	49.94	49.62	50.25	49.68	50.06	49.68	50.02	49.49	49.73	49.91	49.65	49.88	49.63	49.20	48.71	49.77	48.73	49.41	49.32	49.65
TiO_2	0.07	0.08	0.08	0.03	0.05	0.05	0.05	0.10	0.10	0.11	0.11	0.10	0.09	0.06	0.05	0.09	0.04	0.07	0.07	0.06	0.07
Al_2O_3	0.56	0.58	0.50	0.58	0.63	0.48	0.53	0.58	0.45	0.48	0.61	0.61	0.48	0.54	0.51	0.62	0.45	0.46	0.64	0.52	0.54
Cr_2O_3	0.00	0.00	0.00	0.00	0.00	0.00	0.00	0.07	0.05	0.06	0.06	0.06	0.07	0.00	0.00	0.01	0.00	0.01	0.00	0.01	0.02
FeO	33.32	33.83	33.35	33.08	33.19	33.06	33.36	33.47	33.45	33.06	33.07	33.05	33.48	33.48	33.54	33.52	33.52	33.50	33.98	33.59	33.40
MnO	0.69	0.70	0.69	0.71	0.71	0.71	0.69	0.82	0.73	0.73	0.73	0.74	0.80	0.77	0.76	0.74	0.81	0.78	0.82	0.77	0.74
NiO	0.00	0.00	0.00	0.07	0.06	0.03	0.04	0.09	0.07	0.06	0.08	0.07	0.09	0.03	0.04	0.03	0.01	0.03	0.00	0.01	0.04
MgO	14.02	13.82	13.89	13.81	13.91	13.90	13.96	13.73	13.86	14.16	13.77	13.70	13.67	13.73	13.82	13.81	13.83	13.75	13.67	13.83	13.83
CaO	0.80	0.77	0.70	0.84	0.74	0.76	0.77	0.87	0.83	0.69	0.85	0.85	0.80	0.77	0.76	0.77	0.71	0.69	0.83	0.74	0.78
Na_2O	0.03	0.02	0.03	0.00	0.02	0.00	0.00	0.00	0.00	0.00	0.00	0.00	0.00	0.00	0.01	0.01	0.00	0.01	0.00	0.00	0.01
K_2O	0.00	0.00	0.00	0.00	0.00	0.00	0.00	0.00	0.00	0.00	0.00	0.00	0.00	0.00	0.00	0.00	0.00	0.00	0.00	0.00	0.00
TOTAL	99.86	99.75	98.86	99.37	98.99	99.05	99.08	99.75	99.03	99.08	99.19	98.83	99.36	99.01	98.69	98.31	99.14	98.03	99.42	98.85	99.08
Formula per 6 oxygens																					
Si	1.99	1.98	1.98	1.99	1.98	1.99	1.98	1.98	1.98	1.98	1.98	1.98	1.98	1.98	1.97	1.96	1.98	1.97	1.97	1.98	1.98
Al^{IV}	0.01	0.02	0.02	0.01	0.02	0.01	0.02	0.02	0.02	0.02	0.02	0.02	0.02	0.02	0.02	0.03	0.02	0.02	0.03	0.02	0.02
Al^{VI}	0.01	0.01	0.01	0.02	0.01	0.01	0.01	0.01	0.00	0.00	0.01	0.01	0.01	0.01	0.00	0.00	0.01	0.00	0.00	0.00	0.01
Fe	1.10	1.12	1.11	1.10	1.11	1.10	1.11	1.11	1.12	1.10	1.10	1.10	1.11	1.12	1.13	1.13	1.12	1.13	1.13	1.13	1.11
Mn	0.02	0.02	0.02	0.02	0.02	0.02	0.02	0.03	0.02	0.02	0.02	0.02	0.03	0.03	0.03	0.03	0.03	0.03	0.03	0.03	0.03
Mg	0.82	0.82	0.83	0.82	0.83	0.82	0.83	0.81	0.83	0.84	0.82	0.82	0.81	0.82	0.83	0.83	0.82	0.83	0.81	0.83	0.82
Ca	0.03	0.03	0.03	0.04	0.03	0.03	0.03	0.04	0.04	0.03	0.04	0.04	0.03	0.03	0.03	0.03	0.03	0.03	0.04	0.03	0.03
Fe/Fe+Mg	0.57	0.58	0.57	0.57	0.57	0.57	0.57	0.58	0.57	0.57	0.57	0.57	0.58	0.58	0.58	0.58	0.58	0.58	0.58	0.58	0.58

NDF 70 - Fine grained granulite, Valley Trust Formation.

	1 C	2 C	3 C	4 C	5 M	6 C	7 C	8 C	9 C	10 C	Average
SiO_2	47.00	46.71	46.91	46.57	46.34	46.48	45.87	46.87	46.53	45.74	46.50
TiO_2	0.06	0.04	0.07	0.06	0.06	0.07	0.06	0.04	0.06	0.05	0.06
Al_2O_3	6.26	6.56	6.33	6.42	5.88	6.53	6.44	6.09	5.93	6.09	6.25
Cr_2O_3	0.00	0.01	0.00	0.03	0.02	0.02	0.00	0.01	0.01	0.02	0.01
FeO	26.36	26.70	26.45	26.20	25.91	25.72	25.41	25.19	25.93	25.62	25.95
MnO	0.19	0.45	0.43	0.45	0.41	0.49	0.45	0.44	0.50	0.47	0.43
NiO	0.03	0.00	0.00	0.00	0.00	0.00	0.00	0.00	0.00	0.00	0.00
MgO	17.27	17.47	17.09	17.52	17.93	17.42	17.21	17.31	17.50	17.64	17.44
CaO	0.03	0.03	0.01	0.06	0.05	0.04	0.05	0.05	0.03	0.05	0.04
Na_2O	0.00	0.00	0.00	0.00	0.02	0.00	0.01	0.00	0.00	0.00	0.00
K_2O	0.00	0.00	0.00	0.00	0.00	0.00	0.00	0.00	0.00	0.00	0.00
TOTAL	97.20	97.97	97.29	97.31	96.62	96.77	95.50	96.00	96.49	95.68	96.68
Formula per 6 oxygens											
Si	1.84	1.82	1.84	1.83	1.83	1.83	1.83	1.85	1.84	1.82	1.83
Al^{IV}	0.16	0.18	0.16	0.17	0.17	0.17	0.17	0.15	0.16	0.18	0.17
Al^{VI}	0.13	0.12	0.13	0.12	0.10	0.13	0.13	0.14	0.11	0.11	0.12
Fe	0.86	0.87	0.87	0.86	0.86	0.85	0.85	0.83	0.86	0.85	0.86
Mn	0.02	0.01	0.01	0.01	0.01	0.02	0.02	0.02	0.02	0.02	0.02
Mg	1.01	1.02	1.00	1.02	1.06	1.02	1.02	1.02	1.03	1.05	1.02
Fe/Fe+Mg	0.46	0.46	0.47	0.46	0.45	0.45	0.45	0.45	0.46	0.45	0.46

NDF 67

	1 C	2 C	3 C	4 C	5 C	Average
SiO_2	48.25	48.72	48.50	48.11	48.55	48.43
TiO_2	0.05	0.04	0.04	0.05	0.04	0.04
Al_2O_3	5.27	5.71	5.71	5.67	5.23	5.52
Cr_2O_3	0.02	0.00	0.01	0.00	0.00	0.00
FeO	26.01	24.39	24.48	24.44	25.14	24.89
MnO	0.33	0.20	0.28	0.23	0.28	0.26
NiO	0.01	0.00	0.00	0.00	0.00	0.00
MgO	18.60	19.20	18.75	19.22	19.12	18.98
CaO	0.04	0.02	0.03	0.03	0.03	0.03
Na_2O	0.00	0.00	0.00	0.00	0.00	0.00
K_2O	0.00	0.00	0.00	0.00	0.00	0.00
TOTAL	98.58	98.28	97.80	97.75	98.39	98.16
Formula per 6 oxygens						
Si^{IV}	1.86	1.86	1.87	1.85	1.87	1.86
Al^{IV}	0.14	0.14	0.13	0.15	0.13	0.14
Al^{VI}	0.10	0.12	0.13	0.11	0.10	0.11
Fe	0.84	0.78	0.79	0.79	0.81	0.80
Mn	0.01	0.01	0.01	0.01	0.01	0.01
Mg	1.07	1.09	1.08	1.10	1.09	1.09
Fe/Fe+Mg	0.44	0.42	0.42	0.42	0.43	0.42

NDF 67a - Fine grained granulite, Valley Trust Formation.

	1 C Assoc with garnet	2 C Assoc with garnet	3 C Assoc with garnet	4 C Assoc with garnet	5 C Assoc with garnet	6 C Assoc with garnet	7 C Assoc with garnet	8 C Assoc with garnet	9 C From biotite poor zone
SiO_2	49.17	48.25	48.56	48.93	48.95	48.39	47.77	47.29	48.26
TiO_2	0.07	0.07	0.07	0.05	0.08	0.18	0.12	0.05	0.09
Al_2O_3	6.54	6.51	6.70	6.61	6.53	6.04	6.51	6.54	6.41
Cr_2O_3	0.02	0.00	0.00	0.00	0.01	0.00	0.00	0.01	0.01
FeO	23.15	24.15	23.55	23.20	23.09	23.65	24.47	23.97	24.82
MnO	0.10	0.14	0.09	0.12	0.10	0.15	0.15	0.19	0.21
NiO	0.00	0.00	0.00	0.00	0.00	0.00	0.00	0.00	0.01
MgO	20.30	19.70	19.96	20.32	20.30	20.20	19.41	20.05	19.22
CaO	0.03	0.03	0.03	0.03	0.03	0.02	0.02	0.02	0.03
Na_2O	0.01	0.01	0.01	0.00	0.02	0.00	0.00	0.00	0.00
K_2O	0.00	0.00	0.00	0.00	0.00	0.00	0.00	0.00	0.00
TOTAL	99.39	98.86	98.97	99.26	99.11	98.63	98.45	98.12	99.05
Formula per 6 oxygens									
Si	1.85	1.83	1.84	1.84	1.84	1.84	1.83	1.81	1.84
AlIV	0.15	0.17	0.16	0.16	0.16	0.16	0.17	0.19	0.16
AlVI	0.14	0.13	0.14	0.13	0.13	0.11	0.12	0.11	0.12
Ti	0.00	0.00	0.00	0.00	0.00	0.01	0.00	0.00	0.00
Fe	0.73	0.77	0.75	0.73	0.73	0.75	0.78	0.77	0.79
Mn	0.00	0.00	0.00	0.00	0.00	0.00	0.00	0.01	0.01
Mg	1.14	1.12	1.13	1.14	1.14	1.15	1.11	1.15	1.09
Fe/Fe+Mg	0.39	0.41	0.40	0.39	0.39	0.39	0.41	0.40	0.42

Table continued.

10 C From biotite poor zone	11 C From biotite poor zone	12 C From biotite poor zone	13 C From biotite rich zone	14 C From biotite rich zone	Average	Average (Associated with garnet)	Average (No associated biotite)	Average (Associated biotite)
48.11	48.34	47.44	47.49	48.22	48.23	48.41	48.04	47.86
0.05	0.05	0.06	0.06	0.07	0.08	0.09	0.06	0.07
6.38	6.25	6.37	6.37	6.25	6.43	6.50	6.35	6.31
0.00	0.02	0.01	0.01	0.00	0.01	0.00	0.01	0.01
24.54	24.20	24.91	24.70	24.64	24.07	23.65	24.62	24.67
0.18	0.20	0.25	0.26	0.29	0.17	0.13	0.21	0.28
0.01	0.00	0.00	0.00	0.00	0.00	0.00	0.01	0.00
19.45	19.37	19.06	19.33	19.35	19.71	20.03	19.28	19.34
0.01	0.02	0.03	0.03	0.03	0.03	0.03	0.02	0.03
0.00	0.00	0.00	0.00	0.00	0.00	0.01	0.00	0.00
0.00	0.00	0.00	0.00	0.00	0.00	0.00	0.00	0.00
98.73	98.45	98.13	98.25	98.85	98.73	98.85	98.59	98.56
1.84	1.85	1.83	1.83	1.84	1.84	1.84	1.84	1.84
0.16	0.15	0.17	0.17	0.16	0.16	0.17	0.16	0.17
0.12	0.13	0.12	0.11	0.12	0.12	0.13	0.12	0.12
0.00	0.00	0.00	0.00	0.00	0.00	0.00	0.00	0.00
0.78	0.77	0.80	0.79	0.79	0.77	0.75	0.79	0.79
0.01	0.01	0.01	0.01	0.01	0.01	0.00	0.01	0.01
1.11	1.10	1.09	1.11	1.10	1.12	1.14	1.10	1.11
0.41	0.41	0.42	0.42	0.42	0.41	0.40	0.42	0.42

UND 74 - Charnockite, Mlahlanja Suite.

	1 C	2 C
SiO_2	46.16	46.14
TiO_2	0.06	0.05
Al_2O_3	0.46	0.46
Cr_2O_3	0.00	0.00
FeO	43.14	43.20
MnO	1.49	1.56
NiO	0.02	0.00
MgO	5.28	5.16
CaO	0.83	0.82
Na_2O	0.00	0.00
K_2O	0.00	0.00
TOTAL	97.44	97.39
Formula per 6 oxygens		
Si^{IV}	1.99	1.99
Al^{IV}	0.01	0.01
Al^{VI}	0.01	0.01
Fe	1.55	1.56
Mn	0.05	0.06
Mg	0.34	0.33
Ca	0.04	0.04
Fe/Fe+Mg	0.82	0.83

Garnet

NDF 8 - Pelitic gneiss, Nagle Dam Formation.

	1 C	2 C	3 C	4 C	5 C	6 C	7 C	8 C	9 C	10 C	11 C
SiO_2	37.51	37.63	37.49	37.62	38.13	38.11	37.52	37.55	37.63	37.68	37.53
TiO_2	0.00	0.00	0.00	0.00	0.00	0.00	0.00	0.01	0.00	0.00	0.00
Al_2O_3	20.84	20.55	20.79	20.95	20.44	20.86	21.13	20.96	21.13	20.31	21.00
Cr_2O_3	0.00	0.00	0.00	0.00	0.00	0.00	0.00	0.00	0.00	0.00	0.00
FeO	30.22	30.24	30.17	30.10	30.29	30.87	30.18	31.00	31.28	31.65	30.84
MnO	4.80	5.03	5.00	4.71	4.93	5.00	4.88	4.63	4.56	5.59	4.66
MgO	4.45	4.16	4.22	4.42	4.45	4.32	4.21	4.62	4.36	3.49	4.29
CaO	1.62	1.56	1.78	1.80	1.74	1.69	1.90	1.85	1.72	1.66	1.66
TOTAL	99.44	99.17	99.45	99.60	99.98	100.85	99.82	100.62	100.68	100.38	99.98
Formula per 24 oxygens											
Si	6.02	6.06	6.02	6.02	6.09	6.04	6.00	5.97	5.98	6.05	6.00
Al^{IV}	0.00	0.00	0.00	0.00	0.00	0.00	0.00	0.03	0.02	0.00	0.00
Al^{VI}	3.94	3.90	3.94	3.95	3.84	3.90	3.98	3.90	3.94	3.84	3.96
Fe	4.05	4.07	4.05	4.03	4.04	4.09	4.04	4.12	4.16	4.25	4.12
Mn	0.65	0.69	0.68	0.64	0.67	0.67	0.66	0.62	0.61	0.76	0.63
Mg	1.06	1.00	1.01	1.05	1.06	1.02	1.00	1.10	1.03	0.83	1.02
Ca	0.28	0.27	0.31	0.31	0.30	0.29	0.33	0.31	0.29	0.28	0.28
Alm	0.671	0.675	0.670	0.668	0.666	0.674	0.670	0.670	0.683	0.694	0.681
Py	0.175	0.166	0.167	0.174	0.175	0.168	0.166	0.179	0.169	0.136	0.169
Spess	0.108	0.114	0.112	0.106	0.110	0.110	0.109	0.101	0.100	0.124	0.104
Gross	0.046	0.045	0.051	0.052	0.049	0.048	0.055	0.050	0.048	0.046	0.046

Table continued.

12 C	13 C Adjacent to biotite	14 M Adjacent to biotite	15 C	16 C	17 C	18 M Adjacent to biotite	19 C	Average	Average Core	Average Margin
37.60	37.02	34.79	36.84	37.63	37.47	35.25	36.77	37.25	37.51	35.02
0.01	0.02	0.01	0.01	0.00	0.01	0.01	0.00	0.00	0.00	0.00
20.93	20.13	21.75	20.73	20.96	20.70	21.12	20.91	20.85	20.78	21.43
0.00	0.00	0.00	0.00	0.00	0.00	0.00	0.00	0.00	0.00	0.00
31.48	32.56	31.48	32.03	31.59	31.37	32.03	31.81	31.12	31.04	31.75
4.47	4.43	7.72	4.49	4.59	4.16	6.12	4.12	4.94	4.71	6.92
4.59	4.17	1.73	4.45	4.37	4.42	2.66	4.57	4.10	4.33	2.20
1.67	1.88	1.81	1.80	1.78	1.83	1.83	1.71	1.75	1.74	1.82
100.75	100.21	99.29	100.35	100.92	99.96	99.02	99.89	100.02	100.12	99.16
5.98	5.97	5.74	5.91	5.98	6.00	5.80	5.91	5.98	6.00	5.77
0.02	0.03	0.26	0.09	0.02	0.00	0.20	0.09	0.04	0.02	0.23
3.90	3.79	3.97	3.84	3.90	3.91	3.90	3.88	3.90	3.90	3.94
4.19	4.39	4.34	4.30	4.20	4.20	4.41	4.28	4.18	4.15	4.38
0.60	0.61	1.08	0.61	0.62	0.56	0.85	0.56	0.67	0.64	0.97
1.09	1.00	0.43	1.07	1.04	1.05	0.65	1.09	0.98	1.03	0.54
0.29	0.32	0.32	0.31	0.30	0.31	0.32	0.29	0.30	0.30	0.32
0.679	0.695	0.703	0.684	0.682	0.686	0.708	0.688	0.682	0.678	0.705
0.177	0.158	0.070	0.170	0.169	0.172	0.104	0.175	0.160	0.168	0.087
0.097	0.096	0.175	0.097	0.100	0.091	0.137	0.090	0.109	0.105	0.156
0.047	0.051	0.052	0.049	0.049	0.051	0.051	0.047	0.049	0.049	0.052

NDF 56 - Pelitic gneiss, Valley Trust Formation.

	1 C	2 M	3 M Adjacent to biotite	4 C	5 C	6 C	7 C	8 C	9 C	10 C	11 C	12 C	13 C	14 C
SiO_2	37.39	37.49	37.63	37.75	37.28	36.90	36.82	37.34	37.32	37.47	37.58	36.77	36.93	37.03
TiO_2	0.05	0.00	0.02	0.02	0.06	0.04	0.01	0.02	0.01	0.02	0.00	0.01	0.02	0.01
Al_2O_3	21.42	21.49	21.77	21.45	21.31	21.22	21.25	21.35	21.29	21.41	20.85	21.24	21.29	21.49
Cr_2O_3	0.07	0.07	0.06	0.08	0.04	0.06	0.03	0.06	0.08	0.04	0.00	0.00	0.00	0.00
FeO	32.02	32.29	32.10	32.06	32.31	32.63	33.71	32.35	32.40	32.74	33.48	34.65	33.00	33.80
MnO	0.66	0.61	0.67	0.63	0.65	0.62	0.71	0.69	0.64	0.71	0.62	0.67	0.67	0.61
MgO	6.34	6.61	6.31	6.30	6.36	6.54	5.77	6.45	6.42	6.36	5.85	4.98	6.21	5.79
CaO	1.15	0.96	1.02	1.05	1.18	1.04	0.95	1.02	0.91	0.93	0.89	0.86	1.13	0.88
TOTAL	99.10	99.52	99.58	99.34	99.19	99.05	99.25	99.28	99.07	99.68	99.27	99.18	99.25	99.61
Formula per 24 oxygens														
Si	5.95	5.94	5.95	5.98	5.94	5.90	5.90	5.94	5.95	5.94	6.00	5.92	5.90	5.91
Al^{IV}	0.05	0.06	0.05	0.02	0.06	0.10	0.10	0.06	0.05	0.06	0.00	0.08	0.10	0.09
Al^{VI}	3.97	3.95	4.01	3.99	3.94	3.90	3.92	3.94	3.95	3.95	3.93	3.96	3.91	3.95
Ti	0.01	0.00	0.00	0.00	0.01	0.01	0.00	0.00	0.00	0.00	0.00	0.00	0.00	0.00
Cr	0.01	0.01	0.01	0.01	0.01	0.01	0.00	0.01	0.01	0.00	0.00	0.00	0.00	0.00
Fe	4.26	4.28	4.24	4.25	4.30	4.36	4.52	4.30	4.32	4.34	4.47	4.67	4.41	4.51
Mn	0.09	0.08	0.09	0.08	0.09	0.08	0.10	0.09	0.09	0.09	0.08	0.09	0.09	0.08
Mg	1.50	1.56	1.49	1.49	1.51	1.56	1.38	1.53	1.52	1.50	1.39	1.19	1.48	1.38
Ca	0.20	0.16	0.17	0.18	0.20	0.18	0.16	0.17	0.15	0.16	0.15	0.15	0.19	0.15
Alm	0.704	0.704	0.708	0.709	0.705	0.706	0.734	0.706	0.710	0.713	0.734	0.765	0.715	0.737
Py	0.248	0.257	0.249	0.248	0.247	0.252	0.224	0.251	0.250	0.246	0.228	0.195	0.240	0.225
Spess	0.015	0.013	0.015	0.013	0.015	0.013	0.016	0.015	0.015	0.015	0.013	0.015	0.014	0.013
Gross	0.033	0.026	0.028	0.030	0.033	0.029	0.026	0.028	0.025	0.026	0.025	0.025	0.031	0.025

Table continued.

15 C	16 C	17 C	18 M	19 C	20 C	21 C	22 C	23 M Adjacent to biotite	24 C	25 C	26 M Adjacent to biotite	27 M Adjacent to biotite	28 C	Average	Average Core	Average Margin
36.39	37.58	37.48	37.38	37.50	37.76	37.64	37.86	37.56	37.63	38.09	36.82	37.70	37.92	37.39	37.38	37.43
0.00	0.09	0.07	0.00	0.04	0.03	0.04	0.00	0.03	0.03	0.01	0.04	0.02	0.02	0.03	0.03	0.02
21.56	21.31	21.29	21.98	21.18	21.30	21.29	21.19	21.45	21.37	20.73	21.48	21.18	21.28	21.34	21.28	21.56
0.00	0.00	0.00	0.00	0.00	0.00	0.00	0.00	0.00	0.00	0.00	0.00	0.00	0.00	0.02	0.02	0.02
34.69	32.88	32.84	33.95	32.79	33.14	32.90	32.99	33.05	32.90	32.64	33.60	32.59	32.66	32.97	32.98	32.93
0.67	0.62	0.62	0.62	0.64	0.65	0.64	0.67	0.67	0.68	0.69	0.68	0.69	0.62	0.65	0.65	0.66
4.99	6.37	6.26	6.13	6.21	6.33	6.23	6.38	6.16	6.23	6.28	5.76	6.35	6.29	6.15	6.13	6.22
0.85	1.23	1.23	0.84	1.11	1.07	1.01	0.91	0.91	0.93	0.84	0.89	0.84	0.96	0.99	1.01	0.91
99.15	100.08	99.79	100.90	99.47	100.28	99.75	100.00	99.83	99.77	99.28	99.27	99.37	99.75	99.54	99.48	99.73
5.87	5.94	5.94	5.88	5.96	5.96	5.97	5.98	5.95	5.96	6.05	5.89	5.99	6.00	5.95	5.95	5.93
0.13	0.06	0.06	0.12	0.04	0.04	0.03	0.02	0.05	0.04	0.00	0.11	0.01	0.00	0.06	0.05	0.07
3.97	3.91	3.92	3.95	3.93	3.92	3.94	3.93	3.96	3.95	3.88	3.95	3.95	3.96	3.94	3.94	3.96
0.00	0.01	0.01	0.00	0.01	0.00	0.00	0.00	0.00	0.00	0.00	0.00	0.00	0.00	0.00	0.00	0.00
0.00	0.00	0.00	0.00	0.00	0.00	0.00	0.00	0.00	0.00	0.00	0.00	0.00	0.00	0.00	0.00	0.00
4.68	4.35	4.35	4.47	4.36	4.37	4.36	4.36	4.38	4.36	4.34	4.50	4.33	4.32	4.38	4.39	4.37
0.09	0.08	0.08	0.08	0.09	0.09	0.09	0.09	0.09	0.09	0.09	0.09	0.09	0.08	0.09	0.09	0.09
1.20	1.50	1.48	1.44	1.47	1.49	1.47	1.50	1.46	1.47	1.49	1.38	1.50	1.48	1.46	1.45	1.47
0.15	0.21	0.21	0.14	0.19	0.18	0.17	0.15	0.15	0.16	0.14	0.15	0.14	0.16	0.17	0.17	0.15
0.765	0.709	0.711	0.729	0.713	0.713	0.716	0.715	0.720	0.717	0.716	0.735	0.714	0.715	0.718	0.719	0.719
0.196	0.244	0.242	0.235	0.241	0.243	0.241	0.246	0.240	0.242	0.246	0.225	0.248	0.245	0.239	0.238	0.242
0.015	0.013	0.013	0.013	0.015	0.015	0.015	0.015	0.015	0.015	0.015	0.015	0.015	0.013	0.015	0.015	0.015
0.024	0.034	0.034	0.023	0.031	0.029	0.028	0.024	0.025	0.026	0.023	0.025	0.023	0.027	0.028	0.028	0.024

UND 374 - Pelitic gneiss, Valley Trust Formation.

	1 C	2 C	3 C	4 C	5 C	6 C	7 C	8 C	9 C	10 C	Average
SiO_2	37.09	37.48	36.89	37.46	36.57	36.93	37.22	37.16	37.16	37.49	37.15
TiO_2	0.01	0.02	0.02	0.04	0.03	0.02	0.03	0.04	0.03	0.02	0.03
Al_2O_3	21.47	21.61	20.79	21.37	21.05	21.42	21.21	21.04	21.16	21.17	21.23
Cr_2O_3	0.01	0.02	0.02	0.01	0.02	0.02	0.03	0.02	0.00	0.05	0.02
FeO	34.47	34.13	34.57	34.43	34.36	34.41	34.00	33.80	33.74	33.88	34.18
MnO	1.12	1.07	0.90	1.04	1.03	1.05	1.07	0.96	1.02	0.98	1.02
MgO	4.44	4.66	4.54	4.65	4.57	4.54	4.66	4.70	4.74	4.69	4.62
CaO	1.13	1.32	1.21	1.14	1.22	1.23	1.18	1.40	1.24	1.16	1.22
TOTAL	99.74	100.31	98.94	100.14	98.85	99.62	99.40	99.12	99.09	99.44	99.47
Formula per 24 oxygens											
Si	5.94	5.96	5.97	5.97	5.92	5.93	5.97	5.98	5.98	6.00	5.96
Al^{IV}	0.06	0.04	0.03	0.03	0.08	0.07	0.03	0.02	0.02	0.00	0.04
Al^{VI}	4.00	4.00	3.93	3.98	3.94	3.98	3.98	3.97	3.99	4.00	3.98
Ti	0.00	0.00	0.00	0.01	0.00	0.00	0.00	0.01	0.00	0.00	0.00
Cr	0.00	0.00	0.00	0.00	0.00	0.00	0.00	0.00	0.00	0.01	0.00
Fe	4.62	4.54	4.68	4.59	4.66	4.62	4.56	4.55	4.54	4.54	4.59
Mn	0.15	0.14	0.12	0.14	0.14	0.14	0.15	0.13	0.14	0.13	0.14
Mg	1.06	1.10	1.10	1.11	1.10	1.09	1.12	1.13	1.14	1.12	1.11
Ca	0.19	0.23	0.21	0.20	0.21	0.21	0.20	0.24	0.21	0.20	0.21
Alm	0.767	0.756	0.766	0.760	0.763	0.762	0.756	0.752	0.753	0.758	0.759
Py	0.176	0.183	0.180	0.184	0.180	0.180	0.186	0.187	0.189	0.187	0.183
Spess	0.025	0.023	0.020	0.023	0.023	0.023	0.025	0.021	0.023	0.022	0.023
Gross	0.032	0.038	0.034	0.033	0.034	0.035	0.033	0.040	0.035	0.033	0.035

NDF 92A - Garnet granite.

	1 C	2 C	3 C	4 C	5 C	6 C	7 C	8 C	9 C	10 C	Average
SiO_2	37.28	37.55	37.12	37.45	37.66	36.99	37.18	36.87	36.87	37.41	37.24
TiO_2	0.03	0.03	0.02	0.01	0.03	0.01	0.02	0.00	0.03	0.00	0.02
Al_2O_3	21.70	21.34	21.51	21.45	21.36	21.47	21.69	21.59	21.64	21.65	21.54
Cr_2O_3	0.05	0.04	0.06	0.04	0.06	0.03	0.04	0.03	0.07	0.05	0.05
FeO	34.03	34.18	33.98	34.21	34.19	34.42	34.34	34.22	33.79	34.17	34.15
MnO	1.05	0.97	1.02	1.12	1.09	1.23	1.19	1.17	1.06	1.15	1.11
MgO	4.96	5.05	5.00	5.01	4.84	4.43	4.87	5.05	5.02	4.92	4.92
CaO	1.10	1.08	1.11	1.09	1.10	1.04	1.05	1.02	0.98	0.89	1.05
TOTAL	100.20	100.24	99.82	100.38	100.33	99.62	100.38	99.95	99.46	100.24	100.06
Formula per 24 oxygens											
Si	5.93	5.97	5.93	5.95	5.98	5.94	5.91	5.89	5.91	5.95	5.94
Al^{IV}	0.07	0.03	0.07	0.05	0.02	0.06	0.09	0.11	0.09	0.05	0.07
Al^{VI}	3.99	3.97	3.98	3.97	3.98	4.00	3.98	3.96	3.99	4.00	3.98
Ti	0.00	0.00	0.00	0.00	0.00	0.00	0.00	0.00	0.00	0.00	0.00
Cr	0.01	0.01	0.01	0.01	0.01	0.00	0.01	0.00	0.01	0.01	0.01
Fe	4.53	4.54	4.54	4.55	4.54	4.62	4.57	4.57	4.53	4.54	4.55
Mn	0.14	0.13	0.14	0.15	0.15	0.17	0.16	0.16	0.14	0.16	0.15
Mg	1.18	1.20	1.19	1.19	1.15	1.06	1.16	1.20	1.20	1.17	1.17
Ca	0.19	0.18	0.19	0.19	0.19	0.18	0.18	0.18	0.17	0.15	0.18
Alm	0.750	0.750	0.749	0.748	0.753	0.766	0.753	0.748	0.750	0.754	0.752
Py	0.195	0.198	0.197	0.196	0.191	0.176	0.191	0.196	0.199	0.194	0.193
Spess	0.023	0.022	0.023	0.025	0.025	0.028	0.026	0.026	0.023	0.027	0.025
Gross	0.032	0.030	0.031	0.031	0.031	0.030	0.030	0.030	0.028	0.025	0.030

UND 93 - Garnet granite.

	1 C	2 C	3 C	4 C	5 C	6 C	7 C	8 C	9 C	10 C	Average
SiO_2	36.74	36.65	36.55	37.10	37.29	36.41	36.81	36.50	36.65	37.12	36.78
TiO_2	0.03	0.00	0.03	0.03	0.01	0.01	0.04	0.01	0.01	0.00	0.02
Al_2O_3	20.98	20.86	20.89	21.06	21.19	20.71	20.96	20.86	21.01	21.17	20.97
Cr_2O_3	0.02	0.00	0.00	0.00	0.00	0.00	0.00	0.00	0.00	0.00	0.00
FeO	35.24	35.59	35.84	35.58	35.18	35.02	34.94	34.75	35.24	35.35	35.27
MnO	1.09	1.11	1.03	0.98	1.05	1.16	1.03	0.97	1.07	1.00	1.05
MgO	3.34	3.38	3.37	3.46	3.56	3.49	3.50	3.43	3.53	3.65	3.47
CaO	1.88	1.90	1.89	2.03	2.12	2.04	2.32	2.34	2.25	1.95	2.07
TOTAL	99.32	99.49	99.60	100.24	100.40	98.84	99.60	98.86	99.76	100.24	99.64
Formula per 24 oxygens											
Si	5.96	5.95	5.93	5.96	5.97	5.94	5.95	5.94	5.92	5.96	5.95
Al^{IV}	0.04	0.06	0.07	0.04	0.03	0.06	0.05	0.06	0.08	0.05	0.05
Al^{VI}	3.97	3.93	3.92	3.95	3.97	3.92	3.94	3.95	3.93	3.96	3.94
Ti	0.00	0.00	0.00	0.00	0.00	0.00	0.01	0.00	0.00	0.00	0.00
Cr	0.00	0.00	0.00	0.00	0.00	0.00	0.00	0.00	0.00	0.00	0.00
Fe	4.78	4.83	4.86	4.78	4.71	4.78	4.72	4.73	4.76	4.74	4.77
Mn	0.15	0.15	0.14	0.13	0.14	0.16	0.14	0.13	0.15	0.14	0.14
Mg	0.81	0.82	0.82	0.83	0.85	0.85	0.84	0.83	0.85	0.87	0.84
Ca	0.33	0.33	0.33	0.35	0.36	0.36	0.40	0.41	0.39	0.34	0.36
Alm	0.788	0.788	0.790	0.785	0.777	0.777	0.774	0.776	0.774	0.778	0.781
Py	0.133	0.134	0.133	0.136	0.140	0.138	0.138	0.136	0.138	0.143	0.137
Spess	0.025	0.024	0.023	0.021	0.023	0.026	0.023	0.021	0.025	0.023	0.023
Gross	0.054	0.054	0.054	0.058	0.060	0.059	0.065	0.067	0.063	0.056	0.059

NDF 70 - Fine grained granulite, Valley Trust Formation.

	1 C	2 C	3 C	4 M Adjacent to biotite	5 C	6 M Adjacent to biotite	7 M Adjacent to biotite	8 C	9 C	10 C	11 C	Average	Average Core	Average Margin
SiO_2	38.62	37.91	40.52	41.35	40.12	38.05	38.88	38.66	38.39	38.59	38.37	39.04	38.90	39.43
TiO_2	0.00	0.01	0.01	0.01	0.00	0.01	0.00	0.00	0.00	0.00	0.00	0.00	0.00	0.00
Al_2O_3	21.29	21.43	20.80	20.83	20.89	21.10	21.13	21.64	21.44	21.52	21.75	21.26	21.34	21.02
Cr_2O_3	0.00	0.00	0.00	0.00	0.00	0.00	0.00	0.00	0.00	0.00	0.00	0.00	0.00	0.00
FeO	29.63	29.63	29.17	28.18	29.27	31.63	31.69	29.88	29.67	29.86	29.88	29.86	29.62	30.50
MnO	1.18	1.29	1.27	1.18	1.24	1.45	1.40	1.19	1.13	1.19	1.19	1.25	1.21	1.34
MgO	8.92	8.79	8.03	8.13	8.63	7.09	7.07	8.64	8.82	8.64	8.48	8.29	8.62	7.43
CaO	1.08	1.08	1.11	1.07	1.14	1.16	1.10	1.04	1.10	1.12	1.03	1.09	1.09	1.11
TOTAL	100.72	100.14	100.91	100.75	101.29	100.49	101.27	101.05	100.55	100.92	100.70	100.80	100.79	100.84
Formula per 24 oxygens														
Si	5.98	5.91	6.22	6.31	6.14	5.97	6.04	5.96	5.95	5.96	5.94	6.03	6.01	6.11
Al^{IV}	0.02	0.09	0.00	0.00	0.00	0.03	0.00	0.04	0.05	0.04	0.06	0.03	0.04	0.01
Al^{VI}	3.86	3.85	3.76	3.74	3.77	3.88	3.87	3.90	3.87	3.88	3.91	3.84	3.85	3.83
Fe	3.83	3.87	3.74	3.59	3.75	4.15	4.12	3.86	3.85	3.86	3.87	3.86	3.83	3.95
Mn	0.15	0.17	0.16	0.15	0.16	0.19	0.18	0.16	0.15	0.16	0.16	0.16	0.16	0.17
Mg	2.06	2.04	1.84	1.85	1.97	1.66	1.64	1.99	2.04	1.99	1.96	1.91	1.99	1.72
Ca	0.18	0.18	0.18	0.18	0.19	0.19	0.18	0.17	0.18	0.18	0.17	0.18	0.18	0.18
Alm	0.616	0.618	0.632	0.622	0.618	0.670	0.673	0.625	0.619	0.624	0.628	0.632	0.622	0.655
Py	0.331	0.326	0.311	0.321	0.325	0.268	0.268	0.322	0.328	0.321	0.318	0.313	0.323	0.286
Spess	0.024	0.027	0.027	0.026	0.026	0.031	0.030	0.026	0.024	0.026	0.026	0.026	0.026	0.029
Gross	0.029	0.029	0.030	0.031	0.031	0.031	0.029	0.027	0.029	0.029	0.028	0.029	0.029	0.030

NDF 67a - Fine grained granulite, Valley Trust Formation.

	1 C	2 C	3 C	4 C	5 C	6 C	7 C	8 C	9 C	10 C	11 C	12 C	13 C	14 C	15 C
SiO_2	39.20	39.43	38.73	39.21	39.07	39.13	38.82	38.84	39.08	39.05	39.13	39.19	39.08	39.20	39.15
TiO_2	0.01	0.01	0.01	0.00	0.00	0.01	0.00	0.01	0.01	0.01	0.02	0.01	0.00	0.00	0.00
Al_2O_3	22.22	22.53	22.32	22.19	22.26	22.33	22.22	22.19	22.43	22.33	22.22	22.28	21.81	22.11	22.05
Cr_2O_3	0.01	0.01	0.01	0.00	0.01	0.00	0.00	0.01	0.01	0.01	0.01	0.00	0.00	0.00	0.01
FeO	27.54	27.51	29.33	28.44	29.19	26.38	27.46	28.92	28.05	27.91	27.83	28.09	27.71	28.04	28.13
MnO	0.45	0.46	0.41	0.44	0.40	0.42	0.42	0.58	0.58	0.53	0.49	0.44	0.47	0.53	0.50
MgO	10.41	10.32	9.02	9.12	8.96	10.51	9.84	9.60	9.91	9.82	9.95	9.72	9.87	9.40	9.63
CaO	0.62	0.62	0.62	0.56	0.59	0.58	0.58	0.61	0.65	0.65	0.61	0.65	0.66	0.65	0.64
TOTAL	100.46	100.89	100.45	99.96	100.48	99.36	99.34	100.76	100.72	100.31	100.26	100.38	99.60	99.93	100.11
Formula per 24 oxygens															
Si	5.98	5.98	5.96	6.03	6.00	6.00	5.99	5.95	5.96	5.98	5.99	6.00	6.02	6.03	6.01
Al^{IV}	0.02	0.02	0.04	0.00	0.00	0.00	0.01	0.05	0.04	0.02	0.01	0.00	0.00	0.00	0.00
Al^{VI}	3.98	4.01	4.01	4.02	4.03	4.04	4.03	3.96	4.00	4.01	4.00	4.02	3.96	4.01	3.99
Fe	3.51	3.49	3.78	3.66	3.75	3.38	3.54	3.71	3.58	3.57	3.56	3.59	3.57	3.61	3.61
Mn	0.06	0.06	0.05	0.06	0.05	0.05	0.05	0.08	0.07	0.07	0.06	0.06	0.06	0.07	0.06
Mg	2.37	2.33	2.07	2.09	2.05	2.40	2.26	2.19	2.25	2.24	2.27	2.22	2.27	2.15	2.20
Ca	0.10	0.10	0.10	0.09	0.10	0.10	0.10	0.10	0.11	0.11	0.10	0.11	0.11	0.11	0.11
Alm	0.581	0.583	0.630	0.621	0.630	0.570	0.595	0.610	0.596	0.596	0.594	0.600	0.594	0.608	0.604
Py	0.392	0.390	0.345	0.354	0.345	0.405	0.380	0.360	0.374	0.374	0.379	0.371	0.378	0.362	0.368
Spess	0.010	0.010	0.008	0.010	0.008	0.008	0.008	0.013	0.012	0.012	0.010	0.010	0.010	0.012	0.010
Gross	0.017	0.017	0.017	0.015	0.017	0.017	0.017	0.017	0.018	0.018	0.017	0.019	0.018	0.018	0.018

Table continued.

16 C	17 M	18 M Adjacent to opx	19 M	20 M Adjacent to opx	21 M Adjacent to biotite	22 M	23 M	24 M	25 M	26 M	27 M	28 M	Average core	Average Margin	Average (Assoc. with opx)	Average (Assoc. with bio)
38.92	38.50	38.67	38.71	38.38	39.08	38.66	39.19	39.03	38.94	39.11	39.01	38.67	39.08	38.83	38.56	38.96
0.00	0.01	0.02	0.04	0.01	0.03	0.01	0.00	0.01	0.01	0.01	0.01	0.01	0.01	0.01	0.02	0.01
21.96	22.36	22.17	22.35	21.96	22.09	22.03	22.17	22.22	22.23	22.49	22.39	21.91	22.22	22.20	22.21	22.19
0.00	0.01	0.00	0.01	0.02	0.00	0.00	0.00	0.00	0.00	0.00	0.00	0.01	0.01	0.00	0.01	0.00
27.06	28.87	28.69	28.42	29.55	30.09	30.12	27.30	30.40	29.11	29.28	28.69	28.96	27.97	29.12	28.89	29.24
0.42	0.53	0.55	0.61	0.63	0.45	0.47	0.44	0.49	0.54	0.56	0.50	0.50	0.47	0.52	0.58	0.49
10.23	9.17	9.86	10.09	8.70	8.37	8.23	10.27	7.79	9.34	8.86	9.22	9.43	9.77	9.11	9.45	8.94
0.63	0.66	0.65	0.64	0.65	0.60	0.64	0.66	0.61	0.61	0.60	0.63	0.65	0.62	0.63	0.65	0.62
99.22	100.11	100.61	100.87	99.90	100.71	100.16	100.03	100.55	100.78	100.91	100.45	100.14	100.14	100.43	100.37	100.46
6.00	5.94	5.93	5.92	5.96	6.02	5.99	6.00	6.03	5.97	5.99	5.98	5.97	5.99	5.98	5.94	5.99
0.00	0.06	0.07	0.08	0.04	0.00	0.01	0.00	0.00	0.03	0.01	0.02	0.03	0.01	0.03	0.06	0.01
3.99	4.01	3.94	3.94	3.98	4.01	4.02	4.00	4.04	3.99	4.04	4.03	3.95	4.00	4.00	3.97	4.01
3.49	3.73	3.68	3.63	3.84	3.87	3.90	3.50	3.93	3.73	3.75	3.68	3.74	3.59	3.75	3.72	3.76
0.05	0.07	0.07	0.08	0.08	0.06	0.06	0.06	0.06	0.07	0.07	0.07	0.06	0.06	0.07	0.08	0.06
2.35	2.11	2.26	2.30	2.01	1.92	1.90	2.34	1.79	2.13	2.02	2.11	2.17	2.23	2.09	2.17	2.05
0.10	0.11	0.11	0.10	0.11	0.10	0.11	0.11	0.10	0.10	0.10	0.10	0.10	0.10	0.10	0.11	0.10
0.583	0.620	0.601	0.594	0.636	0.650	0.653	0.583	0.669	0.618	0.631	0.617	0.616	0.600	0.624	0.612	0.630
0.392	0.350	0.369	0.377	0.333	0.323	0.318	0.389	0.304	0.353	0.340	0.354	0.358	0.373	0.348	0.357	0.343
0.008	0.012	0.012	0.013	0.013	0.010	0.010	0.010	0.010	0.012	0.012	0.012	0.010	0.010	0.012	0.013	0.010
0.017	0.018	0.018	0.016	0.018	0.017	0.019	0.018	0.017	0.017	0.017	0.017	0.016	0.017	0.017	0.018	0.017

NDF 69 - Fine grained granulite, Valley Trust Formation.

	1 C	2 C	3 C	4 C	5 C	6 C Isolated garnet	7 C Isolated garnet	8 C Isolated garnet	9 C Main band	10 C Main band	11 C Main band	12 C Main band	13 C Main band	14 M Main band	15 C Main band	16 M Main band	17 C Main band	18 C Main band
SiO_2	38.91	38.25	38.21	38.81	38.77	39.14	38.70	38.24	38.90	38.73	38.79	38.64	38.52	38.70	38.41	38.60	38.53	38.05
TiO_2	0.00	0.00	0.00	0.00	0.00	0.02	0.02	0.02	0.02	0.00	0.00	0.00	0.01	0.03	0.01	0.00	0.01	0.02
Al_2O_3	22.17	22.42	22.26	22.35	22.28	22.23	22.14	21.90	22.25	22.30	22.27	22.09	21.89	21.91	21.94	21.89	21.89	22.05
Cr_2O_3	0.04	0.05	0.01	0.01	0.01	0.02	0.01	0.02	0.00	0.00	0.00	0.00	0.01	0.00	0.01	0.01	0.01	0.00
FeO	28.72	29.23	29.51	29.49	29.16	28.68	29.62	30.28	31.02	29.78	30.09	30.33	29.36	30.51	29.32	29.66	29.72	29.69
MnO	0.27	0.23	0.24	0.26	0.23	0.26	0.27	0.29	0.17	0.18	0.23	0.18	0.28	0.24	0.22	0.24	0.21	0.19
MgO	9.07	8.95	9.18	8.97	9.26	9.52	9.35	8.89	7.81	8.98	8.68	8.68	9.17	7.72	8.92	8.63	8.66	8.66
CaO	0.85	0.84	0.85	0.84	0.90	0.81	0.82	0.78	0.79	0.88	0.86	0.94	0.78	0.78	0.80	0.80	0.91	0.86
Total	100.03	99.97	100.26	100.73	100.61	100.68	100.93	100.42	100.96	100.85	100.92	100.86	100.02	99.89	99.63	99.83	99.94	99.52
Formula per 24 oxygens																		
Si	6.00	5.92	5.91	5.96	5.95	5.99	5.94	5.92	5.99	5.95	5.96	5.95	5.96	6.02	5.97	5.99	5.98	5.93
Al^{IV}	0.00	0.08	0.09	0.04	0.05	0.01	0.06	0.08	0.01	0.05	0.04	0.05	0.04	0.00	0.03	0.01	0.02	0.07
Al^{VI}	4.02	4.01	3.96	4.00	3.99	3.99	3.94	3.92	4.04	3.98	3.99	3.96	3.96	4.02	3.98	3.99	3.98	3.99
Ti	0.00	0.00	0.00	0.00	0.00	0.00	0.00	0.00	0.00	0.00	0.00	0.00	0.00	0.00	0.00	0.00	0.00	0.00
Cr	0.01	0.01	0.00	0.00	0.00	0.00	0.00	0.00	0.00	0.00	0.00	0.00	0.00	0.00	0.00	0.00	0.00	0.00
Fe	3.70	3.78	3.81	3.79	3.74	3.67	3.80	3.92	4.00	3.82	3.87	3.91	3.80	3.97	3.81	3.85	3.86	3.87
Mn	0.03	0.03	0.03	0.03	0.03	0.03	0.04	0.04	0.02	0.02	0.03	0.02	0.04	0.03	0.03	0.03	0.03	0.02
Mg	2.08	2.07	2.12	2.05	2.12	2.17	2.14	2.05	1.79	2.06	1.99	1.99	2.12	1.79	2.07	2.00	2.00	2.01
Ca	0.14	0.14	0.14	0.14	0.15	0.13	0.13	0.13	0.13	0.14	0.14	0.16	0.13	0.13	0.13	0.13	0.15	0.14
Alm	0.622	0.628	0.625	0.631	0.619	0.611	0.622	0.638	0.673	0.632	0.642	0.643	0.624	0.671	0.631	0.641	0.639	0.641
Py	0.350	0.344	0.347	0.341	0.351	0.362	0.350	0.334	0.302	0.341	0.330	0.327	0.348	0.302	0.343	0.333	0.331	0.333
Spess	0.005	0.005	0.005	0.005	0.005	0.005	0.007	0.007	0.003	0.004	0.005	0.003	0.007	0.005	0.005	0.005	0.005	0.003
Gross	0.023	0.023	0.023	0.023	0.025	0.022	0.021	0.021	0.022	0.023	0.023	0.026	0.021	0.022	0.021	0.021	0.025	0.023

Table continued.

19 C Main band	20 C Main band	21 C Main band	22 C	23 C	24 C	25 M Adjacent to biotite	26 M Adjacent to biotite	27 M Adjacent to biotite	28 M Adjacent to biotite	Average	Average Core	Average Margin
37.95	38.12	38.20	39.05	38.52	38.85	38.66	38.76	38.66	38.68	38.58	38.59	38.68
0.01	0.01	0.01	0.00	0.00	0.00	0.00	0.02	0.01	0.00	0.01	0.01	0.01
22.00	21.91	22.08	22.17	22.14	22.17	21.65	21.93	21.95	21.71	22.07	22.13	21.84
0.00	0.00	0.00	0.00	0.02	0.00	0.02	0.01	0.00	0.02	0.01	0.01	0.01
30.16	29:28	29.56	29.55	29.47	29.58	29.71	30.91	29.34	29.55	29.69	29.62	29.95
0.22	0.21	0.20	0.20	0.17	0.21	0.21	0.26	0.16	0.17	0.22	0.22	0.21
8.38	8.44	8.48	8.70	8.82	8.63	8.10	7.30	8.47	8.47	8.67	8.83	8.12
0.82	0.83	0.85	0.83	0.84	0.80	0.83	0.81	0.86	0.83	0.84	0.84	0.82
99.54	98.80	99.38	100.50	99.98	100.24	99.18	100.00	99.45	99.43	100.09	100.22	99.63
5.93	5.98	5.96	6.01	5.96	6.00	6.04	6.03	6.01	6.02	5.97	5.96	6.02
0.00	0.00	0.00	0.00	0.00	0.00	0.00	0.00	0.00	0.00	0.00	0.03	0.00
3.98	4.02	4.02	4.02	4.00	4.03	3.99	4.02	4.02	3.98	3.99	3.99	4.00
0.00	0.00	0.00	0.00	0.00	0.00	0.00	0.00	0.00	0.00	0.00	0.00	0.00
0.00	0.00	0.00	0.00	0.00	0.00	0.00	0.00	0.00	0.00	0.00	0.00	0.00
3.94	3.84	3.85	3.80	3.81	3.82	3.88	4.02	3.82	3.85	3.84	3.83	3.89
0.03	0.03	0.03	0.03	0.02	0.03	0.03	0.03	0.02	0.02	0.03	0.03	0.03
1.95	1.97	1.97	2.00	2.03	1.98	1.89	1.69	1.96	1.97	2.00	2.03	1.88
0.14	0.14	0.14	0.14	0.14	0.13	0.14	0.13	0.14	0.14	0.14	0.14	0.14
0.650	0.642	0.643	0.637	0.635	0.641	0.653	0.685	0.643	0.644	0.639	0.635	0.655
0.322	0.330	0.329	0.335	0.339	0.332	0.318	0.288	0.330	0.330	0.333	0.337	0.316
0.005	0.005	0.005	0.005	0.003	0.005	0.005	0.005	0.003	0.003	0.005	0.005	0.005
0.023	0.023	0.023	0.023	0.023	0.022	0.024	0.022	0.024	0.023	0.023	0.023	0.024

UND 330 - Granitic enclave.

	1 C	2 C	3 C	4 C	5 C	6 C	7 M	8 M	9 M	Average Core	Average Margin
SiO_2	37.37	36.97	37.33	37.12	36.89	36.49	37.54	37.18	37.67	37.03	37.46
TiO_2	0.00	0.00	0.01	0.02	0.00	0.00	0.01	0.00	0.01	0.01	0.01
Al_2O_3	20.58	20.38	20.67	20.69	20.93	20.86	21.46	20.83	21.21	20.69	21.17
Cr_2O_3	0.00	0.01	0.00	0.01	0.01	0.00	0.03	0.00	0.00	0.01	0.01
FeO	33.83	33.19	33.18	33.82	33.85	34.48	32.55	32.80	32.96	33.73	32.77
MnO	2.25	2.16	2.28	2.14	2.04	2.16	3.72	2.29	2.81	2.17	2.94
MgO	1.10	1.09	0.90	1.20	1.21	1.25	0.50	0.94	0.70	1.13	0.71
CaO	5.28	5.32	5.28	4.24	4.84	3.87	4.86	5.26	5.23	4.81	5.12
TOTAL	100.41	99.12	99.65	99.20	99.70	99.11	100.60	99.30	100.59	99.58	100.19
Formula per 24 oxygens											
Si	6.03	6.04	6.06	6.05	5.99	5.98	6.03	6.05	6.05	6.03	6.04
Al^{IV}	0.00	0.00	0.00	0.00	0.01	0.02	0.00	0.00	0.00	0.00	0.00
Al^{VI}	3.92	3.92	3.95	3.97	3.99	4.00	4.06	3.99	4.01	3.96	4.02
Fe	4.57	4.54	4.50	4.61	4.60	4.72	4.37	4.46	4.43	4.59	4.42
Mn	0.31	0.30	0.31	0.30	0.28	0.30	0.51	0.32	0.38	0.30	0.40
Mg	0.26	0.26	0.22	0.29	0.29	0.30	0.12	0.23	0.17	0.27	0.17
Ca	0.91	0.93	0.92	0.74	0.84	0.68	0.84	0.92	0.90	0.84	0.89
Alm	0.756	0.753	0.756	0.776	0.765	0.787	0.748	0.752	0.753	0.765	0.752
Py	0.043	0.043	0.037	0.049	0.048	0.050	0.021	0.039	0.029	0.045	0.029
Spess	0.051	0.050	0.052	0.050	0.047	0.050	0.087	0.054	0.065	0.050	0.068
Gross	0.150	0.154	0.155	0.125	0.140	0.113	0.144	0.155	0.153	0.140	0.151

XS 4 - Biotite garnet granite, Ximba Suite.

	1 C	2 C	3 C	4 C	5 C	6 C	7 C	8 C	9 C	10 C	11 M	12 C
SiO_2	36.75	37.13	37.07	36.80	37.01	36.55	36.81	36.82	36.63	36.90	36.17	36.73
TiO_2	0.02	0.01	0.00	0.02	0.00	0.02	0.01	0.02	0.01	0.02	0.04	0.01
Al_2O_3	20.57	20.72	20.52	20.59	20.60	20.59	20.75	20.70	20.73	20.97	20.62	20.75
Cr_2O_3	0.00	0.00	0.00	0.00	0.00	0.00	0.00	0.00	0.00	0.00	0.00	0.00
FeO	33.35	33.39	32.98	33.53	33.15	33.01	32.97	32.54	32.96	33.37	32.41	33.46
MnO	2.16	2.14	2.25	2.26	2.20	2.16	2.12	2.17	2.10	2.31	2.72	2.28
MgO	0.86	0.86	0.85	0.89	0.83	0.76	0.86	0.82	0.92	0.72	0.67	0.86
CaO	6.39	6.36	6.66	6.27	6.31	6.40	6.44	6.43	6.29	6.46	6.98	6.51
TOTAL	100.10	100.61	100.33	100.36	100.10	99.49	99.96	99.50	99.64	100.75	99.61	100.60
Formula per 24 oxygens												
Si	5.97	5.99	6.00	5.97	6.00	5.97	5.97	5.99	5.97	5.95	5.92	5.94
Al^{IV}	0.03	0.01	0.00	0.03	0.00	0.03	0.03	0.01	0.03	0.05	0.08	0.06
Al^{VI}	3.91	3.93	3.91	3.90	3.94	3.93	3.94	3.97	3.94	3.94	3.89	3.90
Fe	4.53	4.51	4.46	4.55	4.50	4.51	4.47	4.43	4.49	4.50	4.43	4.53
Mn	0.30	0.29	0.31	0.31	0.30	0.30	0.29	0.30	0.29	0.32	0.38	0.31
Mg	0.21	0.21	0.21	0.22	0.20	0.18	0.21	0.20	0.22	0.17	0.16	0.21
Ca	1.11	1.10	1.16	1.09	1.10	1.12	1.12	1.12	1.10	1.12	1.22	1.13
Alm	0.737	0.738	0.726	0.737	0.738	0.738	0.734	0.732	0.736	0.737	0.716	0.733
Py	0.034	0.034	0.034	0.036	0.033	0.030	0.034	0.033	0.036	0.028	0.026	0.034
Spess	0.049	0.048	0.051	0.050	0.049	0.049	0.048	0.050	0.048	0.052	0.061	0.050
Gross	0.180	0.180	0.189	0.177	0.180	0.183	0.184	0.185	0.180	0.183	0.197	0.183

Table continued.

13 M	14 C	15 C	16 M	17 M	18 C	19 M	20 C	21 C Adjacent to biotite	22 C	23 C	24 M	Average	Average Core	Average Margin
36.57	36.66	36.37	36.86	36.60	36.82	36.31	36.77	37.35	36.27	36.33	35.39	36.65	36.77	36.32
0.00	0.03	0.05	0.02	0.03	0.01	0.02	0.02	0.03	0.03	0.04	0.03	0.02	0.02	0.02
20.10	20.64	20.46	21.16	21.05	20.45	20.39	20.15	19.59	20.61	20.19	21.05	20.58	20.53	20.73
0.00	0.00	0.00	0.00	0.00	0.00	0.00	0.00	0.00	0.00	0.00	0.00	0.00	0.00	0.00
32.86	33.50	33.53	32.19	32.65	33.74	33.66	33.40	33.47	32.14	33.02	32.17	33.06	33.20	32.66
2.33	2.20	2.20	2.37	2.54	2.03	2.02	2.10	2.11	2.27	2.09	2.36	2.23	2.18	2.39
0.73	0.84	0.76	0.72	0.66	0.86	0.79	0.86	0.64	0.65	0.74	0.68	0.78	0.81	0.71
6.85	6.31	6.35	7.24	6.71	6.75	6.42	6.14	6.67	7.03	6.96	7.68	6.61	6.49	6.98
99.44	100.18	99.72	100.56	100.24	100.66	99.61	99.44	99.86	99.00	99.37	99.36	99.95	99.98	99.86
5.97	5.96	5.95	5.94	5.93	5.96	5.94	6.01	6.09	5.95	5.96	5.81	5.96	5.98	5.92
0.03	0.04	0.05	0.06	0.07	0.04	0.06	0.00	0.00	0.05	0.04	0.19	0.04	0.03	0.08
3.89	3.91	3.89	3.96	3.95	3.86	3.88	3.88	3.76	3.93	3.86	3.88	3.91	3.91	3.91
4.48	4.55	4.58	4.34	4.42	4.57	4.61	4.57	4.56	4.41	4.53	4.42	4.50	4.51	4.45
0.32	0.30	0.30	0.32	0.35	0.28	0.28	0.29	0.29	0.32	0.29	0.33	0.31	0.30	0.33
0.18	0.20	0.19	0.17	0.16	0.21	0.19	0.21	0.16	0.16	0.18	0.17	0.19	0.20	0.17
1.20	1.10	1.11	1.25	1.16	1.17	1.13	1.08	1.16	1.24	1.22	1.35	1.15	1.13	1.22
0.725	0.740	0.741	0.714	0.726	0.733	0.742	0.743	0.739	0.720	0.728	0.705	0.732	0.735	0.721
0.029	0.032	0.031	0.028	0.026	0.034	0.031	0.034	0.026	0.026	0.029	0.027	0.031	0.033	0.028
0.052	0.049	0.048	0.053	0.057	0.045	0.045	0.047	0.047	0.052	0.047	0.053	0.050	0.049	0.053
0.194	0.179	0.180	0.205	0.191	0.188	0.182	0.176	0.188	0.202	0.196	0.215	0.187	0.184	0.198

UND 22 - Granite vein.

	1 C	2 C	3 C	4 M	5 M	6 M	Average Core	Average Margin
SiO_2	37.08	36.91	37.08	36.92	36.43	36.87	37.02	36.74
TiO_2	0.03	0.02	0.02	0.02	0.00	0.01	0.02	0.01
Al_2O_3	20.58	20.57	20.71	20.35	20.32	20.29	20.62	20.32
Cr_2O_3	0.00	0.00	0.00	0.00	0.00	0.02	0.00	0.01
FeO	27.58	28.24	28.12	27.68	27.88	28.13	27.98	27.89
MnO	10.26	10.42	10.35	10.69	10.92	10.65	10.34	10.76
MgO	0.68	0.69	0.69	0.73	0.72	0.70	0.69	0.72
CaO	2.79	2.76	2.71	2.67	2.68	2.54	2.75	2.63
TOTAL	98.99	99.61	99.68	99.06	98.95	99.21	99.43	99.08
Formula per 24 oxygens								
Si	6.08	6.04	6.05	6.07	6.02	6.06	6.06	6.05
Al^{IV}	0.00	0.00	0.00	0.00	0.00	0.00	0.00	0.00
Al^{VI}	3.98	3.97	3.98	3.94	3.96	3.93	3.98	3.94
Fe	3.78	3.97	3.99	3.95	3.96	3.94	3.91	3.95
Mn	1.43	1.44	1.43	1.49	1.53	1.48	1.43	1.50
Mg	0.17	0.17	0.17	0.18	0.18	0.17	0.17	0.18
Ca	0.49	0.48	0.47	0.47	0.47	0.45	0.48	0.46
Alm	0.644	0.655	0.658	0.649	0.645	0.652	0.653	0.649
Py	0.029	0.028	0.028	0.029	0.029	0.028	0.028	0.029
Spess	0.244	0.238	0.236	0.245	0.249	0.245	0.239	0.246
Gross	0.083	0.079	0.078	0.077	0.077	0.075	0.080	0.076

UND 19 - Nqwadolo Suite.

	1 C	2 C	3 C	4 C	5 C	6 C
SiO_2	35.87	35.90	36.15	35.59	35.86	35.76
TiO_2	0.00	0.02	0.01	0.00	0.01	0.01
Al_2O_3	19.99	20.56	20.15	20.14	20.43	20.14
Cr_2O_3	0.00	0.00	0.00	0.00	0.00	0.00
FeO	37.73	37.83	37.94	38.64	38.01	38.08
MnO	0.61	0.62	0.57	0.57	0.56	0.55
MgO	0.24	0.19	0.25	0.25	0.26	0.27
CaO	2.19	2.06	2.47	2.26	2.39	2.45
TOTAL	96.63	97.18	97.54	97.45	97.52	97.26

UND 90 - Biotite garnet granite, Ximba Suite.

	1 C	2 C	3 C	4 C	5 C	6 C	7 C	8 C	9 C	10 C	11 C	12 C	13 C	Average
SiO_2	36.53	37.04	36.97	36.86	36.43	36.84	36.87	36.49	36.68	37.06	36.53	36.71	36.74	36.75
TiO_2	0.01	0.00	0.01	0.03	0.01	0.02	0.04	0.01	0.01	0.02	0.00	0.01	0.00	0.01
Al_2O_3	20.95	20.99	20.54	20.86	20.48	20.77	20.83	20.53	20.80	21.06	20.60	20.80	20.86	20.77
Cr_2O_3	0.00	0.00	0.00	0.00	0.00	0.00	0.00	0.00	0.00	0.00	0.00	0.00	0.00	0.00
FeO	34.59	34.88	34.67	34.11	34.73	35.06	34.45	35.21	34.73	34.47	35.21	34.57	33.60	34.64
MnO	1.49	1.45	1.37	1.34	1.35	1.49	1.39	1.52	1.40	1.44	1.47	1.53	1.43	1.44
MgO	0.96	0.98	0.94	0.96	0.86	0.85	0.95	0.88	0.91	0.93	0.99	0.84	0.94	0.92
CaO	5.40	5.48	5.64	5.28	5.31	5.25	5.35	4.87	5.37	5.27	5.05	5.36	5.53	5.32
TOTAL	99.93	100.82	100.14	99.44	99.17	100.28	99.88	99.51	99.90	100.25	99.85	99.82	99.10	99.91
Formula per 24 oxygens														
Si	5.94	5.97	6.00	6.00	5.98	5.98	5.99	5.98	5.97	5.99	5.96	5.98	5.98	5.98
Al^{IV}	0.06	0.03	0.00	0.00	0.02	0.02	0.01	0.02	0.03	0.01	0.04	0.02	0.03	0.02
Al^{VI}	3.96	3.96	3.93	4.00	3.94	3.95	3.98	3.94	3.96	4.00	3.92	3.97	3.97	3.96
Ti	0.00	0.00	0.00	0.00	0.00	0.00	0.01	0.00	0.00	0.00	0.00	0.00	0.00	0.00
Cr	0.00	0.00	0.00	0.00	0.00	0.00	0.00	0.00	0.00	0.00	0.00	0.00	0.00	0.00
Fe	4.71	4.70	4.71	4.65	4.77	4.76	4.68	4.82	4.73	4.66	4.81	4.71	4.66	4.72
Mn	0.21	0.20	0.19	0.19	0.19	0.21	0.19	0.21	0.19	0.20	0.20	0.21	0.20	0.20
Mg	0.23	0.24	0.23	0.23	0.21	0.21	0.23	0.22	0.22	0.22	0.24	0.20	0.23	0.22
Ca	0.94	0.95	0.98	0.92	0.93	0.91	0.93	0.85	0.94	0.91	0.88	0.94	0.96	0.93
Alm	0.773	0.772	0.771	0.776	0.782	0.782	0.776	0.790	0.778	0.778	0.785	0.777	0.770	0.778
Py	0.038	0.039	0.038	0.038	0.035	0.034	0.038	0.036	0.036	0.037	0.039	0.033	0.038	0.036
Spess	0.035	0.033	0.031	0.032	0.031	0.035	0.032	0.035	0.031	0.033	0.032	0.035	0.033	0.033
Gross	0.154	0.156	0.160	0.154	0.152	0.149	0.154	0.139	0.155	0.152	0.144	0.155	0.159	0.153

APPENDIX 3

CHEMICAL ANALYSES

Large, c.50 kg samples were collected in the field, with individual samples collected from construction sites and quarries. The majority of the pelitic gneisses and biotite garnet granites were collected after blasting. After collection the samples were washed, and split into c.5kg pieces. These were washed again, and the weathered material removed using a rock splitter, which had been cleaned with a wire brush, then vacuumed and washed with acetone. The fresh material was then crushed in a jaw crusher, which had been cleaned and then precontaminated with the removed weathered material from the individual samples. The sample was then subdivided in a sampler splitter, which had been air blasted clean, and c.50g further crushed in an agate mill, which had been washed with distilled water and then acetone.

Major and trace element analyses were undertaken at the Geological Survey, Pretoria using the methodology of Frick and Walraven (1985) as discussed by Kuyper (1979) and the University of Natal, Pietermaritzburg (Krynauw 1986) on an XRF using Norrish fusion discs and pressed powder pellets. Precision is estimated at 2% for the major elements above 0.1% concentration and 5% above 10 ppm concentration for trace elements for the analyses at the Geological Survey, Pretoria (Frick and Walraven 1985) and 0.6%-7% for major elements above 1% and 2-10% for trace elements at the University of Natal, Pietermaritzburg (Krynauw 1986). REE analyses were undertaken at Royal Holloway and New Bedford College, London, on an ICP using the methods of Walsh *et al.* (1981), with an estimated precision of 1-2%.

GEOCHEMICAL SAMPLE SITES

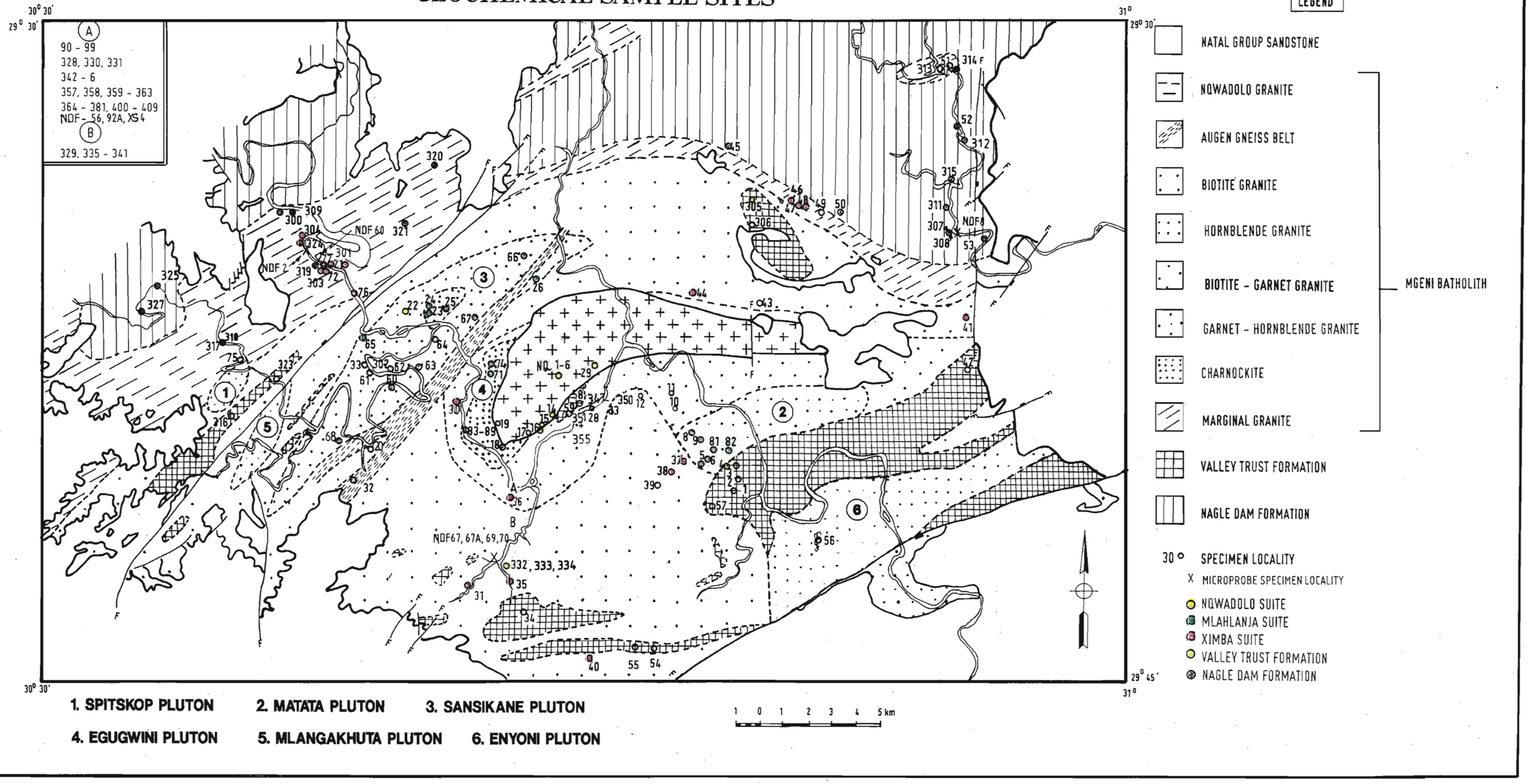

Amphibolite - Nagle Dam Formation.

	UND 307	UND 308	UND 314	UND 320	UND 324
SiO_2 (wt%)	49.89	47.17	51.89	51.69	50.68
TiO_2	0.83	1.25	0.87	0.46	1.43
Al_2O_3	14..63	13.60	14.56	13.21	15.44
Fe_2O_3	9.72	12.91	12.04	2.59	3.83
FeO	0.00	0.00	0.00	6.07	8.25
MnO	0.16	0.17	0.26	0.19	0.19
MgO	9.21	10.65	8.71	8.19	8.41
CaO	11.00	11.13	8.77	12.77	9.06
Na_2O	2.77	2.05	0.80	2.52	2.65
K_2O	0.89	0.98	2.13	0.89	0.47
P_2O_5	0.11	0.10	0.08	0.14	0.34
Cr_2O_3	0.00	0.00	0.00		
H_2O^+				0.51	0.35
H_2O^-				0.09	0.07
CO_2				0.09	0.12
S				0.00	0.16
LOI	0.86	0.73	2.22		
TOTAL	99.21	100.00	100.11	99.41	101.46
Trace elements in ppm					
Rb	15	32	88	58	11
Sr	133	172	184	172	306
Zr	54	59	62	66	67
Ni	115	291	167	66	183
Cr	636	717	456	511	433
Zn	69	81	195	89	106
Pb	13	4	13	34	13
Y	19	19	23	31	29
Nb	11	5	3	6	5
Ba	184	575	928	201	176
Th	3	0	4	8	5
U	2	2	3	15	13
Mo				1	1
Ga	15	17	18	17	21
Cu	7	30	0	21	59
V	249	288	298	250	307
La	10	5	9		
Co	52	63	53		
Sc	46	42	45		

Biotite hornblende gneiss - Nagle Dam Formation.

	UND 45	UND 50	UND 52	UND 53	UND 300	UND 312	UND 315	UND 317	UND 317a
SiO_2 (wt%)	55.59	67.09	60.84	64.04	69.77	64.05	64.13	52.26	51.91
TiO_2	1.25	0.43	0.87	0.34	0.39	0.69	0.39	1.27	1.35
Al_2O_3	16.69	14.48	16.69	14.24	15.38	16.91	14.46	20.27	19.37
Fe_2O_3	2.08	1.59	2.29	2.95	3.51	5.37	7.01	9.03	3.77
FeO	5.90	3.84	4.26	3.19	0.00	0.00	0.00	0.00	5.21
MnO	0.15	0.09	0.10	0.14	0.07	0.08	0.13	0.12	0.12
MgO	4.76	3.17	2.97	3.44	1.38	2.26	3.22	3.08	3.31
CaO	8.48	4.27	5.04	4.97	3.62	5.19	6.20	8.40	8.48
Na_2O	2.04	1.72	2.72	2.59	3.74	3.41	2.84	4.44	3.89
K_2O	1.52	1.79	2.09	1.86	1.96	1.76	1.57	0.66	0.66
P_2O_5	0.27	0.21	0.27	0.24	0.16	0.17	0.18	0.38	0.45
Cr_2O_3	0.01	0.01	0.01	0.01	0.00	0.00	0.00	0.00	
H_2O^+	1.10	0.87	0.44	0.86					1.06
H_2O^-	0.12	0.17	0.11	0.10					0.07
CO_2	0.09	0.07	0.04	0.03					0.16
S									0.35
LOI					0.31	0.78	0.69	1.37	
TOTAL	100.05	99.80	98.74	99.00	99.98	99.89	100.12	99.91	100.16
Trace elements in ppm									
Rb	70	102	86	61	107	84	32	23	20
Sr	479	372	466	395	402	609	520	948	>800
Zr	166	149	151	83	128	111	77	212	200
Ni	23	5	8	14	10	14	12	12	1
Cr					17	30	60	7	43
Zn	80	55	81	56	49	63	38	101	110
Pb	12	13	10	7	21	9	10	23	23
Y	36	23	15	16	24	13	17	30	41
Nb	14	12	12	8	11	4	3	6	9
Ba	489	680	760	408	544	642	387	346	346
Th	15	9	5	9	13	0	0	0	5
U					2	2	1	1	11
Mo									4
Ga					16	18	14	25	25
Cu					3	14	3	22	52
V					50	108	154	169	251
La					35	14	17	21	
Co					11	15	20	15	
Sc					13	11	24	21	

Biotite hornblende gneiss (continued).

	UND 325	UND 327
SiO_2 (wt%)	60.86	60.95
TiO_2	1.04	0.50
Al_2O_3	16.47	14.78
Fe_2O_3	0.00	1.91
FeO	6.55	5.49
MnO	0.11	0.13
MgO	2.94	5.21
CaO	5.64	6.81
Na_2O	2.69	0.27
K_2O	2.15	2.72
P_2O_5	0.34	0.12
Cr_2O_3		
H_2O^+	0.99	1.32
H_2O^-	0.09	0.15
CO_2	0.16	0.12
S	0.08	0.00
LOI		
TOTAL	100.11	100.19
Trace elements in ppm		
Rb	150	166
Sr	484	252
Zr	98	95
Ni	11	42
Cr	44	189
Zn	87	63
Pb	26	27
Y	36	27
Nb	9	6
Ba	641	418
Th	10	11
U	14	14
Mo	1	2
Ga	22	21
Cu	56	27
V	202	249
La		
Co		
Sc		

Quartzo-feldspathic gneiss - Nagle Dam Formation.

	UND 309	UND 311	UND 311a	UND 311b	UND 318	UND 319	UND 321
SiO_2 (wt%)	77.93	71.65	75.17	77.55	74.85	75.98	76.21
TiO_2	0.01	0.01	0.04	0.07	0.11	0.19	0.02
Al_2O_3	12.92	15.22	14.09	12.83	13.79	13.23	13.71
Fe_2O_3	0.00	0.25	0.64	1.16	0.00	1.38	0.17
FeO	1.21	0.00	0.00	0.00	1.39	0.00	0.10
MnO	0.00	0.01	0.01	0.01	0.02	0.03	0.00
MgO	0.00	0.06	0.17	0.19	0.28	0.68	0.08
CaO	1.36	0.72	1.06	1.36	1.21	2.25	0.27
Na_2O	2.34	1.84	2.49	2.62	2.42	2.90	3.12
K_2O	4.11	8.93	6.52	4.19	6.17	3.44	5.15
P_2O_5	0.06	0.01	0.02	0.02	0.09	0.05	0.06
Cr_2O_3		0.00	0.00	0.00		0.00	
H_2O^+	0.12				0.24		0.29
H_2O^-	0.01				0.03		0.06
CO_2	0.04				0.07		0.05
S	0.00				0.00		0.00
LOI		0.56	0.85	1.05		1.13	
TOTAL	100.12	98.70	100.21	100.01	100.68	100.11	99.28
Trace elements in ppm							
Rb	133	174	129	85	143	105	208
Sr	307	349	318	278	196	485	46
Zr	55	25	43	70	117	39	57
Ni	1	0	0	0	1	5	1
Cr	11	1	0	1	15	4	9
Zn	7	3	5	8	24	21	9
Pb	52	27	21	15	50	27	68
Y	14	2	3	4	17	3	34
Nb	5	0	1	0	5	1	8
Ba	1067	1196	946	688	711	1158	102
Th	17	1	1	3	16	0	11
U	13	0	0	2	13	3	15
Mo	2				1		2
Ga	15	12	11	9	16	11	19
Cu	6	0	13	33	5	0	11
V	15	5	8	16	20	31	11
La		6	7	11		9	
Co		1	3	5		2	
Sc		1	2	1		2	

Amphibolite - Valley Trust Formation.

	UND 54	UND 55	UND 56	UND 57	UND 58	UND 59	UND 332	UND 334	UND 347
SiO_2 (wt%)	51.10	47.33	51.50	46.29	48.94	45.91	52.54	53.95	48.33
TiO_2	3.24	2.68	1.82	2.24	1.31	3.43	0.67	0.88	1.55
Al_2O_3	11.72	13.25	14.90	13.51	12.67	6.24	15.02	16.01	11.07
Fe_2O_3	1.38	0.10	2.42	0.28	0.10	0.10	0.00	0.00	0.00
FeO	13.37	15.38	8.09	13.27	10.81	15.31	9.89	9.62	13.96
MnO	0.23	0.23	0.14	0.22	0.20	0.28	0.23	0.17	0.24
MgO	4.95	5.93	5.92	7.06	9.34	10.32	4.17	4.73	10.08
CaO	9.26	9.59	9.32	11.49	13.40	14.72	12.79	9.65	13.30
Na_2O	2.01	2.23	3.67	2.07	1.04	1.42	0.10	2.70	0.97
K_2O	0.41	0.37	0.71	0.41	0.25	0.28	1.43	0.51	0.13
P_2O_5	0.25	0.27	0.28	0.20	0.10	0.10	0.33	0.27	0.16
Cr_2O_3									
H_2O^+	0.64	0.35	0.37	0.01	0.09	0.23	1.22	0.28	0.39
H_2O^-	0.17	0.14	0.13	0.16	0.22	0.22	0.08	0.02	0.04
CO_2	0.06	0.19	0.01	0.04	0.20	0.14	2.03	0.19	0.36
S							0.00	0.00	0.04
LOI									
TOTAL	98.80	98.04	99.28	97.25	98.67	98.70	100.51	98.98	100.62
Trace elements in ppm									
Rb	15	23	21	8	12	12	109	11	11
Sr	157	179	460	168	170	65	126	207	128
Zr	201	143	145	91	50	132	62	53	58
Ni	20	48	45	81	84	102	21	29	94
Cr	100	200	200	400	500	400	341	151	563
Zn	125	127	63	109	86	163	78	84	102
Pb	13	5	5	5	5	6	15	14	16
Y	46	34	31	27	20	37	34	29	36
Nb	22	20	12	15	12	18	5	5	5
Ba							831	218	95
Th							5	5	5
U							14	13	15
Mo							1	1	1
Ga							19	20	19
Cu							17	126	39
V							123	297	507
La									
Co									
Sc									

Amphibolite (continued).

	UND 348	UND 349	UND 350	UND 357	UND 358
SiO_2 (wt%)	49.51	49.17	48.81	48.20	48.42
TiO_2	1.52	1.41	1.57	2.17	2.19
Al_2O_3	10.56	10.93	10.39	12.19	12.06
Fe_2O_3	0.18	4.16	3.33	0.63	0.03
FeO	12.22	8.52	10.23	13.55	14.42
MnO	0.22	0.22	0.24	0.22	0.23
MgO	9.86	10.05	10.33	8.36	8.00
CaO	13.35	13.67	12.87	11.35	10.50
Na_2O	1.23	1.28	1.11	1.66	1.79
K_2O	0.13	0.12	0.17	0.52	0.34
P_2O_5	0.13	0.12	0.14	0.14	0.21
Cr_2O_3					
H_2O^+	0.32	0.26	0.31	0.30	0.51
H_2O^-	0.06	0.07	0.07	0.03	0.07
CO_2	0.68	0.31	0.37	0.33	0.50
S	0.05	0.04	0.03	0.11	0.07
LOI					
TOTAL	100.01	100.34	99.98	99.76	99.32
Trace elements in ppm					
Rb	8	5	6	14	8
Sr	120	121	106	147	140
Zr	59	57	60	69	98
Ni	98	98	100	80	73
Cr	527	550	608	377	362
Zn	97	95	102	113	120
Pb	14	11	10	16	11
Y	35	33	43	35	42
Nb	6	5	6	7	9
Ba	47	46	83	88	90
Th	5	5	5	5	5
U	15	11	11	14	12
Mo	1	1	1	1	1
Ga	19	19	18	23	23
Cu	59	46	42	83	54
V	514	498	535	735	625
La					
Co					
Sc					

Quartzo-feldspathic gneiss - Valley Trust Formation.

	UND 1	UND 3	UND 4	UND33	UND34	UND 42
SiO_2 (wt%)	74.36	75.85	72.72	77.61	74.86	72.04
TiO_2	0.20	0.21	0.25	0.03	0.14	0.44
Al_2O_3	13.30	12.02	15.00	11.98	13.20	13.42
Fe_2O_3	1.76	1.57	0.56	0.48	0.23	1.12
FeO	0.11	0.19	1.02	0.19	1.09	1.95
MnO	0.01	0.01	0.02	-0.02	-0.02	0.06
MgO	0.14	0.10	0.13	0.49	0.62	1.04
CaO	0.07	0.14	0.51	0.60	0.98	1.77
Na_2O	4.11	3.34	2.87	3.39	3.52	3.48
K_2O	5.15	6.72	5.60	5.05	5.00	4.22
P_2O_5	0.13	0.07	0.14	-0.10	-0.10	0.20
Cr_2O_3						
H_2O^+	0.12	0.26	0.33			0.40
H_2O^-	0.13	0.23	0.12	0.10	0.14	0.10
CO_2	0.01	0.01	0.04	0.06	0.09	0.06
S						
LOI				0.24	0.38	
TOTAL	99.68	100.78	99.43	100.20	100.20	100.31
Trace elements in ppm						
Rb	176	185	174	171	123	160
Sr	63	62	191	18	135	154
Zr	149	93	125	162	118	258
Ni						
Cr						
Zn	35	32	59	12	32	
Pb	25	33	41			3
Y	0	7	0	13	15	
Nb	7	5	8	5	5	
Ba	500	300	900	47	743	786
Th	15	11	38	6	11	
U	3	2	3			
Mo						
Ga						
Cu						
V						
La						
Co						
Sc						

Quartzo-feldspathic gneiss (continued).

	UND 302	UND 305	UND 306	UND 316	UND 323
SiO_2 (wt%)	77.90	75.68	80.90	79.18	80.34
TiO_2	0.01	0.04	0.18	0.06	0.02
Al_2O_3	12.33	14.02	10.95	12.12	12.04
Fe_2O_3	0.70	0.46	0.22	0.32	0.58
FeO	0.00	0.00	0.00	0.35	0.04
MnO	0.00	0.00	0.00	0.01	0.00
MgO	0.07	0.04	0.03	0.08	0.02
CaO	0.46	0.37	0.08	0.16	0.35
Na_2O	2.86	3.21	3.41	2.80	2.91
K_2O	5.54	5.98	3.89	3.26	2.93
P_2O_5	0.00	0.01	0.04	0.07	0.05
Cr_2O_3					
H_2O^+				0.27	0.27
H_2O^-				0.02	0.08
CO_2				0.05	0.06
S				0.00	0.00
LOI	0.14	0.52	0.51		
TOTAL	99.87	99.80	99.70	98.76	99.70
Trace elements in ppm					
Rb	190	184	138	134	111
Sr	12	83	24	39	35
Zr	95	29	124	64	48
Ni	0	1	1	1	1
Cr	0	0	1	16	9
Zn	6	8	8	19	35
Pb	73	46	57	57	46
Y	9	3	79	18	16
Nb	8	1	23	6	5
Ba	70	647	285	188	142
Th	5	2	26	6	6
U	2	1	4	13	11
Mo				1	2
Ga	19	18	12	18	18
Cu	0	0	0	4	14
V	2	2	3	16	11
La	12	11	169		
Co	1	0	1		
Sc	1	1	9		

Pelitic gneiss - Valley Trust Formation.

	UND 328	UND333	UND335	UND336	UND342	UND343	UND344	UND 345	UND346
SiO_2(wt%)	70.38	60.65	75.48	75.49	57.83	58.91	71.09	68.56	78.55
TiO_2	0.83	0.86	0.76	0.71	1.03	1.09	0.99	1.06	0.78
Al_2O_3	14.83	15.93	11.88	11.69	20.33	18.43	13.47	13.89	9.93
Fe_2O_3	2.28	0.17	0.38	1.28	4.32	1.62	0.00	2.26	0.80
FeO	3.78	8.43	4.01	2.86	5.72	7.12	6.44	4.37	3.24
MnO	0.07	0.13	0.07	0.06	0.10	0.10	0.10	0.08	0.06
MgO	1.67	4.19	1.19	1.00	3.05	2.63	1.74	2.03	0.93
CaO	1.02	5.86	0.85	0.54	0.51	0.67	1.29	0.59	0.78
Na_2O	1.25	0.68	1.61	1.11	0.79	2.31	1.41	1.45	1.53
K_2O	3.00	1.56	2.92	3.32	5.06	4.27	3.03	3.12	3.01
P_2O_5	0.17	0.31	0.15	0.16	0.16	0.13	0.15	0.17	0.12
Cr_2O_3									
H_2O^+	0.43	1.67	0.54	0.70	0.82	1.08	0.62	0.88	0.79
H_2O^-	0.13	0.10	0.14	0.25	0.10	0.20	0.06	0.07	0.09
CO_2	0.03	0.32	0.11	0.20	0.04	0.08	0.07	0.10	0.18
S	0.00	0.00	0.00	0.00	0.00	0.00	0.00	0.00	0.00
LOI									
TOTAL	99.89	100.87	100.07	99.37	99.87	98.65	100.45	98.63	100.78
Trace elements in ppm									
Rb	145	60	131	151	251	176	123	138	102
Sr	123	197	128	121	66	115	124	109	130
Zr	198	72	217	231	193	214	244	246	288
Ni	22	32	11	5	56	43	14	26	7
Cr	89	237	77	65	166	150	98	108	75
Zn	118	93	60	68	214	183	95	126	70
Pb	28	19	29	38	53	59	37	40	29
Y	51	33	48	51	78	65	58	60	50
Nb	13	5	13	11	16	16	14	15	13
Ba	593	362	651	778	793	848	642	667	582
Th	14	5	16	16	18	17	17	18	15
U	15	14	15	14	16	16	15	16	16
Mo	1	1	2	1	2	3	2	2	3
Ga	21	21	19	17	31	29	21	21	17
Cu	12	27	12	20	27	25	13	18	10
V	150	237	124	107	237	225	152	163	117
La									
Co									
Sc									

Pelitic gneiss (continued).

	UND 351	UND 352	UND 353	UND 354	UND 355	UND 364
SiO_2(wt%)	70.36	72.56	64.94	67.87	72.09	61.76
TiO_2	1.12	0.98	0.94	1.08	0.85	1.08
Al_2O_3	15.48	14.54	18.01	15.75	14.13	17.43
Fe_2O_3	1.87	2.24	2.02	2.23	0.61	2.38
FeO	3.19	3.31	4.30	4.47	3.97	6.07
MnO	0.09	0.07	0.10	0.07	0.10	0.10
MgO	1.33	1.65	1.86	2.36	1.40	2.57
CaO	0.43	0.57	0.66	0.58	0.70	1.31
Na_2O	0.77	0.98	1.00	0.87	0.94	1.49
K_2O	4.34	3.50	3.22	2.40	4.01	3.38
P_2O_5	0.09	0.11	0.13	0.15	0.13	0.15
Cr_2O_3						
H_2O^+	1.43	1.09	1.09	1.01	0.84	0.81
H_2O^-	0.57	0.26	0.07	0.34	0.19	0.11
CO_2	0.13	0.12	0.16	0.17	0.09	0.55
S	0.00	0.02	0.00	0.68	0.06	0.90
LOI						
TOTAL	101.21	102.01	98.51	100.03	100.12	100.09
Trace elements in ppm						
Rb	154	122	152	139	129	144
Sr	95	105	118	88	120	121
Zr	212	228	186	230	221	237
Ni	1	1	1	118	1	31
Cr	119	114	135	140	96	152
Zn	90	110	109	150	100	160
Pb	39	40	42	40	42	42
Y	62	60	69	54	72	82
Nb	18	15	13	15	13	17
Ba	858	752	919	630	689	744
Th	19	21	14	19	15	26
U	13	14	13	16	16	18
Mo	2	2	1	3	2	7
Ga	26	22	26	24	20	28
Cu	22	26	34	49	22	61
V	177	173	208	193	147	229
La						
Co						
Sc						

Pelitic gneiss (continued).

	UND 365	UND 366	UND 367	UND 368	UND 369	UND 370	UND 371	UND 372	UND 373
SiO_2 (wt%)	56.82	57.41	57.72	59.98	57.86	59.46	57.62	59.57	58.16
TiO_2	0.89	0.95	0.92	0.88	0.94	0.87	0.84	0.76	0.87
Al_2O_3	18.91	18.51	18.21	17.33	18.57	17.47	18.27	17.27	18.42
Fe_2O_3	8.99	8.52	8.59	8.05	8.65	8.17	8.43	7.57	7.92
FeO									
MnO	0.08	0.07	0.08	0.07	0.08	0.07	0.05	0.06	0.08
MgO	2.61	2.59	2.66	2.48	2.85	2.64	2.45	2.16	2.65
CaO	0.56	0.68	0.44	1.03	0.60	0.63	0.91	0.91	0.54
Na_2O	2.35	2.33	2.01	2.31	1.85	1.95	2.36	2.16	1.94
K_2O	8.75	8.66	9.16	7.60	8.52	8.67	8.83	8.52	9.15
P_2O_5	0.13	0.14	0.13	0.12	0.10	0.11	0.13	0.14	0.11
Cr_2O_3									
H_2O^+									
H_2O^-									
CO_2									
S									
LOI	1.30	0.68	0.71	0.69	0.87	0.84	0.96	0.80	0.83
TOTAL	100.08	99.86	99.91	99.86	100.01	100.05	99.88	99.11	99.84
Trace elements in ppm									
Rb	251	268	273	242	244	256	289	274	260
Sr	72	86	71	99	63	74	98	112	68
Zr	157	173	170	183	173	167	157	151	161
Ni	39	40	33	29	36	33	35	28	31
Cr	89	87	95	89	94	87	79	72	85
Zn	151	169	152	157	152	147	182	165	139
Pb	51	54	46	52	39	40	59	55	47
Y	38	47	45	45	47	43	42	42	43
Nb	15	16	16	18	17	16	16	19	16
Ba	718	754	652	671	655	611	692	724	674
Th	13	17	18	12	18	16	15	11	18
U	3	1	2	1	1	3	2	2	2
Mo									
Ga	27	27	26	24	27	25	26	29	27
Cu	38	25	26	26	35	32	41	31	31
V	152	146	154	131	143	133	129	115	131
La	27	30	25	31	42	32	23	26	31
Co	16	17	16	11	17	15	16	11	13
Sc	20	20	19	18	21	19	19	16	19

Pelitic gneiss (continued).

	UND 374	UND 375	UND 376	UND 377	UND 378	UND 379	UND 380	UND 381
SiO_2 (wt%)	59.75	56.05	57.13	57.65	58.88	57.74	58.52	57.47
TiO_2	0.97	1.16	1.03	1.00	1.09	0.88	0.87	0.95
Al_2O_3	18.97	18.49	18.71	19.26	18.24	19.96	19.56	19.69
Fe_2O_3	9.31	10.63	9.39	9.77	9.08	6.10	6.11	6.55
FeO								
MnO	0.09	0.11	0.09	0.09	0.10	0.06	0.05	0.05
MgO	2.80	3.18	2.87	2.93	2.52	1.37	1.33	1.51
CaO	0.64	1.43	1.10	0.70	1.54	4.08	3.97	4.08
Na_2O	1.83	2.80	2.46	1.77	2.99	4.60	4.49	4.48
K_2O	5.56	5.86	6.91	6.17	5.12	4.39	4.34	4.30
P_2O_5	0.11	0.16	0.14	0.11	0.12	0.22	0.21	0.23
Cr_2O_3								
H_2O^+								
H_2O^-								
CO_2								
S								
LOI	1.44	0.94	0.99	1.38	0.98	1.10	1.20	1.39
TOTAL	100.04	99.87	99.82	99.43	99.69	99.41	99.46	9.31
Trace elements in ppm								
Rb	188	241	251	214	184	155	156	150
Sr	76	98	96	81	140	344	363	342
Zr	181	247	208	192	268	653	623	597
Ni	39	40	41	45	33	0	0	1
Cr	110	114	103	113	117	7	4	6
Zn	152	205	184	167	185	142	133	134
Pb	38	43	47	44	34	30	32	43
Y	45	89	69	62	77	39	35	35
Nb	16	19	18	17	19	41	20	18
Ba	795	807	854	853	706	1211	1285	1243
Th	17	27	25	22	19	63	56	57
U	1	4	3	3	2	9	7	9
Mo								
Ga	28	31	27	29	26	32	27	28
Cu	42	40	36	41	25	0	0	0
V	181	193	179	190	176	76	63	67
La	30	67	56	45	46	191	182	178
Co	20	19	16	20	18	6	9	7
Sc	20	28	27	23	24	12	10	11

Garnet granite.

	UND 93	UND 94	UND 95	UND 96	UND 97	UND 409
SiO_2 (wt%)	68.61	68.67	69.93	70.68	68.25	68.61
TiO_2	0.36	0.39	0.36	0.30	0.44	0.41
Al_2O_3	16.40	16.17	15.58	15.50	16.30	15.79
Fe_2O_3	2.98	3.14	3.15	3.48	3.20	3.48
FeO						
MnO	0.06	0.07	0.07	0.09	0.06	0.07
MgO	0.41	0.47	0.41	0.35	0.48	0.43
CaO	2.02	2.23	2.22	2.28	2.20	2.33
Na_2O	2.66	2.74	2.75	2.75	2.68	3.00
K_2O	6.12	5.60	5.11	4.29	5.86	5.25
P_2O_5	0.26	0.32	0.23	0.12	0.32	0.22
Cr_2O_3						
H_2O^+						
H_2O^-						
CO_2						
S						
LOI	0.14	0.21	0.12	0.21	0.24	0.42
TOTAL	99.89	99.81	99.81	99.84	99.81	99.58
Trace elements in ppm						
Rb	167	154	141	112	164	137
Sr	228	220	210	214	223	242
Zr	306	349	363	346	362	367
Ni	1	2	1	0	2	1
Cr	0	0	0	0	0	2
Zn	47	46	41	32	59	55
Pb	48	51	44	42	47	47
Y	60	71	63	60	53	61
Nb	15	14	14	14	16	14
Ba	2426	2218	2038	1847	2337	1995
Th	5	7	12	14	17	9
U	0	0	2	1	0	1
Mo						
Ga	24	22	22	22	25	27
Cu	0	0	0	0	0	1
V	13	14	10	10	14	14
La	25	36	40	43	56	37
Co	2	0	4	1	1	2
Sc	7	6	7	8	6	9

Fine grained granulite - Valley Trust Formation.

	UND 329	UND 331	UND 339	UND 341	UND 359	UND 360	UND 361	UND 362	UND 363
SiO_2 (wt%)	65.08	56.13	63.71	66.31	55.05	64.13	65.46	58.52	61.49
TiO_2	0.81	0.88	1.04	1.00	1.29	1.04	0.89	1.00	1.06
Al_2O_3	14.52	15.07	17.19	16.28	18.42	14.91	16.58	16.34	16.15
Fe_2O_3	0.00	4.47	0.00	5.77	1.77	0.79	0.83	1.86	0.34
FeO	7.10	7.25	12.35	4.55	10.81	7.08	7.63	8.70	9.01
MnO	0.03	0.11	0.31	0.38	0.27	0.13	0.16	0.22	0.10
MgO	5.99	9.05	2.19	2.09	6.35	3.64	3.99	5.20	4.04
CaO	1.24	1.92	1.47	1.24	1.20	2.48	1.84	1.98	3.32
Na_2O	0.35	0.57	0.66	0.50	2.41	4.71	0.10	3.57	0.10
K_2O	4.41	1.94	1.68	1.35	2.20	0.97	2.09	1.30	2.28
P_2O_5	0.25	0.32	0.29	0.13	0.40	0.32	0.27	0.26	0.31
Cr_2O_3									
H_2O^+	0.62	0.60	0.48	0.61	0.36	0.27	0.45	0.28	0.32
H_2O^-	0.10	0.13	0.10	0.06	0.05	0.11	0.04	0.02	0.06
CO_2	0.08	0.08	0.06	0.05	0.05	0.08	0.08	0.08	0.15
S	0.00	0.00	0.00	0.00	0.03	0.02	0.04	0.02	0.37
LOI									
TOTAL	100.59	98.52	101.55	100.33	100.67	100.68	100.44	99.35	99.10
Trace elements in ppm									
Rb	82	73	53	58	54	23	52	26	62
Sr	60	81	155	129	178	274	72	331	140
Zr	74	81	234	210	113	118	77	57	78
Ni	1	1	22	19	1	1	1	1	1
Cr	115	45	100	116	43	59	35	53	33
Zn	62	207	124	117	171	90	100	118	160
Pb	13	14	27	22	16	14	14	17	21
Y	31	40	67	53	42	39	33	32	38
Nb	5	5	10	10	6	8	5	5	5
Ba	557	573	1063	864	302	242	231	193	435
Th	5	5	10	5	5	5	5	5	5
U	14	14	12	14	12	13	10	13	11
Mo	1	2	2	1	2	1	2	2	6
Ga	19	20	28	26	28	19	22	22	23
Cu	33	23	42	68	51	29	40	51	148
V	179	205	163	156	296	201	223	300	236
La									
Co									
Sc									

Fine grained amphibolitic granulite - Valley Trust Formation.

	UND 337	UND 338	UND 340
SiO_2 (wt%)	49.30	49.70	51.85
TiO_2	1.12	1.30	1.20
Al_2O_3	13.18	14.31	14.22
Fe_2O_3	8.27	3.46	2.09
FeO	5.50	9.45	9.79
MnO	0.21	0.25	0.37
MgO	9.22	7.57	7.16
CaO	11.94	12.26	11.44
Na_2O	1.47	1.57	0.95
K_2O	0.14	0.14	0.19
P_2O_5	0.10	0.12	0.12
Cr_2O_3			
H_2O^+	0.19	0.23	0.21
H_2O^-	0.01	0.06	0.07
CO_2	0.11	0.16	0.15
S	0.02	0.02	0.00
LOI			
TOTAL	100.79	100.58	99.81
Trace elements in ppm			
Rb	6	6	18
Sr	131	164	68
Zr			
Ni	133	88	82
Cr	285	214	195
Zn	91	90	85
Pb	11	16	14
Y	30	35	33
Nb	5	5	5
Ba	81	76	85
Th	5	5	5
U	13	8	13
Mo	1	1	2
Ga	20	21	25
Cu	97	98	98
V	368	398	386
La			
Co			
Sc			

Marginal granite - Ximba Suite.

	UND 21	UND 46	UND 47	UND 48	UND 49	UND 51	UND 72	UND 72a	UND 75
SiO_2 (wt%)	61.55	59.60	59.03	66.95	70.11	70.41	63.46	64.50	63.57
TiO_2	1.32	1.21	1.94	0.87	1.59	0.42	1.17	1.20	0.54
Al_2O_3	16.27	16.61	13.12	13.71	14.09	14.74	14.96	13.82	16.67
Fe_2O_3	4.06	2.25	4.92	1.63	1.59	0.62	6.78	2.84	1.11
FeO	3.57	4.30	7.52	4.18	1.96	1.87	0.00	3.52	2.06
MnO	0.15	0.13	0.26	0.11	0.06	0.03	0.12	0.12	0.07
MgO	0.60	1.29	2.20	1.12	1.60	1.56	1.58	1.49	1.11
CaO	4.20	2.76	5.30	2.83	2.68	2.42	3.90	3.94	2.24
Na_2O	3.62	3.52	3.47	2.64	3.02	2.77	3.05	2.95	2.57
K_2O	2.83	5.73	1.81	4.43	4.41	3.80	3.58	3.49	7.02
P_2O_5	0.71	0.34	0.62	0.31	0.23	0.18	0.49	0.53	0.66
Cr_2O_3	0.02								
H_2O^+	0.27	0.74	0.17	0.29	0.40	0.48		1.16	0.52
H_2O^-	0.16	0.16	0.15	0.13	0.14	0.34		0.10	0.09
CO_2	0.03	0.07	0.06	0.03	0.03	0.03		0.39	0.07
S								0.14	0.00
LOI							1.21		
TOTAL	99.51	98.74	100.62	99.26	101.93	99.69	99.08	100.20	98.30
Trace elements in ppm									
Rb	88	158	81	119	109	127	94		179
Sr	497	318	314	262	603	297	522	477	196
Zr	311	691	937	581	285	246	443	376	286
Ni					5	5	2	1	
Cr							8	32	
Zn	140				62	40	118	118	48
Pb	36				25	23	33	41	54
Y	30				27	16	51	49	57
Nb	21				13	14	17	15	16
Ba	1500	2341	863	1937	2532	846	2318	2289	1244
Th	5				18	11	9	11	35
U	0						2	6	4
Mo								3	
Ga							22	22	20
Cu							3	30	
V							66	135	
La							49		
Co							9		
Sc							18		

Marginal granite (continued).

	UND 76	UND 77	UND 301	UND 303	UND 304	UND 313
SiO_2 (wt%)	70.15	61.11	75.35	63.38	73.57	70.80
TiO_2	0.33	1.22	0.19	1.17	0.22	0.43
Al_2O_3	14.69	15.46	12.80	14.81	14.02	15.11
Fe_2O_3	0.15	2.97	2.14	7.08	1.75	3.61
FeO	1.86	3.65	0.00	0.00	0.00	0.00
MnO	0.03	0.14	0.02	0.14	0.02	0.05
MgO	0.27	1.73	0.11	1.75	0.31	0.94
CaO	1.44	3.88	0.61	4.21	1.55	2.54
Na_2O	2.91	2.99	2.30	3.32	2.75	2.93
K_2O	6.79	4.39	6.05	3.17	5.26	3.29
P_2O_5	0.10	0.56	0.03	0.51	0.06	0.11
Cr_2O_3						
H_2O^+	0.43	0.68				
H_2O^-	0.02	0.10				
CO_2	0.29	0.10				
S	0.01	0.09				
LOI			0.41	0.73	0.58	0.97
TOTAL	99.48	99.07	99.59	99.55	99.51	99.80
Trace elements in ppm						
Rb	152	103	159	97	194	111
Sr	286	531	138	447	158	267
Zr	149	397	176	323	169	256
Ni			0	5	2	3
Cr			1	10	5	13
Zn	47	116	27	115	25	55
Pb	34	32	42	33	50	27
Y	11	42	4	51	15	16
Nb	8	20	1	16	8	11
Ba	2334	2717	369	1432	852	910
Th	17	7	4	9	38	17
U	2	2	1	2	1	2
Mo						
Ga	23	26	15	22	16	21
Cu			0	4	0	0
V			14	76	20	46
La			20	53	35	36
Co			3	11	2	8
Sc			1	19	4	11

Biotite granite - Ximba Suite.

	UND 2	UND 10	UND 11	UND 12	UND 13	UND 20	UND 31	UND 32	UND 35
SiO_2 (wt%)	74.09	71.57	71.11	71.96	70.05	69.80	71.65	72.01	74.09
TiO_2	0.17	0.29	0.39	0.04	0.38	0.46	0.37	0.73	0.25
Al_2O_3	13.98	14.64	15.71	13.34	15.77	15.42	13.79	12.58	12.64
Fe_2O_3	0.91	0.41	0.37	0.90	0.85	1.24	0.45	1.31	0.48
FeO	0.34	1.58	2.34	2.18	2.21	1.79	2.66	2.91	1.83
MnO	0.03	0.03	0.04	0.05	0.04	0.05	0.05	0.06	0.03
MgO	0.26	0.41	0.10	0.10	0.14	0.10	0.79	1.08	0.65
CaO	0.88	1.36	1.80	1.92	1.70	1.70	1.92	2.06	1.54
Na_2O	3.29	2.61	2.91	3.15	3.07	3.86	3.03	2.75	2.51
K_2O	5.06	5.66	4.23	6.12	4.72	4.87	4.76	4.15	4.73
P_2O_5	0.14	0.22	0.24	0.17	0.25	0.24	0.13	0.17	0.10
Cr_2O_3									
H_2O^+	0.21	0.22	0.11	0.26	0.10	0.20			
H_2O^-	0.14	0.07	0.04	0.03	0.04	0.11	0.16	0.10	0.13
CO_2	0.01	0.10	0.01	0.09	0.03	0.01	0.07	0.09	0.12
S									
LOI							0.20	0.40	0.32
TOTAL	99.56	99.31	99.57	100.45	99.48	99.97	100.00	100.30	99.20
Trace elements in ppm									
Rb	144	168	159	155	167	158	136	160	138
Sr	83	165	170	221	163	160	151	171	149
Zr	154	215	191	299	288	246	243	291	228
Ni									
Cr									
Zn	52	71	90	79	89	89	72	93	57
Pb	32	46	42	37	34	35			
Y	4	9	34	12	21	27	52	80	38
Nb	7	13	13	13	18	14	15	25	15
Ba	438	1100	1400	1100	1100	900	1456	992	1235
Th	28	16	9	6	9	9	11	13	12
U	5	3	2	1	0	2			
Mo									
Ga									
Cu									
V									
La									
Co									
Sc									

Biotite granite (continued).

	UND 37	UND 38	UND 39	UND 40	UND 41	UND 43	UND 44
SiO_2 (wt%)	72.76	75.04	72.70	70.75	69.40	76.84	71.74
TiO_2	0.30	0.27	0.40	0.26	0.70	0.22	0.44
Al_2O_3	13.86	12.57	11.94	14.73	13.81	12.16	14.07
Fe_2O_3	0.29	0.50	1.10	0.11	1.97	0.58	0.60
FeO	2.33	1.70	2.43	2.18	1.48	1.49	2.62
MnO	0.03	0.03	0.04	0.03	0.05	0.03	0.05
MgO	0.74	0.77	0.69	0.26	1.49	0.66	0.96
CaO	1.65	1.16	1.53	1.66	1.54	0.70	1.58
Na_2O	2.75	2.59	2.64	2.93	3.08	2.24	2.75
K_2O	5.04	4.74	5.14	5.68	5.31	5.13	5.00
P_2O_5	0.12	0.10	0.10	0.16	0.32	0.10	0.17
Cr_2O_3							
H_2O^+					0.45	0.55	0.42
H_2O^-	0.11	0.16	0.14	0.15	0.29	0.13	0.14
CO_2	0.29	0.17	0.06	0.10	0.06	0.07	0.06
S							
LOI	0.58	0.68	0.43	0.36			
TOTAL	100.50	100.50	99.20	99.40	99.98	101.10	100.62
Trace elements in ppm							
Rb	158	128	155	150	168	108	120
Sr	146	147	126	168	201	92	182
Zr	234	379	301	221	326	198	345
Ni							
Cr							
Zn	63	50	68	54			
Pb							
Y	36	16	56	33			
Nb	16	14	17	15			
Ba	1242	1205	994	1459	2393	679	1537
Th	8	7	29	7			
U							
Mo							
Ga							
Cu							
V							
La							
Co							
Sc							

Biotite garnet granite - Ximba Suite.

	UND 28	UND 30	UND 36	UND 90	UND 91	UND 92
SiO_2 (wt%)	71.08	69.25	67.84	69.25	69.59	69.31
TiO_2	0.31	0.39	0.36	0.37	0.36	0.37
Al_2O_3	14.64	14.65	16.01	15.79	15.61	15.55
Fe_2O_3	0.42	0.68	0.27	3.45	3.34	3.50
FeO	2.11	2.31	2.67			
MnO	0.04	0.05	0.04	0.04	0.05	0.05
MgO	0.29	0.86	0.78	0.34	0.34	0.34
CaO	1.64	1.73	2.28	2.30	2.20	2.25
Na_2O	3.16	3.31	3.11	2.91	2.80	2.65
K_2O	5.04	4.86	4.91	5.27	5.42	5.15
P_2O_5	0.18	0.24	0.18	0.11	0.11	0.11
Cr_2O_3	0.03	0.03	0.01			
H_2O^+	0.20	0.25	0.48			
H_2O^-	0.04	0.04	0.12			
CO_2	0.01	0.10	0.10			
S						
LOI				0.43	0.22	0.38
TOTAL	99.19	98.75	99.16	99.83	99.82	99.27
Trace elements in ppm						
Rb	146	139	110	137	141	136
Sr	160	158	241	227	226	226
Zr	315	354	314	321	348	368
Ni				0	0	1
Cr				5	1	0
Zn	81	95	68	71	71	71
Pb	38	32		37	35	37
Y	23	33	41	27	31	28
Nb	13	14	16	17	17	18
Ba	1000	1000	2330	2062	2098	2049
Th	10	2	10	11	9	16
U	1	4		1	0	1
Mo						
Ga				24	24	25
Cu				0	0	0
V				16	14	12
La				64	62	71
Co				0	3	1
Sc				4	5	5

Biotite garnet granite - within contamination zone.

	UND 400	UND 401	UND 402	UND 403	UND 404	UND 405	UND 406	UND 407	UND 408
SiO_2 (wt%)	67.56	62.10	68.35	68.66	68.13	67.28	65.72	67.72	68.70
TiO_2	0.39	0.62	0.38	0.40	0.40	0.41	0.48	0.40	0.40
Al_2O_3	16.33	18.10	15.50	15.67	15.76	16.24	16.91	16.03	15.60
Fe_2O_3	3.52	5.61	3.58	3.70	3.88	3.81	4.18	3.75	3.87
FeO									
MnO	0.05	0.08	0.05	0.05	0.06	.0.06	0.05	0.04	0.05
MgO	0.38	0.60	0.35	0.36	0.36	0.42	0.49	0.37	0.37
CaO	2.57	3.18	2.40	2.46	2.43	2.46	2.82	2.50	2.53
Na_2O	3.49	3.66	2.99	3.12	3.17	3.03	3.49	3.23	3.10
K_2O	5.45	5.34	5.38	5.31	5.49	5.74	5.42	5.49	5.15
P_2O_5	0.12	0.18	0.11	0.13	0.13	0.13	0.16	0.12	0.13
Cr_2O_3									
H_2O^+									
H_2O^-									
CO_2									
S									
LOI	0.80	1.07	0.84	0.68	0.95	0.98	0.61	0.57	0.50
TOTAL	99.84	99.48	99.10	99.86	99.81	99.57	99.72	99.66	99.90
Trace elements in ppm									
Rb	134	148	132	134	138	142	138	137	131
Sr	264	283	251	253	255	258	273	257	252
Zr	369	551	360	396	364	368	471	367	380
Ni	0	0	1	1	0	0	0	2	0
Cr	1	1	0	2	0	1	0	3	3
Zn	76	124	76	79	79	79	95	84	83
Pb	41	38	34	40	41	44	38	38	37
Y	30	50	29	26	29	43	38	29	23
Nb	16	23	16	16	17	18	18	17	17
Ba	2103	2162	2082	2081	2168	2225	2188	2139	2074
Th	9	21	7	1	3	6	18	10	1
U	1	1	0	0	2	1	2	1	0
Mo									
Ga	22	29	24	20	22	24	24	23	27
Cu	5	1	0	0	0	0	4	0	0
V	19	28	18	16	15	16	20	17	17
La	57	99	47	26	26	46	78	56	51
Co	6	5	5	5	3	5	4	0	2
Sc	4	6	4	5	3	5	6	4	4

Biotite garnet granite - within contamination zone (continued).

	UND 98	UND 99
SiO_2 (wt%)	69.92	62.46
TiO_2	0.33	0.58
Al_2O_3	15.58	18.34
Fe_2O_3	3.65	5.01
FeO		
MnO	0.09	0.06
MgO	0.43	0.64
CaO	2.26	3.17
Na_2O	2.95	3.74
K_2O	4.66	5.50
P_2O_5	0.18	0.19
Cr_2O_3		
H_2O^+		
H_2O^-		
CO_2		
S		
LOI	0.39	0.78
TOTAL	100.06	99.69
Trace elements in ppm		
Rb	119	147
Sr	231	291
Zr	371	567
Ni	4	3
Cr	1	3
Zn	38	103
Pb	47	34
Y	66	51
Nb	13	22
Ba	1935	2106
Th	11	13
U	0	0
Mo		
Ga	20	24
Cu	2	1
V	10	31
La	34	64
Co	4	6
Sc	10	7

Charnockite and green hornblende granite (subcharnockite) - Mlahlanja Suite.

	UND 18	UND 23	UND 24	UND 25	UND 71	UND 71a	UND 74	UND 74a	UND 83
SiO_2 (wt%)	64.18	65.63	64.51	64.95	75.51	78.11	70.66	73.13	71.68
TiO_2	0.67	1.03	0.91	0.92	0.25	0.25	0.47	0.46	0.25
Al_2O_3	17.20	14.71	15.81	14.69	12.55	11.96	14.20	13.64	14.04
Fe_2O_3	1.05	1.99	1.71	1.56	2.19	0.33	3.61	0.00	0.24
FeO	4.60	5.19	4.71	4.85	0.00	1.66	0.00	3.96	1.86
MnO	0.09	0.13	0.12	0.13	0.03	0.02	0.05	0.05	0.03
MgO	0.45	0.10	0.10	0.74	0.26	0.11	0.42	0.34	0.13
CaO	3.16	3.47	3.07	3.11	1.47	1.47	2.15	2.17	1.73
Na_2O	3.11	3.21	3.66	3.41	2.40	2.36	2.88	2.63	2.98
K_2O	4.45	3.86	4.31	3.99	4.79	4.79	4.93	4.15	5.26
P_2O_5	0.32	0.42	0.42	0.41	0.07	0.10	0.13	0.16	0.11
Cr_2O_3									
H_2O^+	0.15	0.05	0.48	0.07		0.31		0.30	0.45
H_2O^-	0.11	0.10	0.12	0.10		0.02		0.08	0.02
CO_2	0.17	0.03	0.01	0.03		0.10		0.12	0.09
S						0.00		0.01	0.02
LOI					0.23		0.13		
TOTAL	99.92	100.13	100.15	99.15	99.52	101.59	99.47	101.21	98.89
Trace elements in ppm									
Rb	97	101	98	105	132	132	129	129	153
Sr	295	298	304	286	153	145	194	183	165
Zr	712	607	638	698	246	219	372	332	238
Ni					2	1	2	1	
Cr					1	16	4	22	
Zn	116	144	141	144	50	52	74	76	56
Pb	31	33	34	33	34	34	29	37	33
Y	35	52	46	69	28	30	46	45	29
Nb	23	25	24	31	7	6	13	11	11
Ba	1900	1900	1800	1600	1126	1121	1405	1352	1533
Th	2	2	2	1	7	6	8	7	9
U	1	2	1	2	2	6	3	6	2
Mo						7		6	
Ga					1	21	22	23	26
Cu					0	9	0	15	
V					10	33	19	52	
La					59		60		
Co					3		5		
Sc					5		8		

Charnockite and green hornblende granite (subcharnockite) (continued).

	UND 84	UND 85	UND 86	UND 87	UND 88	UND 89
SiO_2 (wt%)	69.05	73.57	74.00	73.74	75.28	74.38
TiO_2	0.36	0.28	0.26	0.30	0.24	0.30
Al_2O_3	14.93	13.08	13.18	13.15	12.56	13.64
Fe_2O_3	0.00	0.00	0.00	0.00	0.00	0.40
FeO	3.40	2.96	2.60	2.96	2.30	2.04
MnO	0.04	0.03	0.03	0.03	0.02	0.03
MgO	0.42	0.09	0.11	0.07	0.09	0.13
CaO	1.89	1.61	1.65	1.79	1.66	1.88
Na_2O	2.68	2.52	2.29	2.59	2.29	2.63
K_2O	5.10	6.34	5.55	6.81	5.64	5.60
P_2O_5	0.15	0.10	0.10	0.11	0.09	0.12
Cr_2O_3						
H_2O^+	0.42	0.56	0.28	0.27	0.29	0.32
H_2O^-	0.08	0.05	0.08	0.04	0.04	0.01
CO_2	0.06	0.13	0.06	0.10	0.08	0.05
S	0.21	0.01	0.02	0.02	0.03	0.00
LOI						
TOTAL	98.80	101.34	100.20	101.98	100.61	101.53
Trace elements in ppm						
Rb	144	142	139	144	129	148
Sr	155	156	142	143	135	166
Zr	348	242	231	268	227	243
Ni						1
Cr						15
Zn	75	54	54	62	51	60
Pb	30	31	30	30	30	40
Y	39	27	26	30	26	33
Nb	14	12	11	13	10	7
Ba	1458	1423	1288	1336	1205	1317
Th	13	11	10	12	11	7
U	2	2	2	2	2	6
Mo						6
Ga	27	25	24	25	23	23
Cu						10
V						36
La						
Co						
Sc						

Hornblende granite - Mlahlanja Suite.

	NDF 26	UND 60	UND 61	UND 62	UND 63	UND 64	UND 65	UND 66
SiO_2 (wt%)	61.33	65.26	66.31	64.85	60.36	63.63	65.89	63.91
TiO_2	1.31	0.70	0.62	0.71	1.15	0.84	0.58	0.90
Al_2O_3	16.25	14.04	14.16	14.57	14.19	14.09	14.23	14.03
Fe_2O_3	2.29	2.67	1.89	0.44	2.90	1.28	0.80	2.65
FeO	5.88	3.83	3.93	5.92	6.45	6.03	5.00	5.25
MnO	0.16	0.07	0.06	BD	0.10	0.10	0.06	0.05
MgO	0.81	0.88	0.69	0.81	1.43	1.01	0.73	1.13
CaO	3.93	3.50	3.14	3.39	4.85	3.80	3.00	3.91
Na_2O	3.00	3.05	3.34	3.26	3.14	3.30	3.39	2.90
K_2O	3.17	4.76	5.08	4.36	3.63	4.20	5.00	4.26
P_2O_5	0.65	0.54	0.48	0.54	0.84	0.63	0.45	0.69
Cr_2O_3	0.03							
H_2O^+	0.14	0.43	0.70	0.76	0.50	0.75	0.65	0.53
H_2O^-	0.07	0.10	BD	0.12	0.08	0.08	0.05	0.11
CO_2	0.05	0.05	0.05	0.05	0.10	0.12	0.20	0.90
S								
LOI								
TOTAL	99.07	99.88	100.45	99.78	99.72	99.86	100.03	101.22
Trace elements in ppm								
Rb	92	107	102	86	84	104	120	101
Sr	340	321	320	356	376	336	298	325
Zr	508	387	422	426	468	443	454	446
Ni		3	1	3	3	7	1	14
Cr								
Zn	165	91	99	102	156	110	105	121
Pb	34	38	37	38	34	35	38	35
Y	65	71	62	63	96	83	81	87
Nb	28	18	16	18	19	19	18	20
Ba	1500	1977	2315	2168	1841	1936	2072	1927
Th	3	5	6	2	9	5	10	5
U		1	1	1	4	1	1	1
Mo		11	14	12	16	11	16	13
Ga		16	16	17	17	17	18	18
Cu		1	1	1	6	1	1	1
V		124	103	122	189	146	107	157
La								
Co		15	10	21	20	19	9	19
Sc								

Hornblende granite (continued).

	UND 67	UND 68
SiO_2 (wt%)	70.40	70.13
TiO_2	0.38	0.43
Al_2O_3	13.71	13.64
Fe_2O_3	1.65	0.53
FeO	2.37	3.68
MnO	0.05	0.05
MgO	0.62	0.68
CaO	2.07	2.23
Na_2O	3.06	2.95
K_2O	5.20	5.37
P_2O_5	0.37	0.38
Cr_2O_3		
H_2O^+	0.32	0.32
H_2O^-	BD	BD
CO_2	0.10	0.10
S		
LOI		
TOTAL	100.30	100.49
Trace elements in ppm		
Rb	176	159
Sr	188	202
Zr	225	285
Ni	1	6
Cr		
Zn	68	67
Pb	38	38
Y	79	85
Nb	16	16
Ba	1242	1422
Th	6	3
U	1	1
Mo	7	8
Ga	18	19
Cu	1	1
V	79	91
La		
Co	8	8
Sc		

Garnet hornblende granite - Mlahlanja Suite.

	UBD 5	UND 6	UND 8	UND 9	UND 81	UND 82
SiO_2 (wt%)	67.16	67.78	65.41	65.90	72.58	67.87
TiO_2	0.65	0.72	0.80	0.64	0.32	0.65
Al_2O_3	15.33	15.17	15.44	16.27	12.84	13.66
Fe_2O_3	1.97	1.20	1.81	1.32	0.00	0.00
FeO	4.03	4.93	5.37	4.28	2.75	5.66
MnO	0.13	0.12	0.12	0.10	0.04	0.11
MgO	0.61	0.58	1.44	1.21	0.14	0.46
CaO	2.31	2.30	2.61	2.78	1.66	2.78
Na_2O	2.28	2.19	2.44	2.56	2.13	2.28
K_2O	3.93	3.32	3.42	3.79	6.53	4.35
P_2O_5	0.37	0.36	0.41	0.33	0.14	0.28
Cr_2O_3	0.02	0.02	0.02	0.02		
H_2O^+	0.55	0.98	0.31	0.12	0.39	0.41
H_2O^-	0.04	0.15	0.14	0.06	0.05	0.02
CO_2	0.08	0.12	0.01	0.19	0.28	0.30
S					0.00	0.07
LOI						
TOTAL	99.46	99.94	99.75	99.57	99.84	98.90
Trace elements in ppm						
Rb	148	144	143	131	203	173
Sr	280	279	270	305	258	260
Zr	585	634	602	523	178	519
Ni						
Cr						
Zn	153	163	174	136	66	125
Pb	35	34	33	39	41	32
Y	54	54	74	50	26	61
Nb	28	29	31	25	18	30
Ba	1300	1300	1300	1400	1682	1745
Th	10	11	12	8	16	14
U	1	0	2	1	2	2
Mo						
Ga					23	27
Cu						
V						
La						
Co						
Sc						

Nqwadolo Suite.

	UND 14	UND 15	UND 16	UND 17	UND 19	UND 22	UND 29	NQG 1	NQG 2
SiO_2 (wt%)	76.65	75.26	75.45	74.93	74.73	75.19	74.80	76.94	76.63
TiO_2	0.16	0.12	0.15	0.11	0.07	0.07	0.06	0.12	0.11
Al_2O_3	11.55	14.21	12.66	13.10	13.91	13.36	14.21	12.52	12.54
Fe_2O_3	0.31	0.31	0.34	0.47	0.10	0.12	0.51	0.18	0.17
FeO	1.02	1.02	0.99	0.73	1.03	0.63	0.54	1.48	1.37
MnO	0.03	0.17	0.02	0.02	0.03	0.03	0.01	0.03	0.02
MgO	0.10	0.48	0.37	0.11	0.10	0.10	0.16	0.09	0.02
CaO	0.89	0.76	0.75	0.77	0.47	0.30	0.62	0.80	0.83
Na_2O	3.17	3.72	3.39	3.54	3.76	5.36	4.48	2.89	2.93
K_2O	5.84	4.33	4.80	4.93	5.05	3.96	3.62	5.28	5.39
P_2O_5	0.12	0.19	0.14	0.15	0.15	0.14	0.14	0.01	0.01
Cr_2O_3	0.01	0.02	0.02	0.03	0.03	0.03	0.02	0.00	0.00
H_2O^+	0.07	0.05	0.12	0.04	0.08	0.21	0.10		
H_2O^-	0.07	0.10	0.04	0.11	0.04	0.14	0.07		
CO_2	0.04	0.01	0.02	0.02	0.04	0.02	0.08		
S									
LOI									
TOTAL	100.03	100.75	99.26	99.06	99.59	99.66	99.42	100.34	100.02
Trace elements in ppm									
Rb	224	231	225	175	231	99	249	180	205
Sr	11	13	11	12	11	13	10	16	6
Zr	128	143	132	120	79	100	75	129	110
Ni									
Cr									
Zn	88	106	102	89	90		136	98	88
Pb	58	59	57	56	68		75	49	49
Y	61	67	74	46	152		216	53	85
Nb	17	18	17	12	39		40	14	18
Ba	100	100	100	100	600	100	100	129	16
Th	17	21	19	14	35		20	17	16
U	7	9	6	4	21		14	6	6
Mo									
Ga									
Cu									
V									
La									
Co									
Sc									

Nqwadolo Suite (continued).

	NQG 3	NQG 4	NQG 5	NQG 6
SiO_2 (wt%)	77.42	77.43	76.39	74.49
TiO_2	0.11	0.07	0.15	0.15
Al_2O_3	12.41	12.60	12.48	13.57
Fe_2O_3	0.16	0.13	0.19	0.20
FeO	1.31	1.05	1.52	1.58
MnO	0.01	0.02	0.02	0.02
MgO	0.07	0.00	0.08	0.10
CaO	0.83	0.75	1.01	0.95
Na_2O	2.89	3.19	2.93	3.31
K_2O	5.26	5.14	5.23	5.69
P_2O_5	0.02	0.01	0.03	0.03
Cr_2O_3	0.00	0.00	0.00	0.00
H_2O^+				
H_2O^-				
CO_2				
S				
LOI				
TOTAL	100.49	100.39	100.03	100.09
Trace elements in ppm				
Rb	176	229	180	204
Sr	15	6	31	35
Zr	127	90	134	131
Ni				
Cr				
Zn	83	78	80	90
Pb	44	64	45	48
Y	89	179	73	84
Nb	14	56	17	19
Ba	128	25	318	379
Th	16	47	16	17
U	7	13	5	6
Mo				
Ga				
Cu				
V				
La				
Co				
Sc				

REE Analyses.

A. Ximba Suite.

	UND 10	UND 20	UND 28	UND 36	UND 38
La (ppm)	78.70	67.43	86.10	52.80	40.10
Ce	157.65	146.74	178.09	101.67	79.34
Pr	17.63	17.16	19.89	11.84	8.83
Nd	71.60	67.48	85.20	52.60	36.20
Sm	11.77	12.42	13.86	10.11	6.12
Eu	2.42	2.06	2.73	4.14	2.03
Gd	8.83	11.18	10.39	9.81	4.68
Dy	5.46	8.26	7.82	8.41	2.97
Ho	1.01	1.62	1.45	1.63	0.55
Er	2.30	4.06	2.61	4.48	1.44
Yb	1.44	2.61	2.46	3.53	1.13
Lu	0.26	0.34	0.38	0.53	0.20

B. Mlahlanja Suite.

	UND 6	UND 8	UND 18	UND 23	UND 24	UND 26	UND 61	UND 66	UND 67
La (ppm)	94.20	72.00	63.20	51.04	57.75	59.60	49.83	60.20	49.50
Ce	193.96	153.32	125.67	128.01	131.56	135.85	114.14	132.35	105.29
Pr	23.33	19.05	14.85	16.62	16.97	17.64	14.88	16.76	13.03
Nd	102.20	88.30	67.20	78.02	73.47	83.50	64.51	79.70	59.20
Sm	19.54	19.23	12.51	14.91	14.31	17.59	12.90	16.92	13.37
Eu	4.54	4.28	5.08	4.17	4.24	4.01	4.17	4.13	2.21
Gd	17.53	19.13	11.52	14.36	13.68	16.92	12.36	16.42	13.50
Dy	15.78	16.82	9.39	12.47	11.64	15.13	10.51	14.47	12.89
Ho	3.41	3.30	1.85	2.63	2.45	2.98	2.18	2.87	2.52
Er	11.22	9.25	5.21	6.56	6.71	8.52	5.98	8.13	7.02
Yb	13.42	7.95	4.65	6.13	5.98	7.51	5.05	7.06	5.64
Lu	2.00	1.20	0.75	0.85	0.83	1.13	0.69	1.08	0.81

C. Nqwadolo Suite.

	UND 15	NQG 1	NQG 2	NQG 3	NQG 4	NQG 5	NQG 6
La (ppm)	49.76	60.80	55.90	60.20	22.90	71.60	81.30
Ce	129.09	137.19	137.64	137.07	58.50	157.87	183.93
Pr	17.39	17.15	18.39	17.29	8.87	19.38	22.92
Nd	76.21	77.10	86.80	79.30	46.40	84.70	100.90
Sm	19.41	17.22	23.25	20.18	19.75	18.90	23.23
Eu	0.21	0.39	0.21	0.42	0.15	0.69	0.71
Gd	18.21	14.45	22.48	21.41	28.04	18.03	22.37
Dy	15.76	10.75	19.78	19.99	32.96	16.16	19.36
Ho	3.23	2.08	3.81	3.80	6.56	3.11	3.73
Er	8.76	5.93	10.63	10.14	18.22	8.53	9.73
Yb	7.19	5.11	8.49	7.50	13.44	6.20	7.76
Lu	0.94	0.78	1.20	1.06	1.82	0.85	1.12

APPENDIX 4

STATISTICS

Definitions (after Rollinson 1993).

Correlation coefficient - Measures the strength of the linear relationship between two variables in a population.

Standard deviation - The spread of values about the mean.

Mean - The *n*th root of the product of positive values.

Variance - The square of the standard deviation.

1. MAJOR ELEMENT CORRELATION COEFFICIENTS

A. Nagle Dam Formation.

	SiO_2	TiO_2	Al_2O_3	FeO_{TOT}	MnO	MgO	CaO	Na_2O	K_2O	P_2O_5
SiO_2	1									
TiO_2	-0.87	1								
Al_2O_3	-0.46	0.67	1							
FeO_{TOT}	-0.96	0.87	0.36	1						
MnO	-0.61	0.51	0.06	0.66	1					
MgO	-0.89	0.66	0.02	0.91	0.67	1				
CaO	-0.96	0.77	0.30	0.93	0.66	0.91	1			
Na_2O	0.02	0.17	0.49	-0.12	-0.15	-0.29	-0.04	1		
K_2O	0.75	-0.75	-0.38	-0.81	-0.61	-0.67	-0.80	-0.22	1	
P_2O_5	-0.57	0.78	0.8	0.57	0.24	0.22	0.47	0.43	-0.67	1

B. Amphibolite - Valley Trust Formation.

	SiO_2	TiO_2	Al_2O_3	FeO_{TOT}	MnO	MgO	CaO	Na_2O	K_2O	P_2O_5
SiO_2	1									
TiO_2	-0.58	1								
Al_2O_3	0.66	-0.55	1							
FeO_{TOT}	-0.77	0.83	-0.65	1						
MnO	-0.63	0.46	-0.77	0.72	1					
MgO	-0.63	0.08	-0.77	0.35	0.45	1				
CaO	-0.40	-0.17	-0.65	0.04	0.56	0.76	1			
Na_2O	0.17	0.28	0.37	-0.06	-0.66	-0.38	-0.76	1		
K_2O	0.53	-0.3	0.59	-0.49	-0.24	-0.74	-0.26	-0.06	1	
P_2O_5	0.61	-0.15	0.75	-0.33	-0.41	-0.93	-0.72	0.35	0.75	1

C. Quartzo-feldspathic gneiss - Valley Trust Formation.

	SiO_2	TiO_2	Al_2O_3	FeO_{TOT}	MnO	MgO	CaO	Na_2O	K_2O	P_2O_5
SiO_2	1									
TiO_2	-0.69	1								
Al_2O_3	-0.82	0.35	1							
FeO_{TOT}	-0.45	0.45	0.12	1						
MnO	-0.52	0.80	0.34	0.76	1					
MgO	-0.57	0.60	0.20	0.70	0.4	1				
CaO	-0.58	0.56	0.34	0.67	0.50	0.93	1			
Na_2O	-0.35	0.40	0.02	0.40	0.02	0.35	0.10	1		
K_2O	-0.52	0.10	0.39	0.18	-0.10	-0.06	-0.08	0.21	1	
P_2O_5	-0.42	0.71	0.33	0.62	0.91	0.07	0.14	0.06	-0.11	1

D. Pelitic gneiss - Valley Trust Formation.

	SiO_2	TiO_2	Al_2O_3	FeO_{TOT}	MnO	MgO	CaO	Na_2O	K_2O	P_2O_5
SiO_2	1									
TiO_2	-0.33	1								
Al_2O_3	-0.94	0.43	1							
FeO_{TOT}	-0.90	0.51	0.89	1						
MnO	-0.26	0.54	0.29	0.48	1					
MgO	-0.85	0.36	0.77	0.89	0.51	1				
CaO	-0.11	-0.06	-0.04	0.22	0.55	0.51	1			
Na_2O	-0.61	0.12	0.45	0.42	-0.14	0.31	-0.15	1		
K_2O	-0.70	-0.13	0.62	0.40	-0.34	0.35	-0.32	0.66	1	
P_2O_5	0.03	-0.13	-0.17	0.16	0.43	0.38	-0.85	-0.31	-0.45	1

E. Pelitic fine grained granulite - Valley Trust Formation.

	SiO_2	TiO_2	Al_2O_3	FeO_{TOT}	MnO	MgO	CaO	Na_2O	K_2O	P_2O_5
SiO_2	1									
TiO_2	-0.46	1								
Al_2O_3	-0.34	0.77	1							
FeO_{TOT}	-0.65	0.58	0.72	1						
MnO	0.04	0.51	0.68	0.6	1					
MgO	-0.74	-0.16	-0.23	0.14	-0.53	1				
CaO	-0.04	0.02	-0.26	-0.26	-0.46	-0.05	1			
Na_2O	-0.26	0.40	-0.01	-0.02	-0.05	0.01	0.13	1		
K_2O	0.10	-0.40	-0.27	-0.36	-0.57	0.35	-0.25	-0.5	1	
P_2O_5	-0.68	0.50	0.30	0.35	-0.33	0.49	0.24	0.31	0.04	1

F. Ximba Suite.

	SiO_2	TiO_2	Al_2O_3	FeO_{TOT}	MnO	MgO	CaO	Na_2O	K_2O	P_2O_5
SiO_2	1									
TiO_2	-0.72	1								
Al_2O_3	-0.61	0.05	1							
FeO_{TOT}	-0.82	0.87	0.12	1						
MnO	-0.79	0.87	0.09	0.97	1					
MgO	-0.50	0.79	-0.19	0.66	0.67	1				
CaO	-0.88	0.81	0.37	0.90	0.87	0.61	1			
Na_2O	-0.62	0.34	0.61	0.43	0.39	0.03	0.51	1		
K_2O	0.29	-0.64	0.21	-0.64	-0.64	-0.59	-0.62	-0.18	1	
P_2O_5	-0.73	0.75	0.21	0.71	0.78	0.61	0.70	0.31	-0.46	1

G. Mlahlanja Suite.

	SiO_2	TiO_2	Al_2O_3	FeO_{TOT}	MnO	MgO	CaO	Na_2O	K_2O	P_2O_5
SiO_2	1									
TiO_2	-0.91	1								
Al_2O_3	-0.75	0.64	1							
FeO_{TOT}	-0.95	0.95	0.62	1						
MnO	-0.70	0.80	0.69	0.73	1					
MgO	-0.73	0.62	0.43	0.75	0.42	1				
CaO	-0.92	0.91	0.52	0.94	0.57	0.70	1			
Na_2O	-0.61	0.52	0.38	0.50	0.22	0.27	0.64	1		
K_2O	0.68	-0.79	-0.63	-0.75	-0.75	-0.61	-0.64	-0.23	1	
P_2O_5	-0.90	0.87	0.46	0.93	0.54	0.78	0.94	0.59	-0.63	1

H. Nqwadolo Suite.

	SiO_2	TiO_2	Al_2O_3	FeO_{TOT}	MnO	MgO	CaO	Na_2O	K_2O	P_2O_5
SiO_2	1									
TiO_2	0.06	1								
Al_2O_3	-0.76	-0.50	1							
FeO_{TOT}	0.26	0.66	-0.34	1						
MnO	-0.19	0.09	0.42	-0.07	1					
MgO	-0.43	0.23	0.44	-0.19	0.74	1				
CaO	0.36	0.77	-0.56	0.78	-0.07	-0.16	1			
Na_2O	-0.73	-0.52	0.79	-0.73	0.21	0.41	-0.66	1		
K_2O	0.42	0.56	-0.7	0.61	-0.30	-0.51	0.55	-0.81	1	
P_2O_5	-0.67	-0.09	0.51	-0.67	0.49	0.71	-0.53	0.74	-0.56	1

2. SILICA-TRACE ELEMENT CORRELATION COEFFICIENTS.

A. Nagle Dam Formation.

	SiO_2	Rb	Sr	Zr	Ni	Cr	Zn	Pb	Y	Nb	Ba
SiO_2	1										
Rb	0.7	1									
Sr	-0.17	-0.37	1								
Zr	-0.31	-0.31	0.71	1							
Ni	-0.66	-0.45	-0.38	-0.28	1						
Cr	-0.76	-0.51	-0.47	-0.27	0.9	1					
Zn	-0.83	-0.51	0.19	0.36	0.53	0.55	1				
Pb	0.51	0.65	-0.29	-0.17	-0.37	-0.4	-0.42	1			
Y	-0.57	-0.19	0.17	0.55	0.13	0.21	0.56	0.14	1		
Nb	-0.36	-0.16	0.1	0.6	-0.06	0.23	0.29	-0.09	0.64	1	
Ba	0.52	0.42	0.02	-0.3	-0.21	-0.36	-0.28	0.01	-0.69	-0.46	1

B. Amphibolite - Valley Trust Formation.

	SiO_2	Rb	Sr	Zr	Ni	Cr	Zn	Pb	Y	Nb	Ba
SiO_2	1										
Rb	0.42	1									
Sr	0.41	-0.004	1								
Zr	-0.08	-0.06	0.3	1							
Ni	-0.71	-0.55	-0.42	-0.43	1						
Cr	-0.45	-0.2	-0.49	-0.68	0.86	1					
Zn	-0.68	-0.3	-0.59	0.43	0.29	-0.03	1				
Pb	0.43	0.23	-0.34	-0.35	-0.13	0.1	-0.15	1			
Y	-0.03	-0.04	-0.3	0.43	-0.05	-0.08	0.45	0.39	1		
Nb	-0.36	-0.14	0.1	0.86	-0.26	-0.54	0.58	-0.6	0.12	1	
Ba	0.63	0.98	0.02	-0.1	-0.8	-0.4	-0.67	0.31	-0.25	-0.26	1

C. Quartzo-feldspathic gneiss - Valley Trust Formation.

	SiO_2	Rb	Sr	Zr	Zn	Pb	Y	Nb	Ba
SiO_2	1								
Rb	-0.45	1							
Sr	-0.84	0.03	1						
Zr	-0.54	0.13	0.38	1					
Zn	-0.59	-0.12	0.76	0.18	1				
Pb	0.72	-0.09	-0.63	-0.7	-0.64	1			
Y	0.65	-0.37	-0.28	0.34	-0.27	0.22	1		
Nb	0.45	-0.21	-0.21	0.36	-0.19	0.3	0.97	1	
Ba	-0.82	0.08	0.95	0.32	0.59	-0.65	-0.09	-0.14	1

D. Pelitic gneiss - Valley Trust Formation.

	SiO_2	Rb	Sr	Zr	Ni	Cr	Zn	Pb	Y	Nb	Ba
SiO_2	1										
Rb	-0.67	1									
Sr	-0.07	-0.37	1								
Zr	-0.07	-0.27	0.7	1							
Ni	-0.34	0.34	-0.35	-0.39	1						
Cr	0.01	-0.17	-0.32	-0.7	0.45	1					
Zn	-0.82	0.71	0.08	-0.06	0.57	0.13	1				
Pb	-0.46	0.74	-0.49	-0.27	0.32	-0.01	0.63	1			
Y	0.1	-0.05	-0.12	-0.2	0.14	0.44	0.31	0.16	1		
Nb	-0.37	0.2	0.51	0.67	-0.13	-0.55	0.33	0.06	-0.06	1	
Ba	-0.3	0.02	0.46	0.84	-0.35	-0.62	0.17	0.1	-0.05	0.66	1

E. Pelitic gneiss - excluding the biotite gneiss.

	SiO_2	Rb	Sr	Zr	Ni	Cr	Zn	Pb	Y	Nb	Ba
SiO_2	1										
Rb	-0.75	1									
Sr	0.14	-0.41	1								
Zr	0.52	-0.34	0.25	1							
Ni	-0.48	0.3	-0.17	-0.13	1						
Cr	-0.21	-0.4	0.25	-0.27	0.29	1					
Zn	-0.85	0.71	-0.11	-0.13	0.6	0.15	1				
Pb	-0.55	0.75	-0.44	-0.14	0.26	-0.23	0.66	1			
Y	0	-0.13	0.22	0.63	-0.01	0.25	0.32	0.08	1		
Nb	-0.44	0.64	-0.18	0.3	0.22	-0.36	0.65	0.59	0.38	1	
Ba	-0.19	0.31	-0.24	0.29	-0.07	-0.15	0.35	0.54	0.55	0.58	1

F. Pelitic fine grained granulite - Valley Trust Formation.

	SiO_2	Rb	Sr	Zr	Zn	Pb	Y	Nb	Ba
SiO_2	1								
Rb	0.67	1							
Sr	0.45	-0.23	1						
Zr	0.57	0.34	0.22	1					
Zn	0.57	0.58	0.29	0.33	1				
Pb	0.79	0.51	0.43	0.82	0.6	1			
Y	0.78	0.53	0.36	0.92	0.61	0.94	1		
Nb	0.76	0.37	0.43	0.95	0.4	0.86	0.94	1	
Ba	0.53	0.61	-0.05	0.87	0.37	0.78	0.84	0.78	1

G. Ximba Suite.

	SiO_2	Rb	Sr	Zr	Ni	Cr	Zn	Pb	Y	Nb	Ba
SiO_2	1										
Rb	0.38	1									
Sr	-0.68	-0.64	1								
Zr	-0.74	-0.4	0.34	1							
Ni	-0.01	-0.4	0.51	-0.24	1						
Cr	-0.24	-0.59	0.63	-0.1	0.28	1					
Zn	-0.74	-0.47	0.54	0.59	-0.16	0.33	1				
Pb	0.03	0.5	-0.38	-0.05	-0.52	-0.14	-0.2	1			
Y	-0.45	-0.21	0.22	0.44	0.14	0.31	0.41	0.24	1		
Nb	-0.62	-0.25	0.31	0.69	-0.16	0.01	0.71	-0.07	0.66	1	
Ba	-0.53	-0.25	0.59	0.35	-0.25	-0.04	0.39	-0.05	0.31	0.48	1

H. Mlahlanja Suite.

	SiO_2	Rb	Sr	Zr	Ni	Cr	Zn	Pb	Y	Nb	Ba
SiO_2	1										
Rb	0.61	1									
Sr	-0.92	-0.59	1								
Zr	-0.77	-0.5	0.7	1							
Ni	-0.42	-0.4	0.24	0.37	1						
Cr	0.2	0.16	0.01	-0.08	-0.94	1					
Zn	-0.83	-0.42	0.79	0.89	-0.03	0.31	1				
Pb	-0.12	0.13	0.35	-0.11	-0.74	0.62	0.03	1			
Y	-0.73	-0.35	0.69	0.4	0.06	0.22	0.56	0.33	1		
Nb	-0.73	-0.24	0.69	0.88	0.36	-0.08	0.91	-0.03	0.41	1	
Ba	-0.67	-0.54	0.74	0.38	0.01	0.18	0.31	0.26	0.46	0.31	1

I. Nqwadolo Suite.

	SiO_2	Rb	Sr	Zr	Zn	Pb	Y	Nb	Ba
SiO_2	1								
Rb	-0.34	1							
Sr	-0.2	-0.47	1						
Zr	0.16	-0.53	0.53	1					
Zn	-0.51	0.55	-0.3	-0.3	1				
Pb	-0.42	0.83	-0.6	-0.76	0.6	1			
Y	-0.12	0.66	-0.39	-0.89	0.41	0.75	1		
Nb	0.01	0.65	-0.4	-0.83	0.13	0.72	0.9	1	
Ba	-0.48	0.01	0.51	-0.18	-0.16	0.05	0.11	0.1	1

3. RANGE, STANDARD DEVIATION, AVERAGE, MEAN AND VARIANCE.

A. Nagle Dam Formation.

	Maximum	Minimum	Number of samples	Sample Standard deviation	Population standard devation	Average	Mean	Variance
SiO_2	77.93	47.17	23	10.31	10.08	63.14	62.32	106.3
TiO_2	1.43	0.01	23	0.49	0.48	0.6	0.3	0.24
Al_2O_3	20.27	12.83	23	1.92	1.88	15.09	14.98	3.7
FeO	11.7	0.23	23	3.75	3.67	5.53	3.52	14.06
MnO	0.3	0	23	0.08	0.08	0.11	-	0.01
MgO	10.65	0	23	3.33	3.26	3.58	-	11.1
CaO	12.77	0.27	23	3.72	3.64	5.57	3.89	13.9
Na_2O	4.44	0.27	23	0.91	0.89	2.6	2.3	0.83
K_2O	8.93	0.47	23	2.19	2.14	2.72	2.03	4.8
P_2O_5	0.45	0.01	23	0.12	0.12	0.17	0.12	0.02
Rb	208	11	23	55.4	54.2	91	70	3,069
Sr	948	46	23	211.5	206.9	377	318	44,747
Zr	212	25	23	51.4	50.3	95	83	2,646
Ni	291	0	23	75.4	73.7	43	-	5,683
Cr	717	0	19	245.7	239.1	168	-	60,353
Zn	195	3	23	45.4	44.4	61	40	2,059
Pb	68	4	23	15.8	15.5	23	18	251
Y	41	2	23	11.3	11.1	21	16	128
Nb	14	0	23	4	3.9	6	-	16
Ba	1,196	102	23	315.2	308.3	591	498	99,369

B. Amphibolite - Nagle Dam Formation.

	Maximum	Minimum	Number of samples	Sample Standard deviation	Population standard deviation	Average	Mean	Variance
SiO_2	51.89	47.17	5	1.91	1.71	50.26	50.23	3.6
TiO_2	1.43	0.46	5	0.38	0.34	0.97	0.9	0.14
Al_2O_3	15.44	13.21	5	0.89	0.79	14.29	14.27	0.79
FeO	11.7	8.4	5	1.58	1.41	10.26	10.16	2.5
MnO	0.26	0.16	5	0.04	0.03	0.19	0.19	0.002
MgO	10.65	8.19	5	0.98	0.88	9.03	8.99	0.96
CaO	12.77	8.77	5	1.65	1.47	10.55	10.44	2.71
Na_2O	2.77	0.8	5	0.81	0.72	2.16	1.98	0.65
K_2O	2.13	0.47	5	0.62	0.56	1.07	0.95	0.39
P_2O_5	0.34	0.08	5	0.11	0.09	0.15	0.13	0.01
Rb	88	11	5	32.2	28.8	41	31	1,039
Sr	306	133	5	65.8	58.9	193	186	4,333
Zr	67	54	5	5.3	4.8	62	61	28
Ni	291	66	5	84.4	75.5	164	147	7,126
Cr	717	433	5	121.8	108.9	551	540	14,832
Zn	195	69	5	50.5	45.1	108	101	2,546
Pb	34	4	5	11.1	9.9	15	12	123
Y	31	19	5	5.6	5	24	24	31
Nb	11	3	5	3	2.7	6	5	9
Ba	928	176	5	333.6	283.3	413	322	111,256

C. Biotite hornblende gneiss - Nagle Dam Formation.

	Maximum	Minimum	Number of samples	Sample Standard deviation	Population standard deviation	Average	Mean	Variance
SiO_2	69.77	51.91	11	5.75	5.48	60.04	60.79	33.07
TiO_2	1.35	0.34	11	0.4	0.38	0.77	0.68	0.16
Al_2O_3	20.27	14.24	11	2	1.91	16.34	16.23	4
FeO	8.6	3.16	11	1.58	1.51	6.36	6.16	2.49
MnO	0.15	0.07	11	0.03	0.02	0.11	0.11	0.001
MgO	5.21	1.38	11	1.04	0.99	3.25	3.09	1.08
CaO	8.48	3.62	11	1.73	1.65	6.1	5.88	3.01
Na_2O	4.44	0.27	11	1.15	1.1	2.76	2.33	1.33
K_2O	2.72	0.66	11	0.61	0.58	1.7	1.57	0.37
P_2O_5	0.45	0.12	11	0.1	0.1	0.25	0.24	0.01
Rb	166	20	11	48.1	45.9	82	67	2,313
Sr	948	252	11	199.7	190.4	521	489	39,867
Zr	212	77	11	46.1	43.9	134	127	2,121
Ni	42	1	11	10.9	10.4	14	10	118
Cr	189	7	7	61.4	56.8	56	36	3,769
Zn	110	38	11	22.4	21.4	71	68	504
Pb	27	7	11	7.5	7.2	16	15	57
Y	41	13	11	9.6	9.1	25	24	92
Nb	14	3	11	3.5	3.4	9	8	12
Ba	760	346	11	146.7	139.8	515	496	21,513

D. Quatrzo-feldspathic gneiss - Nagle Dam Formation.

	Maximum	Minimum	Number of samples	Sample Standard deviation	Population standard deviation	Average	Mean	Variance
SiO_2	77.93	71.65	7	2.09	1.93	75.62	75.59	4.35
TiO_2	0.19	0.01	7	0.07	0.06	0.06	0.04	0.004
Al_2O_3	15.22	12.83	7	0.82	0.76	13.68	13.66	0.68
FeO	1.39	0.23	7	0.49	0.45	0.85	0.69	0.24
MnO	0.3	0	7	0.11	0.1	0.05	-	0.01
MgO	0.68	0	7	0.23	0.21	0.21	-	0.05
CaO	2.25	0.27	7	0.61	0.57	1.18	1.01	0.38
Na_2O	3.12	1.84	7	0.41	0.38	2.53	2.5	0.17
K_2O	8.93	3.44	7	1.88	1.74	5.5	5.25	3.54
P_2O_5	0.09	0.01	7	0.03	0.03	0.04	0.03	0.001
Rb	208	85	7	41.2	38.2	139.6	134.4	1,701
Sr	485	46	7	135.8	125.8	282.7	236.5	18,453
Zr	117	25	7	29.7	27.5	58	52.3	885
Ni	5	0	7	1.8	1.6	1.1	-	3.1
Cr	15	0	7	5.8	5.4	5.9	-	34
Zn	24	3	7	8.1	7.5	11	8.7	66
Pb	68	15	7	19.6	18.1	37.1	32.8	382
Y	34	2	7	11.8	10.9	11	6.7	139
Nb	8	0	7	3.1	2.9	2.9	-	9.8
Ba	1,196	102	7	381.9	353.6	838.3	683.6	145,832

E. Amphibolite - Valley Trust Formation.

	Maximum	Minimum	Number of samples	Sample Standard deviation	Population standard deviation	Average	Mean	Variance
SiO_2	53.95	45.91	14	2.29	2.2	49.29	49.24	5.23
TiO_2	3.43	0.67	14	0.81	0.78	1.91	1.74	0.66
Al_2O_3	16.01	6.24	14	2.44	2.35	12.18	11.91	5.96
FeO	15.47	9.62	14	2.01	1.94	12.86	12.71	4.05
MnO	0.28	0.14	14	0.03	0.03	0.22	0.22	0.001
MgO	10.33	4.17	14	2.29	2.21	7.79	7.45	5.25
CaO	14.72	9.26	14	1.87	1.8	11.8	11.66	3.5
Na_2O	3.67	0.1	14	0.87	0.83	1.66	1.35	0.75
K_2O	1.43	0.12	14	0.34	0.33	0.41	0.32	0.11
P_2O_5	0.33	0.1	14	0.08	0.07	0.19	0.18	0.006
Rb	109	5	14	26.8	25.5	19	13	701
Sr	460	65	14	91.8	88.4	165	149	8,423
Zr	201	50	14	46.5	44.8	91	82	2,164
Ni	102	20	14	30.6	29.5	70	61	937
Cr	608	100	14	163.7	157.8	377	335	26,812
Zn	163	63	14	24.9	23.9	105	102	617
Pb	16	5	14	4.4	4.3	10	9	19
Y	46	20	14	6.7	6.4	34	34	45
Nb	22	5	14	6.1	5.9	10	9	38
Ba	831	46	8	265.6	248.4	187	112	70,524

F. Quartzo-feldspathic gneiss - Valley Trust Formation.

	Maximum	Minimum	Number of samples	Sample Standard deviation	Population standard deviation	Average	Mean	Variance
SiO_2	80.9	72.04	11	2.95	2.81	76.49	76.44	8.7
TiO_2	0.44	0.01	11	0.13	0.12	0.14	0.09	0.02
Al_2O_3	15	10.95	11	1.14	1.09	12.76	12.72	1.31
FeO	2.96	0.2	11	0.81	0.77	1.1	0.86	0.65
MnO	0.06	-0.02	11	0.02	0.02	0.01	-	0.0005
MgO	1.04	0.02	11	0.33	0.31	0.25	0.12	0.11
CaO	1.77	0.07	11	0.5	0.48	0.5	0.32	0.25
Na_2O	4.11	2.8	11	0.39	0.37	3.26	3.24	0.15
K_2O	6.72	2.93	11	1.16	1.11	4.85	4.71	1.35
P_2O_5	0.2	-0.1	11	0.09	0.09	0.05	-	0.01
Rb	190	111	11	27.5	26.3	159	156	759
Sr	191	12	11	60.3	57.5	74	53	3,638
Zr	258	29	11	62.7	59.8	115	99	3,937
Ni	1	0	5	0.4	0.4	0.8	-	0.2
Cr	16	0	5	7.3	6.5	5	-	63
Zn	59	6	10	17	16.1	25	19	288
Pb	73	3	9	20.4	19.2	42	33	417
Y	79	3	8	24.4	22.8	20	13	593
Nb	23	1	10	5.9	5.6	7	6	34
Ba	900	47	11	308.5	294.2	419	291	95,196

G. Pelitic gneiss - Valley Trust Formation.

	Maximum	Minimum	Number of samples	Sample Standard deviation	Population standard deviation	Average	Mean	Variance
SiO_2	78.55	56.05	29	6.95	6.83	63.47	63.12	48.31
TiO_2	1.16	0.71	29	0.12	0.11	0.94	0.93	0.01
Al_2O_3	20.33	9.93	29	2.61	2.56	16.63	16.41	6.8
FeO	9.61	0.96	29	1.9	1.86	6.93	6.51	3.6
MnO	0.13	0.05	29	0.02	0.02	0.08	0.08	0
MgO	4.19	0.93	29	0.73	0.72	2.31	2.18	0.54
CaO	5.86	0.43	29	0.99	0.97	0.97	0.8	0.98
Na_2O	2.99	0.68	29	0.65	0.64	1.7	1.57	0.42
K_2O	9.16	1.56	29	2.49	2.45	5.44	4.87	6.19
P_2O_5	0.31	0.09	29	0.04	0.04	0.14	0.14	0
Rb	289	60	29	63.8	62.7	191	180	4,072
Sr	342	63	29	52.5	51.6	110	103	2,760
Zr	288	72	29	43.2	42.4	200	195	1,862
Ni	118	1	29	22.8	22.4	30	18	521
Cr	237	65	29	35.3	34.7	109	104	1,247
Zn	214	60	29	41.4	40.7	140	133	1,716
Pb	59	19	29	9.4	9.2	42	41	89
Y	89	33	29	14.2	14	56	54	203
Nb	19	5	29	2.8	2.8	15	15	7.9
Ba	919	362	29	111.2	109.3	713	703	12,363

H. Biotite gneiss - Valley Trust Formation.

	Maximum	Minimum	Number of samples	Sample Standard deviation	Population standard deviation	Average	Mean	Variance
SiO_2	58.52	57.47	3	0.55	0.45	57.91	57.91	0.3
TiO_2	0.95	0.87	3	0.04	0.03	0.9	0.9	0.002
Al_2O_3	19.96	19.56	3	0.2	0.17	19.74	19.74	0.04
FeO	5.9	5.49	3	0.23	0.19	5.63	5.62	0.05
MnO	0.06	0.05	3	0.01	0.005	0.05	0.05	0.00003
MgO	1.51	1.33	3	0.09	0.08	1.4	1.4	0.009
CaO	4.08	3.97	3	0.06	0.05	4.04	4.04	0.004
Na_2O	4.6	4.48	3	0.07	0.05	4.52	4.52	0.004
K_2O	4.39	4.3	3	0.05	0.04	4.34	4.34	0.002
P_2O_5	0.23	0.21	3	0.01	0.01	0.22	0.22	0.0001
Rb	156	150	3	3.4	2.8	154	154	11.9
Sr	363	140	3	123.7	101	282	259	15,300
Zr	653	597	3	28.2	23	624	624	794
Ni	1.2	0	3	0.6	0.5	0.5	-	0.4
Cr	7	4	3	1.5	1.2	6	6	2.3
Zn	142	133	3	4.7	3.9	136	136	23
Pb	43	30	3	7	5.7	35	35	49
Y	39	35	3	2	1.6	36	36	3.8
Nb	41	18	3	12.6	10.3	27	25	159
Ba	1,285	1,211	3	37.1	30.3	1,246	1,246	1,377

I. Fine grained granulite - Valley Trust Formation.

	Maximum	Minimum	Number of samples	Sample Standard deviation	Population standard deviation	Average	Mean	Variance
SiO_2	66.31	55.05	9	4.21	3.97	61.76	61.63	17.77
TiO_2	1.29	0.81	9	0.14	0.13	1	0.99	0.02
Al_2O_3	18.42	14.52	9	1.22	1.15	16.16	16.12	1.48
FeO	12.4	7.1	9	1.91	1.81	9.86	9.69	3.67
MnO	0.38	0.03	9	0.11	0.11	0.19	0.15	0.01
MgO	9.05	2.09	9	2.2	2.07	4.73	4.28	4.84
CaO	3.32	1.2	9	0.7	0.66	1.85	1.75	0.49
Na_2O	4.71	0.1	9	1.7	1.61	1.44	0.67	2.9
K_2O	4.41	0.97	9	1	0.94	2.02	1.85	1
P_2O_5	0.4	0.13	9	0.07	0.07	0.28	0.27	0.01
Rb	82	23	9	19.3	18.2	54	50	372
Sr	331	60	9	92.1	86.9	158	136	8,486
Zr	234	57	9	63.5	59.8	116	103	4,026
Ni	22	1	9	8.6	8.1	5	2	75
Cr	116	33	9	34.1	32.1	67	59	1,162
Zn	207	62	9	44.6	42.1	128	121	1,992
Pb	27	13	9	1.8	4.5	18	17	23
Y	67	31	9	11.6	10.9	42	40	135
Nb	10	5	9	2.2	2.1	7	6	4.8
Ba	1,063	193	9	303	285.7	496	421	91,809

J. Fine grained amphibolite - Valley Trust Formation.

	Maximum	Minimum	Number of samples	Sample Standard deviation	Population standard deviation	Average	Mean	Variance
SiO_2	51.85	49.3	3	1.37	1.12	50.28	50.27	1.88
TiO_2	1.3	1.12	3	0.09	0.07	1.21	1.2	0.01
Al_2O_3	14.31	13.18	3	0.63	0.51	13.9	13.89	0.39
FeO	12.94	11.67	3	0.65	0.53	12.39	12.38	0.43
MnO	0.37	0.21	3	0.08	0.07	0.28	0.27	0.01
MgO	9.22	7.16	3	1.09	0.89	7.98	7.94	1.19
CaO	12.26	11.44	3	0.41	0.34	11.88	11.88	0.17
Na_2O	1.57	0.95	3	0.33	0.27	1.33	1.3	0.11
K_2O	0.19	0.14	3	0.03	0.02	0.16	0.16	0.001
P_2O_5	0.12	0.1	3	0.01	0.01	0.11	0.11	0.0001
Rb	18	6	3	6.9	5.7	10	9	48
Sr	164	59	3	53.7	43.8	118	108	2,883
Zr	69	59	3	5.5	4.5	65	65	30
Ni	133	82	3	27.9	22.8	101	99	777
Cr	285	195	3	49.6	40.5	228	225	2,457
Zn	91	85	3	3.2	2.62	89	89	10
Pb	16	11	3	2.5	2.1	14	14	6.3
Y	35	30	3	2.5	2.1	33	33	6.3
Nb	5	5	3	0	0	5	5	0
Ba	85	76	3	4.5	3.7	81	81	20

K. Ximba Suite.

	Maximum	Minimum	Number of samples	Sample Standard deviation	Population standard deviation	Average	Mean	Variance
SiO_2	76.84	59.03	48	4.2	4.16	68.79	68.66	17.68
TiO_2	1.94	0.04	48	0.4	0.4	0.55	0.44	0.16
Al_2O_3	18.34	11.94	48	1.45	1.43	14.88	14.81	2.09
FeO	11.95	1.16	48	1.85	1.83	3.63	3.3	3.42
MnO	0.26	0.02	48	0.04	0.04	0.06	0.05	0.002
MgO	2.2	0.1	48	0.53	0.52	0.72	0.54	0.28
CaO	5.3	0.61	48	0.96	0.95	2.3	2.11	0.91
Na_2O	3.86	2.24	48	0.36	0.36	3.02	3	0.13
K_2O	7.02	1.81	48	0.96	0.95	4.92	4.8	0.91
P_2O_5	0.71	-0.1	48	0.18	0.18	0.21	-	0.03
Rb	194	81	48	24.7	24.5	136	134	612
Sr	603	83	48	117.1	115.9	248	226	13,718
Zr	937	149	48	142.3	140.8	341	318	20,259
Ni	5	0	22	1.8	1.74	2	-	3.2
Cr	32	0	20	7.4	7.2	5	-	55
Zn	140	25	42	26.2	25.8	76	72	684
Pb	54	23	34	6.5	6.4	37	37	42
Y	80	4	42	17.1	16.9	33	28	293
Nb	25	1	42	4.3	4.2	15	14	18
Ba	2,717	369	48	624.4	617.8	1,614	1,473	389,831

L. Mlahlanja Suite.

	Maximum	Minimum	Number of samples	Sample Standard deviation	Population standard deviation	Average	Mean	Variance
SiO_2	78.11	60.36	31	4.61	4.53	68.62	68.47	21.2
TiO_2	1.31	0.24	31	0.29	0.29	0.59	0.52	0.09
Al_2O_3	17.2	11.96	31	1.19	1.17	14.22	14.18	1.4
FeO	9.06	1.96	31	2.03	1.99	4.88	4.43	4.1
MnO	0.16	0	31	0.04	0.04	0.07	-	0
MgO	1.44	0.07	31	0.41	0.4	0.54	0.37	0.17
CaO	4.85	1.47	31	0.88	0.86	2.6	2.46	0.77
Na_2O	3.66	2.13	31	0.43	0.42	2.8	2.77	0.18
K_2O	6.81	3.17	31	0.91	0.9	4.71	4.63	0.83
P_2O_5	0.84	0.07	31	0.21	0.21	0.33	0.26	0.04
Rb	203	84	31	28.4	28	129	126	809
Sr	376	135	31	76.7	75.5	246	234	5,887
Zr	712	178	31	160.7	158.1	411	379	25,843
Ni	2	1	5	0.5	0.49	1	1	0.3
Cr	22	1	5	8.8	7.86	12	7	77.3
Zn	174	50	31	40.6	40	100	92	1,652
Pb	41	29	31	3.3	3.2	34	34	10.7
Y	96	26	31	21.6	21.2	53	49	467
Nb	31	6	31	7.8	7.7	18	16	60.6
Ba	2,315	1,121	31	326.6	321.3	1,577	1,546	106,694

M. Nqwadolo Suite.

	Maximum	Minimum	Number of samples	Sample Standard deviation	Population standard deviation	Average	Mean	Variance
SiO_2	77.43	74.49	12	1.09	1.05	75.93	75.92	1.2
TiO_2	0.16	0.06	12	0.03	0.03	0.12	0.11	0.001
Al_2O_3	14.21	11.55	12	0.83	0.79	12.98	12.96	0.68
FeO	1.76	1	12	0.25	0.24	1.37	1.35	0.06
MnO	0.17	0.01	12	0.04	0.04	0.03	0.02	0.002
MgO	0.48	0	12	0.14	0.14	0.14	-	0.02
CaO	1.01	0.47	12	0.14	0.14	0.79	0.77	0.02
Na_2O	4.48	2.89	12	0.47	0.45	3.35	3.32	0.22
K_2O	5.84	3.62	12	0.6	0.57	5.05	5.01	0.36
P_2O_5	0.19	0.01	12	0.07	0.07	0.08	0.05	0.005
Rb	249	175	12	26	24.9	209	208	674
Sr	35	6	12	9.3	8.9	14	12	87
Zr	142	75	12	22.7	21.8	116	114	517
Ni	0.9	0.9	1	-	0	0.9	0.9	-
Zn	136	78	12	15.6	15	94	93	245
Pb	75	44	12	9.6	9.2	56	55	92
Y	216	46	12	54	51.7	98	87	2,918
Nb	56	12	12	13.8	13.2	23	21	190
Ba	600	16	12	171.3	164	175	114	29,356

APPENDIX 5

FRACTIONATION MODELLING

Major element fractionation modelling was undertaken using the least-squares major element approximation method, with average microprobe mineral compositions (Appendix 2) utilised for the appropriate unit, or where unavailable, mineral compositions from the literature, as referenced in the individual model tables. Trace element variations were modeled with the Rayleigh distilation law, using the KD utilised by Ramo (1991), after Arth (1976) and given below.

	Horn	Bio	Plag	K-feld	Opx	Cpx	Quartz	Magnetite	Ilmenite	Apatite
Rb	0.014	2.24	0.041	0.34	0.003	0.032	0.014	0.5	0	0
Sr	0.022	0.12	4.4	3.87	0.009	0.516	0	0.7	0	5
Ba	0.044	6.4	0.308	6.12	0.003	0.131	0.023	0.4	0	0

F : Fraction of residual liquid remaining

SSR : Sum of the squares of the residuals

APPENDIX 5.1. BIOTITE HORNBLENDE GNEISS - LOW SILICA SERIES.

CUMULATE MODEL.

a) Major Elements (wt%).

	Initial	Model	Evolved	(Minerals after Pitcher *et al.* 1985, Lachize *et al.* 1996, Ramo 1991)
SiO_2	57.64	57.42	60.95	SSR 0.06
TiO_2	1.1	1.01	0.5	Hornblende - 0.05
Al_2O_3	17.06	17.05	14.78	Plagioclase - 0.2875
FeO	7.44	7.42	7.21	Magnetite - 0.0175
MnO	0.14	0.13	0.13	Ilmenite - 0.014
MgO	3.97	4	5.21	Apatite - 0.00475
CaO	7.3	7.33	6.81	F - 0.62625
Na_2O	2.28	2.36	0.27	
K_2O	1.78	1.76	2.72	
P_2O_5	0.28	0.28	0.12	

b) Trace Elements (ppm).

	Melt			Cumulate		
F	Rb	Sr	Ba	Rb	Sr	Ba
0.95	107	477	493	3.5	1755	117
0.9	113	418	513	3.6	1649	120
0.8	127	313	561	3.8	1453	125
0.7	144	226	621	4	1277	131
0.6	167	155	698	4.3	1120	138
0.5	199	99	801	4.7	983	147
0.4	247	57	949	5.1	863	158
0.3	327	28	1179	5.7	761	172
0.2	483	10	1603	6.7	674	192
0.1	944	2	2710	8.4	601	226

APPENDIX 5.2. BIOTITE HORNBLENDE GNEISS - HIGH SILICA SERIES.

FRACTIONATION MODEL.

a) Major Elements (wt%).

	Initial	Model	Evolved	(Minerals after Pitcher *et al.* 1985, Lachize *et al.* 1996, Ramo, 1991)
SiO_2	64.13	69.95	69.77	SSR 0.16
TiO_2	0.39	0.44	0.39	Hornblende - 0.075
Al_2O_3	14.46	15.67	15.38	Biotite - 0.005
FeO	6.31	3.25	3.16	Plagioclase - 0.1575
MnO	0.13	0.03	0.07	K-feldspar - 0.0275
MgO	3.22	1.42	1.38	Clinopyroxene - 0.06
CaO	6.2	3.58	3.62	Orthopyroxene - 0.0225
Na_2O	2.84	3.57	3.74	Magnetite - 0.025
K_2O	1.57	1.95	1.96	Apatite - 0.0021
P_2O_5	0.18	0.16	0.16	Quartz - 0.06
				F - 0.5654

b) Trace Elements (ppm).

	Melt		
F	Rb	Sr	Ba
0.95	34	495	395
0.9	35	471	404
0.8	39	421	423
0.7	45	372	447
0.6	51	321	475
0.5	61	271	511
0.4	75	219	559
0.3	98	167	627
0.2	143	114	738
0.1	273	59	975

APPENDIX 5.3. BIOTITE HORNBLENDE GNEISS - HIGH SILICA SERIES.

CUMULATE MODEL.

a) Major Elements (wt%).

	Initial	Model	Evolved	(Minerals after Pitcher *et al.* 1985, Lachize *et al.* 1996, Ramo1991)
SiO_2	65.82	65.81	69.77	SSR 0.26
TiO_2	0.45	0.44	0.39	Hornblende - 0.1
Al_2O_3	15.09	14.7	15.38	Biotite - 0.0075
FeO	5.08	5.05	3.16	Plagioclase - 0.05
MnO	0.1	0.14	0.07	K-feldspar - 0.0125
MgO	2.69	2.69	1.38	Oxide - 0.0014
CaO	4.85	4.89	3.62	Quartz - 0.005
Na_2O	2.86	3.27	3.74	F - 0.8236
K_2O	1.79	1.86	1.96	
P_2O_5	0.19	0.19	0.16	

b) Trace Elements (ppm).

	Melt			Cumulate		
F	Rb	Sr	Ba	Rb	Sr	Ba
0.95	81	449	538	10	670	409
0.9	84	438	545	10	662	411
0.8	94	414	561	11	645	417
0.7	105	388	579	12	627	423
0.6	120	361	600	12	608	430
0.5	141	331	627	13	589	437
0.4	171	298	660	14	568	446
0.3	220	260	707	16	546	457
0.2	312	214	778	18	521	471
0.1	571	154	916	22	494	489

APPENDIX 5.4. QUARTZO-FELDSPATHIC GNEISS - HIGH Zr/Y SERIES - VALLEY TRUST FORMATION.

FRACTIONATION MODEL.

a) Major Elements (wt%).

	Initial	Model	Evolved	(Minerals after Pitcher *et al.* 1985, oxide and apatite after Ramo 1991)
SiO_2	74.86	77.82	77.9	SSR 0.03
TiO_2	0.14	0.03	0.01	Hornblende - 0.015
Al_2O_3	13.2	12.37	12.33	Biotite - 0.0195
FeO	1.3	0.62	0.63	Plagioclase - 0.11
MnO	0.02	0	0	Oxide - 0.001
MgO	0.62	0.2	0.07	Apatite - 0.0025
CaO	0.98	0.45	0.46	F - 0.825
Na_2O	3.52	2.9	2.86	
K_2O	5	5.47	5.54	
P_2O_5	0.1	0	0	

b) Trace Elements (ppm).

	Melt		
F	Rb	Sr	Ba
0.95	127	120	740
0.9	132	105	737
0.8	143	80	730
0.7	156	58	723
0.6	173	40	714
0.5	196	26	705
0.4	228	15	692
0.3	277	8	678
0.2	363	3	657
0.1	579	1	623

APPENDIX 5.5. QUARTZO-FELDSPATHIC GNEISS - HIGH Zr/Y SERIES - VALLEY TRUST FORMATION.

CUMULATE MODEL.

a) Major Elements (wt%).

	Initial	Model	Evolved	(K-feldspar and biotite after Pitcher *et al.* 1985, plagioclase from Ramo 1991)
SiO_2	76.38	76.37	77.9	SSR 0.05
TiO_2	0.09	0.08	0.01	Biotite -.0.0185
Al_2O_3	12.71	12.84	12.33	Plagioclase - 0.085
FeO	0.91	0.91	0.63	K-feldspar - 0.085
MnO	0	0.01	0	Quartz - 0.064
MgO	0.26	0.28	0.07	F - 0.7475
CaO	0.51	0.59	0.46	
Na_2O	3.26	3.09	2.86	
K_2O	5.66	5.63	5.54	
P_2O_5	0	0	0	

b) Trace Elements (ppm).

	Melt			Cumulate		
F	Rb	Sr	Ba	Rb	Sr	Ba
0.95	177	57	332	51	165	912
0.9	184	51	304	52	158	874
0.8	200	42	251	54	144	802
0.7	220	33	202	56	130	733
0.6	245	25	157	59	118	667
0.5	279	18	116	63	106	606
0.4	327	12	81	67	95	548
0.3	401	7	51	72	85	494
0.2	534	3	26	80	77	445
0.1	872	1	8	93	69	400

APPENDIX 5.6. LOW Zr/Y AMPHIBOLITE - VALLEY TRUST FORMATION.

FRACTIONATION MODEL - IRON ENRICHMENT TREND.

a) Major Elements (wt%).

	Initial	Model	Evolved	(Mineral chemistries from Wood 1978, apatite, ilmenite and magnetite from Ramo 1991)
SiO_2	48.81	48.62	48.2	SSR 0.42
TiO_2	1.57	1.86	2.17	Plagioclase - 0.033
Al_2O_3	10.39	12.2	12.19	Clinopyroxene - 0.2175
FeO	13.23	14.14	14.12	Olivine - 0.03
MnO	0.24	0.32	0.22	Apatite - 0.0009
MgO	10.33	8.3	8.36	F - 0.7186
CaO	12.87	11.23	11.35	
Na_2O	1.11	1.47	1.66	
K_2O	0.17	0.24	0.52	
P_2O_5	0.14	0.14	0.14	

APPENDIX 5.7. LOW Zr/Y AMPHIBOLITE - VALLEY TRUST FORMATION.

FRACTIONATION MODEL - IRON DEPLETION TREND.

a) Major Elements (wt%).

	Initial	Model	Evolved	(Mineral chemistries from Ramo 1991, plagioclase from Wood 1978)
SiO_2	48.2	53.33	53.95	SSR 0.67
TiO_2	2.17	0.75	0.88	Plagioclase - 0.106
Al_2O_3	12.19	15.95	16.01	Clinopyroxene - 0.252
FeO	14.12	9.6	9.62	Olivine - 0.107
MnO	0.22	0.15	0.17	Apatite - 0.0001
MgO	8.36	4.44	4.73	Magnetite - 0.0025
CaO	11.35	9.68	9.65	Ilmenite - 0.0275
Na_2O	1.66	2.79	2.7	F - 0.5049
K_2O	0.52	0.92	0.51	
P_2O_5	0.14	0.27	0.27	

APPENDIX 5.8. HIGH Zr/Y AMPHIBOLITE - VALLEY TRUST FORMATION.

FRACTIONATION MODEL - IRON ENRICHMENT TREND - PHASE 1.

a) Major Elements (wt%).

	Initial	Model	Evolved	(Plagioclase and olivine from Wood 1978, clinopyroxene from Fram and Lesher 1997)
SiO_2	48.94	48.42	46.29	SSR 5.55
TiO_2	1.31	1.74	2.24	Plagioclase - 0.1
Al_2O_3	12.67	13.5	13.51	Clinopyroxene - 0.225
FeO	10.9	13.54	13.52	Olivine - 0.025
MnO	0.2	0.28	0.22	F - 0.65
MgO	9.34	7.09	7.06	
CaO	13.4	11.21	11.49	
Na_2O	1.04	1.25	2.07	
K_2O	0.25	0.32	0.41	
P_2O_5	0.1	0.15	0.2	

APPENDIX 5.9. HIGH Zr/Y AMPHIBOLITE - VALLEY TRUST FORMATION.

FRACTIONATION MODEL - IRON ENRICHMENT TREND - PHASE 2.

a) Major Elements (wt%).

	Initial	Model	Evolved	(Plagioclase and olivine from Wood 1978, clinopyroxene from Fram and Lesher 1997)
SiO_2	46.29	46.49	49.22	SSR 8.01
TiO_2	2.24	2.7	2.96	Plagioclase - 0.16
Al_2O_3	13.51	12.52	12.49	Clinopyroxene - 0.14
FeO	13.52	15.07	15.04	Olivine - 0.0425
MnO	0.22	0.31	0.23	Apatite - 0.001
MgO	7.06	5.41	5.44	Magnetite - 0.0175
CaO	11.49	9.4	9.43	F - 0.639
Na_2O	2.07	2.82	2.12	
K_2O	0.41	0.54	0.39	
P_2O_5	0.2	0.25	0.26	

APPENDIX 5.10. HIGH Zr/Y AMPHIBOLITE - VALLEY TRUST FORMATION.

FRACTIONATION MODEL - IRON DEPLETION TREND.

a) Major Elements (wt%).

	Initial	Model	Evolved	(Plagioclase and olivine from Wood 1978, clinopyroxene from Fram and Lesher 1997)
SiO_2	46.29	48.79	51.5	SSR 7.84
TiO_2	2.24	1.83	1.82	Plagioclase - 0.12
Al_2O_3	13.51	14.85	14.9	Clinopyroxene - 0.20
FeO	13.52	10.2	10.27	Olivine - 0.035
MnO	0.22	0.19	0.14	Apatite - 0.001
MgO	7.06	5.9	5.92	Magnetite - 0.04
CaO	11.49	9.46	9.32	F - 0.604
Na_2O	2.07	3	3.67	
K_2O	0.41	0.59	0.71	
P_2O_5	0.2	0.26	0.28	

APPENDIX 5.11. MARGINAL GRANITE - BIOTITE GRANITE SERIES.

CUMULATE MODEL - 1.

a) Major Elements (wt%).

	Initial	Model	Evolved	(Apatite and ilmenite after Ramo 1991)
SiO_2	70.18	70.15	74.09	SSR 0.33
TiO_2	0.57	0.52	0.17	Hornblende - 0.065
Al_2O_3	14.8	14.52	13.98	Plagioclase - 0.065
FeO	2.81	2.96	1.16	K-feldspar - 0.0425
MnO	0.04	0.07	0.03	Ilmenite - 0.005
MgO	0.8	0.45	0.26	Apatite - 0.002
CaO	1.96	1.9	0.88	F - 0.8205
Na_2O	3.07	3.38	3.29	
K_2O	4.86	4.88	5.06	
P_2O_5	0.2	0.2	0.14	

b) Trace Elements (ppm).

	Melt			Cumulate		
F	Rb	Sr	Ba	Rb	Sr	Ba
0.95	149	247	1514	15	663	2422
0.9	156	227	1467	15	636	2386
0.8	174	189	1371	16	585	2312
0.7	196	153	1269	17	537	2235
0.6	225	120	1161	18	490	2156
0.5	265	90	1045	19	446	2073
0.4	324	63	919	21	404	1985
0.3	419	40	779	23	366	1893
0.2	604	21	616	26	330	1795
0.1	1127	7	413	33	297	1686

APPENDIX 5.12. MARGINAL GRANITE - BIOTITE GRANITE SERIES.

CUMULATE MODEL - 2.

a) Major Elements (wt%).

	Initial	Model	Evolved	(Apatite after Ramo 1991)
SiO_2	70.18	70.22	74.09	SSR 0.36
TiO_2	0.57	0.32	0.17	Hornblende - 0.055
Al_2O_3	14.8	14.62	13.98	Plagioclase - 0.07
FeO	2.81	2.98	1.16	K-feldspar - 0.04
MnO	0.04	0.07	0.03	Apatite - 0.002
MgO	0.8	0.47	0.26	Quartz - 0.05
CaO	1.96	1.81	0.88	F - 0.783
Na_2O	3.07	3.37	3.29	
K_2O	4.86	4.95	5.06	
P_2O_5	0.2	0.2	0.14	

b) Trace Elements (ppm).

	Melt			Cumulate		
F	Rb	Sr	Ba	Rb	Sr	Ba
0.95	148	248	1479	44	645	3087
0.9	154	229	1398	46	621	3005
0.8	167	192	1238	47	573	2842
0.7	183	157	1079	50	527	2680
0.6	204	125	920	52	483	2517
0.5	231	95	762	55	441	2356
0.4	270	68	605	59	401	2195
0.3	329	44	450	63	364	2034
0.2	436	24	296	70	329	1875
0.1	704	8	145	81	297	1716

APPENDIX 5.13. MARGINAL GRANITE - BIOTITE GRANITE SERIES.

CUMULATE MODEL - 3.

a) Major Elements (wt%).

	Initial	Model	Evolved	(Apatite after Ramo 1991)
SiO_2	72.44	72.43	74.09	SSR 0.31
TiO_2	0.33	0.3	0.17	Hornblende - 0.0525
Al_2O_3	13.89	13.44	13.98	Biotite - 0.0225
FeO	2.57	2.85	1.16	Plagioclase - 0.07
MnO	0.04	0.06	0.03	K-feldspar - 0.09
MgO	0.56	0.43	0.26	Apatite - 0.0009
CaO	1.59	1.54	0.88	Quartz - 0.1075
Na_2O	2.83	2.91	3.29	F - 0.6566
K_2O	4.92	4.95	5.06	
P_2O_5	0.13	0.13	0.14	

b) Trace Elements (ppm).

	Melt			Cumulate		
F	Rb	Sr	Ba	Rb	Sr	Ba
0.95	153	158	986	37	314	2123
0.9	159	150	930	38	306	2064
0.8	174	135	817	39	291	1946
0.7	192	119	706	41	276	1829
0.6	216	103	597	43	261	1712
0.5	248	87	489	46	245	1597
0.4	293	70	383	50	230	1483
0.3	364	54	280	54	214	1370
0.2	494	37	180	60	198	1259
0.1	834	19	84	71	182	1150

APPENDIX 5.14. MARGINAL GRANITE - BIOTITE GRANITE SERIES.

CUMULATE MODEL - 4.

a) Major Elements (wt%).

	Initial	Model	Evolved	(Apatite after Ramo 1991)
SiO_2	72.09	72.09	74.09	SSR 0.18
TiO_2	0.4	0.3	0.17	Hornblende - 0.051
Al_2O_3	13.93	13.66	13.98	Plagioclase - 0.07
FeO	2.62	2.81	1.16	Biotite - 0.0215
MnO	0.04	0.06	0.03	K-feldspar - 0.09
MgO	0.64	0.43	0.26	Apatite - 0.0011
CaO	1.63	1.6	0.88	Quartz - 0.0915
Na_2O	2.85	2.97	3.29	F - 0.6749
K_2O	5	5.03	5.06	
P_2O_5	0.14	0.14	0.14	

b) Trace Elements (ppm).

	Melt			Cumulate		
F	Rb	Sr	Ba	Rb	Sr	Ba
0.95	153	183	1158	38	385	2617
0.9	159	173	1086	39	374	2537
0.8	174	153	944	40	354	2380
0.7	192	133	805	42	333	2225
0.6	215	113	670	45	313	2072
0.5	247	93	539	47	293	1923
0.4	291	74	413	51	272	1776
0.3	361	55	294	55	252	1633
0.2	489	36	181	62	232	1493
0.1	820	17	79	72	213	1359

APPENDIX 5.15. HORNBLENDE GRANITE - SUBCHARNOCKITE - CHARNOCKITE - MLAHLANJA SUITE.

FRACTIONATION MODEL - BASIC - INTERMEDIATE.

a) Major Elements (wt%).

	Initial	Model	Evolved	(Apatite and oxide after Ramo 1991)
SiO_2	60.36	69.51	70.06	SSR 0.91
TiO_2	1.15	0.39	0.4	Hornblende - 0.15
Al_2O_3	14.19	14.62	14.12	Plagioclase - 0.135
FeO	9.06	3.53	3.67	Biotite - 0.02
MnO	0.1	-0.11	0.05	K-feldspar - 0.02
MgO	1.43	1.01	0.54	Clinopyroxene - 0.025
CaO	4.85	1.94	2.09	Orthopyroxene - 0.025
Na_2O	3.14	2.8	2.89	Apatite - 0.016
K_2O	3.63	4.91	5.15	Oxide - 0.01
P_2O_5	0.84	0.26	0.26	F - 0.599

b) Trace Elements (ppm).

	Melt		
F	Rb	Sr	Ba
0.95	88	359	1864
0.9	92	341	1890
0.8	102	306	1945
0.7	114	271	2011
0.6	130	235	2089
0.5	151	199	2185
0.4	183	162	2309
0.3	234	124	2479
0.2	330	85	2740
0.1	595	45	3252

APPENDIX 5.16. HORNBLENDE GRANITE - SUBCHARNOCKITE - CHARNOCKITE - MLAHLANJA SUITE.

FRACTIONATION MODEL - INTERMEDIATE - ACID.

a) Major Elements (wt%).

	Initial	Model	Evolved	(Apatite and oxide after Ramo 1991)
SiO_2	70.06	75.52	75.51	SSR 0.06
TiO_2	0.4	0.11	0.25	Hornblende - 0.025
Al_2O_3	14.12	12.63	12.55	Plagioclase - 0.105
FeO	3.67	2.12	1.97	Biotite - 0.05
MnO	0.05	0.03	0.03	K-feldspar - 0.075
MgO	0.54	0.26	0.26	Apatite - 0.005
CaO	2.09	1.4	1.47	F - 0.74
Na_2O	2.89	2.45	2.4	
K_2O	5.15	4.83	4.79	
P_2O_5	0.26	0.06	0.07	

b) Trace Elements (ppm).

	Melt		
F	Rb	Sr	Ba
0.95	156	167	1240
0.9	159	150	1105
0.8	168	118	860
0.7	179	90	648
0.6	192	66	467
0.5	208	46	317
0.4	230	29	197
0.3	262	16	107
0.2	315	7	45
0.1	432	2	10

APPENDIX 5.17. HORNBLENDE GRANITE - SUBCHARNOCKITE - CHARNOCKITE - MLAHLANJA SUITE.

CUMULATE MODEL.

a) Major Elements (wt%).

	Initial	Model	Evolved	(Apatite and oxide after Ramo 1991)
SiO_2	70.06	70.05	75.51	SSR 0.11
TiO_2	0.4	0.37	0.25	Hornblende - 0.04
Al_2O_3	14.12	13.91	12.55	Plagioclase - 0.125
FeO	3.67	3.71	1.97	Biotite - 0.025
MnO	0.05	0.07	0.03	K-feldspar - 0.135
MgO	0.54	0.51	0.26	Orthopyroxene - 0.0125
CaO	2.09	2.33	1.47	Clinopyroxene - 0.005
Na_2O	2.89	2.85	2.4	Apatite - 0.005
K_2O	5.15	5.16	4.79	Quartz - 0.0375
P_2O_5	0.26	0.26	0.07	F - 0.615

b) Trace Elements (ppm).

	Melt			Cumulate		
F	Rb	Sr	Ba	Rb	Sr	Ba
0.95	158	168	1269	43	506	3535
0.9	164	152	1159	44	482	3386
0.8	178	123	953	46	437	3100
0.7	197	95	762	48	395	2828
0.6	220	71	589	51	356	2571
0.5	250	51	435	54	319	2329
0.4	294	33	300	57	286	2103
0.3	362	20	186	62	256	1895
0.2	484	9	94	69	229	1704
0.1	798	3	30	80	205	1532

APPENDIX 5.18. NQWADOLO SUITE.

FRACTIONATION MODEL.

a) Major Elements (wt%).

	Initial	Model	Evolved	(Biotite and apatite from Ramo 1991)
SiO_2	74.71	76.45	77.42	SSR 0.96
TiO_2	0.13	0.12	0.11	Biotite- 0.0075
Al_2O_3	13.34	12.39	12.41	Plagioclase - 0.075
FeO	1.47	1.37	1.45	K-feldspar - 0.05
MnO	0.02	0.02	0.01	Apatite - 0.00175
MgO	0.11	0.12	0.07	F - 0.86575
CaO	0.86	0.76	0.83	
Na_2O	3.43	2.88	2.89	
K_2O	5.31	5.22	5.26	
P_2O_5	0.09	0.02	0.02	

b) Trace Elements (ppm).

	Melt		
F	Rb	Sr	Ba
0.95	197	21	219
0.9	205	18	198
0.8	223	12	160
0.7	246	8	126
0.6	275	5	95
0.5	314	3	68
0.4	369	2	46
0.3	455	1	27
0.2	611	0.2	13
0.1	1009	0	4

APPENDIX 5.19. NQWADOLO SUITE.

CUMULATE MODEL.

a) Major Elements (wt%).

	Initial	Model	Evolved	(Biotite, apatite and ilmenite from Ramo 1991)
SiO_2	76.02	76.34	77.42	SSR 0.148
TiO_2	0.13	0.17	0.11	Biotite - 0.005
Al_2O_3	12.78	12.86	12.41	Plagioclase - 0.04
FeO	1.45	1.59	1.45	K-feldspar - 0.02
MnO	0.04	0.01	0.01	Ilmenite - 0.001
MgO	0.16	0.07	0.07	Apatite - 0.0015
CaO	0.84	0.91	0.83	F - 0.9325
Na_2O	3.2	3.18	2.89	
K_2O	5.19	5.24	5.26	
P_2O_5	0.08	0.08	0.02	

b) Trace Elements (ppm).

	Melt			Cumulate		
F	Rb	Sr	Ba	Rb	Sr	Ba
0.95	207	15	141	59	61	362
0.9	216	13	130	60	57	348
0.8	234	9	109	63	49	322
0.7	258	6	90	66	42	297
0.6	287	4	72	69	37	272
0.5	327	2	55	73	32	249
0.4	383	1	40	78	28	227
0.3	470	0.5	26	84	24	206
0.2	626	0.2	14	93	21	186
0.1	1023	0.02	5	109	19	168